FACULTAD DE CIENCIAS

DEPARTAMENTO DE QUÍMICA ORGÁNICA

SUBPHTHALOCYANINE-BASED SYSTEMS FOCUSED ON MOLECULAR PHOTOVOLTAICS

GERMÁN ZANGO CASADO

Doctoral Thesis

Madrid, 2016

The present work has been developed at the Organic Chemistry Department of Universidad Autónoma de Madrid, under the supervision of Dr. Mª Victoria Martínez Díaz and Prof. Tomás Torres Cebada.

Agradecimientos

Resumir todo un doctorado en un “librito” no es tarea fácil. Pero más complicado es recordar a todos los que han compartido estos cinco largos años contigo en unas pocas líneas. Aún así, lo intentaré.

Quiero empezar expresando mi más sincero agradecimiento a mis directores por su apoyo y confianza constantes. A **Tomás**, por darme la oportunidad de llevar a cabo este trabajo. Eres un gran ejemplo profesional y personal para mí. Gracias a **Mariví** por ayudarme a convertirme en el científico que hoy puedo decir que soy, por enseñarme a ser riguroso y objetivo en mi investigación y por transmitirme la pasión por nuestra labor. En este párrafo, quiero incluir al “tercer director” de esta tesis. **Christian**, una buena parte de este trabajo está inspirado en algunas de tus grandes ideas. Espero que, allí donde estés, te sientas orgulloso de lo que hemos conseguido. Creo que habrías disfrutado mucho leyendo esta tesis.

Gracias a todos los colaboradores de los grupos del **Profesor Shu Seki** en Kyoto, **Tom Aernouts** en Leuven, el **Profesor René Janssen** en Eindhoven y el **Profesor Dirk Guldi** en Erlangen, que han aportado su (enorme) granito de arena en esta tesis. Sin su esfuerzo, este trabajo no habría salido adelante.

En nuestro grupo de investigación, he tenido la oportunidad de coincidir con excelentes profesionales y mejores personas. A **Puri, Gema, Salomé, David, Gianni, Max, Andrés y Esmeralda**, gracias por vuestra ayuda y consejos durante estos años. A **Miguelito** e **Isma**, por las charlas científicas y los buenos ratos en esta última etapa. A **Giulia** y a **Lara**, por hacer tan fácil y agradable la convivencia en el 301. A todos los demás, a los que han pasado, a los que están y a los que acaban de llegar: ha sido un placer trabajar a vuestro lado y compartir el día a día con vosotros.

Hay personas especiales que se cruzan en tu vida en situaciones concretas pero que llegan para quedarse. A **Dani**, **Pablito**, **Jorge**, **Vio** y **Carlos**, gracias por hacerme recordar la Autónoma con cariño para siempre. A **Raquel** y **Miguel**, porque los cafés saben mejor con vosotros. A **Romi**, por su fidelidad y amistad. A **Hoyito**, por enseñarme a afrontar todo con una sonrisa. A **Alja**, por aguantarme en el laboratorio y por todo lo que te queda en el futuro. A **Eveline**, porque todo lo que me hace rabiar, me lo hace reír, y eso solo lo hacen los hermanos. A **Jose**, **Manu**, **Lau**, **Irene** y **Pau**, por haberme acogido como uno más en vuestra pequeña familia. Sois geniales. Y especialmente, a los doctores **Javi** y **Edu**. Ahora que se nos ha acabado una etapa, me doy cuenta más que nunca de la suerte que he tenido de compartir estos años con

vosotros. Sé que conseguiréis todo lo que os propongáis, y pienso estar ahí para celebrarlo con vosotros.

Mil gracias a **mi madre** y a **mi padre**. Sois los pilares en los que me he podido apoyar siempre para crecer y llegar hasta donde estoy hoy. Esta tesis es tan mía como vuestra. Por eso y por mil motivos más, gracias. A mi hermano **Daniel**, porque siguiendo tu ejemplo desde pequeño todo ha sido mucho más fácil. A mi abuela **Ofelia**, que aunque no pare de decirme que no piensa venir a verme, sé que va a ser la abuela más orgullosa del mundo. A **Salomé**, por su apoyo constante e incondicional.

Para acabar, a veces la química te reserva sorpresas maravillosas. A **Sara**. Porque tú mejor que nadie entiendes lo que significa esto para mí. Por regalarme tu apoyo, confianza y cariño cada día. Por hacerme ver este momento no solo como un final feliz, sino como el comienzo de una gran aventura. Gracias.

Abbreviations and acronyms

We have used standard Organic Chemistry abbreviations and acronyms following the recommendation of the "Guidelines for authors", *J. Org. Chem.* **2016**, which can be found in the journal webpage:
http://pubs.acs.org/paragonplus/submission/joceah/joceah_authguide.pdf

In addition, the following abbreviations have been employed during this dissertation:

A	Acceptor
AS	Admittance Spectroscopy
BCP	Bathocuproine
BHJ	Bulk Heterojunction
CNT	Carbon Nanotube
CT	Charge Transfer
D	Donor
DIP	Diindeno[1,2,3-cd:1',2',3'-lm]perylene
DPV	Differential Pulse Voltammetry
DSSC	Dye-Sensitized Solar Cell
EBL	Exciton-Blocking Barrier
E_{DA}	Interface gap energy
$E_{g,opt}$	Optical band gap
EQE	External Quantum Efficiency
ETL	Electron Transport Layer
Fc	Ferrocene
FET	Field-Effect Transistor
FF	Fill Factor
FP-TRMC	Flash-Photolysis Time-Resolved Microwave Conductivity
γ	Field-dependence factor
HCL	Hole Collection Layer
HTL	Hole Transport Layer
IPCE	Incident Photon-to-Current Efficiency
I_{SC}	Short-circuit current

J_{SC}	Short-circuit current density
K	Association constant
LED	Light-Emitting Diode
μ	Mobility
M_{PP}	Maximum Power Point
η	Power conversion efficiency
NFA	Non-Fullerene Acceptor
NLO	Non-Linear Optics
o-DCB	*ortho*-Dichlorobenzene
OSC	Organic Solar Cell
φ	Photocarrier generation yield
ϕ_F	Fluorescence quantum yield
P3HT	Poly(3-hexylthiophene-2,5-diyl)
PA	Photo-absorption
Pc	Phthalocyanine
PCBM	Phenyl-C_n-Butyric acid Methyl ester
PCE	Power Conversion Efficiency
PEDOT:PSS	Poly(3,4-ethylenedioxythiophene)-poly(styrenesulfonate)
PHJ	Planar Heterojunction
P	Porphyrin
PSC	Perovskite Solar Cell
PTB7	Poly({4,8-bis[(2-ethylhexyl)oxy]benzo[1,2-b:4,5-b']dithiophene-2,6-diyl}{3-fluoro-2-[(2-ethylhexyl)carbonyl]thieno[3,4-*b*]thiophenediyl})
PV	Photovoltaics
Pz	Porphyrazine
SCRF	Self-Consistent Reaction Field
SubNc	Subnaphthalocyanine
SubPc	Subphthalocyanine
SubP	Subporphyrin
SubPz	Subporphyrazine

SWV	Square-Wave Voltammetry
TAS	Transient Absorption Spectroscopy
$TBAPF_6$	Tetrabutylammonium hexafluorophosphate
TEM	Transmission Electron Microscopy
V_{OC}	Open-circuit voltage

To date, the results reported in the present work have led to the following publications:

(i) "Decreased Recombination Through the Use of a Non-Fullerene Acceptor in a 6.4% Efficient Organic Planar Heterojunction Solar Cell", Verreet, B.; Cnops, K.; Cheyns, D.; Heremans, P.; Stesmans, A.; Zango, G.; Claessens, C. G.; Torres, T.; Rand, B. P. *Adv. Energy Mater.* **2014**, *4*, 1301413.

(ii) "A Push-Pull Unsymmetrical Subphthalocyanine Dimer", Zango, G.; Zirzlmeier, J.; Claessens, C. G.; Clark, T.; Martinez-Diaz, M. V.; Guldi, D. M.; Torres, T. *Chem. Sci*. **2015**, *6*, 5571.

(iii) "Energy Level Tuning of Non-fullerene Acceptors in Organic Solar Cells", Cnops, K.; Zango, G.; Genoe, J.; Heremans, P.; Martínez-Díaz, M. V.; Torres, T.; Cheyns, D. *J. Am. Chem. Soc.* **2015**, *137*, 8991.

(iv) "The role of the axial substituent in subphthalocyanine acceptors for bulk-heterojunction solar cells", Zango, G.; Duan, C.; García Iglesias, M.; Colberts, F. J. M.; Wienk, M. M.; Martínez-Díaz, M. V.; Janssen, R. A. J.; Torres, T. *Angew. Chem. Int. Ed.* **2016**, DOI: 10.1002/anie.201608644R1.

Table of Contents

Introduction

Nanoscience, Nanotechnology and Organic Molecular Materials

"…I would like to describe a field, in which little has been done, but in which an enormous amount can be done in principle. This field is not quite the same as the others in that it will not tell us much of fundamental physics (in the sense of, 'What are the strange particles?') but it is more like solid-state physics in the sense that it might tell us much of great interest about the strange phenomena that occur in complex situations. Furthermore, a point that is most important is that it would have an enormous number of technical applications. What I want to talk about is the problem of manipulating and controlling things on a small scale..."

"...I am not afraid to consider the final question as to whether, ultimately-in the great future-we can arrange the atoms the way we want; the very atoms, all the way down! What would happen if we could arrange the atoms one by one the way we want them..."[1]

These words pronounced by Nobel laureate Richard Feynman in 1959 preluded the concepts that seeded the fields of Nanoscience and Nanotechnology. More than fifty years later, daily life in developed countries cannot be understood without the huge impact of plenty of scientific and technological advances triggered by Nanotechnology on it.

Nanoscience is an emerging and interdisciplinary science that integrates chemistry, physics, biology, materials science, engineering, earth science and computer science. Nanotechnology, as the straightforward application of Nanoscience, can be defined as the research and technology development at the atomic, molecular or macromolecular levels, in the length scale of approximately 1-100 nanometer range, to provide a fundamental understanding of phenomena and materials at the nanoscale and to create and use structures, devices and systems that have novel properties and functions because of their small and/or intermediate size.[2] With this purpose in mind, Nanotechnology is helping to considerably improve, even revolutionize, many technology and industry sectors: materials industry, electronics and information technology, energy conversion, environmental science, medicine, homeland security, food safety, and transportation, among many others.[3]

---

[1] Richard Feynman, "There's Plenty of Room at the Bottom" at the American Physical Society meeting at Caltech, December 29th, **1959**.

[2] Roco, M. C.; Murday, J.; Teague, C.; Hays, S.; Merzbacher, C. *The national nanotechnology initiative: Strategic plan*; National Science and Technology Council Committee on technology, NSET, 2004.

[3] www.nano.gov

Although the term Nanotechnology was coined by Norio Taniguchi in 1974,[4] it was not until 1980s decade that some major scientific breakthroughs, with the development of the scanning tunneling microscope (STM)[5] in 1981 in the lead, sparked the growth of Nanotechnology as a prominent research field.

In order to produce old and new nanoscaled materials, two main strategies can be followed, namely *top-down* and *bottom-up* approaches (Figure 1).[6] The *top-down* approach involves traditional microfabrication methods that cut, etch, mill, grind and shape large pieces of materials into the desired shape and order without atomic-level control, and nanolithography techniques where a bulk material is reduced in size to nanoscale pattern, such as optical, electron-beam, multiphoton, X-ray, scanning probe and nanoimprint lithography.[7] On the other hand, the *bottom-up* approach entails building materials and devices from smaller building blocks such as atoms or molecules. *Bottom-up* techniques include gas-phase processes such as chemical vapor deposition, atomic layer deposition, molecular beam epitaxy and metallo-organic vapor phase epitaxy (MOCVD), and liquid-phase methods such as electrodeposition, anodizing and molecular self-assembly.[8] This last strategy utilizes the concepts of chemical synthesis, molecular recognition and supramolecular chemistry for the formation of highly ordered two- and three-dimensional nanoscale structures.[9] In this regard, Nature is a continuous source of inspiration, as almost all biological processes, like the photosynthetic process or protein synthesis by ribosomes, can be considered as sophisticated

[4] Taniguchi, N. On the Basic Concept of 'Nano-Technology'. *Proc. Intl. Conf. Prod. Eng. Tokyo, Part II*, Japan Society of Precision Engineering, 1974.

[5] a) Binnig, G.; Rohrer, H. *IBM Journal of Research and Development* **1986**, *30*, 355. b) Chiang, S. Imaging Small Molecules by Scanning Probe Microscopy. In *Fundamentals of Picoscience*; Sattler, K. D., Ed.; CRC Press: Boca Raton, Florida, 2013; pp. 139-160.

[6] a) Iqbal, P.; Preece, J. A.; Mendes, P. M. Nanotechnology: the "top-down" and "bottom-up" approaches. In *Supramolecular Chemistry: From Molecules to Nanomaterials*; Gale, P. A., Steed, J. W., Eds.; John Wiley & Sons Ltd.: Chichester, UK, 2012; Vol. 8, pp 3589-3602. b) Parak, W. J.; Simmel, F. C.; Holleitner, A. W. Top-down versus bottom-up. In *Nanotechnology*; Schmid, G., Ed.; Wiley-VCH: Weinheim, Germany, 2008; pp. 41-71.

[7] a) Venugopal, G.; Kim, S. -J. Nanolithography. In *Advances in Micro/Nano Electromechanical Systems and Fabrication Technologies*; Takahata, K., Ed.; InTech: Rijeka, Croatia, 2013; pp. 187-206. b) Henzie, J.; Barton, J.E.; Stender, C. L.; Odom, T. W. *Acc. Chem. Res.* **2006**, *39*, 249.

[8] a) Hornyak, G. L.; Tibbals, H. F.; Dutta, J.; Moore, J. J. *Introduction to Nanoscience and Nanotechnology*; CRC Press: Boca Raton, Florida, 2009; pp. 210–224. b) He, C.; Zhao, N.; Shi, C: Liu, E.; Li, J. *Adv. Mater.* **2015**, *27*, 5422. c) Sobel, N.; Hess, C. *Angew. Chem. Int. Ed.* **2015**, *54*, 15014.

[9] *Core Concepts in Supramolecular Chemistry and Nanochemistry*; Steed, J. W., Turner, D. R., Wallace, K. J., Eds.; John Wiley & Sons, Ltd: Chichester, West Sussex, England, 2007; pp. 229-271.

nanotechnological systems based on *bottom-up* self-assembly strategies ruled by supramolecular interactions.[10]

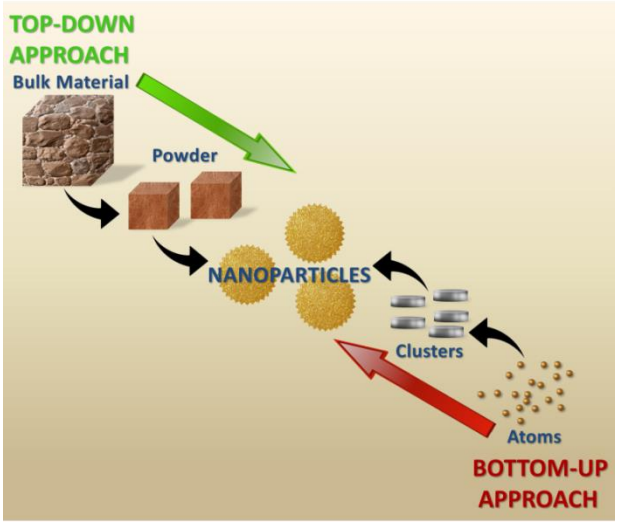

Figure 1. Schematic representation of the *bottom-up* and *top-down* synthesis.

The innovative focus, scientific breakthroughs and novel technologies resulting from the Nanoscience and Nanotechnology revolutionary perspective have unleashed a scorching pace of growth in Materials Science,[11] an interdisciplinary research field that combines chemistry for the design and synthesis of new materials, physics for the measuring and understanding of its properties, and engineering for its technological application (Figure 2). Over the last decades, inorganic, organic or metallo-organic molecules have been synthesized and, in a second stage, organized into condensed phases with controlled morphology and well-defined properties to form the so-called Molecular Materials, thus allowing their incorporation as active components in functional devices.[12] In particular, there is an increasing interest in organic or hybrid molecular materials due to the fact that they present some advantages over classical inorganic materials. First of all, the versatility provided by organic synthesis offers vast

[10] Drexler, K. E. *Phys. Educ.* **2005**, *40*, 339.

[11] a) *Advances in materials science research*; Wythers, M. C., Ed.; Nova Science Publishers, Inc.: Hauppauge, N. Y., 2011. b) Callister, W. D.; Rethwisch, D. G. *Materials Science and Engineering: An Introduction*, 7th ed.; John Wiley & Sons Ltd.: Chichester, UK, 2012.

[12] a) *Molecular Materials*; Bruce, D. W., O'Hare, D., Walton, R. I., Eds.; John Wiley & Sons Ltd.: Chichester, UK, 2010. b) *Functional Materials: Preparation, Processing and Applications*; Banerjee, S., Tyagi, A. K., Eds.; Elsevier Ltd.: London, UK, 2012.

possibilities to introduce properly selected modifications in the molecular structure in order to fine-tune the desired properties. In addition, organic molecular entities are designed in such a way that they can be arranged into different kinds of condensed phases depending on the organization at the supramolecular level, which may facilitate both their processing and incorporation into devices.

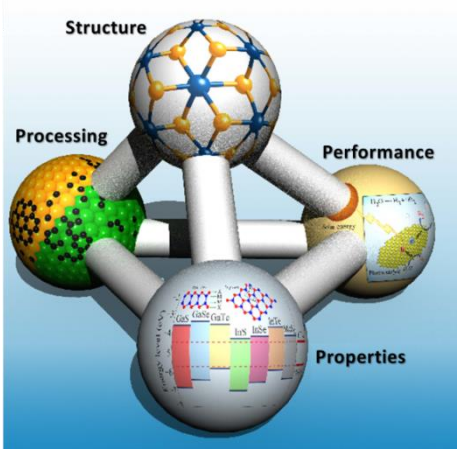

Figure 2. Traditional materials science tetrahedron.

The desired properties and applications of the material crucially determine the type of condensed phase needed, being high stability and high order the primary requirements of these systems. These condensed phases may be obtained in the form of engineered crystals,[13] liquid crystals,[14] a more sought-after arrangement in which molecules are ordered in a quasi-liquid medium that combines the anisotropy of a crystal and the fluidity of an anisotropic liquid, and thin films.[15] Several techniques have been extensively developed to produce high-quality thin films. Langmuir-Blodgett (LB) technique,[16] based on the organization of

[13] a) Desiraju, G. R.; Vittal, J. J.; Ramanan, A.; *Crystal Engineering: A Textbook*; World Scientific: Singapore, 2011. b) Desiraju, G. R. *J. Am. Chem. Soc.* **2013**, *135*, 9952.

[14] a) *Handbook of Liquid Crystals*, 2nd ed.; Goodby, J. W., Collings, P. J., Kato, T., Tschierske, C., Gleeson, H. F., Raynes, P., Eds.; Wiley-VCH: Weinheim, Germany, 2014. b) Woehrle, T.; Wurzbach, I.; Kirres, J.; Kostidou, A.; Kapernaum, N.; Litterscheidt, J.; Haenle, J. C.; Staffeld, P.; Baro, A.; Giesselmann, F.; Laschat, S. *Chem. Rev.* **2016**, *116*, 1139.

[15] a) *Handbook of Nanostructured Thin Films and Coatings*; Zhang, S., Ed.; CRC Press: Boca Raton, Florida, 2010. b) Khan, R. U. A.; Kwon, O.; Tapponnier, A.; Rashid, A. N.; Günter, P. *Adv. Funct. Mater.* **2006**, *16*, 180.

[16] a) Petty, M. C. *Langmuir-Blodgett films: An introduction*; Cambridge University Press: Cambridge, UK, 1996. b) Ulman, A. *An Introduction to Ultrathin Organic Films: from Langmuir-Blodgett to Self-assembly*; Academic Press: San Diego, 1991. c) Ariga, K.; Yamauchi, Y.; Mori, T.; Hill, J. P. *Adv. Mater.* **2013**, *25*, 6477.

amphiphilic molecules at an air/water interface and their subsequent transfer to a solid support, and self-assembled monolayers (SAMs),[16b,17] consisting of densely packed molecular supperlatices spontaneously formed by the interaction of a specific substrate and suitably functionalized organic molecules, follow a certain *bottom-up* conception based on molecular self-assembly principles.[18] On the other hand, hybrid fabrication methods that combine *top-down* and *bottom-up* mechanisms (generally starting from a bulk phase to produce thin films with high morphology control) include vapor-based deposition techniques such as chemical vapor deposition, atomic layer deposition and molecular beam epitaxy among others, and solution-based deposition techniques such as spin-coating, drop-casting, printing and meniscus-guided coating.[15a,b,19]

Organic or hybrid molecular materials present unconventional electronic, electrical, magnetic, optical, biological, and chemical properties suitable for several actual and potential applications.[20] Some real-life applications where functional molecular materials displaying one or more of these properties are already making an impact are:

- Optical data storage and transmission: organometallic and organic molecules and polymers with nonlinear optical (NLO) properties are able to manipulate and process optical signals and constitute important components in photonic devices.[21]
- Chemical and biological sensing: from graphene-based electrochemical biosensors to chiral sensing of chiral polymers or metal-organic frameworks (MOFs) and semiconductor materials sensing, many molecular materials have been developed for highly sensitive, cost-effective, miniature sensing devices.[22]

---

[17] a) Ulman, A. *Chem. Rev.* **1996**, *96*, 1533. b) Gooding, J. J.; Ciampi, S. *Chem. Soc. Rev.* **2011**, *40*, 2704. c) Heimel, G.; Rissner, F.; Zojer, E. *Adv. Mater.* **2010**, *22*, 2494.

[18] Sakakibara, K.; Hill, J. P.; Ariga, K. *Small* **2011**, *7*, 1288.

[19] a) Diao, Y.; Shaw, L.; Bao, Z.; Mannsfeld, S. C. B. *Energy Environ. Sci.* **2014**, *7*, 2145. b) Angusmacleod, H. Recent developments in deposition techniques for optical thin films and coatings. In *Optical Thin Films and Coatings: From Materials to Applications*; Piegari, A., Flory, F., Eds.; Woodhead Publ. Ser. Electron. Opt. Mater., Vol. 49; Woodhead Publishing: Cambridge, UK, 2013; pp 3-25.

[20] *Functional Materials: Electrical, Dielectric, Electromagnetic, Optical and Magnetic Applications*; Chung, D. D. L., Ed.; Eng. Mater. Technol. Needs, Vol.2; World Scientific: Singapore, 2010.

[21] a) *Essentials of Nonlinear Optics*; Murti, Y. V. G. S., Vijayan, C., Eds.; John Wiley & Sons, Inc.: Hoboken, NJ, USA, 2014. b) Stegeman, G. I.; Stegeman, R. A. *Nonlinear Optics: Phenomena, Materials and Devices*; Boreman, G., Ed.; Wiley Series in Pure and Applied Optics; John Wiley & Sons: Hoboken, NJ, 2012.

[22] a) *Advanced Sensor and Detection Materials*; Tiwari, A., Demir, M. M., Eds.; John Wiley & Sons: Hoboken, NJ, 2014. b) Zopfl, A.; Patterson, W.; Hirsch, T. Graphene for Biosensor Applications. In *Handbook of Carbon*

- Nanobiotechnology and medicine: nanostructured materials, for example, dye photosensitizers, dendrimers, polymers, quantum dots and biomimetic materials, are some of the building blocks to be employed as nanocarriers, targeting, labelling or therapeutic agents in medical applications such as drug delivery and theranostics.[23]
- Catalysis: MOF-based catalysis, photocatalytic water splitting for hydrogen production and biomimetic photo- and electrocatalysis by porphyrinoid macrocycles are only some of the applications of molecular materials in this subject.[24]
- Electronics and information storage: the development of electroluminescent polymers and organic materials for use in Organic Light-Emitting Diodes (OLEDs) and semiconducting π-conjugated systems, charge-transfer salts and polymers for use in Organic Field-Effect Transistors (OFETs) has demonstrated commercial applications of these devices in digital displays and in communications and information industry, respectively.[25]
- Energy storage: CNTs hybrid nanostructures, biopolymer-based and organic electrode materials are already showing promising results in their utilization in high energy/power density and environmentally friendly supercapacitors, Li-ion batteries and 3D-microbatteries.[26]
- Energy conversion: semiconducting highly extended π-conjugated systems, polymers and organic small molecules, which can absorb light in the visible part of the

---

Nano Materials; D'Souza, F., Kadish, K. M., Eds. World Scientific: Singapore, 2014; Vol. 6, pp 83-145. c) Kreno, L. E.; Leong, K.; Farha, O. K.; Allendorf, M.; Van Duyne, R. P.; Hupp, J. T. *Chem. Rev.* **2012**, *112*, 1105.

[23] a) Doane T. L.; Burda, C. *Chem. Soc. Rev.* **2012**, *41*, 2885. b) Elsabahy, M.; Wooley, K. L. *Chem. Soc. Rev.* **2012**, *41*, 2545. c) Kelkar, S. S.; Reineke, T. M. *Bioconjugate Chem.* **2011**, *22*, 1879.

[24] a) Supramolecular Catalysis, Reactivity and Chemical Biology. In *Supramolecular Chemistry: From Molecules to Nanomaterials*; Gale, P. A., Steed, J. W., Eds.; John Wiley & Sons Ltd.: Chichester, UK, 2012; Vol. 4, pp 1381-1496. b) Zagal, J. H.; Griveau, S.; Silva, J. F.; Nyokong, T.; Bedioui, F. *Coord. Chem. Rev.* **2010**, *254*, 2755. c) Lee, J. Y.; Farha, O. K.; Roberts, J.; Scheidt, K. A.; Nguyen, S. B. T.; Hupp, J. T. *Chem. Soc. Rev.* **2009**, *38*, 1450.

[25] a) Nguyen, T. P.; Molinie, P.; Destruel, P. Organic and polymer-based light-emitting diodes. In *Handbook of Advanced Electronic and Photonic Materials and Devices*; Nalwa, H. S., Ed.; Springer-Verlag: Heidelberg, Germany, 2001; Vol. 10, pp. 1-51. b) *Organic Electronics: Structural And Electronic Properties Of OFETs*; Woell, C., Ed.; Wiley-VCH: Weinheim, Germany, 2009. c) Guo, Y.; Yu, G.; Liu, Y. *Adv. Mater.* **2010**, *22*, 4427.

[26] a) Reddy, A. L. M.; Gowda, S. R.; Shaijumon, M. M.; Ajayan, P. M. *Adv. Mater.* **2012**, *24*, 5045. b) Song, Z.; Zhou, H. *Energy Environ. Sci.* **2013**, *6*, 2280. c) Liang, Y.; Tao, Z.; Chen, J. *Adv. Energy Mater.* **2012**, *2*, 742.

electromagnetic spectrum, are being extensively studied as active elements for the conversion of solar energy into electricity in photovoltaic cell devices.[27]

Among the wide variety of organic components that can give rise to molecular materials, organic chromophores based on nature-inspired pyrrolic macrocycles hold a privileged position due to their synthetic versatility, allowing a fine tunability of their photophysical properties, the possibility of organization into different condensed systems and their multiple technological applications (Chart 1).[28] Tetrapyrrolic macrocycles common structure consists of four pyrrole units forming an aromatic, planar structure linked through a *meso* atom. This family can be subdivided into Porphyrins (Ps)[29] or Porphyrazines (Pzs)[30] depending on whether the pyrrole rings are linked through a carbon or a nitrogen atom, respectively. Among the great number of expanded or extended porphyrinoid systems intensively explored for the last decades,[31] Phthalocyanines (Pcs),[32] comprising four benzene rings fused to the *β*-carbons of a tetraazaporphyrin, can be considered as a category themselves, based on their interesting electronic and physicochemical properties, the vast number of studies on these compounds and their numerous applications in different industrial fields. Finally, a family of contracted Ps and Pcs containing three pyrrole or isoindole units arranged around a boron atom that present unique spectral and electronic features includes Subporphyrins (SubPs),[33] Subporphyrazines

[27] a) Darling, S. B.; You, F. *RSC Adv.* **2013**, *3*, 17633. b) For more details and numerous general and specific examples in this subject, see *Chapter 1* in this Thesis.

[28] Schultz, H.; Lehmann, H.; Rein, M.; Hanack, M. Metal Complexes with Tetrapyrrole Ligands II. In *Structure and Bonding*; Buchler, J. W., Ed.; Springer-Verlag: Berlin, Germany, 1991; Vol. 74, pp. 41-146.

[29] a) *Handbook of Porphyrin Science*; Kadish, K. M., Smith, K. M., Guilard, R., Eds.; World Scientific: Singapore, 2013. b) Urbani, M.; Gratzel, M.; Nazeeruddin, M. K.; Torres, T. *Chem. Rev.* **2014**, *114*, 12330.

[30] a) Michel, S. L. J.; Hoffman, B. M.; Baum, S. M.; Barrett, A. G. M. *Prog. Inorg. Chem.* **2001**, *50*, 473. b) Rio, Y.; Rodríguez-Morgade, M. S.; Torres, T. *Org. Biomol. Chem.* **2008**, *6*, 1877.

[31] Saito, S.; Osuka, A. *Angew. Chem. Int. Ed.* **2011**, *50*, 4342.

[32] a) *Phthalocyanines. Properties and Applications*; Leznoff, C. C., Lever, A. B. P., Eds; VCH Publishers (LSK) Ltd.: Cambridge, UK, 1996; Vols. 1-4. b) Martínez-Díaz, M. V.; Torres, T. *Handbook of Porphyrin Science*; Kadish, K. M., Smith, K. M., Guilard, R., Eds.; World Scientific: Singapore, 2010; Vol. 10, Chapter 45, pp. 141-181. c) de la Torre, G.; Claessens, C. G.; Torres, T. *Chem. Commun.* **2007**, 2000. d) Claessens, C. G.; Hahn, U.; Torres, T. *Chem. Rec.* **2008**, *8*, 75. e) *Phthalocyanine Materials. Synthesis, Structure and Function*; McKeown, N. B., Ed.; Cambridge University Press: Cambridge, UK, 1998. f) Mack, J.; Kobayashi, N. *Chem. Rev.* **2011**, *111*, 281.

[33] a) Takeuchi, Y.; Matsuda, A.; Kobayashi, N. *J. Am. Chem. Soc.* **2007**, *129*, 8271. b) Inokuma, Y.; Osuka, A. *Dalton Trans.* **2008**, 2517. c) Tsurumaki, E.; Sung, J.; Kim, D.; Osuka, A. *J. Am. Chem. Soc.* **2015**, *137*, 1056.

(SubPzs),[34] and the best known of these contracted porphyrinoid species, **Subphthalocyanines**.[35]

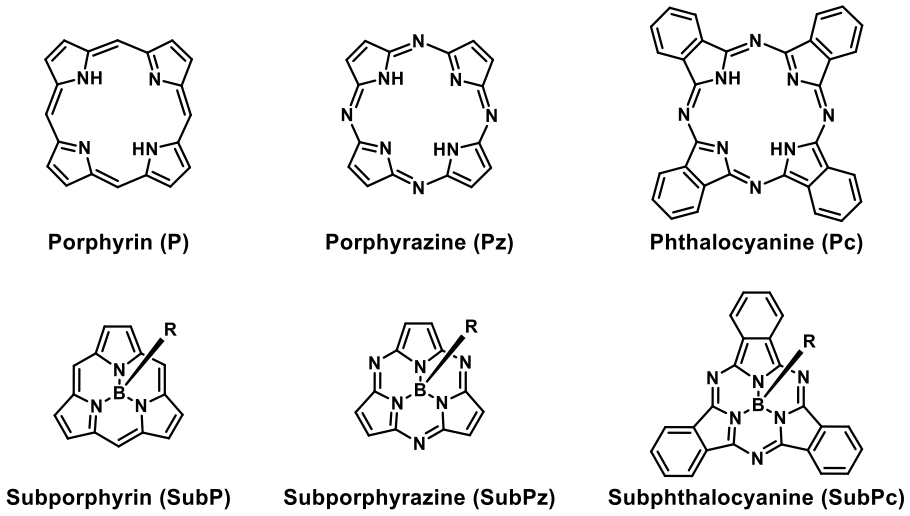

Chart 1. Chemical structure of diverse pyrrole-based macrocycles.

[34] a) Rodriguez-Morgade, M. S.; Esperanza, S.; Torres, T.; Barbera, J. *Chem. Eur. J.* **2005**, *11*, 354. b) Rahman, G. M. A.; Lueders, D.; Rodriguez-Morgade, M. S.; Caballero, E.; Torres, T.; Guldi, D. M. *ChemSusChem* **2009**, *2*, 330.

[35] Claessens, C. G.; González-Rodríguez, D.; Rodríguez-Morgade, M. S.; Medina, A.; Torres, T. *Chem. Rev.* **2014**, *114*, 2192.

Subphthalocyanines as Molecular Materials

Subphthalocyanines (SubPcs)[35,36] are aromatic macrocycles composed of three N-fused 1,3-diiminoisoindole units (Figure 3). In the middle of their central cavity, a boron atom is linked to three nitrogen atoms of the isoindole units and a fourth substituent (Cl in SubPc **1**) that occupies the so-called axial position of the molecule. The tetrahedral coordination of this central boron atom confers their characteristic nonplanar cone-shaped geometry to SubPcs. The 14 π-electrons conjugated system of these macrocycles is essentially located in the inner ring, while the peripheral benzenes virtually preserve their electronic structure. These unique structural features make the SubPcs one of the few known examples of heteroatomic non-planar aromatic compounds.

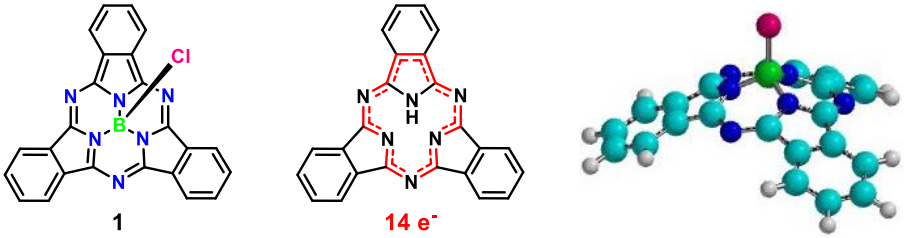

Figure 3. Chemical structure of SubPc **1**, electronic delocalization in the aromatic core and ball-and-spoke model.

Subphthalocyanines were serendipitously discovered in 1972 by Meller and Ossko[37] while attempting the synthesis of a boron phthalocyanine by the condensation reaction of phthalonitrile in the presence of boron trichloride. Instead, they obtained a pink-colored compound unequivocally characterized by elemental analysis and mass spectrometry. Two years later, X-ray crystal structure characterization[38] confirmed the proposed geometry. Subsequent X-ray diffraction studies of other axially substituted SubPcs have all shown cone-shaped structure.[35]

---

[36] a) Claessens, C. G.; González-Rodríguez, D.; Torres, T. *Chem. Rev.* **2002**, *102*, 835. b) Medina, A.; Claessens, C. G. *J. Porphyrins Phthalocyanines* **2009**, *13*, 447. c) del Rey, B.; Keller, U.; Torres, T.; Rojo, G.; Agullo-Lopez, F.; Nonell, S.; Marti, C.; Brasselet, S.; Ledoux, I.; Zyss, J. *J. Am. Chem. Soc.* **1998**, *120*, 12808. d) Geyer, M.; Plenzig, F.; Rauschnabel, J.; Hanack, M.; del Rey, B.; Sastre, A.; Torres, T. *Synthesis* **1996**, 1139. e) Torres, T. *Angew. Chem. Int. Ed.* **2006**, *45*, 2834.

[37] Meller, A.; Ossko, A. *Monatsh. Chem.* **1972**, *103*, 150.

[38] Kietaibl, H. *Monatsh. Chem.* **1974**, *105*, 405.

Synthesis of subphthalocyanines

Nowadays, SubPc synthesis[39] is typically carried out by cyclotrimerization reaction of a phthalonitrile derivative in the presence of stoichiometric amounts of a boron trihalide (BX_3), generally boron trichloride (BCl_3) or boron tribromide (BBr_3), at high temperatures (140-200 °C), in high boiling point aromatic solvents such as *p*-xylene,[39] *o*-xylene,[40] chloronaphthalene,[36c,d,41] *o*-dichlorobenzene[42] and 1,2,4-trichlorobenzene[43] (Scheme 1). For this purpose, commercially available 1 M solution of BX_3 in different solvents (CH_2Cl_2, heptane or *p*-xylene) can be readily employed to precisely control the stoichiometry of the reactants.[44] Other boron-based Lewis acids, for instance BF_3,[45] BPh_3,[36d] $PhBF_2$,[37] $PhBCl_2$[36d,37] or $BuBBr_2$,[36d] have been utilized in specific cases. The reactivity of these trisubstituted boron compounds toward phthalonitrile derivatives follows, as observed experimentally, the order $B(Alkyl)_3$ < BPh_3 < BF_3 < BCl_3 < BBr_3, which is closely related to their Lewis acidity.[46]

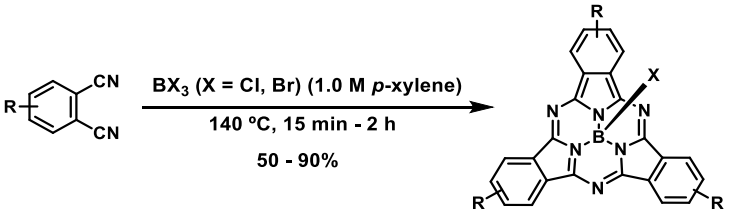

Scheme 1. General synthesis of SubPcs.

[39] Claessens, C. G.; González-Rodríguez, D.; del Rey, B.; Torres, T.; Mark, G.; Schuchmann, H. -P.; von Sonntag, C.; MacDonald, G.; Nohr, R. S. *Eur. J. Org. Chem.* **2003**, 2547.

[40] Jacquot de Rouville, H.-P.; Garbage, R.; Ample, F.; Nickel, A.; Meyer, J.; Moresco, F.; Joachim, C.; Rapenne, G. *Chem. Eur. J.* **2012**, *18*, 8925.

[41] Ohno-Okumura, E.; Sakamoto, K.; Kato, T.; Hatano, T.; Fukui, K.; Karatsu, T.; Kitamura, A.; Urano, T. *Dyes Pigm.* **2002**, *53*, 57.

[42] a) Morse, G. E.; Helander, M. G.; Maka, J. F.; Lu, Z. -H.; Bender, T. P. *ACS Appl. Mat. Interfaces* **2010**, *2*, 1934. b) Fulford, M. V.; Jaidka, D.; Paton, A. S.; Morse, G. E.; Brisson, E. R. L.; Lough, A. J.; Bender, T. P. *J. Chem. Eng. Data* **2012**, *57*, 2756.

[43] Shimizu, S.; Otaki, T.; Yamazaki, Y.; Kobayashi, N. *Chem. Commun.* **2012**, *48*, 4100.

[44] See ref. 36a for examples published before 2002, when BCl_3 used to be previously condensed before addition to the corresponding phthalonitrile derivative.

[45] Potz, R.; Göldner, M.; Hückstädt, H.; Cornelissen, U.; Tutaβ, A.; Homborg, H. *Z. Anorg. Allg. Chem.* **2000**, *626*, 588.

[46] *Comprehensive Inorganic Chemistry*; Bailar, J. C., Emeleus, H. J., Nyholm, R., Trotman-Dickenson, A. F., Eds.; Pergamon: New York, 1973; Vol. 1.

Although these synthetic conditions limit the number of peripheral functional groups that can be initially introduced in the SubPc structure, the current optimized methodology has allowed for the incorporation of various and diverse substituents, such as halogens, nitro groups, ethers, thioethers, alkyl groups and sulphonyl groups.[35]

Starting phthalonitriles that possess C_{2v} symmetry give rise to a single SubPc isomer. Those that lack C_{2v} symmetry, however, yield a mixture of two SubPc regioisomers with C_1 and C_3 symmetries (Figure 4). The separation of these isomers, which can be accomplished by HPLC[47] or more conveniently by column chromatography,[48] results very relevant when property/structure relationships are requested. In the case of *meta*-substituted SubPcs, the C_3/C_1 ratio does not seem to be influenced by electronic or steric factors and follows a statistical distribution (1:3, respectively). This is no longer the case of *ortho*-substituted SubPcs, since their peripheral substituents are closer to the core of this aromatic molecule and steric and electronic factors play here an important role.[47b,48a,49]

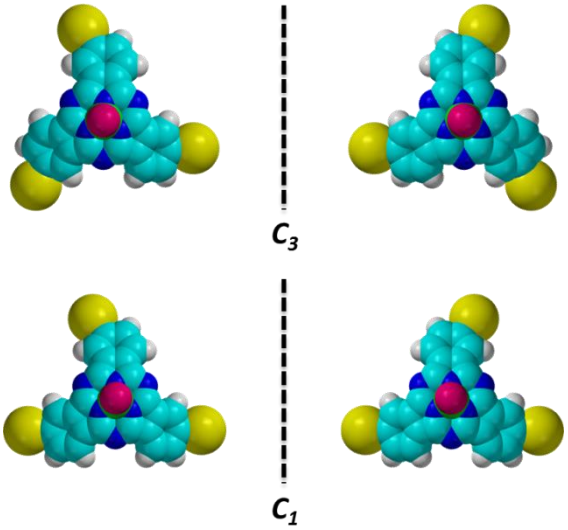

Figure 4. *metha*-substituted SubPc regioisomers and stereoisomers.

[47] a) Hanack, M.; Geyer, M. *J. Chem. Soc., Chem. Commun.* **1994**, 2253. b) Kobayashi, N.; Nonomura, T. *Tetrahedron Lett.* **2002**, *43*, 4253.
[48] a) Claessens, C. G.; Torres, T. *Eur. J. Org. Chem.* **2000**, 1603. b) Claessens, C. G.; Torres, T. *Tetrahedron Lett.* **2000**, *41*, 6361.
[49] Iida, N.; Tokunaga, E.; Saito, N.; Shibata, N. *J. Fluorine Chem.* **2015**, *171*, 120.

The conical shape of SubPcs makes them intrinsically non-centrosymmetric, which results in molecular chirality when unsymmetrically-substituted phthalonitriles are used. In fact, each of the C_1/C_3 regioisomers consists on a racemic mixture of enantiomers (Figure 4) that can be separated on an analytical[48b] or semi-preparative[47b,50] chiral HPLC.

The crossover condensation of two different phthalonitriles (A and B) leads to a mixture of four SubPc derivatives (A_3, A_2B, AB_2 and B_3) with a different substitution pattern in each of the isoindole units regarding the nature, number or position of the substituents (Figure 5), which can be frequently separated by column chromatography.[51] These compounds may possess not only physical properties halfway in between the two related symmetrically substituted SubPcs, but also new properties that may arise from a particular cooperation between the different substituents (e.g., donor-acceptor interactions). Even though there are not many reports on this subject so as to draw a clear tendency, it looks that the selectivity in the formation of unsymmetrically substituted SubPcs depends on steric factors and on the relative reactivity of the phthalonitrile precursors toward the boron reagent. In all cases a mixture of the four possible compounds is obtained but the yield of the desired unsymmetrically substituted SubPc can be optimized by choosing the appropriate relative ratio of starting phthalonitriles.

[50] Guilleme, J.; Mayoral, M. J.; Calbo, J.; Aragó, J.; Viruela, P. M.; Ortí, E.; Torres, T.; González-Rodríguez, D. *Angew. Chem. Int. Ed.* **2015**, *54*, 2543.

[51] a) Ali, H.; Sim, S. K.; van Lier, J. E. *J. Chem. Res.* **1999**, 496. b) Claessens, C. G.; Torres, T. *Chem. Eur. J.* **2000**, *6*, 2168. c) Stork, J. R.; Potucek, R. J.; Durfee, W. S.; Noll, B. C. *Tetrahedron Lett.* **1999**, *40*, 8055. d) Zyskowski, C. D.; Kennedy, V. O. *J. Porphyrins Phthalocyanines* **2000**, *4*, 707. e) González-Rodríguez, D.; Claessens, C. G.; Torres, T.; Liu, S. -G.; Echegoyen, L.; Vila, N.; Nonell, S. *Chem. Eur. J.* **2005**, *11*, 3881. f) Iglesias, R. S.; Claessens, C. G.; Herranz, M. A.; Torres, T. *Org. Lett.* **2007**, *9*, 5381. g) González-Rodríguez, D.; Claessens, C. G.; Torres, T. *J. Porphyrins Phthalocyanines* **2009**, *13*, 203.

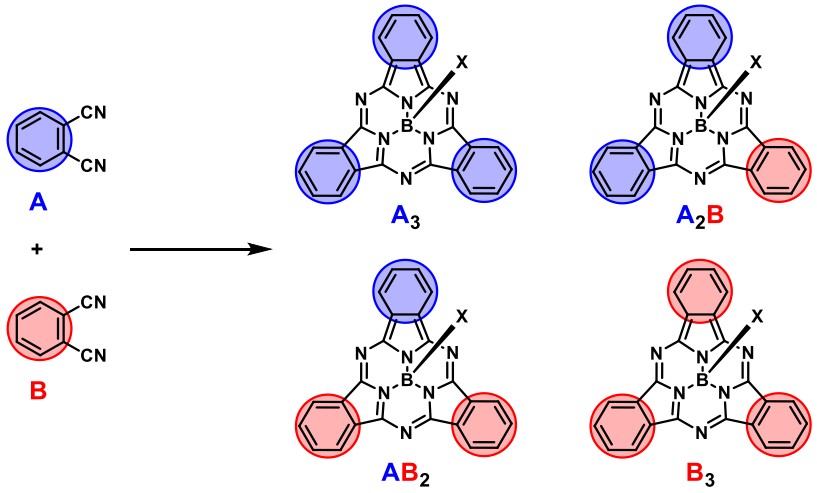

Figure 5. Mixture of SubPcs obtained via statistical cyclotrimerization of two differently functionalized phthalonitriles, A and B.

A mechanistic study of chloro-SubPc formation, together with quantum-chemical computations, suggests that the rearrangement of the initial phthalonitrile-BCl_3 adduct (**I**) produces intermediate (1*Z*)-3-chloro-*N*-(dichloroboryl)-1H-isoindol-1-imine (**II**). Intermediate **II** would cyclotrimerize to afford the dichlorosubstituted macrocycle **III** that, after concerted elimination of molecular chlorine assisted by BCl_3, gives rise to chloro-SubPc (Figure 6).[52]

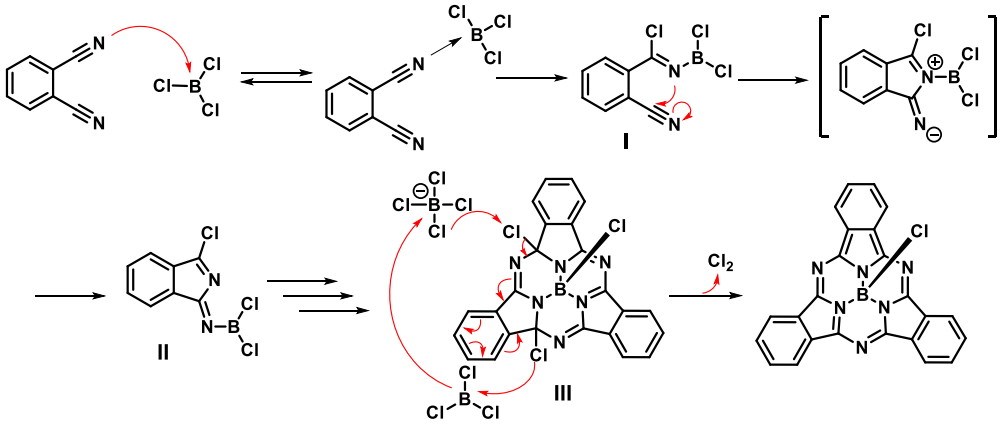

Figure 6. Key steps of the mechanism of SubPc formation.

[52] a) Claessens, C. G.; González-Rodríguez, D.; McCallum, C. M.; Nohr, R. S.; Schuchmann, H. –P.; Torres, T. *J. Porphyrins Phthalocyanines* **2000**, 11, 18. b) Nohr, R. S.; McCallum, C. M.; Schuchmann, H. –P. *J. Porphyrins Phthalocyanines* **2010**, *14*, 271.

Reactivity of subphthalocyanines

Due to the functional group limitation imposed by the use of boron reagents, the progress of synthetic modifications of SubPcs at both the levels of the boron atom and of the peripheral aromatic units is of utmost importance. This approach may allow the fine-tuning of their physical properties, the modification of their solubility characteristics, the extension of their π-conjugated structure, the incorporation of SubPcs as units into other electroactive systems, or their organization into supramolecular assemblies.

In this sense, SubPc reactivity may be classified in three main groups (Figure 7): (a) axial reactivity, (b) peripheral reactivity, and (c) ring expansion reactions. The three of them differ in the reactive center: (a) the axial B-X bond, (b) the functional groups placed at the aromatic carbon atoms, or (c) the imine-type core, respectively. Both axial and peripheral reactions produce modified SubPcs, while ring expansion results in the opening of the SubPc constrained ring and incorporation of an additional isoindole unit, thus leading to the formation of low-symmetry A_3B Pcs.

An additional mode of reactivity that cannot be classified within any of the groups mentioned above was reported by Rodríguez-Morgade, Torres, Sessler and coworkers.[53] It consists in the formation of ruthenoarene π-complexes of SubPcs by reaction of the aromatic rings in the macrocycle with $[CpRu(MeCN)_3]PF_6$ (Cp = pentamethylcyclopentadienyl). The coordination of Cp*Ru to axially phenoxy-substituted SubPcs can result in three different products where the metal binds either to the phenoxy ligand, the SubPc concave side, or the SubPc convex side. It was shown that this reaction displays high selectivities for electron-rich aromatic rings and, to a lesser extent, for metal π coordination to the SubPc convex side rather than to the concave side.

[53] Caballero, E.; Fernández-Ariza, J.; Lynch, V. M.; Romero-Nieto, C.; Rodríguez-Morgade, M. S.; Sessler, J. L.; Guldi, D. M.; Torres, T. *Angew. Chem. Int. Ed.* **2012**, *51*, 11337.

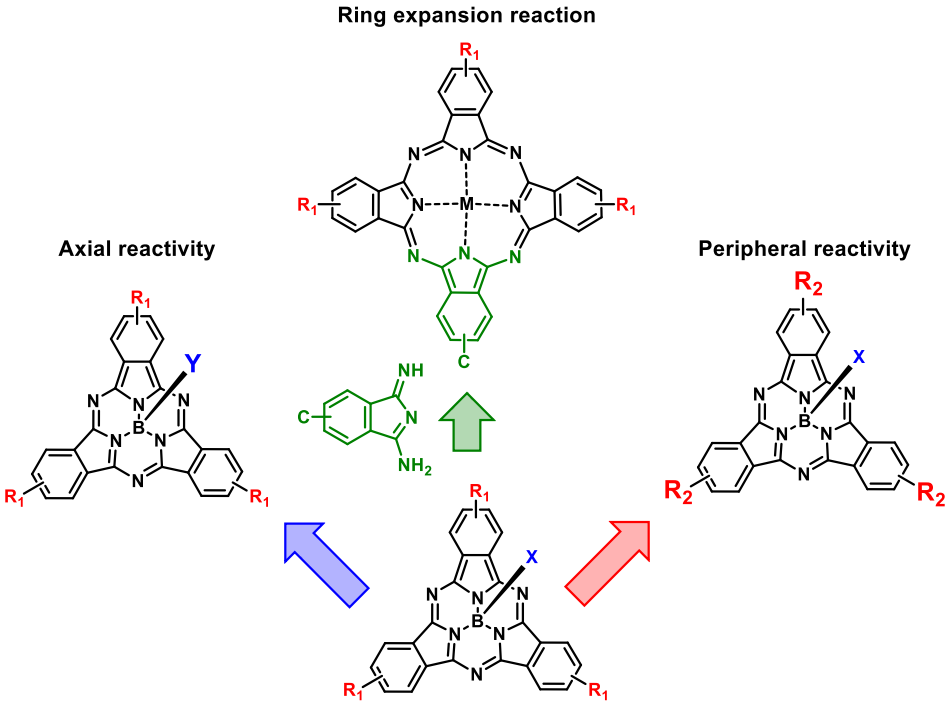

Figure 7. Three main different modes of SubPc reactivity.

a) Axial reactivity

Substitution at the boron atom in SubPcs is a recurrent method employed for the incorporation of these macrocycles into systems of increasing complexity. Generally, the axial functionalization of SubPcs does not alter the electronic characteristics of the π-conjugated macrocycle, which are mainly determined by the nature of the substituents on the benzene rings.

Among the many possible substituting groups, phenol derivatives offer, for experimental reasons, many advantages: (i) they are available in large quantities, (ii) they increase the stability and solubility of the SubPc when compared to the same compound with an axial halogen atom, and (iii) they may be useful for introducing new functional groups.[35,54] The

[54] a) Çoşut, B.; Yeşilot, S.; Durmuş, M.; Kiliç, A. *Dyes Pigm.* **2013**, *98*, 442. b) Viswanath, L. C. K.; Shirtcliff, L. D.; Berlin, K. D. *J. Porphyrins Phthalocyanines* **2013**, *17*, 1167. c) KC, C. B.; Lim, G. N.; Zandler, M. E.; D'Souza, F. *Org. Lett.* **2013**, *15*, 4612. d) Çetindere, S.; Çoşut, B.; Yeşilot, S.; Durmuş, M.; Kiliç, A. *Dyes Pigm.* **2014**, *101*, 234. e) Morse, G. E.; Gantz, J. L.; Steirer, K. X.; Armstrong, N. R.; Bender, T. P. *ACS Appl. Mater. Interfaces* **2014**, *6*, 1515. f) Ince, M.; Medina, A.; Yum, J. -H.; Yella, A.; Claessens, C. G.; Martínez-Díaz, M. V.; Grätzel, M.;

reaction is typically carried out by heating a mixture of the SubPc and the phenol in high-boiling point aromatic solvents (toluene, chlorobenzene, etc.). In certain cases, weak bases like trialkylamines or pyridine have been added to the reaction mixture in order to neutralize the hydrogen halide acid released. Very recently, an insight into the mechanism of the axial ligand exchange reaction between chloro-SubPcs and phenols has been provided by Guilleme *et al*.[55] Their combined experimental and theoretical results support an unusual bimolecular *σ*-bond metathesis mechanism in which the phenolic proton assists in weakening the boron-halogen bond concomitantly with substitution at the boron center. This mechanism would also explain that (i) bromo-SubPcs react faster than chloro and fluoro-SubPcs, since the boron-halogen bond is longer and weaker in that series; (ii) SubPcs substituted with electron-donating groups at the periphery react faster as a result of the stabilization of the positive charge developed at the B atom in the transition state; and (iii) more acidic phenols accelerate the reaction, since they are able to bind more efficiently to the leaving halogen atom via proton coordination.

Chloro- and bromo-SubPcs have been reported to react as well with carboxylic acids[56] and benzyl[57] or alkyl[56a,58] alcohols to yield the corresponding B-O bond SubPc. Hydroxy-SubPcs have been obtained by refluxing a suspension of the starting SubPc in water,[59] pyridine/water[60] mixtures, and acetonitrile/water[61] mixtures. Finally, symmetrical[62] or

---

Nazeeruddin, M. K.; Torres, T. *Chem. Eur. J.* **2014**, *20*, 2016. g) Mori, S.; Ogawa, N.; Tokunaga, E.; Shibata, N. *Dalton Trans.* **2015**, *44*, 19451. h) Mori, S.; Ogawa, N.; Tokunaga, E.; Tsuzuki, S.; Shibata, N. *Dalton Trans.* **2016**, *45*, 908. i) Bandi, V.; D'Souza, F. P.; Gobeze, H. B.; D'Souza, F. *Chem. Commun.* **2016**, *52*, 579.

[55] Guilleme, J.; Martínez-Fernández, L.; González-Rodríguez, D.; Corral, I.; Yáñez, M.; Torres, T. *J. Am. Chem. Soc.* **2014**, *136*, 14289.

[56] a) Solntsev, P. V.; Spurgin, K. L.; Sabin, J. R.; Heikal, A. A.; Nemykin, V. N. *Inorg. Chem.* **2012**, *51*, 6537. b) Lessard, B. H.; Bender, T. P. *Macrom. Rapid Commun.* **2013**, *34*, 568.

[57] a) Romero-Nieto, C.; Medina, A.; Molina-Ontoria, A.; Claessens, C. G.; Echegoyen, L.; Martín, N.; Torres, T.; Guldi, D. M. *Chem. Commun.* **2012**, *48*, 4953. b) Ren, Y.; Hiszpanski, A. M.; Loo, Y. -L. *Chem. Mater.* **2015**, *27*, 4008. c) Konarev, D. V:; Troyanov, S. I.; Lyubovskaya, R. N. *CrystEngComm* **2015**, *17*, 3923.

[58] a) Adachi, K.; Watarai, H. *Anal. Chem.* **2006**, *78*, 6840. b) Xu, H.; Ng, D. K. P. *Chem. Asian J.* **2009**, *4*, 104. c) Xu, H.; Ermilov, E. A.; Röder, B.; Ng, D. K. P. *Phys. Chem. Chem. Phys.* **2010**, *12*, 7366. d) Biyiklioglu, Z.; Alp, H. *Dalton Trans.* **2016**, *45*, 3838. e) Gotfredsen, H.; Jevric, M.; Kadziola, A.; Nielsen, M. B. *Eur. J. Org. Chem.* **2016**, 17.

[59] Martínez-Díaz, M. V.; del Rey, B.; Torres, T.; Agricole, B.; Mingotaud, C.; Cuvillier, N.; Rojo, G.; Agulló-López, F. *J. Mat. Chem.* **1999**, *9*, 1521.

[60] Kudrevich, S. V.; Gilbert, S.; van Lier, J. E. *J. Org. Chem.* **1996**, *61*, 5706.

[61] del Rey, B.; Martínez-Díaz, M. V.; Barberá, J.; Torres, T. *J. Porphyrins Phthalocyanines* **2000**, *4*, 569.

[62] a) Kobayashi, N.; Ishizaki, T.; Ishii, K.; Konami, H. *J. Am. Chem. Soc.* **1999**, *121*, 9096. b) Yamasaki, Y.; Mori, T. *Bull. Chem. Soc. Jpn.* **2011**, *84*, 1208.

unsymmetrical[63] μ-oxo-bridged SubPc dimers have been synthesized by dehydration of hydroxyl-SubPc or by reaction of hydroxyl-SubPc with halo-SubPc respectively.

In the last decade, other general methodologies for the axial functionalization of SubPcs with different nucleophiles have been published. First, in 2008, Rodríguez-Morgade *et al.* described the formation of fluoro-SubPcs in moderate yields by treatment of SubPcs bearing axial chlorine, bromine or phenoxy groups with a large excess of $Et_2O{\cdot}BF_3$.[64] In the same year, the first efficient synthesis of ethynyl-boron SubPcs via replacement of the chloride ligand on the boron atom in the presence of Grignard reagents was reported by Ziessel *et al*.[65] A similar protocol was more recently employed by Yamasaki *et al.* to prepare a series of SubPcs having direct B-C bonds.[66] The procedure basically relied on the reaction between bromo-SubPcs and primary alkyl, secondary alkyl, or aryl Grignard reagents.

In 2011 Guilleme *et al.* achieved a breakthrough in the axial functionalization of SubPcs when publishing a one-pot, two-step synthetic methodology to efficiently exchange the chlorine atom in SubPc products with a wide range of nucleophiles.[67] The first step consists in the irreversible generation of an activated triflate-SubPc intermediate by reaction with AgOTf or Me_3SiOTf reagents. In the second step, the nucleophile is added and the reaction is completed within a few hours at mild temperatures. This approach allowed for the first time the incorporation of nitrogen and sulfur nucleophiles to the SubPc axial position. In 2012 Bender *et al.* communicated another strategy for the activation of the axial position of SubPcs by treatment of chloro- or bromo-SubPcs with aluminum chloride ($AlCl_3$) prior to the addition of the nucleophile, although the scope of the reaction was limited to aromatic nucleophiles.[68]

Very recently, two different mild and versatile synthetic routes that employ TMS-protected nucleophiles as starting materials to carry out the axial ligand exchange reaction in SubPcs in one step have been described,[69] granting the access to new axial derivatives of singular importance within the chemistry of SubPcs.

---

[63] Dang, J. D.; Fulford, M. V.; Kamino, B. A.; Paton, A. S.; Bender, T. P. *Dalton Trans.* **2015**, *44*, 4280.

[64] Rodríguez-Morgade, M. S.; Claessens, C. G.; Medina, A.; González-Rodríguez, D.; Gutiérrez-Puebla, E.; Monge, A.; Alkorta, I.; Elguero, J.; Torres, T. *Chem. Eur. J.* **2008**, *14*, 1342.

[65] Camerel, F.; Ulrich, G.; Retailleau, P.; Ziessel, R. *Angew. Chem. Int. Ed.* **2008**, *47*, 8876.

[66] Yamasaki, Y.; Mori, T. *Chem. Lett.* **2010**, *39*, 1108.

[67] Guilleme, J.; González-Rodríguez, D.; Torres, T. *Angew. Chem. Int. Ed.* **2011**, *50*, 3506.

[68] Morse, G. E.; Bender, T. P. *Inorg. Chem.* **2012**, *51*, 6460.

[69] a) Guilleme, J.; Martínez-Fernández, L.; Corral, I.; Yáñez, M.; González-Rodríguez, D.; Torres, T. *Org. Lett.* **2015**, *17* , 4722. b) Gotfredsen, H.; Jevric, M.; Broman, S. L.; Petersen, A. U.; Nielsen, M. B. *J. Org. Chem.* **2016**, *81*, 1.

b) Peripheral reactivity

"Peripheral reactivity" refers to any reaction that produces a chemical modification of the substituents placed at the benzene rings of the isoindole units. Generally, these are conventional reactions that are not characteristic of SubPcs. However, owing to the relative chemical instability of these constrained macrocycles, the synthetic procedures employed must be carefully selected in order to preserve the structure of the ring.

Metal-catalyzed cross-coupling reactions constitute the most frequently employed methodology to functionalize SubPcs at the isoindole rings or at the aromatic axial substituents.[70] These are mild approaches that have been highly useful to introduce a wide range of chemical functionalities that are not compatible with the SubPc synthetic protocol, to produce SubPc oligomers, or to couple these chromophores to other photoactive units. Iodo-substituted SubPcs have been the precursors of choice in palladium-catalyzed Sonogashira,[51e,f,65,71] Suzuki,[72] Stille,[72c] and Heck[73] C-C bond formation reactions, Buchwald-Hartwig amination reactions,[72c,74] or borylation reactions.[72c] Furthermore, *ortho*-diethynyl-substituted SubPcs have been used as monomers in palladium-mediated homocoupling reactions leading to SubPc trimers with a dehydro[18]annulene core.[51f]

Other protocols have been successfully employed to transform functional groups attached to the SubPc core. With the aim of increasing SubPc water solubility, axial and peripheral pyridine or tertiary amine groups have been transformed into their respective quaternized salts via

[70] Martínez-Díaz, M. V.; Quintiliani, M.; Torres, T. *Synlett* **2008**, *1*, 1.

[71] a) del Rey, B.; Torres, T. *Tetrahedron Lett.* **1997**, *38*, 5351. b) Claessens, C. G.; Torres, T. *Chem. Commun.* **2004**, 1298. c) Ziessel, R.; Ulrich, G.; Elliott, K. J.; Harriman, A. *Chem. Eur. J.* **2009**, *15*, 4980. d) Lapok, L.; Claessens, C. G.; Wöhrle, D.; Torres, T. *Tetrahedron Lett.* **2009**, *50*, 2041. e) Morisue, M.; Wataru, S.; Kuroda, Y. *Tetrahedron Lett.* **2012**, *53*, 313.

[72] a) Claessens, C. G.; Torres, T. *J. Am. Chem. Soc.* **2002**, *124*, 14522. b) González-Rodríguez, D.; Carbonell, E.; Guldi, D. M.; Torres, T. *Angew. Chem. Int. Ed.* **2009**, *48*, 8032. c) González-Rodríguez, D.; Torres, T. *Eur. J. Org. Chem.* **2009**, 1871. d) González-Rodríguez, D.; Martínez-Díaz, M. V.; Abel, J.; Perl, A.; Huskens, J.; Echegoyen, L.; Torres, T. *Org. Lett.* **2010**, *12*, 2970. e) González-Rodríguez, D.; Carbonell, E.; de Miguel Rojas, G.; Atienza Castellanos, C.; Guldi, D. M.; Torres, T. *J. Am. Chem. Soc.* **2010**, *132*, 16488. f) Mauldin, C. E.; Piliego, C.; Poulsen, D.; Unruh, D. A.; Woo, C.; Ma, B.; Mynar, J. L.; Fréchet, J. M. J. *Appl. Mater. Interfaces* **2010**, *2*, 2833.

[73] Sánchez-Molina, I.; Soriano, A.; Claessens, C. G.; Torres, T.; Bolink, H. J. *J. Porphyrins Phthalocyanines* **2013**, *17*, 1017.

[74] a) González-Rodríguez, D.; Torres, T.; Guldi, D. M.; Rivera, J.; Herranz, M. A.; Echegoyen, L. *J. Am. Chem. Soc.* **2004**, *126*, 6301. b) González-Rodríguez, D.; Torres, T.; Herranz, M. A.; Echegoyen, L.; Carbonell, E.; Guldi, D. M. *Chem. Eur. J.* **2008**, *14*, 7670.

alkylation reactions.[71d,73,75] Dicyclohexylcarbodiimide (DCC)-mediated acylation reactions[72c,d,e] have been employed to introduce new ester functions in hydroxy-substituted SubPcs. Different deprotection conditions have also been tested for *tert*-butyl esters[76] and silylether[72c] groups to yield the corresponding carboxylic acid- and hydroxy-substituted SubPcs, respectively. The oxidation of sulfides to sulfoxides or sulfones with *m*-chloroperbenzoic acid (*m*-CPBA) has been conducted.[77] The reduction of triple bonds attached around the SubPc core with molecular hydrogen has also been shown to proceed with moderate yields.[71d] Finally, to couple C_{60} fullerene to SubPc-based macrocycles, the well-known 1,3-dipolar cycloaddition or Prato reaction[74,78] and cyclopropanation or Bingel reaction[72c,e] have been successfully utilized.

c) Ring expansion reaction

In 1990, nearly twenty years after their discovery, Kobayashi *et al.* renewed the interest for SubPcs by devising a method for the synthesis of unsymmetrical A_3B-type Pcs through ring opening reaction of SubPc macrocycle (A_3) in the presence of 1,3-diiminoisoindoline derivatives (B) and subsequent ring closure.[79] This method was claimed to afford reasonable yields and good A_3B selectivity, with a simple purification process.

After intense research by several groups it was clear that the efficiency and thus the convenience of this promising procedure depends dramatically on a number of factors, such as the nature of the peripheral substituents of the SubPc and the diiminoisoindoline precursor, the solvent, and the reaction temperature.[60,62a,80] During the last 10 years, further research has been devoted to the study and optimization of this procedure in diverse conditions.[81] Best yields obtained for the target A_3B-type Pcs, in the order of 40-60%, were reported by Chauhan *et al.*[81d]

---

[75] a) Spesia, M. B.; Durantini, E. N. *Dyes Pigm.* **2008**, *77*, 229. b) Tolbin, A. Y.; Tomilova, L. G. *Mendeleev Commun.* **2008**, *18*, 286.

[76] Palomares, E.; Martínez-Díaz, M. V.; Torres, T.; Coronado, E. *Adv. Funct. Mater.* **2006**, *16*, 1166.

[77] González-Rodríguez, D.; Torres, T. *Tetrahedron Lett.* **2009**, *50*, 860.

[78] a) El-Khouly, M. E.; Shim, S. H; Araki, Y.; Ito, O.; Kay, K. -Y. *J. Phys. Chem. B* **2008**, *112*, 3910. b) Shibata, N.; Das, B.; Tokunaga, E.; Shiro, M.; Kobayashi, N. *Chem. Eur. J.* **2010**, *16*, 7554.

[79] Kobayashi, N.; Kondo, R.; Nakajima, S. -I.; Osa, T. *J. Am. Chem. Soc.* **1990**, *112*, 9640.

[80] a) Weitemeyer, A.; Kliesch, H.; Wöhrle, D. *J. Org. Chem.* **1995**, *60*, 4900. b) Sastre, A.; Torres, T.; Hanack, M. *Tetrahedron Lett.* **1995**, *36*, 8501. c) Sastre, A.; del Rey, B.; Torres, T. *J. Org. Chem.* **1996**, *61*, 8591. d) Kudrevich, S.; Brasseur, N.; La Madeleine, C.; Gilbert, S.; van Lier, J. E. *J. Med. Chem.* **1997**, *40*, 3897.

[81] a) Matlaba, P.; Nyokong, T. *Polyhedron* **2002**, *21*, 2463. b) Sharman, W. M.; van Lier, J. E. *J. Porphyrins Phthalocyanines* **2005**, *9*, 651. c) Padmaja, K.; Youngblood, J. W.; Wei, L.; Bocian, D. F.; Lindsey, J. S. *Inorg. Chem.* **2006**, *45*, 5479. d) Chauhan, S. M. S.; Kumari, P. *Tetrahedron* **2009**, *65*, 2518. e) Tempesti, T. C.; Álvarez, M. G.; Durantini, E. N. *Dyes Pigm.* **2011**, *91*, 6.

Properties and applications of subphthalocyanines

The cone-shaped structure of SubPcs provides a chromophore with distinctive photophysical properties that, in some cases, compare favorably to those shown by other related planar aza aromatic macrocycles.

The UV-vis spectra of SubPcs are comparable to those exhibited by Pcs in that they both show two main transitions, a weaker absorption at the 260-370 nm region corresponding to the Soret or *B* band that originates from the $S_0 \rightarrow S_2$ transition and a stronger absorption band in the 460-580 nm region that is parallel to the $S_0 \rightarrow S_1$ transition (Figure 8).

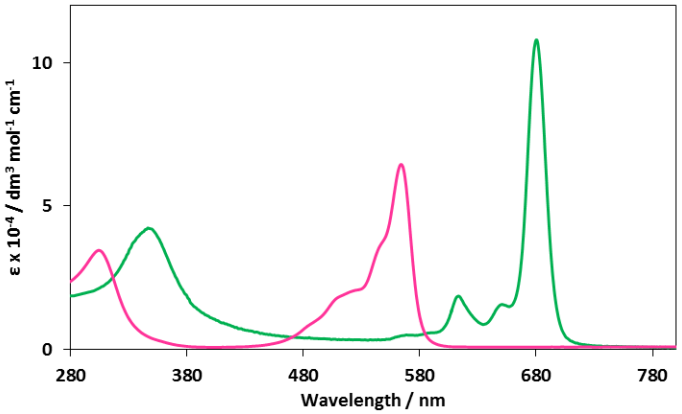

Figure 8. UV-vis spectra in chloroform of SubPc **1** (pink line) compared to that of a Zn(II) Pc (green line).

Both Soret and *Q* bands are significantly blue shifted with respect to the corresponding Pc transitions (λ_{max} = 300-400 and 600-800 nm, respectively) as a consequence of the reduction in the number of π-electrons in the aromatic circuit, from 18 for Pcs to 14 in SubPcs. Absorption coefficients (ε) in both Soret band and *Q* band also decrease on going from Pcs to SubPcs due to the nonplanar structure of the latter,[62a] being the ε values of the *Q* bands of SubPcs around 5-6 × 10^4 dm^3 mol^{-1} cm^{-1}.

Axial substituents have none or only a very small effect on the position of the bands. On the contrary, peripheral donor and acceptor substituents able to slightly extend the π-conjugation of the ring tend to shift the *Q* band of SubPcs toward longer wavelengths. The effect is particularly dramatic in SubPcs substituted with π-donor atoms, such as sulfur, oxygen, or nitrogen, and it is enhanced with the increasing number of such substituents at the SubPc

periphery.[41,72c,74,82] In addition, these substituents produce supplementary bands in the 400-500 nm region attributable to n→π* transitions due to π-donation from the heteroatom lone pair to the macrocycle.[36c,51e,72c]

SubPcs are fluorescent, with λ_{max} = 575-670 nm, emission and excitation spectra generally being in a mirror image relationship, although fluorescence emission only takes place from the lowest singlet excited state. SubPcs, as their parent Pcs, exhibit very small Stokes shifts (typically around 10-15 nm) and unusually narrow widths at half of the maximum intensity,[83] what indicates very small geometric distortion of the excited state. From the intersection between the two bands, singlet excited state energies of *ca.* 2.1-2.0 eV are typically derived for SubPcs, higher than those found for Pcs (~1.7 eV), and consistent with the HOMO-LUMO gaps derived from cyclic voltammetry measurements. Fluorescence quantum yields (ϕ_F) of SubPcs are typically around 0.2-0.5, but they can reach up to 0.95 for certain compounds,[78b] or go down to < 0.1 radiative yields due to molecular aggregation,[75b] fast intersystem crossing in heavy-atom-substituted aromatic compounds,[51e] or intramolecular energy or electron transfer singlet-excited state deactivation.[78b,82,84]

The triplet excited state energy level in SubPcs is located in the near-infrared region (~845 nm), and based on these maxima, SubPc triplet energies of 1.45 eV can be derived.[51e] Thus, singlet-triplet energy gaps in SubPcs (*ca.* 0.65 eV) are only slightly larger than those of Pcs (0.5-0.6 eV).

The first oxidative or reductive half-wave potentials of SubPcs are both one electron processes. The reduction is frequently reversible, while on the other hand, oxidation processes appear to give rise to less stable charged species. Scanning at more positive or negative potentials typically reveals several redox events, some of them multielectronic, which usually are electrochemically irreversible or quasi-reversible.

The first oxidative or reductive half-wave potential of SubPcs, and hence their electron-donor/acceptor ability, do not vary much with the nature of the axial ligand, but they are considerably affected and can be predictably tuned by the peripheral substitution on the isoindole rings. For instance, the first reductive event is typically observed between -1.58 V[74]

[82] González-Rodríguez, D.; Torres, T.; Olmstead, M. M.; Rivera, J.; Herranz, M. A.; Echegoyen, L.; Atienza Castellanos, C.; Guldi, D. M. *J. Am. Chem. Soc.* **2006**, *128*, 10680.

[83] Díaz, D. D.; Bolink, H. J.; Cappelli, L.; Claessens, C. G.; Coronado, E.; Torres, T. *Tetrahedron Lett.* **2007**, *48*, 4657.

[84] Xu, H.; Jiang, X. -J.; Chan, E. Y. M.; Fong, W. -P.; Ng, D. K. P. *Org. Biomol. Chem.* **2007**, *5*, 3987.

and -0.82 V[82] whereas first oxidative half-wave values were as high as +1.15 V[82] and as low as +0.37 V,[74] *vs.* the Fc/Fc^+ internal reference.

The redox gap of SubPcs (~2.1 eV) is therefore clearly larger than that of Pcs (~1.7 eV). Absolute HOMO and LUMO energy levels have been estimated for several SubPcs via different techniques such as cyclic voltammetry in solution, or photoelectron spectroscopy onto HOPG substrates.[42a,85] Interestingly, Bender *et al.* recently described a mathematical model for the prediction of HOMO and LUMO energy levels in SubPc macrocycles from semiempirical (PM3 or RM1) or DFT (B3LYP) computational data,[85] validated by a combination of cyclic voltammetry, absorption spectroscopy, and ultraviolet photoelectron spectroscopy techniques. Thus, HOMO values of SubPcs vary between -6.8 and -5.3 eV whereas the LUMO level is normally situated between -3.3 and -4.7 eV.

During the past few years, due to their outstanding electronic and photophysical properties, together with an increasing understanding of the morphology at the nanometer-scale of the SubPc-based molecular materials, SubPcs have already begun to have a profound impact in many high-technology areas, finding applications and commercial utility as active units in chemical sensors,[76,86] optical information recording media,[87] supramolecular chemistry,[50,71b,72a,88] nonlinear optics, molecular electronics[89] and photonics, photodynamic therapy (PDT), and organic photovoltaic devices (OPVs), among others.

---

[85] Morse, G. E.; Helander, M. G.; Stanwick, J.; Sauks, J. M.; Paton, A. S.; Lu, Z.-H.; Bender, T. P. *J. Phys. Chem. C* **2011**, *115*, 11709.

[86] a) Xu, S.; Chen, K.; Tian, H. *J. Mat. Chem.* **2005**, *15*, 2676. b) Ros-Lis, J. V.; Martínez-Máñez, R.; Soto, J. *Chem. Commun.* **2005**, 5260.

[87] a) Wang, Y.; Gu, D.; Gan, F. *Phys. Status Solidi* **2001**, *186*, 71. b) Wang, Y.; Gan, F. *Chin. Sci. Bull.* **2001**, 46, 2013. c) Wang, Y.; Gu, D.; Gan, F. *Proc. SPIE* **2003**, *5060*, 15. d) Natarajan, A.; Boden, E. P.; Chan, K. P.; McCloskey, P. J.; Ostroverkhov, V. P.; Kim, E. M.; Gascoyne, D. G.; Perry, R. J.; Jean-Gilles, R. P.; Lee, J. L.; Lawrence, B. L. US 8,182,967 B2, issued on May 22, 2012, Filed on Aug. 31, 2009, Prior Publication US 2011/0051586A1, March 03, 2011. e) Compositions, optical data storage media and methods for using the optical data storage media. Boden, E. P.; Chan, K. P.; Jean-Gilles, R. P.; Kim, E. M.; Lawrence, B. L.; Lee, J. L.; McCloskey, P. J.; Natarajan, A.; Ostroverkhov, V. P.; Perry, R. J. EP2290651 B1, issued on October 10, 2012, priority date August 31, 2009. Also published as US20110053055. f) Natarajan, A.; Mccloskey, P. J.; Chan, K.-P.; Kim, E. M.; Colborn, R. E.; Boden, E. P. European Patent, EP2595155 (A2), 2013.

[88] a) Claessens, C. G.; Vicente-Arana, M.; Torres, T. *Chem. Commun.* **2008**, 6378. b) Claessens, C. G.; Sánchez-Molina, I.; Torres, T. *Supramol. Chem.* **2009**, *21*, 44. c) Sánchez-Molina, I.; Grimm, B.; Krick Calderon, R. M.; Claessens, C. G.; Guldi, D. M.; Torres, T. *J. Am. Chem. Soc.* **2013**, *135*, 10503.

[89] a) Guilleme, J.; Aragó, J.; Ortí, E.; Cavero, E.; Sierra, T.; Ortega, J.; Folcia, C. L.; Etxebarria, J.; González-Rodríguez, D.; Torres, T. *J. Mater. Chem. C* **2015**, *3*, 985. b) Guilleme, J.; Cavero, E.; Sierra, T.; Ortega, J.; Folcia, C. L.; Etxebarria, J.; Torres, T.; González-Rodríguez, D. *Adv. Mater.* **2015**, *27*, 4280.

SubPcs, with their highly delocalized π-electron systems and both dipolar and octupolar characters, have been intensively investigated as NLO materials.[90] The second harmonic generation (SHG) properties of a series of SubPcs tri- or hexasubstituted with electron-donor and electron-acceptor groups have been extensively studied toward this end, obtaining quadratic hyperpolarizability β values well comparable to the best values obtained so far with other organic molecules.[36c,91] Third-order harmonic generation (THG) studies have also been performed on SubPcs,[92] the cubic susceptibility $\chi^{(3)}$ values recorded being three times higher than those measured for Pcs in the same frequency range. Besides, SubPcs are potential optical limiters since they can exhibit strong excited-state absorption, high triplet yields and long excited-state lifetimes.[93]

OFETs are the basic building blocks for many flexible integrated circuits and displays. OFETs consisting of vacuum sublimed thin films of SubPc **1**[94] and three phenoxy-SubPcs,[95] have been prepared, and electron mobilities were determined to be in the range of *ca.* 10^{-5}-10^{-4} cm^2 V^{-1} s^{-1}. In addition, Forrest *et al.*[96] have demonstrated an imaging passive pixel sensor circuit consisting of a bottom-gate, top-contact pentacene organic thin-film transistor (OTFT) integrated with a top-illuminated, inverted SubPc/C_{60} organic photodetector (OPD) (Figure 9). By integrating the two components, a 12-bit dynamic range passive pixel sensor is achieved, with an off current of 31 ± 5 *p*A and a pixel readout time of 0.4 ± 0.05 ms, with potential for use in large-scale focal plane array imagers.

---

[90] a) de la Torre, G.; Vázquez, P.; Agulló-López, F.; Torres, T. *J. Mater. Chem.* **1998**, *8*, 1671. b) de la Torre, G.; Vázquez, P.; Agulló-López, F.; Torres, T. *Chem. Rev.* **2004**, *104*, 3723. c) Díaz-García, M. A. *J. Porphyrins Phthalocyanines* **2009**, *13*, 652.

[91] a) Sastre, A.; Torres, T.; Díaz-García, M. A.; Agulló-López, F.; Dhenaut, C.; Brasselet, S.; Ledoux, I.; Zyss, J. *J. Am. Chem. Soc.* **1996**, *118*, 2746. b) Torres Cebada, T.; Sastre Santos, A.; Del Rey Alvarez, B. (Universidad Autónoma de Madrid, Spain) Spain ES 2116867, 1998. c) Olbrechts, G.; Clays, K.; Wostyn, K.; Persoons, A. *Synth. Met.* **2000**, *115*, 207. d) Martín, G.; Rojo, G.; Hierro, A.; Agulló-López, F.; Ferro, V. R.; García de la Vega, J. M.; Martínez-Díaz, M. V.; Torres, T.; Ledoux, I.; Zyss, J. *J. Phys. Chem. B* **2002**, *106*, 13139. e) Claessens, C. G.; González-Rodríguez, D.; Torres, T.; Martín, G.; Agulló-López, F.; Ledoux, I.; Zyss, J.; Ferro, V. R.; García de la Vega, J. M. *J. Phys. Chem.* **2005**, *109*, 3800. f) Kim, H. M.; Cho, B. R. *J. Mater. Chem.* **2009**, *19*, 7402.

[92] a) Díaz-García, M. A.; Agulló-López, F.; Sastre, A.; Torres, T.; Torruellas, W. E.; Stegeman, G. I. *J. Phys. Chem.* **1995**, *99*, 14988. b) Liang, Z.; Gan, F.; Sun, Z.; Yang, X.; Ding, L.; Wang, Z. *Opt. Mater.* **2000**, *14*, 13. c) Liang, Z. -J.; Tang, F .-L.; Gan, F. -X.; Xun, Z. -R.; Yang, X. -H.; Ding, L. -E.; Wang, Z. -G. *Wuli Xuebao* **2000**, *49*, 252.

[93] a) Gu, Y.; Gan, F.; Yin, G.; Yu, B. *Guangxue Xuebao* **2002**, *22*, 144. b) Dini, D.; Vagin, S.; Hanack, M.; Amendola, V.; Meneghetti, M. *Chem. Commun.* **2005**, 3796.

[94] Yasuda, T.; Tsutsui, T. *Mol. Cryst. Liq. Cryst.* **2007**, *462*, 3.

[95] Castrucci, J. S.; Helander, M. G.; Morse, G. E.; Lu, Z.-H.; Yip, C. M.; Bender, T. P. *Cryst. Growth Des.* **2012**, *12*, 1095.

[96] a) Renshaw, C. K.; Xu, X.; Forrest, S. R. *Org. Electron.* **2010**, *11*, 175. b) Tong, X.; Forrest, S. R. *Org. Electron.* **2011**, *12*, 1822.

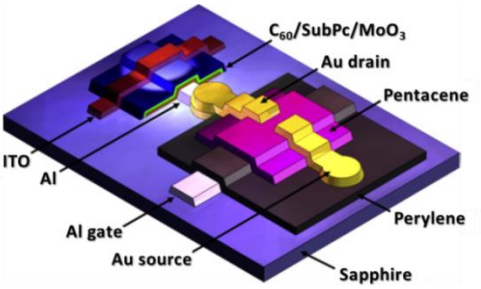

Figure 9. Schematic diagram of the integrated passive pixel sensor consisting of a top-illuminated SubPc/C_{60} OPD with an indium-tin-oxide (ITO) top contact in series with a pentacene OTFT.

SubPcs are a promising class of orange emitters with a remarkably narrow emission width and excellent electrical performance in OLEDs.[42a,83,97] Recently, Bender *et al.* have reported a class of axially substituted phthalimido-SubPcs,[97d] which exhibit a high quantum yield for photoluminescence (ϕ_F), maintain a high molar extinction coefficient (ε) and have bipolar electrochemical stability, resulting in OLEDs with comparable maximum efficiencies as electron transport and hole transport emitters (Figure 10).

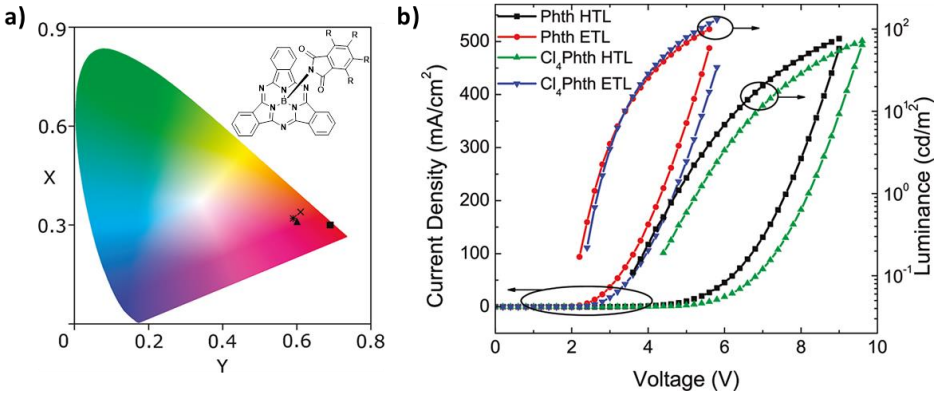

Figure 10. a) Structure of phthalimido-SubPcs and CIE color coordinates (symbol; *x*, *y*) for the light emission produced by the OLED devices; b) Luminance and current density as a function of voltage for OLED devices including SubPc as a hole transport layer (HTL) and an electron transport layer (ETL).

[97] a) Chen, Y. -H.; Chang, J. -H.; Lee, G. -R.; Wu, I. -W.; Fang, J. -H.; Wu, C. -I.; Pi, T. -W. *Appl. Phys. Lett.* **2009**, *95*, 133302/1. b) Chen, Y. -H.; Chang, Y. -J.; Lee, G. -R.; Chang, J. -H.; Wu, I. -W.; Fang, J. -H.; Hsu, S. -H.; Liu, S. -W.; Wu, C. -I.; Pi, T. –W. *Org. Electron.* **2010**, *11*, 445. c) Helander, M. G.; Morse, G. E.; Qiu, J.; Castrucci, J. S.; Bender, T. P.; Lu, Z. -H. *ACS Appl. Mater. Interfaces* **2010**, *2*, 3147. d) Morse, G. E.; Castrucci, J. S.; Helander, M. G.; Lu, Z. -H.; Bender, T. P. *ACS Appl. Mater. Interfaces* **2011**, *3*, 3538. e) Morse, G. E.; Bender, T. P. *ACS Appl. Mater. Interfaces* **2012**, *4*, 5055.

In recent years, there has been a growing interest in the use of Pcs, Ps, and related compounds as photosensitizers in PDT.[98] In this context, SubPcs have potential as high-sensitivity probes dye in the visible region or as chromophores in PDT due to their high extinction coefficients around 600 nm, long triplet lifetimes in the order of 100 μs, and their characteristic cone-shaped structure that prevents aggregation and facilitates water solubility.[99] Singlet oxygen quantum yields in SubPcs can be relatively high (ϕ_Δ = 0.5−0.7),[51e,75a,b,84] and water-soluble SubPcs have demonstrated an efficient cellular uptake and phototoxicity against *Escherichia coli*[75a] or *HepG2* human hepatocarcinoma and *HT29* human colon adenocarcinoma cells.[84] Finally, Decréau *et al.* have described the use of SubPcs as fluorophores for the *in vitro* fluorescence imaging of *B16* melanoma cells with no cytotoxicity by nano-encapsulation in liposomes for hydrophobic species or by increasing water-solubility by the introduction of alkyl sulfonate chains (Figure 11).[100]

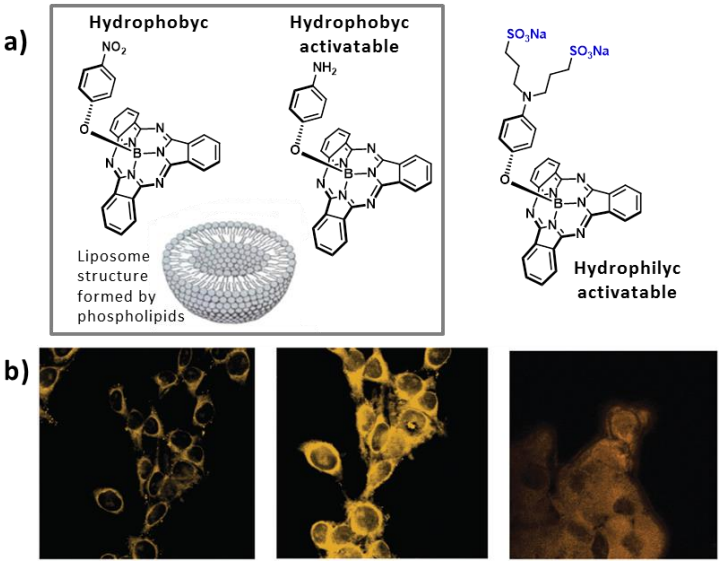

Figure 11. a) General structure of hydrophobic/hydrophilic activatable SubPcs and liposome structure; b) Fluorescence microscopy images of *B16* melanoma cells upon incubation for 1 h with fluorescent SubPc probes and fixation (methanol).

[98] a) Bonnett, R. *Chem. Soc. Rev.* **1995**, *24*, 19. b) Allen, C. M.; Sharman, W. M.; van Lier, J. E. *J. Porphyrins Phthalocyanines* **2001**, *5*, 161.
[99] Roy, I.; Shetty, D.; Hota, R.; Baek, K.; Kim, J.; Kim, C.; Kappert, S.; Kim, K. *Angew. Chem. Int. Ed.* **2015**, *54*, 15152.
[100] Bernhard, Y.; Winckler, P.; Chassagnon, R.; Richard, P.; Gigot, E.; Perrier-Cornet, J. –M.; Decréau, R. A. *Chem. Commun.* **2014**, *50*, 13975.

Apart from the above applications, during the past few years, SubPcs have emerged as a class of high performing materials in Organic Photovoltaic (OPV) cells.[35,97e] SubPcs can be now considered as both donor and acceptor materials in OPV solar cells with an absorption in the visible comparable to that of well-known Pcs. The state-of-the-art of the photovoltaic technologies and the application of SubPcs in OPVs will be extensively discussed in *Chapter 1* of the present thesis.

Subphthalocyanine-based extended systems

The extension of the conjugated system of the SubPc structure is an appealing strategy to develop expanded curved π surfaces with enlarged concave geometries or with different complex topologies and to give rise to analogous macrocycles with distinct optical and photophysical properties.

The conjugated system of SubPcs may be straightforwardly extended by the addition of extra benzene rings to the isoindole units, by direct condensation of a π-expanded phthalonitrile derivative such as naphthalonitrile using the same conditions employed for SubPc synthesis. In this way, different symmetrical SubPc derivatives fused with additional aromatic moieties have been synthesized thus far, including benzene-fused 1,2- and 2,3-Subnaphthalocyanines (SubNcs),[36d,51d,62a,91d,101] and tetrathiafulvalene-annulated or phenanthro[4,5-*fgh*]quinoxaline-fused SubPcs (Chart 2).[102] Besides, mixed condensation reactions of these largely fused dicarbonitriles with other phthalonitrile precursors have been reported to yield A_2B- and AB_2-type low-symmetry SubPc analogues.[51c,d,102,103] In all cases, the more extended conjugation of these derivatives results in a red shift of the absorption compared to related SubPcs, going from the characteristic pink or purple color of SubPcs to green.

---

[101] a) Rauschnabel, J.; Hanack, M. *Tetrahedron Lett.* **1995**, *36*, 1629. b) Rubio, N.; Jiménez-Banzo, A.; Torres, T.; Nonell, S. *J. Photochem. Photobiol. A* **2007**, *187*, 214. c) Shimizu, S.; Miura, A.; Khene, S.; Nyokong, T.; Kobayashi, N. *J. Am. Chem. Soc.* **2011**, *133*, 17322. d) Takao, Y.; Masuoka, T.; Yamamoto, K.; Mizutani, T.; Matsumoto, F.; Moriwaki, K.; Hida, K.; Iwai, T.; Ito, T.; Mizuno, T.; Ohno, T. *Tetrahedron Lett.* **2014**, *55*, 4564. e) Yamamoto, K.; Takagi, A.; Hada, M.; Taniwaki, R.; Mizutani, T.; Kimura, Y.; Takao, Y.; Moriwaki, K.; Matsumoto, F.; Ito, T.; Iwai, T.; Hida, K.; Mizuno, T.; Ohno, T. *Tetrahedron* **2016**, *72*, 4918.

[102] a) Shimizu, S.; Yamazaki, Y.; Kobayashi, N. *Chem. Eur. J.* **2013**, *19*, 7324. b) Pan, H.; Liu, W.; Wang, C.; Wang, K.; Jiang, J. *Chem. Eur. J.* **2016**, *22*, 9488.

[103] a) Zhu, H.; Shimizu, S.; Kobayashi, N. *Angew. Chem. Int. Ed.* **2010**, *49*, 8000. b) Shimizu, S.; Nakano, S.; Hosoya, T.; Kobayashi, N. *Chem. Commun.* **2011**, *47*, 316. c) Mack, J.; Otaki, T.; Durfee, W. S.; Kobayashi, N.; Stillman, M. J. *J. Inorg. Biochem.* **2014**, *136*, 122. d) Shimizu, S.; Nakano, S.; Kojima, A.; Kobayashi, N. *Angew. Chem. Int. Ed.* **2014**, *53*, 2408.

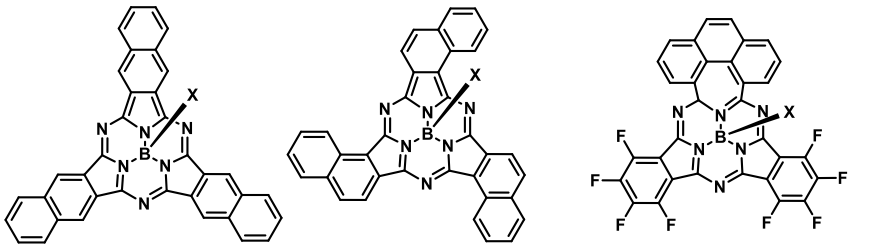

Chart 2. Chemical structure of diverse extended SubPc systems.

Cyclic SubPc trimers built by fusing SubPc units around a dehydro[18]annulene core were prepared by Iglesias *et al.* in 2007.[51f] These trimers must be in fact a mixture of two topoisomers[104] that could not be separated or differentiated from the characterization data. Their extended π-conjugation is reflected in UV-vis absorption and cyclic voltammetry ground-state measurements. Shimizu *et al.* have recently prepared novel pyrene-bridged SubPc dimers from a mixed-condensation reaction of 2,7-di-*tert*-butyl-4,5,9,10-tetracyanopyrene and tetrafluorophthalonitrile, giving rise to their corresponding *syn* and *anti* isomers.[105] Expansion of the conjugated system of SubPc through the pyrene bridge was observed by the red shift of the *Q* band absorption relative to the parent pyrene-fused monomer.

A different type of SubPc-based conjugated systems was envisioned by Kobayashi in 1991,[106] when he described the synthesis of a fused dimer of SubPc, that is, a π-extended molecule comprising two SubPc units sharing a common benzene ring, though without any spectroscopic support. It was eleven years later when Claessens *et al.* and Kobayashi *et al.*[107] simultaneously reported the preparation of a peripherally fluorinated SubPc dimer **2** (Chart 3) by crossover condensation of tetrafluorophthalonitrile and 1,2,4,5-benzenetetracarbonitrile in the presence of BCl_3. The geometry of the constituent SubPcs endows the corresponding dimers with an unusual bowl-shape topology, in which two topoisomers, the *syn* and the *anti*, are formed in equal amounts. Few more SubPc dimers bearing different peripheral and axial functionalization have been reported.[108] Photophysical and electrochemical studies have

[104] Topoisomers or topological isomers are molecules with the same chemical formula and stereochemical bond connectivities but different topologies.

[105] Nakano, S.; Kage, Y.; Furuta, H.; Kobayashi, N.; Shimizu, S. *Chem. Eur. J.* **2016**, *22*, 7706.

[106] Kobayashi, N. *J. Chem. Soc., Chem. Commun.* **1991**, 1203.

[107] a) Claessens, C. G.; Torres, T. *Angew. Chem. Int. Ed.* **2002**, *41*, 2561. b) Fukuda, T.; Stork, J. R.; Potucek, R. J.; Olmstead, M. M.; Noll, B. C.; Kobayashi, N.; Durfee, W. S. *Angew. Chem. Int. Ed.* **2002**, *41*, 2565.

[108] a) Iglesias, R. S.; Claessens, C. G.; Torres, T.; Herranz, M. A.; Ferro, V. A.; García de la Vega, J. M. *J. Org. Chem.* **2007**, *72*, 2967. b) Giribabu, L.; Kumar, C. V.; Surendar, A.; Reddy, V. G.; Chandrasekharam, M.; Reddy,

revealed that there is good communication between the SubPc moieties within the oligomeric structures. *Chapter 2* of the present thesis is devoted to the development of some approaches for the peripheral and axial functionalization of these systems, in order to study and modify their interesting physicochemical properties and to employ their compelling unique topologies for molecular recognition.

Finally, SubPc-based multicomponent systems where two or more SubPc units are bonded by peripheral or axial positions but no extension of the conjugated core of SubPc is produced have been prepared. Herein, SubPc μ-oxo dimers,[62,63] SubPc bisphenoxy dimers,[54b,g,h,109] axially linked SubPc polymers,[56b,110] SubPc diabolos[111] and wheels,[40] and cyclophane-fused SubPc dimers[112] (Chart 3) are representative examples.

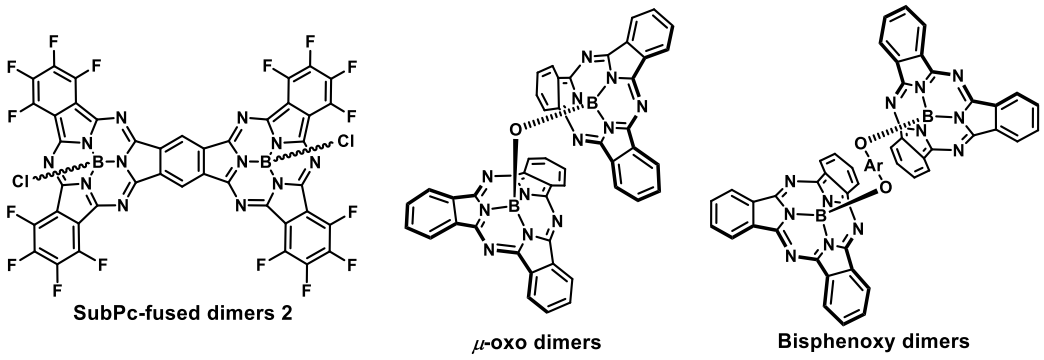

Chart 3. Chemical structure of diverse fused π-extended or multicomponent SubPc dimers.

P. Y. *Synth. Commun.* **2007**, *37*, 4141. c) Shibata, N.; Mori, S.; Hayashi, M.; Umeda, M.; Tokunaga, E.; Shiro, M.; Sato, H.; Hoshi, T.; Kobayashi, N. *Chem. Commun.* **2014**, *50*, 3040.

[109] a) Fukuda, T.; Olmstead, M. M.; Durfee, W. S.; Kobayashi, N. *Chem. Commun.* **2003**, 1256. b) Morse, G. E.; Paton, A. S.; Lough, A.; Bender, T. P. *Dalton Trans.* **2010**, *9*, 3915.

[110] Dang, J. D.; Virdo, J. D.; Lessard, B. H.; Bultz, E.; Paton, A. S.; Bender, T. P. *Macromolecules* **2012**, *45*, 7791.

[111] Eckert, A. K.; Rodríguez-Morgade, M. S.; Torres, T. *Chem. Commun.* **2007**, 4104.

[112] Liu, Q.; Shimizu, S.; Kobayashi, N. *Angew. Chem. Int. Ed.* **2015**, *54*, 5187.

General Objectives

The aim of this Thesis is the preparation of new subphthalocyanine based systems for their application as photo- and electroactive materials in organic photovoltaics.

Chapter 1 is devoted to the development and study of novel SubPc derivatives as acceptor materials in organic solar cells. For this purpose, new routes towards the introduction of electron-withdrawing substituents in the SubPc periphery will be explored.

From the pool of existing SubPcs, selected derivatives will be incorporated in vacuum-evaporated planar heterojunction and solution-processed bulk heterojunction solar cells. These SubPcs should fulfil specific requirements. They must exhibit (i) intense absorption of solar light with complementary profiles to the donor materials, (ii) suitable HOMO and LUMO energy levels, (iii) appropriate conducting properties and (iv) adequate aggregation behavior to control the morphology of the systems.

The aim of **Chapter 2** is the synthesis and characterization of novel curved π-extended systems based on SubPc fused oligomers and the study of selected properties and potential photovoltaic applications.

A stepwise rationally designed synthetic strategy for the preparation of unsymmetrical SubPc fused dimers differently functionalized in each SubPc unit will be presented, with the goal of modulating further the optoelectronic properties of this family of molecular building blocks.

In addition, the axial functionalization of SubPc dimers to generate SubPc-based multicomponent systems for molecular recognition and supramolecular artificial photosynthetic systems will be explored. The suitability of the novel π-extended curved aromatic structures obtained for the complexation of carbon nanostructures will be analysed.

Specific objectives to be met in the research will be listed in each chapter.

Chapter I

Subphthalocyanine Derivatives as Electron Acceptor Components of Organic Solar Cells

1.1 Photovoltaics: direct light-to-electric energy conversion

During the last decades, numerous scientific reports[113] delivered by several governmental and non-governmental international organizations for the assessment of climate change and its potential environmental and socio-economic impacts have disclosed a shattering fact: the existing dependence of global economy on fossil fuels as the primary source of world's energy production has driven greenhouse gas atmospheric concentrations to critical maximum levels in at least the last 800,000 years, leading to an uptake of energy by the climate system. In 2013, nearly 82% world's energy supply was coming from fossil fuels.[113b] Besides, the ongoing use of oil supplies by human society is performed at a much higher rate than the minimum rate at which reserves can be geophysically renewed while experts predictions augur global population growth and economic development will at least double the current energy demand by 2050.[114] This disturbing scenario evinces the rapid development and deployment of renewable energies, such as solar, wind, hydropower, tidal, geothermal and biomass, are essential for mankind progress.

Sunlight is the most abundant and sustainable source of energy available to humanity. Earth receives solar energy at the rate of approximately 120,000 TW (1 TW = 10^{12} W) in a highly reliable and distributed fashion. This vastly exceeds the current annual worldwide energy consumption rate of ~15 TW.[115] Solar energy can be transformed into electricity either thermodynamically or electronically. Solar thermal systems generate electricity by using mirrors to heat up a working fluid that in turn drives a turbine connected to an electrical generator.[116] Photovoltaics is a method based on the direct conversion of solar light into electricity by photovoltaic effect[117] using devices called solar cells.

The search for low cost highly efficient photovoltaics has led researchers to the quest for both inorganic and organic semiconducting materials as possible candidates for their application in

---

[113] a) *IPCC, 2014: Climate Change 2014: Synthesis Report. Contribution of Working Groups I, II and III to the Fifth Assessment Report of the Intergovernmental Panel on Climate Change*; Pachauri, R.K., Meyer, L.A., Eds.; IPCC: Geneva, Switzerland, 2014. b) *2015 Key World Energy Statistics*; International Energy Agency, Ed.; OECD/IEA: Paris, France, 2015. c) *Commission of the European Communities. Green Paper: A European Strategy for Sustainable, Competitive and Secure Energy*; Brussels, 2006.

[114] Service, R. F. *Science* **2005**, *309*, 548.

[115] Blankenship, R. E.; Tiede, D. M.; Barber, J.; Brudvig, G. W.; Fleming, G.; Ghirardi, M.; Gunner, M. R.; Junge, W.; Kramer, D. M.; Melis, A.; Moore, T. A.; Moser, C. C.; Nocera, D. G.; Nozik, A. J.; Ort, D. R.; Parson, W. W.; Prince, R. C.; Sayre, R. T. *Science* **2011**, *332*, 805.

[116] Norton, B. *Harnessing Solar Heat*; Lecture in Energy 18; Springer: Dordrecht, 2014.

[117] Becquerel, A. E. *C. R. Hebd. Seances Acad. Sci.***1839**, *9*, 561.

these devices. In this regard, solar cells can be broadly classified depending on the nature of the semiconducting material they are made of, the manufacturing technique, and the type of junction formed.

1.1.1 Classification of solar cells

a) Inorganic solar cells

First modern solar cell, based on the use of a single-crystal silicon wafer, was demonstrated in 1954 by Chapin, Fuller, and Pearson at Bell Laboratories, with an efficiency of ~5%.[118] During the ensuing decades, due to the natural abundance of this material, extensive research and progressive improvement in silicon-based devices gave rise to the *first generation* of solar cells. The majority of today's commercial solar cells still utilizes a silicon wafer in either single-crystal or polycrystalline form, with maximum efficiencies of 25.6 and 21.3% respectively.[119] However, the high production cost of highly pure silicon materials promoted the quest for alternative and cheaper inorganic systems. The *second generation*[120] solar cells apply thin-film techniques to produce devices based primarily on polycrystalline absorber materials, such as cadmium telluride (CdTe), copper indium gallium diselenide (CIGS), gallium arsenide (GaAs) and amorphous silicon. Record efficiencies of ~29%[119] and lower production costs make them competitive compared to *first generation* devices. The main drawbacks of these cells are the scarcity and high toxicity of the materials needed.

The constraints and handicaps of these two approaches encouraged the appearance of a *third generation*[121] of solar cells, encompassing organic and hybrid devices, that makes use of synthetically-tuned, easy-processable materials and are based on novel concepts like hot-carrier solar cells, multi-exciton generation, multi-junction or tandem solar cells, with excellent

[118] Chapin, D. M.; Fuller, C. S.; Pearson, G. L. *J. Appl. Phys.* **1954**, *25*, 676.
[119] Green, M. A.; Emery, K.; Hishikawa, Y.; Warta, W.; Dunlop, E. D. *Prog. Photovolt: Res. Appl.* **2016**, *24*, 3.
[120] a) Peter, L.M. *Phil. Trans. R. Soc. A*, **2011**, *369*, 1840. b) Schmidtke, J. *Opt. Express* **2010**, *18*, A477.
[121] a) Green, M.A. *Third Generation Photovoltaics*; Springer-Verlag: Berlin, Germany, 2003. b) Conibeer, G. *Mater. Today* **2007**, *10*, 42. c) Brunetti, F. G.; Kumar, R.; F. Wudl, *J. Mater. Chem*. **2010**, *20*, 2934. d) Delgado, J. L.; Bouit, P. -A.; Filippone, S.; Herranz, M. A.; Martin, N. *Chem. Comm*. **2010**, *46*, 4853. e) Yan, J.; Saunders, B. R. *RSC Adv*. **2014**, *4*, 43286. f) Mazzio, K. A.; Luscombe, C. K. *Chem. Soc. Rev*. **2015**, *44*, 78. g) Ragoussi, M. -E.; Torres, T. *Chem. Commun*. **2015**, *51*, 3957.

potential for large-scale solar electricity generation. This generation has the aim of reducing production costs, as well as exceeding the Shockley and Queisser efficiency limit.[122]

b) Organic solar cells

Studies on all-organic photovoltaics started in the 1950s, when simple organic dyes, like chlorophyll or magnesium Pcs, were investigated, with reported power conversion efficiencies (*PCE*) not surpassing 0.1%.[123] The main weakness of these single-layer architectures was the extensive charge recombination, attributed to the fact that excitons (localized and bound electron-hole pairs), formed upon light illumination, do not dissociate readily in most organic semiconductors.[121f] In 1986, Tang fabricated the first two-component donor/acceptor (D/A) active layer solar cell with an efficiency approaching 1%,[124] which was a milestone in the development of OPVs. In this device, the pioneering example of *Planar Heterojunction (PHJ*, Figure 12a*)* solar cells*,* exciton dissociation at the heterojunction (interface) of the two molecules was favored due to the substantially different electron affinities and ionization potentials among them and the recombination chances of the charge carriers were minimized by ensuring the connectivity between the active layers to the correct electrode. Nevertheless, a significant hurdle for the performance of OPVs based on this architecture is the short exciton diffusion length in organic materials (typically 5-20 nm),[125] that limits the maximum thickness of the active layer and thus the maximum fraction of the incident light that the cell can absorb and convert into electricity.

To circumvent this limitation, Yu *et al.*[126] introduced in 1995 the concept of *Bulk Heterojunction (BHJ*, Figure 12b*)* solar cells, consisting on a blend of bicontinuous and interpenetrating donor and acceptor components, creating a network that significantly increases the interfacial D/A area, leading to a substantial enhancement of the number of generated excitons as well as their dissociation into free charge carriers and hence to a rise of efficiency of the OPV devices.[127]

There exists also another approach to improve OPVs efficiencies, the so-called *Tandem or Multijunction Solar Cells* (Figure 12c). In this cell design, two or even more single

---

[122] a) Green, M. A. *Prog. Photovoltaics* **2001**, *9*, 123. b) Nelson, C. A.; Monahan, N. R.; Zhu, X. -Y. *Energy Environ. Sci.* **2013**, *6*, 3508.
[123] Kearns D.; Calvin, M. J. *Chem. Phys.* **1958**, *29*, 950.
[124] Tang, C.W. *Appl. Phys. Lett.* **1986**, *48*, 183.
[125] Lunt, R. R.; Giebink, N. C.; Belak, A. A.; Benziger, J. B.; Forrest, S. R. *J. Appl. Phys.,* **2009**, *105*, 053711.
[126] Yu, G.; Gao, J.; Hummelen, J. C.; Wudl, F.; Heeger, A. J. *Science* **1995**, *270* , 1789.
[127] Brabec, C. J.; Sariciftci, N. S.; Hummelen, J. C. *Adv. Funct. Mater.* **2001**, *11*, 15.

heterojunction cells can be stacked on top of each other to form a tandem structure, which enables one to resolve two limiting factors existing intrinsically among organic semiconductor molecules: poor charge carrier mobility and a narrow light absorption range.[128]

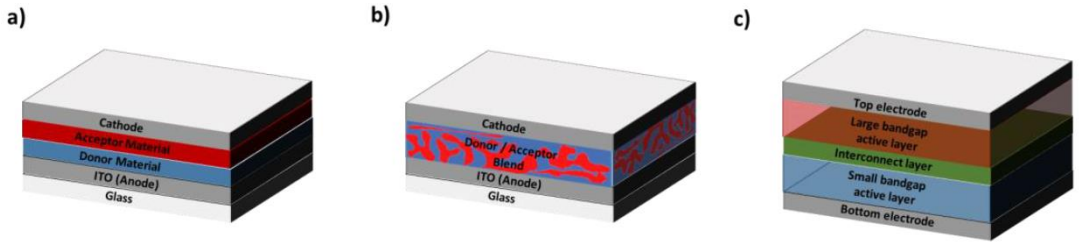

Figure 12. Schematic representation of a) PHJ solar cell, b) BHJ solar cell and c) tandem solar cell architectures.

c) Hybrid solar cells

Hybrid solar cells combine organic and inorganic materials with the aim of incorporating the advantages associated with both material groups. Organic materials are inexpensive, easily processable and their functionality can be tailored by molecular design and chemical synthesis. On the other hand, inorganic semiconductors can be manufactured as nanoparticles and inorganic semiconductor nanoparticles offer the advantage of having high absorption coefficients and size tunability.[129]

Among all, the most studied device of this generation is the *Dye-Sensitized Solar Cell* (*DSSC*, Figure 13),[130] being a low-cost and high efficiency solar energy-to-electricity converter. This pioneering architecture was introduced by O'Regan and Grätzel[131] and its development of DSSCs in the 1990s opened up new horizons in the area of photovoltaics, showing a tremendous potential as an alternative to the standard silicon photovoltaics,[132] with the

[128] a) Kim, J. Y.; Lee, K.; Coates, N. E.; Moses, D.; Nguyen, T.-Q.; Dante, M.; Heeger, A. J. *Science* **2007**, *317*, 222. b) Hadipour, A.; de Boer, B.; Blom, P. W. M. *Adv. Funct. Mater.* **2008**, *18*, 169. c) Riede, M.; Uhrich, C.; Widmer, J.; Timmreck, R.; Wynands, D.; Schwartz, G.; Gnehr, W. -M.; Hildebrandt, D.; Weiss, A.; Hwang, J.; Sundarraj, S.; Erk, P.; Pfeiffer, M.; Leo, K. *Adv. Funct. Mater.* **2011**, *21*, 3019. d) Ameri, T.; Li, N.; Brabec, C. J. *Energy Environ. Sci.* **2013**, *6*, 2390.

[129] a) Günes, S.; Sariciftci, N. S. *Inorg. Chim. Acta* **2008**, *361*, 581. b) Wright, M.; Uddin, A. *Sol. Energ. Mat. Sol. Cells* **2012**, *107*, 87.

[130] a) Hagfeldt, A.; Boschloo, G.; Sun, L.; Kloo, L.; Pettersson, H. *Chem. Rev*. **2010**, *110*, 6595. b) Nazeeruddin, M. K.; Baranoff, E.; Grätzel, M. *Solar Energy* **2011**, *85*, 1172. c) Albero, J.; Atienzar, P.; Corma, A.; García, H. *Chem. Rec*. **2015**, *15*, 803.

[131] O'Regan, B.; Grätzel, M. *Nature* **1991**, *353*, 737.

[132] Jung, H. S.; Lee, J. -K. *J. Phys. Chem. Lett.* **2013**, *4*, 1682.

obtained efficiencies growing from 7% in the seminal report[131] to 13% recently.[133] DSSCs are unique compared with almost all other kinds of solar cells in that electron transport, light absorption and hole transport are each handled by different materials in the cell. In a classical DSSC device configuration, an organic light-absorbing sensitizing dye is anchored to a wide-bandgap semiconductor such as TiO_2, SnO_2 or ZnO. When the dye absorbs light, the photoexcited electron rapidly transfers to the conduction band of the semiconductor, which carries the electron to one of the electrodes. A redox couple, usually comprised of iodide/triiodide (I^-/I^{3-}), then reduces the oxidized dye back to its neutral state and transports the positive charge to the platinized counter-electrode. Research on light-absorbing dyes is very much developed, with different benchmark molecules ranging from expensive and toxic ruthenium complexes to organic chromophores such as Ps and Pcs.[134]

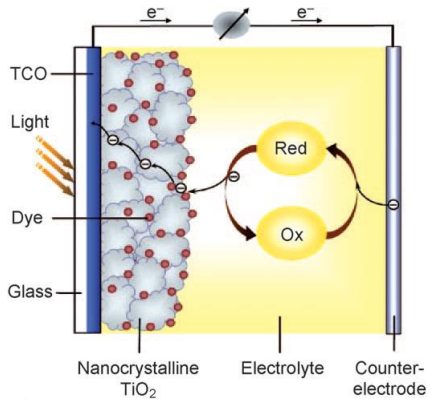

Figure 13. Schematic representation and fundamental processes in a DSSC.

d) Perovskite solar cells

The past few years have seen the unprecedentedly rapid emergence of a new class of solar cell based on mixed organic-inorganic halide perovskites sensitized devices (*Perovskite Solar Cells* or *PSCs*).[135] Perovskites have the general formula of AMX_3 (Figure 14). In this structure, A is a

[133] Mathew, S.; Yella, A.; Gao, P.; Humphry-Baker, R.; Curchod, B. F. E.; Ashari-Astani, N.; Tavernelli, I.; Rothlisberger, U.; Nazeeruddin, M. K.; Grätzel, M. *Nat. Chem.* **2014**, *6*, 242.

[134] a) Robertson, N. *Angew. Chem. Int. Ed.* **2006**, *45*, 2338. b) Mishra, A.; Fischer, M. K. R.; Bäuerle, P. *Angew. Chem. Int. Ed.* **2009**, *48*, 2474. c) Martínez-Díaz, M. V.; de la Torre G.; Torres, T. *Chem. Commun.* **2010**, *46*, 7090. d) Wu Y.; Zhu, W. *Chem. Soc. Rev.* **2013**, *42*, 2039.

[135] a) Snaith, H. J. *J. Phys. Chem. Lett.* **2013**, *4*, 3623. b) Loi, M. A.; Hummelen, J. C. *Nat. Mater.* **2013**, *12*, 1087. c) Kazim, S.; Nazeeruddin, M. K.; Gratzel, M.; Ahmad, S. *Angew. Chem. Int. Ed.* **2014**, *53*, 2812. d) Green, M. A.; Ho-Baillie, A.; Snaith, H. J. *Nature Photon.* **2014**, *8*, 506. e) Gao, P.; Grätzel, M.; Nazeeruddin, M. K. *Energy Environ. Sci*. **2014**, *7*, 2448.

monovalent cation, generally an organic ammonium salt; M is a metallic divalent cation, generally Pb^{+2}; and X is, for solar cell applications, a halogen.

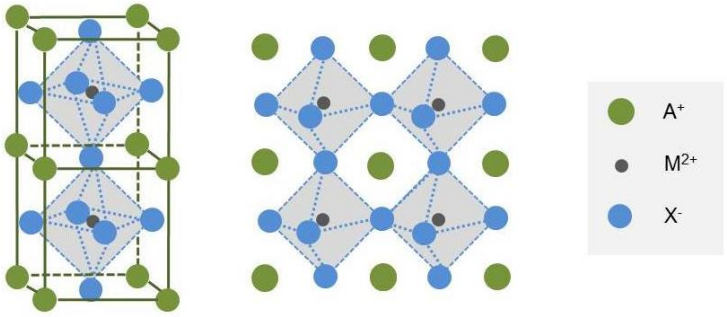

Figure 14. Structure of a common perovskite currently employed in solar cell applications.

This new generation of solar cells offers tantalizing prospects on both higher energy conversion efficiencies and significantly lower processing costs fronts, due to their ease of fabrication, strong solar absorption and low non-radiative carrier recombination rates for such simply prepared materials. Since the first 3.81% *PCE* reported on devices based on mesoporous TiO_2 photoanodes in 2009,[136] efficiencies have grown exponentially and rapidly surpassed those of all other organic or hybrid solar cells by engineering the selective contacts, optimizing the device morphology and improving the stability,[135e,137] reaching an outstanding 22.1% (KRICT/UNIST). One negative aspect of PSCs is the fact that lead has been a major constituent of all highly performing devices to date, raising toxicity issues during device fabrication, deployment and disposal. Also, they generally undergo relatively rapid degradation on exposure to moisture and ultraviolet radiation.

In a nutshell, the U.S. National Renewable Energy Laboratory (NREL) maintains a plot of compiled values of highest confirmed conversion efficiencies for research cells reported on a standardized basis that provides a general view of the comparative evolution and current state-of-the-art of the different photovoltaic devices (Figure 15).

[136] Kojima, A.; Teshima, K.; Shirai, Y.; Miyasaka, T. *J. Am. Chem. Soc.* **2009**, *131*, 6050.
[137] a) Burschka, J.; Pellet, N.; Moon, S. -J.; Humphry-Baker, R.; Gao, P.; Nazeeruddin, M. K.; Grätzel, M. *Nature* **2013**, *499*, 316. b) Eperon, G. E.; Stranks, S. D.; Menelaou, C.; Johnston, M. B.; Herz, L. M.; Snaith, H. J. *Energy Environ. Sci.* **2014**, *7*, 982. c) Lin, Q.; Armin, A.; Burn, P. L.; Meredith, P. *Acc. Chem. Res.* **2016**, *49*, 545.

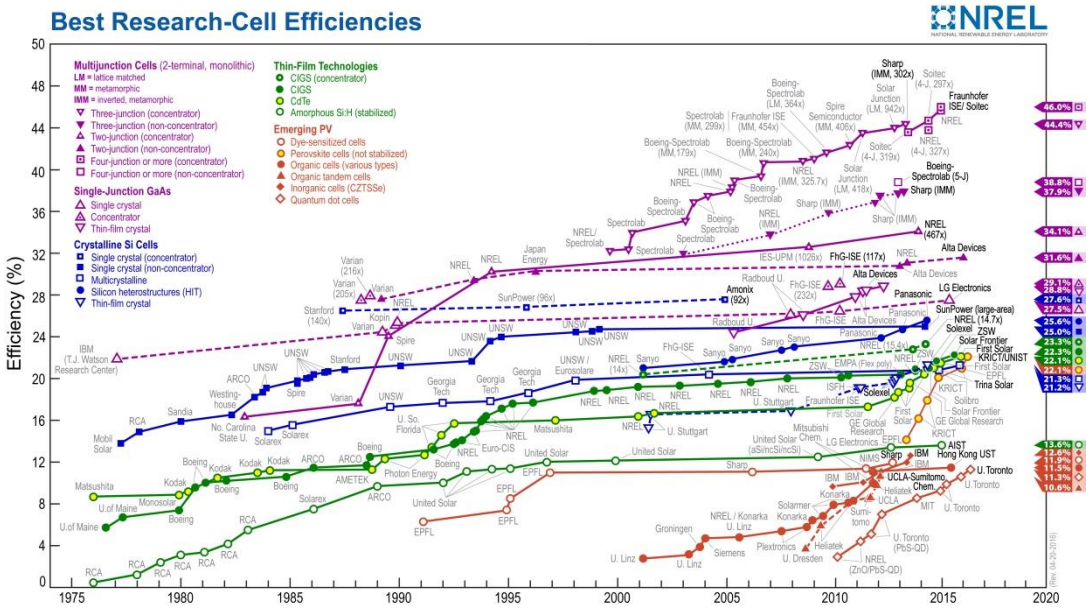

Figure 15. Efficiency of photovoltaic devices updated to May 2016.

1.2 Organic solar cells

As mentioned before, organic solar cells are basically constituted by semiconducting organic materials formed by contacting electron donor and acceptor compounds. In this regard, transformation of solar energy into electricity occurs through a series of optical and electronic processes that are common to any type of OSC and differ from those in inorganic photovoltaics.

1.2.1 Device configuration and operational principles in organic solar cells

The configuration of a conventional OSC involves a photoactive layer interposed between a high-work function anode, typically a modified transparent ITO (indium tin oxide) layer, and a relatively low-work function metal cathode, such as Ca or Al, to collect holes and electrons respectively (Figure 16). To a lesser extent, devices with an inverted structure,[138] that is with an ITO bottom cathode and a high-work function metal anode, have also been studied, and will be properly expounded in due time.

The function of a typical OPV system follows four basic steps,[139] as shown in Figure 16.

[138] a) Ameri, T.; Dennler, G.; Waldauf, C.; Denk, P.; Forberich, K.; Scharber, M. C.; Brabec, C. J.; Hingerl, K. *J. Appl. Phys.* **2008**, *103*, 084506. b) Ameri, T.; Dennler, G.; Waldauf, C.; Azimi, H.; Seemann, A.; Forberich, K.; Hauch, J.; Scharber, M.; Hingerl, K.; Brabec, C. J. *Adv. Funct. Mater.* **2010**, *20*, 1592. c) Wang, K.; Liu, C.; Meng, T.; Yi, C.; Gong, X. *Chem. Soc. Rev*. **2016**, *45*, 2937.

[139] a) Spanggaard, H.; Krebs, F. C. *Sol. Energy Mater. Sol. Cells* **2004**, *83*, 125. b) *Organic Photovoltaics: Materials, Device Physics and Manufacturing Technologies*; Brabec, C. J., Dyakonov V., Dcherf, U., Eds.; Wiley-VCH: Weinheim, Germany, 2008. c) Kippelen, B.; Brédas, J. L. *Energy Environ. Sci.* **2009**, *2*, 251. d) Clarke, T. M; Durrant, J. R. *Chem. Rev.* **2010**, *110*, 6736.

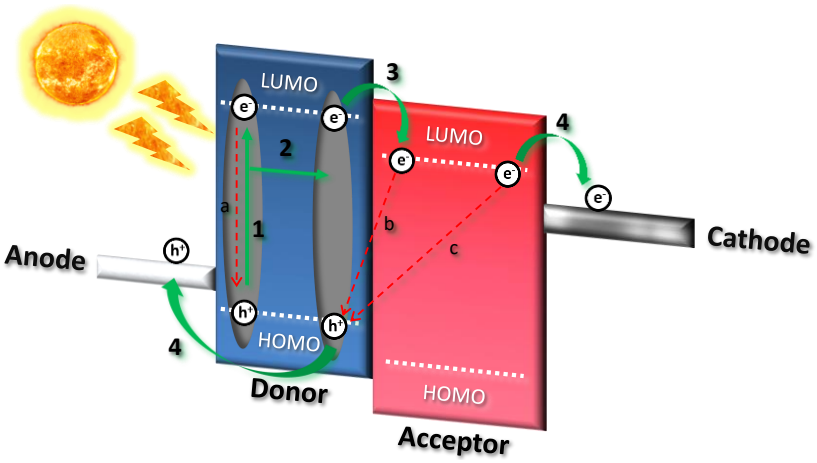

Figure 16. Schematic of the operating principles of OPV, highlighting the desired transport of charge pairs (green arrows) through the donor and acceptor materials and undesired phenomena (red arrows) that may take place in the process.

Upon photoabsorption, an electron can be excited from the donor HOMO to its LUMO, forming an exciton (photoinduced exciton generation; **step 1**, Figure 16). The strong Coulombic attraction between generated electron and hole can cause them to directly recombine, voiding the process (intra-molecular electron-hole recombination; step a, Figure 16). However, this exciton can also diffuse to a D/A interface via a chemical potential gradient (exciton diffusion to the interface; **step 2**, Figure 16) where the electron can transfer to the LUMO of the acceptor material, forming a charge transfer complex. This phenomenon will be favorable to occur when the energy difference between the donor LUMO and the acceptor LUMO is greater than the binding energy of the exciton, typically on the order of a couple hundred meV, depending on the materials employed. The charge transfer state can then become a charge separated state, or free charge carriers (exciton dissociation; **step 3**, Figure 16). However, if unable to escape the coulomb capture radius (*i.e.* the mutual separation of two charges at which the Coulombic attraction is less than thermal energy κT), the geminate pair will recombine across the D/A interface (geminate recombination; step b, Figure 16), which constitutes another loss mechanism in these devices. Any dissociated charges can then be transported through p-type or n-type domains to the electrodes, with holes being collected at the anode and electrons being collected at the cathode (charge collection; **step 4**, Figure 16), where they can be used to do work in an external circuit. The final and leading loss mechanism in OPV is that of charge recombination, whereby free charge carriers recombine with unassociated charge carriers (non-geminate recombination; step c, Figure 16). The

ultimate performance of an OPV device is reflected in a set of parameters that are summarized in detail in the next section.

1.2.2 Characteristic parameters of solar cells

The properties of photovoltaic devices can be characterized by plotting the measured current density output *J* of the cell versus the voltage output *V* of the cell (*J*-*V* graph, Figure 17). In the dark, this *J*-*V* curve passes through the origin, since at that moment no current is flowing through the device and no potential is present. By exposing the photovoltaic device to light, the *J*-*V* curve shifts downwards. The most important characteristic parameters of photovoltaic devices can be found on this *J*-*V* curve.

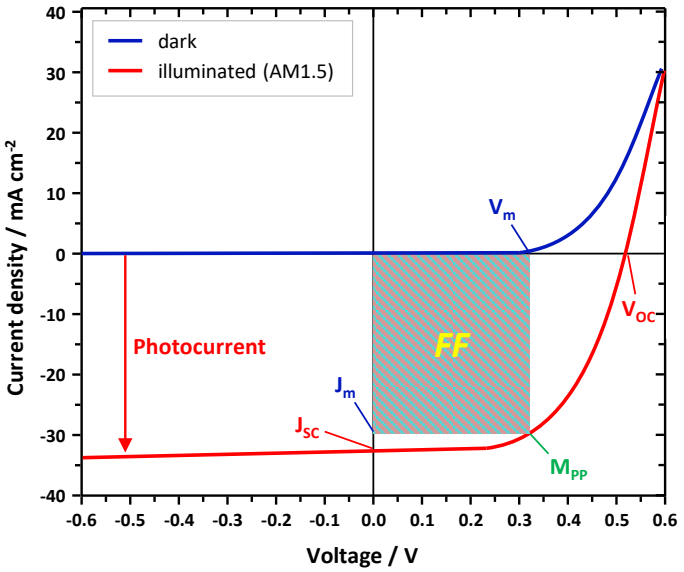

Figure 17. Current-voltage (*J*-*V*) characteristics of a typical solar cell. Essential parameters determining the cell performance are shown.

a) Open-circuit voltage (V_{OC})

It is the maximum possible voltage across a photovoltaic device. This is the voltage across the cell, under sunlight, when no current is flowing through the device. The V_{OC} in organic

photovoltaics has been found to be dependent to a first approximation on the difference between the HOMO of the donor and the LUMO of the acceptor.[140]

b) Short-circuit current (I_{SC})

It is the current that flows through an illuminated solar cell when there is no external resistance *i.e.* when the electrodes are simply connected or short-circuited. I_{SC} is the maximum current that a photovoltaic device is able to produce. Under an external load, the current will always be less than I_{SC}. The short-circuit current depends on a number of factors, such as the area of the solar cell. To remove the dependence of the solar cell area, it is more common to list the short-circuit current density (J_{SC}, in mA cm^{-2}), rather than the short-circuit current (I_{SC}, in mA).

c) Maximum power point (M_{PP})

This magnitude makes reference to the point on the *J-V* curve (V_m, J_m) at which the maximum power is produced. Power is the product of current *J* and voltage *V*. On the graph in Figure 17, it is represented by the rectangle formed between the point on the *J-V* illuminated graph and the axes where the area is maximum.

d) Fill factor (*FF*)

It is the ratio of its actual maximum power output to its theoretical power output, if current and voltage would be at their maxima, J_{SC} and V_{OC}, respectively. This is a very important property used to measure photovoltaic device performance. It is a measure of the 'squareness' of the *J-V* curve. *FF* can be written down as follows:

$$FF = \frac{J_m \times V_m}{J_{SC} \times V_{OC}} \qquad \text{(Eqn. 1)}$$

It has been recently demonstrated that the competition between recombination and extraction of free charges ultimately determines the *FF* of organic solar cells.[141]

e) Power conversion efficiency (*PCE* or η)

It is the ratio of power output (P_{out}), to power input (P_{in}). *PCE* measures the amount of power produced by a photovoltaic device relative to the power available in the incident solar

[140] Qi, B.; Wang, J. *J. Mater. Chem.* **2012**, *22*, 24315.
[141] Bartesaghi, D.; del Carmen Pérez, I.; Kniepert, J.; Roland, S.; Turbiez, M.; Neher, D.; Koster, L. J. A. *Nat. Commun.* **2015**, *6*, 7083.

radiation. P_{in} is the sum over all wavelengths, which usually has a value of 100 mW cm^{-2} when solar simulators are used. This is the most general way to define the efficiency of a photovoltaic device. *PCE* can be written down as follows:

$$PCE\ (\eta) = \frac{P_{out}}{P_{in}} \times 100\% = \frac{J_m \times V_m}{P_{in}} \times 100\% = \frac{J_{SC} \times V_{OC} \times FF}{P_{in}} \times 100\% \qquad \text{(Eqn. 2)}$$

PCE is one of the most important parameters to characterize solar cell performances. In order to compare results from various devices, regardless of the design and active material, photovoltaic cells are all subjected to the same standard test conditions. The cells are typically illuminated at a constant density of roughly 100 mW cm^{-2}, which is defined as the standard "1 Sun" value, with a spectrum consistent to an air-mass global value of 1.5 (AM 1.5G), at a temperature of 25 °C. Air mass describes the spectrum of radiation and can be defined as the amount of atmosphere through which sunlight has to travel to reach the Earth's surface. This is abbreviated as AM x, in which x is the inverse of the cosine of the zenith angle of the sun. The above mentioned AM 1.5G conditions correspond to the spectrum and irradiance of sunlight incident with a zenith angle of 48.2° (Figure 18).

f) External quantum efficiency (*EQE*)

It is one of the two ways to measure the Incident photon-to-current efficiency (*IPCE)*. It is calculated by the number of electrons extracted in an external circuit, divided by the number of incident photons at a certain wavelength under short-circuit conditions. *EQE* can be written down as follows:

$$EQE = \frac{number\ of\ electrons}{number\ of\ incident\ photons} = \frac{J_{SC}(\lambda)/e}{P_{in}(\lambda)/(hc/\lambda)} = \frac{J_{SC}(\lambda)hc}{P_{in}(\lambda)e\lambda} \qquad \text{(Eqn. 3)}$$

where λ is the wavelength, e is the elementary charge, h is the Planck constant and c is the speed of light in vacuum.

IPCE is an important parameter because it comprises the overall efficiency of the four main processes in OSCs, and it can be described as follows:

$$IPCE = \eta_{abs}(\lambda) \times \eta_{diff}(\lambda) \times \eta_{ct}(\lambda) \times \eta_{coll}(\lambda) \qquad \text{(Eqn. 4)}$$

where η_{abs} is the photoabsorption efficiency, η_{diff} is the exciton diffusion efficiency to the D/A interface, η_{ct} is the charge transfer efficiency, η_{coll} is the charge collection efficiency, and λ is the wavelength of interest.

The molecular orbital levels, the absorption coefficients, the morphology of the layers and the exciton diffusion lengths, are therefore the main factors that control the device performance.

Research on these aspects during the last decade, based on rational design of newly optimized materials, has led to up of 11.0% *PCE* for single-junction OSCs.[119]

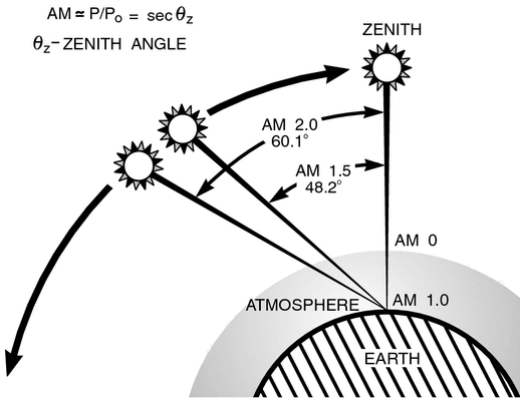

Figure 18. The air-mass value AM 0 equates to insolation at sea level with the Sun at its zenith. AM 1.0 represents sunlight with the Sun at zenith above the Earth's atmosphere. AM 1.5 is the same, but with the Sun at an oblique angle of 48.2°, which simulates a longer optical path through the Earth's atmosphere; AM 2.0 extends that oblique angle to 60.1°.

1.2.3 Active organic molecules for solar cells

Organic semiconductor materials for OPV applications can be broadly classified as either polymers or conjugated small molecules/oligomers. Polymer-based solar cells, also known as plastic solar cells,[127,142] are constituted by solution-processable conjugated polymers that improve the charge-carrier migration from the D/A interface to the corresponding electrodes. Plastic solar cells represent the vast majority of systems studied due to the possibility of chemically manipulating the material properties of polymers, combined with a variety of easy and cheap processing techniques. The most commonly used configurations with the highest efficiencies are BHJ consisting on donor polymers with fullerenes as acceptor counterpart,[142b] yet different ways to decrease the band gap of semiconducting polymers have arisen, allowing for the preparation of polymer/polymer solar cells and organic/inorganic hybrid solar cells.[143] The main drawback of polymer-based OPVs is batch to batch variations in molecular

[142] a) Peet, J.; Senatore, M. L.; Heeger, A. J.; Bazan, G. C. *Adv. Mater*. **2009**, *21*, 1521. b) Brabec, C. J.; Gowrisanker, S.; Halls, J. J. M.; Laird, D.; Jia, S.; Williams, S. P. *Adv. Mater*. **2010**, *22*, 3839. c) Peet, J.; Heeger, A. J.; Bazan, G. C. *Acc. Chem. Res*. **2009**, *42*, 1700. d) Gendron, D.; Leclerc, M. *Energy Environ. Sci*. **2011**, *4*, 1225. e) Lu, L.; Zheng, T.; Wu, Q.; Schneider, A. M.; Zhao, D.; Yu, L. *Chem. Rev.* **2015**, *115*, 12666.
[143] McGehee, M. D. *MRS Bull.* **2009**, *34*, 95.

weight/polydispersity, solubility, and purity[144] that can result in different device performance and even in different processing properties. On the other hand, small-molecule photovoltaic devices[145] are based on discrete chromophores that form the active layers. Small molecular semiconductors for OPVs have recently attracted considerable attention owing to their advantages over their polymer counterparts, which include well-defined molecular structure, definite molecular weight, and high purity with full synthetic reproducibility.

The distinctions between these classes of materials become most important in determining the processing that is required in making films and devices and for the subsequent molecular arrangements that are obtained. In principle, there are two processing techniques for the fabrication of OPV devices, vacuum deposition and solution processing. The latter is simpler, cheaper and offers the possibility to work on large areas of substrates by low energy-demanding technologies. On the other hand, vacuum deposition makes possible the use of insoluble materials often more stable than their soluble analogues, and promotes more precise control of the morphology and the thickness of the active layers, giving rise to higher efficiency devices. However, vacuum-processing is more costly because of the more sophisticated equipment needed. Heating of polymers to high temperatures generally results in a decrease in molecular weight and even changes to local chemistry,[146] limiting the manufacturing methods of polymer OPVs mostly to solution processing techniques. Conversely, low weight semiconducting molecules and oligomers are typically vaporizable and thermally stable during the sublimation process and, at the same time, they can be chemically modified to tune their solubility in common organic solvents, allowing for a direct comparison between the two organic solar cell production technologies when the same material is used.

1.2.3.1 Small molecule semiconductors for organic solar cells

Small molecular semiconductors can be generally classified as hole transporting (also called donor or p-type) materials or electron transporting (acceptor or n-type) materials, according to the type of orderly transferring charge carriers, under a given set of conditions, stemming

[144] Nikiforov, M. P.; Lai, B.; Chen, W.; Chen, S.; Schaller, R. D.; Strzalka, J.; Maser J.; Darling, S. B. *Energy Environ. Sci.* **2013**, *6*, 1513.

[145] a) Roncali, J. *Acc. Chem. Res.* **2009**, *42*, 1719. b) Walker, B.; Kim, C.; Nguyen, T. -Q. *Chem. Mater.* **2011**, *23*, 470. c) Mishra, A.; Bäuerle, P. *Angew. Chem. Int. Ed.* **2012**, *51*, 2020. d) Lin, Y.; Li, Y.; Zhan, X. *Chem. Soc. Rev.* **2012**, *41*, 4245.

[146] a) Gritsenko, K. P.; Krasovsky, A. M. *Chem. Rev.* **2003**, *103*, 3607. b) Kovacik, P.; Sforazzini, G.; Cook, A. G.; Willis, S. M.; Grant, P. S.; Assender, H. E.; Watt, A. A. R. *ACS Appl. Mater. Interfaces* **2011**, *3*, 11.

from removal of electrons from the filled molecular orbitals or from the addition of electrons to empty orbitals, respectively.

Many small molecular p-type semiconductors have been studied for decades.[145,147] Among these molecules, only a fraction has been applied successfully as electron donors in OPV devices due to the various optical, electrical, and stability requirements demanded The properties of materials, such as hole mobility (*i.e.*, the distance over which holes are transported per second under the unit electric field), exciton diffusion length, thin film morphology, frontier energy level alignment band gap, and absorption coefficient, all greatly affect the performance of OSCs. The wide range of donor materials tested in a variety of device configurations, either in PHJs or BHJs, by vacuum or solution processing, includes different classes of chromophores, such as oligothiophenes and oligothiophene-based molecules with D^1-A-D^2-A-D^1 architecture,[148] oligoacenes, triphenylamines,[149] squaraines,[150] borondipyrromethene (BODIPY),[151] diketopyrrolopyrroles,[152] Ps, Pcs,[134c] SubPcs,[97e] and other π-conjugated molecules (Chart 4).[121d,g,145c]

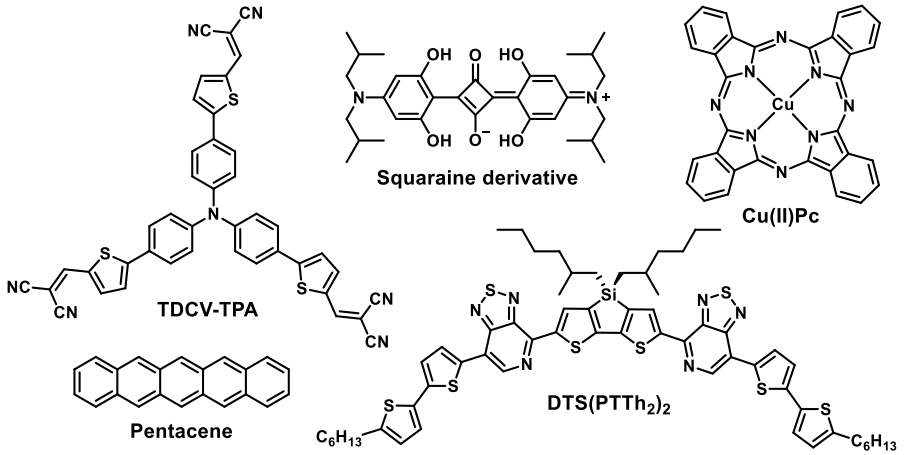

Chart 4. Some examples of donor small molecules typically used in organic solar cells.

[147] Roncali, J.; Leriche, P.; Blanchard, P. *Adv. Mater.* **2014**, *26*, 3821.

[148] a) Mishra, A.; Ma, C. -Q.; Bäuerle, P. *Chem. Rev.* **2009**, *109*, 1141. b) Chen, Y.; Wan, X.; Long, G. *Acc. Chem. Res.* **2013**, *46*, 2645. c) Coughlin, J. E.; Henson, Z. B.; Welch, G. C.; Bazan, G. C. *Acc. Chem. Res.* **2014**, *47*, 257. d) Malytskyi, V.; Simon, J. -J.; Patrone, L.; Raimundo, J. -M. *RSC Adv.* **2015**, *5*, 354. e) Ni, W.; Wan, X.; Li, M.; Wang, Y.; Chen, Y. *Chem. Commun.* **2015**, *51*, 4936.

[149] Lin, Y.; Zhan, X. *Acc. Chem. Res.* **2016**, *49*, 175.

[150] Beverina, L.; Salice, P. *Eur. J. Org. Chem.* **2010**, 1207.

[151] Bessette, A.; Hanan, G. S. *Chem. Soc. Rev.* **2014**, *43*, 3342.

[152] Qua, S.; Tian, H. *Chem. Commun.* **2012**, *48*, 3039.

In contrast to the development of this broad spectrum of donor materials, the current acceptor materials research landscape is largely dominated by C_{60} and C_{70} fullerenes and their derivatives, such as solution-processable phenyl-C_{61}(C_{71})-butyric acid methyl ester (PCBM) derivatives.[121d,153] Their predominance in OPV applications stems from advantageous properties including (i) the ability to accept and transport electrons in three dimensions thanks to a LUMO that is delocalized over the whole surface of the molecule, (ii) high electron mobilities,[154] (iii) multiple reversible electrochemical reductions, and (iv) the ability to aggregate in bulk heterojunctions to form both pure and mixed domains of the appropriate length scale for charge separation. For this reason, over several years, research has been focused on developing appropriate and efficient donor materials optimized specifically for these fullerenes, reaching record efficiencies that exceed 10% *PCE* values[155] by following this design strategy. Nevertheless, fullerene-based acceptors have some significant limitations including (i) weak absorption in the abundant region of the incident solar spectrum, which limits their ability to harvest light, (ii) limited tunability in terms of spectral absorption, (iii) high synthetic costs, especially for the high performing C_{70} derivative, and (iv) morphological instability due to fullerene diffusion and aggregation in the thin film over time.

1.2.3.2 Non-fullerene electron acceptors for organic solar cells

In this regard, a more modular and dynamic approach focused on the development of new kinds of n-type semiconducting materials known as *Non-Fullerene Acceptors* (NFAs)[145c,d,153,156] to overcome prevalent fullerene acceptors insufficiencies has been recently addressed by several research groups as a worthwhile alternative to further enhance OPV devices in conjunction with the large number of small molecule and polymeric donor materials that have been developed over the past decade.

New NFAs should obviously retain the advantageous properties of the fullerenes, such as efficient charge transfer with a low possibility of back transfer and good blend morphology with the donor material. They should also display greater ease of synthesis, improved

---

[153] Chochos, C. L.; Tagmatarchis, N.; Gregoriou, V. G. *RSC Adv.* **2013**, *3*, 7160.

[154] a) von Hauff, E.; Dyakonov, V.; Parisi, R. *Sol. Energy Mater. Sol. Cells* **2005**, *87*, 149. b) Woebkenberg, P. H.; Bradley, D. D. C.; Kronholm, D.; Hummelen, J. C.; de Leeuw, D. M.; Coelle, M.; Anthopoulos, T. D. *Synth. Met.* **2008**, *158*, 468.

[155] Liu, Y.; Zhao, J.; Li, Z.; Mu, C.; Ma, W.; Hu, H.; Jiang, K.; Lin, H.; Ade, H.; Yan, H. *Nat. Commun.* **2014**, *5*, 5293.

[156] a) Sonar, P.; Lim, J. P. F.; Chan, K. L. *Energy Environ. Sci.* **2011**, *4*, 1558. b) Eftaiha, A. F.; Sun, J. -P.; Hill, I. G.; Welch, G. C. *J. Mater. Chem. A* **2014**, *2*, 1201. c) Nielsen, C. B.; Holliday, S.; Chen, H. -Y.; Cryer, S. J.; McCulloch, I. *Acc. Chem. Res.* **2015**, *48*, 2803. d) Zhan, C.; Zhang, X.; Yao, J. *RSC Adv.* **2015**, *5*, 93002.

solubility and processability from environmentally friendlier solvents, and increased optical absorptivity and introduce a structural flexibility that allows for favorable matching of frontier energy levels of donor and acceptor materials.

The most widely investigated NFA molecules to date have been perylene diimide (PDI) and other rylene-diimide derivatives (Chart 5), which have been shown to possess many desirable design features for OPV electron acceptors, such as large absorption coefficients, high electron mobilities and high electron affinities similar to widely used fullerene acceptors.[157] The three functionalization positions available in PDI can be exploited to tailor their optoelectronic properties and to synthesize PDI-oligomers or to increase their solubility in order to restrict their tendency to π-π stack and form micrometer-sized crystallites where excitons get trapped. Efficiencies over 7% have been accomplished employing PDI derivatives in BHJs.[158]

Apart from the rylene-based derivatives, other π-conjugated small molecules with n-type semiconducting behavior have been developed and studied as NFAs in high throughput devices (Chart 5). One method of increasing the electron affinities of molecules is to introduce electron-withdrawing units, such as fluorine, chlorine and cyano, to the periphery of the aromatic rings.[159] For instance, while Cu(II)Pc has been extensively studied as an archetypical small molecule donor, hexadecafluorinated Cu(II)PcF_{16} showed electron mobilities of up to 5 x 10^{-3} cm^2 V^{-1} s^{-1} and was incorporated in PHJs as an acceptor, obtaining moderate *PCE* values of 0.18%.[160] Some n-type semiconducting π-conjugated small molecules that have shown great promise in OPV applications are truxenone derivatives,[161] decacyclene-based triimides,[162] and SubPc derivatives, that hold the best record efficiencies for this kind of acceptor materials.[163]

[157] Li, C.; Wonneberger, H. *Adv. Mater.* **2012**, *24*, 613.
[158] Sun, D.; Meng, D.; Cai, Y.; Fan, B.; Li, Y.; Jiang, W.; Huo, L.; Sun, Y.; Wang, Z. *J. Am. Chem. Soc.* **2015**, *137*, 11156.
[159] Tang, M. L.; Oh, J. H.; Reichardt, A. D.; Bao, Z. *J. Am. Chem. Soc.* **2009**, *131*, 3733.
[160] Jiang, X.; Dai, J.; Wang, H.; Geng, Y.; Yan, D. *Chem. Phys. Lett.* **2007**, *446*, 329.
[161] a) Nielsen, C. B.; Voroshazi, E.; Holliday, S.; Cnops, K.; Rand, B. P.; McCulloch, I. *J. Mater. Chem. A* **2013**, *1*, 73. b) Nielsen, C. B.; Voroshazi, E.; Holliday, S.; Cnops, K.; Cheyns, D.; McCulloch, I. *J. Mater. Chem. A* **2014**, *2*, 12348.
[162] a) Pho, T. V.; Toma, F. M.; Chabinyc, M. L.; Wudl, F. *Angew. Chem. Int. Ed.* **2013**, *52*, 1446. b) Pho, T. V.; Toma, F. M.; Tremolet de Villers, B. J.; Wang, S.; Treat, N. D.; Eisenmenger, N. D.; Su, G. M.; Coffin, R. C.; Douglas, J. D.; Fréchet, J. M. J.; Bazan, G. C.; Wudl, F.; Chabinyc, M. L. *Adv. Energy Mater.* **2014**, *4*, 1301007.
[163] Cnops, K.; Rand, B. P.; Cheyns, D.; Verreet, B.; Empl, M. A.; Heremans, P. *Nat. Commun.* **2014**, *5*, 3406.

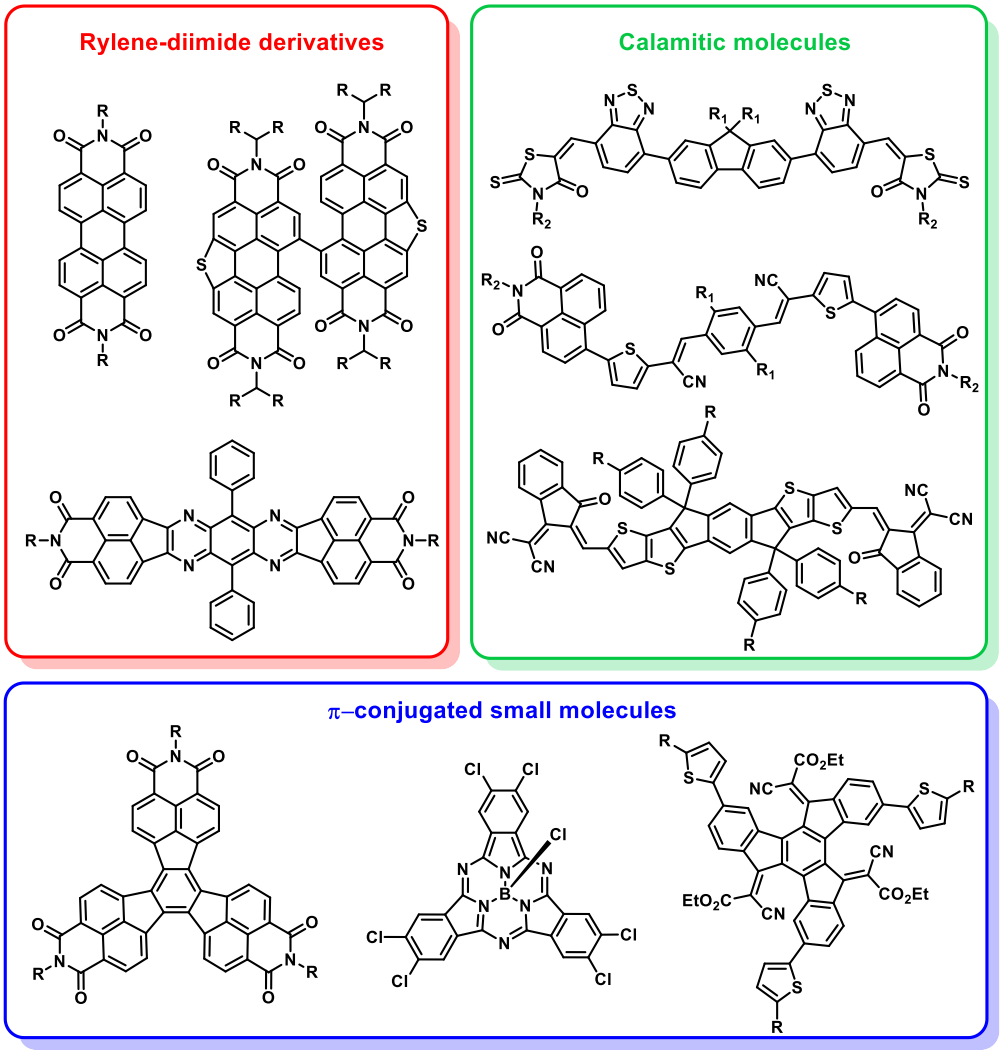

Chart 5. Some examples of NFA small molecules used in organic solar cells.

Finally, a new type of small molecules that have received attention recently as a promising class of NFAs are calamitic shaped structures, with discrete separation of electron rich and poor sections (Chart 5). A conjugated push-pull structure can be achieved by combining electron rich and electron poor structural units, thereby reducing the optical bandgap via molecular orbital hybridization, which helps to extend the absorption, as well as offering control over the separation of the HOMO and LUMO electron density in the molecule in order

to facilitate charge transfer. The inclusion of terminal acceptor units such as rhodanine,[164] diketopyrrolopyrrole[165] and naphthalimide[166] provides a large and sterically exposed electron accepting component on the periphery of these structures.

To sum up, numerous studies have hitherto demonstrated the anticipated advantages of NFAs in terms of enhanced optical absorptivity and ease of frontier energy level engineering relative to fullerene acceptors. These results should pave the way for further improvements in the performance of small molecule acceptor materials for OSCs.

[164] Holliday, S.; Ashraf, R. S.; Nielsen, C. B.; Kirkus, M.; Röhr, J. A.; Tan, C. -H.; Collado-Fregoso, E.; Knall, A. -C.; Durrant, J. R.; Nelson, J.; McCulloch, I. *J. Am. Chem. Soc.* **2015**, *137*, 898.
[165] Shi, H.; Fu, W.; Shi, M.; Ling, J.; Chen, H. *J. Mater. Chem. A* **2015**, *3*, 1902.
[166] Kwon, O. K.; Park, J. -H.; Kim, D. W.; Park, S. K.; Park, S. Y. *Adv. Mater.* **2015**, *27*, 1951.

1.3 Specific objectives of *Chapter I*

The main goal of this chapter is to develop novel SubPc derivatives bearing electron-withdrawing substituents and to assess their potential application as acceptor materials in OSCs. This chapter is divided in three different sections.

In the **first section**, a new synthetic methodology for the preparation of SubPcs bearing cyano groups at the peripheral positions will be presented. Halogenated SubPcs bearing different number of F or Cl have been already reported and successfully tested as acceptor materials in OSCs. The introduction of novel π-conjugated electron-withdrawing groups, such as CN, at the periphery of the SubPc structure has been contemplated as an appealing strategy for tuning both the optical properties and the n-type semiconducting behavior of these derivatives.[167] In particular, a set of unreported SubPc bearing different number of cyano groups will be prepared by a two-step synthetic methodology consisting on the preparation of iodo-functionalized SubPc precursors and subsequent palladium-catalyzed cross-coupling cyanation reaction (Figure 19). The preparation of peripherally cyanated SubPc derivatives represents a challenging task inasmuch as SubPcs with electron-withdrawing groups have been reported to decompose in the presence of relatively low concentrations of cyanide anion.[76]

The electrochemical and photophysical characterization of the novel SubPc derivatives obtained will be carried out and compared with other related SubPc derivatives to evaluate the influence of the cyano groups in the SubPcs properties, aiming at achieving a set of potential acceptor materials with a fine-tuning of the HOMO and LUMO levels. Finally, charge carrier mobility measurements of selected derivatives will be conducted in the laboratory of Professor Shu Seki in Kyoto University.

[167] For examples on the influence of cyano groups in the properties of various semiconducting materials, see: a) Jones, B. A.; Ahrens, M. J.; Yoon, M. -H.; Facchetti, A.; Marks, T. J.; Wasielewski, M. R. *Angew. Chem. Int. Ed.* **2004**, *43*, 6363. b) Chang, J.; Ye, Q.; Huang, K. -W.; Zhang, J.; Chen, Z. -K.; Wu, J.; Chi, C. *Org Lett.* **2012**, *14*, 2964. c) Gao, J.; Xiao, C.; Jiang, W.; Wang, Z. *Org. Lett.* **2014**, *16*, 394. d) Zhang, C.; Shi, K.; Cai, K.; Xie, J.; Lei, T.; Yan, Q.; Wang, J. -Y.; Pei, J.; Zhao, D. *Chem. Commun.* **2015**, *51*, 7144.

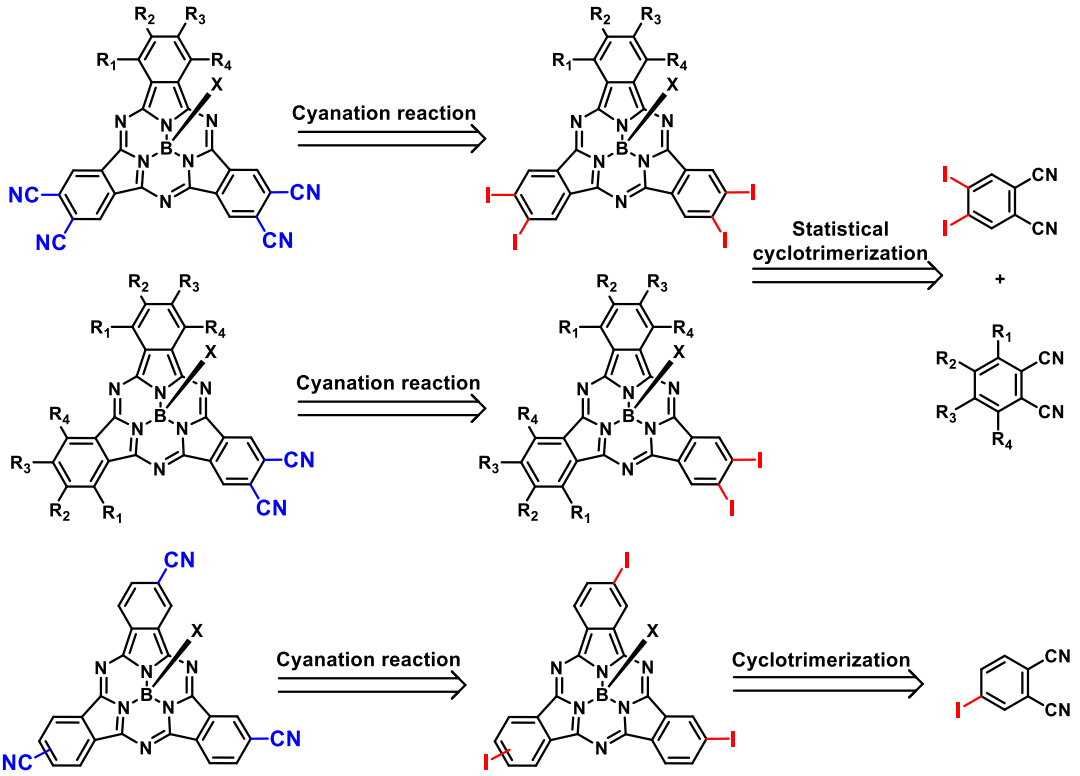

Figure 19. Retrosynthetic approach to unsymmetrical cyanated SubPc derivatives.

The **second section** of this chapter is focused on the incorporation of SubPc derivatives as acceptor materials in vacuum-evaporated PHJ solar cells (Figure 20).[168] The use of these NFA derivatives in these devices is expected to lead to enhanced efficiencies due to increased V_{OC} and improved absorption of solar light. As mentioned, the electronic properties of SubPcs can be easily tuned by introduction of peripheral substituents. For this study, four different peripherally substituted SubPc derivatives have been selected relying on the knowledge acquired from the first section of this chapter, namely easy evaporable SubPcs bearing different number of electron-withdrawing substituents (F, Cl, CN) that help lowering their LUMO energy level. They will be combined with four carefully selected small-band-gap donor materials with suitable HOMO energy levels and complementary absorption profiles in order to optimize the interface energetics of the D/A planar heterojunctions and the photocurrent

[168] Cnops, K.; Zango, G.; Genoe, J.; Heremans, P.; Martínez-Díaz, M. V.; Torres, T.; Cheyns, D. *J. Am. Chem. Soc.* **2015**, *137*, 8991.

generation. In addition, the role of the charge transport layers in the device architecture will be explored.

The fabrication of the devices and the measurements of their performance will be carried out in the laboratory of Tom Aernouts in the IMEC in Leuven.

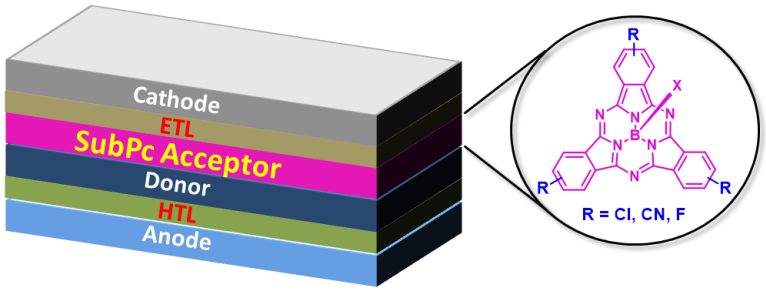

Figure 20. Schematic representation of the PHJ solar cells studied in this Thesis.

The **third section** of this chapter deals with the fabrication of solution-processed BHJ devices from SubPc units as the acceptor component and selected polymeric donor materials (Figure 21).[169] For this purpose, several derivatives of SubPc bearing peripheral electron-withdrawing groups (Cl, CN) and various axial substituents, namely fluorine, chlorine and differently substituted phenoxy groups, will be employed. While modification of the axial substituent does not alter the absorption spectra and results in a slight variation of the electron-accepting character of each SubPc derivative, it can greatly affects its aggregation and crystallization behavior, critical factors in solar cells performance optimization.

The fabrication of the devices and the measurements of their performance will be carried out in the laboratory of Professor René Janssen in the Technische Universiteit Eindhoven.

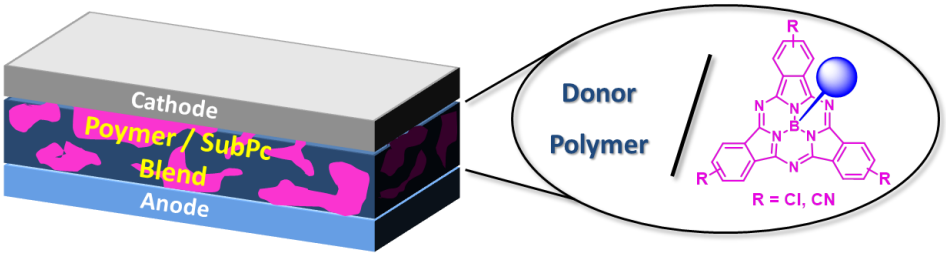

Figure 21. Schematic representation of the BHJ solar cells studied in this Thesis.

[169] Zango, G.; Duan, C.; García Iglesias, M.; Colberts, F. J. M.; Wienk, M. M.; Martínez-Díaz, M. V.; Janssen, R. A. J.; Torres, T. *Angew. Chem. Int. Ed.* **2016**, DOI: 10.1002/anie.201608644R1.

1.4 Synthesis and characterization of novel subphthalocyanine derivatives bearing peripheral cyano groups

1.4.1 Background

As many other functionalized SubPcs, the synthesis of unsymmetrical SubPc derivatives bearing one *ortho*-dicyano functionality in their peripheral positions has been pursued in our research group, not only because of their expected physicochemical properties, but also due to the high synthetic value these sought-after structures present as a unique type of phthalonitrile derivatives for the synthesis of multicomponent SubPc-based systems (see *Chapter 2* of the present thesis).

The attempts for their preparation made use of the direct synthesis by statistical condensation reaction between 1,2,4,5-tetracyanobenzene and another phthalonitrile. Unfortunately, previous attempts in this approach[170] only rendered very low yields of the desired *ortho*-dicyano-SubPc (< 5%), mainly due to the partial hydrolysis of the dinitrile groups under the condensation reaction conditions, giving rise to large amounts of phthalimide and phthalimido-SubPc derivatives as side products (Scheme 2).

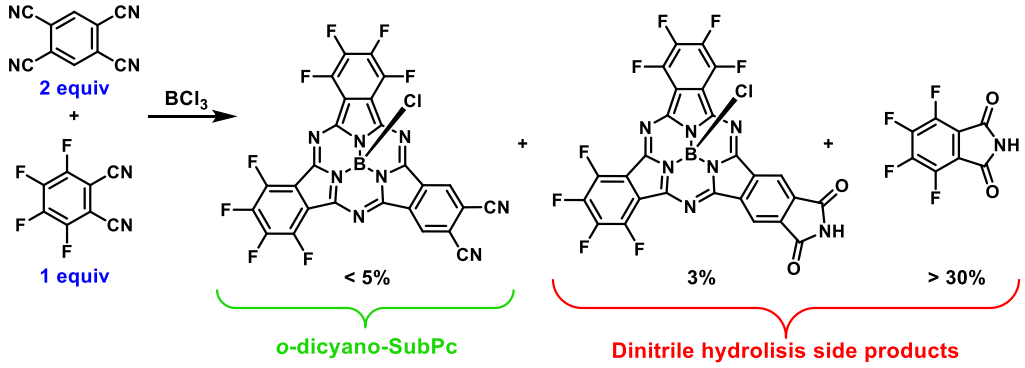

Scheme 2. Major products obtained in the direct synthesis of *ortho*-dicyano-SubPc.

Thus, a new synthetic approach was envisioned, relying on the transformation of previously synthesized *ortho*-diiodo substituted SubPcs. The condensation reaction for the preparation of these unsymmetrical SubPc precursors, that entails the use of 4,5-diiodophthalonitrile instead

[170] Medina, A. Ph.D. Thesis, Universidad Autónoma de Madrid: Madrid, Spain, 2011.

of tetracyanobenzene, is expected to proceed in higher yields and enables the obtainment of diiodo- and tetraiodo-SubPcs at the same time.

It is well known in the field that, compared to Pcs, the cone-shaped structure of SubPcs prevents macrocycle aggregation, making easier the isolation of the different compounds formed (even regioisomers)[51b,g] in a mixed macrocyclization[51] by standard laboratory chromatographic techniques. However, when trying to maximize the formation of a particular unsymmetrical SubPc, since each specific example differs in the starting phthalonitriles relative ratio, a deep survey on the influence of the nature of the substituents of the phthalonitrile precursors in the selectivity in the formation of unsymmetrical SubPcs has not yet been performed.

In a second step, the substitution of the iodo substituents by cyano groups must be tackled in order to obtain the desired *ortho*-dicyano functionalities in the SubPc structure. Since metal-catalyzed cross-coupling reactions have proven to be an efficient method to functionalize SubPcs at the isoindole rings,[70,71,72] a Pd-catalyzed cyanation reaction was conceived for the incorporation of nitrile substituents at the SubPc periphery.

1.4.2 Palladium-catalyzed cyanation of aryl halides: General aspects

The reaction of copper(I) cyanide with aryl halides, known as the Rosenmund-von Braun reaction, is, together with the Sandmeyer reaction of aromatic amino groups,[171] one of the general methods for the synthesis of aryl nitriles.[171d,172] Despite its widely demonstrated utility, the Rosenmund-von Braun reaction presents some important drawbacks, like the use of stoichiometric amounts of copper(I) cyanide as a cyanating agent, which leads to equimolar amounts of heavy metal waste, the relatively high temperature (150-250 °C) and the low reactivity of aryl chlorides and bromides compared to expensive aryl iodides.[173]

A useful alternative for the preparation of substituted benzonitriles constitute the transition metal-catalyzed cyanation of aryl-X compounds (X = Cl, Br, I, OTf and H) with cheap and readily

---

[171] a) Sandmeyer, T. *Ber. Dtsch. Chem. Ges.* **1884**, *17*, 1633. b) Hodgson, H. H. *Chem. Rev.* **1947**, *40*, 251. c) Galli, C. *Chem. Rev.* **1988**, *88*, 765. d) Mowry, D. T. *Chem. Rev.* **1948**, *42*, 189.

[172] Ellis, G. P.; Romney-Alexander, T. M. *Chem. Rev.* **1987**, *87*, 779.

[173] a) Anbarasan, P.; Schareina, T.; Beller, M. *Chem. Soc. Rev.*, **2011**, *40*, 5049. b) Schareina, T.; Beller, M. Copper-Catalyzed Cyanations of Aryl Halides and Related Compounds. In *Copper-Mediated Cross-Coupling Reactions*; Evano, G, Blanchard, N., Eds.; John Wiley & Sons, Inc.: Hoboken, NJ, USA, 2014; pp 313-334.

available cyanation agents like sodium or potassium cyanide.[174] The first palladium-catalyzed cyanation of aryl-X derivatives was introduced in 1973 by Takagi *et al.* using aryl bromides and iodides with potassium cyanide as cyanating agent and palladium(II) cyanide or palladium(II) acetate as catalyst (Scheme 3).[173,175,176]

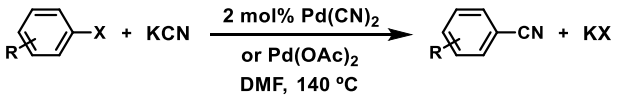

Scheme 3. First Takagi's palladium-catalyzed cyanation of aryl iodides and bromides.

The catalytic cycle of the palladium-catalyzed cyanations was assumed to be similar to other standard coupling reactions (Scheme 4, green box). This assumption is supported by various findings, *e.g.* that the reactivity of aryl halides follows the order ArI > ArBr > ArCl, and electron-rich aromatic rings react slower than electron-poor ones, which is consistent with the pattern commonly observed in other Pd-catalyzed coupling reactions, too. At first, a Pd(0) species undergoes oxidative addition to the aryl halide, resulting in an arylPd(II) halide complex (Scheme 4, step 1). Subsequent anion exchange (Scheme 4, Step 2) results in the corresponding cyano complex, from which the product benzonitriles is formed by reductive elimination (Scheme 4, Step 3) to re-form the active Pd(0) species.

---

[174] a) *Transition Metal Reagents and Catalysts-Innovations in Organic Synthesis*; Tsuji, J., Ed.; John Wiley & Sons, Chichester, 2000. b) Brandsma, L.; Vasilevsky, S. F.; Verkruijsse, H. D. *Application of Transition Metal Catalysts in Organic Synthesis*; Springer Verlag, Berlin, Heidelberg, 1999, pp. 149-177.

[175] a) Takagi, K.; Okamoto, T.; Sakakibara, Y.; Oka, S. *Chem. Lett.* **1973**, 471. b) Takagi, K.; Okamoto, T.; Sakakibara, Y.; Ohno, A.; Oka, S.; Hayama, N. *Bull. Chem. Soc. Jpn.* **1976**, *49*, 3177.

[176] a) Takagi, K. Palladium-Catalyzed Cross-Coupling Involving α-Hetero-Substituted Organometals: Palladium-Catalyzed Cross-Coupling Involving Metal Cyanides. In *Handbook of Organopalladium Chemistry for Organic Synthesis;* Negishi, E.i., Ed.; John Wiley & Sons, Inc.: New York, USA, 2002; pp 657-672. b) Sundermeier, M.; Zapf, A.; Beller, M. *Eur. J. Inorg. Chem.* **2003**, *2003*, 3513. c) Schareina, T.; Zapf, A.; Beller, M. *Chem. Commun.* **2004**, 1388. d) Zanon, J.; Klapars, A.; Buchwald, S. L. *J. Am. Chem. Soc.* **2003**, *125*, 2890. e) Weissman, S. A.; Zewge, D.; Chen, C. *J. Org. Chem.* **2005**, *70*, 1508. f) Ushkov, A. V.; Grushin, V. V. *J. Am. Chem. Soc.* **2011**, *133*, 10999. g) Arvela, R. K.; Leadbeater, N. E. *J. Org. Chem.* **2003**, *68*, 9122. h) Cristau, H. J.; Ouali, A.; Spindler, J. F.; Taillefer, M. *Chem. Eur. J.* **2005**, *11*, 2483. i) Schareina, T.; Zapf, A.; Magerlein, W.; Muller, N.; Beller, M. *Chem. Eur. J.* **2007**, *13*, 6249. j) Senecal, T. D.; Shu, W.; Buchwald, S. L. *Angew. Chem. Int. Ed.* **2013**, *52*, 10035.

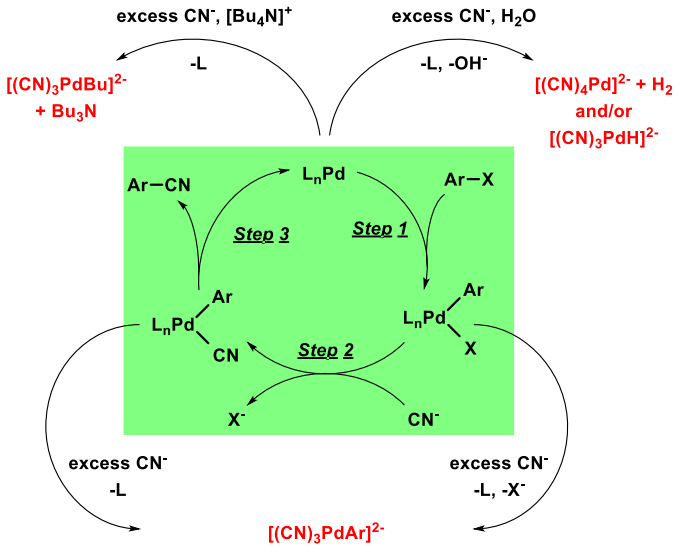

Scheme 4. Catalytic cycle of cyanation (green box), with deactivation pathways (outside of box).

Nonetheless, since the original work of Takagi's group in the 1970s, problems with facile deactivation of the Pd catalyst by excess cyanide were observed.[175] More recently, some detailed mechanistical investigations performed by Grushin *et al.*[177] shed light on the mechanisms of catalyst poisoning during cyanation of haloarenes (Scheme 4, outside of box). The presence of moisture in the reaction medium is one of the greatest dangers for the catalysis employing readily ionizable sources of cyanide that easily generate HCN upon hydrolysis. It has been demonstrated that phosphine-stabilized Pd(0) is highly reactive toward HCN, undergoing transformations to catalytically inactive $[(CN)_4Pd]^{2-}$ and/or $[(CN)_3PdH]^{2-}$. Besides, cyanide concentration in the liquid phase of the reaction mixture must be comparable to that of the Pd catalyst. Low $[CN^-]$ can starve the catalyst for cyanide, resulting in slower reaction rates and possibly side-processes at the metal center. On the other hand, the X/CN exchange (step 2) and reductive elimination (step 3) of the loop (Scheme 4) can be easily disrupted by excess cyanide due to facile phosphine displacement with CN^-, leading to $[(CN)_3PdAr]^{2-}$. Being reluctant to undergo Ar-CN reductive elimination in the presence of extra CN^-, this dianionic palladium aryl is another dead end for the catalytic process.

The most economical and extensively used sources of cyanide are KCN and NaCN. However, these ionic salts are hygroscopic, highly soluble in water, easily hydrolyzable, and hence most

[177] a) Dobbs, K. D.; Marshall, W. J.; Grushin, V. V. *J. Am. Chem. Soc.* **2007**, *129*, 30. b) Erhardt, S.; Grushin, V. V.; Kilpatrick, A. H.; Macgregor, S. A.; Marshall, W. J.; Roe, D. C. *J. Am. Chem. Soc.* **2008**, *130*, 4828.

potentially poisonous to the palladium catalyst. Other cyanide sources that are better tolerated by the catalyst are mainly metal- or metalloid-bound cyanide sources, such as zinc cyanide $Zn(CN)_2$,[178] trimethylsilyl cyanide TMSCN,[179] potassium ferrocyanide $K_4[Fe(CN)_6]$[176c,e,i,j,180] and acetone cyanohydrin.[181] Particularly widely used are $Zn(CN)_2$ and $K_4[Fe(CN)_6]$, both of which are considerably less capable of producing free CN^- and consequently deactivating the catalyst.

$Zn(CN)_2$ in particular is the second most used cyanide source till date, since the first report of a palladium-catalyzed cyanation of aryl bromides and iodides with $Zn(CN)_2$ in 1994 (Scheme 5).[178a] Some advantages associated with its use are the low solubility in most organic solvents, a factor that keeps the concentration of cyanide ions at the required low level, and the capability of transforming both cyanide ions to the product. In addition, it has been demonstrated that $Zn(CN)_2$ afforded higher yields in several cyanation reactions than KCN or NaCN as a result of the lower concentration of cyanide ions (due to the highly covalent nature of the zinc cyanide bond) in the catalytic reaction mixture. Hence, it allows for lower level catalyst loading by decreasing the catalyst poisoning.

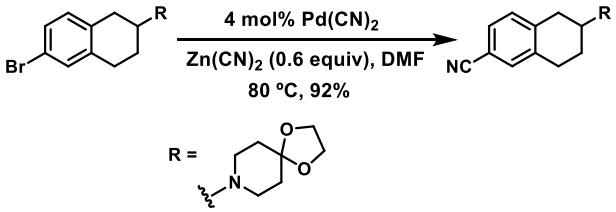

Scheme 5. First palladium-catalyzed cyanation with zinc cyanide.

---

[178] a) Tschaen, D. M.; Desmond, R.; King, A. O.; Fortin, M. C.; Pipik, B.; King, S.; Verhoeven, T. R. *Synth. Commun.* **1994**, *24*, 887. b) Maligres, P. E.; Waters, M. S.; Fleitz, F.; Askin, D. *Tetrahedron Lett.* **1999**, *40*, 8193. c) Alterman, M.; Hallberg, A. *J. Org. Chem.* **2000**, *65*, 7984. d) Chidambaram, R. *Tetrahedron Lett.* **2004**, *45*, 1441. e) Jensen, R. S.; Gajare, A. S.; Toyota, K.; Yoshifuji, M.; Ozawa, F. *Tetrahedron Lett.* **2005**, *46*, 8645. f) Buono, F. G.; Chidambaram, R.; Mueller, R. H.; Waltermire, R. E. *Org. Lett.* **2008**, *10*, 5325. g) Martin, M. T.; Liu, B.; Cooley, B. E., Jr.; Eaddy, J. F. *Tetrahedron Lett.* **2007**, *48*, 2555. h) Cohen, D. T.; Buchwald, S. L. *Org. Lett.* **2015**, *17*, 202.

[179] a) Chatani, N.; Hanafusa, T. *J. Org. Chem.* **1986**, *51*, 4714. b) Sundermeier, M.; Mutyala, S.; Zapf, A.; Spannenberg, A.; Beller, M. *J. Organomet. Chem.* **2003**, *684*, 50.

[180] a) Zhang, J.; Chen, X.; Hu, T.; Zhang, Y.; Xu, K.; Yu, Y.; Huang, J. *Catal. Lett.* **2010**, *139*, 56. b) Yeung, P. Y.; So, C. M.; Lau, C. P.; Kwong, F. Y. *Angew. Chem. Int. Ed.* **2010**, *49*, 8918. c) Yeung, P. Y.; So, C. M.; Lau, C. P.; Kwong, F. Y. *Org. Lett.* **2011**, *13*, 648. d) Yeung, P. Y.; So, C. M.; Lau, C. P.; Kwong, F. Y. *Tetrahedron Lett.* **2011**, *52*, 7038. e) Xu, Z.; Xiao, Y.; Ding, H.; Cao, C.; Li, H.; Pang, G.; Shi, Y. *Synthesis*, **2015**, *47*, 1560. f) Mondal, B.; Acharyya, K.; Howlader, P.; Mukherjee, P. S. *J. Am. Chem. Soc.* **2016**, *138*, 1709.

[181] a) Sundermeier, M.; Zapf, A.; Beller, M. *Angew. Chem. Int. Ed.* **2003**, *42*, 1661. b) Ouchaou, K.; Georgin, D.; Taran, F. *Synlett* **2010**, 2083.

1.4.2.1 Microwave-assisted cyanation of aryl halides

Traditionally, organic synthesis is carried out by conductive heating with an external heat source (for example, an oil bath). However, in the past decades, heating and driving chemical reactions by microwave irradiation has been established as a heavily used technique in both academia and industry.[182]

Microwave-enhanced chemistry is based on the efficient heating of materials by "microwave dielectric heating" effects. The magnitude of heating depends on the dielectric properties of the molecules (solvents, reagents, catalysts) that are present in the reaction mixture. This very efficient and homogeneous internal heat transfer results in an inverted temperature gradient compared to conventional thermal heating (Figure 22).[183]

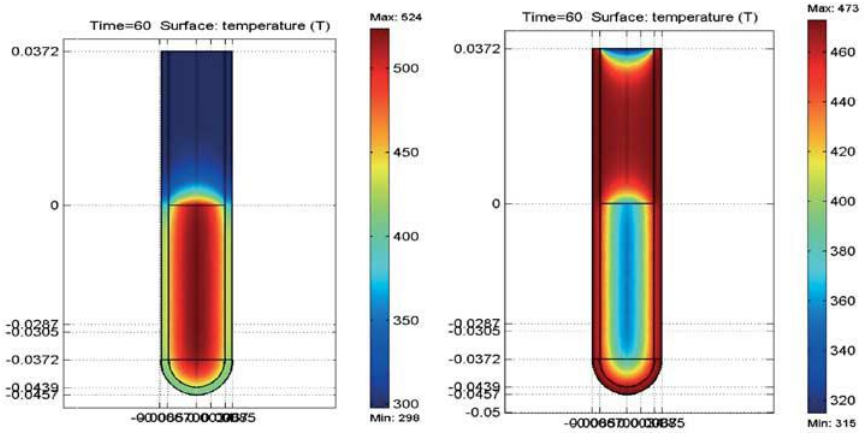

Figure 22. The temperature profile after 60 sec as affected by microwave irradiation (left) compared to treatment in an oil-bath (right). Microwave irradiation raises the temperature of the whole reaction volume simultaneously, whereas in the oil heated tube, the reaction mixture in contact with the vessel wall is heated first. Temperature scale in Kelvin. '0' on the vertical scale indicates the position of the meniscus.

---

[182] a) Leadbeater, N. E. Organic Synthesis Using Microwave Heating. In *Comprehensive Organic Synthesis,* 2nd ed.; Knochel, P., Molander, G. A., Eds.; Elsevier B.V.: Amsterdam, Netherlands, 2014; pp 234-286. b) Kappe, C. O.; Stadler, A.; Dallinger, D.; *Microwaves in Organic and Medicinal Chemistry*, 2nd ed.; Wiley-VCH: Weinheim, Germany, 2012. c) *Microwave Assisted Organic Synthesis*; Lidstrom, P., Tierney, J. P., Eds.; Blackwell Publishing Ltd.: Oxford, UK, 2004. d) *Microwaves in Organic Synthesis*, 3rd ed.; Loupy, A., de la Hoz, A., Eds.; Wiley-VCH: Weinheim, Germany, 2012. e) *Microwave-Assisted Synthesis of Heterocycles*; Eycken, E. v. d., Kappe, C. O., Almqvist, F., Eds.; Springer: Berlin, 2006. f) Kappe, C. O. *Angew. Chem. Int. Ed.* **2004**, *43*, 6250.

[183] Schanche, J. S. *Mol. Diversity* **2003**, *7*, 291.

As a result, microwave processing frequently leads to dramatically reduced reaction times, higher yields, and cleaner reaction profiles. Additionally, microwave-assisted synthesis has mostly standardized sealed-vessel reaction conditions, allowing for the heating of low boiling point solvents high above their boiling point temperature, enhancing reaction rates even more.

Among the many types of chemical transformations that can be carried out successfully under microwave conditions, transition-metal-catalyzed C-C bond formation reactions represent one of the most important and best studied reaction types.[182] Typically needing hours or days to reach completion with traditional heating under reflux conditions and inert atmosphere, these reactions can be performed within minutes by employing microwave heating under sealed-vessel conditions, obtaining even better products yields.

In this context, first microwave-assisted palladium-catalyzed preparation of aryl and vinyl nitriles was developed by Hallberg and Alterman in 2000 reacting aryl bromides with zinc cyanide heating at 60 W in DMF as solvent with reaction times ranging from 2 to 2.5 min.[178c] Since then, several reports have illustrated the effectiveness of this methodology in the cyanation reaction of a variety of substrates of diverse nature, employing different cyanide sources, relatively mild reaction conditions and severely reduced reaction times.[173a,184]

In our research group, previous experience in the application of a palladium-catalyzed cyanation strategy using $Zn(CN)_2$ in DMF under microwave irradiation was reported in the preparation of 5,6-dicyanoazulene for the synthesis of azulenocyanines.[185] In this case, slightly higher yield, from 83 to 85%, in dramatically shorter reaction time, from 17 h to 10 min, at lower temperature, from DMF reflux to 90 °C, was obtained in comparison with the previously reported synthesis consisting on a classical Rosenmund-von Braun reaction.[186]

---

[184] a) Chobanian, H. R.; Fors, B. P.; Lin, L. S. *Tetrahedron Lett.* **2006**, *47*, 3303. b) Velmathi, S.; Leadbeater, N. E. *Tetrahedron Lett.* **2008**, *49*, 4693. c) Arvela, R. K.; Leadbeater, N. E.; Torenius, H. M.; Tye, H. *Org. Biomol. Chem.* **2003**, *1*, 1119.

[185] Ince, M.; Hausmann, A.; Martıínez-Díaz, M. V.; Guldi, D. M.; Torres, T. *Chem. Commun,* **2012**, *48*, 4058.

[186] Muranaka, A.; Yonehara, M.; Uchiyama, M. *J. Am. Chem. Soc.* **2010**, *132*, 7844.

1.4.3 Results and discussion

1.4.3.1 Synthesis of partially iodinated subphthalocyanines

In order to obtain a set of unsymmetrical SubPcs bearing one or two *ortho*-diiodo functionalities at the periphery, one of the starting phthalonitriles must always be 4,5-diiodophthalonitrile (phthalonitrile **A**). On the other hand, for this study, a variety of starting phthalonitriles **B** that differ in the electron-donating or electron-withdrawing character of their substituents were employed in the mixed macrocyclization reaction. The chosen phthalonitriles **B** were 4,5-dioctylthiophthalonitrile, 4-*tert*-butylphthalonitrile, 1,2-dicyanobenzene, 4,5-dichlorophthalonitrile and 3,4,5,6-tetrafluorophthalonitrile (Figure 23).

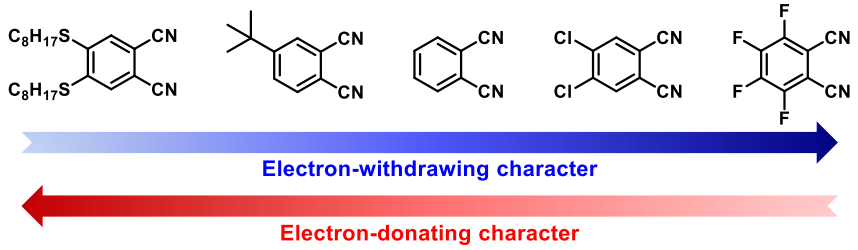

Figure 23. Starting phthalonitriles **B**.

SubPcs **3a-c** to **7a-c** and **9** were initially synthesized from 1 equiv of 4,5-diiodophthalonitrile **A** and 2 equiv of each of the phthalonitriles **B** (Scheme 6). These starting materials ratio corresponds to the stoichiometric amounts proportional to *ortho*-diiodo-SubPcs **3-7b**. In all cases standard condensation reaction conditions using BCl_3 (3 equiv, 1.0 M in *p*-xylene) at reflux led to the formation of the four symmetrical and unsymmetrical SubPc products, although the reaction time for each series differed depending on the nature of the phthalonitrile **B**, as it could be seen by monitoring the consumption of the starting materials by TLC.

Successive substitution of the axial chlorine atom by 4-*tert*-butylphenol in excess under toluene reflux was carried out in order to ease the isolation of each compound by column chromatography on silica gel and to increase the stability and solubility of the SubPcs for further functionalization reactions (see *Experimental Section*). In fact, optimized chromatographic conditions allowed for the separation of all compounds formed in each

series. In particular, SubPc **4b** was obtained as a mixture of three different regioisomers, as observed by TLC.[187]

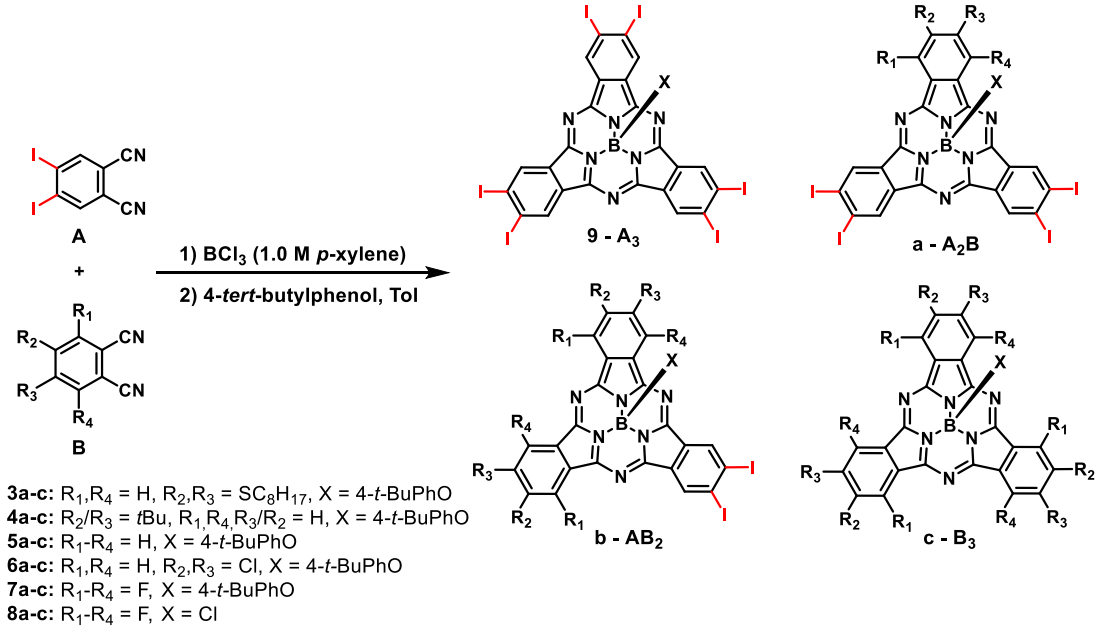

Scheme 6. Synthesis of SubPcs **3-9**.

Reaction mixture of partially peripherally fluorinated SubPcs **7** exhibited a noticeable lack of reactivity toward axial substitution by 4-*tert*-butylphenol. For this reason, an alternative method implying the isolation of axially chlorinated SubPcs **8a** and **8b** by column chromatography on silica gel and later reaction with 4-*tert*-butylphenol was followed in this case, obtaining SubPcs **7a** and **7b** respectively in moderate yields.

The structures of the new SubPcs were determined by ^{1}H-NMR, ^{13}C-NMR, UV-vis, infrared spectroscopy (FT-IR), mass spectrometry (MS) and exact mass (HR-MS) characterization. In ^{1}H-NMR spectra all unsymmetrical SubPcs exhibit characteristic signals appearing between 9.0 and 9.5 ppm which correspond to the downfield shifted protons of the diiodo-substituted benzene rings. Thus, the assignment of each structure was made on the basis of the number (1 for diiodo-SubPcs **3-8b** or 2 for tetraiodo-SubPcs **3-8a**) and the integration of these signals (Figure 24). Besides, the axial phenoxy group protons show their distinctive signals at $\delta \approx 6.8$

[187] The isolation of each of the three different regioisomers of SubPc **3b** will be carried out in *Chapter 2*.

and 5.3 ppm. The latter appear strongly upfield shifted due to the SubPc anisotropic ring current.

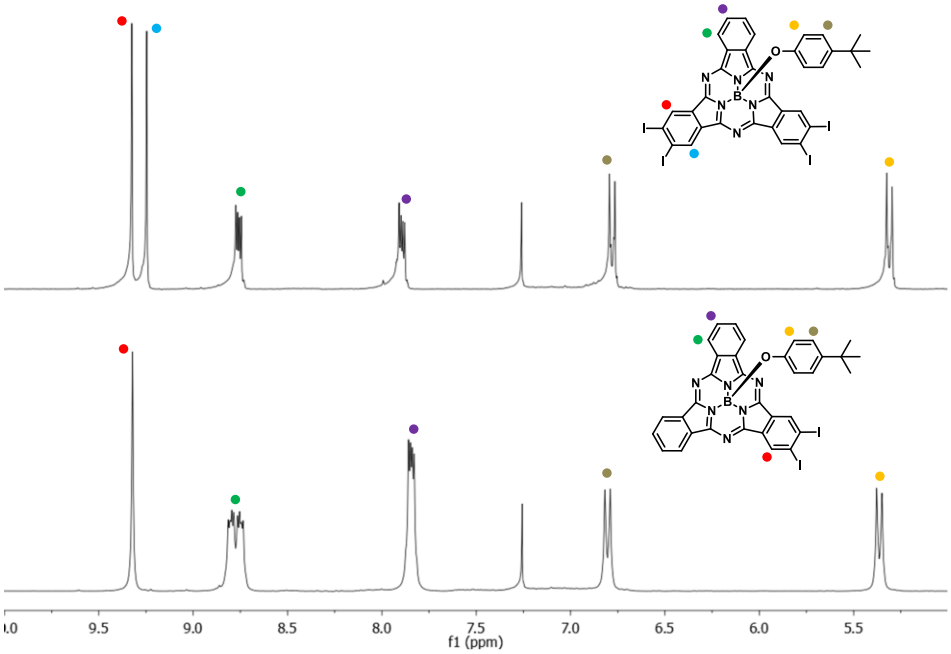

Figure 24. Partial ^{1}H-NMR (300 MHz) spectra in $CDCl_3$ of SubPc **5a** (top) and SubPc **5b** (down).

Thereupon, with the aim of maximizing the formation of unsymmetrical SubPcs (**a** and **b**) compared to the symmetrical SubPcs (**c** and **9**), the cross condensation reaction of each phthalonitrile **B** with 4,5-diiodophthalonitrile **A** was performed at different A:B ratios. All other reaction parameters were kept constant during this study. The yields of each SubPc **a-c** and **9** obtained for each series **3** to **8** at each phthalonitriles ratio are summarized in Table 1.[188]

[188] The method to calculate yields in the synthesis of unsymmetrical SubPcs is not standardized in literature. Ref 51a expresses the yield of unsymmetrical SubPcs as the mass fraction of each SubPc to the total mass of SubPc obtained, so the addition of all SubPc yields equals 100% yield. Refs 51b and 51g defines each unsymmetrical SubPc yield as the amount of that SubPc compound formed from starting phthalonitriles based on a statistical distribution of reactants. In refs 51c and 51e, yields of unsymmetrical SubPcs are only given with respect to one of the two starting phthalonitriles or with respect to the limiting reactant. In this study, yields of unsymmetrical SubPcs shown in Table 1 were calculated as follows: each SubPc, symmetrical A_3 and B_3 and unsymmetrical A_2B and AB_2, is considered as the only reaction product from the cross-condensation reaction of its constituent parts. For instance, by this method, reaction of 1 mmol of 4,5-diiodophthalonitrile **A** with 2 mmol of phthalonitrile **B** considering a 100% yield could produce: 0.33 mmol of SubPc A_3, 0.50 mmol of

Table 1. Yields of SubPcs **3**, **4**, **5**, **6** and **8** obtained employing different starting phthalonitriles ratio.

SubPcs series	A:B ratio	Yield (%)			
		9 – A_3	a – A_2B	b – AB_2	c – B_3
3 (R = SC_8H_{17})	1:2	5	19	27	28
	2:3	5	34	26	20
	1:1	7	29	14	20
4 (R = *t*Bu)	1:3	<1	4	24	18
	1:2	6	25	33	8
	1:1	8	26	13	6
5 (R = H)	1:2	3	21	25	20
	2:3	3	22	15	12
	1:1	5	28	6	10
6 (R = Cl)	1:2	5	7	8	29
	2:3	7	15	23	22
	1:1	8	17	15	15
8 (R = F)	1:2	<1	2	11	39
	1:1	<1	5	14	30
	2:1	<1	7	16	27

As can be seen, for SubPcs series **3**-**5**, 1:1 ratios of 4,5-diiodophthalonitrile **A** and phthalonitrile **B** lead to low yields of diiodo-SubPcs **b**. On the other hand, raising the proportion of phthalonitrile **B** results in a significant increase of the yield of these SubPcs at the same time that tetraiodo-SubPcs **a** are still obtained in reasonably good yields. However, when an excess of phthalonitrile **B** respect to stoichiometric amounts of starting materials for the synthesis of diiodo-SubPcs **b** was used, a general decrease in unsymmetrical SubPcs **a-b** yields was observed.

Phthalonitriles bearing electron-withdrawing substituents, as in SubPcs series **6** and **8**, show a different reactivity trend. Partially chlorinated SubPcs **6a-b** are obtained in better yields at A:B ratios of 2:3 or 1:1. Lastly, an A:B ratio of 2:1 results in the best yields for SubPcs **8a-b**, but a more synthetically efficient 1:1 ratio was chosen with very little variations in final yields.

SubPc A_2B, 1 mmol of SubPc AB_2 and 0.66 mmol of SubPc B_3. From our understanding, this calculation method sets out the best reactants ratio to maximize the yield of one or more reaction products respect to the others precisely.

In the light of the results obtained, it seems that a higher load of 4,5-diiodophthalonitrile **A** is required in the cross condensation reaction with electron-poor phthalonitriles than with electron-rich phthalonitriles. Although we do not have a clear mechanistic explanation for this effect, it is known that the first ones tend to react faster, at lower temperatures and with better yields to give the corresponding symmetrical SubPcs than the latter ones.[189] Besides, it is also reported that the cyclotrimerization reaction of 4,5-diiodophthalonitrile in the presence of BCl_3 gives rise to very low yields of the symmetrical hexaiodo-SubPc-Cl, under 2%,[189] probably due to a combination of poor solubility and low reactivity of the starting phthalonitrile. In this way, it could be justified that, in SubPc series **6-8**, an initial higher concentration of 4,5-diiodophthalonitrile (**A**) promotes the formation of diiodo and tetraiodo-SubPcs **a-b** before the entire amount of the corresponding phthalonitrile **B** is exhausted in the formation of the favored symmetrical SubPc **c**. It is also worth mentioning that, to our surprise, mixed-condensation reactions of phthalonitriles **A** and **B** render in all cases higher yields of hexaiodo-SubPc **9** than the one obtained for hexaiodo-SubPc-Cl from the direct cyclotrimerization of 4,5-diidophthalonitrile in BCl_3. Up to this point, it could only be conjectured that the presence of reactive intermediates coming from phthalonitrile **B** might foster the reactivity of 4,5-diiodophthalonitrile **A** toward a second molecule of **A**.

Additionally, in order to modify the functionalization pattern and study the influence of the number and relative position of the nitrile groups in the SubPc properties, precursor triiodo-SubPc **10** was prepared by refluxing a mixture of 4-iodophthalonitrile in 1 M BCl_3 in *p*-xylene and, after *in situ* treatment with 4-*tert*-butylphenol, triiodo-SubPc **11** was generated as a 1:3 mixture of regioisomers C_3/C_1 (Scheme 7). During the purification of this SubPc derivative by column chromatography, the two possible regioisomers ***C*$_3$-11** and ***C*$_1$-11** were separated.[88a]

[189] González-Rodríguez, D. Ph.D. Thesis, Universidad Autónoma de Madrid: Madrid, Spain, 2003.

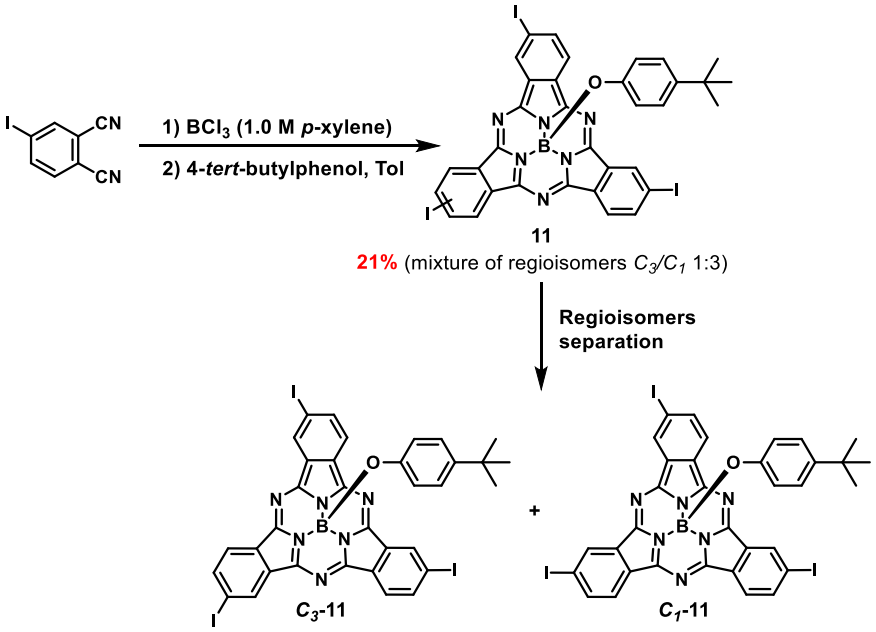

Scheme 7. Synthesis of SubPcs **11**.

1.4.3.2 Synthesis of partially cyanated subphthalocyanines

As it has been mentioned before, the only record of the interaction between SubPcs and cyano groups found in literature consists in the use of a perfluorinated SubPc as a highly sensitive, selective colorimetric and fluorometric molecular sensor for the detection of cyanide or fluoride anions in aqueous samples.[76] SubPcs with electron-withdrawing groups at their periphery are selectively opened in the presence of these anions initially giving rise, most probably, to blue-colored open compounds (diiminoisoindoline-type trimers), whose presence was pointed out by UV-vis spectroscopy. The possibility of an initial nucleophilic attack of the corresponding anion on the boron atom of the SubPc cannot be ruled out, since the SubPc absorption would remain unaltered.

On account of this, seeking for a general and efficient method for the cyanation of the iodinated SubPcs previously synthesized, three different catalytic systems found in literature involving $Zn(CN)_2$ as the cyanating agent for the reaction with aryl halides were initially tested, based on the mildness of the reaction conditions and the ready availability of the reagents. Preliminary results using SubPc **4b** as substrate and employing conventional thermal heating are shown in Table 2.

Table 2. Comparison of the different methods tested in the cyanation reaction of SubPc **4b**.

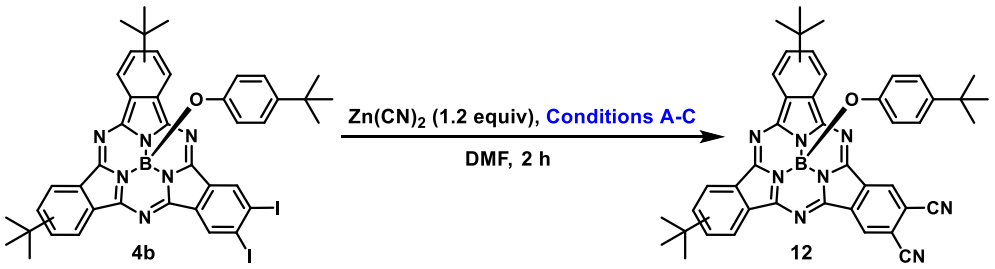

Entry	Reaction conditions	Results observed by TLC after 2 h
A	$Pd_2(dba)_3$ (0.04 equiv), dppf (0.06 equiv), Zn (0.20 equiv), 120 °C[178b,190]	Unreacted starting materials
B	$Pd_2(dba)_3$ (0.05 equiv), *t*-Bu_3P (0.05 equiv), Zn (0.20 equiv), 50 °C[191]	Starting material and complex mixture of products
C	$Pd(PPh_3)_4$ (0.10 equiv), 100 °C[178a,192]	Starting material and detection of two new purple spots

Subsequent chromatographic purification on silica gel did not allow the isolation of any product from the reaction mixture obtained in methods **A** and **B** aside from the starting SubPc. On the other hand, the two new purple compounds spotted in the reaction with $Pd(PPh_3)_4$ as catalyst (entry **C**) could be isolated and identified as SubPc **12** and the corresponding *ortho*-monocyano-monoiodo-SubPc, but low yields were obtained (less than 30% for each SubPc). Although in some cases, reaction times in between 1 and 24 h are reported for the experimental conditions tested, in our case, longer reaction times only led to an increase in the degree of SubPc decomposition.

Next, the best performing catalytic system **C** was reproduced employing microwave-assisted synthesis under sealed-vessel conditions. It could be promptly verified that microwave heating strongly accelerates the reaction rate, yielding SubPc **12** as the major product with no trace of the starting SubPc **4b** after only 20 min reaction time and greatly avoiding SubPc decomposition. Several reaction parameters, namely $Zn(CN)_2$ ratio, catalytic load, temperature and reaction time, were screened for the synthesis of **12**, leading to the optimized reaction conditions in Scheme 8, that rendered this SubPc with 85% yield.

[190] Jin, F.; Confalone, P. N. *Tetrahedron Lett.* **2000**, *41*, 3271.
[191] Ramnauth, J.; Bhardwaj, N.; Renton, P.; Rakhit, S.; Maddaford, S. P. *Synlett* **2003**, 2237.
[192] Selnick, H. G.; Smith, G. R.; Tebben, A. J. *Synth. Commun.* **1995**, *25*, 3255.

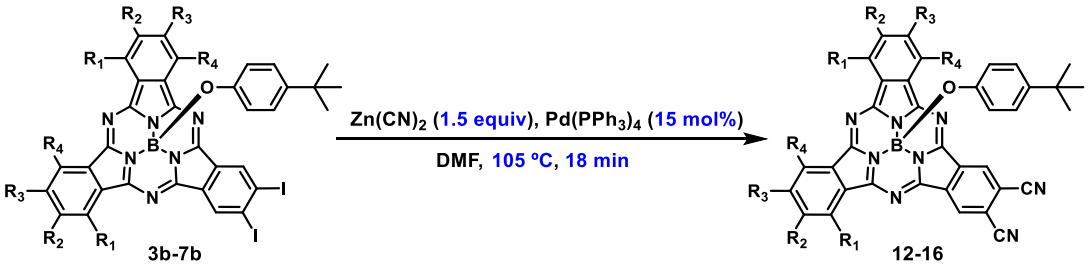

4b: R_2/R_3 = *t*Bu, $R_1,R_4,R_3/R_2$ = H
3b: R_1,R_4 = H, R_2,R_3 = SC_8H_{17}
5b: R_1-R_4 = H
6b: R_1,R_4 = H, R_2,R_3 = Cl
7b: R_1-R_4 = F

12: R_2/R_3 = *t*Bu, $R_1,R_4,R_3/R_2$ = H; **85%**
13: R_1,R_4 = H, R_2,R_3 = SC_8H_{17}; **76%**
14: R_1-R_4 = H; **89%**
15: R_1,R_4 = H, R_2,R_3 = Cl; **69%**
16: R_1-R_4 = F; **40%**

Scheme 8. Synthesis of SubPcs **12-16**.

The scope of this reaction could be extended to the synthesis of *ortho*-dicyano-SubPcs **12-16** with diverse yields (Scheme 8). This procedure rendered SubPcs **12-14**, bearing no substituents or electron-donating substituents in the other two isoindole units, in very good yields (76-89%). Instead, SubPcs **15** and, particularly **16**, bearing additional electron-withdrawing groups at their periphery, are obtained in lower yields (69% and 40% respectively), presumably due to a higher degree of decomposition derived from the nucleophilic attack of cyanide anions to SubPc peripheral positions.[76] However, yields obtained in the synthesis of SubPc **15** are remarkably good considering its high eletron-acceptor character. It should be noted that, during all these reactions, the microwave power input was not fixed to a specific value in order to reach the desired temperature as soon as possible, what was observed to sparingly improve final yields.

Encouraged by these results, the synthesis of tetracyano-SubPcs **17-21** from tetraiodo-SubPcs **3a-7a** was tackled (Scheme 9). Microwave assisted cyanation procedure implemented in the preparation of dicyano-SubPcs was successfully reproducible in the synthesis of SubPcs **17-19** with good yields, keeping all the reaction conditions constant and doubling $Zn(CN)_2$ and $Pd(PPh_3)_4$ load. SubPc **20** was obtained with very low yields (8%) due to a high degree of decomposition during the reaction and additional partial decomposition of the final product during the isolation by column chromatography on silica gel. Cyanation reaction of SubPc **7a** only afforded decomposition products.

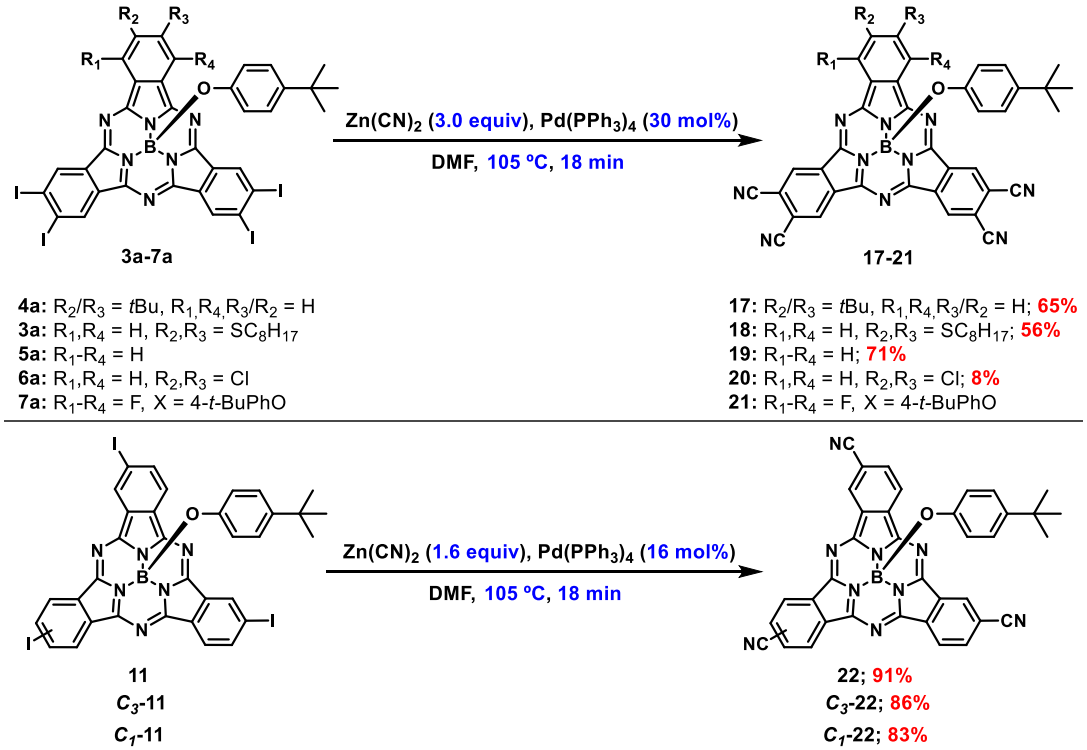

Scheme 9. Synthesis of SubPcs **17-20** and SubPcs **22**.

Same way, microwave assisted reaction of SubPcs **11**, ***C*$_3$-11** and ***C*$_1$-11** with 1.6 equiv of $Zn(CN)_2$, 16 mol% $Pd(PPh_3)_4$, at 105 °C in 18 min afforded tricyano-SubPcs **22**, ***C*$_3$-22** and ***C*$_1$-22** with 91%, 86% and 83% respectively (Scheme 9).

The structures of the new SubPcs were determined by ^{1}H-NMR, ^{13}C-NMR, UV-vis, FT-IR, MS and HR-MS characterization. In ^{1}H-NMR spectra, the signals of α-protons adjacent to cyano substituents in all unsymmetrical SubPcs **12-22** appear appreciably upfield shifted in comparison with these same protons in precursor iodinated SubPcs (Figure 25a). In addition, axial phenoxy group protons signals confirm the axial substituent remains unaltered during the cyanation reaction. ^{13}C-NMR spectra and FT-IR exhibit characteristic nitrile carbon signal (between 115 and 110 ppm) and C≡N stretch (around 2230 cm^{-1}) features that confirm the presence of cyano groups in the SubPc structure (Figure 25b).

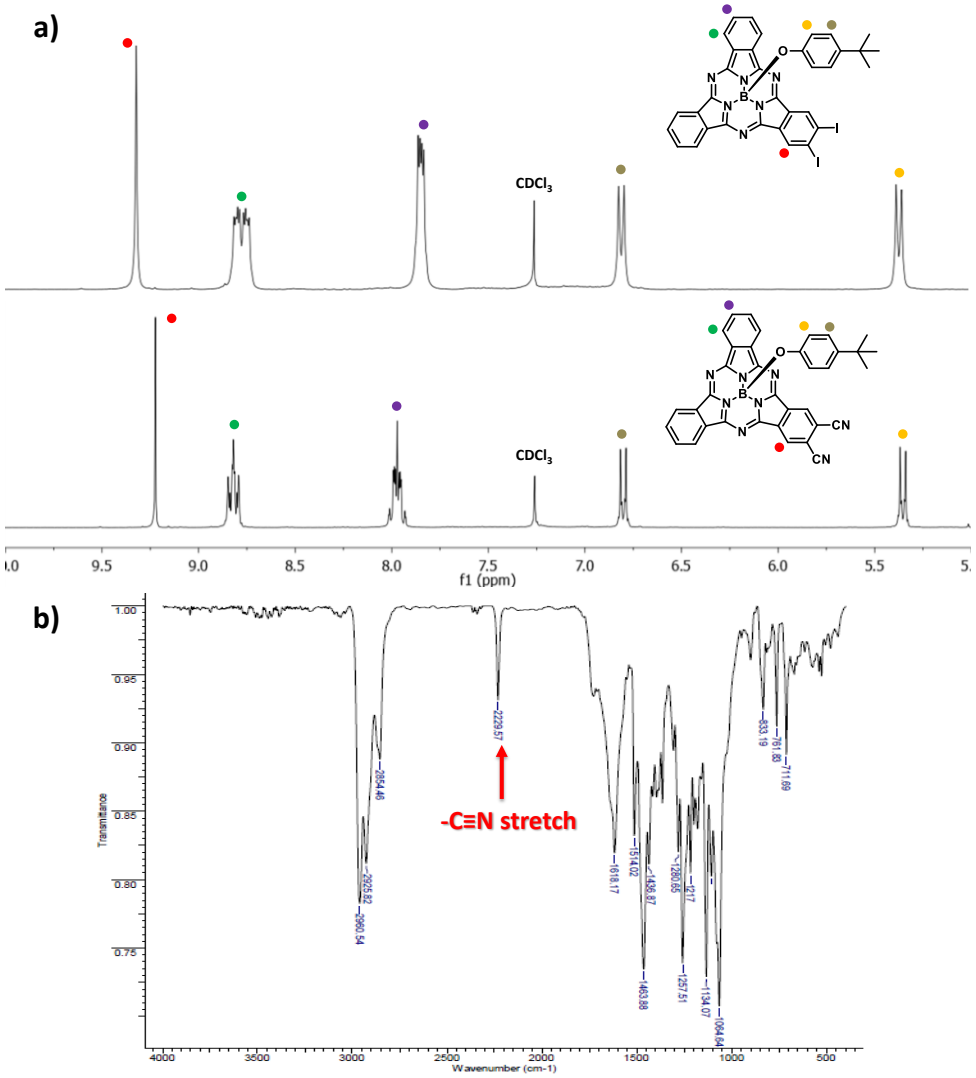

Figure 25. a) Partial ^{1}H-NMR (300 MHz) spectra in $CDCl_3$ of SubPc **5b** (top) and SubPc **14** (down). b) FT-IR spectrum of SubPc **14** featuring the characteristic C≡N stretch band.

Finally, the synthesis of hexacyano-SubPc **23** from hexaiodo-SubPc **9** was tackled (Scheme 10). Several attempts were carried out modifying the reagents ratio and the reaction conditions. In particular, monitoring by TLC of the reaction of **9** with 6.0 equiv of $Zn(CN)_2$ and 60 mol% $Pd(PPh_3)_4$, at 105 °C in 15 min, suggested the formation of SubPc **23** as a dark purple product in the reaction mixture. However, any attempt to isolate and purify the target compound was unsuccessful as the product seemed to darken and decompose during any work up procedure

implying liquid-liquid extraction, percolation, silica gel chromatography, reversed phase chromatography or size exclusion chromatography.

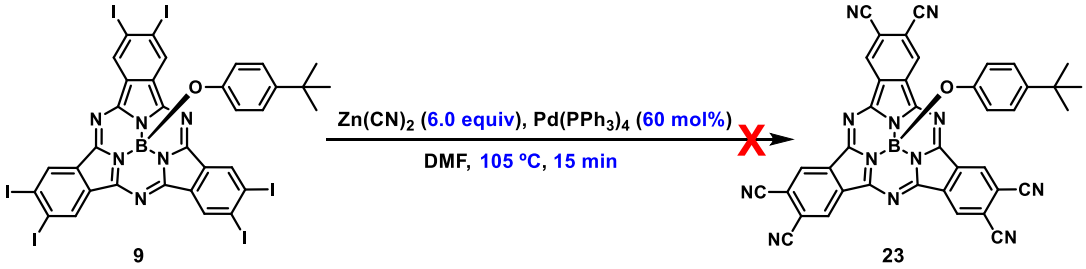

Scheme 10. Unsuccessful synthesis of SubPc **23**.

Despite these results, the interest of C_3-symmetrical hexacyanated SubPc **23** as a potential n-type material for photovoltaic applications prompted us to attempt the synthesis of related hexacyano-SubNc **24** (Scheme 11). Precursor hexabromo-SubNc **25** was obtained from commercial 2,3-dibromo-6,7-dicyanonaphthalene through cyclotrimerization reaction in 1 M BCl_3 in refluxing *p*-xylene and *in situ* treatment with 4-*tert*-butylphenol. In contrast to SubPc synthesis, condensation reaction of unsusbstituted naphthalenedicarbonitrile with BCl_3 is known to produce a mixture of SubNc derivatives with a considerable amount of chlorination at the bay positions.[193] In our case, the formation of two minor and one major green compounds was spotted in the cyclotrimerization reaction. Upon axial substitution reaction by 4-*tert*-butylphenol, reaction mixture was subjected to column chromatography on silica gel to isolate the major green product in 13% yield, which could be identified as SubNc **25** with traces of peripherally chlorinated SubNc derivatives by ^{1}H-NMR and HR-MS characterization.

[193] a) Endres, J.; Pelczer, I.; Rand, B. P.; Kahn, A. *Chem. Mater.* **2016**, *28*, 794. b) Dang, J. D.; Josey, D. S.; Lough, A. J.; Li, Y.; Sifate, A.; Lu, Z. -H.; Bender, T. P. *J. Mater. Chem. A* **2016**, *4*, 9566.

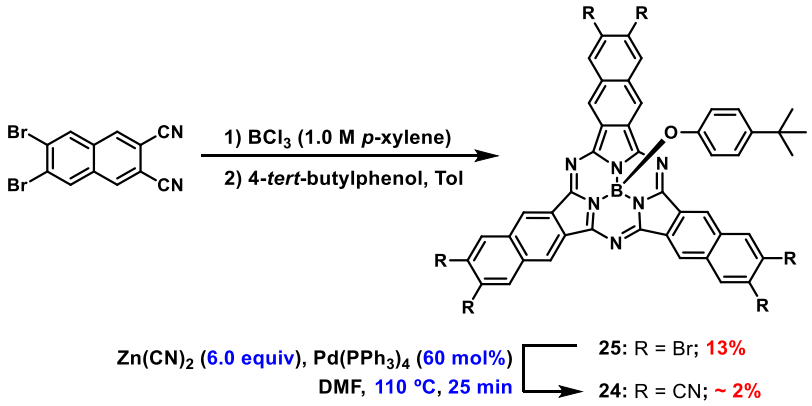

Scheme 11. Attempted synthesis of SubNc **24**.

Pd-catalyzed cyanation reaction of SubPc **25** employing optimized reaction conditions (Scheme 11) led in this case to the evident formation of a highly polar new green compound in the reaction mixture. Unfortunately, this compound, which was identified as SubNc derivative **24** on the basis of its ^{1}H-NMR and MS features, could only be obtained in 2% yield after unavoidable chromatographic work up on silica gel, due to the low stability that it exhibited in solution.

The photodegradation and the high moisture and silica gel sensitivity that compounds **23** and **24** displayed might be consequence of the presumably low-lying LUMOs they would present. For this reason, further attempts on the synthesis of compounds **23** or **24** were discarded.

1.4.3.3 Optical properties of subphthalocyanines 3-22

The UV-vis absorption spectra of the novel unsymmetrical dicyano- and tetracyano-SubPcs and tricyano-SubPcs were recorded and compared to the corresponding precursor iodinated SubPcs in each case (Figure 26). The absorption spectra of the diiodo-SubPcs **3b-7b** and tetra-iodo SubPcs **3a-7a** (dashed lines, Figures 26a-e) are significantly influenced by the peripheral substitution in the macrocycle. In general, diiodo-SubPcs **4b**, **5b**, **6b** and **7b** present analogous characteristic features, a *Q* band in between 573 and 580 nm with ε values in the order of 4 x 10^4 M^{-1} cm^{-1}, with a number of less intense shoulders in the blue region of this band due to their low symmetry, and a Soret band splitted in two main components, at around 270 and 320 nm. Thiooctyl substituted diiodo-SubPc **3b** renders a broader and more intense *Q* band bathochromically shifted around 15 nm with respect to previous ones, as could be expected due to the π-donor character of the thiooctyl substituents. Besides, a broad charge transfer

band (CT-band) appears at around 420 nm, attributable to n→π* transitions that arise from the nonbonding electrons associated to the peripheral sulphur atoms.

In a similar fashion, *Q* band of tetraiodo-SubPcs **4a-7a** show a slightly red shifted maximum (577-585 nm) with respect to their corresponding diiodo-SubPcs. In contrast, tetraiodo-SubPc **3a** displays an hypsochromically shifted *Q* band at 590 nm in comparison with SubPc **3b** and a less prominent CT-band at 436 nm as a consequence of the decrease in the number of thiooctyl substituents at the SubPc periphery.

When going from unsymmetrical iodinated SubPcs to unsymmetrical cyanated SubPcs (solid lines, Figures 26a-e), a general trend can be easily spotted. The substitution of iodo substituents by cyano groups, either in one or two of the SubPc isoindole units, leads to a remarkable shift of the maxima of both the *Q* band and the *B* band to longer wavelengths and an increase in the absorption coefficient, with values in the order of 8-10 x 10^4 M^{-1} cm^{-1} for the *Q* band. These variations in the UV-vis absorption spectra are a indicator of the more extended π-conjugation in the dicyano- and tetracyano-SubPcs, involving the *ortho*-dinitrile functionalities in the electronic delocalization. Besides, cyano-SubPcs present a more acute splitting in the blue region of the *Q* band that results in three or four relatively intense and better resolved peaks or shoulders. Thus, *Q* band maxima of dicyano-SubPcs appear at 598 nm for **12**, 617 nm for **13**, 593 nm for **14**, 592 nm for **15** and 588 nm for **16**, making up bathochromic shifts of 15-22 nm with respect to their corresponding diiodo-SubPcs. Tetracyano-SubPcs show *Q* band maxima at 609 nm for **17**, 619 nm for **18**, 604 nm for **19** and 598 nm for **20**, which means an important red shift of 20-29 nm in comparison with their corresponding tetraiodo-SubPcs. It must be noticed the almost panchromatic absorption that thiooctyl substituted SubPcs **13** and **18** (solid lines, Figure 26b) display due to the wide broadening of the *Q* band overlapping an also broad CT-band.

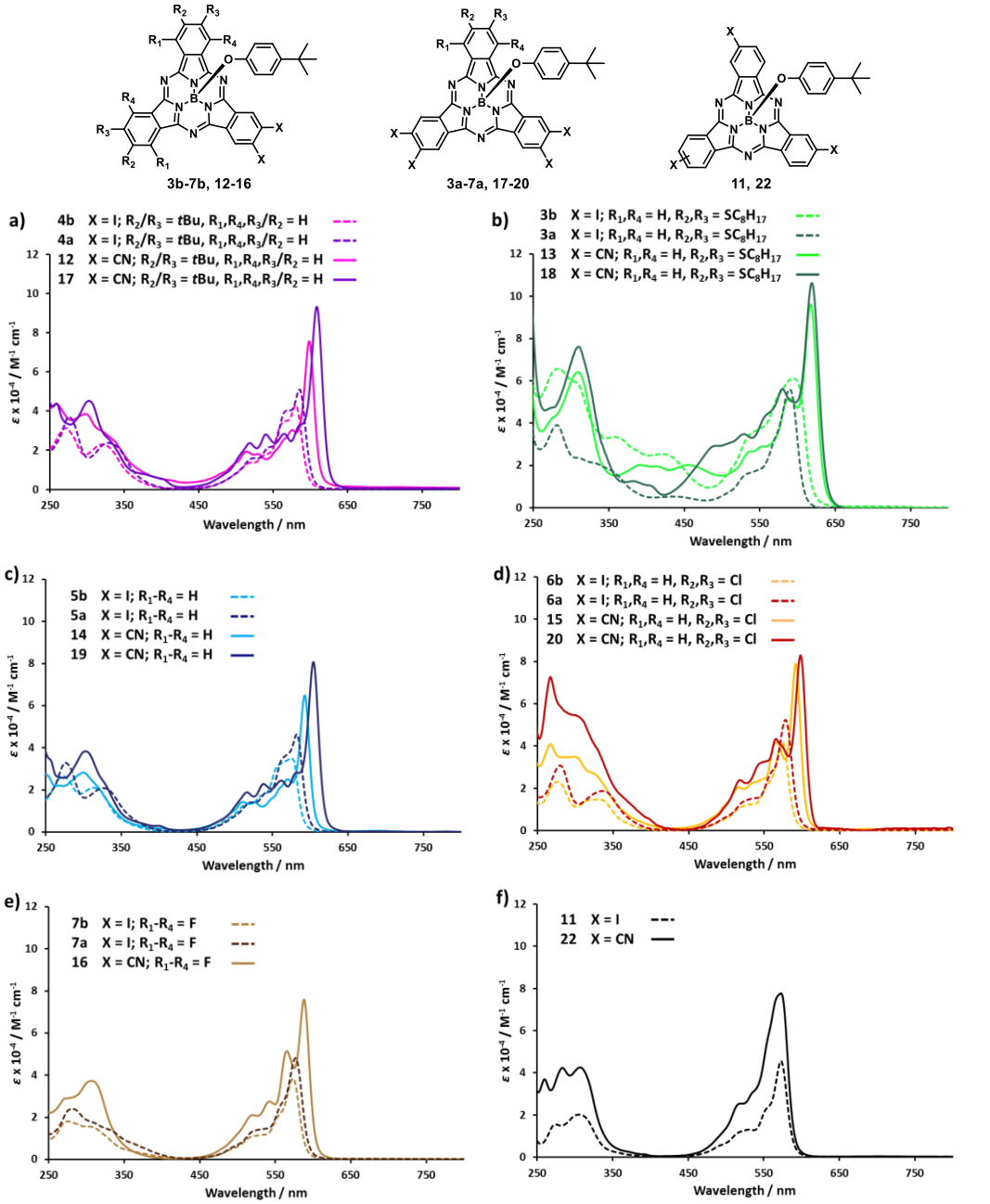

Figure 26. UV-vis absorption spectra in chloroform of: a) SubPcs **4b**, **4a**, **12** and **17**, b) SubPcs **3b**, **3a**, **13** and **18**, c) SubPcs **5b**, **5a**, **14** and **19**, d) SubPcs **6b**, **6a**, **15** and **20**, e) SubPcs **7b**, **7a** and **16** and f) SubPcs **11** and **22**.

Interestingly, the pattern described for the effect of the incorporation of cyano substituents to the periphery of the SubPcs in the absorption features is not observed in tricyano-SubPcs **21**. In this case, UV-vis absorption spectra of both regioisomeric mixture and regioisomerically pure precursor triiodo-SubPcs **10** exhibit a sharp *Q* band at 573 nm and a *B* band at 317 nm (dashed line, Figure 26f). Unexpectedly, the substitution of the iodo substituents by nitrile groups does not entail any visible change in the shifts of the main absorption bands, but only an increase in the ε values, from 4 x 10^4 M^{-1} cm^{-1} for **10** to 8 x 10^4 M^{-1} cm^{-1} for **21**. Hence, in view of these results, it seems that the introduction of an *ortho*-dicyano functionality is required to further extend the π-conjugation of the SubPc structure. However, we do not have a clear explanation for this effect, as it has been previously demonstrated that other peripheral substituents able to slightly extend the π-conjugation, such as diphenylamino groups, produce a strong and progressive red shift of the *Q* band even when only one of these substituents is introduced in each benzene ring.[72c]

In a similar way to ground state absorption, the substitution model around the SubPc macrocycle tunes the properties of their excited states. Figure 27 displays the absorption and singlet excited states emission of SubPcs **4b**, **12**, **15** and **20** as representative examples of the optical properties of unsymmetrical iodinated SubPcs **3-7** and cyanated SubPcs **12-20**. The shifts of the fluorescence emission maxima are parallel to those of the absorption *Q* band and exhibit small Stokes shifts of around 8-20 nm. However, emission spectra are not mirror images of the splitted *Q* band in the absorption spectra since fluorescence emission only takes place from the lowest singlet excited state. Fluorescence quantum yields of these SubPcs have been measured in toluene, using as reference a ϕ_F value of 0.71 for SubPc **1**.[42b] Diiodo- and tetraiodo-SubPcs present low ϕ_F values around 0.05-0.15 due to the highly efficient intersystem crossing characteristic of iodine substituted aromatic compounds. Dicyano-SubPcs and tetracyano-SubPcs ϕ_F values were calculated to be around 0.25-0.40 and 0.05-0.15, respectively.

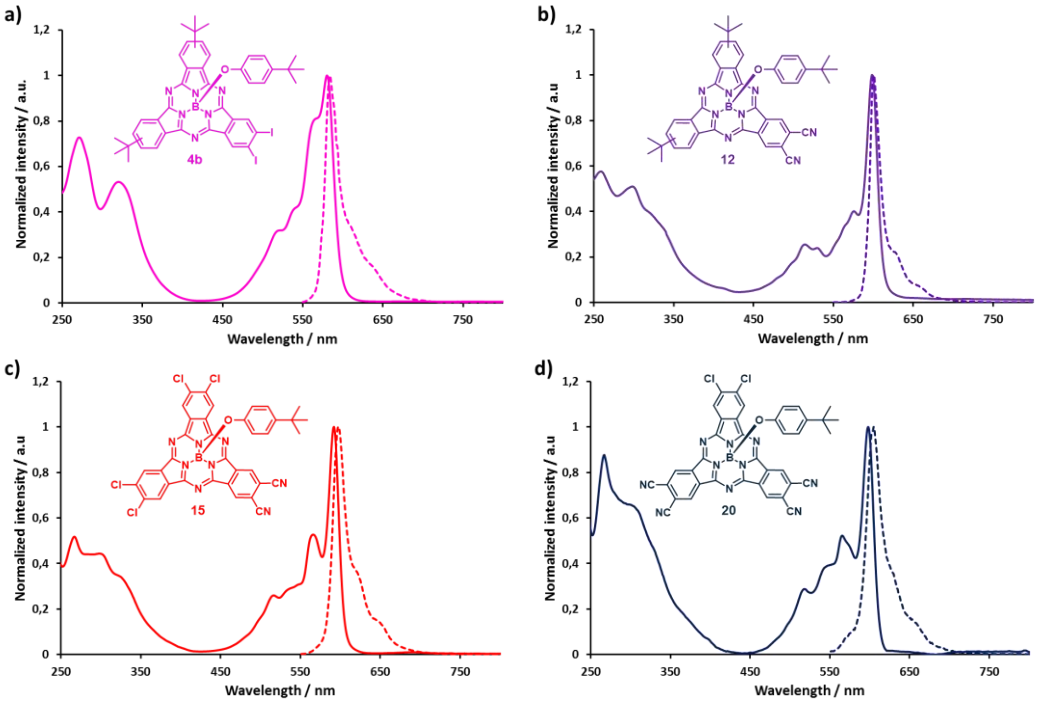

Figure 27. Normalized absorption (solid line) and emission (dashed line) spectra (exc. wavelength = 520 nm) in chloroform of: a) SubPc **4b**, b) SubPc **12**, c) SubPc **15** and d) SubPc **20**.

1.4.3.4 Electrochemical studies of subphthalocyanines 3-22

Electrochemical experiments (cyclic voltammetry (CV), Osteryoung square-wave voltammetry (OSWV) and differential pulse voltammetry (DPV)) in THF solution (0.1 M $TBAPF_6$) were conducted to investigate the influence of the peripheral functionalization on the redox properties of the novel iodinated and cyanated SubPcs. Electrochemical measurements of symmetrical SubPcs **5c**, **6c**, **7c** and **9** were also performed in the same experimental conditions to assess the relative electron-accepting and electron-donating capability of new SubPcs. All potential values quoted throughout this section have been referred to the Fc/Fc^+ couple.

Figures 28, 29, 30 and 31 show the voltammograms of the compounds studied and the electrochemical data are summarized in Table 3. First thing to be noticed is that, as expected, cyclic voltammograms of all SubPcs in the study present a reversible first reduction process and several successive redox events at more negative potentials, which are electrochemically reversible, quasi-reversible or irreversible depending on the peripheral substitution of each SubPc as well. Thus, potential values obtained in the cathodic window in CV, OSWV and DPV

experiments reasonably agree with each other. The first oxidation process on the contrary is irreversible and, in some cases, cannot be easily detected in CV experiments when anodic peaks are too close to the solvent threshold. For this reason, OSWV or DPV experiments and values of the oxidative potentials are shown in those cases where CV anodic window did not display any remarkable feature.

Reference SubPcs **5c**, **6c**, **7c** and **9** exhibit two well resolved reduction waves, each of them involving one electron (Figure 28). These two reduction processes are reversible except in the case of the second reduction peak of **9**. The peripheral substitution of the SubPc structure with electron-withdrawing groups provokes a clear shift of the cathodic peaks to less negative potentials, which implies an easier reduction. Thus, perfluorinated SubPc **7c** and non-substituted SubPc **5c** respectively render the easiest and the hardest first reduction, these processes occurring at half-wave potentials $E^{1}_{1/2,red}$ of -1.03 and -1.55 V in each case. SubPcs **6c** and **9** display intermediate first reduction potential values. The same trend but in the opposite way is followed in the anodic window, where these compounds feature an irreversible oxidation peak at around 0.64-1.05 V.

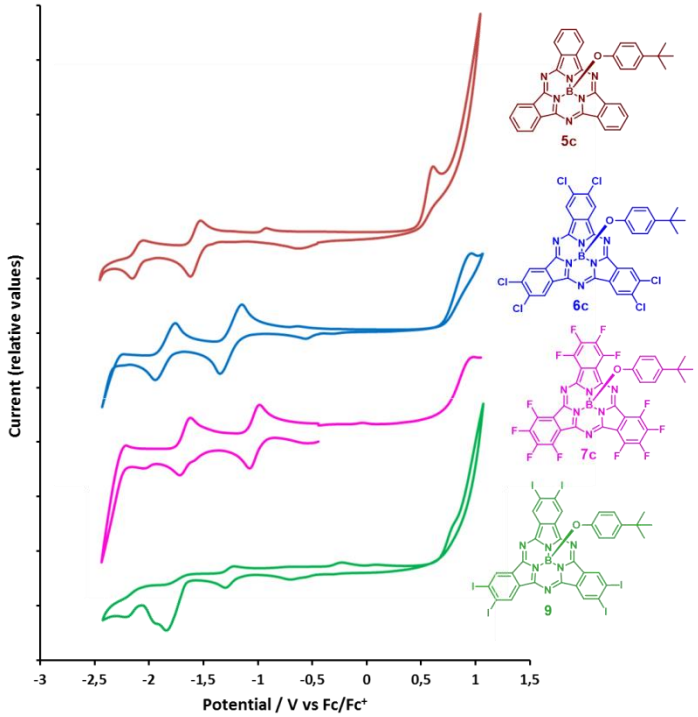

Figure 28. Cyclic voltammograms (OSW voltammogram in the anodic window of **7c**) of reference compounds **5c**, **6c**, **7c** and **9** in THF.

Electrochemical CV studies of unsymmetrical diiodo-SubPcs **3-6b**, tetraiodo-SubPcs **3-6c** and triiodo-SubPcs ***C*$_3$-11** and ***C*$_1$-11** are shown in Figure 29. These SubPcs have in common a reversible first reduction process and irreversible second and third cathodic peaks. In fact, in comparison with reference SubPcs **5c** and **6c**, the peripheral substitution with iodine atoms to yield **5a-b** and **6a-b** seems to favor the irreversibility of these processes. The first reduction half-wave potentials of diiodo-SubPcs **3-6b** appear at -1.43, -1.48, -1.46 and -1.26 V respectively, while tetraiodo-SubPcs **3-6a** present first reduction values of -1.36, -1.37, -1.34 and -1.24 V. The second and third reduction half-wave potentials follow a similar evolution.

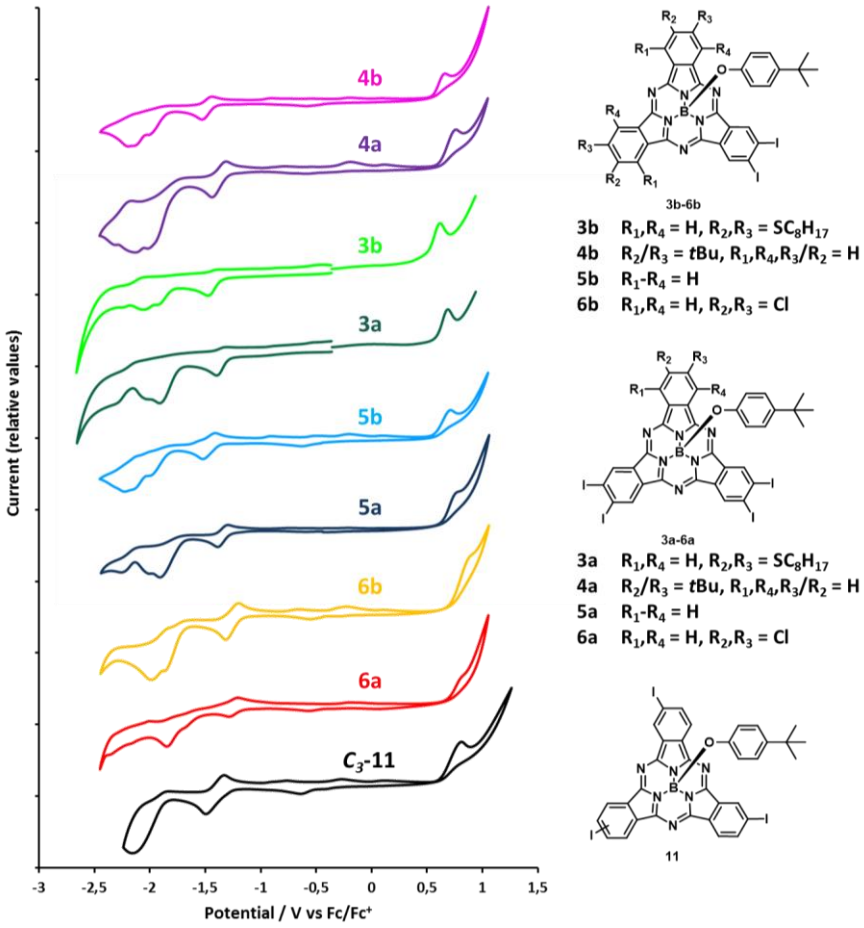

Figure 29. Cyclic voltammograms (OSW voltammogram in the anodic window of **3a** and **3b**) of diiodo-SubPcs **3b-6b**, tetraiodo-SubPcs **3a-6a** and triiodo-SubPc ***C*$_3$-11** in THF.

These results underline the influence of the peripheral substitution of SubPcs in their redox properties, as SubPcs **6a-b**, bearing chlorine atoms in the non-iodinated isoindole units, exhibit a remarkably easier reduction than SubPcs **3a-b**, **4a-b** and **5a-b**, bearing electron-donating thiooctyl or *tert*-butyl groups or unsubstituted in their periphery. Besides, in these SubPc series, a shift of more than 100 mV to less negative potentials is detected in the first reduction process when going from diiodo-SubPcs **3-5b** to **3-5a**. The anodic scans of all these compounds reveal one irreversible oxidation process at potential values in between 0.62-0.85 V inversely influenced by the substituents nature. Triiodo-SubPcs ***C*$_3$-11** and ***C*$_1$-11** display almost identical CV voltammograms that feature a reversible first reduction at -1.42V and an irreversible second event at -2.18 V, and an oxidation peak at 0.81-0.89 V.

CV voltammograms of unsymmetrical dicyano-SubPcs **12-15**, tetracyano-SubPcs **17-20** and tricyano-SubPcs ***C*$_3$-22** and ***C*$_1$-22** are displayed in Figure 30. Interestingly, all these SubPcs feature up to three reversible or quasi-reversible reduction waves, in contrast with precursor iodinated SubPcs. This fact points out the effect that the incorporation of cyano groups in the SubPc periphery causes when more than one electron is captured by the SubPc. In addition, first cathodic waves of cyanated SubPcs are clearly shifted to less negative potentials with respect to the corresponding iodinated SubPcs. Thus, dicyano-SubPcs **12-15** render $E^1_{1/2,red}$ values of -1.22, -1.17, -1.17 and -0.99 V, anodically shifted 260, 266, 289 and 267 mV when compared with diiodo-SubPc **3-6b**. In a similar way, first reduction waves of tricyano-SubPcs ***C*$_3$-22** and ***C*$_1$-22** emerge at -1.15 and -1.16 V, around 265 mV anodically shifted with respect to ***C*$_3$-11** and ***C*$_1$-11**. This effect is even more pronounced in tetracyano-SubPcs **17-20**, that present a first reduction event at -0.90, -0.89, -0.89 and -0.86 V, that is, 473, 461, 443 and 385 mV less negative potential values than tetraiodo-SubPcs **3-6a**. Incorporation of cyano groups in peripheral positions of the SubPc structure entails then a substantial increase of the acceptor character of the molecules, giving rise to easier reduction phenomena. In fact, tetracyano-SubPcs **17-20** display first cathodic waves more than 130 mV shifted to less negative potentials compared to the reference SubPc **7c** and very similar values than the SubPc with the lowest reduction potential in THF reported in literature.[82] Predictably, cyanated SubPcs present an anodic shift of the first oxidation wave with respect to the corresponding iodinated SubPcs, as the cyano substituents also affect the donating capability of the SubPc derivatives.

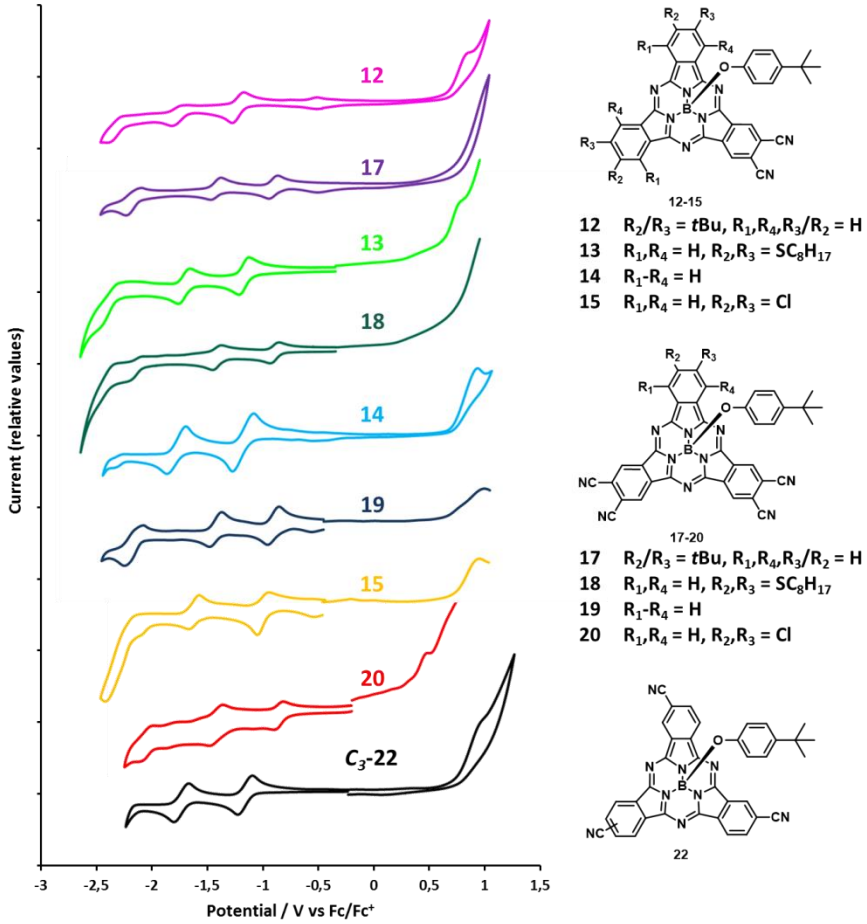

Figure 30. Cyclic voltammograms (OSW voltammogram in the anodic window of **13**, **15**, **18**, **19** and **20**) of dicyano-SubPcs **12-15**, tetracyano-SubPcs **17-20** and tricyano-SubPc ***C*$_3$-22** in THF.

Figure 31 shows the voltammograms of the SubPc series **5b**, **5a**, **14** and **19**, bearing no substituents in the other SubPc benzene rings and the evolution of the first reduction and the first oxidation events when going from the diiodo- to the tetraiodo-SubPc, and the effect of the incorporation of one or two *ortho*-dicyano functionalities in these processes.

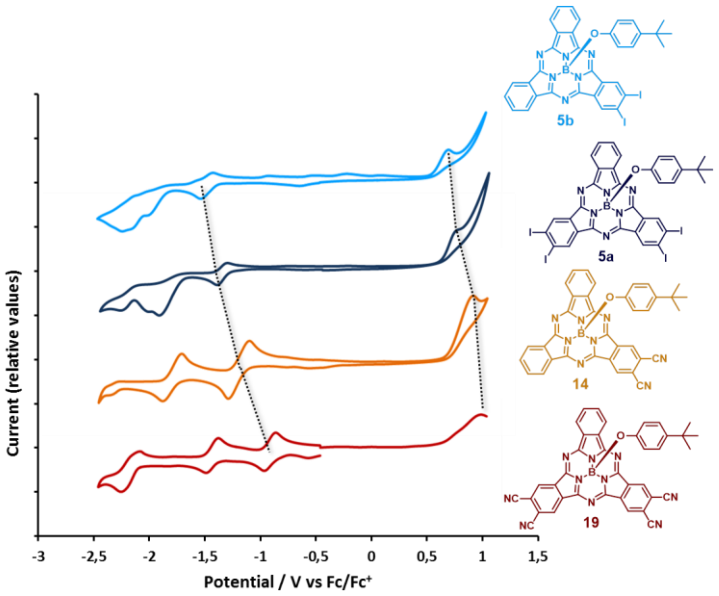

Figure 31. Cyclic voltammograms (OSW voltammogram in the anodic window of **19**) of diiodo-SubPc **5b**, tetraiodo-SubPc **5a**, dicyano-SubPc **14** and tetracyano-SubPc **19** in THF comparing the shift of the first reduction and oxidation processes upon successive introduction of peripheral electron-withdrawing groups.

Table 3. Electrochemical data (in mV *vs.* Fc/Fc^{+}) in THF of reference compounds **5-7c** and **9**, diiodo-SubPcs **3-6b**, tetraiodo-SubPcs **3-6a**, dicyano-SubPcs **12-15**, tetracyano-SubPcs **17-20**, triiodo-SubPcs ***C*$_3$-11** and ***C*$_1$-11** and tricyano-SubPcs ***C*$_3$-22** and ***C*$_1$-22**.

Subphthalocyanine		$E^1_{1/2,red}$ (mV)	$E^2_{1/2,red}$ (mV)	$E^3_{1/2,red}$ (mV)	E^1_{ox} [a] (mV)
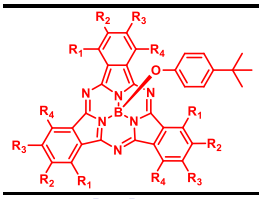	**5c**	-1545	-2074		643
	6c	-1244	-1849		969
	7c	-1027	-1667		1057[c]
	9	-1263	-1847[b]	-2225[b]	783
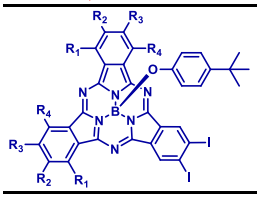	**3b**	-1433	-1906[b]	-2003[b]	623[c]
	4b	-1481	-2008[b]		668
	5b	-1462	-1989[b]	-2221[b]	717
	6b	-1261	-1855[b]	-1985[b]	853
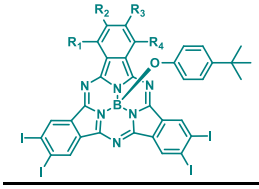	**3a**	-1357	-1871[b]	-1952[b]	702[c]
	4a	-1373	-1960[b]	-2161[b]	765
	5a	-1338	-1907[b]	-2164[b]	765
	6a	-1244	-1844[b]		808
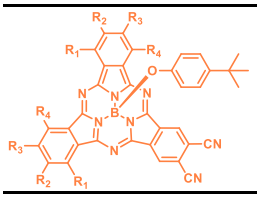	**12**	-1221	-1744	-2289[b]	806
	13	-1167	-1710	-2385[b]	769[c]
	14	-1173	-1774	-2264[b]	939
	15	-994	-1615	-2281[b]	948
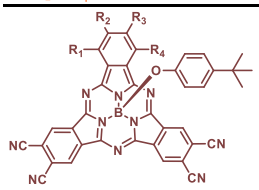	**17**	-900	-1418	-2157	996
	18	-896	-1415	-2138[b]	
	19	-895	-1414	-2151	993[c]
	20	-859	-1421	-2059	
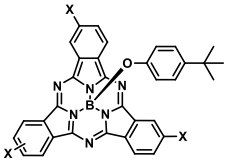	***C*$_3$-11**	-1417	-2181[b]		807
	***C*$_1$-11**	-1422	-2183[b]		890
	***C*$_3$-22**	-1157	-1732		913
	***C*$_1$-22**	-1150	-1702		952

[a] Since these oxidation processes are irreversible, only anodic peak potentials are reported. [b] Since these reduction processes are irreversible, only cathodic peak potentials are reported. [c] Peak oxidation potential by OSWV.

1.4.3.5 Calculation of HOMO/LUMO levels of subphthalocyanines 3-22

Calculation of the energy level of HOMO and LUMO orbitals of an organic semiconductor with potential applicability in OSCs is essential as the frontier orbitals levels alignment of the donor and the acceptor active materials plays a key role in the performance of the device. HOMO and LUMO energy values can be acquired from different experimental techniques, either in solution by electrochemistry studies or on thin film, by highly accurate techniques like Ultraviolet Photoelectron Spectroscopy (UPS), X-ray Photoelectron Spectroscopy (XPS) or Photoelectron Spectroscopy in Air (PESA).

In our case, the energy level values *vs.* vacuum were obtained from CV experiments, using the approximation depicted in Equation 5, based on the revised potential of the Fc/Fc^+ redox couple considering the influence of the different reference electrodes employed described by Cardona *et al.*:[194]

$$E_{HOMO/LUMO} = -5.1 - E^1_{1/2,ox/red}(vs.\,Fc/Fc^+)(eV) \qquad \text{(Eqn. 5)}$$

As it has been analyzed before, SubPcs render irreversible first oxidation processes that impede the correct assignment of half-wave potential values. On the other hand, all SubPcs on this study display reversible first reduction events whose half-wave potentials can be easily extracted. For this reason, Equation 5 was used to calculate the energy LUMO level E_{LUMO} for each SubPc derivative.

Then, in order to obtain reliable HOMO energy values, the optical band gap $E_{g,opt}$, that can be directly related to the HOMO-LUMO energy gap, was estimated from the intersection of the normalized absorption and emission spectra,[195] and directly added to E_{LUMO} values applying Equation 6:

$$E_{HOMO} = E_{LUMO} + E_{g,opt}(eV) \qquad \text{(Eqn. 6)}$$

It is very important to notice that this process implies a series of unavoidable approximations that must be taken into account when comparing the HOMO and LUMO levels calculated with other SubPc derivatives molecular energy levels found in literature. SubPc researchers employ many different approaches for measuring and reporting molecular energy levels, either in the equation developed to estimate the HOMO energy level from CV measurements[42b,85,196] or in

[194] Cardona, C. M.; Li, W.; Kaifer, A. E.; Stockdale, D.; Bazan, G. C. *Adv. Mater.* **2011**, *23*, 2367.
[195] Djurovich, P. I.; Mayo, E. I.; Forrest, S. R.; Thompson, M. E. *Org. Electron.* **2009***, 10***,** 515.
[196] a) Trasatti, S. *Pure & AppL Chem.* **1986**, *58*, 955. b) D'Andrade, B. W.; Datta, S.; Forrest, S. R.; Djurovich, P.; Polikarpov, E.; Thompson, M. E. *Org. Electron.* **2005**, *6*, 11.

the way to obtain the wavelength value considered in the $E_{g,opt}$ calculation,[42b,85,97c,197] that substantially differ from the one followed in this section. Therefore, the HOMO and LUMO levels and $E_{g,opt}$ values indicated in this Thesis serve only to reflect the relative positions of the transport energy levels for the different SubPc derivatives rather than representing the absolute values of these energy levels.

Finally, in order to further investigate the geometries and electronic properties of the new SubPc derivatives, computational studies were performed using Spartan '14 applying density functional theory (DFT) at the B3LYP/6-31G* level for the geometry optimization and the calculation of the energy levels and the potential and energy surfaces in vacuum. In order to assess the viability of the mathematical model proposed by Bender *et al.* for the prediction of HOMO and LUMO energy levels in SubPc macrocycles from DFT (B3LYP) computational data,[85] estimation of the theoretical E_{HOMO} and E_{LUMO} values were carried out applying Equation 7 and Equation 8 to the molecular orbitals energy values computationally obtained:

$$E_{HOMO} = 1.284 \times E_{HOMO}^{B3LYP} + 1.132 \pm 0.188 \qquad \text{(Eqn. 7)}$$

$$E_{LUMO} = 1.176 \times E_{LUMO}^{B3LYP} - 0.499 \pm 0.163 \qquad \text{(Eqn. 8)}$$

Experimental and theoretical calculations have been carried out for all SubPc derivatives **3-22**. The experimental and computational data obtained for the HOMO-LUMO levels of reference SubPcs **6c** and **7c**, dicyano-SubPcs **12-15**, tetracyano-SubPcs **17-20** and tricyano-SubPcs ***C*$_3$-22** and ***C*$_1$-22** is summarized in Table 4 and is shown schematically in Figure 32.

The trend in LUMO energy levels calculated with Equation 5 is obviously similar to the trend in $E^1_{1/2,red}$ seen in CV measurements. On the other hand, experimental E_{HOMO} values obtained from E_{LUMO} and $E_{g,opt}$ data with Equation 6 differ slightly from the relative values of E^1_{ox} due to the previously mentioned uncertainty associated to the experimental observation of SubPc oxidation processes by voltammetric measurements. Thus, E_{LUMO} of dicyano-SubPc derivatives ranges from around -3.9 eV for SubPcs **12-14** to -4.1 eV for SubPc **15**. This lowering denotes the influence of the electron-withdrawing peripheral substituents in **15** to increase the electron-acceptor character of these derivatives. In contrast, E_{LUMO} of tetracyano-SubPcs **17-20** barely spans 0.04 eV, from -4.20 to -4.24 eV, suggesting that the sensitivity of the acceptor character of tetracyano-SubPcs to additional peripheral substitution is reduced due to the prevailing effect of two *ortho*-dicyano functionalities. A range in E_{HOMO} from -5.92 to -6.19 eV

[197] Sullivan, P.; Duraud, A.; Hancox, I.; Beaumont, N.; Mirri, G.; Tucker, J. H. R.; Hatton, R. A.; Shipman, M.; Jones, T. S. *Adv. Energy Mater.* **2011**, *1*, 352.

for dicyano-SubPcs **12-15** and from -6.18 to -6.30 eV for tetracyano-SubPcs **17-20** can be extracted from Equation 6.

Table 4. Experimental and theoretical HOMO-LUMO energy levels data (in eV) of reference SubPc **6c** and **7c**, dicyano-SubPcs **12-15**, tetracyano-SubPcs **17-20** and tricyano-SubPcs C_3-**22** and C_1-**22**.

SubPc	Experimental data			Computational data	
	E_{LUMO} (eV)	E_{HOMO} (eV)	$E_{g,opt}$ [a] (eV)	E_{LUMO} [b] (eV)	E_{HOMO} [c] (eV)
6c	-3.86	-6.02	2.16 (573)	-4.13	-6.30
7c	-4.07	-6.23	2.16 (575)	-4.30	-6.38
12	-3.88	-5.95	2.07 (599)	-4.16	-6.12
13	-3.93	-5.92	1.98 (625)	-4.24	-6.11
14	-3.93	-6.01	2.08 (595)	-4.24	-6.24
15	-4.11	-6.19	2.09 (594)	-4.67	-6.73
17	-4.20	-6.22	2.02 (615)	-4.89	-6.69
18	-4.20	-6.18	1.98 (626)	-4.90	-6.58
19	-4.21	-6.24	2.03 (609)	-4.92	-6.92
20	-4.24	-6.30	2.06 (602)	-5.11	-7.14
C_3-**22**	-3.94	-6.11	2.16 (573)	-4.47	-6.64
C_1-**22**	-3.95	-6.11	2.16 (573)	-4.51	-6.64

[a] Intersection wavelength in nm of the normalized absorption and emission spectra in brackets. [b] Calculated using Equation 8. [c] Calculated using Equation 7.

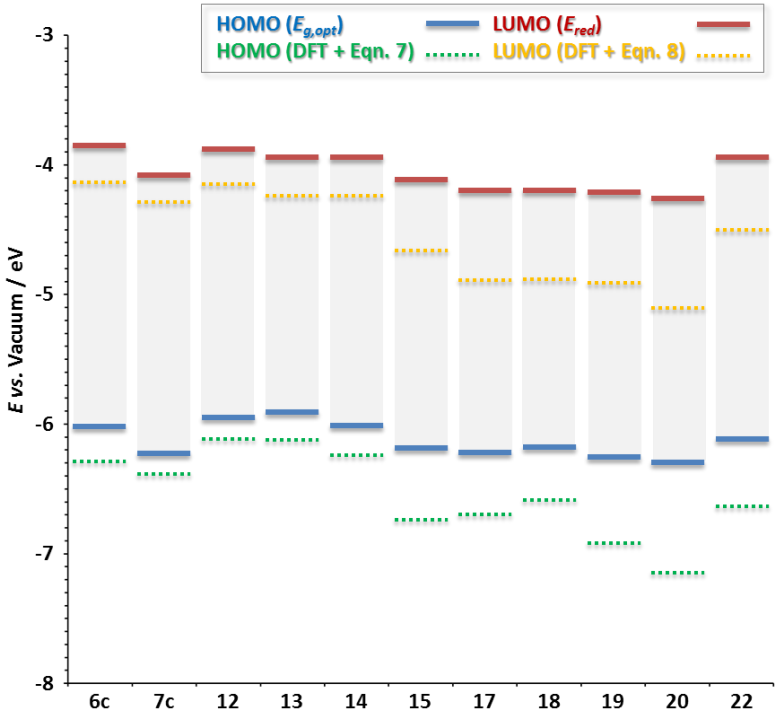

Figure 32. Schematic representation of the calculated HOMO and LUMO energy levels of reference SubPc **6c** and **7c**, dicyano-SubPcs **12-15**, tetracyano-SubPcs **17-20** and tricyano-SubPcs ***C*$_3$-22** and ***C*$_1$-22**.

From computational E_{LUMO} and E_{HOMO} data in Table 4 and Figure 32, it can be easily spotted that estimates provided by the mathematical model proposed by Bender *et al.* does not fit well with the new substitution pattern introduced by cyano-SubPcs, giving rise to very disparate values. As a result, in all cases, experimental HOMO and LUMO values lie between 0.2 and 0.9 eV higher in energy when compared to the value obtained by computational calculations.

With the aim at determining a correlation between computational results obtained from B3LYP calculations and experimental data from CV measurements for the influence of the incorporation of one or two *ortho*-dicyano functionalities to the molecular orbital energy levels of SubPc derivatives, the same procedure as the one described by Bender *et al.* was followed. When plotting the computational estimates from each method against the experimental data for dicyano-SubPcs **12-15** and tetracyano-SubPcs **17-20** (tricyano-SubPcs **22** were excluded from this study as the substitution pattern is different), a linear regression of

each data set produced goodness of fit (R^2) values of 0.946 for E_{HOMO} values and 0.988 for E_{LUMO} values (Figure 33). From the linear regressions, the following equations were generated to estimate the molecular orbitals energies of these SubPc derivatives using B3LYP method:

$$E_{HOMO} = 0.4764 \times E_{HOMO}^{B3LYP} - 3.2701 \quad \text{(Eqn. 9)}$$

$$E_{LUMO} = 0.4669 \times E_{LUMO}^{B3LYP} - 2.4435 \quad \text{(Eqn. 10)}$$

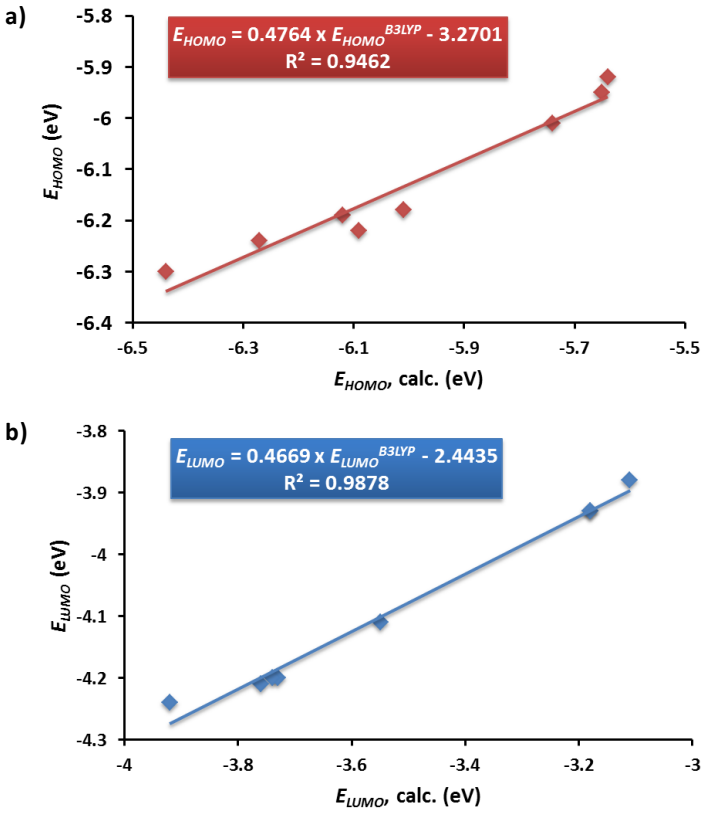

Figure 33. a) Calculated E_{HOMO}, calc. (eV) using B3LYP versus E_{HOMO} (eV) measured experimentally by CV for dicyano-SubPcs **12-15** and tetracyano-SubPcs **17-20**. b) Calculated E_{LUMO}, calc. (eV) using B3LYP versus E_{LUMO} (eV) measured experimentally by CV for dicyano-SubPcs **12-15** and tetracyano-SubPcs **17-20**.

The good correlation determined between experimentally and computationally acquired E_{LUMO} values is especially relevant, since these peripherally cyanated SubPc derivatives might be potentially applicable as n-type materials in OPV devices. Through these correlations, we

would be able to rapidly predict structural factors which influence the HOMO and LUMO energy levels of other cyanated SubPcs.

Figure 34 shows the HOMO and LUMO orbitals of a series of unsymmetrical SubPcs, namely diiodo-SubPc **5b**, tetraiodo-SubPc **5a**, dicyano-SubPc **14** and tetracyano-SubPc **19**, calculated by DFT. Among these compounds, both the HOMO and LUMO are situated entirely on the SubPc core with no contribution from axial substituent. The HOMO is evenly distributed on the carbon atoms of the macrocycle, comprising the three isoindole units, while the LUMO encompasses both the nitrogen and carbon atoms comprising the 14 π-electron system. In iodinated SubPcs **5a** and **5b**, no contribution from the halogen atoms is observed to the HOMO or the LUMO. On the other hand, cyano groups in SubPcs **14** and **19** are slightly involved in the HOMO orbital delocalization, while they contribute to a greater extent in the LUMO orbital density. These patterns are reproduced in the other unsymmetrical SubPc series.

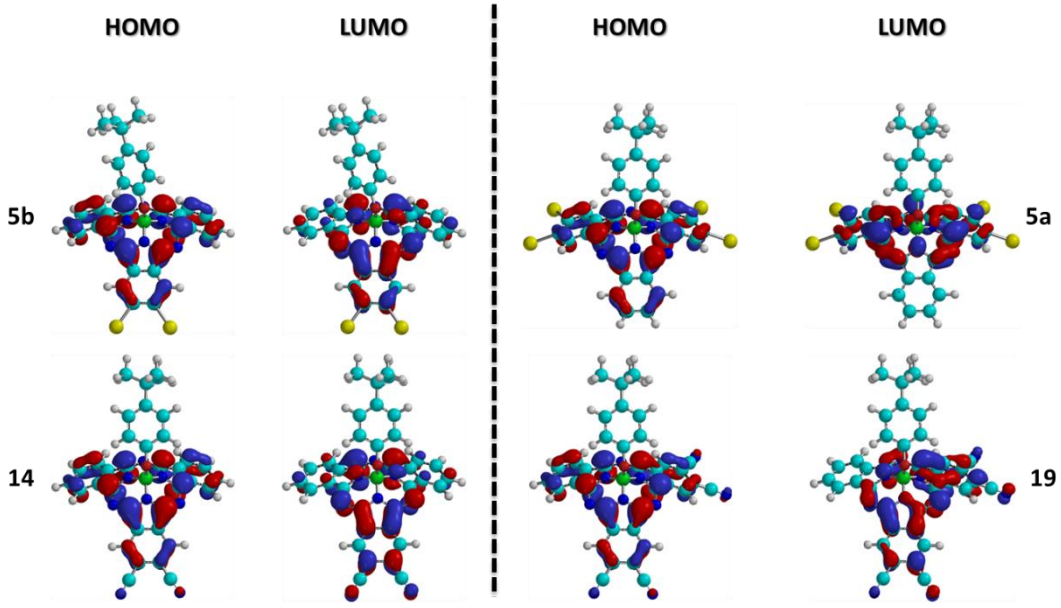

Figure 34. Frontier orbitals (HOMO and LUMO) of unsymmetrical SubPcs **5a**, **5b**, **14** and **19** calculated at the B3LYP/6-31G* computational level.

It can be noticed that, for the LUMO orbital in tetraiodo and tetracyano substituted SubPcs **5a** and **19**, the unsubstituted peripheral benzene does not exhibit any participation in the orbital delocalization. Interestingly, all tetracyanated SubPcs **17-20** follow the same trend (Figure 35). This observation visually confirms the previously mentioned limited influence of the peripheral

substituents occupying the non-cyanated benzene ring in the LUMO energy level. Finally, in SubPc **18**, HOMO orbital density is entirely centered in the electron-donating thioalkyl substituents of the periphery, accordingly with the presence of intense CT-bands in the UV-vis absorption spectrum of this compound.

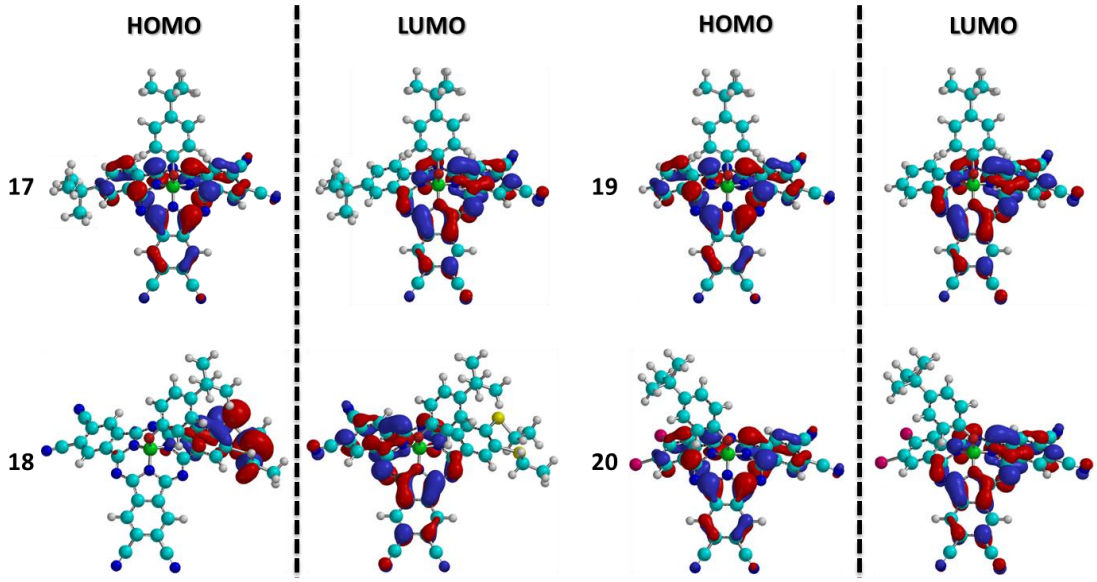

Figure 35. Frontier orbitals (HOMO and LUMO) of tetracyano-SubPcs **17-20** calculated at the B3LYP/6-31G* computational level. In SubPc **18**, thiooctyl groups have been substituted by thioethyl groups to speed up calculations.

1.4.3.6 Charge carriers mobility measurements of selected subphthalocyanines

The intrinsic charge carrier transporting ability of a novel organic molecular semiconductor is a key parameter in order to asses its potential applicability as n-type active material in OPVs. In this regard, the quantification of the charge carrier mobility μ of a material can be carried out *via* a number of techniques, such as direct measurement in Field-Effect Transistors (FET) or using the time-of-flight (TOF) method[198] or admittance spectroscopy (AS)[199] in specially constructed single carrier devices. However, these techniques present several limitations that make notoriously difficult to extract reliable mobility measurements from the current/voltage characteristics of single-carrier devices, as they all reflect the charge carrier mobility as a

[198] Kaneto, K. *Thin Solid Films* **2001**, *393*, 249.
[199] Tsang, S. W.; So, S. K.; Xu, J. B. *J. Appl. Phys.* **2006**, *99*, 013706.

function of electric field in films and they are sensitive to charge-injection constraints at the metal-organic contacts due to the use of electrodes.

Probably for this reason, the sparse reports in the literature of the charge transport properties of SubPcs are contradictory, ranging across many orders of magnitude. SubPc **1** charge carrier transport properties have been determined within a thin film transistor (TFT), with electron and hole mobilities of $\sim 10^{-5}$ cm^2 V^{-1} s^{-1}.[200] Using single-carrier devices, Poole-Frenkel-type hole mobilities of $\mu_0 = 4.5 \times 10^{-8}$ cm^2 V^{-1} s^{-1} and electron mobilities of $\mu_0 = 5.2 \times 10^{-10}$ cm^2 V^{-1} s^{-1} have been measured for the same SubPc.[201] On the other hand, the dielectric spectroscopy technique has been demonstrated to determine the charge carrier transport properties of SubPc **1** film, reporting an electron mobility of $\sim 10^{-9}$ cm^2 V^{-1} s^{-1}.[202]

Finally, Bender *et al.* have studied the electric field and temperature dependence of the electron mobilities of a group of differently axially and peripherally functionalized SubPcs, using AS technique in vapor-phase-deposited thin films.[95,203] Interestingly, the authors found a correlation between the increase of mobility in response to an increasing electric field and the average molecular spacing (<*d*>) within the crystal. On the basis of these observations, the authors proposed desirable solid-state packing characteristics and good film forming properties to achieve high charge carrier mobility in SubPcs.

As an alternative to a device characterization, non-contact techniques such as transient absorption spectroscopy (TAS)[204] and flash-photolysis time-resolved microwave conductivity (FP-TRMC)[205] are choices to evaluate optoelectronic properties of organic electronic materials without using electrodes. Owing to the direct measurement of transient photoconductivity, a low-power electric field of high-frequency microwave, and a resonant cavity with high sensitivity, FP-TRMC allows for probing the motion of charge carrier before complete deactivation by trapping sites and thus enables the device-less evaluation of charge carrier transport. The TAS experiment provides the transient photo-absorption (PA) spectrum/kinetics

---

[200] Yasuda, T.; Tsutsui, T. *Mol. Cryst. Liq. Cryst.* **2007**, *462*, 3.

[201] Pandey, R.; Gunawan, A. A.; Mkhoyan, K. A.; Holmes, R. J. *Adv. Funct. Mater.* **2012**, *22*, 617.

[202] Singh, M.; Mahajan, A.; Bedi, R. K.; Aswal, D. K.. *Electron. Mater. Lett.* **2013**, *9*, 101.

[203] Beaumont, N.; Castrucci, J. S.; Sullivan, P.; Morse, G. E.; Paton, A. S.; Lu, Z. -H.; Bender, T. P.; Jones, T. S. *J. Phys. Chem. C* **2014**, *118*, 14813.

[204] a) Maurano, A.; Hamilton, R.; Shuttle, C. G.; Ballantyne, A. M.; Nelson, J.; O'Regan, B.; Zhang, W.; McCulloch, I.; Azimi, H.; Morana, M.; Brabec, C. J.; Durrant, J. R. *Adv. Mater.* **2010** , *22*, 4987. b) Clarke, T. M.; Ballantyne, A.; Shoaee, S.; Soon, Y. W.; Duffy, W.; Heeney, M.; McCulloch, I.; Nelson, J.; Durrant, J. R. *Adv. Mater.* **2010**, *22*, 5287.

[205] a) Saeki, A.; Koizumi, Y.; Aida, T.; Seki, S. *Acc. Chem. Res*. **2012**, *45*, 1193. b) Seki, S.; Saeki, A.; Sakurai, T.; Sakamaki, D. *Phys. Chem. Chem. Phys.* **2014**, *16*, 11093.

and the emission spectrum, of which the dependence of the incident photon density is compared with the TRMC results to discuss the dynamics of the excitons and the charge carriers. As a result, the combination of both techniques provides a versatile route toward the elucidation of intrinsic charge carrier mobility in a wide variety of organic and inorganic electronic materials.

In this section, the potential charge carrier transport properties of selected novel peripherally cyanated SubPc derivatives have been studied by means of FP-TRMC and TAS techniques. These measurements have been conducted in the laboratory of Professor Shu Seki in Kyoto University.

With the aim of improving the crystallinity and the solid-state packing of cyanated phenoxy-SubPc derivatives, the axial substitution reaction of the bulky 4-*tert*-butylphenoxy group by a smaller halogen atom would be desirable. The exchange of the axial phenoxy ligand either by chlorine, in the presence of BCl_3,[189] or by fluorine, employing an excess of $Et_2O{\cdot}BF_3$,[42b,64] has already been described.

Reaction of dicyano-SubPcs **12-15** and tetracyano-SubPcs **17-20** with stoichiometric amounts of BCl_3 or $Et_2O{\cdot}BF_3$ at room temperature, in an attempt to prevent the reaction of the *ortho*-dinitrile functionalities with the boron trihalides, led to the partial formation of axially halogenated SubPc derivatives. Unfortunately, the addition of a Lewis acid excess in order to drive the reaction to completion only led to the decomposition of the SubPc compound.

Conversely, reaction of tricyano-SubPcs ***C*$_3$-** and ***C*$_1$-22** with 5 equiv of BCl_3 at CH_2Cl_2 reflux gave rise to axially chlorinated tricyano-SubPcs ***C*$_3$-26** and ***C*$_1$-26** in very good yields (Scheme 12). These results suggest that decomposition of SubPcs **12-15** and **17-20** under these reaction conditions is a consequence of the hydrolysis of the dinitrile groups and/or the ring opening reaction of these highly acceptor SubPcs in the presence of strong Lewis acids such as boron trihalides.

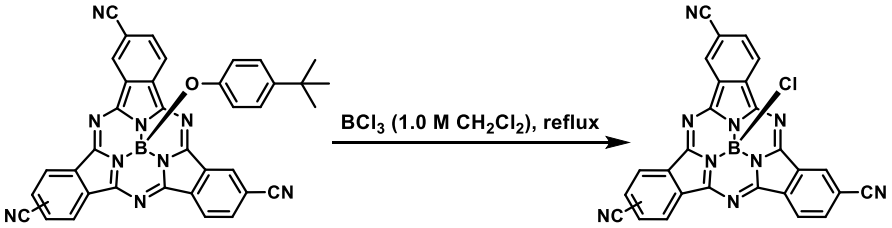

***C*$_3$-22** ***C*$_3$-26; 90%**

***C*$_1$-22** ***C*$_1$-26; 88%**

Scheme 12. Synthesis of SubPcs ***C*$_3$-26** and ***C*$_1$-26**.

For this reason, an alternative synthetic procedure consisting in the treatment of phenoxy-SubPcs with other Lewis acids, namely aluminum or titanium chloride, was attempted. This approach, based on the activation of the axial position of SubPcs by treatment with $AlCl_3$ described by Bender,[68] would presumably avoid the dinitrile groups hydrolysis while generating the corresponding chloro-SubPc.

The synthesis of chloro-dicyano-SubPcs **27** and **28** was carried out by heating a solution of the corresponding phenoxy-SubPcs in toluene in the presence of a slight excess of $AlCl_3$ or $TiCl_4$ (Scheme 13). In both cases, reaction with $TiCl_4$ rendered higher yields. However, while full conversion of initial SubPc into product **27** was observed in the case of SubPc **14**, only partial substitution of the axial phenoxy ligand in SubPc **15** was achieved, probably due to the coordination of the Lewis acid to the peripheral chlorine substituents of SubPcs in addition to their *meso* nitrogen atoms (Scheme 13).[55]

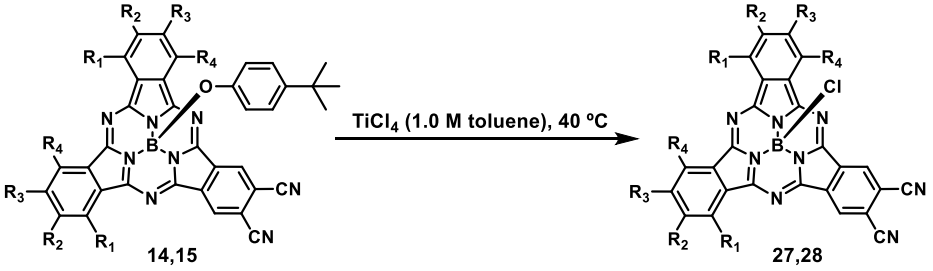

Scheme 13. Synthesis of SubPcs **27** and **28.**

Any attempts on the synthesis of chloro-tetracyano-SubPcs from compounds **17-20** were fruitless, observing a total lack of reactivity of the starting material toward $AlCl_3$ or $TiCl_4$.

Finally, well-known acceptor SubPcs F_{12}-SubPc-Cl **8c**[39] and Cl_6-SubPc-Cl **29**,[109b,206] were synthesized as reference compounds, from 3,4,5,6-tetrafluorophthalonitrile and 4,5-dichlorophthalonitrile respectively according to the procedures previously described (Chart 6).

[206] Verreet, B.; Cnops, K.; Cheyns, D.; Heremans, P.; Stesmans, A.; Zango, G.; Claessens, C. G.; Torres, T.; Rand, B. P. *Adv. Energy Mater.* **2014**, *4*, 1301413.

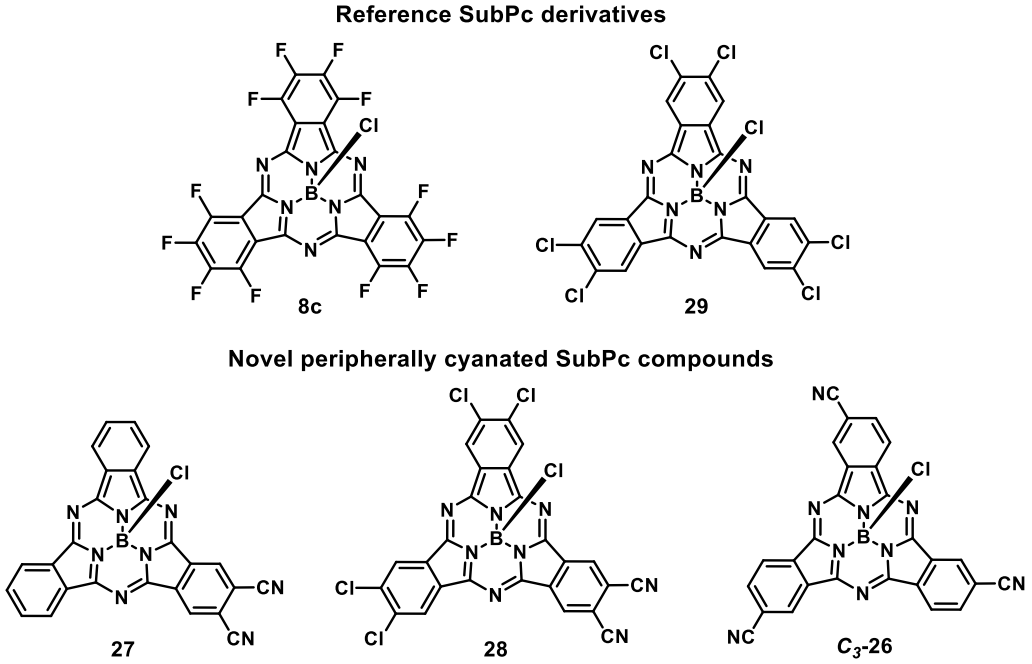

Chart 6. SubPc derivatives studied in the charge carrier mobility measurements.

It is worth mentioning that the axial exchange of the phenoxy ligand by a chloro atom has only a very small effect on the optical spectra, SubPcs **26-28** featuring almost identical absorption and emission spectra than their corresponding phenoxy-SubPcs. Nevertheless, ϕ_F values of *ortho*-dicyano-SubPcs increased from 0.25-0.40 for SubPcs **14-15** to ~ 0.60 for SubPcs **27-28**.

On the other hand, electrochemical properties of cyanated SubPcs are moderately influenced by the axial group. Axial substitution of the phenoxy group provokes an evident increase of the acceptor character of the molecules, giving rise to easier reduction phenomena. Thus, SubPcs ***C*$_3$-26**, **27** and **28** present first cathodic events at -1.08, -1.08 and -0.90 V respectively, anodically shifted 77-93 mV when compared with precursor SubPcs ***C*$_3$-22**, **14** and **15**. The nature of the axial ligand also affects the reversibility of the different redox processes, chloro-SubPcs displaying less reversible phenomena than phenoxy-SubPcs.[207]

A monocrystal of SubPc ***C*$_3$-26** was obtained by slow diffusion of hexane in a THF solution of the compound and its structure was determined by X-Ray diffraction. The X-ray structure of

[207] Ferro, V. R.; Poveda, L. A.; Claessens, C. G.; González-Jonte, R. H.; García de la Vega, J. M. *Int. J. Quantum Chem.* **2003**, *91*, 369.

***C*$_3$-26** exhibits the characteristic cone-shaped geometry of this macrocycle, with a bowl depth of 2.454 Å and a B-Cl bond distance of 1.864 Å (Figure 36a). The solid-state packing mode of ***C*$_3$-26** (Figures 36b-c) is dominated by π-π interactions between adjacent SubPc molecules, displaying concave-concave and convex-convex head-to-head arrangements in the range of 3.70-3.90 Å. Besides, two of the three nitrile groups of each ***C*$_3$-26** molecule are involved in C≡N···C≡N interactions with neighboring SubPc units at a separation of 3.222 Å, less than the sum of the van der Waals radii; the third nitrile group is located nearly in the centre of the concave side of an adjacent molecule beneath the boron atom, at a distance of 3.568 Å.[208]

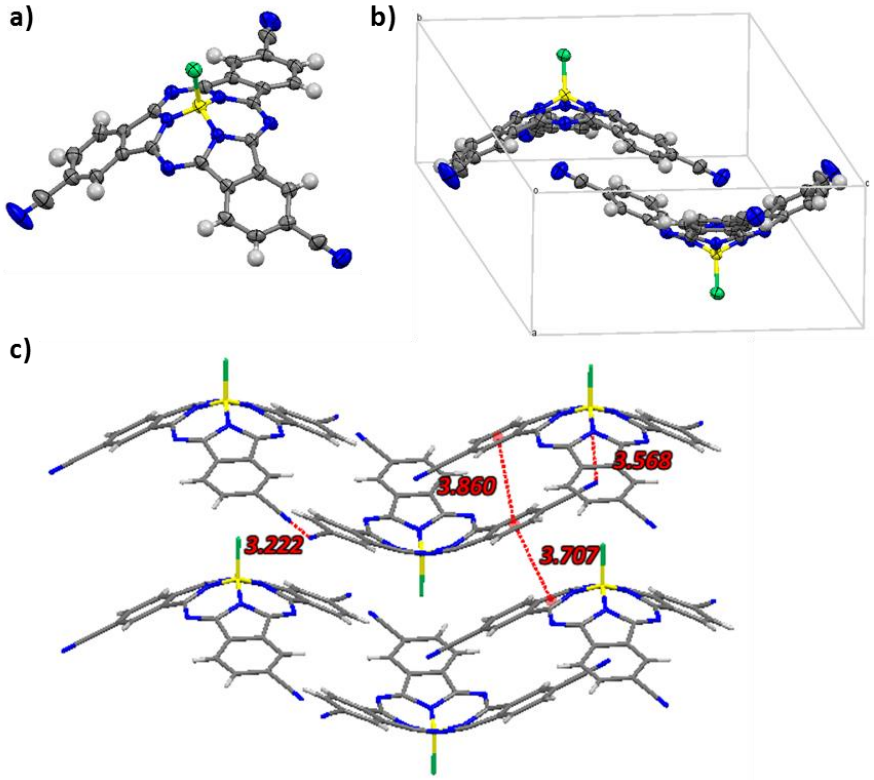

Figure 36. a) ORTEP drawing (50% probability level) of the molecular structure, b) unit cell, and c) solid-state arrangement of SubPc ***C*$_3$-26**.

[208] At this point, it is worth mentioning that preliminary studies on the arrangement of SubPcs ***C*$_3$-26** and ***C*$_1$-26** on an epitaxially grown master of graphene on ruthenium observed by STM have been carried out in collaboration with the research group of Amadez L. Vázquez de Parga. These studies show a different behavior of the two C_3 and C_1 regioisomers (each of them being a mixture of enantiomers) on surface. This work is currently in progress.

For the measurement of charge carrier mobilities of the target SubPc derivatives, drop-casted or spin-coated films from chloroform and toluene solutions of all five different compounds were initially prepared. However, poor solubility of SubPcs ***C*$_3$-26**, **27**, **28** and **29** in most processable solvents precluded the obtention of uniform thin films by this technique.[209] Thus, vapor-deposited films of SubPc derivatives **27**, **28** and **29**were prepared. Unfortunately, SubPc ***C*$_3$-26** decomposed during thermal vapor deposition and was discarded in FP-TRMC measurements. Better solubility of SubPc **8c** in chloroform allowed for the fabrication of both drop-casted and vapor-deposited uniform films of this derivative.

Upon photoexcitation at 355 nm pulses, all the dropcast **8c** and vapor-deposited **8c** and **27-29** displayed transient conductivity with a prompt rise and slow decay in FP-TRMC studies, though the maximum intensities were small (Figure 37). The maximum conductivity values $(\varphi\Sigma\mu)_{max}$, given by a photocarrier generation yield (φ) multiplied by the sum of charge carrier mobilities ($\Sigma\mu$), obtained for each sample are presented in Table 5 (see *Experimental Section* for details).

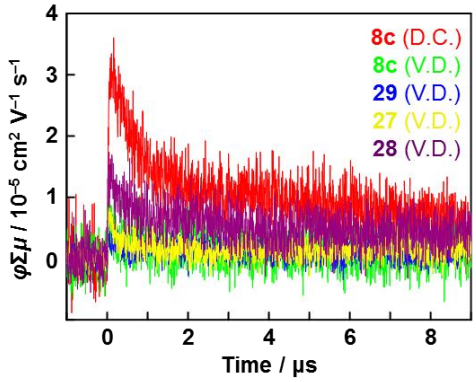

Figure 37. Typical transient conductivity profiles for dropcast film of **8c** (red) and vapor-deposited films of **8c** (green), **29** (blue), **27** (yellow), and **28** (purple) upon photoexcitation of 355 nm pulses.

Identical films used for FP-TRMC measurements were again used in TAS studies to quantify the generation efficiency of radical cations and/or anions. In TAS, all the five films exhibited a characteristic absorption band at around 580-650 nm, while obvious photo-bleach was present at 550-620 nm (see *Experimental Section*). When focusing on the kinetic traces of these absorption and bleach bands, decay profiles were confirmed due to the recombination

[209] For the production of solution-processed uniform thin films by drop-cast or spin-coating techniques, a solubility of *ca.* 20 mg mL^{-1} of the SubPc derivative in the processing solvent is highly advisable. Solubility tests of the SubPc derivatives studied in this section revealed solubility values under 5 mg mL^{-1} in all cases (except SubPc **8c**) in chloroform, acetone, toluene, xylene, chlorobenzene and dichlorobenzene.

of transient radical species. Although the appeared absorption band corresponds to the radical cation and/or anion species, the assignment has not been achieved. Thus, we focused on the photo-bleach to estimate the maximum charge carrier generation efficiency φ_{max}. Firstly, the kinetic similarity between the appeared absorption and photo-bleach suggests that the number of the generated radical cation/anion species mostly corresponds to that of converted neutral species. Furthermore, the kinetic profiles were almost similar between transient conductivity and transient absorption spectra at the photo-bleach band. After comparing the absorption coefficient of each SubPc derivative at its *Q* band maximum wavelength with the observed maximum TAS intensity, values of φ_{max} of 1.8-7.8 × 10^{-2} could be estimated.

Finally, from the values of these φ_{max} as well as $(\varphi\Sigma\mu)_{max}$, the sum of the charge carriers mobilities were evaluated. The calculated mobility values were 4.1 × 10^{-4} and 2.6 × 10^{-4} cm^2 V^{-1} s^{-1} for drop-cast and vapor-deposited films of reference SubPc F_{12}-SubPc-Cl **8c** respectively, 7.6 × 10^{-5} cm^2 V^{-1} s^{-1} for vapor-deposited films of reference SubPc Cl_6-SubPc-Cl **29** and 9.8 × 10^{-5} and 1.0 × 10^{-3} cm^2 V^{-1} s^{-1} for vapor-deposited films of novel chloro-dicyano-SubPcs **27** and **28** respectively (Table 5).

Table 5. Summary of maximum transient conductivity from FP-TRMC, maximum charge carrier generation efficiency from TAS, and estimated sum of charge carrier intrinsic mobilities.

SubPc	$(\varphi\Sigma\mu)_{max}$ (cm^2 V^{-1} s^{-1})	φ_{max} ($cm^{1/2}$ $V^{-1/2}$)	$\Sigma\mu$ (cm^2 V^{-1} s^{-1})
8c[a]	3.2 × 10^{-5}	7.8 × 10^{-2}	4.1 × 10^{-4}
8c[b]	8.8 × 10^{-6}	3.4 × 10^{-2}	2.6 × 10^{-4}
29[b]	4.7 × 10^{-6}	6.2 × 10^{-2}	7.6 × 10^{-5}
27[b]	7.0 × 10^{-6}	7.1 × 10^{-2}	9.8 × 10^{-5}
28[b]	1.5 × 10^{-5}	1.8 × 10^{-2}	1.0 × 10^{-3}

[a] Drop-cast film from toluene solution. [b] Vapor-deposited film.

First, comparing mobility values of reference SubPc **8c** in drop-cast or vapor-deposited films, it could be assumed that the former afforded higher mobility values because it generally produces films with higher crystallinity.

On the other hand, novel electron deficient dicyano-SubPcs **27** and **28** showed charge carrier intrinsic mobilities comparable to or larger than that observed for reference SubPcs **8c** and **29**.

In particular, while the mobility value of SubPc **27** was in between the two reference SubPcs, the estimated value of intrinsic mobility for SubPc **28** was four-fold and more than ten-fold higher than the values of **8c** and **29**, respectively. This fact, together with their excellent electron-accepting capabilities, confirms the potential of these new peripherally cyanated SubPc derivatives as appealing n-type organic semiconductors for application in the fabrication of photovoltaic devices.

1.5 Subphthalocyanines as acceptor materials in vacuum-evaporated PHJ solar cells

1.5.1 Background

1.5.1.1 Subphthalocyanines as donor material in PHJs

Pioneering work by Thompson and Forrest groups in 2006 introduced the use of SubPc **1** as a donor in combination with C_{60}, in a planar bilayer configuration that exhibited a more than doubled V_{OC} compared to a conventional copper Pc (CuPc)/C_{60} cell under 1 sun AM 1.5G simulated illumination (Figure 38).[210] The lower oxidation potential of SubPc resulted in an increase in the energy difference between the LUMO orbital of the acceptor-like material and the HOMO orbital of the donor-like material referred to as the interface energy gap (E_{DA})[211] by 400 meV that led to a high V_{OC} of 0.97 V and a power conversion efficiency of 2.1%.

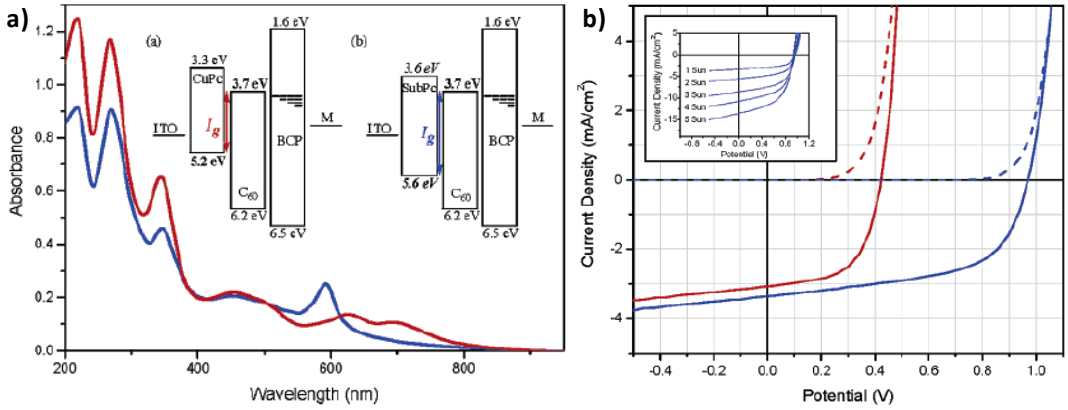

Figure 38. a) Absorbance spectra of stacked CuPc/C_{60}/BCP (red) and of SubPc **1**/C_{60}/BCP (blue). And schematic energy level diagram for devices with (a) CuPc or (b) SubPc as the donor layer. b) *J-V* characteristics of CuPc (red) and SubPc **1** (blue) under 1 sun AM 1.5G simulated illumination (solid) and in the dark (dashed). Inset: Intensity dependence of the SubPc device at 1-5 suns.

[210] Mutolo, K. L.; Mayo, E. I.; Rand, B. P.; Forrest, S. R.; Thompson, M. E. *J. Am. Chem. Soc.* **2006**, *128*, 8108.

[211] a) Wilke, A.; Endres, J.; Hörmann, U.; Niederhausen, J.; Schlesinger, R.; Frisch, J.; Amsalem, P.; Wagner, J.; Gruber, M.; Opitz, A.; Vollmer, A.; Brütting, W.; Kahn, A.; Koch, N. *Appl. Phys. Lett.* **2012**, *101*, 233301. b) Graham, K. R.; Erwin, P.; Nordlund, D.; Vandewal, K.; Li, R.; Ngongang Ndjawa, G. O.; Hoke, E. T.; Salleo, A.; Thompson, M. E.; McGehee, M. D.; Amassian, A. *Adv. Mater.* **2013**, *25*, 6076.

Since then, SubPc **1** has been extensively studied as a paradigmatic example of high-efficiency donor material in vacuum-evaporated PHJ solar cells in combination with fullerenes C_{60} and C_{70} as the acceptor counterpartner.[35,97e,212] Investigations on the interface electronic structure of C_{60} and SubPc **1** and the molecular orientation of SubPc on ITO,[213] or on the exciton diffusion lengths in the SubPc **1**/C_{60} devices, a critical parameter for the optimization of photovoltaic device performance,[139c] and studies directed to improve the performance of the active layer,[214] have been performed to improve these devices efficiencies.

In this regard, contacting layers and electrical contact materials play also a very important role in the correct energy level alignment for charge injection. The major gains from the inclusion of these interlayers result from their ability to reduce electron leakage currents, and increase the built-in potential by modifying the electrode work function. Bathocuproine (BCP) is a wide band gap material that has been used as an exciton-blocking barrier (EBL) between the acceptor C_{60} and the top electrode that prohibits excitons diffusing toward the cathode where they would otherwise be quenched, and it has been tested in SubPc-based OPV cells, notably increasing the *PCE*.[215] On the other hand, the incorporation of different small molecule hole selective contacts,[216] hole transporting polymer layers such as PEDOT:PSS,[217] and metal oxide hole extracting layers, namely MoO_3 and V_2O_x,[218] has shown to be an effective way of increasing both V_{OC} and J_{SC} in these devices. The sum of all these efforts has led to SubPc **1**/C_{60} devices with *PCE*s above 5%.[219]

---

[212] a) Gommans, H.; Cheyns, D.; Aernouts, T.; Girotto, C.; Poortmans, J.; Heremans, P. *Adv. Funct. Mater.* **2007**, *17*, 2653. b) Heremans, P.; Cheyns, D.; Rand, B. P. *Acc. Chem. Res.* **2009**, *42*, 1740.

[213] Cho, S. W.; Piper, L. F. J.; DeMasi, A.; Preston, A. R. H.; Smith, K. E.; Chauhan, K. V.; Sullivan, P.; Hatton, R. A.; Jones, T. S. *J. Phys. Chem. C* **2010**, *114*, 1928.

[214] Ryu, I. -H.; Kim, J.; Yim, S. -G. *J. Nanoelectron. Optoelectron.* **2010**, *5*, 191.

[215] a) Gommans, H.; Verreet, B.; Rand, B. P.; Muller, R.; Poortmans, J.; Heremans, P.; Genoe, J. *Adv. Funct. Mater.* **2008**, *18*, 3686. b) Liu, S. -W.; Lee, C. -C.; Su, W. -C.; Yuan, C. -H.; Shu, Y. -S.; Chang, W. -C.; Guo, J. -Y.; Chiu, C. -F.; Li, Y. -Z.; Su, T. -H.; Chen, K. -T.; Chang, P. -C.; Yeh, T. -H.; Liu, Y. -H. *ACS Appl. Mater. Interfaces* **2015**, *7*, 9262.

[216] a) Kulshreshtha, C.; Choi, J. W.; Kim, J. K.; Jeon, W. S.; Suh, M. C.; Park, Y.; Kwon, J. H. *Appl. Phys. Lett.* **2011**, *99*, 023308. b) Kulshreshtha, C.; Kim, G.-W.; Lampande, R.; Huh, D. -H.; Chaeb, M.; Kwon, J. -H. *J. Mater. Chem. A* **2013**, *1*, 4077.

[217] Huang, J.; Yu, J.; Qi, Y.; Jiang, Y. *Energy Procedia* **2011**, *12*, 508.

[218] a) Hancox, I.; Sullivan, P.; Chauhan, K. V.; Beaumont, N.; Rochford, L. A.; Hatton, R. A.; Jones, T. S. *Org. Electron.* **2010**, *11*, 2019. b) Girotto, C.; Voroshazi, E.; Cheyns, D.; Heremans, P.; Rand, B. P. *ACS Appl. Mater. Interfaces* **2011**, *3*, 3244. c) Hancox, I.; Rochford, L. A.; Clare, D.; Sullivan, P.; Jones, T. S. *Appl. Phys. Lett.* **2011**, *99*, 013304.

[219] Lin, C. -F.; Nichols, V. M.; Cheng, Y. -C.; Bardeen, C. J.; Wei, M. -K.; Liu, S. -W.; Lee, C. -C.; Su, W. -C.; Chiu, T. -L.; Han, H. -C.; Chen, L. -C.; Chen, C. -T.; Lee, J. -H. *Sol. Energy Mater. Sol. Cells* **2014**, *122*, 264.

PHJ solar cells employing donor SubPc **1** and a non-fullerene acceptor have also been reported. Copper hexadecafluoro-Pc (F_{16}CuPc) has been used as an electron accepting layer in vacuum-evaporated bilayer small molecule OPV cells.[220] Solution-processable electron deficient truxenone-based derivatives have been synthesized and studied in PHJ devices with evaporated SubPc **1** as the donor counterpart by Nielsen *et al.*,[221] and an N-ethylated barbituric acid end-capped bithiophene derivative has been also investigated as electron acceptor in SubPc donor based PHJs, with *PCEs* as high as 2.6%.[222]

On the other hand, a few other SubPc derivatives aside from SubPc **1** have been tested as p-type materials in conjunction with acceptor C_{60} in PHJs (Chart 7). Bender *et al.* have demonstrated that vacuum-evaporated pentafluorophenoxy boron SubPc SubPc-OPhF_5 can function either as an electron donor or an electron acceptor in PHJ cells when matched with C_{60} or SubPc **1** respectively in devices that display V_{OC} close to or in excess of 1 V and reasonable *PCEs* around 1-1.5%.[54e] The same group has recently described the preparation of a family of aryl-substituted SubPcs in their axial position and their dual functionality in OPV devices as p-type or n-type materials.[223]

Other SubPc derivatives with enhanced solubility and low tendency to aggregate have been prepared to enable the formation of high quality thin films via solution processing for OPVs application. Thus for example, by using a soluble axially substituted 2-allylphenol SubPc derivative as donor and C_{60} as acceptor, PHJ solar cells have been demonstrated with power conversion efficiencies of over 1.7%, which represented one of the highest efficiencies for devices with solution processable small molecules to that date.[224] Thin films of axially substituted SubPcs with bithiophene and quaterthiophene moieties, prepared also via solution processing, can act as the electron donor in bilayer OPVs with evaporated C_{60} as the electron acceptor, with modest efficiencies around 1%.[72f] Finally, our group has described the synthesis of a tricationic SubPc that can be employed as light-harvesting and donor material in a solution-processed ionic solid-state OPV, with an efficiency of 0.5%.[73] Regarding SubPc derivatives with extended conjugation, subnaphthalocyanine chloride SubNcCl was introduced as a new donor material concurrently by Verret *et al.* and Ma *et al.* in evaporated and solution-

[220] Yang, J. L.; Schumann, S.; Hatton, R. A.; Jones, T. S. *Org. Electron.* **2010**, *11*, 1399.
[221] a) Nielsen, C. B.; Voroshazi, E.; Holliday, S.; Cnops, K.; Rand, B. P.; McCulloch, I. *J. Mater. Chem. A* **2013**, *1*, 73. b) Nielsen, C. B.; Voroshazi, E.; Holliday, S.; Cnops, K.; Cheyns, D.; McCulloch, I. *J. Mater. Chem. A* **2014**, *2*, 12348.
[222] Sullivan, P.; Collis, G. E.; Rochford, L. A.; Arantes, J. F.; Kemppinen, P.; Jones, T. S.; Winzenberg, K. N. *Chem. Commun.* **2015**, *51*, 6222.
[223] Bonnier, C.; Josey, D. S.; Bender, T. P. *Aust. J. Chem.* **2015**, *68*, 1750.
[224] Ma, B.; Miyamoto, Y.; Woo, C. H.; Frechet, J. M. J.; Zhang, F.; Liu, Y. *Proc. SPIE* **2009**, *7416*, 74161E/1.

processed PHJ cells of with acceptor C_{60}.[225] The combination of a strong red absorption, close to 700 nm, and high V_{OC} makes SubNcCl an interesting material for organic solar cells.[206,216b,226]

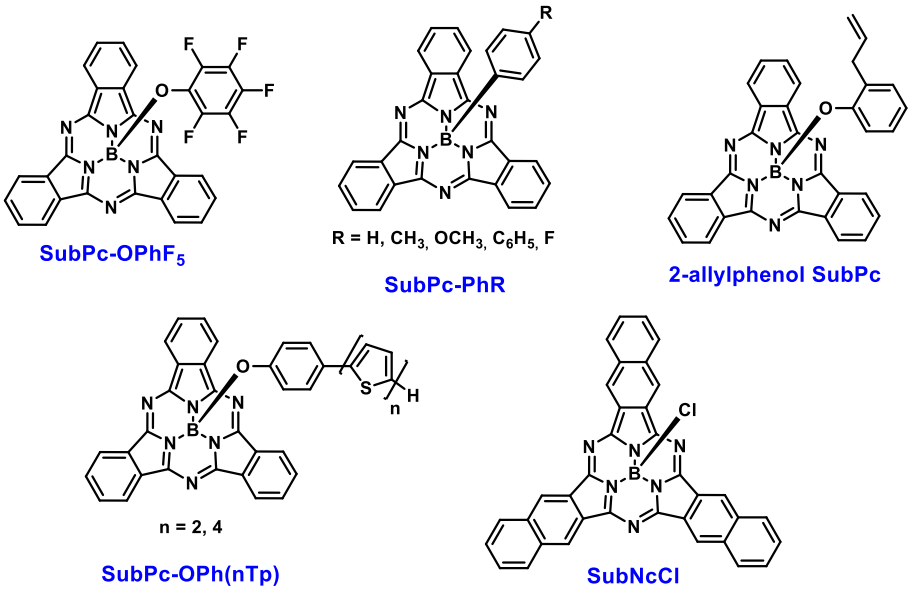

Chart 7. Chemical structure of different SubPc derivatives reported in the literature that have been applied as donor materials in PHJ solar cells.

1.5.1.2 Subphthalocyanines as acceptor material in PHJs

As mentioned before, SubPc derivatives can behave both as donor or acceptor as a function of the counter-partner. Germinal work on the performance of fullerene-free OPVs or "all SubPc-based devices" made using electron deficient SubPcs as the acceptor material instead of C_{60}, and SubPc **1** as the donor one, was reported by Aernouts, Torres and co-workers.[227] In this first report, the photovoltaic performance of peripherally perfluorinated F_{12}-SubPc-Cl **8c** and F_{12}-SubPc-F as acceptor materials was characterized in a range of D/A heterojunctions, using SubPc **1**, SubNcCl, AlPcCl, CuPc, and pentacene as donors. Both electron and hole transfer

[225] a) Verreet, B.; Schols, S.; Cheyns, D.; Rand, B. P.; Gommans, H.; Aernouts, T.; Heremans, P.; Genoe, J. *J. Mater Chem.* **2009**, *19*, 5295. b) Ma, B.; Woo, C. H.; Miyamoto, Y.; Fréchet, J. M. J. *Chem. Mater.* **2009**, *21*, 1413.
[226] Cheyns, D.; Rand, B. P.; Heremans, P. *Appl. Phys. Lett.* **2010**, *97*, 033301.
[227] Gommans, H.; Aernouts, T.; Verreet, B.; Heremans, P.; Medina, A.; Claessens, C. G.; Torres, T. *Adv. Funct. Mater.* **2009**, *19*, 3435.

between donor and acceptor materials were demonstrated and *PCEs* of 0.96% were found for the configuration ITO/SubPc **1**/F_{12}-SubPc-F/BCP/Al, with an open-circuit bias of 940 mV.

Another example of high-voltage fullerene-free OPVs has been reported by Jones *et al.*[197] The authors demonstrated the use of selective halogenation as a method to tune the energy levels of SubPc derivatives in order to maximize V_{OC} when used as an acceptor material in an organic heterojunction device with SubPc **1** as donor (Figure 39). In particular, they presented peripherally hexachlorinated Cl_6-SubPc-Cl **29** as the most promising contender for the replacement of C_{60} in small molecule, photovoltaic devices in conjunction with SubPc donors, due to an exceptionally high V_{OC}, *ca.* 1.3 V, resulting from a maximized E_{DA}. However, low quantum efficiencies and the overlapping absorption profiles of the donor and acceptor materials resulted in low photocurrent generation.

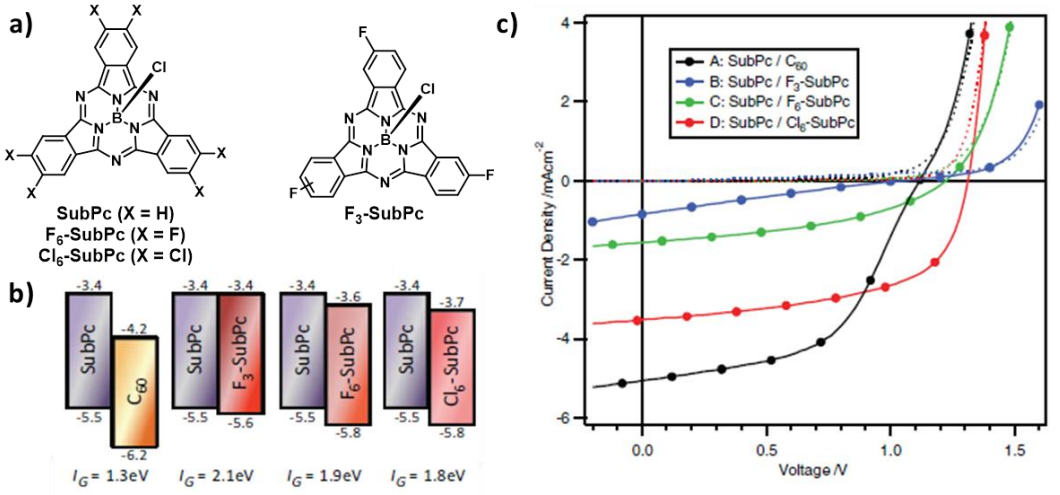

Figure 39. a) Chemical structure of SubPc derivatives used in ref 197. b) Frontier orbital energy level diagrams of a typical SubPc **1**/C_{60} heterojunction and the series of SubPc **1**/halogenated-SubPc heterojunctions showing the resulting interface gap energy, E_{DA} (HOMO and LUMO energy values directly extracted from ref. 197). c) *J-V* curves under 1 sun AM 1.5G simulated illumination for the series of heterojunction devices A-D. Respective dark current curves are shown as dotted lines.

Verreet *et al.* have demonstrated that fluorinated SubPc fused dimer **2** as a mixture of the *syn* and *anti* topoisomers is an exceptional novel acceptor material with complementary absorption to the donor material SubPc **1**.[228] The 120 nm red shift of the absorption maximum

[228] Verreet, B.; Rand, B. P.; Cheyns, D.; Hadipour, A.; Aernouts, T.; Heremans, P.; Medina, A.; Claessens, C. G.; Torres, T. *Adv. Energy Mater.* **2011**, *1*, 565.

of **2** with respect to that of its parent F_{12}-SubPc-Cl led to an enhanced J_{SC} while preserving the high V_{OC} characteristic of SubPc-based devices. In order to integrate this new material in PHJ solar cells, the authors compared multiple solar cell architectures and they found that it is crucial to optimize the electron extracting contact. Thus, the best efficiency was achieved by introducing a C_{60} interlayer in between SubPc dimer and BCP yielding a *PCE* of 4%, with a V_{OC} of 950 mV. The spectral response and reflection data showed that the SubPc **1**/SubPc dimer **2** interface is the photoactive one, whereas the fullerene mainly functions as a transport layer which enhances electron extraction.

Other fullerene-free OPVs based on a SubPc combined with other kinds of small molecules have been reported. Thus, regarding acceptor SubPc-based devices, single-heterojunction OPV cells consisting of tetracene and pentacene as donor materials and SubPc **1** or Cl_6-SubPc-Cl **29** as acceptor compounds have been described by the groups of Jones and Bender,[203,229] demonstrating the ambipolar characteristics of SubPc derivatives. Besides, perchlorinated Cl_{12}-SubPc-Cl, with deep HOMO and LUMO levels, has been used as an efficient triplet harvester when paired with pentacene in OPV devices, giving rise to more than tripled J_{SC} when compared with other SubPc acceptors.[230] An impressive example of a three-layer architecture comprising two non-fullerene acceptors, namely SubNcCl and SubPc **1**, and donor α-sexithiophene (α-6T), in which an energy-relay cascade enables an efficient two-step exciton dissociation process, has been reported by Cnops *et al*.[163] *PCEs* as high as 8.40%, record efficiencies for non-fullerene OSCs, are achieved due to a high V_{OC} of 0.96 V, a J_{SC} of 14.55 mA cm^{-2}, and a *FF* of 61%. The three photoactive materials have complementary optical absorption profiles and both *IQE* and *EQE* spectra importantly show efficient photocurrent generation by all three absorbing materials (Figure 40).

[229] Beaumont, N.; Cho, S. W.; Sullivan, P.; Newby, D.; Smith, K. E.; Jones, T. S. *Adv. Funct. Mater.* **2012**, *22*, 561.
[230] Castrucci, J. S.; Josey, D. S.; Thibau, E.; Lu, Z. -H.; Bender, T. P. *J. Phys. Chem. Lett.* **2015**, *6*, 3121.

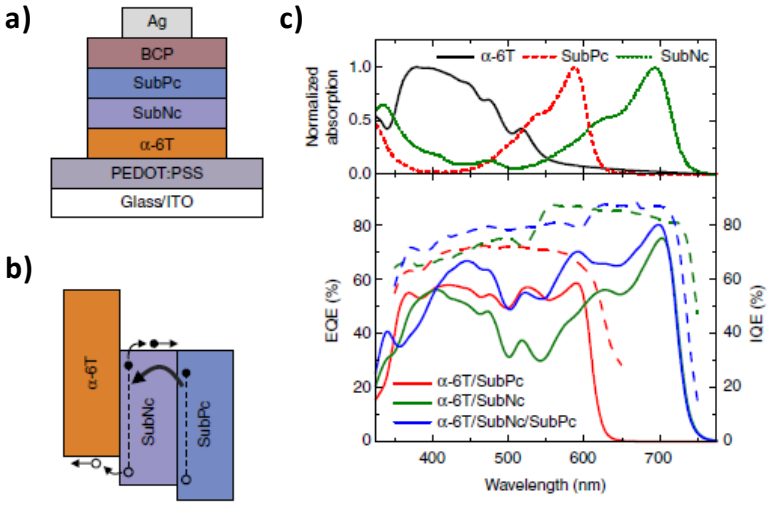

Figure 40. a) Schematic representation of the device architecture. b) Energy-level diagram of the active layers illustrating the two-step exciton dissociation mechanism. c) Spectral response of fullerene-free OPV devices: the absorption spectra of the three active materials complement each other to effectively harvest solar light (top); the measured *EQE* (solid lines) and *IQE* (dashed lines) spectra show efficient photocurrent generation by all three absorbing materials (down).

Recently, we have presented together with Cheyns and co-workers an optimization of several aspects of PHJ solar cells based on SubNcCl as a donor material and hexachlorinated Cl_6-SubPc-Cl **29** as an acceptor material.[206] This configuration allows for the simultaneous increase of the J_{SC}, *FF*, and V_{OC} compared to cells with fullerene acceptors, due to the complementary absorption of Cl_6-SubPc-Cl versus SubNcCl, reduced recombination at the heterointerface, either of CT-states or of trapped charges, and improved energetic alignment. Furthermore, insertion of a thin layer of diindeno[1,2,3-cd:1′,2′,3′-lm]perylene (DIP), previously used as a donor material in organic solar cells,[231] at the anode results in a very significant 60% increase in photocurrent owing to reduced exciton quenching at the PEDOT:PSS/SubNcCl interface. The simultaneous improvement of all three solar cell parameters results in a high *PCE* of 6.4% for a non-fullerene PHJ cell (Figure 41).

[231] a) Verreet, B.; Malinowski, P. E.; Niesen, B.; Cheyns, D.; Heremans, P.; Stesmans, A.; Rand, B. P. *Appl. Phys. Lett.* **2013**, *102*, 043301. b) Wagner, J.; Gruber, M.; Wilke, A.; Tanake, Y.; Topczak, K.; Steindamm, A.; Hörmann, U.; Opitz, A.; Nakayama, Y.; Ishii, H.; Pflaum, J.; Koch, N.; Brütting, W. *J. Appl. Phys.* **2012**, *111*, 054509.

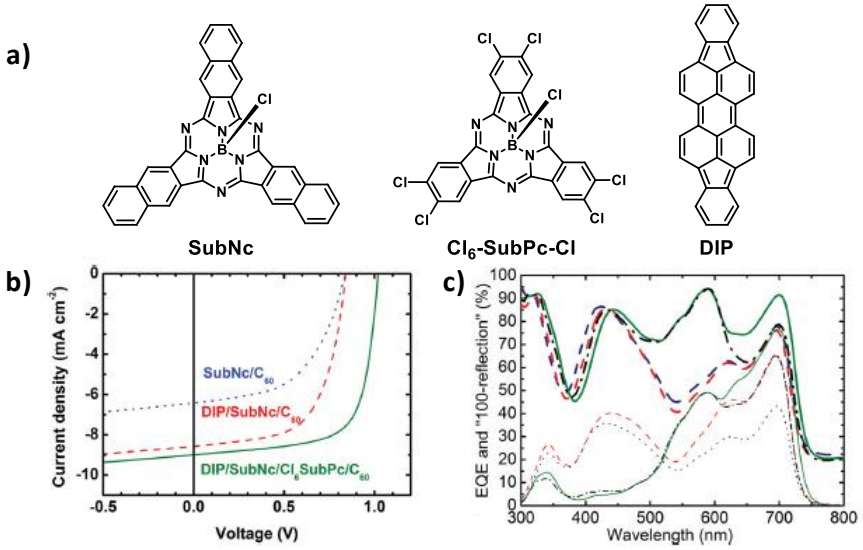

Figure 41. a) Molecular structure of SubNc, Cl_6-SubPc-Cl and DIP. b) *J-V* characteristics under 100 mW cm^{-2} AM 1.5G simulated solar illumination. c) *EQE* (thin curves) and absorption spectra (100 – R, in %, thick curves) of solar cells with the structure: ITO/PEDOT:PSS/8 nm SubNc/C_{60}/BCP/Ag (blue dotted curve); ITO/PEDOT:PSS/DIP/8 nm SubNc/C_{60}/BCP/Ag (red dashed curve) and ITO/PEDOT:PSS/DIP/x nm SubNc/Cl_6SubPc/C_{60}/BCP/Ag (x = 8: black dash-dotted curve; x = 12: green solid curve).

To sum up, several reports in the literature confirm that SubPc derivatives can be employed as well-performing acceptor materials, provided that the selected donor material supplies sufficient energy offsets to enable efficient exciton dissociation at the heterojunction. On the other hand, the V_{OC} of OPV devices has been shown to scale with the E_{DA}. The electronic properties and the n-type character of SubPc molecules can be modulated by the introduction of electron-withdrawing substituents in the isoindole units, being peripheral halogenation the strategy followed to shift the molecular orbital energy levels of SubPcs. Because neither peripheral nor axial substitutions alter the conjugated system of the molecule, the optical band gap and absorption spectrum of SubPc derivatives remain largely unchanged. As a consequence, the class of SubPc molecules is highly suited for use in investigating the influence of the acceptor's energetic position on OPV device performance. Moreover, the easy tunability of their energy levels simplifies the optimization of interface energetics in D/A heterojunctions. Selecting donor materials with absorption profiles complementary to those of the SubPc acceptors and improving energetic alignment have already resulted in efficiencies over 6%, employing the extended SubPc derivative, SubNcCl, and partially chlorinated Cl_6SubPCl as donor and acceptor materials respectively.[206]

It is our strong belief that further efficiency enhancement could be achieved by fine-tuning the HOMO level and especially the LUMO level of the acceptor compound in the corresponding active layer. Herein, we describe the results obtained in the systematic study of the combination of four small-band-gap donor materials with four peripherally substituted SubPc derivatives that have been carefully designed as acceptors in vacuum-evaporated PHJ organic solar cells and we explore how the device performance depends on the LUMO energy level of these acceptors. This work has been developed in collaboration with the research group of Tom Aernouts in the IMEC in Leuven.

1.5.2 Results and discussion

In our research group, two different SubPc-Cl derivatives have been already described as n-type materials in fullerene-free OPVs: F_{12}-SubPc-Cl **8c**[227] and Cl_6-SubPc-Cl **29**.[206] In halogenated SubPcs, the electronegativity of the halogen atoms has the effect of lowering the energy levels compared to unsubstituted SubPc **1**. An increase in the number of halogen atoms leads to an increase in the magnitude of this shift.[197] As a consequence, perfluorinated F_{12}-SubPc-Cl **8c** results in a large shift of around 0.6 eV in the frontier orbital energies compared to **1**, which is in the threshold for the attainment of reasonable V_{OC} values when matched with SubPc-based donors. On the other hand, Cl_6-SubPc-Cl **29** generates a HOMO and LUMO offset of at least 0.3 eV when faced with **1**. Besides, these two SubPcs present analogous *Q* band features, peaking at wavelengths around 570 nm, so they constituted ideal acceptor molecules to include them in this study. The choice of other two SubPc derivatives was imposed then by two aspects, a similar absorption spectra and a slightly lower or an intermediate electron-withdrawing character compared to SubPcs **8c** and **29**. With this aim, two novel SubPc derivatives were envisioned, an unsymmetrically substituted SubPc bearing two chlorine atoms at two isoindole units, Cl_4-SubPc-Cl **30**, as a compound with a slight increase in the LUMO energy relative to Cl_6-SubPc-Cl **29**, and the evaporable analogous of tricyano-SubPc **22**, $(CN)_3$-SubPc-F **31**, bearing a fluorine atom in the axial position, with an electron-withdrawing character presumably intermediate between those of Cl_6-SubPc-Cl and F_{12}-SubPc-Cl.

1.5.2.1 Synthesis and characterization of subphthalocyanines 8c, 29, 30, and 31

Unsymmetrical Cl_4-SubPc-Cl **30** was prepared by a statistical condensation reaction of 4,5-dichlorophthalonitrile and phthalonitrile in a 2:1 ratio in 1 M BCl_3 in refluxing *p*-xylene, observing the formation of all four symmetrical and unsymmetrical SubPcs by TLC. SubPc **30** was subsequently separated from the crude mixture by column chromatography on silica gel, obtaining the desired product in 19% yield (Scheme 14).

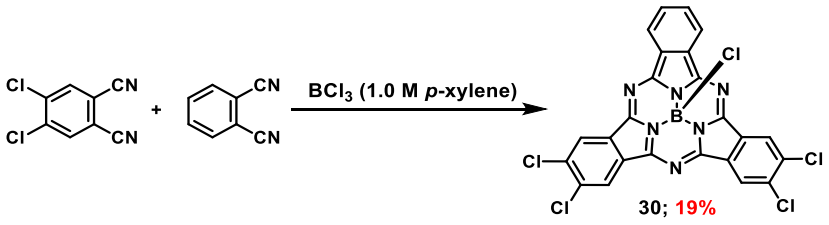

Scheme 14. Synthesis of SubPc **30**.

The synthesis of $(CN)_3$-SubPc-F **31** (as a 1:3 mixture of regioisomers C_3/C_1) was carried out by adapting the method of M. V. Fulford *et al.*[42b,64] Thus, the reaction of SubPc **22** with 25 equiv of $Et_2O{\cdot}BF_3$ in refluxing toluene for 5 h gave rise to SubPc **31** in 91% yield (Scheme 15).

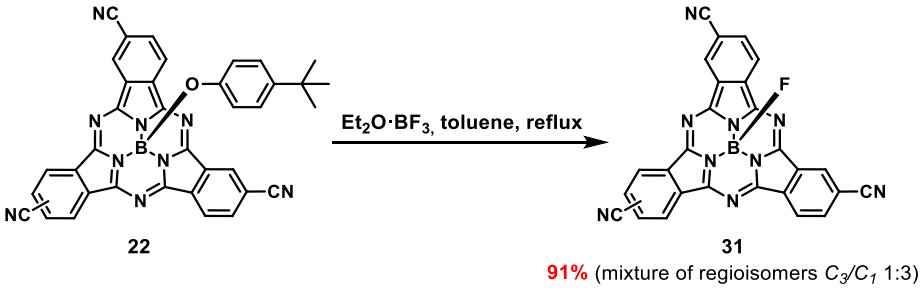

Scheme 15. Synthesis of SubPc **31**.

The structure of SubPcs **30** and **31** was established on the basis of their spectroscopic features, namely ^{1}H-NMR, ^{19}F-NMR, UV-vis, FT-IR, MS and HR-MS.

Figure 42 shows the normalized absorption spectra of $(CN)_3$-SubPc-F **31**, Cl_6-SubPc-Cl **29**, Cl_4-SubPc-Cl **30** and F_{12}-SubPc-Cl **8c**. As expected, all four SubPc compounds feature almost identical absorption spectra due to the scarce influence of the peripheral substituents in the π-conjugated system of the macrocycle, with *Q* band maxima peaking at 572, 572, 573 and 574 nm respectively. Furthermore, *Q* band *ε* values present minor differences, going from 3-4 x 10^4 M^{-1} cm^{-1} in SubPcs **8c**, **29** and **30** to 5 x 10^4 M^{-1} cm^{-1} in SubPc **31**.

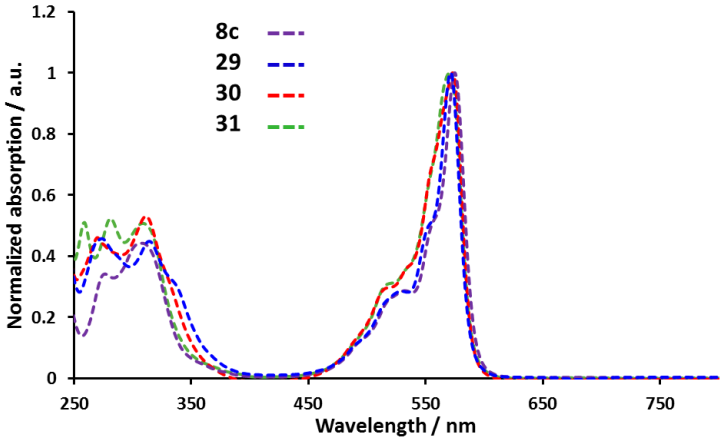

Figure 42. Normalized UV-vis absorption spectra in chloroform of SubPcs **8c**, **29**, **30** and **31**.

1.5.2.2 Electrochemical studies and calculation of HOMO and LUMO levels of subphthalocyanines 8c, 29, 30 and 31

Electrochemical properties of SubPcs **8c**, **29**, **30** and **31** were investigated by cyclic voltammetry, square-wave voltammetry and differential pulse voltammetry measurements in THF solution (0.1 M $TBAPF_6$). All potential values quoted throughout this section have been referred to the Fc/Fc^+ couple.

Figure 43 shows the voltammograms of the compounds studied and the electrochemical data is summarized in Table 6. As expected, in halogenated SubPcs **8c**, **29** and **30**, first reduction potentials can be correlated with the number of halogen substituents in the periphery of the macrocycle. As a result, novel Cl_4-SubPc-Cl **30** display a first reduction wave at -1.26 V, while half-wave potentials of Cl_6-SubPc-Cl **29** and F_{12}-SubPc-Cl **8c** appear at -1.19 and -0.95 V respectively. Interestingly, compared to their SubPc analogous **6c** and **7c** bearing a 4-*tert*-butylphenoxy group in axial position, the effect of the axial chlorine atom provokes a 60-80 mV shift of this first reduction process to less negative potentials. $(CN)_3$-SubPc-F **31** features up to three reversible reduction waves, with a first wave emerging at -1.09 V. As it was envisaged, this novel SubPc presents a reduction capability in between SubPcs **29** and **8c**, arising then as a very suitable compound for this study. The anodic scans of all these compounds reveal one irreversible oxidation process at potential values in between 0.87-1.06 V inversely influenced by the substituents nature.

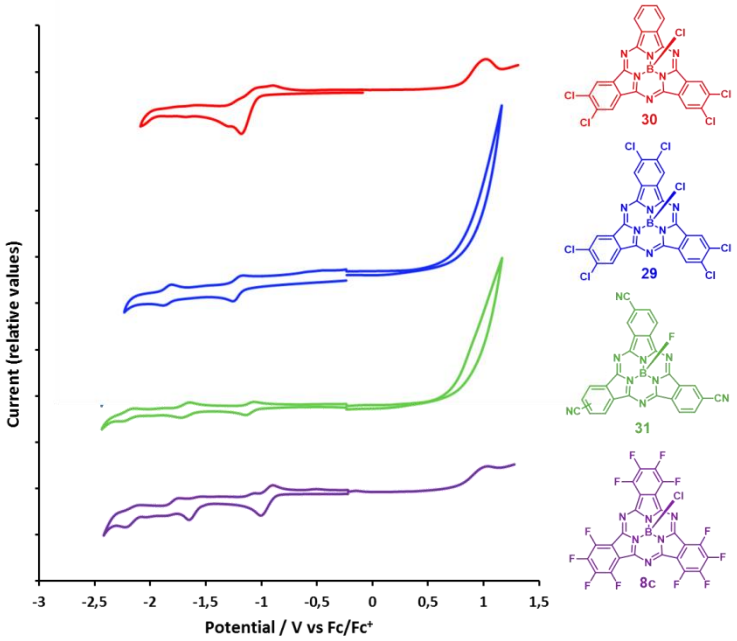

Figure 43. Cyclic voltammograms (OSW voltammogram in the anodic window of **30** and **8c**) of SubPcs **8c**, **29**, **30** and **31** in THF.

Calculation of the energy level of LUMO orbitals of SubPcs **8c**, **29**, **30** and **31** *vs.* vacuum were obtained from CV experiments. However, unlike the numerical relation depicted in section 1.4.3.5 (Equation 5), in this particular case the LUMO levels were calculated using the Ferrocene couple HOMO value of - 4.8 eV:[196]

$$E_{HOMO/LUMO} = -4.8 - E^{1}_{1/2,ox/red}(vs.\,Fc/Fc^{+})(eV) \qquad \text{(Eqn. 11)}$$

As it has been mentioned before, this value has been revised some times since it was calculated. Nonetheless, energy levels of the donor counterparts employed in this study were taken from literature and, from our understanding, energy levels of acceptor SubPcs were more conveniently estimated in such a way to allow comparison. HOMO energy values were indirectly calculated from the LUMO energy value and the optical band gap $E_{g,opt}$, applying Equation 6. Molecular orbitals energy values are summarized in Table 6.

Table 6. Electrochemical data (in mV *vs.* Fc/Fc^+) in THF and experimental HOMO-LUMO energy levels data (in eV) of SubPcs **8c**, **29**, **30** and **31**.

SubPc	$E^1_{1/2,red}$ (mV)	$E^2_{1/2,red}$ (mV)	$E^3_{1/2,red}$ (mV)	E^1_{ox} [a] (mV)	E_{LUMO} (eV)	E_{HOMO} (eV)	$E_{g,opt}$ [b] (eV)
30	-1261	-	-	869[d]	-3.54	-5.70	2.16 (575)
29	-1186	-1820	-	1060[d]	-3.61	-5.77	2.16 (575)
31	-1091	-1675	-2190	928[d]	-3.71	-5.87	2.16 (574)
8c	-945	-1617[c]	-	1044[d]	-3.85	-6.00	2.15 (577)

[a] Since these oxidation processes are irreversible, only anodic peak potentials are reported. [b] Intersection wavelength in nm of the normalized absorption and emission spectra in brackets. [c] Since these reduction processes are irreversible, only cathodic peak potentials are reported. [d] Peak oxidation potential by OSWV.

1.5.2.3 Photovoltaic performance of PHJ solar cells containing subphthalocyanines 8c, 29, 30 and 31 as acceptor materials

Planar-heterojunction devices containing the SubPc derivatives **8c**, **29**, **30** and **31** as acceptors, with LUMO energies ranging from -3.54 to -3.85 eV, were fabricated. These non-fullerene acceptors were combined with the small-band-gap donor materials shown in Figure 44b, namely lead phthalocyanine (PbPc), zinc phthalocyanine (ZnPc), SubNc, and zinc tetrafluorophthalocyanine (F_4-ZnPc). These donor molecules were selected to span a range of HOMO energy levels (-5.0, -5.11, -5.37, and -5.46 eV, respectively)[232] (Figure 44). Because of their smaller band gaps, all of the donor materials have absorption spectra complementary to those of the SubPc acceptors (Figure 45).

[232] a) Ikushima, A. J.; Kanno, T.; Yoshida, S.; Maeda, A. *Thin Solid Films* **1996**, *273*, 35. b) Riede, M. K.; Uhrich, C.; Widmer, J.; Timmreck, R.; Wynands, D.; Schwartz, G.; Gnehr, W. -M.; Hildebrandt, D.; Weiß, A.; Hwang, J.; Sundarraj, S.; Erk, P.; Pfeiffer, M.; Leo, K. *Adv. Funct. Mater.* **2011**, *21*, 3019. c) Barito, A.; Sykes, M. E.; Huang, B.; Bilby, D.; Frieberg, B.; Kim, J.; Green, P. F.; Shtein, M. *Adv. Energy Mater.* **2014**, *4*, 1400216.

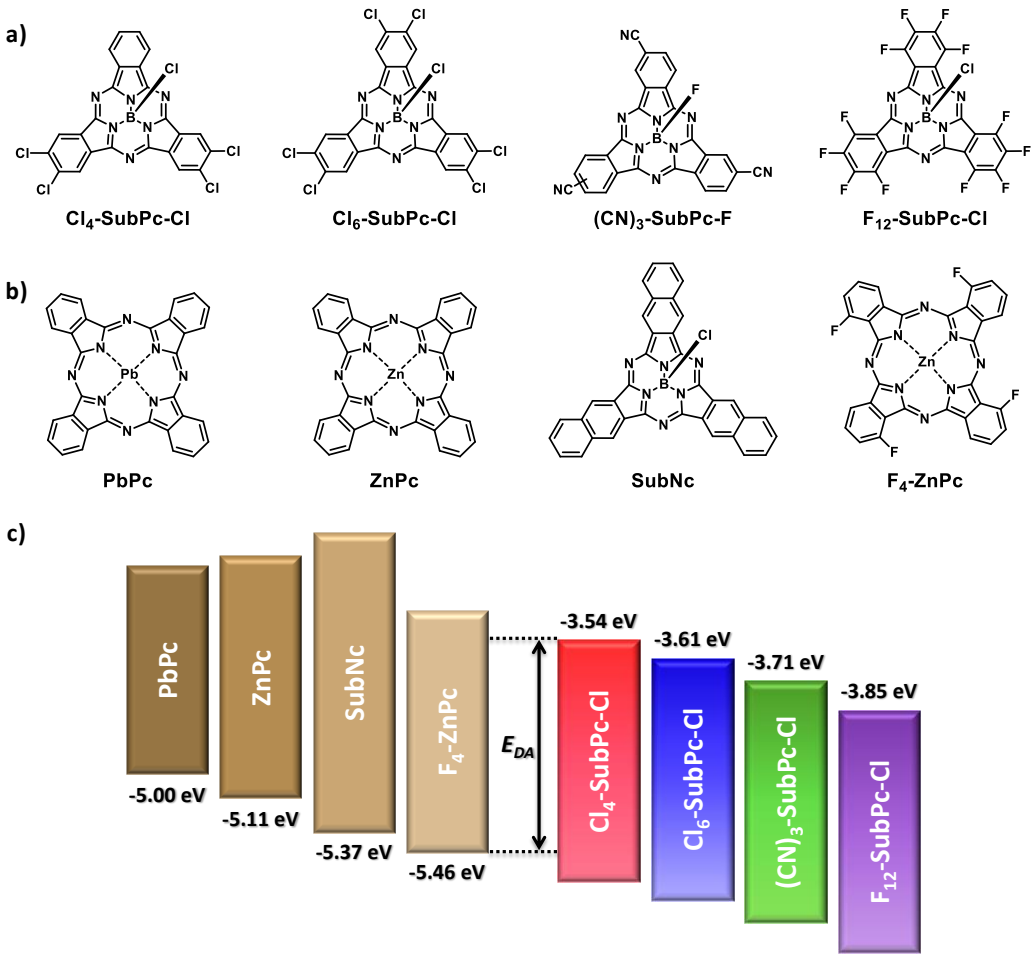

Figure 44. Structural and energetic properties of the active organic molecules used in this work. a) Molecular structures of the SubPc acceptors. b) Molecular structures of the donor materials. c) Schematic representation of the LUMO energy levels of the SubPc acceptors, the HOMO energy levels of the donor materials, and the interface band gap E_{DA}.

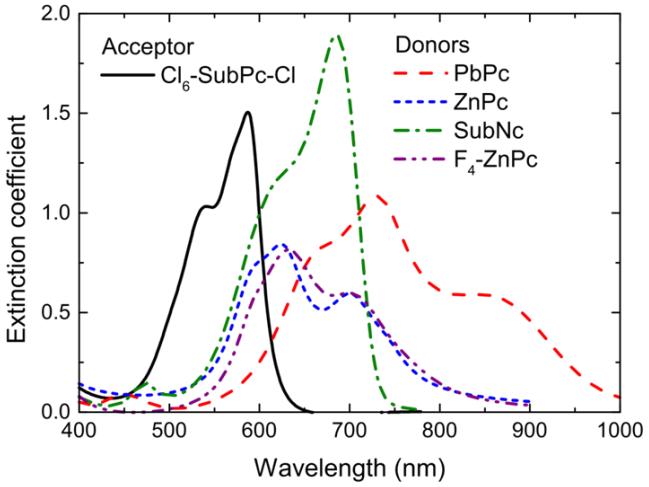

Figure 45. Extinction coefficients of the donor materials, determined by spectroscopic ellipsometry on thin films on Si/SiO_2 substrates (acceptor material Cl_6-SubPc-Cl is included for comparison).

A 14 nm thick donor layer was deposited for SubNc, while a thickness of 40 nm was chosen for the other phthalocyanine donors. The thickness of the acceptor layer was set at 8 nm, irrespective of which SubPc derivative was used. Insertion of 5 nm of MoO_3 at the anode interface ensured good hole extraction due to an improved energy level alignment with the donor materials.[233] A 50 nm thick 1:1 blend of bathocuproine (BCP) and fullerene C_{60} was used as the electron transport layer (ETL). The low optical absorption and high conductivity of this layer ensured sufficient optical spacer thickness without compromising electron extraction.[234] It has been shown that the presence of fullerene in the ETL does not actively contribute to the photocurrent generation in devices with a SubPc derivative as the acceptor.[206,228] The effect of the SubPc acceptor on device performance was studied by current density-voltage (*J-V*) measurements under simulated solar illumination of 100 mW cm^{-2} (Figure 46) and by external quantum efficiency (*EQE*) measurements (Figure 47). The combination of each SubPc derivative with several donor materials resulted in a large set of data (Table 7), enabling us to assess the impact of the heterojunction energetics on the V_{OC}, *FF*, and photocurrent.

[233] Hancox, I.; Sullivan, P.; Chauhan, K. V.; Beaumont, N.; Rochford, L. A.; Hatton, R. A.; Jones, T. S. *Org. Electron.* **2010**, *11*, 2019.
[234] Bartynski, A. N.; Trinh, C.; Panda, A.; Bergemann, K. J.; Lassiter, B. E.; Zimmerman, J. D.; Forrest, S. R.; Thompson, M. E. *Nano Lett.* **2013**, *13*, 3315.

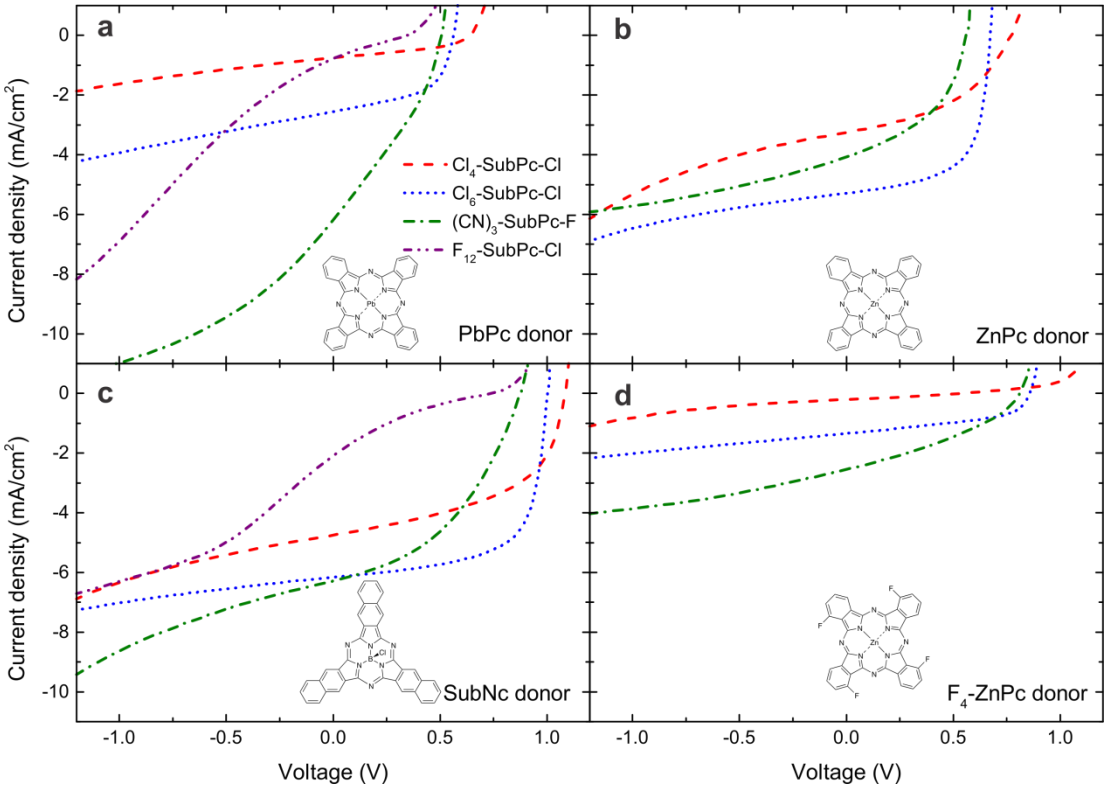

Figure 46. Current density-voltage measurements under simulated solar illumination of all heterojunction devices tested in this work. In each panel several SubPc derivative acceptors are combined with a small-bandgap donor material: a) PbPc, b) ZnPc, c) SubNc, and d) F_4-ZnPc.

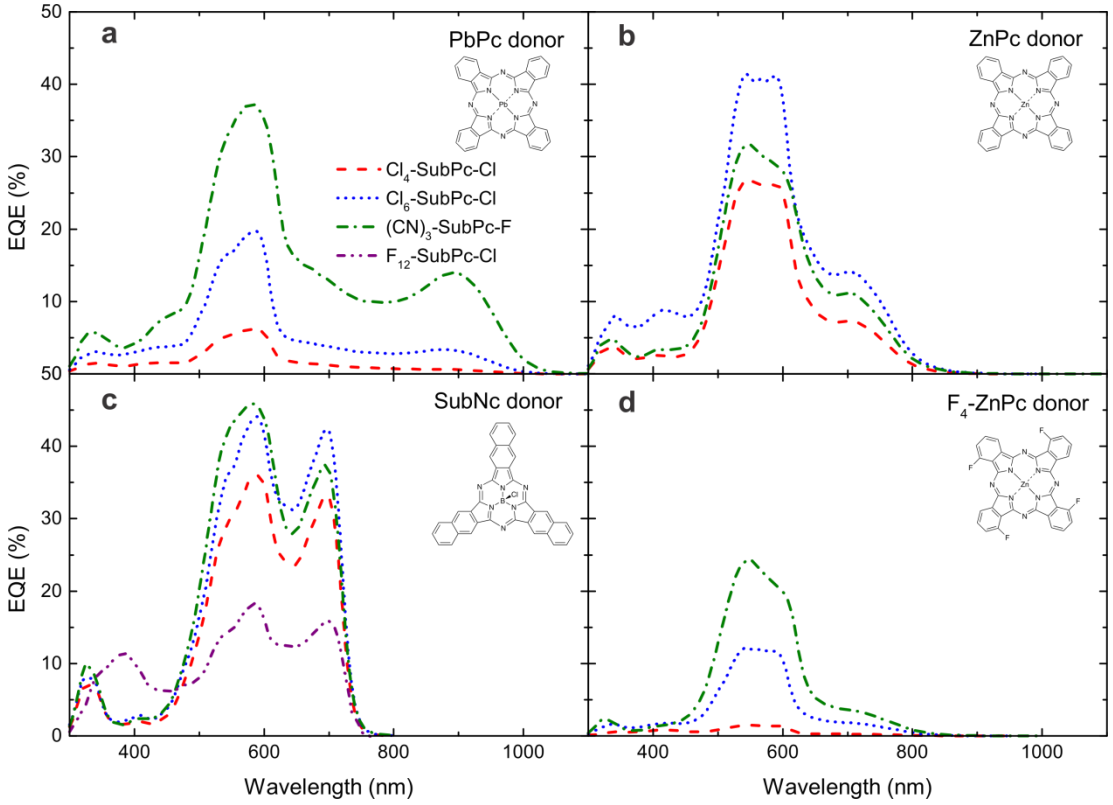

Figure 47. External quantum efficiency *EQE* of all heterojunction devices tested in this work. In each panel several SubPc derivative acceptors are combined with a small-bandgap donor material: a) PbPc, b) ZnPc, c) SubNc, and d) F_4-ZnPc.

Table 7. Interface energy gap (E_{DA}) and *J-V* characteristics for each heterojunction device studied in this work. Average values (and standard deviations) of V_{OC}, J_{SC}, *FF*, and *PCE* are calculated for at least 3 devices on a single substrate.

Donor	Acceptor	E_{DA} (eV)	V_{OC} (V)	J_{SC} (mA cm^{-2})	*FF* (%)	*PCE* (%)
PbPc	**F_{12}-SubPc-Cl**	1.15	0.33 (± 0.01)	0.88 (± 0.07)	23.4 (± 0.2)	0.07 (± 0.01)
	$(CN)_3$-SubPc-F	1.29	0.50 (± 0.01)	6.00 (± 0.1)	32.5 (± 0.4)	0.97 (± 0.02)
	Cl_6-SubPc-Cl	1.39	0.57 (± 0.01)	2.51 (± 0.03)	53.9 (± 0.5)	0.76 (± 0.01)
	Cl_4-SubPc-Cl	1.46	0.64 (± 0.01)	0.76 (± 0.01)	40.1 (± 1.4)	0.19 (± 0.01)
ZnPc	**$(CN)_3$-SubPc-F**	1.40	0.56 (± 0.01)	4.07 (± 0.04)	43.5 (± 0.7)	0.97 (± 0.02)
	Cl_6-SubPc-Cl	1.50	0.67 (± 0.01)	5.28 (± 0.01)	62.6 (± 1.2)	2.23 (± 0.03)
	Cl_4-SubPc-Cl	1.57	0.77 (± 0.01)	3.25 (± 0.01)	43.9 (± 1.0)	1.10 (± 0.02)
SubNc	**F_{12}-SubPc-Cl**	1.52	0.75 (± 0.01)	2.4 (± 0.2)	17.2 (± 0.3)	0.30 (± 0.03)
	$(CN)_3$-SubPc-F	1.66	0.89 (± 0.01)	6.18 (± 0.08)	43.2 (± 0.6)	2.36 (± 0.03)
	Cl_6-SubPc-Cl	1.76	1.00 (± 0.01)	6.12 (± 0.04)	65.3 (± 0.4)	3.89 (± 0.04)
	Cl_4-SubPc-Cl	1.83	1.08 (± 0.01)	4.83 (± 0.07)	48.2 (± 3.0)	2.44 (± 0.14)
F_4-ZnPc	**$(CN)_3$-SubPc-F**	1.75	0.81 (± 0.01)	2.52 (± 0.04)	34.8 (± 0.4)	0.70 (± 0.01)
	Cl_6-SubPc-Cl	1.85	0.87 (± 0.01)	1.34 (± 0.01)	47.4 (± 0.5)	0.53 (± 0.01)
	Cl_4-SubPc-Cl	1.92	0.66 (± 0.1)	0.21 (± 0.02)	26.3 (± 1.1)	0.04 (± 0.01)

In this set of bilayer heterojunction devices, the V_{OC} ranges from 0.3 to 1.1 V. For a single donor material, the V_{OC} can be tuned by 0.3 V depending on the choice of the SubPc acceptor. Figure 48a shows that V_{OC} increases linearly with the interface energy gap E_{DA}. This corresponds to the well-known trend previously reported in the literature[211] correlating V_{OC} with the interface energetics. The upper limit for V_{OC} is determined by the energy of the CT-state,[235] which is closely related to the interface gap E_{DA}. However, the measured V_{OC} in organic heterojunction devices never reaches this upper limit because of energy losses resulting from charge carrier recombination. The linear increase in V_{OC} with E_{DA} suggests that the different recombination processes occurring in these PHJ devices generally do not influence V_{OC}. Only devices with a F_4-ZnPc donor yielded a reduced V_{OC} compared with the other donor materials, possibly resulting from significantly increased recombination losses. However, the reduced V_{OC} could also be a related to dipole formation at the F_4-ZnPc interface, as was suggested after similar observations for fullerene-based devices.[236] The remarkably low V_{OC} for the device with the largest interface gap, *i.e.*, the combination of F_4-ZnPc and Cl_4-SubPc-Cl, is a consequence of the lack of photocurrent generation at this heterojunction. With no free charge carriers available, no considerable photovoltage can be generated in this device structure. Disregarding the F_4-ZnPc-based devices, the average difference between E_{DA} and $q \cdot V_{OC}$ is 0.8 eV. This value corresponds to those in previous literature reports,[211] considering that the estimated interface energy gap E_{DA} exceeds the energy of the CT-state by the CT-state binding energy. The advantage of the SubPc acceptors hence lies in the facile tuning of E_{DA} rather than reducing the energy losses at the active heterojunction.

[235] Vandewal, K.; Tvingstedt, K.; Gadisa, A.; Inganäs, O.; Manca, J. V. *Phys. Rev. B* **2010**, *81*, 125204.
[236] Meiss, J.; Merten, A.; Hein, M.; Schuenemann, C.; Schäfer, S.; Tietze, M.; Uhrich, C.; Pfeiffer, M.; Leo, K.; Riede, M. K. *Adv. Funct. Mater.* **2012**, *22*, 405.

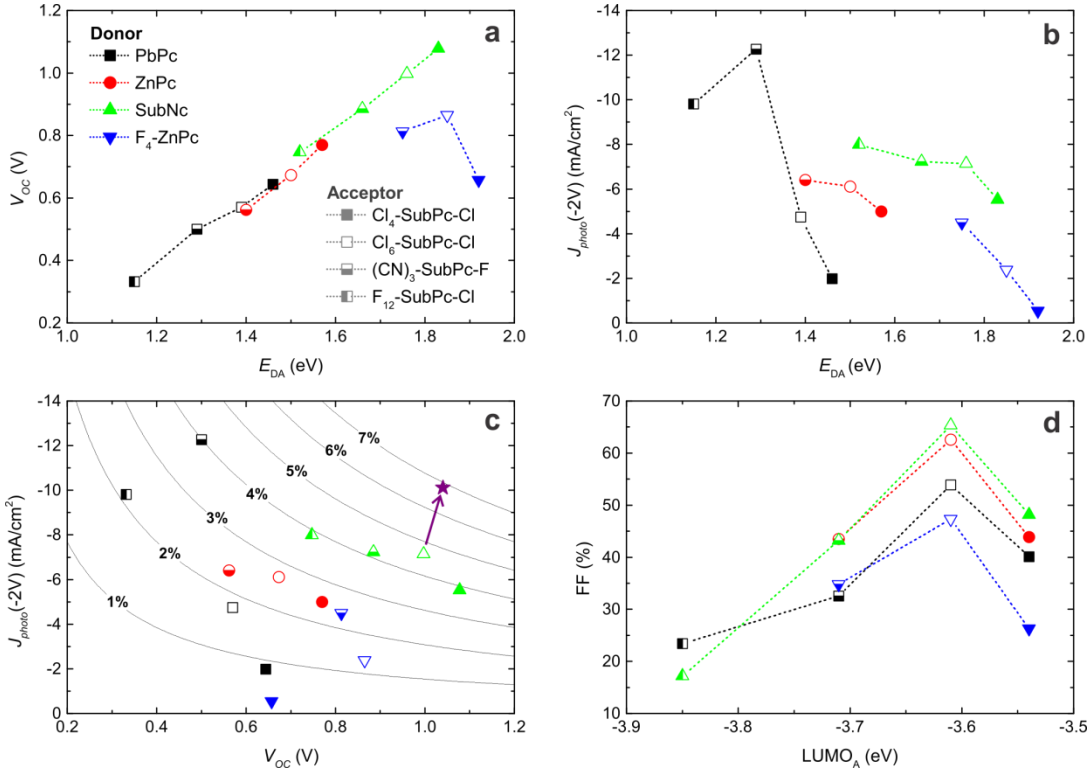

Figure 48. Relation of OPV performance parameters to the heterojunction energetics. a) V_{OC} scales linearly with the interface band gap energy E_{DA}. b) The photocurrent at reverse bias generally decreases with E_{DA}. c) The trade-off between photocurrent and V_{OC} limits the *PCE* of organic heterojunction devices. The contour lines represent *PCEs* calculated assuming a 65% *FF* and a voltage-independent photocurrent. The arrow indicates a device with an exciton-blocking hole transport layer, which increases the photocurrent and consequently the *PCE*. d) The *FF* is related to the LUMO energy of the acceptor.

The lack of photocurrent generation in the F_4-ZnPc/Cl_4-SubPc-Cl device warranted further investigation of the dependence of the photocurrent on the heterojunction energetics. Dissociation of bound excitons into free charge carriers is assumed to proceed through an intermediate CT-state. A high quantum yield of free charge carriers is obtained only if this CT process is energetically favorable. As the interface energy gap E_{DA} is closely related to the energy of the CT-state, a correlation of E_{DA} with photocurrent generation is expected. Figure 48b shows the photocurrents for all of the studied D/A heterojunctions in relation to their interface gaps. The photocurrent generation differs significantly for devices with different donor materials, depending on the absorption and spectral response of the specific donor

material (*EQE* curves in Figure 47). In contrast, the different SubPc derivatives all have similar absorption spectra, and the variation in photocurrent density upon changing the acceptor material in these devices is therefore a good indication of their *IQEs*. We evaluated the photocurrent density at reverse bias (-2 V), as the photocurrent under short-circuit conditions is reduced by charge extraction issues in some device structures (see below). Figure 48b reveals a general trend toward low photocurrent generation at large E_{DA} for all of the donor materials. Similar to previous reports,[237] the reduced photocurrent is a consequence of the smaller free energy driving the CT process. The maximal interface gap where efficient CT still occurs differs for every donor material and depends on the optical band gap of the donor. For example, devices with SubNc as the donor, which has the largest band gap of the studied donor materials, generated reasonable photocurrents with all of the SubPc acceptors. In contrast, for devices containing PbPc, the donor with the smallest band gap in our study, the photocurrent was significantly reduced as E_{DA} increased. In case of the F_4-ZnPc/Cl_4-SubPc-Cl heterojunction, E_{DA} is too large and the energy of the CT-state equals or exceeds the donor exciton energy. As a consequence, no free charges were generated at the heterojunction, and nearly no photocurrent was produced in this device structure. These observations confirm the correlation between the heterojunction energetics and the charge generation kinetics at the D/A interface. Besides the heterojunction energetics, other material properties determine the total photocurrent extraction in these devices, such as charge mobility, bulk recombination, layer morphology, and crystallinity. However, the degree to which these parameters affect the photocurrent requires further material characterization and is therefore a subject for future research.

Figure 48a-b makes clear that V_{OC} and the photocurrent exhibit opposite trends with respect to the interface energy gap E_{DA}: while V_{OC} linearly increases with E_{DA}, the photocurrent generally decreases for large E_{DA}. As a result of this trade-off between V_{OC} and photocurrent, efficiency enhancement of a heterojunction OPV device relies on optimization of the interface energy gap. Both E_{DA} and V_{OC} should be maximized without substantial reduction of the photocurrent. Figure 48c illustrates this trade-off for the presented PHJ devices. With the contour lines indicating *PCEs* calculated assuming a 65% *FF* and a voltage-independent

[237] a) Ohkita, H.; Cook, S.; Astuti, Y.; Duffy, W.; Tierney, S.; Zhang, W.; Heeney, M.; Mcculloch, I.; Nelson, J.; Bradley, D. D. C.; Durrant, J. R. *J. Am. Chem. Soc.* **2008**, *130*, 3030. b) Shoaee, S.; Clarke, T. M.; Huang, C.; Barlow, S.; Marder, S. R.; Heeney, M.; Mcculloch, I.; Durrant, J. R. *J. Am. Chem. Soc.* **2010**, *132*, 12919. c) Hoke, E. T.; Vandewal, K.; Bartelt, J. A.; Mateker, W. R.; Douglas, J. D.; Noriega, R.; Graham, K. R.; Fréchet, J. M. J.; Salleo, A.; McGehee, M. D. *Adv. Energy Mater.* **2012**, *3*, 220. d) Vandewal, K.; Ma, Z.; Bergqvist, J.; Tang, Z.; Wang, E.; Henriksson, P.; Tvingstedt, K.; Andersson, M. R.; Zhang, F.; Inganäs, O. *Adv. Funct. Mater.* **2012**, *22*, 3480.

photocurrent, we expect the highest *PCE* for the combination of a SubNc donor with a Cl_6-SubPc-Cl acceptor. Disregarding possible variations in *FF*, all of the remaining D/A pairs yield either a reduced V_{OC} or photocurrent and consequently cannot obtain higher efficiencies. For a specific donor material, however, the *PCE* can easily be maximized by selecting the most appropriate acceptor material. The LUMO level tunability of the SubPc derivatives thus offers an additional advantage in *PCE* enhancement of heterojunction OPV devices.

With an average *FF* of 65.3%, the SubNc/Cl_6-SubPc-Cl heterojunction indeed yields the highest *PCE* in this systematic study, as expected from Figure 48c. As a result of the voltage-dependent photocurrent, the average *PCE* is yet limited to 3.9% in the general device structure, comprising MoO_3 as the HTL and BCP:C_{60} as the ETL. However, specific modification of these transport layers can further enhance the performance of these PHJ devices. Figure 49 shows the *J-V* curves for some selected device structures with adjusted electron and hole transport layers.

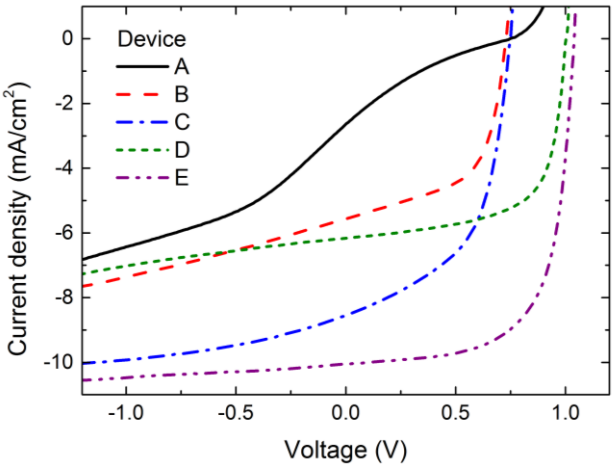

Figure 49. Current density-voltage measurements under simulated solar illumination for PHJ devices with different electron and hole transport layers: (A) MoO_3/SubNc/F_{12}-SubPc-Cl/BCP:C_{60}; (B) MoO_3/SubNc/F_{12}-SubPc-Cl/BCP:Yb; (C) PEDOT:PSS/DIP/SubNc/F_{12}-SubPc-Cl/BCP:Yb; (D) MoO_3/SubNc/Cl_6-SubPc-Cl/BCP:C_{60}; and (E) PEDOT:PSS/DIP/SubNc/Cl_6-SubPc-Cl/BCP:C_{60}.

Table 8 summarizes the performance parameters of the best-performing cell for each device structure.

Table 8. Solar cell performance parameters for PHJ devices with different electron and hole transport layers.[a]

Device structure	V_{OC} (V)	J_{SC} (mA cm^{-2})	*FF* (%)	*PCE* (%)
A: MoO_3/SubNc/F_{12}-SubPc-Cl/BCP:C_{60}	0.75	2.64	17.4	0.34
B: MoO_3/SubNc/F_{12}-SubPc-Cl/BCP:Yb	0.73	5.57	57.6	2.25
C: PEDOT:PSS/DIP/SubNc/F_{12}-SubPc-Cl/BCP:Yb	0.75	8.55	53.4	3.31
D: MoO_3/SubNc/Cl_6-SubPc-Cl/BCP:C_{60}	1.00	6.17	65.9	3.96
E: PEDOT:PSS/DIP/SubNc/Cl_6-SubPc-Cl/BCP:C_{60}	1.04	10.1	66.6	6.86

[a] For each device structure, the open-circuit voltage (V_{OC}), short-circuit current density (J_{SC}), fill factor (*FF*), and power conversion efficiency (*PCE*) of the best-performing cell are given.

In Cl_6-SubPc-Cl-based devices, optimization of the ETL and HTL led to further efficiency enhancement for the champion SubNc/Cl_6-SubPc-Cl heterojunction, with a V_{OC} above 1 V, a J_{SC} of 10.1 mA cm^{-2} and a *FF* of 67%, resulting in a *PCE* of 6.9%, among the highest reported efficiencies for bilayer OPV devices with a non-fullerene acceptor.

1.6 Subphthalocyanines as acceptor materials in solution-processed BHJ solar cells

1.6.1 Background

Whilst planar bilayer configurations have been effectively used to produce solar cells from SubPc derivatives, the number of reports describing bulk heterojunction devices employing SubPc **1** or SubPc derivatives as active materials is still scarce. Work on the performance of SubPc-based BHJ OPV cells has indeed been focused on the optimization of the SubPc **1**/fullerene D/A heterojunction. SubPc **1** is sparingly soluble in most organic solvents and therefore is incorporated into BHJ devices by vapor deposition as opposed to solution processing.

Film morphology optimization for cells containing SubPc **1** as a donor and fullerene C_{60} as an acceptor has been accomplished by continuously graded D/A heterojunction (GHJ).[238] The GHJ permits the formation of a network of donor and acceptor materials for optimized exciton diffusion and charge carrier transport, leading to a significant improvement in device performance relative to that of planar and uniformly mixed OPVs. Using this architecture, an efficiency of 4.2% has been demonstrated. OPV cells constructed using mixed films of SubPc **1**:C_{60} with an optimum ratio of 80 wt.% C_{60}, provided a *PCE* of 3.7%.[201] This optimum composition also coincides with a peak in the *FF* and the J_{SC} density. The performance of BHJ cells based on the electron D/A pairing of SubPc **1** and C_{70} fullerene has been also reported.[239] C_{70}, due to its red shifted absorption edge and larger extinction coefficient compared to C_{60}, substantially increased the J_{SC} density. Recently, *PCEs* up to 6% have been claimed in planar-mixed OPV devices prepared from SubPc **1** and C_{70}.[240] The effect of a SubPc interfacial layer on the performance of inverted polymer solar cells based on P3HT/PC_{71}BM has been also reported.[241]

While uncommon, a few examples of solution deposition of SubPc derivatives in BHJ solar cells can be found in the literature. SubNc has been used as an electron donor, combined with a

---

[238] Pandey, R.; Holmes, R. J. *Adv. Mater.* **2010**, *22*, 5301.

[239] a) Pandey, R.; Zou, Y.; Holmes, R. J. *Appl. Phys. Lett.* **2012**, *101*, 033308. b) Zheng, Y. -Q.; Potscavage, W. J.; Komino, T.; Hirade, M.; Adachi, J.; Adachi, C. *Appl. Phys. Lett.* **2013**, *102*, 143304. c) Lee, C. -C.; Liu, S. -W.; Cheng, C. -W.; Su, W. -C.; Chou, C. -C.; Lin, C. -F.; Chen, C. -T. *Int. J. Photoenergy* **2013**, 585196.

[240] Liu, S. -W.; Su, W. -C.; Lee, C. -C.; Cheng, C. W.; Chou, C. -C.; Lin, C. -F. *J. Electrochem. Soc.* **2013**, *160*, G14.

[241] Kim, J. Y.; Noh, S.; Nam, Y. M.; Kim, J. Y.; Roh, J.; Park, M.; Amsden, J. J.; Yoon, D. Y.; Lee, C.; Jo, W. H. *ACS Appl. Mater. Interfaces* **2011**, *3*, 4279.

$PC_{71}BM$ acceptor in BHJ cells.[242] In spite of the limited solubility of SubNc in organic solvents, the solution processed device exhibited an efficiency of 4.0% under 1 sun, AM 1.5G solar irradiation at room temperature. First report of solution processable SubPcs in BHJ solar cells described the use of perfluorinated SubPc **8c** as acceptor and typical polymer poly[2-methoxy-5-(3′,7′-dimethyloctyloxy)-1,4-phenylene vinylene] (MDMO-PPV) as donor, leading to fully solution processed OPVs with efficiencies over 0.1%.[224] Bender *et al.* have tested the effect of a highly soluble tri-*n*-hexylsilyl oxide boron SubPc derivative and other three different phenoxy-SubPcs as additives in a P3HT:$PC_{61}BM$ cascade ternary BHJ OPV,[243] and, while the SubPc chromophores had the correct frontier orbital energies to produce a cascade electron transfer between P3HT and $PC_{61}BM$ phases, none of them was proven to facilitate the desired electron transfer effect.

Very recently, the fabrication of solution-processed BHJ devices from halogenated SubPc units, namely F_6-SubPc-OPhF_5 and Cl_6-SubPc-OPh, as the acceptor component and conventional polymeric donor materials such as MEHPPV, P3HT and PTB7 has been demonstrated (Figure 50).[244] The high solubility of the SubPc derivatives facilitated the formation of efficient D/A networks and provided *PCEs* of 0.4% with MEH-PPV, 1.1% with P3HT and 3.5% with PTB7. A clear contribution of photon harvesting by the acceptor was identified from the *EQE* spectra. Analysis of the *J-V* characteristics and photoluminescence quenching revealed trap-assisted and geminate recombination as a loss mechanism. These results show that solution-processable SubPcs are a promising alternative to fullerenes for polymer solar cells.

[242] Chen, G.; Sasabe, H.; Sano, T.; Wang, X. -F.; Hong, Z.; Kido, J.; Yang, Y. *Nanotechnology* **2013**, *24*, 484007.
[243] Lessard, B. H.; Dang, J. D.; Grant, T. M.; Gao, D.; Seferos, D. S.; Bender, T. P. *ACS Appl. Mater. Interfaces* **2014**, *6*, 15040.
[244] Ebenhoch, B.; Prasetya, N. B. A.; Rotello, V. M.; Cooke, G.; Samuel, I. D. W. *J. Mater. Chem. A* **2015**, *3*, 7345.

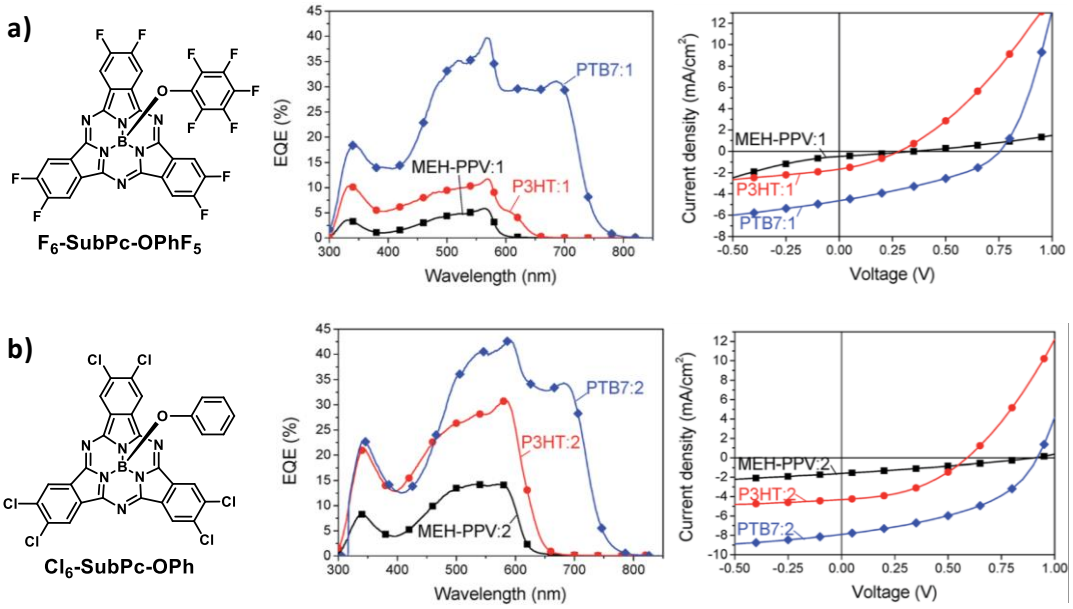

Figure 50. a) Molecular structure (left) of SubPc derivative F_6-SubPc-OPhF_5, *EQE* spectra (middle) and *J-V* characteristics (right) of MEH-PPV (squares), P3HT (circles) and PTB7 (diamonds) blended with F_6-SubPc-OPhF_5. b) Molecular structure (left) of SubPc derivative Cl_6-SubPc-OPh, *EQE* spectra (middle) and *J-V* characteristics (right) of MEH-PPV (squares), P3HT (circles) and PTB7 (diamonds) blended with Cl_6-SubPc-OPh.

1.6.2 Results and discussion

In the previous section of this chapter, Cl_6-SubPc-Cl **29** has demonstrated great potential as the best performing n-type SubPc derivative in combination with diverse small-band-gap donor materials in PHJ OSCs. For this reason, five hexachloro-substituted SubPcs bearing distinct axial substituents, *i.e.* chlorine, fluorine and differently substituted phenoxy groups, were selected as electron acceptors in BHJ solar cells. While modification of the axial substituent does not alter the absorption spectra and results in a slight variation of its electron-accepting character, it can greatly affect its aggregation and crystallization behavior. On the other hand, the novelty and good results obtained in the use of compound **31** in PHJ devices prompted us to include chloro-tricyano-SubPc derivative **26** in this study. This work has been developed in collaboration with the research group of Professor René Janssen in the Technische Universiteit Eindhoven.

1.6.2.1 Synthesis and characterization of subphthalocyanines 32-35

Five axially substituted Cl_6-SubPc-X derivatives were used in this study. Synthesis of Cl_6-SubPc-Cl **29** has been previously described.[109b,206] Reaction with selected phenol derivatives with electron-donating or electron-withdrawing substituents provided Cl_6-SubPc-OPh$(OMe)_3$ **32**, Cl_6-SubPc-OPh^{t}Bu **33** and Cl_6-SubPc-OPhF_5 **34** in good yields (Scheme 16). Finally, Cl_6-SubPc-F **35** was prepared starting from SubPc **33** by adapting the method of M. V. Fulford *et al.*[42b,64]

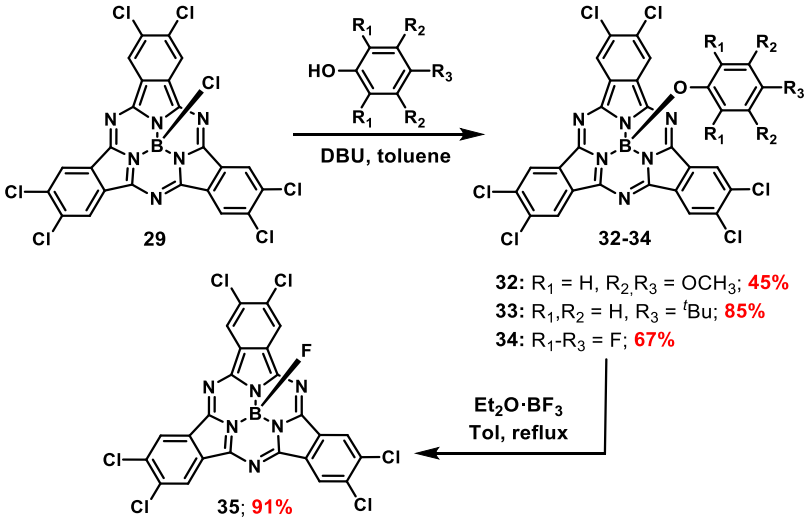

Scheme 16. Synthesis of SubPcs **32-35**.

All five SubPc compounds feature almost identical absorption spectra in toluene due to the scarce influence of the axial substituents in the π-conjugated system of the macrocycle, *Q* band maxima peaking at wavelengths around 570 nm with absorption coefficient values up to 4.0-4.5 × 10^4 M^{-1} cm^{-1} (Figure 51a, Table 9). The absorption spectra of Cl_6-SubPc-X in films prepared by spin-coating of a chlorobenzene solution display a bathochromic shift of around 10 nm (Figure 51b, Table 9) compared to the spectra in solution. Remarkably, the Cl_6-SubPc-Cl **29** absorption spectrum in film displays a broader *Q* band with an additional intense maximum at 558 nm, that could be attributed to the formation of head-to-tail columnar stacks (H-type like aggregates) in the solid state, favored by the presence of a small chlorine atom in axial position. Axial substitution with bulky phenoxy groups in the other three Cl_6-SubPc-X derivatives **32-34** precludes this behavior. On the other hand, Cl_6-SubPc-F **35** evidenced solubility problems in most organic solvents during films fabrication, so this SubPc derivative was discarded in further studies.

The fluorescence quantum yield ϕ_F of Cl_6-SubPc-Cl, Cl_6-SubPc-OPh^{t}Bu and Cl_6-SubPc-OPhF_5 is around 0.35-0.65 in toluene, and it is reduced to 0.003 in Cl_6-SubPc-OPh$(OMe)_3$ (Table 9). The strongly quenched fluorescence in Cl_6-SubPc-OPh$(OMe)_3$ is attributed to an intramolecular photo-induced electron transfer process from axial electron rich phenoxy substituent to the SubPc acceptor.

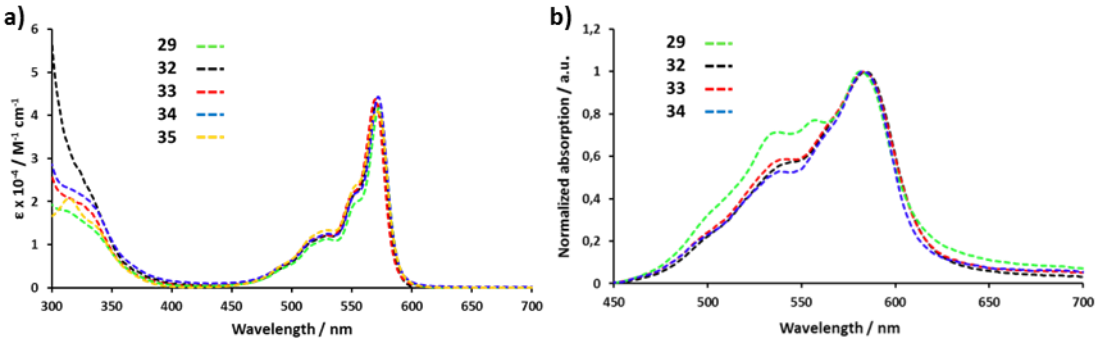

Figure 51. a) UV-vis absorption spectra in toluene and b) normalized UV-vis absorption spectra in films of SubPcs **29**, **32-35**.

Electrochemical properties of four Cl_6-SubPc-X derivatives were investigated by CV and SWV measurements in THF (Figure 52 and Table 9). The LUMO and HOMO energy levels were estimated from the reduction potentials obtained by CV measurements and optical bandgap $E_{g,opt}$ values (~2.15 eV), employing Equations 5 and 6. While peripheral electron-withdrawing chlorine substituents govern Cl_6-SubPc-X electron affinities, axial substitution allows fine-

tuning of LUMO and HOMO levels in a 0.1 eV range, resulting in LUMO and HOMO energies spanning from -3.84 and -6.00 eV for Cl_6-SubPc-OPh$(OMe)_3$ to -3.93 and -6.08 eV for Cl_6-SubPc-OPhF_5, respectively (Table 9).

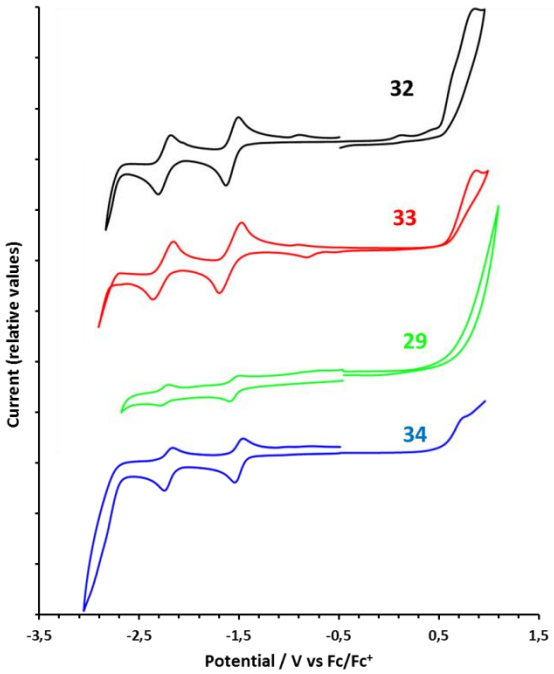

Figure 52. Cyclic voltammograms (OSW voltammogram in the anodic window of **34**) of SubPcs **29**, **32-34** in THF.

Table 9. Electrochemical data (in mV *vs.* Fc/Fc^+) in THF and experimental HOMO-LUMO energy levels data (in eV) of SubPcs **8c**, **29**, **30** and **31**.

Cl_6-SubPc-X	λ_{max} (nm)		$E_{g,opt}$ [a] (eV)	E_{LUMO} (eV)	E_{HOMO} (eV)	Φ_F
	solution	film				
32 (X = OPh$(OMe)_3$)	572	584	2.16 (575)	-3.84	-6.00	0.003
33 (X = OPh^{t}Bu)	571	584	2.16 (575)	-3.86	-6.02	0.351
29 (X = Cl)	574	582	2.15 (578)	-3.90	-6.06	0.643
34 (X = OPhF_5)	572	582	2.15 (576)	-3.93	-6.08	0.429

[a] Intersection wavelength in nm of the normalized absorption and emission spectra in brackets.

1.6.2.2 Photovoltaic performance of BHJ solar cells containing subphthalocyanines 29, 32-34 as acceptor materials

Initially, devices with three different donor polymers, P3HT, PTB7-Th and PTB7-F20 (Figure 53), were fabricated to explore the usability of the SubPcs as acceptors. Surprisingly, solar cells with conventional structure ITO/HCL/polymer:Cl_6-SubPc-X/LiF/Al that use either PEDOT:PSS or MoO_x as hole collection layer (HCL) all produced very poor results even with optimized active layer processing conditions, possibly caused by an unfavorable vertical phase segregation. This fact is in contradiction with the recent report of Ebenhoch *et al.*[244] and only efficiencies under 0.1% could be obtained with P3HT even by reproducing identical device fabrication conditions. *PCEs* under 1.0% were also recorded for the combination of PTB7-Th and PTB7-F20 with all Cl_6-SubPc-X derivatives.

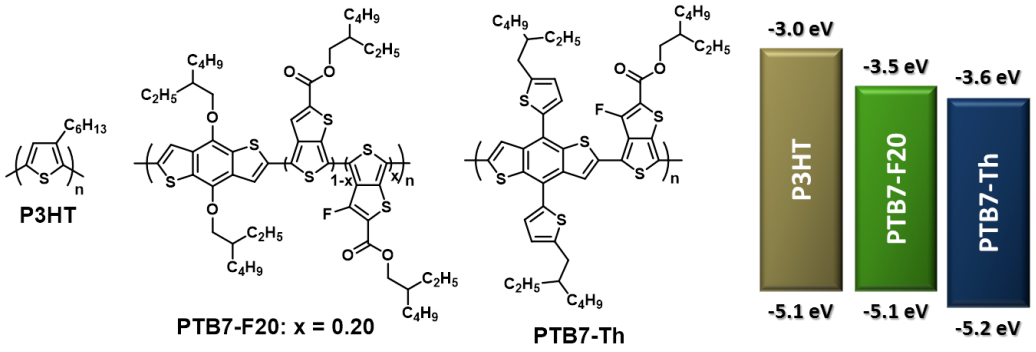

Figure 53. Molecular structures of the donor polymers tested in this work and schematic representation of their energy levels. HOMO and LUMO values extracted from literature.

For this reason, studies were redirected to the fabrication of devices with an inverted structure (Figure 54). In this OSC architecture, the ITO acts as the cathode and the high-work function metals act as the anode, respectively. Also, the polarity of charge collection is reversed in inverted OPVs, which allows the utilization of more ambient stable and high-work function metals such as gold, silver and copper as the top anode, making it possible for printing technologies to deposit the metal anode instead of the conventional energy consuming thermal deposition. Meanwhile the acidic PEDOT:PSS buffer layer is also eliminated to avoid the proton etching ITO or the cation derogating the organics.

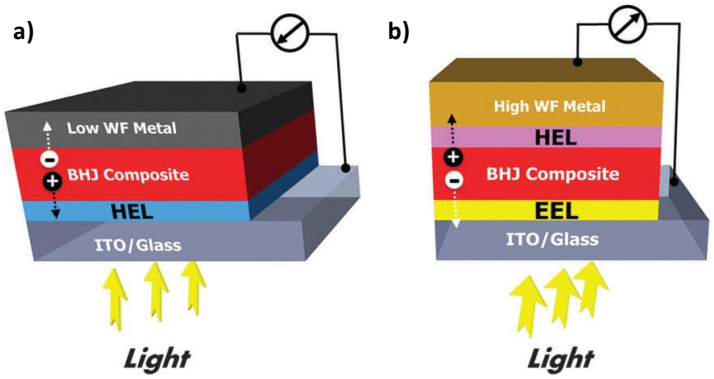

Figure 54. Bottom-illuminated OPVs with a) conventional device structure and b) inverted structure.

Early tests in inverted solar cell devices employing PTB7-Th as the electron donor resulted in higher efficiencies than devices containing P3HT or PTB7-F20. Thus, our efforts were focused on the screening of the fabrication conditions and optimization of the device parameters for all PTB7-Th/Cl_6-SubPc-X D/A pairs. The photovoltaic properties of the SubPc molecules as acceptors were evaluated in solar cells with an inverted architecture of ITO/ZnO/PTB7-Th:Cl_6-SubPc-X/MoO_x/Ag. The solar cells were tested under simulated AM 1.5G illumination (100 mW cm^{-2}). *EQE* calibrated current densities were used to accurately estimate the *PCEs* of the solar cells. The *J-V* characteristics and *EQE* spectra of the optimized devices are shown in Figure 55.

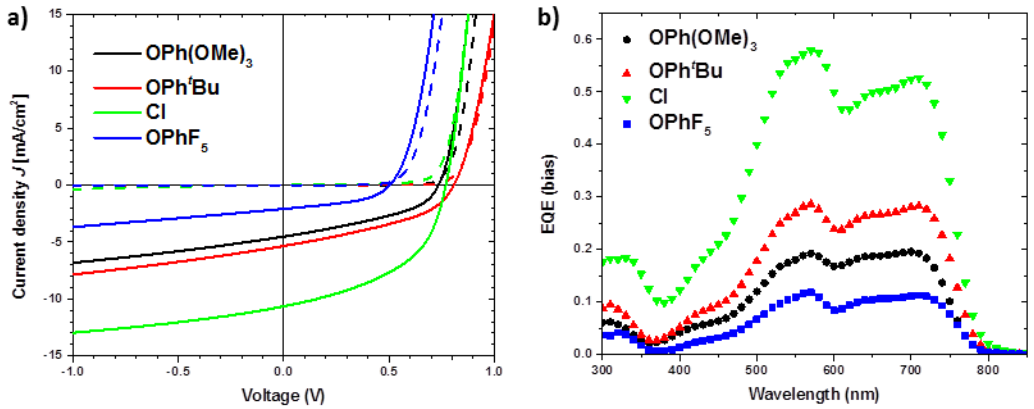

Figure 55. a) *J-V* curves of the PTB7-Th:Cl_6-SubPc-X solar cells in dark (dashed lines) and under illumination (solid lines). b) Corresponding *EQE* spectra.

A summary of the device statistics of the solar cells based on each SubPc molecule under optimized fabricating conditions and device statistics of the optimized devices are collected in

Table 10. The highest *PCE* value was measured for Cl_6-SubPc-Cl, which offered a *PCE* of 4.0%, along with a J_{SC} of 10.7 mA cm^{-2}, a V_{OC} of 0.77 V, and a *FF* of 0.48.

Table 10. Performance parameters of the PTB7-Th:Cl_6-SubPc-X solar cells measured with white light (100 mW cm^{-2}) in device structure of ITO/ZnO (40 nm)/PTB7-Th:Cl_6-SubPc-X/MoO_x (10 nm)/Ag (100 nm) under optimized conditions.

Cl_6-SubPc-X	D:A ratio	Solvent	Annealing	$J_{SC}(EQE)$[a] (mA cm^{-2})	V_{OC} (V)	*FF* (%)	*PCE*[b] (%)	EQE_{max}
32	1:1.5	CB (2% DIO)	-	3.6	0.74	40	1.1	0.20
33	1:1.5	CB (2% CN)	90 °C, 5 min	5.3	0.81	41	1.8	0.29
29	1:1.5	CB (2% CN)	90 °C, 5 min	10.7	0.77	48	4.0	0.58
34	1:1.5	CB (2% CN)	90 °C, 5 min	2.1	0.50	45	0.5	0.12

[a] Determined by integrating the EQE spectrum with the AM1.5G spectrum. [b] Calculated using $J_{SC}(EQE)$. CB = chlorobenzene. DIO = 1,8-diiodooctane. CN = 1-chloronaphthalene.

Importantly, both the polymer donor and the SubPc acceptor contribute substantially to the photocurrent for each SubPc derivative (Figure 55b). The *EQE* maxima located at about 710 nm originate from the absorption of PTB7-Th, while the *EQE* maxima located at around 570 nm are close to the absorption peaks of the SubPc molecules (Figure 55 and Table 9). The lack of light absorption of both PTB7-Th and SubPc acceptors in the high photon energy region, from 350 to 450 nm, results in rather uncommon shape in the *EQE* spectra, where all curves show a valley in this region. At higher wavelengths, however, an impressive *EQE* maximum of 0.58 was achieved for Cl_6-SubPc-Cl, but the solar cells based on the other SubPc molecules produced significantly lower *EQE* and J_{SC}. As a result, these devices all afforded *PCEs* lower than 2.0%. Notably, except for Cl_6-SubPc-$OPhF_5$, the solar cells based on other SubPc acceptors exhibit similar V_{OC} (~0.8 V) as that of corresponding fullerene-based devices. Although an encouraging J_{SC} and *PCE* have been achieved by Cl_6-SubPc-Cl, a common limitation of these solar cells is their low *FF* (<0.5), which is considerably lower than that of the state-of-the-art fullerene-based devices.

Therefore, an understanding on the low *FF* of these devices is crucial to the further development of SubPc-based acceptors. The charge carrier transport properties and bimolecular charge recombination of the PTB7-Th:Cl_6-SubPc-X blend films were thus investigated. Electron mobilities were estimated from electron-only devices of PTB7-Th:Cl_6-SubPc-X blends by fitting the data using the space-charge-limited current (SCLC) model. The

current density versus voltage characteristics are shown in Figure 56, and the mobility values are listed in Table 11. All PTB7-Th:Cl_6-SubPc-X films possess an electron mobility around 10^{-6} cm^2 V^{-1} s^{-1}. Keeping in mind that the PTB7-Th:fullerene blends in similar devices exhibit an electron mobility of about 10^{-3}-10^{-2} cm^2 V^{-1} s^{-1},[245] the considerably lower electron mobility of the PTB7-Th:Cl_6-SubPc-X films should be responsible for the low *FF* of the resulting solar cells.

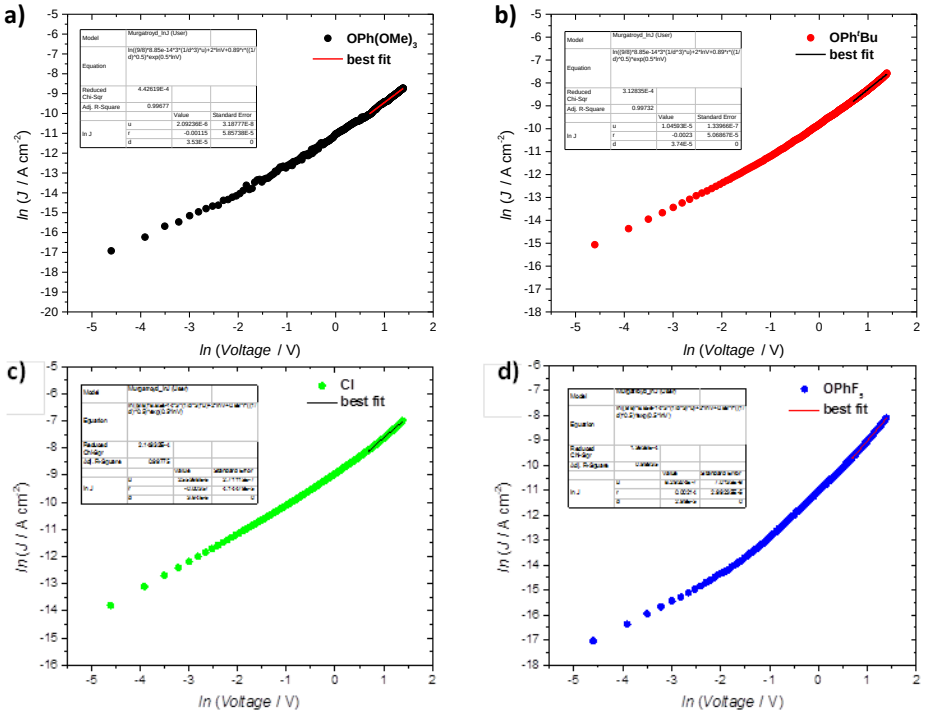

Figure 56. Current density versus voltage characteristics of electron-only devices with a configuration of ITO/ZnO (40 nm)/PTB7-Th:Cl_6-SubPc-X/LiF (1 nm)/Al (100 nm) plotted in the format of ln*J* ~ ln*V* for SubPcs: a) **32**, b) **33**, c) **29**, and d) **34**.

[245] Huang, J.; Carpenter, J. H.; Li, C. -Z.; Yu, J. -S.; Ade, H.; Jen, A. K. Y. *Adv. Mater.* **2016**, *28*, 967.

Table 11. Summary of the derived fitting data for the electron-only devices of ITO/ZnO (40 nm)/PTB7-Th:Cl_6-SubPc-X/LiF (1 nm)/Al (100 nm) based on Mott-Gurneys law with field-dependent mobility.

Cl_6-SubPc-X	Zero-field mobility μ_0 ($cm^2\ V^{-1}\ s^{-1}$)	Field-dependence factor γ ($cm^{1/2}\ V^{-1/2}$)	μ_e at $E = 1 \times 10^5$ V cm^{-1} ($cm^2\ V^{-1}\ s^{-1}$)
32	2.1×10^{-6}	-1.2×10^{-3}	1.5×10^{-6}
33	1.1×10^{-5}	-2.3×10^{-3}	5.1×10^{-6}
29	2.6×10^{-5}	-3.6×10^{-3}	8.3×10^{-6}
34	8.3×10^{-7}	2.1×10^{-4}	1.6×10^{-6}

In agreement with the low electron mobilities, all solar cells of PTB7-Th:Cl_6-SubPc-X exhibit substantial bimolecular charge recombination losses. These losses are evidenced by the large differences between the *EQE* measured with light bias (which affords the short-circuit current density equivalent to AM 1.5G illumination) and the *EQE* measured without light bias (Figure 57). To clarify this point, the average values of the ratio between the *EQE* measured with light bias and the *EQE* measured without light bias (denoted as $\rho = EQE_{bias}/EQE_{nobias}$) were plotted for each device (Figure 58). Since the bimolecular recombination efficiency can be approximated as $\eta_{BR} = 1 - \rho$, a low ρ indicates considerable bimolecular recombination loss.[246]

For state-of-the-art polymer:fullerene solar cells ρ approaches unity and the low ρ values of these PTB7-Th:Cl_6-SubPc-X devices suggest severe bimolecular recombination losses. It is notable that bimolecular recombination is relatively less severe for PTB7-Th:Cl_6-SubPc-Cl, which is consistent with the higher electron mobility of Cl_6-SubPc-Cl among the four SubPc acceptors and the highest *FF* and *PCE* of the solar cells. We speculate that the higher performance of Cl_6-SubPc-Cl originates from the H-type like aggregates of Cl_6-SubPc-Cl in the solid state, which are favorable for charge transport.

[246] Koster, L. J. A.; Kemerink, M.; Wienk M. M.; Maturová, K.; Janssen, R. A. J. *Adv. Mater.* **2011**, *23*, 1670.

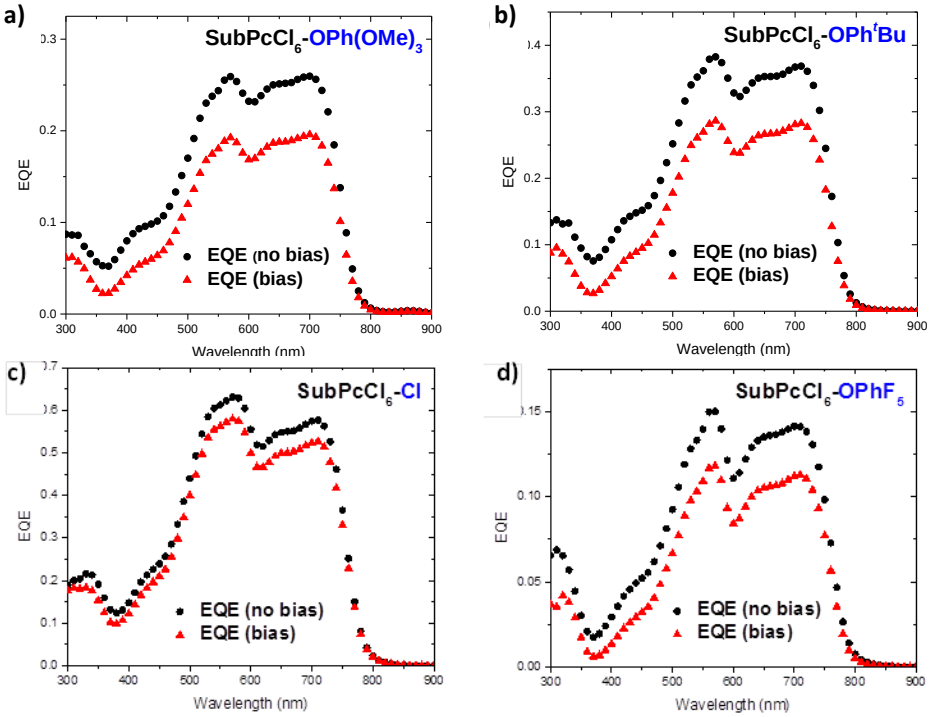

Figure 57. *EQE* spectra measured with and without light bias of the ITO/ZnO (40 nm)/PTB7-Th:Cl_6-SubPc-X/MoO_x (10 nm)/Ag (100 nm) solar cells for SubPcs: a) **32**, b) **33**, c) **29**, and d) **34**.

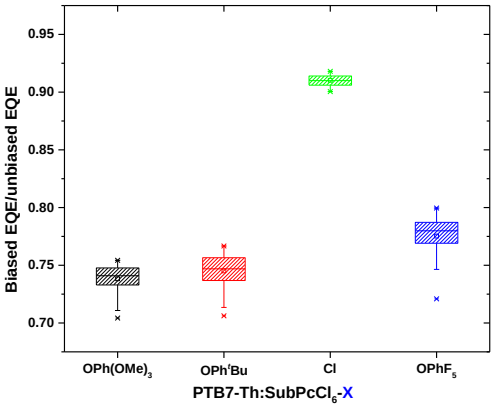

Figure 58. Average EQE_{bias}/EQE_{nobias} values of PTB7-Th:Cl_6-SubPc-X solar cells.

The morphology of PTB7-Th:Cl_6-SubPc-X blend films was investigated by transmission electron microscopy (TEM). As shown in Figure 59, the blends based on Cl_6-SubPc-OPh^{t}Bu and Cl_6-SubPc-Cl show homogeneous films without noteworthy phase separation. In such intimately mixed blends, charge separation is prevented because the lack of pure domains. High domain purity is well known to be beneficial for the dissociation of photogenerated charges from the D/A interface, while low domain purity will cause serious geminate recombination.[247] In the films based on Cl_6-SubPc-OPh$(OMe)_3$ and Cl_6-SubPc-OPhF_5, there is a slightly increased contrast between the light and dark regions, indicative of more distinct phase separation, but these films lack long-enough fibrillary structure (Figure 59). The transport of charge carrier in such films may thus be impeded because of a poor interconnectivity between neighboring domains. Combined, the electron mobility measurements, the charge recombination analysis, and the morphology study explain why these PTB7-Th: Cl_6-SubPc-X show low *FF* in BHJ solar cells.

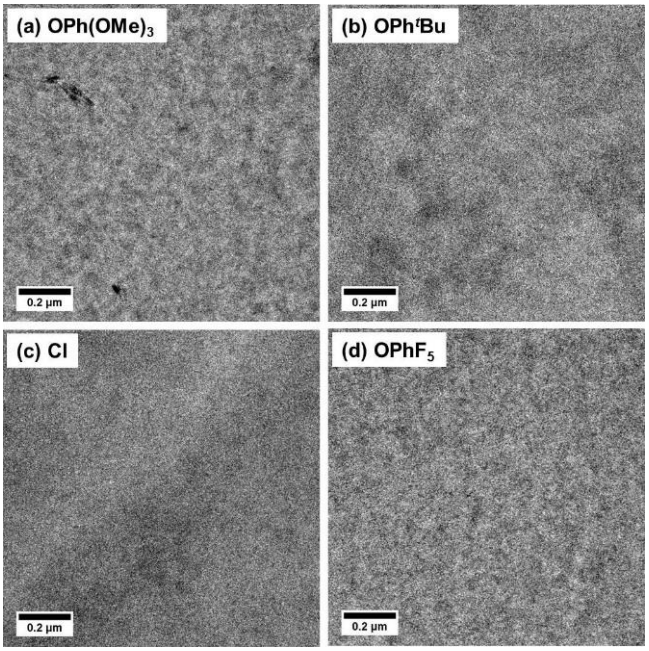

Figure 59. Bright field TEM images of the PTB7-Th:Cl_6-SubPc-X blend films deposited with the same methods as those for OSCs fabrication for SubPcs a) **32**, b) **33**, c) **29**, and d) **34**. Image size: 1.5 × 1.5 μm^2; scale bar: 200 nm.

[247] a) Veldman, D.; İpek, O. z.; Meskers, S. C. J.; Sweelssen, J. r.; Koetse, M. M.; Veenstra, S. C.; Kroon J. M.; Bavel, S. S. v.; Loos, J.; Janssen, R. A. J. *J. Am. Chem. Soc.* **2008**, *130*, 7721. b) Ma, W.; Tumbleston, J. R.; Wang, M.; Gann, E.; Huang, F.; Ade, H. *Adv. Energy Mater*. **2013**, *3*, 864.

1.6.2.3 Photovoltaic performance of BHJ solar cells containing subphthalocyanine 26 as acceptor material

Encouraged by the good results obtained in BHJ devices based on PTB7-Th/Cl_6-SubPc-Cl **29** pair, preliminary studies on the performance of devices comprising of chloro-tricyano-SubPc derivative **26** as the acceptor component and PTB7-Th as the polymeric donor were carried out. Three different samples of SubPc **26**, namely regioisomerically pure ***C_3*-26** and ***C_1*-26** and a C_3/C_1 1:3 mixture, were tested in order to assess the possible influence of the molecular symmetry on the film forming properties of the compound.

However, it could be promptly verified that SubPc **26**, either as a regioisomeric mixture or a single regioisomer, presents scarce solubility in all processing solvents. For this reason, optimized devices with an inverted architecture of ITO/ZnO/PTB7-Th:$(CN)_3$-SubPc-Cl/MoO_x/Ag for each SubPc **26** sample underperformed in comparison with BHJ cells based on Cl_6-SubPc-X derivatives (Figure 60 and Table 12).

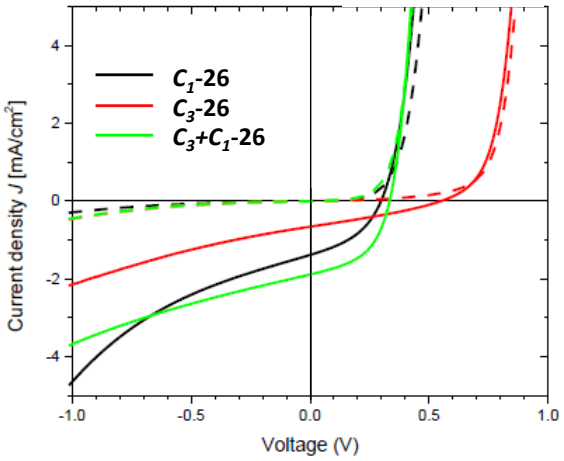

Figure 60. *J-V* curves of the PTB7-Th-$(CN)_3$-SubPc-Cl solar cells in dark (dashed lines) and under illumination (solid lines).

Table 12. Performance parameters of the PTB7-Th:$(CN)_3$-SubPc-Cl solar cells measured with white light (100 mW cm^{-2}) in device structure of ITO/ZnO (40 nm)/PTB7-Th:$(CN)_3$-SubPc-Cl/MoO_x (10 nm)/Ag (100 nm) under optimized conditions.

$(CN)_3$-SubPc-Cl	D:A ratio	J_{SC} (mA cm^{-2})	V_{OC} (V)	*FF* (%)	*PCE* (%)
C_3-26	1:1.5	0.66	0.549	30	0.11
C_1-26	1:1.5	1.38	0.298	40	0.17
C_3+C_1-26	1:1.5	1.88	0.334	48	0.31

1.7 Summary and conclusions

In this chapter, the synthesis, study and application of different SubPc derivatives as potential non-fullerene acceptor materials in organic photovoltaics have been presented.

In the first section, a novel family of SubPc derivatives bearing π-conjugated electron-withdrawing cyano groups in their periphery has been synthesized by means of a two-step synthetic methodology, consisting on the preparation of iodo-functionalized SubPc precursors and subsequent palladium-catalyzed cross-coupling cyanation reaction. The use of microwave irradiation in the cyanation reaction is essential for the success of the method. Optimization of this procedure has allowed the preparation of a series of unsymmetrical *ortho*-dicyano- and tetracyano-SubPcs additionaly functionalized with either electron-accepting or electron-donating groups, and of symmetrical tricyano-SubPcs, with reasonable yields.

The electronic and redox features of these derivatives and the influence of the introduction of cyano groups in their properties have been studied by comparison with their iodo-substituted precursors. In general, it has been observed that the presence of cyano substituents in the SubPcs periphery produces a remarkable bathocromic shift of the absorption maxima, together with higher absorption coefficients, and a substantial increase of the acceptor character of the molecules, confirming the extension of the conjugation of the SubPc π-system through the cyano substituents. Estimation of the HOMO and LUMO energy levels based in experimental data and in DFT calculations demonstrates that these SubPc derivatives cover a wide range of frontier orbitals energy levels, depending on the additional peripheral substituents. Finally, the intrinsic charge carrier transporting ability of selected cyano-SubPcs has been measured through novel non-contact flash-photolysis time-resolved microwave conductivity technique, displaying charge carrier mobility values comparable to or larger than other known well-performing acceptor SubPcs (Figure 61).

The remarkable properties of these novel peripherally cyanated SubPc derivatives represent a promising prospect for the application of these compounds as appealing n-type organic semiconductors in the fabrication of photovoltaic devices.

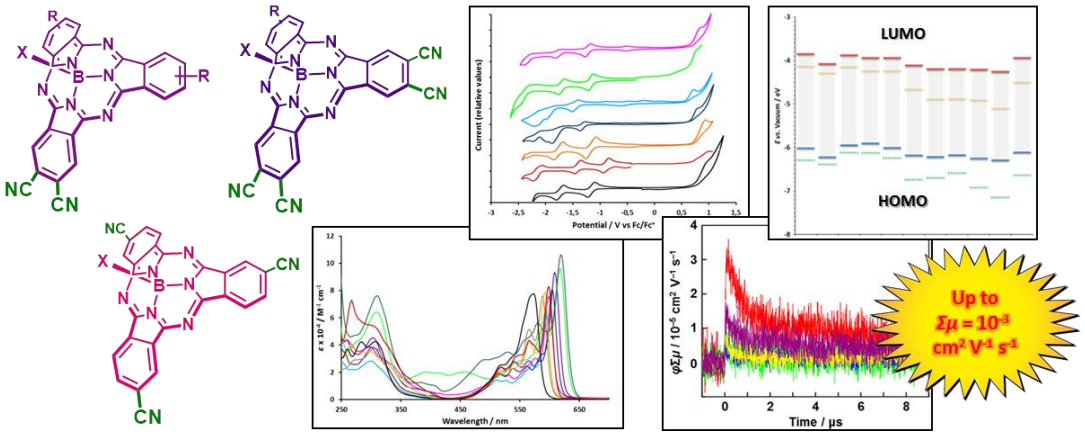

Figure 61. Graphical abstract of the results obtained in section 1.4.

In the second section, the efficient use of SubPc derivatives as non-fullerene acceptors in bilayer heterojunction devices has been demonstrated.

The electronic properties and the n-type character of selected SubPc molecules have been modulated by the introduction of electron-withdrawing substituents, namely halogen atoms and cyano groups, in the periphery, that allow to span a wide range of LUMO energy levels. They have been combined with four small-band-gap donor materials with suitable HOMO energy levels and complementary absorption profiles.

In a systematic study, the dependence of the device performance on the interface energetics of the D/A planar heterojunctions has been explored. The observations confirm that the open-circuit voltage and the photocurrent exhibit opposite trends with respect to the interface energy gap E_{DA}: while V_{OC} linearly increases with E_{DA}, the photocurrent generally decreases for large E_{DA}. As a result of this trade-off between V_{OC} and photocurrent, efficiency enhancement of a heterojunction OPV device relies on optimization of the interface energy gap. The facile LUMO level tunability of the SubPc derivatives thus offers an additional advantage in *PCE* enhancement of heterojunction OPV devices. Finally, it has been found that non-fullerene acceptors require adjusted buffer layers with aligned electron transport levels to enable efficient charge extraction, while the insertion of an exciton-blocking layer at the anode interface further boosts photocurrent generation. These adjustments result in a PHJ OPV device with an efficiency of 6.9% and a V_{OC} above 1 V (Figure 62).

This study thus shows that the use of non-fullerene acceptors is a successful method to enhance the performance of organic solar cells.

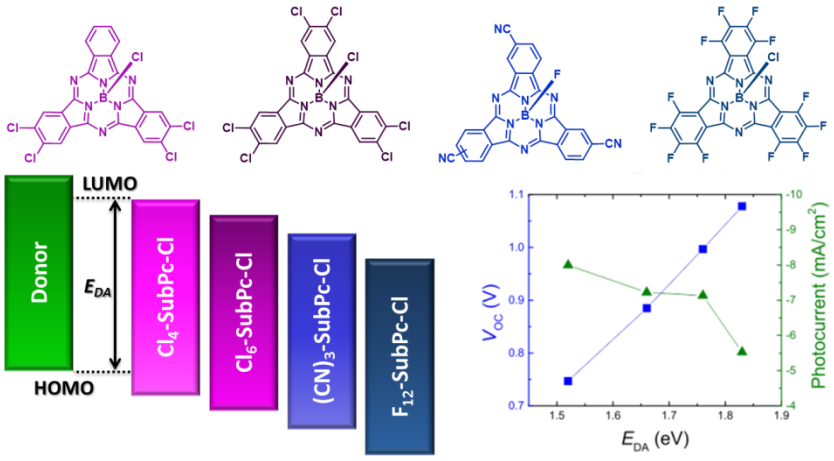

Figure 62. Graphical abstract of the results obtained in section 1.5.

In the last part of this chapter, a group of hexachloro-SubPcs bearing fluorine, chlorine and differently substituted axial phenoxy substituents have been synthesized and used as electron acceptors in BHJ solar cells in combination with selected polymeric donor materials.

This study evidences that, while modification of the axial substituent does not alter the absorption spectra and results in a slight variation of the electron-accepting character of each SubPc derivative, it affects its aggregation and crystallization behavior. The employment of BHJ solar cells with inverted architectures has been proven to be critical to obtain appreciable efficiency values. A *PCE* up to 4.0% has been achieved, which is the highest reported value for solution processed SubPc-based solar cells. Both the polymer donor and the SubPc acceptor contribution to the photocurrent has been experimentally verified, indicating the promising acceptor properties of SubPcs. The main limitation of these SubPc-based solar cells has been found in their low fill factor, which is a collective result of a low electron mobility, serious bimolecular recombination, and suboptimal BHJ morphology (Figure 63).

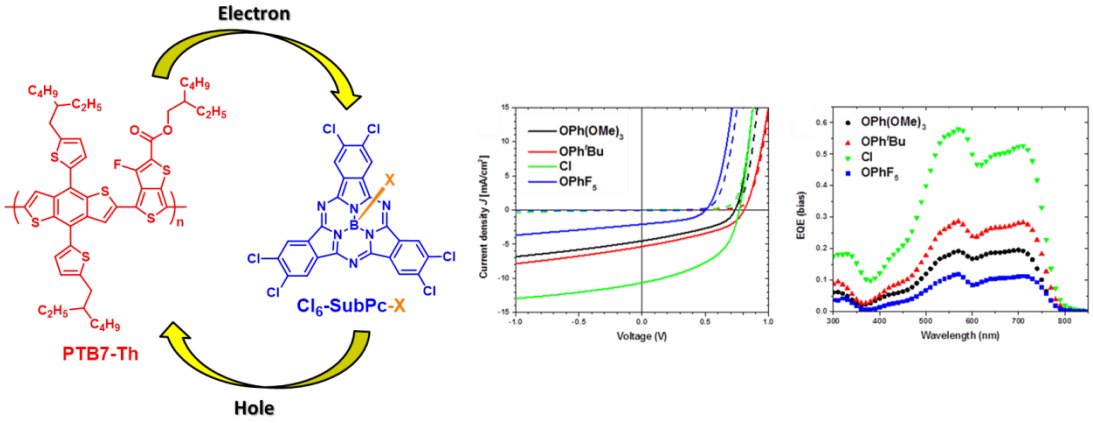

Figure 63. Graphical abstract of the results obtained in section 1.6.

1.8 Experimental section

In this *Experimental section*, the preparation and characterization of the compounds has been organized following the order as they appear in the text. Isomeric compounds (C_3/C_1 or unsymmetrically substituted SubPcs) have been listed following their chromatographic elution order.

1.8.1 Materials and general methods

Chemical reagents were purchased from Aldrich Chemical Co., Alfa Aesar, Acros Organics or Fluka Chemie and were used without further purification. "Synthetic grade" solvents were used for chemical reactions and column chromatography purifications and "anhydric grade" for reactions under dry conditions. Additionally, some solvents were further dried by distillation with Na/benzophenone (THF), or with previously activated molecular sieves (3 or 4 Å), or with a solvent purifying system by Innovative Technology Inc. MD-4-PS.

Microwave irradiation technique: microwave reactions were carried out in a Biotage Initiator+ system. All reactions were performed in capped glass vials under argon atmosphere.

Chromatography: the monitoring of the reactions has been carried out by thin layer chromatography (TLC), employing aluminum sheets coated with silica gel type 60 F254 (0.2 mm thick, E. Merck). The analysis of the TLCs was carried out with an UV lamp of 254 and 365 nm. Purification and separation of the synthesized products was performed by column chromatography, using silica gel (230-400 mesh, 0.040-0.063 mm, Merck). Eluents and relative proportions of the solvents are indicated for each particular case. Size exclusion chromatography was performed using Bio-Beads S-X1 (200-400 mesh, Bio-Rad).

Melting point (MP): melting points were measured in open-end capillary tubes by using a Büchi 504392-S apparatus, and are uncorrected.

Nuclear Magnetic Resonance (NMR): monodimensional and/or bidimensional NMR spectra (^{1}H-NMR, ^{13}C-NMR and ^{19}F-NMR) were recorded on a Bruker AC-300 (300 MHz) or a Bruker XRD-500 (500 MHz) instruments either in the Organic Chemistry Department or in SIdI (Servicio Interdepartamental de Investigación, Interdepartmental Investigation Service). In each case, the deuterated solvent employed is indicated between brackets. Chemical shifts (δ) are reported in ppm and calibrated relative to residual solvent signals using literature

reference values,[248] and coupling constants (J) are reported in hertz (Hz). The following abbreviations are used to indicate the multiplicity in ^{1}H-NMR spectra: s, singlet; d, doublet; t, triplet; q, quartet; quint, quintet; m, multiplet; bs, broad signal.

Mass Spectrometry (MS) and High Resolution Mass Spectrometry (HRMS): mass spectra were recorded in SIdI, employing Electronic Impact (EI), Fast Atom Bombardment (FAB-MS) or Matrix Assisted Laser Desorption/Ionization-Time of Flight (MALDI-TOF), using a VG-AutoSpec spectrometer for EI and FAB-MS and a Bruker Reflex III spectrometer, with a nitrogen laser operating at 337 nm, for MALDI-TOF. The different matrixes employed are indicated for each spectrum. Mass spectrometry data are expressed in *m/z* units.

Ultraviolet–visible spectroscopy (UV-Vis) and Fluorescence Spectroscopy: spectroscopic grade solvents were used for spectroscopic measurements. UV-Vis spectra were recorded in the Organic Chemistry Department of UAM, employing a JASCO-V660 UV-Vis spectrophotometer. Fluorescence studies were carried out with a JASCO-V8600 fluorometer.

Infrared Spectroscopy (FT-IR): infrared spectra were recorded in the Organic Chemistry Department on a Bruker Vector 22 spectrophotometer, employing in all cases solid samples (KBr pressed disks).

Cyclic Voltammetry (CV) and Square Wave Voltammetry (SWV): electrochemical measurements were performed on an Autolab PGStat 30 equipment using a three electrode configuration system. The measurements were carried out using freshly distilled THF solutions containing 0.1 M tetrabutylammonium hexafluorophosphate ($TBAPF_6$) and a concentration of approximately 10^{-4} M of the corresponding compound. A glassy carbon electrode (3 mm diameter) was used as the working electrode, and a platinum wire and an $Ag/AgNO_3$ (in CH_3CN) electrode were employed as the counter and the reference electrodes, respectively. Ferrocene (Fc) was used as an external reference and all the potentials were given relative to the Fc/Fc^+ couple. Scan rate was 100 mV s^{-1} unless otherwise specified.

X-Ray Spectroscopy: X-Ray diffraction spectra were done in SIdi with a Bruker KAPPA APEX II CCD goniometer with kappa geometry and Mo source (λ = 0.71073 Å). Data were collected at different temperatures, specified in each case, utilizing a system equipped with an Oxford Cryosystems dispositive. The distance between the sample and the detector is 3.5 cm. The data harvesting is done over 99% and the redundancy value is over 3. Data are corrected then

[248] Fulmer, G. R.; Miller, A. J. M.; Sherden, N. H.; Gottlieb, H. E.; Nudelman, A.; Stoltz, B. M.; Bercaw, J. E.; Goldberg, K. I. *Organometallics* **2010**, *29*, 2176.

with SADABS program. The intensities are calculated with SAINT program. Finally, the structures are resolved with SHELXS and refined with SHELXL.

1.8.2 Synthesis of precursor phthalonitriles

1.8.2.1 Synthesis of 4,5-diiodophthalonitrile[249]

4,5-Diiodophthalimide[249]

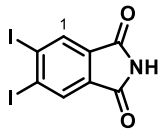

To a suspension of phthalimide (14.7 g, 100 mmol) in 60 mL of 30% fuming sulfuric acid was added iodine (50.8 g, 200 mmol). The reaction mixture was heated to 70 °C for 24 h. After cooling to room temperature, the mixture was poured onto 400 g of ice. The precipitated brown solid was filtered and washed with water (2 x 100 mL), a 2% solution of K_2CO_3 (100 mL), a saturated solution of $Na_2S_2O_3$ (100 mL) and water (100 mL) again. The solid was extracted with acetone (1 L) in a Soxhlet extractor for 48 h. The precipitate formed in the solvent vessel was filtered from the acetone and 100 mL of water was added. This solution was concentrated to 500 mL and the solid obtained was filtered off and vacuum-dried, yielding 32.3 g (81.0 mmol) of 4,5-diiodophthalimide as a white solid. Yield: 81%.

^{1}H-NMR (300 MHz, Acetone-d_6): δ (ppm) = 8.26 (s, 2H; H-1).

4,5-Diiodophthalamide[249]

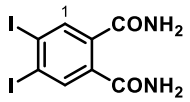

A suspension of 4,5-diiodophthalimide (12.0 g, 30.0 mmol) in 33% aqueous ammonia (100 mL) was heated to 60 °C for 1 h. The white solid obtained was filtered, washed with water (3 x 25 mL) and MeOH (2 x 25 mL) and vacuum-dried over P_2O_5. In so doing, 9.4 g (22.6 mmol) of 4,5-diiodophthalamide were isolated as a white solid. Yield: 75%.

^{1}H-NMR (300 MHz, DMSO-d_6): δ (ppm) = 7.92 (s, 2H; H-1), 7.8, 7.4 (2xs (broad), 4H, NH_2).

4,5-Diiodophthalonitrile[249]

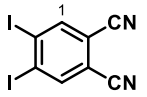

To an ice-cooled stirred suspension of 4,5-diiodophthalamide (8.3 g, 20 mmol) in 80 mL of dry dioxane and 18 mL of dry pyridine was added 16 mL of trifluoroacetic anhydride at 0-5 °C. After the addition was complete, the reaction mixture was warmed to room temperature, stirred for 16 h, and poured onto ice. The product was extracted with EtOAc (3 x 50 mL). The organic layer was washed with water (100 mL), 1 M HCl (2 x 100 mL), a dilute solution of Na_2CO_3 (2 x 200 mL) and water (50 mL) again and dried over $MgSO_4$. After filtration of the drying agent, the solvent was vacuum-evaporated and the yellow solid obtained was subjected to column

[249] Terekhov, D. S.; Nolan, K. J. M.; McArthur, C. R.; Leznoff, C. C. *J. Org. Chem.* **1996**, *61*, 3034.

chromatography on silica gel using Toluene/$CHCl_3$ 3:2 as eluent. In this way, 4.1 g (10.8 mmol) of 4,5-diiodophthalonitrile were obtained as a white solid. Yield: 54%.

^{1}H-NMR (300 MHz, $CDCl_3$): δ (ppm) = 8.19 (s, 2H; H-1).

1.8.2.2 Synthesis of 4,5-dichlorophthalonitrile[250]

4,5-Dichlorophthalic anhydride[250]

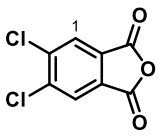

A solution of 4,5-dichlorophthalic acid (15 g, 63.5 mmol) in acetic anhydride (25 mL) was heated to reflux while distilling the acetic acid being formed in the reaction. After 5 h the remaining acetic acid was eliminated by vacuum distillation. The solid obtained was stirred over 12 h in petroleum ether, obtaining a solid that was filtered and thoroughly washed with the same solvent (3 x 20 mL). In this way, 13.5 g (62.2 mmol) of 4,5-dichlorophthalic anhydride were obtained. Yield: 98%.

^{1}H-NMR (300 MHz, $CDCl_3$): δ (ppm) = 8.12 (s, 2H; H-1).

4,5-Dichlorophthalimide[250]

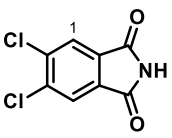

A mixture of 4,5-dichlorophthalic anhydride (13.5 g, 62.5 mmol) and formamide (20 mL) was heated to 200 °C over 3 h. After cooling to room temperature, the solid obtained was filtered, washed with water (1 x 20 mL) and vacuum-dried, yielding 12.4 g (57.4 mmol) of 4,5-dichlorophtalimide as a white solid. Yield: 92%.

^{1}H-NMR (300 MHz, DMSO-d_6): δ (ppm) = 8.10 (s, 2H; H-1).

4,5-Dichlorophthalamide[250]

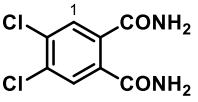

A suspension of 4,5-dichlorophthalimide (12.4 g, 57.7 mmol) in 33% aqueous ammonia (225 mL) was stirred for 36 h at room temperature. The white solid obtained was filtered, washed with water (3 x 15 mL) and vacuum-dried. In so doing, 11.9 g (51.1 mmol) of 4,5-dichlorophthalamide were isolated as a white solid. Yield: 89%.

^{1}H-NMR (300 MHz, DMSO-d_6): δ (ppm) = 7.95 (s (broad), 2H; NH_2), 7.72 (s, 2H; H-1), 7.45 (s (broad), 2H; NH_2).

[250] Wöhrle, D.; Eskes, M.; Shigehara, K.; Yamada, A. *Synthesis* **1993**, 194.

4,5-Dichlorophthalonitrile[250]

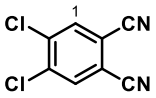

Freshly distilled thionyl chloride (42 mL) was cautiously poured over dry DMF (60 mL) at 0 °C under argon atmosphere. The mixture was vigorously stirred for 2 h at that temperature and then 4,5-dichlorophthalamide (11.9 g, 51.3 mmol) was added. After stirring for 12 h at room temperature the reaction mixture was poured onto crushed ice (100 mL), resulting in the precipitation of a slightly gray solid which was filtered and washed with water (1 x 20mL). Upon recrystallization from MeOH, 8.8 g (45 mmol) of 4,5-dichlorophthalonitrile were obtained. Yield: 88%.

^{1}H-NMR (300 MHz, $CDCl_3$): δ (ppm) = 7.94 (s, 2H; H-1).

1.8.2.3 Synthesis of 4,5-dioctylthiophthalonitrile[36c]

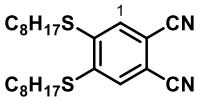

In a 100-ml two-necked round-bottomed flask, equipped with a magnetic stirrer, rubber seal and globe, 4,5-dichlorophthalonitrile (2.4 g, 12.2 mmol), dry K_2CO_3 (5.0 g, 36.2 mmol) and dry dimethylacetamide (30 mL) were placed. A stream of argon was passed through the slurry in order to remove oxygen, and then 1-octanethiol (4.6 mL, 26.8 mmol) was added. The resulting mixture was stirred at 90 °C during 8 h and poured onto 100 mL of cold water. The precipitate was filtered and collected in CH_2Cl_2. This solution was then washed with bleach (3 x 50 mL), water (3 x 50 mL) and brine solution (50 mL) and dried over $MgSO_4$. After filtration of the drying agent, the solvent was vacuum-evaporated and the yellow solid obtained was recrystallized from EtOH, obtaining 4.0 g (9.6 mmol) of 4,5-dioctylthiophthalonitrile as white needles. Yield: 79%.

^{1}H-NMR (300 MHz, $CDCl_3$): δ (ppm) = 7.40 (s, 2H; H-1), 3.0 (m, 4H; $SC\underline{H_2}$), 1.85-1.60 (m, 4H; $SCH_2C\underline{H_2}$), 1.60-1.35 (m, 4H; $S(CH_2)_2C\underline{H_2}$), 1.35-1.15 (m, 16H; $S(CH_2)_3(C\underline{H_2})_4$), 0.88 (m, 6H; CH_3).

1.8.2.4 Synthesis of 4-iodophthalonitrile[251]

4-Aminophthalonitrile[251a]

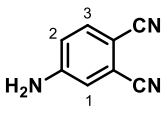

To a mixture of MeOH (450 mL) and concentrated HCl (96 mL), 4-nitrophthalonitrile (20 g, 115 mmol) was added. Upon heating to reflux, when total dissolution of the solid was observed, iron powder (22 g, 392 mmol) was added in small portions over 1 h. After 1 h refluxing, the brown solution was cooling down to room temperature. Cold water (600 mL) was then poured onto the mixture resulting in the precipitation of a yellow-green solid which was filtered, washed

[251] a) Griffiths, J.; Roozpeikar, B. *J. Chem. Soc., Perkin Trans. 1* **1976**, 42. b) Mauriccio, M.S.; Polina, I.; Greenberg, S.; Lever, A. B. P.; Leznoff, C. C.; Tomer, B. *Can. J. Chem.* **1985**, *63*, 3057.

with water and vacuum-dried. Recrystallization from toluene led to 12.6 g (88.0 mmol) of 4-aminophthalonitrile as ocher crystalline needles. Yield: 76%.

^{1}H-NMR (300 MHz, DMSO-d_6): δ (ppm) = 7.65 (d, J_o = 8.7 Hz, 1H; H-3), 7.00 (d, J_m = 2.5 Hz, 1H; H-1), 6.85 (dd, J_o = 8.7 Hz, J_m = 2.5 Hz, 1H; H-2), 6.70 (s (broad), 2H; NH_2).

4-Iodophthalonitrile[251b]

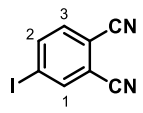

A suspension of 4-aminophthalonitrile (5 g, 35 mmol) in H_2SO_4 2.5 M (70 mL) was cooled to -10 °C and a solution of $NaNO_2$ (2.8 g, 39 mmol) in water (10 mL) was added dropwise under constant stirring. After total addition, the mixture was further stirred for 30 min at 0 °C and then poured over a solution of KI (6.5 g, 39 mmol) in cold water (40 mL). The resulting mixture was stirred for 45 min at room temperature and the brown solid was filtered, washed with water and dissolved in $CHCl_3$ (200 mL). This solution was then washed with a saturated solution of $Na_2S_2O_3$ (30 mL) and water (30 mL) and dried over Na_2SO_4. After filtration of the drying agent, the solvent was vacuum-evaporated and the yellow solid obtained was subjected to column chromatography on silica gel using CH_2Cl_2 as eluent. In this way, 6.1 g (24.0 mmol) of 4-iodophthalonitrile were obtained as a white solid. Yield: 69%.

^{1}H-NMR (300 MHz, $CDCl_3$): δ (ppm) = 8.17 (d, J_m = 1.6 Hz, 1H; H-1), 8.12 (dd, J_o = 8.2 Hz, J_m = 1.6 Hz, 1H; H-2), 7.49 (d, J_o = 8.6 Hz 1H; H-3).

1.8.3 Synthesis of peripherally iodinated subphthalocyanines

1.8.3.1 Synthesis of unsymmetrical di- and tetraiodo-subphthalocyanines

General procedure:

To a 25 ml round-bottom two-neck flask equipped with a reflux condenser and magnetic stirrer, a 1.0 M solution of BCl_3 in *p*-xylene (1 mL for each mmol of phthalonitriles employed) was added to a mixture of 4,5-diiodophthalonitrile (380 mg, 1 mmol) and of the corresponding dry phthalonitrile (2 mmol of 4,5-dioctylthiophthalonitrile for SubPc series **3**; 2 mmol of 4-*tert*-butylphthalonitrile for SubPc series **4**; 2 mmol of phthalonitrile for SubPc series **5**; 1.5 mmol of 4,5-dichlorophthalonitrile for SubPc series **6**; 1 mmol of 3,4,5,6-tetrafluorophthalonitrile for SubPc series **7-8**), under argon atmosphere. The mixture was stirred and heated to reflux (136-138 °C) for 45-150 min, depending on the phthalonitrile employed. The crude was cooled down to room temperature and flushed with argon. After evaporation of *p*-xylene, 4-*tert*-butylphenol (750 mg, 5 mmol) was added. The mixture was dissolved in *ca.* 3 mL of dry toluene and refluxed for 4-16 hours. After cooling down to room temperature, the excess of phenol was removed by washing the crude with a 3:1 MeOH/water solution. The resulting dark solid was subjected to column chromatography on silica gel using a suitable eluent, as described in each case.

*1.8.3.1.1 Subphthalocyanines **3a** and **3b***

Subphthalocyanines formation reaction time: 150 min. Axial substitution reaction time: 2 h. The mixture of subphthalocyanines formed (**9**, **3a**, **3b**, **3c**) was separated by column chromatography on silica gel using toluene/heptane from 2:3 to 3:2 as eluent. Each compound was further purified washing with cold hexane. The products in this series are listed following their elution order.

(4-*tert*-Butylphenoxy)-2,3,9,10-tetraiodo-16,17-dioctylthiosubphthalocyaninateboron(III) (3a)

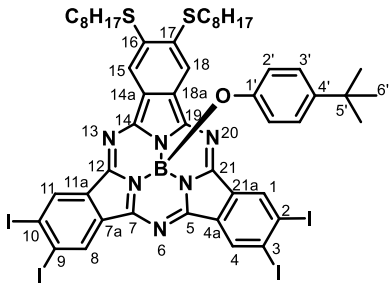

Compound **3a** was obtained as a dark purple solid. Yield: 34%.

^{1}H-NMR (300 MHz, $CDCl_3$): δ (ppm) = 9.18 (s, 2H; H-1, H-11), 9.12 (s, 2H; H-4, H-8), 8.45 (s, 2H; H-15, H-18), 6.81 (d, J_o = 8.6 Hz, 2H; H-3'), 5.37 (d, J_o = 8.6 Hz, 2H; H-2'), 3.35-3.10 (m, 4H; $S\underline{CH_2}$), 1.94-1.79 (tt, J_1 = 7.5 Hz, J_2 = 7.3 Hz, 4H; $SCH_2\underline{CH_2}$), 1.67-1.50 (tt, J_1 = 7.7 Hz, J_2 = 7.3 Hz, 4H; $S(CH_2)_2\underline{CH_2}$), 1.46-1.22 (m, 16H; $S(CH_2)_3(\underline{CH_2})_4$), 1.11 (s, 9H; H-6'), 0.94-0.85 (m, 6H; $S(CH_2)_7\underline{CH_3}$).

^{13}C-NMR (75.5 MHz, $CDCl_3$): δ (ppm) = 152.6 (C-14, C-19), 150.0 (C-5, C-7), 149.9 (C-1'), 148.8 (C-12, C-21), 144.2, 141.6 (C-1, C-4, C-8, C-11, C-14a, C-18a), 132.6, 132.5 (C-4'), 130.9, 130.7 (C-4a, C-7a, C-11a, C-21a), 128.5 (C-16, C-17), 126.0 (C-3'), 119.4 (C-15, C-18), 117.9 (C-2'), 109.5, 109.3 (C-2, C-3, C-9, C-10), 34.0 (C-5'), 33.7, 32.0, 31.5 (C-6'), 29.4, 29.3, 29.3, 28.6, 22.8 ($S\underline{(CH_2)_7}CH_3$), 14.3 ($S(CH_2)_7\underline{CH_3}$).

MS (MALDI-TOF, DCTB): *m/z* = 1335.9 $[M]^+$, 1186.9 [M - axial group]$^+$.

HRLSI-MS: m/z Calcd for $[C_{50}H_{53}BI_4N_6OS_2]$: 1335.9997; Found: 1335.9985.

UV-vis ($CHCl_3$): λ_{max} (nm) (log ε (dm^3 mol^{-1} cm^{-1})) = 590 (4.7), 542 (sh), 436 (3.7), 311 (sh), 282 (4.6).

(4-*tert*-Butylphenoxy)-2,3-diiodo-9,10,16,17-tetraoctylthiosubphthalocyaninateboron(III) (3b)

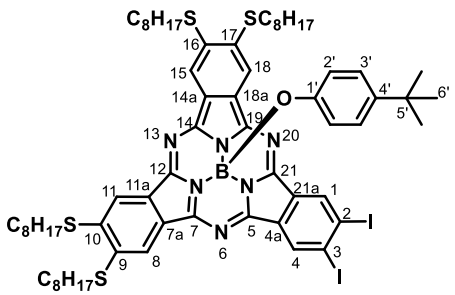

Compound **3b** was obtained as a greenish solid. Yield: 26%.

^{1}H-NMR (300 MHz, $CDCl_3$): δ (ppm) = 9.27 (s, 2H; H-1, H-4), 8.56 (s, 2H; H-11, H-15), 8.52 (s, 2H; H-8, H-18), 6.78 (d, J_o = 8.7 Hz, 2H; H-3'), 5.34 (d, J_o = 8.7 Hz, 2H; H-2'), 3.35-3.13 (m, 8H; $S\underline{CH_2}$), 1.94-1.79 (m, 8H; $SCH_2\underline{CH_2}$), 1.67-1.51 (m, 8H; $S(CH_2)_2\underline{CH_2}$), 1.46-1.24 (m, 32H; $S(CH_2)_3(\underline{CH_2})_4$), 1.10 (s, 9H; H-6'), 0.93-0.85 (m, 12H; $\underline{CH_3}$).

^{13}C-NMR (75.5 MHz, $CDCl_3$): δ (ppm) = 152.3, 151.2 (C-7, C-12, C-14, C-19), 150.1 (C-1'), 148.5 (C-5, C-21), 144.0, 141.4, 140.7 (C-1, C-4, C-7a, C-11a, C-14a, C-18a), 132.5 (C-4'), 130.8 (C-4a, C-21a), 128.8, 128.3 (C-9, C-10, C-16, C-17), 125.9 (C-3'), 119.9, 119.4 (C-8, C-11, C-15, C-18), 118.0 (C-2'), 108.6 (C-2, C-3), 34.0 (C-5'), 33.9, 33.7, 32.0, 31.5 (C-6'), 29.4, 29.3, 29.3, 28.6, 28.6, 22.8 ($S\underline{(CH_2)_7}CH_3$), 14.3, 14.2 ($S(CH_2)_7\underline{CH_3}$).

MS (MALDI-TOF, DCTB): *m/z* = 1372.3 $[M]^+$, 1223.3 [M - axial group]$^+$.

HRLSI-MS: m/z Calcd for $[C_{66}H_{87}BI_2N_6OS_4]$: 1372.4012; Found: 1372.4008.

UV-vis ($CHCl_3$): λ_{max} (nm) (log ε (dm^3 mol^{-1} cm^{-1})) = 595 (4.8), 575 (sh), 544 (sh), 421 (4.4), 356 (4.5), 305 (sh), 283 (4.8).

*1.8.3.1.2 Subphthalocyanines **4a** and **4b***

Subphthalocyanines formation reaction time: 120 min. Axial substitution reaction time: 4 h. The mixture of subphthalocyanines formed (**9**, **4a**, **4b**, **4c**) was separated by column chromatography on silica gel using toluene/heptane 3:1 as eluent. Each compound was further

purified washing with cold hexane. The products in this series are listed following their elution order.

(4-*tert*-Butylphenoxy)-2,3,9,10-tetraiodo-16-(*tert*-butyl)-subphthalocyaninateboron(III) (4a)

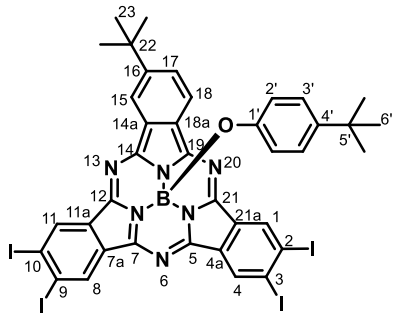

Compound **4a** was obtained as a dark purple solid. Yield: 25%.

Mp > 250 °C.

^{1}H-NMR (300 MHz, $CDCl_3$): δ (ppm) = 9.26 (s, 1H; H-1), 9.23 (s, 1H; H-11), 9.08 (s, 1H; H-4), 9.06 (s, 1H; H-8), 8.80 (d, J_m = 1.7 Hz, 1H; H-15), 8.70 (d, J_o = 8.4 Hz, 1H; H-18), 8.00 (dd, J_o = 8.4 Hz, J_m = 1.7 Hz, 1H; H-17), 6.83 (d, J_o = 8.7 Hz, 2H; H-3'), 5.40 (d, J_o = 8.7 Hz, 2H; H-2'), 1.56 (s, 9H; H-23), 1.12 (s, 9H; H-6').

^{13}C-NMR (75.5 MHz, $CDCl_3$): δ (ppm) = 155.2 (C-14, C-19), 153.6, 153.4 (C-12, C-21), 150.0, 149.9 (C-1'), 149.8 (C-5, C-7), 148.7, 148.6 (C-16), 144.1 (C-1, C-4, C-8, C-11), 132.6 (C-4'), 132.5, 132.4, 131.6, 130.9, 130.8, 130.7, 130.6 (C-4a, C-7a, C-11a, C-14a, C-18a, C-21a), 129.1, 128.9 (C-17), 126.0 (C-3'), 122.3, 119.0 (C-15, C-18), 118.0 (C-2'), 109.5, 109.4, 109.2, 109.1 (C-2, C-3, C-9, C-10), 36.1 (C-22), 34.0 (C-5'), 31.8 (C-23), 31.5 (C-6').

MS (MALDI-TOF, DCTB): *m/z* = 1103.9 $[M]^+$, 954.8 [M - axial group]$^+$.

HRLSI-MS: m/z Calcd for $[C_{38}H_{29}BI_4N_6O]$: 1103.8676; Found: 1103.8663.

UV-vis ($CHCl_3$): λ_{max} (nm) (log ε (dm^3 mol^{-1} cm^{-1})) = 585 (4.7), 570 (4.6), 546 (4.3), 524 (4.2), 328 (4.4), 276 (4.6).

(4-*tert*-Butylphenoxy)-2,3-diiodo-9(10),16(17)-bis(*tert*-butyl)-subphthalocyaninateboron(III) (mixture of three regioisomers) (4b)

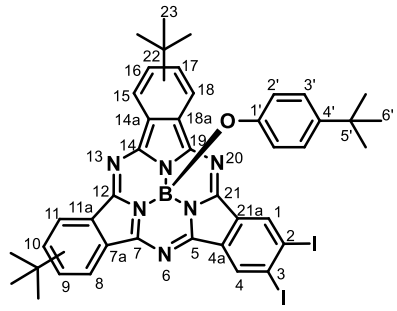

Compound **4b** was obtained as a purple solid. Yield: 33%.

Mp > 250 °C.

^{1}H-NMR (300 MHz, $CDCl_3$): δ (ppm) = 9.38 (s, 1H; H-1/H-4), 9.36 (s, 1H; H-4/H-1), 8.93-8.82 (m, 2H; H-8/H-11, H-15/H-18), 8.78 (d, J_o = 8.4 Hz, 1H; H-8/H-11/H-15/H-18), 8.73 (d, J_o = 8.4 Hz, 1H; H-8/H-11/H-15/H-18), 8.00 (d, J_o = 8.4 Hz, 2H; H-9/H-10, H-16/H-17), 6.75 (d, J_o = 8.8 Hz, 2H; H-3'), 5.29 (d, J_o = 8.8 Hz, 2H; H-2'), 1.55 (m, 18H; H-23), 1.08 (s, 9H; H-6').

^{13}C-NMR (75.5 MHz, $CDCl_3$): δ (ppm) = 154.8, 154.6, 154.5, 153.5, 153.3, 153.2 (C-7, C-12, C-14, C-19), 152.0, 151.8 (C-5, C-21), 150.1 (C-1'), 148.3, 148.2 (C-9/C-10, C-16/C-17), 143.9 (C-1, C-4), 132.5 (C-4'), 131.4, 130.8 (C-4a, C-7a, C-11a, C-14a, C-18a, C-21a), 129.2, 128.6, 128.4 (C-

10/C-9, C-17/C-16), 125.8 (C3'), 122.1, 122.0, 118.9, 118.7 (C-8, C-11, C-15, C-18), 117.9 (C-2'), 108.4, 108.3 (C-2, C-3), 36.0 (C-22), 34.0 (C-5'), 31.8 (C-23), 31.5 (C-6').

MS (MALDI-TOF, DCTB): *m/z* = 908.2 $[M]^+$, 759.1 [M - axial group]$^+$.

HRLSI-MS: m/z Calcd for $[C_{42}H_{39}BI_2N_6O]$: 908.1369; Found: 908.1368.

UV-vis ($CHCl_3$): λ_{max} (nm) (log ε (dm^3 mol^{-1} cm^{-1})) = 580 (4.6), 569 (4.5), 541 (4.2), 522 (4.1), 320 (4.3), 271 (4.4).

FT-IR (KBr), ν (cm^{-1}): 2962, 2866, 1607, 1510, 1454, 1402, 1385, 1259, 1178, 1063 (B-O), 895, 831, 760, 708.

*1.8.3.1.3 Subphthalocyanines **5a** and **5b***

Subphthalocyanines formation reaction time: 90 min. Axial substitution reaction time: 12 h. The mixture of subphthalocyanines formed (**9**, **5**, **5b**, **5c**) was separated by column chromatography on silica gel using toluene/heptane 4:1 as eluent. Each compound was further purified washing with cold hexane. The products in this series are listed following their elution order.

(4-*tert*-Butylphenoxy)-2,3,9,10-tetraiodosubphthalocyaninateboron(III) (5a)

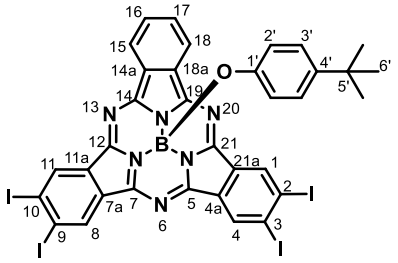

Compound **5a** was obtained as a dark purple solid. Yield: 21%.

Mp > 250 °C.

^{1}H-NMR (300 MHz, $CDCl_3$): δ (ppm) = 9.33 (s, 2H; H-1, H-11), 9.25 (s, 2H; H-4, H-8), 8.82-8.72 (AA'BB' system, 2H; H-15, H-18), 7.92-7.85 (AA'BB' system, 2H; H-16, H-17), 6.78 (d, J_o = 8.7 Hz, 2H; H-3'), 5.31 (d, J_o = 8.7 Hz, 2H; H-2'), 1.10 (s, 9H; H-6').

^{13}C-NMR (75.5 MHz, $CDCl_3$): δ (ppm) = 153.0 (C-14, C-19), 150.0 (C-5, C-7), 149.8 (C-1'), 149.1 (C-12, C-21), 144.3 (C-1, C-4, C-8, C-11), 132.7 (C-16, C-17), 132.6 (C-4'), 131.3 (C-14a, C-18a), 131.0, 130.9, 130.7 (C-4a, C-7a, C-11a, C-21a), 126.0 (C3'), 122.6 (C-15, C-18), 118.0 (C-2'), 109.6, 109.4 (C-2, C-3, C-9, C-10), 34.0 (C-5'), 31.5 (C-6').

MS (MALDI-TOF, DCTB): *m/z* = 1047.8 $[M]^+$, 898.8 [M - axial group]$^+$.

HRLSI-MS: m/z Calcd for $[C_{34}H_{21}BI_4N_6O]$: 1047.8049; Found: 1047.8057.

UV-vis ($CHCl_3$): λ_{max} (nm) (log ε (dm^3 mol^{-1} cm^{-1})) = 582 (4.7), 568 (sh), 543 (4.3), 522 (4.2), 326 (4.3), 276 (4.5).

(4-*tert*-Butylphenoxy)-2,3-diiodosubphthalocyaninateboron(III) (5b)

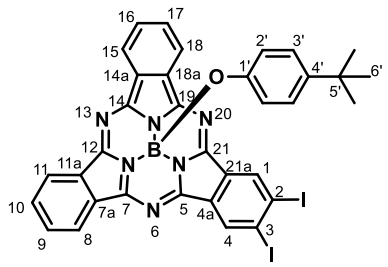

Compound **5b** was obtained as a magenta solid. Yield: 25%.

Mp > 250 °C.

^{1}H-NMR (300 MHz, $CDCl_3$): δ (ppm) = 9.32 (s, 2H; H-1, H-4), 8.85-8.70 (AA'BB' system, 4H; H-8, H-11, H-15, H-18), 7.90-7.80 (AA'BB' system, 4H; H-9, H-10, H-16, H-17), 6.80 (d, J_o = 8.6 Hz, 2H; H-3'), 5.36 (d, J_o = 8.6 Hz, 2H; H-2'), 1.10 (s, 9H; H-6').

^{13}C-NMR (75.5 MHz, $CDCl_3$): δ (ppm) = 152.8, 151.9 (C-7, C-12, C-14, C-19), 150.0 (C-1'), 148.7 (C-5, C-21), 144.0 (C-1, C-4), 132.5 (C-4'), 131.3, 131.1, 130.9 (C-7a, C-11a, C-14a, C-18a), 130.3, 130.2 (C-9, C-10, C-16, C-17), 129.1, 128.3 (C-4a, C-21a), 125.9 (C3'), 122.5, 122.3 (C-8, C-11, C-15, C-18), 118.0 (C-2'), 108.8 (C-2, C-3), 34.0 (C-5'), 31.5 (C-6').

MS (MALDI-TOF, DCTB): *m/z* = 796.1 $[M]^+$, 647.0 [M - axial group]$^+$.

HRLSI-MS: m/z Calcd for $[C_{34}H_{23}BI_2N_6O]$: 796.0116; Found: 796.0123.

UV-vis ($CHCl_3$): λ_{max} (nm) (log ε (dm^3 mol^{-1} cm^{-1})) = 574 (4.5), 567 (sh), 537 (4.2), 518 (4.1), 313 (4.3), 272 (4.4).

*1.8.3.1.4 Subphthalocyanines **6a** and **6b***

Subphthalocyanines formation reaction time: 60 min. Axial substitution reaction time: 16 h. The mixture of subphthalocyanines formed (**9**, **6a**, **6b**, **6c**) was separated by column chromatography on silica gel using heptane/dioxane 8:1 as eluent. Each compound was further purified washing with a 5:1 MeOH/water solution. The products in this series are listed following their elution order.

(4-*tert*-Butylphenoxy)-2,3-diiodo-9,10,16,17-tetrachlorosubphthalocyaninateboron(III) (6b)

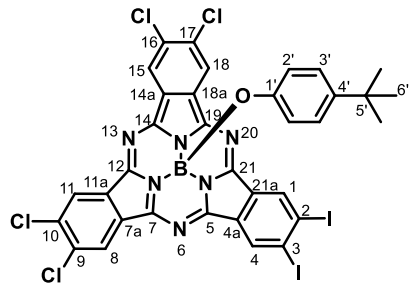

Compound **6b** was obtained as a magenta solid. Yield: 23%.

Mp > 250 °C.

^{1}H-NMR (300 MHz, $CDCl_3$): δ (ppm) = 9.18 (s, 2H; H-1, H-4), 8.76 (s, 2H; H-11, H-15), 8.73 (s, 2H; H-8, H-18), 6.83 (d, J_o = 8.7 Hz, 2H; H-3'), 5.35 (d, J_o = 8.7 Hz, 2H; H-2'), 1.12 (s, 9H; H-6').

^{13}C-NMR (75.5 MHz, $CDCl_3$): δ (ppm) = 150.5, 150.3 (C-7,

C-12, C-14, C-19), 150.2 (C-5, C-21), 149.6 (C-1'), 144.6 (C-1, C-4), 135.1, 135.0 (C-9, C-10, C-16, C-17), 132.7 (C-4'), 130.9 (C-4a, C-21a), 129.8, 129.7 (C-7a, C-11a, C-14a, C-18a), 126.1 (C3'), 123.9 (C-8, C-11, C-15, C-18), 118.0 (C-2'), 110.1 (C-2, C-3), 34.1 (C-5'), 31.5 (C-6').

MS (MALDI-TOF, DCTB): *m/z* = 933.9 $[M]^+$, 784.9 [M - axial group]$^+$.

HRLSI-MS: m/z Calcd for $[C_{34}H_{19}BCl_4I_2N_6O]$: 933.8532; Found: 933.8524.

UV-vis ($CHCl_3$): λ_{max} (nm) (log ε (dm^3 mol^{-1} cm^{-1})) = 574 (4.6), 557 (sh), 528 (sh), 329 (4.2), 276 (4.4).

(4-*tert*-Butylphenoxy)-2,3,9,10-tetraiodo-16,17-dichlorosubphthalocyaninateboron(III) (6a)

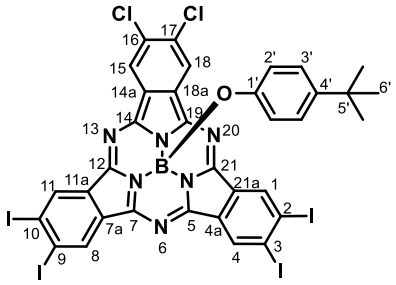

Compound **6a** was obtained as a purple solid. Yield: 15%.

Mp > 250 °C.

^{1}H-NMR (300 MHz, $CDCl_3$): δ (ppm) = 9.29 (s, 2H; H-1, H-11), 9.27 (s, 2H; H-4, H-8), 8.84 (s, 2H; H-15, H-18), 6.78 (d, J_o = 8.7 Hz, 2H; H-3'), 5.28 (d, J_o = 8.7 Hz, 2H; H-2'), 1.12 (s, 9H; H-6').

^{13}C-NMR (75.5 MHz, $CDCl_3$): δ (ppm) = 150.5, 150.4, 150.2 (C-5, C-7, C-12, C-14, C-19, C-21), 149.6 (C-1'), 144.5 (C-1, C-4, C-8, C-11), 135.1 (C-16, C-17), 132.7 (C-4'), 131.1, 131.0 (C-4a, C-7a, C-11a, C-21a), 129.8 (C-14a, C-18a), 126.1 (C3'), 124.0 (C-15, C-18), 118.0 (C-2'), 110.2, 110.1 (C-2, C-3, C-9, C-10), 34.1 (C-5'), 31.5 (C-6').

MS (MALDI-TOF, DCTB): *m/z* = 1115.8 $[M]^+$, 966.7 [M - axial group]$^+$.

HRLSI-MS: m/z Calcd for $[C_{34}H_{19}BCl_2I_4N_6O]$: 1115.7270; Found: 1115.7244.

UV-vis ($CHCl_3$): λ_{max} (nm) (log ε (dm^3 mol^{-1} cm^{-1})) = 578 (4.7), 563 (sh), 529 (sh), 335 (4.3), 280 (4.5).

*1.8.3.1.5 Subphthalocyanines **8a**, **8b**, **7a** and **7b***

Subphthalocyanines formation reaction time: 45 min. In this particular series, subphthalocyanines **8a** and **8b** were isolated prior to axial substitution reaction with 4-*tert*-butylphenol. The mixture of subphthalocyanines formed (**9**, **8a**, **8b**, **8c**) was separated by column chromatography on silica gel using heptane/dioxane 8:1 as eluent. Each compound was further purified washing with cold hexane. The products in this series are listed following their elution order.

For the synthesis of subphthalocyanines **7a** and **7b**, in a round-bottom two-neck flask equipped with a reflux condenser and a magnetic stirrer, 4-*tert*-butylphenol (0.2 mmol) and the corresponding chlorosubphthalocyanine (0.02 mmol; **8a** for **7a**, **8b** for **7b**) were refluxed in

toluene (1 mL) for 18 h. After cooling down to room temperature, the excess of phenol was removed by washing the crude with a 3:1 MeOH/water solution. The resulting dark solid was dissolved in toluene and passed through a short silica plug. The solvent was vacuum-evaporated and the resulting pink solid was purified washing with cold hexane.

Chloro-2,3-diiodo-8,9,10,11,15,16,17,18-octafluorosubphthalocyaninateboron(III) (8b)

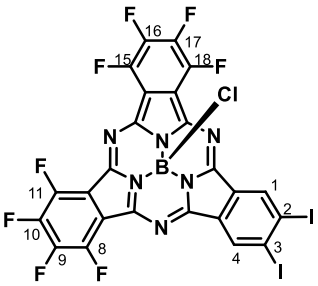

Compound **8b** was obtained as a pink solid. Yield: 14%.

Mp > 250 °C.

^{1}H-NMR (300 MHz, $CDCl_3$): δ (ppm) = 9.39 (s, 2H; H-1, H-4).

^{19}F-NMR (470 MHz, $CDCl_3$): δ (ppm) = -137.0 (AA'BB' system, 4F; F-8, F-11, F-15, F-18), -147.7 (AA'BB' system, 4F; F-9, F-10, F-16, F-17).

MS (MALDI-TOF, DCTB): *m/z* = 825.9 $[M]^+$.

HRLSI-MS: m/z Calcd for $[C_{24}H_2BClF_8I_2N_6]$: 825.8083; Found: 825.8095.

UV-vis ($CHCl_3$): λ_{max} (nm) (log ε (dm^3 mol^{-1} cm^{-1})) = 576 (ε_{max}), 560 (sh), 532 (sh), 300, 280.

Chloro-2,3,9,10-tetraiodo-15,16,17,18-tetrafluorosubphthalocyaninateboron(III) (8a)

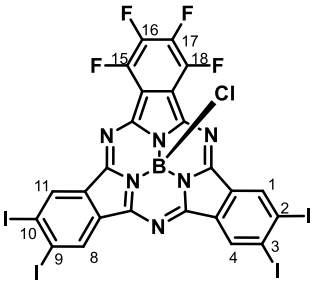

Compound **8a** was obtained as a pink solid. Yield: 5%.

Mp > 250 °C.

^{1}H-NMR (300 MHz, $CDCl_3$): δ (ppm) = 9.43 (s, 2H; H-1, H-11), 9.39 (s, 2H; H-4, H-8).

^{19}F-NMR (470 MHz, $CDCl_3$): δ (ppm) = -137.9 (AA'BB' system, 2F; F-15, F-18), -148.7 (AA'BB' system, 2F; F-16, F-17).

MS (MALDI-TOF, DCTB): *m/z* = 1005.7 $[M]^+$.

HRLSI-MS: m/z Calcd for $[C_{24}H_4BClF_4I_4N_6]$: 1005.6393; Found: 1005.6365.

UV-vis ($CHCl_3$): λ_{max} (nm) (log ε (dm^3 mol^{-1} cm^{-1})) = 581 (ε_{max}), 566 (sh), 528 (sh), 325, 279.

(4-*tert*-Butylphenoxy)-2,3-diiodo-8,9,10,11,15,16,17,18-octafluorosubphthalocyaninateboron(III) (7b)

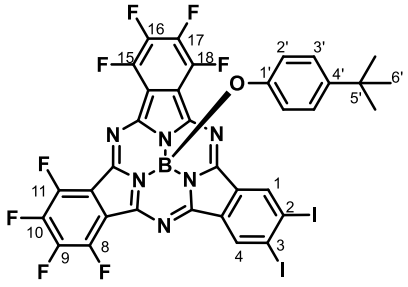

Compound **7b** was obtained as a pink solid. Yield: 78% (from **8b**).

Mp > 250 °C.

^{1}H-NMR (300 MHz, $CDCl_3$): δ (ppm) = 9.38 (s, 2H; H-1, H-4), 6.79 (d, J_o = 8.7 Hz, 2H; H-3'), 5.26 (d, J_o = 8.7 Hz, 2H; H-2'), 1.10 (s, 9H; H-6').

^{19}F-NMR (470 MHz, $CDCl_3$): δ (ppm) = -137.7 (AA'BB' system, 4F; F-8, F-11, F-15, F-18), -148.6 (AA'BB' system, 4F; F-9, F-10, F-16, F-17).

MS (MALDI-TOF, DCTB): *m/z* = 940.0 $[M]^+$ (100%), 790.9 [M - axial group]$^+$.

UV-vis ($CHCl_3$): λ_{max} (nm) (log ε (dm^3 mol^{-1} cm^{-1})) = 573 (4.6), 555 (sh), 523 (sh), 305 (4.2), 276 (4.3).

(4-*tert*-Butylphenoxy)-2,3,9,10-tetraiodo-15,16,17,18-tetrafluorosubphthalocyaninateboron(III) (7a)

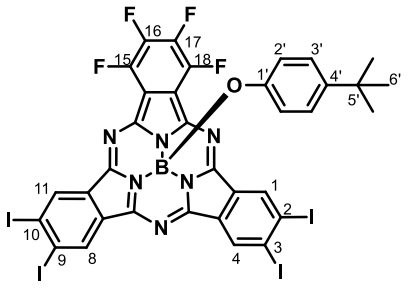

Compound **7a** was obtained as a pink solid. Yield: 70% (from **8a**).

Mp > 250 °C.

^{1}H-NMR (300 MHz, $CDCl_3$): δ (ppm) = 9.38 (s, 2H; H-1, H-11), 9.34 (s, 2H; H-4, H-8), 6.76 (d, J_o = 8.8 Hz, 2H; H-3'), 5.25 (d, J_o = 8.8 Hz, 2H; H-2'), 1.09 (s, 9H; H-6').

MS (MALDI-TOF, DCTB): *m/z* = 1119.8 $[M]^+$, 970.7 [M - axial group]$^+$.

UV-vis ($CHCl_3$): λ_{max} (nm) (log ε (dm^3 mol^{-1} cm^{-1})) = 577 (4.7), 558 (sh), 536 (sh), 327 (sh), 304 (sh), 281 (4.4).

1.8.3.2 Synthesis of triiodo-subphthalocyanines[48b,88a]

Chloro-2,9(10),16-triiodosubphthalocyaninateboron(III) (mixture of regioisomers C_3/C_1 1:3) (10)[48b]

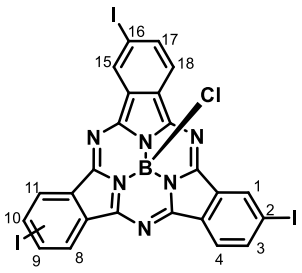

To a 25 ml round-bottom two-neck flask equipped with a reflux condenser and magnetic stirrer, a 1.0 M solution of BCl_3 in *p*-xylene (1.6 mL, 1.6 mmol) was added to 4-iodophthalonitrile (400 mg, 1.57 mmol) under argon atmosphere The mixture was stirred and heated to reflux (136-138 °C) for 2 h. The purple crude was cooled down to room temperature, flushed with argon and the solvent was evaporated under reduced pressure. The product was purified by column chromatography on silica gel using heptane/EtOAc 1:1 as eluent to afford **10** as a purple solid. Yield: 23%.

^{1}H-NMR (300 MHz, $CDCl_3$): δ (ppm) = 9.25-9.21 (m, 3H; H-1, H-8/H-11, H-15), 8.60-8.54 (m, 3H; H-4, H-11/H-8, H-18), 8.27-8.21 (m, 3H; H-3, H-9/H-10, H-17).

UV-vis ($CHCl_3$): λ_{max} (nm) (log ε (dm^3 mol^{-1} cm^{-1})) = 570 (4.5), 520 (sh), 303 (3.9), 270 (4.1).

(4-*tert*-Butylphenoxy)-2,9(10),16-triiodosubphthalocyaninateboron(III) (11)[88a]

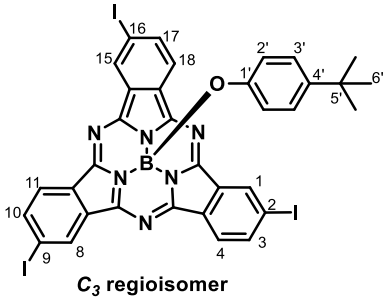

***C_3* regioisomer**

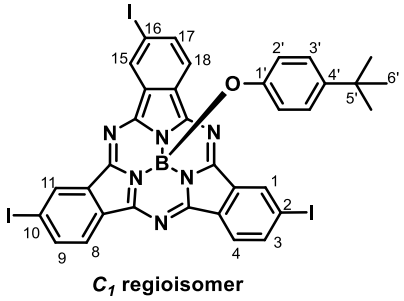

***C_1* regioisomer**

In a round-bottom two-neck flask equipped with a reflux condenser and a magnetic stirrer, 4-*tert*-butylphenol (280 mg, 1.80 mmol), chlorosubphthalocyanine **10** (250 mg, 0.31 mmol) and DBU (45 µL, 0.30 mmol) were refluxed in toluene (3 mL) for 14 h. After cooling down to room temperature, the excess of phenol was removed by washing the crude with a 2:1 MeOH/water solution. The resulting dark solid was purified by column chromatography on silica gel using toluene/heptane 3:1 as eluent, and during the process C_3 and C_1 regioisomers were separated when needed. Compound **11** was isolated as a purple solid. Overall yield: 90%.

***C_3* regioisomer:**

^{1}H-NMR (300 MHz, $CDCl_3$): δ (ppm) = 9.20 (s, 3H; H-1, H-8, H-15), 8.53 (d, J_o = 8.0 Hz, 3H; H-4, H-11, H-18), 8.22 (d, J_o = 8.0 Hz, 3H; H-3, H-10, H-17), 6.73 (d, J_o = 8.2 Hz, 2H; H-3'), 5.24 (d, J_o = 8.2 Hz, 2H; H-2'), 1.08 (s, 9H; H-6').

UV-vis ($CHCl_3$): λ_{max} (nm) (log ε (dm^3 mol^{-1} cm^{-1})) = 573 (4.6), 530 (sh), 340 (4.1), 317 (4.2), 277 (4.3).

***C_1* regioisomer:**

^{1}H-NMR (300 MHz, $CDCl_3$): δ (ppm) = 9.06 (s, 1H; H-1), 9.02 (s, 2H; H-11, H-15), 8.46-8.29 (m, 3H; H-4, H-8, H-18), 8.11-7.95 (m, 3H; H-3, H-9, H-17), 6.84 (d, J_o = 8.2 Hz, 2H; H-3'), 5.41 (d, J_o = 8.2 Hz, 2H; H-2'), 1.12 (s, 9H; H-6').

UV-vis ($CHCl_3$): λ_{max} (nm) (log ε (dm^3 mol^{-1} cm^{-1})) = 573 (4.6), 530 (sh), 340 (4.1), 317 (4.2), 277 (4.3).

1.8.4 Synthesis of peripherally cyanated subphthalocyanines

1.8.4.1 Synthesis of unsymmetrical phenoxy-dicyano-subphthalocyanines

General procedure:

To a 5 mL microwave vial, a solution of the corresponding diiodo-subphthalocyanine **3b-7b** (0.100 mmol) in dry DMF (4 mL), $Zn(CN)_2$ (18 mg, 0.150 mmol) and $Pd(PPh_3)_4$ (17 mg, 0.015 mmol) were added. The reaction tube was sealed and heated to 105 °C under microwave irradiation with a 18 min hold time. Water (20 mL) was added and the product was extracted with dichloromethane (3 × 15 mL). The combined organic extracts were dried over $MgSO_4$ and the solvent was removed by rotary evaporation. The resulting dark solid was subjected to column chromatography on silica gel using a suitable eluent, as described in each case.

(4-*tert*-Butylphenoxy)-2,3-dicyano-9(10),16(17)-bis(*tert*-butyl)-subphthalocyaninateboron(III) (mixture of three regioisomers) (12)

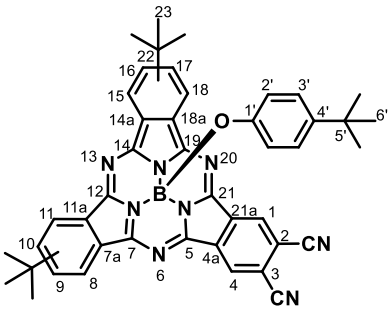

Eluent: toluene/THF 200:1. Compound **12** was obtained as a dark purple solid. Yield: 85%.

Mp > 250 °C.

^{1}H-NMR (300 MHz, $CDCl_3$): δ (ppm) = 9.26 (s, 1H; H-1/H-4), 9.24 (s, 1H; H-4/H-1), 8.92-8.81 (m, 2H; H-8/H-11, H-15/H-18), 8.76 (d, J_o = 8.4 Hz, 1H; H-8/H-11/H-15/H-18), 8.72 (d, J_o = 8.4 Hz, 1H; H-8/H-11/H-15/H-18), 8.11-8.00 (m, 2H; H-9/H-10, H-16/H-17), 6.78 (d, J_o = 8.8 Hz, 2H; H-3'), 5.33 (d, J_o = 8.8 Hz, 2H; H-2'), 1.55 (m, 18H; H-23), 1.08 (s, 9H; H-6').

^{13}C-NMR (75.5 MHz, $CDCl_3$): δ (ppm) = 157.3, 157.1, 156.9, 156.4, 155.7, 155.6 (C-7, C-12, C-14, C-19), 153.0, 152.9, 152.8 (C-5, C-21), 149.8 (C-1'), 145.9, 145.8, 145.7, 144.3 (C-9/C-10, C-16/C-17), 132.6 (C-4'), 131.4, 130.0, 129.8, 129.4, 129.3, 128.9, 128.8 (C-1, C-4, C-4a, C-7a, C-9/C-10, C-11a, C-14a, C-16/C-17, C-18a, C-21a), 126.0 (C-3'), 122.9, 122.4, 119.7, 119.2 (C-8, C-11, C-15, C-18), 117.8 (C-2'), 116.3 (C-2, C-3), 112.6, 112.5 (C≡N), 36.2, 36.1 (C-22), 34.0 (C-5'), 31.7 (C-23), 31.4 (C-6').

MS (MALDI-TOF, DCTB): *m/z* = 706.4 $[M]^+$, 557.3 [M - axial group]$^+$.

HRLSI-MS: m/z Calcd for $[C_{44}H_{39}BN_8O]$: 706.3342; Found: 706.3352.

UV-vis ($CHCl_3$): λ_{max} (nm) (log ε (dm^3 mol^{-1} cm^{-1})) = 598 (4.9), 576 (4.5), 530 (4.3), 514 (4.3), 298 (4.6), 259 (4.6).

FT-IR (KBr), ν (cm^{-1}): 2961, 2926, 2854, 2230 (C≡N), 1618, 1514, 1464, 1437, 1281, 1257, 1217, 1134, 1107, 1065 (B-O), 833, 762, 712.

(4-*tert*-Butylphenoxy)-2,3-dicyano-9,10,16,17-tetraoctylthiosubphthalocyaninateboron(III) (13)

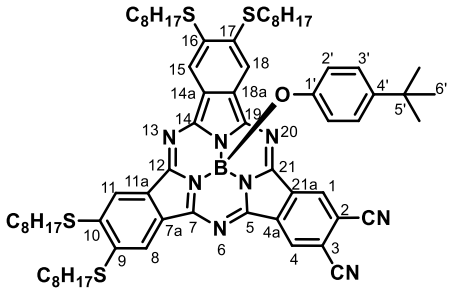

Eluent: toluene/THF 300:1. Compound **13** was obtained as a bluish solid. Yield: 76%.

^{1}H-NMR (300 MHz, $CDCl_3$): δ (ppm) = = 9.16 (s, 2H; H-1, H-4), 8.55 (s, 2H; H-11, H-15), 8.49 (s, 2H; H-8, H-18), 6.80 (d, J_o = 8.7 Hz, 2H; H-3'), 5.36 (d, J_o = 8.7 Hz, 2H; H-2'), 3.37-3.16 (m, 8H; S$\underline{CH_2}$), 1.95-1.80 (m, 8H; $SCH_2\underline{CH_2}$), 1.67-1.52 (m, 8H; $S(CH_2)_2\underline{CH_2}$), 1.46-1.23 (m, 32H; $S(CH_2)_3(\underline{CH_2})_4$), 1.10 (s, 9H; H-6'), 0.94-0.84 (m, 12H; $\underline{CH_3}$).

^{13}C-NMR (75.5 MHz, $CDCl_3$): δ (ppm) = 156.1.3, 152.2 (C-7, C-12, C-14, C-19), 149.8 (C-1'), 146.0 (C-5, C-21), 144.4, 143.4, 141.4 (C-4a, C-7a, C-11a, C-14a, C-18a, C-21a), 129.5 (C-1, C-4), 128.8, 127.9 (C-9, C-10, C-16, C-17), 126.1 (C-3'), 120.2, 118.9 (C-8, C-11, C-15, C-18), 117.9 (C-2'), 116.2 (C-2, C-3), 112.7 (C≡N), 34.0 (C-5'), 33.8, 33.5, 32.0, 31.5 (C-6'), 29.4, 29.3, 29.3, 29.2, 28.6, 28.4, 22.8 ($S(\underline{CH_2})_7CH_3$), 14.3 ($S(CH_2)_7\underline{CH_3}$).

MS (MALDI-TOF, DCTB): *m/z* = 1170.6 $[M]^+$, 1021.5 [M - axial group]$^+$.

HRLSI-MS: m/z Calcd for $[C_{68}H_{87}BN_8OS_4]$: 1170.5984; Found: 1170.5969.

UV-vis ($CHCl_3$): λ_{max} (nm) (log ε (dm^3 mol^{-1} cm^{-1})) = 617 (5.0), 589 (4.7), 552 (sh), 455 (4.3), 413 (4.3), 392 (4.3), 310 (4.8).

(4-*tert*-Butylphenoxy)-2,3-dicyanosubphthalocyaninateboron(III) (14)

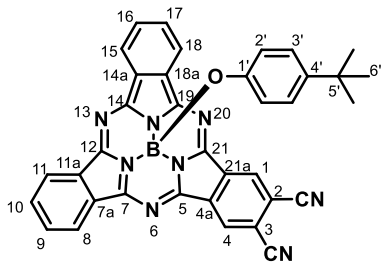

Eluent: toluene/THF 100:1. Compound **14** was obtained as a dark purple solid. Yield: 89%.

Mp > 250 °C.

^{1}H-NMR (300 MHz, $CDCl_3$): δ (ppm) = 9.22 (s, 2H; H-1, H-4), 8.87-8.78 (AA'BB' system, 4H; H-8, H-11, H-15, H-18), 8.01-7.93 (AA'BB' system, 4H; H-9, H-10, H-16, H-17), 6.80 (d, J_o = 8.6 Hz, 2H; H-3'), 5.35 (d, J_o = 8.6 Hz, 2H; H-2'), 1.10 (s, 9H; H-6').

^{13}C-NMR (75.5 MHz, $CDCl_3$): δ (ppm) = 156.5, 152.8 (C-7, C-12, C-14, C-19), 149.7 (C-1'), 146.2 (C-5, C-21), 144.5 (C-4a, C-21a), 132.2 (C-4'), 131.7, 131.1 (C-7a, C-11a, C-14a, C-18a), 129.1 (C-1, C-4), 128.7, 128.3 (C-9, C-10, C-16, C-17), 126.0 (C3'), 123.2, 122.8 (C-8, C-11, C-15, C-18), 117.9 (C-2'), 116.0 (C-2, C-3), 112.9 (C≡N), 34.0 (C-5'), 31.4 (C-6').

MS (MALDI-TOF, DCTB): *m/z* = 594.3 $[M]^+$, 445.2 [M - axial group]$^+$.

HRLSI-MS: m/z Calcd for $[C_{36}H_{23}BN_8O]$: 594.2089; Found: 594.2096.

UV-vis ($CHCl_3$): λ_{max} (nm) (log ε (dm^3 mol^{-1} cm^{-1})) = 593 (4.8), 570 (4.4), 527 (4.1), 511 (4.2), 299 (4.5), 269 (4.3).

FT-IR (KBr), ν (cm^{-1}): 2961, 2926, 2854, 2230 (C≡N), 1612, 1512, 1464, 1437, 1284, 1254, 1238, 1215, 1128, 1107, 1067 (B-O), 779, 748, 702.

(4-*tert*-Butylphenoxy)-2,3-dicyano-9,10,16,17-tetrachlorosubphthalocyaninateboron(III) (15)

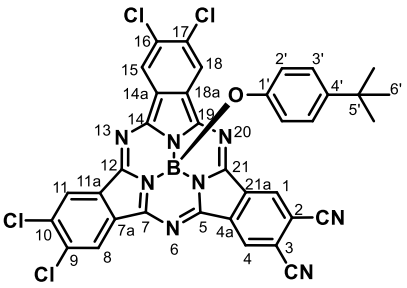

Eluent: toluene/THF from 300:1 to 100:1. Compound **15** was obtained as a dark purple solid. Yield: 69%.

Mp > 250 °C.

^{1}H-NMR (300 MHz, $CDCl_3$): δ (ppm) = 9.23 (s, 2H; H-1, H-4), 8.91 (s, 2H; H-11, H-15), 8.90 (s, 2H; H-8, H-18), 6.78 (d, J_o = 8.7 Hz, 2H; H-3'), 5.28 (d, J_o = 8.7 Hz, 2H; H-2'), 1.10 (s, 9H; H-6').

^{13}C-NMR (75.5 MHz, $CDCl_3$): δ (ppm) = 153.9, 151.3 (C-7, C-12, C-14, C-19), 149.1 (C-1'), 147.7 (C-5, C-21), 145.0 (C-4a, C-21a), 136.6, 136.1 (C-9, C-10, C-16, C-17),130.7 (C-4'), 128.8, 126.6 (C-7a, C-11a, C-14a, C-18a), 126.2 (C3'), 124.6, 124.4 (C-8, C-11, C-15, C-18), 117.9 (C-2'), 115.7 (C-2, C-3), 114.2 (C≡N), 34.1 (C-5'), 31.4 (C-6').

MS (MALDI-TOF, DCTB): *m/z* = 732.1 $[M]^+$, 583.0 [M - axial group]$^+$.

HRLSI-MS: m/z Calcd for $[C_{36}H_{19}BCl_4N_8O]$: 732.0505; Found: 732.0523.

UV-vis ($CHCl_3$): λ_{max} (nm) (log ε (dm^3 mol^{-1} cm^{-1})) = 592 (4.9), 566 (4.6), 535 (sh), 516 (4.3), 318 (sh), 299 (4.5), 267 (4.6).

FT-IR (KBr), ν (cm^{-1}): 2961, 2923, 2853, 2231 (C≡N), 1610, 1512, 1464, 1431, 1408, 1286, 1250, 1211, 1184, 1138, 1097, 1068 (B-O), 821, 762, 710.

(4-*tert*-Butylphenoxy)-2,3-dicyano-8,9,10,11,15,16,17,18-octafluorosubphthalocyaninateboron(III) (16)

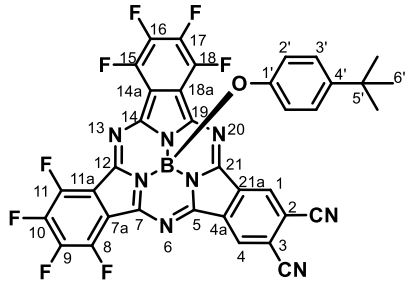

Eluent: toluene/THF 200:1. Compound **16** was obtained as a dark purple solid. Yield: 40%.

Mp > 250 °C.

^{1}H-NMR (300 MHz, $CDCl_3$): δ (ppm) = 9.31 (s, 2H; H-1, H-4), 6.80 (d, J_o = 8.7 Hz, 2H; H-3'), 5.26 (d, J_o = 8.7 Hz, 2H; H-2'), 1.10 (s, 9H; H-6').

^{13}C-NMR (75.5 MHz, $CDCl_3$): δ (ppm) = 150.7, 148.9 (C-7, C-12, C-14, C-19), 148.7 (C-1'), 145.4 (C-5, C-21), 144.7 (C-9, C-10, C-16, C-17), 144.5 (C-4a, C-21a), 141.2 (C-8, C-11, C-15, C-18), 131.2 (C-4'), 128.8 (C-

1, C-4), 126.4 (C3'), 125.7 (C-7a, C-11a, C-14a, C-18a), 117.8 (C-2'), 115.3 (C-2, C-3), 108.9 (C≡N), 34.0 (C-5'), 31.4 (C-6').

^{19}F-NMR (470 MHz, $CDCl_3$): δ (ppm) = -135.9 (AA'BB' system, 4F; F-8, F-11, F-15, F-18), -146.3 (AA'BB' system, 4F; F-9, F-10, F-16, F-17).

MS (MALDI-TOF, DCTB): *m/z* = 738.2 $[M]^+$.

UV-vis ($CHCl_3$): λ_{max} (nm) (log ε (dm^3 mol^{-1} cm^{-1})) = 588 (4.9), 565 (4.7), 542 (4.5), 520 (4.3), 307 (4.6), 278 (sh).

FT-IR (KBr), ν (cm^{-1}): 2961, 2926, 2856, 2233 (C≡N), 1634, 1533, 1485, 1429, 1283, 1217, 1140, 1115, 1090 (B-O), 764, 712.

1.8.4.2 Synthesis of unsymmetrical phenoxy-tetracyano-subphthalocyanines

General procedure:

To a 5 mL microwave vial, a solution of the corresponding tetraiodo-subphthalocyanine **3a-6a** (0.100 mmol) in dry DMF (4 mL), $Zn(CN)_2$ (35 mg, 0.300 mmol) and $Pd(PPh_3)_4$ (35 mg, 0.030 mmol) were added. The reaction tube was sealed and heated to 105 °C under microwave irradiation with a 18 min hold time. Water (20 mL) was added and the product was extracted with dichloromethane (3 × 15 mL). The combined organic extracts were dried over $MgSO_4$ and the solvent was removed by rotary evaporation. The resulting dark solid was subjected to column chromatography on silica gel using a suitable eluent, as described in each case.

(4-*tert*-Butylphenoxy)-2,3,9,10-tetracyano-16-(*tert*-butyl)-subphthalocyaninateboron(III) (17)

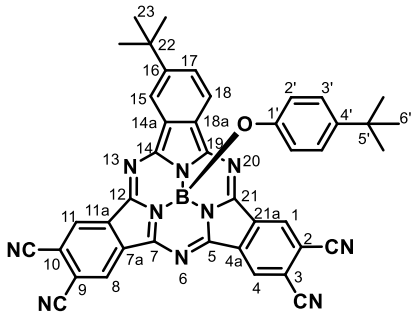

Eluent: toluene/THF 50:1. Compound **17** was obtained as a dark purple solid. Yield: 65%.

Mp > 250 °C.

^{1}H-NMR (300 MHz, $CDCl_3$): δ (ppm) = 9.28 (s, 1H; H-1), 9.24 (s, 1H; H-11), 9.22 (s, 2H; H-4, H-8), 8.88 (d, J_m = 1.6 Hz, 1H; H-15), 8.76 (d, J_o = 8.3 Hz, 1H; H-18), 8.13 (dd, J_o = 8.3 Hz, J_m = 1.6 Hz, 1H; H-17), 6.79 (d, J_o = 8.8 Hz, 2H; H-3'), 5.30 (d, J_o = 8.8 Hz, 2H; H-2'), 1.57 (s, 9H; H-23), 1.10 (s, 9H; H-6').

^{13}C-NMR (75.5 MHz, $CDCl_3$): δ (ppm) = 157.5, 157.2, 157.0 (C-14, C-19), 150.8, 150.7 (C-12, C-21), 149.1 (C-1'), 147.4, 147.3 (C-4a, C-7a, C-11a, C-21a), 145.1 (C-5, C-7), 132.2 (C-4'), 131.9, 131.8, 130.8, 130.7, 130.5, 129.4, 129.1, 129.0 (C-1, C-4, C-8, C-11, C-14a, C-18a), 128.6 (C-17), 126.2 (C-3'), 123.2, 120.1 (C-15, C-18), 117.8 (C-2'), 115.3, 115.2 (C-2, C-3, C-9, C-10), 114.8, 114.7 (C≡N), 36.3 (C-22), 34.1 (C-5'), 31.7 (C-23), 31.4 (C-6').

MS (MALDI-TOF, DCTB): *m/z* = 700.3 $[M]^+$.

HRLSI-MS: m/z Calcd for [$C_{42}H_{29}BN_{10}O$]: 700.2608; Found: 700.2633.

UV-vis ($CHCl_3$): λ_{max} (nm) (log ε (dm^3 mol^{-1} cm^{-1})) = 609 (5.0), 586 (sh), 565 (4.5), 540 (4.5), 519 (4.4), 325 (sh), 302 (4.7), 259 (4.7).

FT-IR (KBr), ν (cm^{-1}): 2963, 2926, 2868, 2231 (C≡N), 1635, 1512, 1468, 1437, 1285, 1248, 1207, 1126, 1103, 1072 (B-O), 839, 764, 710.

(4-*tert*-Butylphenoxy)-2,3,9,10-tetracyano-16,17-dioctylthiosubphthalocyaninateboron(III) (18)

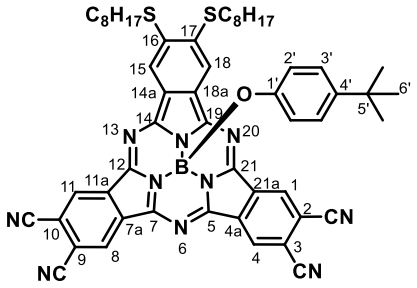

Eluent: toluene/THF from 50:1 to 20:1. Compound **18** was obtained as a bluish solid. Yield: 56%.

^{1}H-NMR (300 MHz, $CDCl_3$): δ (ppm) = 9.19 (d, J_p = 0.8 Hz, 2H; H-1, H-11), 9.17 (d, J_p = 0.8 Hz, 2H; H-4, H-8), 8.52 (s, 2H; H-15, H-18), 6.80 (d, J_o = 8.7 Hz, 2H; H-3'), 5.32 (d, J_o = 8.7 Hz, 2H; H-2'), 3.38-3.17 (m, 4H; $S\underline{CH_2}$), 1.95-1.82 (tt, J_1 = 7.6 Hz, J_2 = 7.2 Hz, 4H; $SCH_2\underline{CH_2}$), 1.66-1.54 (tt, J_1 = 7.5 Hz, J_2 = 7.2 Hz, 4H; $S(CH_2)_2\underline{CH_2}$), 1.48-1.26 (m, 16H; $S(CH_2)_3(\underline{CH_2})_4$), 1.10 (s, 9H; H-6'), 0.94-0.86 (m, 6H; $S(CH_2)_7\underline{CH_3}$).

^{13}C-NMR (75.5 MHz, $CDCl_3$): δ (ppm) = 156.3 (C-14, C-19), 150.8 (C-12, C-21), 149.1 (C-1'), 147.5 (C-5, C-7), 145.1 (C-4a, C-7a, C-11a, C-21a), 143.8 (C-14a, C-18a), 131.8, 130.7 (C-1, C-4, C-8, C-11), 129.0, 128.6, 128.6 (C-16, C-17), 126.2 (C-3'), 119.3 (C-15, C-18), 117.9 (C-2'), 115.4, 115.4, 115.2 (C-2, C-3, C-9, C-10), 114.7 (C≡N), 34.1 (C-5'), 33.6, 32.0, 31.4 (C-6'), 29.4, 29.3, 29.2, 28.4, 22.8 ($S\underline{(CH_2)_7}CH_3$), 14.2 ($S(CH_2)_7\underline{CH_3}$).

MS (MALDI-TOF, DCTB): *m/z* = 932.4 $[M]^+$, 783.4 [M - axial group]$^+$.

HRLSI-MS: m/z Calcd for [$C_{54}H_{53}BN_{10}OS_2$]: 932.3942; Found: 932.3925.

UV-vis ($CHCl_3$): λ_{max} (nm) (log ε (dm^3 mol^{-1} cm^{-1})) = 619 (5.0), 580 (4.7), 557 (sh), 529 (4.5), 488 (sh), 404 (sh), 381 (4.1), 310 (4.9).

(4-*tert*-Butylphenoxy)-2,3,9,10-tetracyanosubphthalocyaninateboron(III) (19)

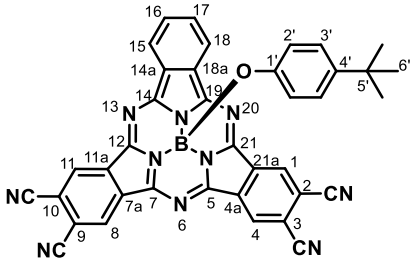

Eluent: toluene/THF from 100:1 to 20:1. Compound **19** was obtained as a dark purple solid. Yield: 71%.

Mp > 250 °C.

^{1}H-NMR (300 MHz, $CDCl_3$): δ (ppm) = 9.25 (s, 2H; H-1, H-11), 9.22 (s, 2H; H-4, H-8), 8.92-8.83 (AA'BB' system, 2H; H-15, H-18), 8.13-8.06 (AA'BB' system, 2H; H-16, H-17), 6.79 (d, J_o = 8.7 Hz, 2H; H-3'), 5.29 (d, J_o = 8.7 Hz,

2H; H-2'), 1.10 (s, 9H; H-6').

^{13}C-NMR (75.5 MHz, $CDCl_3$): δ (ppm) = 156.6 (C-14, C-19), 150.8 (C-12, C-21), 149.0 (C-1'), 147.7 (C-5, C-7), 145.2 (C-4a, C-7a, C-11a, C-21a), 132.5 (C-4'), 131.8, 130.9 (C-14a, C-18a), 129.0, 128.6 (C-1, C-4, C-8, C-11, C-16, C-17), 126.2 (C3'), 123.5 (C-15, C-18), 117.8 (C-2'), 115.4 (C-2, C-3, C-9, C-10), 114.9 (C≡N), 34.1 (C-5'), 31.4 (C-6').

MS (MALDI-TOF, DCTB): *m/z* = 644.3 $[M]^+$.

HRLSI-MS: m/z Calcd for $[C_{38}H_{21}BN_{10}O]$: 644.1994; Found: 644.2005.

UV-vis ($CHCl_3$): λ_{max} (nm) (log ε (dm^3 mol^{-1} cm^{-1})) = 604 (4.9), 582 (sh), 562 (4.4), 538 (4.4), 516 (4.3), 325 (sh), 302 (4.6), 256 (4.5).

FT-IR (KBr), ν (cm^{-1}): 2959, 2924, 2855, 2232 (C≡N), 1632, 1619, 1513, 1466, 1443, 1393, 1312, 1283, 1246, 1210, 1150, 1123, 1073 (B-O), 757, 710.

(4-*tert*-Butylphenoxy)-2,3,9,10-tetracyano-16,17-dichlorosubphthalocyaninateboron(III) (20)

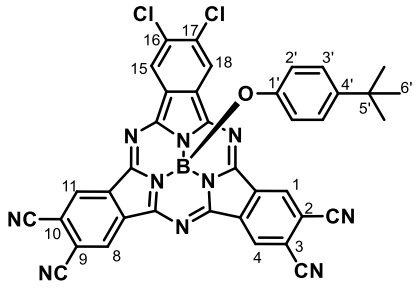

Eluent: toluene/THF from 100:1 to 20:1. Compound **20** was obtained as a dark purple solid. Yield: 8%.

Mp > 250 °C.

^{1}H-NMR (300 MHz, $CDCl_3$): δ (ppm) = 9.26 (s, 4H; H-1, H-4, H-8, H-11), 8.94 (s, 2H; H-15, H-18), 6.79 (d, J_o = 8.7 Hz, 2H; H-3'), 5.26 (d, J_o = 8.7 Hz, 2H; H-2'), 1.09 (s, 9H; H-6').

MS (MALDI-TOF, DCTB): *m/z* = 712.2 $[M]^+$.

UV-vis ($CHCl_3$): λ_{max} (nm) (log ε (dm^3 mol^{-1} cm^{-1})) = 598 (4.9), 565 (4.6), 548 (sh), 518 (4.4), 301 (4.7), 2867 (4.9).

1.8.4.3 Synthesis of phenoxy-tricyano-subphthalocyanines

General procedure:

To a 5 mL microwave vial, a solution of the corresponding triiodo-subphthalocyanine **11** (*C_3* or *C_1*) (92 mg, 0.100 mmol) in dry DMF (4 mL), $Zn(CN)_2$ (19 mg, 0.160 mmol) and $Pd(PPh_3)_4$ (18 mg, 0.016 mmol) were added. The reaction tube was sealed and heated to 105 °C under microwave irradiation with a 18 min hold time. Water (20 mL) was added and the product was extracted with dichloromethane (3 × 15 mL). The combined organic extracts were dried over $MgSO_4$ and the solvent was removed by rotary evaporation. The resulting dark solid was subjected to column chromatography on silica gel using a suitable eluent, as described in each case.

C_3-(4-*tert*-Butylphenoxy)-2,9(10),16-tricyanosubphthalocyaninateboron(III) (C_3-22)

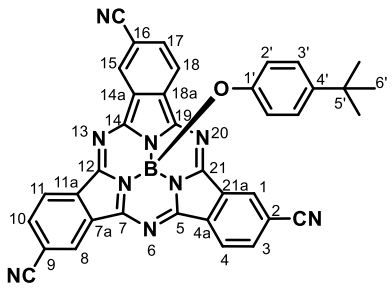

Eluent: toluene/THF 150:1. Compound ***C_3*-22** was obtained as a purple solid. Yield: 86%.

Mp > 250 °C.

^{1}H-NMR (300 MHz, $CDCl_3$): δ (ppm) = 9.12 (s, 3H; H-1, H-8, H-15), 8.95 (d, J_o = 8.2 Hz, 3H; H-4, H-11, H-18), 8.14 (d, J_o = 8.2 Hz, 3H; H-3, H-10, H-17), 6.78 (d, J_o = 8.6 Hz, 2H; H-3'), 5.27 (d, J_o = 8.6 Hz, 2H; H-2'), 1.09 (s, 9H; H-6').

^{13}C-NMR (75.5 MHz, $CDCl_3$): δ (ppm) = 151.4 (C-5, C-7, C-12, C-14, C-19, C-21), 149.3 (C-1'), 144.8 (C-7a, C-14a, C-21a), 133.0 (C-4'), 133.0 (C-3, C-10, C-17), 130.7 (C-4a, C-11a, C-18a), 127.3 (C-1, C-8, C-15), 126.1 (C3'), 123.6 (C-4, C-11, C-18), 118.3 (C-2, C-9, C-16), 117.8 (C-2'), 113.8 (C≡N), 34.1 (C-5'), 31.4 (C-6').

MS (MALDI-TOF, DCTB): *m/z* = 619.3 $[M]^+$, 470.2 [M - axial group]$^+$.

HRLSI-MS: m/z Calcd for $[C_{37}H_{22}BN_9O]$: 619.2041; Found: 619.2058.

UV-vis ($CHCl_3$): λ_{max} (nm) (log ε (dm^3 mol^{-1} cm^{-1})) = 573 (4.9), 520 (4.4), 307 (4.6), 284 (4.6), 260 (4.6).

FT-IR (KBr), ν (cm^{-1}): 2955, 2923, 2830, 2227 (C≡N), 1600, 1512, 1421, 1233, 1216, 1111, 1104, 1065 (B-O), 771, 756, 708.

C_1-(4-*tert*-Butylphenoxy)-2,9(10),16-tricyanosubphthalocyaninateboron(III) (C_1-22)

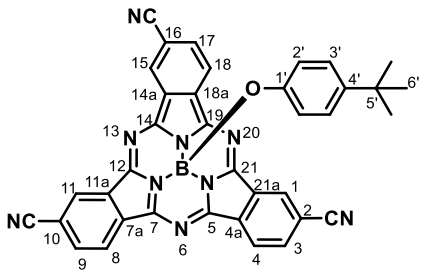

Eluent: toluene/THF 150:1. Compound ***C_1*-22** was obtained as a purple solid. Yield: 83%.

Mp > 250 °C.

^{1}H-NMR (300 MHz, $CDCl_3$): δ (ppm) = 9.13-9.05 (m, 3H; H-1, H-11, H-15), 8.99-8.89 (m, 3H; H-4, H-8, H-18), 8.15-8.03 (m, 3H; H-3, H-9, H-17), 6.80 (d, J_o = 8.7 Hz, 2H; H-3'), 5.30 (d, J_o = 8.7 Hz, 2H; H-2'), 1.10 (s, 9H; H-6').

^{13}C-NMR (75.5 MHz, THF): δ (ppm) = 153.1, 152.9, 152.0, 151.8, 151.6 (C-5, C-7, C-12, C-14, C-19, C-21), 151.4 (C-1'), 144.4 (C-4'), 139.7 (C-4a, C-7a, C-11a, C-14a, C-18a, C-21a), 133.0 (C-3, C-9, C-17), , 127.3 (C-1, C-11, C-15), 126.5 (C3'), 123.6 (C-4, C-8, C-18), 118.8 (C-2'), 118.3 (C-2, C-10, C-16), 96.8 (C≡N), 34.6 (C-5'), 31.8 (C-6').

MS (MALDI-TOF, DCTB): *m/z* = 619.3 $[M]^+$, 470.2 [M - axial group]$^+$.

HRLSI-MS: m/z Calcd for $[C_{37}H_{22}BN_9O]$: 619.2041; Found: 619.2032.

UV-vis ($CHCl_3$): λ_{max} (nm) (log ε (dm^3 mol^{-1} cm^{-1})) = 573 (4.9), 520 (4.4), 307 (4.6), 284 (4.6), 260 (4.6).

FT-IR (KBr), ν (cm^{-1}): 2964, 2936, 2851, 2229 (C≡N), 1624, 1525, 1408, 1224, 1216, 1115, 1110, 1069 (B-O), 756, 734, 713.

1.8.4.4 Synthesis of phenoxy-hexacyano-subnaphthalocyanine 24

(4-*tert*-Butylphenoxy)-4,5,15,16,26,27-hexabromosubnaphthalocyaninateboron(III) (25)

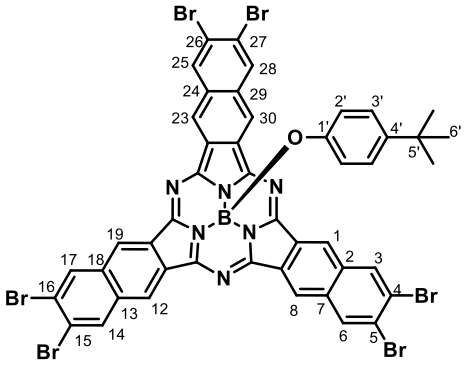

To a 25 ml round-bottom two-neck flask equipped with a reflux condenser and magnetic stirrer, a 1.0 M solution of BCl_3 in *p*-xylene (1.1 mL, 1.1 mmol) was added to 2,3-dibromo-6,7-dicyanonaphthalene (335 mg, 1.0 mmol) under argon atmosphere The mixture was stirred and heated to reflux (136-138 °C) for 1 h. The crude was cooled down to room temperature and flushed with argon. After evaporation of *p*-xylene, 4-*tert*-butylphenol (750 mg, 5 mmol) was added. The mixture was dissolved in *ca.* 3 mL of dry toluene and refluxed for 24 hours. After cooling down to room temperature, the excess of phenol was removed by washing the crude with a 3:1 MeOH/water solution. The product was purified by column chromatography on silica gel using toluene/heptane 3:2 as eluent to afford **25** as a green solid. Yield: 13%.

^{1}H-NMR (300 MHz, $CDCl_3$): δ (ppm) = 9.12 (s, 6H; H-1, H-8, H-12, H-19, H-23, H-30), 8.54 (s, 6H; H-3, H-6, H-14, H-17, H-25, H-28), 6.85 (d, J_o = 8.6 Hz, 2H; H-3'), 5.58 (d, J_o = 8.6 Hz, 2H; H-2'), 1.09 (s, 9H; H-6').

MS (MALDI-TOF, DCTB): *m/z* = 1167.7 $[M]^+$, 1018.7 $[M - \text{axial group}]^+$.

HRLSI-MS: m/z Calcd for $[C_{46}H_{25}BBr_6N_6O]$: 1167.7231; Found: 1167.7205.

UV-vis ($CHCl_3$): λ_{max} (nm) (log ε (dm^3 mol^{-1} cm^{-1})) = 652 (5.0), 593 (4.5), 476 (4.0), 336 (4.7), 292 (4.9).

(4-*tert*-Butylphenoxy)-4,5,15,16,26,27-hexacyanosubnaphthalocyaninateboron(III) (24)

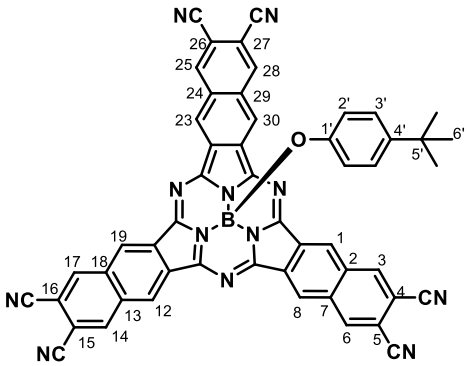

To a 5 mL microwave vial, a solution of hexabromo-subnaphthalocyanine **25** (50 mg, 0.043 mmol) in dry DMF (4 mL), $Zn(CN)_2$ (30 mg, 0.256 mmol) and $Pd(PPh_3)_4$ (30 mg, 0.026 mmol) were added. The reaction tube was sealed and heated to 110 °C under microwave irradiation with a 25 min hold time. Water (20 mL) was added and the product was extracted with dichloromethane (3 × 15 mL). The combined organic extracts were dried over $MgSO_4$ and the solvent was removed by rotary evaporation. The product was purified by column chromatography on silica gel using $CHCl_3$/THF 150:1 from 200:1 to 100:1 as eluent to afford 1 mg (0.0012 mmol) of compound **24** as a green solid. Yield: 2%.

^{1}H-NMR (300 MHz, $CDCl_3$): δ (ppm) = 9.54 (s, 6H; H-1, H-8, H-12, H-19, H-23, H-30), 8.85 (s, 6H; H-3, H-6, H-14, H-17, H-25, H-28), 6.80 (m, 2H; H-3'), 5.60 (m, 2H; H-2'), 1.08 (s, 9H; H-6').

MS (MALDI-TOF, DCTB): *m/z* = 844.3 $[M]^+$.

HRLSI-MS: m/z Calcd for $[C_{52}H_{25}BN_{12}O]$: 844.2370; Found: 844.2355.

1.8.4.5 Synthesis of chloro-tricyano-subphthalocyanines

General procedure:

In a 25 mL two-necked round-bottomed flask, equipped with a condenser, magnetic stirrer and rubber seal, subphthalocyanine **22** (*C_3* or *C_1*) (218 mg, 0.35 mmol) was dissolved in dry CH_2Cl_2 (4 mL) under argon atmosphere. A 1.0 M solution of BCl_3 in CH_2Cl_2 (1.75 mL, 5 molar equiv) was added dropwise. The reaction mixture was stirred under reflux for 1 h. The purple solution was allowed to cool to room temperature and pyridine was added dropwise until the color of the reaction returned to a characteristic SubPc pink color. The flask was placed in an ice bath for one hour, and the precipitate subsequently isolated by vacuum filtration. The resulting dark solid was purified following the methods described in each case.

***C*$_3$-Chloro-2,9(10),16-tricyanosubphthalocyaninateboron(III) (*C*$_3$-26)**

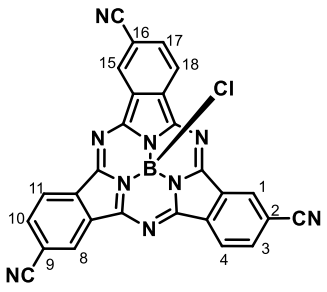

Eluent: toluene/THF 100:1 to 20:1. Compound ***C*$_3$-26** was obtained as a purple solid. Yield: 90%.

Mp > 250 °C.

^{1}H-NMR (300 MHz, $CDCl_3$): δ (ppm) = 9.22 (s, 3H; H-1, H-8, H-15), 9.02 (d, J_o = 8.2 Hz, 3H; H-4, H-11, H-18), 8.22 (d, J_o = 8.2 Hz, 3H; H-3, H-10, H-17).

MS (MALDI-TOF, DCTB): *m/z* = 505.2 $[M]^+$.

HRLSI-MS: m/z Calcd for $[C_{27}H_9BClN_9]$: 505.0762; Found: 505.0753.

UV-vis ($CHCl_3$): λ_{max} (nm) (log ε (dm^3 mol^{-1} cm^{-1})) = 571 (4.7), 552 (sh), 537 (sh), 520 (sh), 312 (4.3).

***C*$_1$-Chloro-2,9(10),16-tricyanosubphthalocyaninateboron(III) (*C*$_1$-26)**

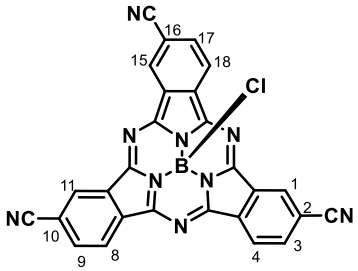

Eluent: toluene/THF 50:1. Compound ***C*$_1$-26** was obtained as a purple solid. Yield: 88%.

Mp > 250 °C.

^{1}H-NMR (300 MHz, $CDCl_3$): δ (ppm) = 9.20-9.09 (m, 3H; H-1, H-11, H-15), 9.05-8.97 (m, 3H; H-4, H-8, H-18), 8.22-8.10 (m, 3H; H-3, H-9, H-17).

MS (MALDI-TOF, DCTB): *m/z* = 505.2 $[M]^+$.

HRLSI-MS: m/z Calcd for $[C_{27}H_9BClN_9]$: 505.0762; Found: 505.0748.

UV-vis ($CHCl_3$): λ_{max} (nm) (log ε (dm^3 mol^{-1} cm^{-1})) = 571 (4.7), 552 (sh), 537 (sh), 520 (sh), 312 (4.3).

1.8.4.6 Synthesis of unsymmetrical chloro-dicyano-subphthalocyanines

General procedure:

In a 25 mL two-necked round-bottomed flask, equipped with a condenser, magnetic stirrer and rubber seal, the corresponding subphthalocyanine **14-15** (0.100 mmol) was dissolved in dry toluene (2 mL) under argon atmosphere. A 1.0 M solution of $TiCl_4$ in toluene (250 µL, 2.5 molar equiv) was added dropwise. The reaction mixture was stirred and heated to 40 °C until completion of the reaction was observed by TLC. The purple solution was allowed to cool to room temperature and pyridine was added dropwise until the color of the reaction returned

to a characteristic SubPc pink color. The flask was placed in an ice bath for one hour, and the precipitate subsequently isolated by vacuum filtration. The resulting dark solid was purified following the methods described in each case.

Chloro-2,3-dicyanosubphthalocyaninateboron(III) (27)

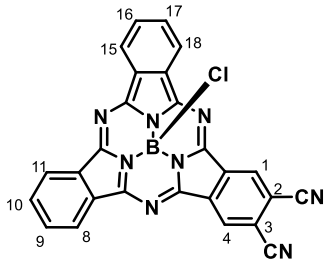

The filter cake was rinsed with methanol followed by ether to give compound **27** as a dark purple solid. Yield: 88%.

Mp > 250 °C.

^{1}H-NMR (300 MHz, $CDCl_3$): δ (ppm) = 9.31 (s, 2H; H-1, H-4), 8.93-8.85 (AA'BB' system, 4H; H-8, H-11, H-15, H-18), 8.11-8.01 (AA'BB' system, 4H; H-9, H-10, H-16, H-17).

MS (MALDI-TOF, DCTB): *m/z* = 480.1 $[M]^+$.

HRLSI-MS: m/z Calcd for $[C_{26}H_{10}BClN_8]$: 480.0809; Found: 480.0816.

UV-vis ($CHCl_3$): λ_{max} (nm) (log ε (dm^3 mol^{-1} cm^{-1})) = 593 (4.8), 569 (4.4), 547 (4.2), 531 (4.1), 514 (4.1), 303 (4.4).

Chloro-2,3-dicyano-9,10,16,17-tetrachlorosubphthalocyaninateboron(III) (28)

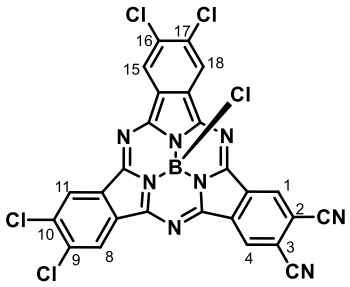

The product was purified by column chromatography on silica gel using toluene as eluent to afford compound **28** as a dark purple solid. Yield: 40%.

Mp > 250 °C.

^{1}H-NMR (300 MHz, $CDCl_3$): δ (ppm) = 9.32 (s, 2H; H-1, H-4), 9.01 (s, 2H; H-11, H-15), 8.99 (s, 2H; H-8, H-18).

MS (MALDI-TOF, DCTB): *m/z* = 618.0 $[M]^+$.

HRLSI-MS: m/z Calcd for $[C_{26}H_6BCl_5N_8]$: 617.9223; Found: 617.9242.

UV-vis ($CHCl_3$): λ_{max} (nm) (log ε (dm^3 mol^{-1} cm^{-1})) = 594 (4.8), 569 (4.6), 547 (4.3), 522 (4.2), 300 (4.5).

1.8.4.7 Synthesis of subphthalocyanines 8c and 29

Chloro-1,2,3,4,8,9,10,11,15,16,17,18-dodecafluorosubphthalocyaninateboron(III) (8c)[39]

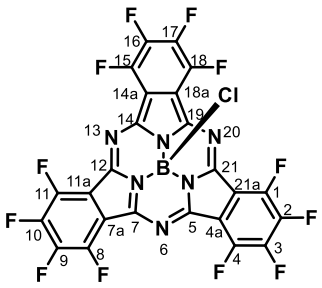

In a 25 mL two-necked round-bottomed flask, equipped with a condenser, magnetic stirrer and rubber seal, a 1.0 M solution of BCl_3 in *p*-xylene (5 mL) was added to 3,4,5,6-tetrafluorophthalonitrile (1 g, 5 mmol) under argon atmosphere. The reaction mixture was stirred under vigorous reflux for 30 min. The purple solution was allowed to cool to room temperature and flushed with argon. The dark purple reaction slurry was dissolved in toluene/THF 10:1 and passed through a short silica plug. The solvent was removed by vacuum distillation and the resulting dark solid was subjected to column chromatography on silica gel using heptane/EtOAc 3:1 as an eluent. By washing with hexane, 810 mg (1.25 mmol) of compound **8c** were obtained as a purple-gold solid. Yield: 75%.

Mp > 250 °C.

^{19}F-NMR (470 MHz, $CDCl_3$): δ (ppm) = -137.0 (AA'BB' system, 6F; F-1, F-4, F-8, F-11, F-15, F-18), -147.7 (AA'BB' system, 6F; F-2, F-3, F-9, F-10, F-16, F-17).

^{13}C-NMR (75.5 MHz, $CDCl_3$): δ (ppm) = 146.9 (C-5, C-7, C-12, C-14, C-19, C-21), 144.8-144.1 (6C; C-F), 141.3-140.6 (6C; C-F), 115.2-114.7 (C-4a, C-7a, C-11a, C-14a, C-18a, C-21a).

MS (MALDI-TOF, DCTB): *m/z* = 646.0 $[M]^+$.

HRLSI-MS: m/z Calcd for $[C_{24}F_{12}N_6BCl]$: 645.9774; Found: 645.9792.

UV-vis ($CHCl_3$): λ_{max} (nm) (log ε (dm^3 mol^{-1} cm^{-1})) = 574 (4.6), 556 (sh), 530 (sh), 311 (4.3), 277 (4.0).

FT-IR (KBr), ν (cm^{-1}): 1655, 1527, 1487, 1419, 1259, 1219, 1178, 1111, 1057, 964 (B-Cl), 883, 816, 714, 662.

Chloro-2,3,9,10,16,17-hexachlorosubphthalocyaninateboron(III) (29)[109b,206]

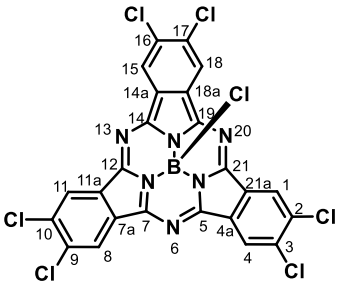

In a 25 mL two-necked round-bottomed flask, equipped with a condenser, magnetic stirrer and rubber seal, a 1.0 M solution of BCl_3 in *p*-xylene (5 mL) was added to 4,5-dichlorophthalonitrile (985 mg, 5 mmol) under argon atmosphere. The reaction mixture was stirred under vigorous reflux for 40 min. The purple solution was allowed to cool to room temperature and flushed with argon. The dark purple reaction slurry was dissolved in toluene/THF 10:1 and passed through a short silica plug. The solvent was removed by vacuum distillation and the resulting dark solid was subjected to column chromatography on

silica gel using toluene as an eluent. By washing with methanol, 659 mg (1.03 mmol) of compound **29** were obtained as a purple-gold solid. Yield: 62%.

Mp > 250 °C.

^{1}H-NMR (300 MHz, $CDCl_3$): δ (ppm) = 8.93 (s, 6H; H-1, H-4, H-8, H-11, H-15, H-18).

^{13}C-NMR (75.5 MHz, $CDCl_3$): δ (ppm) = 150.5 (C-5, C-7, C-12, C-14, C-19, C-21), 135.1 (C-2, C-3, C-9, C-10, C-16, C-17), 129.5 (C-4a, C-7a, C-11a, C-14a, C-18a, C-21a), 123.7 (C-1, C-4, C-8, C-11, C-15, C-18).

MS (MALDI-TOF, DCTB): *m/z* = 637.9 $[M]^+$.

HRLSI-MS: m/z Calcd for $[C_{24}H_6N_6BCl_7]$: 633.8566; Found: 633.8532.

UV-vis ($CHCl_3$): λ_{max} (nm) (log ε (dm^3 mol^{-1} cm^{-1})) = 572 (4.6), 552 (sh), 528 (4.1), 310 (4.3).

FT-IR (KBr), ν (cm^{-1}): 2920, 2851, 1606, 1539, 1456, 1419, 1373, 1278, 1222, 1095 (C-Cl), 1042, 976 (B-Cl), 882, 819.

1.8.4.8 Flash-Photolysis Time-Resolved Microwave Conductivity and Transient Absorption Spectroscopy measurements

FP-TRMC measurements were performed under air at room temperature. Sample films were prepared on a quartz substrate with 9 mm width, 40 mm length, and 1-mm thickness and the substrate was loaded into a TE102 mode microwave cavity. Transient charge carriers were photo-generated upon excitation to laser pulses of third harmonic generation (λ = 355 nm) from a Spectra Physics model INDI-HG Nd:YAG laser with a pulse duration of 5-8 ns. The photon density of a 355 nm pulse, operated at 10 Hz, was 9.1 x 10^{15} photons cm^{-2} $pulse^{-1}$. The probing microwave frequency and power were set at 9.1 GHz and 3 mW, respectively. Photoconductivity transients, demodulated through a GaAs crystal-diode with Schottky-barriers (rise time < 1 ns), were monitored by a Tektronix model TDS3032B digital oscilloscope. The observed conductivities were normalized, given by a photocarrier generation yield (φ) multiplied by sum of the charge carrier mobilities ($\Sigma\mu$), according to the equation,

$$\varphi\Sigma\mu = \frac{\mathrm{A}\Delta P_r}{eI_0 F_{\mathrm{L}} P_r} \qquad \text{(Eqn. 12)}$$

where e, A, I_0, F_{light}, P_r, and ΔP_r are elementary charge, sensitivity factor (S cm^{-1}), incident photon density of the excitation laser (photon cm^{-2}), correction factor (cm^{-1}), and reflected microwave power and its change, respectively.

TAS measurements were carried out at room temperature in air. The sample were photoexcited using the third harmonic generation (λ = 355 nm) from the identical Spectra Physics laser, where the photon density of a 355 nm pulse was 9.1 × 10^{15} photons cm^{-2} $pulse^{-1}$. A white light continuum from a Xe lamp was used as a probe light source for transient absorption spectroscopy. The monochromated probe light was guided into a Hamamatsu model C7700 wide-dynamic-range streak camera system, which collected a two-dimensional

image of the spectral and temporal profiles of light intensity. φ_{max} is estimated by the equation,

$$\varphi = \frac{N_A L d M^{-1} X A^{-1}}{N_p(1-T)} \quad \text{(Eqn. 13)}$$

where N_A, L, d, M, X, A, N_p, T denote Avogadro number, thickness of the film (cm), density of the film (g cm^{-3}), molecular weight of the compound (g mol^{-1}), photo-bleach at a certain wavelength (O.D.), steady state absorption at the wavelength (abs.), incident photon density of 355 nm pulse laser (cm^{-2}), transmittance of 355 nm laser to the sample film, respectively.

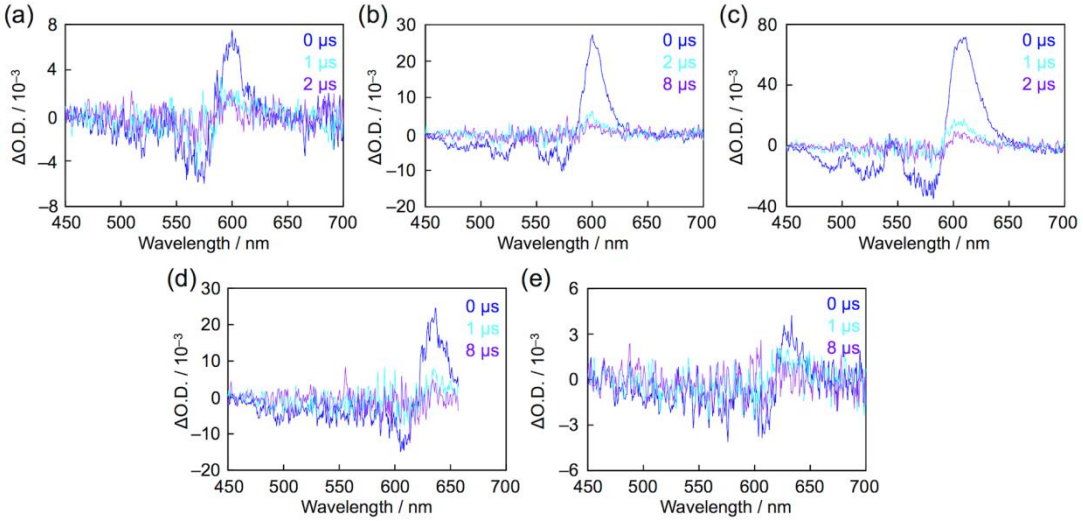

Figure 61. Snapshots of transient absorption spectra for drop-cast film of a) **8c** and vapor-deposited films of b) **8c**, c) **29**, d) **27**, and e) **28** upon photoexcitation of 355 nm pulses.

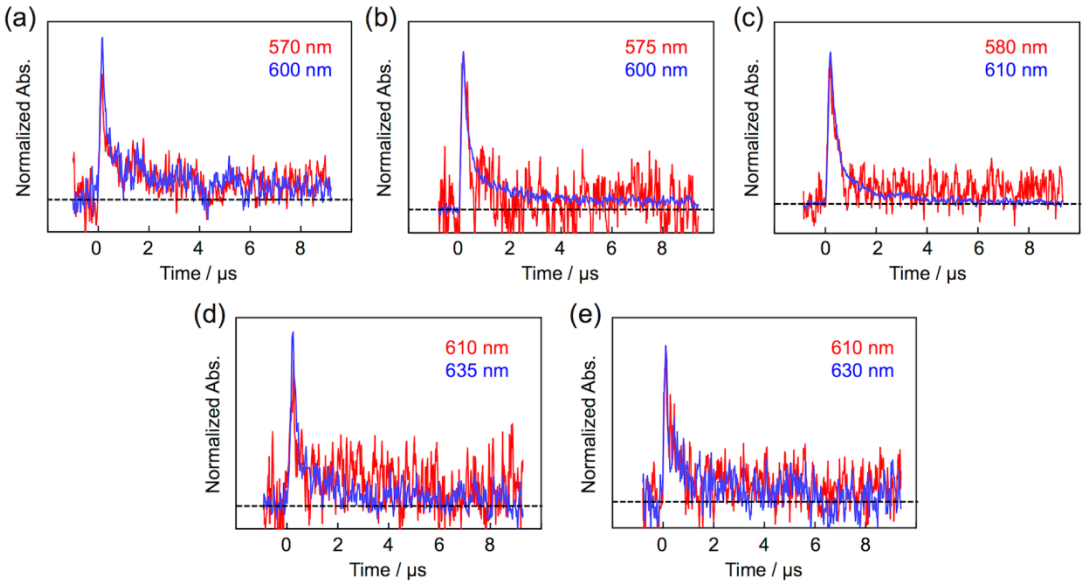

Figure 62. Kinetic traces of transient absorption spectra for drop-cast film of a) **8c** and vapor-deposited films of b) **8c**, c) **29**, d) **27**, and e) **28** upon photoexcitation of 355 nm pulses.

1.8.5 Synthesis of subphthalocyanines as acceptor materials for PHJs

1.8.5.1 Synthesis of subphthalocyanines 30 and 31

Chloro-2,3,9,10-tetrachlorosubphthalocyaninateboron(III) (30)

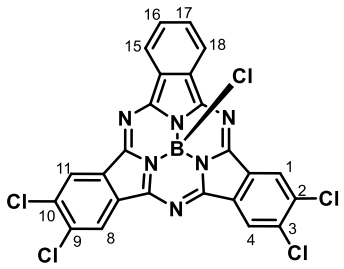

In a 25 mL two-necked round-bottomed flask, equipped with a condenser, magnetic stirrer and rubber seal, a 1.0 M solution of BCl_3 (6 mL) was added to 4,5-dichlorophthalonitrile (788 mg, 4.0 mmol) and phthalonitrile (256 mg, 2.0 mmol) under argon atmosphere. The reaction mixture was stirred under vigorous reflux for 2 h. The purple solution was allowed to cool to room temperature and flushed with argon. The solvent was removed by vacuum distillation and the resulting dark solid was subjected to column chromatography on silica gel using toluene/heptane 3:1 as an eluent. By washing with heptane, 216 mg (0.38 mmol) of compound **30** were obtained as a purple-gold solid. Yield: 19%.

Mp > 250 °C.

^{1}H-NMR (300 MHz, $CDCl_3$): δ (ppm) = 8.98 (s, 2H; H-1, H-11), 8.94 (s, 2H; H-4, H-8), 8.92-8.83 (AA'BB' system, 2H; H-15, H-18), 8.05-7.96 (AA'BB' system, 2H; H-16, H-17).

MS (MALDI-TOF, DCTB): *m/z* = 568.0 $[M]^+$.

HRLSI-MS: m/z Calcd for $[C_{24}H_8BCl_5N_6]$: 567.9317; Found: 567.9345.

UV-vis ($CHCl_3$): λ_{max} (nm) (log ε (dm^3 mol^{-1} cm^{-1})) = 573 (4.5), 539 (sh), 520 (sh), 315 (4.2), 274 (4.2).

Fluoro-2,9(10),16-tricyanosubphthalocyaninateboron(III) (31)

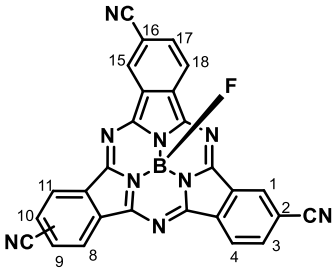

Subphthalocyanine **31** was synthesized by adapting the method of Fulford *et al*.[42b,64] In a 25 mL two-necked round-bottomed flask, equipped with a condenser, magnetic stirrer and rubber seal, subphthalocyanine **22** (218 mg, 0.35 mmol) was dissolved in dry toluene (4 mL) under argon atmosphere. Boron trifluoride diethyl etherate ($Et_2O{\cdot}BF_3$, 1.1 mL, 25 molar equiv) was added dropwise. The reaction mixture was stirred under reflux for 5 h. The purple solution was allowed to cool to room temperature and pyridine was added dropwise until the color of the reaction returned to a characteristic SubPc pink color. The flask was placed in an ice bath for one hour, and the precipitate subsequently isolated by vacuum filtration. The

filter cake was rinsed with methanol followed by ether to give compound **31** (mixture of regioisomers C_3/C_1 1:3) as a purple solid. Yield: 91%.

Mp > 250 °C.

^{1}H-NMR (300 MHz, $CDCl_3$): δ (ppm) = 9.30 (s, 3H; H-1, H-8/H-11, H-15), 9.01 (d, J_o = 8.3 Hz, 3H; H-4, H-11/H-8, H-18), 8.36-8.27 (m, 3H; H-3, H-9/H-10, H-17).

^{19}F-NMR (470 MHz, THF-d_8): δ (ppm) = -159.5 (q, J = 27.8 Hz, 1F; B-F).

MS (MALDI-TOF, DCTB): m/z = 489.2 $[M]^+$.

HRLSI-MS: m/z Calcd for $[C_{27}H_9BFN_9]$: 489.1057; Found: 489.1052.

UV-vis ($CHCl_3$): λ_{max} (nm) (log ε (dm^3 mol^{-1} cm^{-1})) = 572 (4.7), 554 (sh), 537 (sh), 521 (sh), 314 (4.3).

1.8.5.2 Device fabrication and characterization

OPV devices were fabricated on prepatterned indium tin oxide-coated glass substrates. Detergent and solvent cleaning of all substrates was followed by a 5 min oxygen plasma treatment to remove remaining carbon residue. PEDOT:PSS was spin-coated at 5000 rpm and this was followed by a bake-out at 130 °C in N_2. All of the organic materials were purified by thermal gradient sublimation before being loaded into a high-vacuum evaporation chamber. All of the materials were deposited at an evaporation rate of 1 Å s^{-1}. Deposition rates were determined from calibration of the film thickness, measured ex situ by spectroscopic ellipsometry (Sopra GESP-5). The 120 nm thick Ag cathode was evaporated through a shadow mask defining an active area of 13.4 mm^2.

Current density-voltage characteristics were measured under simulated solar illumination using a Keithley 2602 measurement unit and an Abet solar simulator calibrated with a Fraunhofer certified photovoltaic cell to yield a 100 mW cm^{-2} AM 1.5G spectrum. For all device architectures, at least three cells were measured. The device parameters (*FF*, V_{OC}, J_{SC}, and *PCE*) were averaged over these three cells (100% fabrication yield), unless specifically mentioned otherwise.

A commercial set-up (Bentham) was used to measure the *EQE*. Light from a Xe arc lamp (300-670 nm) and a quartz halogen lamp (670-900 nm) was chopped, coupled into a monochromator and aimed at the device. The resulting current was sent through a Bentham477 current pre-amplifier, then arrived at the Bentham485 lock-in amplifier. Calibration was done using a calibrated Si diode.

1.8.6 Synthesis of peripherally chlorinated subphthalocyanines for BHJs

1.8.6.1 Synthesis of phenoxy-substituted hexachloro-subphthalocyanines 32-34

General procedure:

In a round-bottom two-neck flask equipped with a reflux condenser and a magnetic stirrer, the corresponding phenol (2 mmol of 3,4,5-trimethoxyphenol for SubPc **32;** 3 mmol of 4-*tert*-butylphenol for SubPc **33**; 5 mmol of 2,3,4,5,6-pentafluorophenol for SubPc **34**), chlorosubphthalocyanine **29** (320 mg, 0.50 mmol) and DBU (75 µL, 0.50 mmol) were refluxed in toluene (3 mL) for 6-12 h. After cooling down to room temperature, the excess of phenol was removed by washing the crude with a 3:1 MeOH/water solution. The resulting dark solid was subjected to column chromatography on silica gel using a suitable eluent, as described in each case.

(3,4,5-Trimethoxyphenoxy)-2,3,9,10,16,17-hexachlorosubphthalocyaninateboron(III) (32)

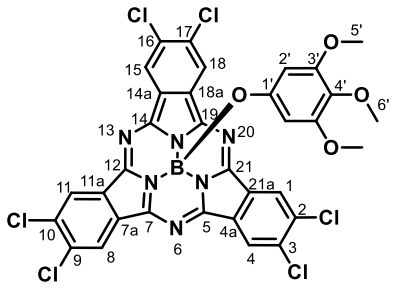

Reaction time: 6 h. Eluent: $CHCl_3$/MeOH 500:1. Compound **32** was obtained as a purple solid. Yield: 45%.

Mp > 250 °C.

^{1}H-NMR (300 MHz, $CDCl_3$): δ (ppm) = 8.61 (s, 6H; H-1, H-4, H-8, H-11, H-15, H-18), 4.55 (s, 2H; H-2'), 3.48 (s, 3H; H-6'), 3.44 (s, 6H; H-5').

^{13}C-NMR (75.5 MHz, $CDCl_3$): δ (ppm) = 152.9 (C-3'), 150.2 (C-5, C-7, C-12, C-14, C-19, C-21), 148.3 (C-1'), 134.9 (C-2, C-3, C-9, C-10, C-16, C-17), 132.8 (C-4'), 129.5 (C-4a, C-7a, C-11a, C-14a, C-18a, C-21a), 123.6 (C-1, C-4, C-8, C-11, C-15, C-18), 95.9 (C-2'), 60.6 (C-6'), 55.8 (C-5').

MS (MALDI-TOF, DCTB): *m/z* = 784.0 $[M]^+$, 618.0 [M - axial group]$^+$.

HRLSI-MS: m/z Calcd for $[C_{33}H_{17}BCl_6N_6O_4]$: 783.9509; Found: 783.9509.

UV-vis ($CHCl_3$): λ_{max} (nm) (log ε (dm^3 mol^{-1} cm^{-1})) = 574 (4.6), 556 (sh), 532 (4.1), 314 (4.3).

FT-IR (KBr), ν (cm^{-1}): 3081, 3002, 2934, 2835, 1735, 1594, 1543, 1504, 1461, 1422, 1379, 1341, 1281, 1221, 1196, 1127, 1095 (C-Cl), 1068 (B-O), 1008, 886, 822, 762, 708.

(4-*tert*-Butylphenoxy)-2,3,9,10,16,17-hexachlorosubphthalocyaninateboron(III) (33)

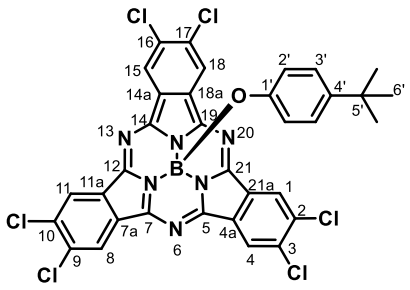

Reaction time: 8 h. Eluent: toluene/heptane 3:1. Compound **33** was obtained as a purple solid. Yield: 85%.

Mp > 250 °C.

^{1}H-NMR (300 MHz, $CDCl_3$): δ (ppm) = 8.84 (s, 6H; H-1, H-4, H-8, H-11, H-15, H-18), 6.80 (d, J_o = 8.6 Hz, 2H; H-3'), 5.31 (d, J_o = 8.6 Hz, 2H; H-2'), 1.11 (s, 9H; H-6').

^{13}C-NMR (75.5 MHz, $CDCl_3$): δ (ppm) = 150.5 (C-5, C-7, C-12, C-14, C-19, C-21), 149.5 (C-1'), 135.2 (C-2, C-3, C-9, C-10, C-16, C-17), 132.5 (C-4'), 129.9 (C-4a, C-7a, C-11a, C-14a, C-18a, C-21a), 126.1 (C3'), 124.0 (C-1, C-4, C-8, C-11, C-15, C-18), 118.0 (C-2'), 34.0 (C-5'), 31.4 (C-6').

MS (MALDI-TOF, DCTB): *m/z* = 750.0 $[M]^+$, 600.9 [M - axial group]$^+$.

HRLSI-MS: m/z Calcd for $[C_{34}H_{19}BCl_6N_6O]$: 749.9819; Found: 749.9821.

UV-vis ($CHCl_3$): λ_{max} (nm) (log ε (dm^3 mol^{-1} cm^{-1})) = 571 (4.6), 522 (sh), 308 (4.3).

FT-IR (KBr), ν (cm^{-1}): 2960, 2924, 2865, 1608, 1513, 1458, 1419, 1256, 1219, 1186, 1096 (C-Cl), 1066 (B-O), 885, 822, 709.

(2,3,4,5,6-Pentafluorophenoxy)-2,3,9,10,16,17-hexachlorosubphthalocyaninateboron(III) (34)

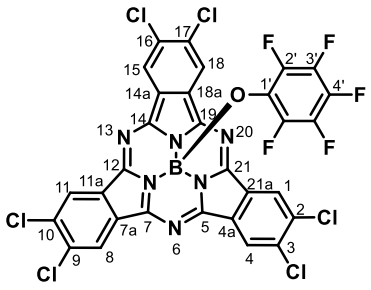

Reaction time: 12 h. Eluent: toluene/heptane 4:1. Compound **34** was obtained as a purple solid. Yield: 67%.

Mp > 250 °C.

^{1}H-NMR (300 MHz, $CDCl_3$): δ (ppm) = 8.90 (s, 6H; H-1, H-4, H-8, H-11, H-15, H-18).

^{19}F-NMR (470 MHz, $CDCl_3$): δ (ppm) = -158.6 (d, J = 21.0 Hz, 2F; F-2'), -163.0 (t, J = 21.5 Hz, 2F; F-3'), -163.6 (d, J = 21.5 Hz, 1F; F-4').

^{13}C-NMR (75.5 MHz, $CDCl_3$): δ (ppm) = 150.2 (C-5, C-7, C-12, C-14, C-19, C-21), 135.7 (C-2, C-3, C-9, C-10, C-16, C-17), 130.8, 130.3, 129.9 (C-4a, C-7a, C-11a, C-14a, C-18a, C-21a), 129.2, 128.7, 124.2 (C-1, C-4, C-8, C-11, C-15, C-18).

MS (MALDI-TOF, DCTB): *m/z* = 783.9 $[M]^+$, 600.9 [M - axial group]$^+$.

HRLSI-MS: m/z Calcd for $[C_{30}H_6BCl_6F_5N_6O]$: 783.8720; Found: 783.8663.

UV-vis ($CHCl_3$): λ_{max} (nm) (log ε (dm^3 mol^{-1} cm^{-1})) = 574 (4.6), 556 (sh), 532 (4.1), 314 (4.3).

FT-IR (KBr), ν (cm^{-1}): 2923, 2853, 1611, 1510, 1458, 1422, 1377, 1280, 1223, 1183, 1096 (C-Cl), 1047 (B-O), 992, 887, 822, 766, 710.

1.8.6.2 Synthesis of fluoro-2,3,9,10,16,17-hexachlorosubphthalocyaninateboron(III) (35)

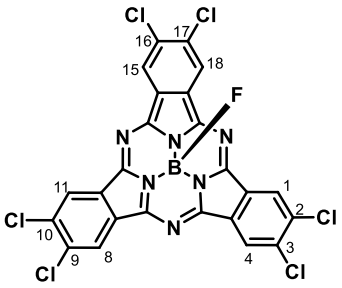

Subphthalocyanine **35** was synthesized by adapting the method of M. V. Fulford *et al*.[42b,64] In a 25 mL two-necked round-bottomed flask, equipped with a condenser, magnetic stirrer and rubber seal, subphthalocyanine **33** (300 mg, 0.40 mmol) was dissolved in dry toluene (4 mL) under argon atmosphere. Boron trifluoride diethyl etherate ($Et_2O{\cdot}BF_3$, 1.3 mL, 25 molar equiv) was added dropwise. The reaction mixture was stirred under reflux for 2 h. The purple solution was allowed to cool to room temperature and pyridine was added dropwise until the color of the reaction returned to a characteristic SubPc pink color. The flask was placed in an ice bath for one hour, and the precipitate subsequently isolated by vacuum filtration. The filter cake was rinsed with methanol followed by ether to give 225 mg (0.36 mmol) of compound **35** as a purple solid. Yield: 91%.

Mp > 250 °C.

^{1}H-NMR (300 MHz, THF-d_8): δ (ppm) = 9.03 (s, 6H; H-1, H-4, H-8, H-11, H-15, H-18).

^{19}F-NMR (470 MHz, $C_2D_2Cl_4$, 120 °C): δ (ppm) = -156.4 (q, *J* = 28.5 Hz, 1F; B-F).

^{11}B-NMR (160.5 MHz, $C_2D_2Cl_4$, 120 °C): δ (ppm) = -13.9 (d, *J* = 28.5 Hz, 1B; B-F)

MS (MALDI-TOF, DCTB): *m/z* = 619.9 $[M]^+$.

HRLSI-MS: m/z Calcd for $[C_{24}H_6BCl_6FN_6]$: 619.8833; Found: 619.8843.

UV-vis ($CHCl_3$): λ_{max} (nm) (log ε (dm^3 mol^{-1} cm^{-1})) = 573 (4.6), 556 (sh), 532 (4.1), 314 (4.3).

1.8.6.3 Measurements of section 1.6

Transmission electron microscopy (TEM) was performed on a Tecnai G^2 Sphera transmission electron microscope (FEI) operated at 200 kV. Space-charge-limited-current electron mobility was acquired through the electron-only devices with a configuration of ITO/ZnO (40 nm)/PTB7-Th:SubPc/LiF (1 nm)/Al (100 nm). The thickness of polymer:SubPc blend films is about 300 nm. The dark current densities of PTB7-Th:SubPc blends were measured by applying a voltage between 0 and 4 V using a computer-controlled Keithley 2400 source meter in N_2atmosphere. These data were analyzed according to the Mott-Gurney laws that includes a Poole-Frenkel-type dependence of mobility on the electric field, given by $J = \frac{9}{8}\varepsilon_r\varepsilon_0\mu_0\frac{V^2}{d^3}\exp(0.89\gamma\sqrt{\frac{V}{d}})$ (Eqn. 14), where ε_0 is the permittivity of free space, ε_r is the

dielectric constant of the polymer which is assumed to be around 3 for the conjugated polymers, μ_0 is the zero-field mobility, *V* is the voltage drop across the device, *d* is the film thickness of active layer, and *γ* is a parameter that describes the strength of the field-dependence effect. The applied voltage is used without correcting from series resistance or built-in voltage, which offers the best fitting of the experimental data following the protocol reported in literature.[252] The electron mobilities are extracted with the fit parameters at an electric field (*E*) of 1×10^5 V cm^{-1} (corresponding to an applied voltage of 3 V across the bulk of a 300 nm device) by the Murgatroyd equation $\mu = \mu_0 \exp(\gamma\sqrt{E})$ (Eqn. 15).

1.8.6.4 Device fabrication and characterization

Photovoltaic devices were made with an inverted architecture (glass/ITO/ZnO/PTB7-Th:SubPc/MoO_x/Ag. Patterned ITO substrates (14 Ω per square) (Naranjo Substrates) were cleaned by sonication in acetone, detergent, deionized water, and isopropanol, followed by UV-ozone treatment. ZnO layers were deposited by spin coating a zinc acetate dehydrate (100 mg) precursor solution (28.3 µL ethanolamine in 0.937 mL 2-methoxyethanol) at 4000 rpm for 60 seconds, followed by annealing at 200 °C for 10-15 min in air, giving layers of 40 nm. The PTB7-Th:SubPc photoactive layers were deposited by spin coating in air from the solutions containing PTB7-Th and corresponding SubPc at room temperature. Active layer thicknesses were about 75 nm. Unless indicated otherwise, Thermal annealing were performed in glovebox at indicated temperature for 5 min. MoO_x (10 nm) and Ag (100 nm) were deposited by vacuum evaporation at $\sim 3 \times 10^{-7}$ mbar as the back electrode. The active area of the cells was 0.09 or 0.16 cm^2, which provided similar results. Current density-voltage (*J-V*) curves were measured under simulated solar light (100 mW cm^{-2}) from a tungsten-halogen lamp filtered by a Hoya LB100 daylight using a Keithley 2400 source meter. No mismatch correction was done. All measurements were conducted in nitrogen-filled glove box. The accurate short-circuit current density (J_{SC}) was determined from the *EQE* by convolution with the AM 1.5G solar spectrum. External quantum efficiency (*EQE*) measurements were performed in a homebuilt set-up, with the devices kept in a nitrogen filled box with a quartz window and illuminated through an aperture of 2 mm. Mechanically modulated (Stanford Research, SR 540) monochromatic (Oriel, Cornerstone 130) light from a 50 W tungsten halogen lamp (Osram 64610) was used as probe light, in combination with continuous bias light from a solid state laser (B&W Tek Inc. 532 nm, 30 mW). The intensity of the bias laser light was adjusted using a variable-neutral density filter. The response was recorded as the voltage over a 50 Ω resistance, using a lock-in amplifier (Stanford Research Systems SR 830). For all devices, the measurements were carried out under representative illumination intensity (AM 1.5G equivalent, provided by the 532 nm laser).

[252] Blakesley, J. C.; Castro, F. A.; Kylberg, W.; Dibb, G. F. A.; Arantes, C.; Valaski, R.; Cremona, M.; Kim, J. S.; Kim, J. -S. *Org. Electron*. **2014**, *15*, 1263.

Chapter II

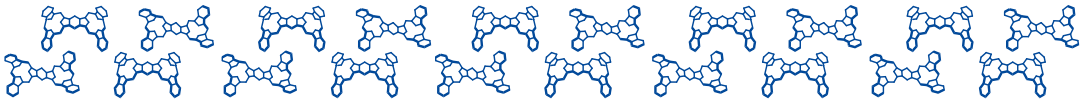

Peripheral and Axial Functionalization of Subphthalocyanine Dimers

2.1 Subphthalocyanine fused oligomers: π-extended curved molecules with unique topologies

For a long time, a planar or near-planar geometry of aromatic carbon-based molecular networks was regarded as necessary for the efficient conjugation of π-electronic systems. However, in the last decades, and particularly encouraged by the discovery of spherical fullerene C_{60}[253] and carbon nanotubes,[254] conjugated molecules bearing a curved surface have attracted significant attention owing to their unique chemical and physical properties, such as enhanced solubility or decreased aggregation by π-π stacking.[255] Curved polyaromatics that exhibit accessible convex and concave surfaces, including fragments of these nanocarbons,[256] like corannulenes, sumanenes,[257] circulenes,[258] and their derivatives[259] have been prepared and intensively investigated.

On the other hand, albeit limited, a number of heteroatomic aromatic compounds exhibiting non-planar structures can be found in literature. While some of these cases evolve from the perturbation of intrinsically planar molecules by structural modifications, steric congestion, or conjugation extension, giving rise to distorted, bent or twisted systems, such as porphyrin oligomers[260] or expanded cyclopyrroles,[261] some rare aromatic molecules present an inherent

---

[253] Kroto, H. W.; Heath, J. R.; O'Brien, S. C.; Curl, R. F.; Smalley, R. E. *Nature* **1985**, *318*, 162.

[254] Iijima, S. *Nature* **1991**, *354*, 56.

[255] a) Hirsch, A.; Brettreich, M. *Fullerenes: Chemistry and Reactions*; Wiley-VCH: Weinheim, Germany, 2005. b) *Chemistry of Nanocarbons*; Akasaka, T., Wudl, F., Nagase, S., Eds.; John Wiley & Sons Ltd.: Chichester, UK, 2010. c) *Carbon Nanotubes and Related Structures: Synthesis Characterization, Functionalization, and Applications*; Guldi, D. M., Martin, N., Eds.; Wiley-VCH: Weinheim, Germany, 2010. d) Yao, T.; Yu, H.; Vermeij, R. J.; Bodwell, G. J. *Pure Appl. Chem.* **2008**, *80*, 533.

[256] a) Wu, Y. -T.; Siegel, J. S. *Chem. Rev.* **2006**, *106*, 4843. b) *Fragments of Fullerenes and Carbon Nanotubes: Designed Synthesis, Unusual Reactions, and Coordination Chemistry*; Petrukhina, M. A., Scott, L. T., Eds.; John Wiley & Sons, Inc.: Hoboken, NJ, USA, 2012.

[257] a) Sakurai, H.; Daiko, T.; Hirao, T. *Science* **2003**, *301*, 1878. b) Amaya, T.; Hirao, T. *Chem. Commun.* **2011**, *47*, 10524.

[258] a) Feng, C. -N.; Kuo, M. -Y.; Wu, Y. -T. *Angew. Chem. Int. Ed.* **2013**, *52*, 7791. b) Sakamoto, Y.; Suzuki, T. *J. Am. Chem. Soc.* **2013**, *135*, 14074.

[259] a) Chen, M. -K.; Hsin, H. -J.; Wu, T. -C.; Kang, B. -Y.; Lee, Y. -W.; Kuo, M. -Y.; Wu, Y. -T. *Chem. Eur. J.* **2014**, *20*, 598. b) Kawasumi, K.; Zhang, Q.; Segawa, Y.; Scott, L. T.; Itami, K. *Nat. Chem.* **2013**, *5*, 739.

[260] a) Senge, M. O. Highly Substituted Porphyrins. In *The Porphyrin Handbook*; Kadish, K. M., Smith, K. M., Guilard, R., Eds.; Academic Press: San Diego, CA, 2000; Vol. 1, pp 239-349. b) Nobukuni, H.; Shimazaki, Y.; Tani, F.; Naruta, Y. *Angew. Chem. Int. Ed.* **2007**, *46*, 8975. c) Song, J.; Aratani, N.; Shinokubo, H.; Osuka, A. *J. Am. Chem. Soc.* **2010**, *132*, 16356. d) Song, J.; Aratani, N.; Shinokubo, H.; Osuka, A. *Chem. Sci.* **2011**, *2*, 748. e) O'Sullivan, M. C.; Sprafke, J. K.; Kondratuk, D. V.; Rinfray, C.; Claridge, T. D. W.; Saywell, A.; Blunt, M. O.; O'Shea, J. N.; Beton, P. H.; Malfois, M.; Anderson, H. L. *Nature* **2011**, *469*, 72.

bowl-shaped geometry, like π-extended tetrathiafulvalenes,[262] and, as it has been already outlined, the cone-shaped SubPcs[35] and SubPs.[33]

Among all these non-planar aromatic systems, SubPcs present two unique physicochemical properties of utmost importance that make them one of the most appealing building blocks for the development of curved extended π-surfaces and supramolecular chemistry. First, their structural features allow for the fine modulation of their optoelectronic properties by chemical functionalization. Second, unlike all the previously cited bowl-shaped aromatic molecules, which undergo cone inversion with relatively low inversion barriers,[256a,257,259a,263] SubPcs possess a rigid tetrahedral structure that do not undergo bowl inversion,[55,101c,264] giving rise to configurationally stable cone-shaped molecules. In this regard, from an early stage of the SubPc chemistry, characteristics arising from the 14 π-electron conjugated curved system, such as difference in aromaticity between the concave and convex surfaces[53,72b,e,103d,265] and concave-convex π-π stacking interaction,[50,64] or inherent molecular chirality of C_3-chiral or unsymmetrically substituted SubPcs,[47b,48,50,51b,101c] have been explored.

One of the research interests in our group has been focused on the development of homo- and heteropolynuclear π-extended ensembles, using Pcs and homologous macrocycles as building blocks, that are achieved by either using rigid alkenyl-alkynyl bridging groups between the macrocyclic units or by the edge-to-edge fusion of two Pcs, resulting in polynuclear systems sharing a common benzene (or naphthalene) ring.[266] Large conjugated molecules may present several interesting properties, as the electronic absorption in the visible region is shifted to the infrared or near-infrared spectral regions (higher than 700 nm), which can be

---

[261] a) Okujima, T.; Jin, G.; Matsumoto, N.; Mack, J.; Mori, S.; Ohara, K.; Kuzuhara, D.; Ando, C.; Ono, N.; Yamada, H.; Uno, H.; Kobayashi, N. *Angew. Chem. Int. Ed.* **2011**, *50*, 5699. b) Roznyatovskiy, V. V.; Lim, J. M.; Lynch, V. M.; Lee, B. S.; Kim, D.; Sessler, J. L. *Org. Lett.* **2011**, *13*, 5620. c) Sarma, T.; Panda, P. K. *Chem. Eur. J.* **2011**, *17*, 13987. d) Okujima, T.; Ando, C.; Mack, J.; Mori, S.; Hisaki, I.; Nakae, T.; Yamada, H.; Ohara, K.; Kobayashi, N.; Uno, H. *Chem. Eur. J.* **2013**, *19*, 13970. e) Okujima, T.; Ando, C.; Agrawal, S.; Matsumoto, H.; Mori, S.; Ohara, K.; Hisaki, I.; Nakae, T.; Takase, M.; Uno, H.; Kobayashi, N. *J. Am. Chem. Soc.* **2016**, *138*, 7540.

[262] a) Martín, N.; Sánchez, L.; Herranz, M. A.; Illescas, B.; Guldi, D. M. *Acc. Chem. Res.* **2007**, 40, 1015. b) Brunetti, F. G.; López, J. L.; Atienza, C.; Martín, N. *J. Mater. Chem.* **2012**, *22*, 4188.

[263] a) Scott, L. T.; Hashemi, M. M.; Bratcher, M. S. *J. Am. Chem. Soc.* **1992**, *114*, 1920. b) Biedermann, P. U.; Pogodin, S.; Agranat, I. *J. Org. Chem.* **1999**, *64*, 3655. c) Seiders, T. J.; Baldridge, K. K.; Grube, G. H.; Siegel, J. S. *J. Am. Chem. Soc.* **2001**, *123*, 517. d) Higashibayashi, S.; Sakurai, H. *J. Am. Chem. Soc.* **2008**, *130*, 8592. e) Yoshida, K.; Osuka, A. *Chem. Eur. J.* **2015**, *21*, 11727.

[264] Samdal, S.; Volden, H. V.; Ferro, V. R.; García de la Vega, J. M.; González-Rodríguez, D.; Torres, T. *J. Phys. Chem. A* **2007**, *111*, 4542.

[265] Claessens, C. G.; González-Rodríguez, D.; Iglesias, R. S.; Torres, T. *C. R. Chim.* **2006**, *9*, 1094.

[266] de la Torre, G.; Bottari, G.; Sekita, M.; Hausmann, A.; Guldi, D. M.; Torres, T. *Chem. Soc. Rev.* **2013**, *42*, 8049.

explored in many applications such as electrolithography, sensitization for photovoltaic devices, or photodynamic therapies. Also, extended π-electronic surfaces are highly polarizable, which is a desired feature for a molecule to present third-order nonlinear optical behavior, and consequently may be employed in nonlinear optical applications.

The extension of this concept to SubPc chemistry led in 2002 to the first synthesis and characterization of a fused dimer of SubPc, consisting of two merged SubPc units that share one benzene ring,[107] as it has been mentioned in the *Introduction* of this Thesis. These systems were prepared by mixed condensation of a phthalonitrile derivative and tetracyanobenzene in the presence of BCl_3. Two binuclear species were separated and identified, corresponding to the formation of the two possible topoisomers that arise from the combination of two cone-shaped SubPc units: the *syn* topoisomer, that presents full hemicircular geometry, and the *anti* topoisomer, that forms a novel S-shaped molecule (Figure 64). Tiny amounts of a SubPc trimer as a mixture of three topoisomers were also obtained. Optimization of the reaction conditions by Claessens *et al.* employing tetrafluorophthalonitrile as the starting phthalonitrile allowed for the obtention of the corresponding dimer **2** as a 1:1 mixture of *syn* and *anti* topoisomers in 20% yield overall.[108a] However, further attempts to prepare a set of fused SubPc dimers bearing donor and acceptor peripheral substituents have revealed that only a few other different dimers can be synthesized, and in very low yields.[108] The central benzene ring conserves its aromatic character in topoisomers *anti* and *syn*, as indicated by the low-field proton resonances for this moiety, which appeared as a "fingerprint" of these species at *ca.* 10.5 ppm. The peripheral substituents have a strong effect on the electronic properties of the macrocycles and the *syn* and *anti* SubPc dimers and the SubPc trimers exhibit a remarkable bathochromic shift of *ca.* 120 and 180 nm of their *Q* band absorptions relative to their parent monomers, respectively (Figure 64b). This, along with their higher intensity, clearly indicates that the SubPc subunits within the dimers and trimers are fully conjugated. The electronic communication between the two macrocyclic units is also evidenced in electrochemistry. SubPc dimers exhibit a first oxidation process 100-150 mV cathodically shifted and a first reduction event 100-250 mV anodically shifted when compared to those of the corresponding monomers. Theoretical calculations at DFT/6-31G(d,p) computational level along with electron density studies support the experimental findings.[108a]

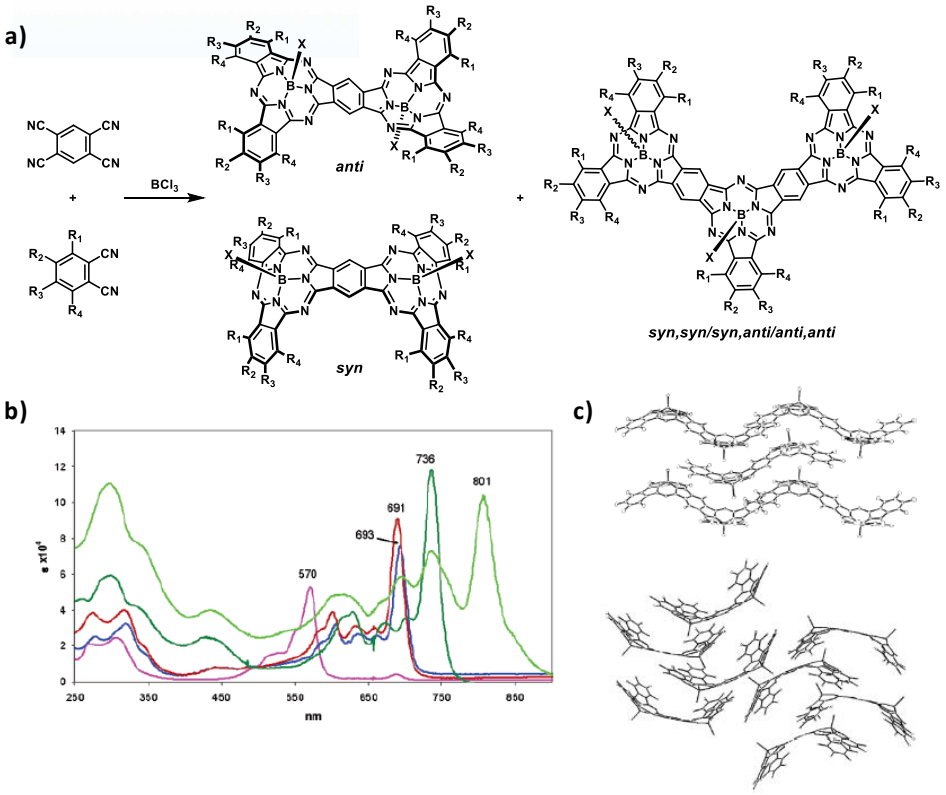

Figure 64. a) Synthesis of SubPc fused dimers (*syn* and *anti*) and trimers (mixture of three topoisomers). b) UV-vis spectra of perfluorinated SubPc (purple line), different axially-substituted perfluorinated SubPc dimers (red and blue line), and thiooctyl substituted SubPc dimer (dark green line) and trimer (light green line). c) Crystal packing of the *anti* (top) and *syn* (bottom) topoisomers of a peripherally fluorinated SubPc dimer.

Challenging issues concerning the inability to synthesize appreciable quantities of other SubPc fused dimers have restricted the reports on the applicability of these systems to the perfluorinated dimer **2**. In particular, it has been employed as an active unit in an artificial photosynthetic system consisting on a covalently linked SubPc *syn* dimer-C_{60} dyad that was prepared through double cycloaddition of the fused dimer, previously functionalized with aldehyde groups at the axial positions to the fullerene.[267] Moreover, highly efficient all SubPc-based photovoltaic devices have been fabricated using perfluorinated fused dimer **2** as

[267] a) Iglesias, R. S.; Claessens, C. G.; Torres, T.; Rahman, G. M. A.; Guldi, D. M. *Chem. Commun.* **2005**, 2113. b) Iglesias, R. S.; Claessens, C. G.; Rahman, G. M. A.; Herranz, M. A.; Guldi, D. M.; Torres, T. *Tetrahedron* **2007**, *63*, 12396.

electron acceptor (Figure 65).[228,268] Finally, the stability and NLO properties of the SubPc fused dimers and trimers were theoretically investigated using ab initio and density functional theory.[269]

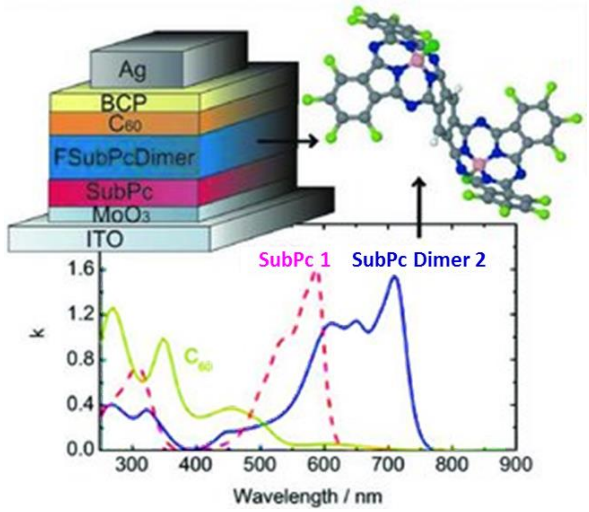

Figure 65. Planar solar cell based on acceptor perfluorinated SubPc fused dimer **2** as represented in ref. 228.

From these examples, it becomes clear that these SubPc fused oligomers exhibit very attractive features for their application in organic photovoltaics, such as an intense absorption in the near-infrared region of the visible spectrum and a rich redox behavior, and a low tendency to aggregate in solution. For this reason, a further insight into the possibilities of functionalizing these π-extended systems and modulating their optoelectronic properties in order to incorporate them as active materials in photovoltaic devices or integrate them as photoactive entities in D-A molecular models is demanded.

Since the last reports on this matter, almost ten years ago, new synthetic methodologies have evolved the peripheral and axial reactivity of SubPcs, giving rise to multiple versatile alternatives to chemically functionalize the SubPc core. Throughout this chapter, some previously unexplored approaches towards the synthesis of novel peripherally and axially functionalized SubPc oligomers with interesting properties and potential usefulness for photovoltaic applications will be discussed.

---

[268] Torres Cebada, T.; Claessens, C.; Medina Martin, A.; Verreet, B.; Aernouts, T. EP2012/057684, WO2012/146672 A2, filed on April 26, 2012.

[269] Yang, Y. J.; Kan, Y. H.; Su, Z. M.; Zhao, L. *J. Mol. Struct. THEOCHEM* **2005**, *725*, 127.

2.2 Specific objectives of *Chapter II*

The main goal of this chapter is the synthesis and characterization of novel curved π-extended systems based on SubPc fused oligomers and the study of selected properties for the potential application of these systems in organic photovoltaics. This chapter is divided in two different sections.

The first part of this chapter is mainly focused on the preparation of unsymmetrical SubPc oligomers with the goal of modulating further the optoelectronic properties of this family of molecular building blocks. It has been proven that, in order to obtain large fused SubPc ensembles, it is essential to design a rational synthetic strategy. In this sense, dicyano- and tetracyano-SubPcs described in *Chapter I* can be contemplated as very interesting phthalonitrile derivatives that would potentially allow the stepwise synthesis of new π-extended curved surfaces (Figure 66). Thus, by condensation reaction of these SubPc derivatives with other phthalonitriles, a series of unsymmetrical fused dimers or trimers could be obtained. Besides, cyclotrimerization reaction of a dicyano-SubPc employing standard SubPc synthesis conditions would purportedly produce a large star-shaped fused tetramer.

Considering the synthesis of unsymmetrical SubPc fused dimers in particular, either electron-donating or electron-accepting substituents will be introduced on each SubPc constituent unit.[270] Electrochemical and photophysical characterization of this unprecedented push-pull π-extended curved aromatic macrocycles, both in the ground and excited states, will be carried out. Finally, other attempts on the synthesis of larger SubPc-based ensembles will be described.

The transient-state photophysical studies of this chapter were carried out in the laboratory of Prof. Dirk Guldi at the Friederich-Alexander University in Erlangen, Germany.

[270] Zango, G.; Zirzlmeier, J.; Claessens, C. G.; Clark, T.; Martinez-Diaz, M. V.; Guldi, D. M.; Torres, T. *Chem. Sci*. **2015**, *6*, 5571.

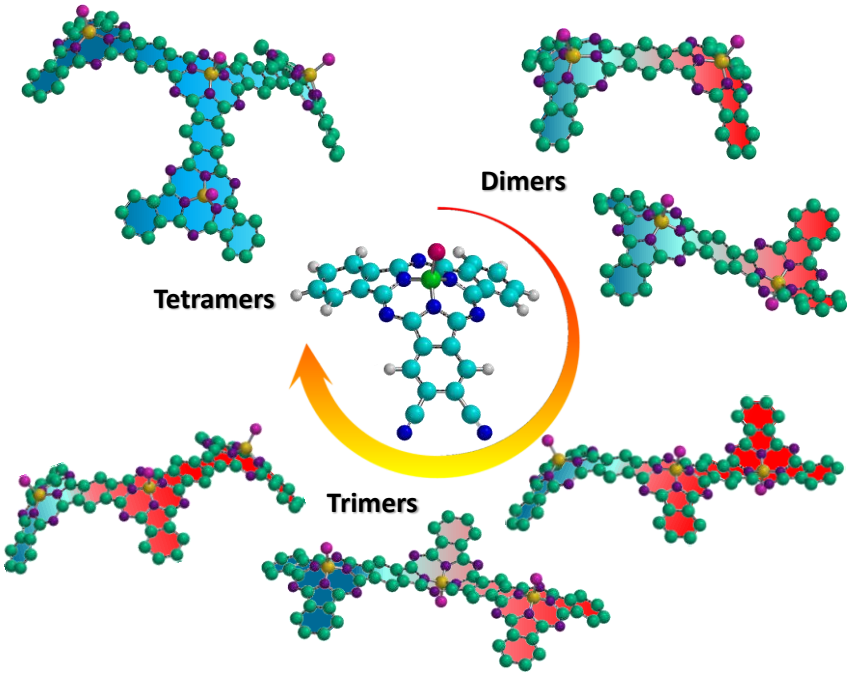

Figure 66. SubPc fused oligomers potentially accessible from a SubPc derivative bearing at least one *ortho*-dicyano functionality (background color gradient represents an unsymmetrical electronic distribution).

The second part of this chapter deals with the preparation of SubPc dimers based multicomponent systems for molecular recognition and supramolecular artificial photosynthetic systems. SubPc fused dimers present two available axial positions that will be employed to attach other photoactive units by means of novel axial functionalization methodologies (Figure 67). The structural features and the properties of the resulting systems will be studied, and their potential application as molecular receptors of carbon nanostructures will be investigated.

Figure 67. Schematic representation of some of the SubPc dimers based multicomponent systems for molecular recognition and supramolecular artificial photosynthetic systems described in this chapter.

2.3 Synthesis and characterization of novel unsymmetrical subphthalocyanine fused oligomers

2.3.1 Results and discussion

2.3.1.1 Synthesis of unsymmetrical SubPc fused dimers

In order to synthesize SubPc fused dimers with an unsymmetrical electronic distribution along their surface, functionalized *ortho*-dicyano-SubPc derivatives described in *Chapter I* could be employed as π-extended phthalonitrile-like precursors in a statistical cross condensation reaction with another phthalonitrile derivative bearing substituents with different electronic nature than the ones present in the SubPc periphery (Scheme 17). As the synthesis of unsymmetrical SubPc derivatives, four different cyclotrimerization products (A_3, A_2B, AB_2 and B_3) can be expected from the macrocyclization. Besides, the series of differently functionalized dicyano-SubPcs prepared enabled to explore the synthesis of SubPc dimers starting from SubPc derivatives bearing either electron-donating or electron-accepting substituents (Scheme 17).

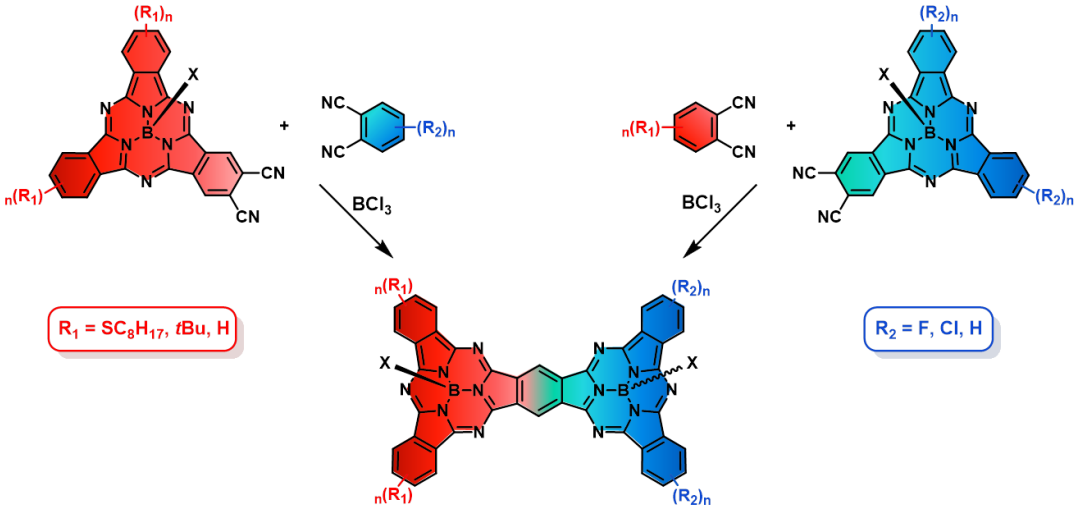

Scheme 17. Synthetic approaches to prepare unsymmetrical SubPc fused dimers from *ortho*-dicyano-SubPcs.

Initially, the synthesis of dimer **36**, bearing *tert*-butyl and fluoro groups, was tackled, starting either from SubPc **12** or SubPc **16** (Scheme 18). First attempts on this dimer, carried out by

reacting 1 equiv of dicyano-SubPc **12** or **16** with 2 equiv of 3,4,5,6-tetrafluorophthalonitrile or 4-*tert*-butylphthalonitrile respectively, in the presence of BCl_3 (3 equiv, 1.0 M in *p*-xylene) at reflux, were unsuccessful. Even varying the dicyano-SubPc/phthalonitrile ratio, reaction led only to the formation of the symmetrical SubPcs F_{12}-SubPc-Cl or t-Bu_3-SubPc-Cl and to decomposition or polymerization side products of SubPcs **12** and **16**. Reaction failure was attributed to a fast reaction of dicyano-SubPcs with boron trihalide. In order to solve this problem, an alternative experimental procedure was followed. Thus, 3 equiv of BCl_3 were initially added to the corresponding phthalonitrile at room temperature and the slurry was stirred for 5 min at room temperature to ensure the formation of the highly reactive phthalonitrile-BCl_3 complex. Then, a solution of dicyano-SubPc **12** or **16** in *p*-xylene was added and the mixture was heated to reflux. In this case, starting from SubPc **12**, the formation of a bluish spot attributed to the sought unsymmetrical binuclear product could be observed by TLC. Subsequent chromatographic work up in silica gel caused decomposition of the product, so purification was performed by size exclusion chromatography, affording dimer **36** in 10% yield as a mixture of *syn* and *anti* topoisomers for an optimized SubPc/phthalonitrile/BCl_3 ratio of 1:4:6. On the other hand, efforts to obtain dimer **36** starting from SubPc **16** were fruitless.

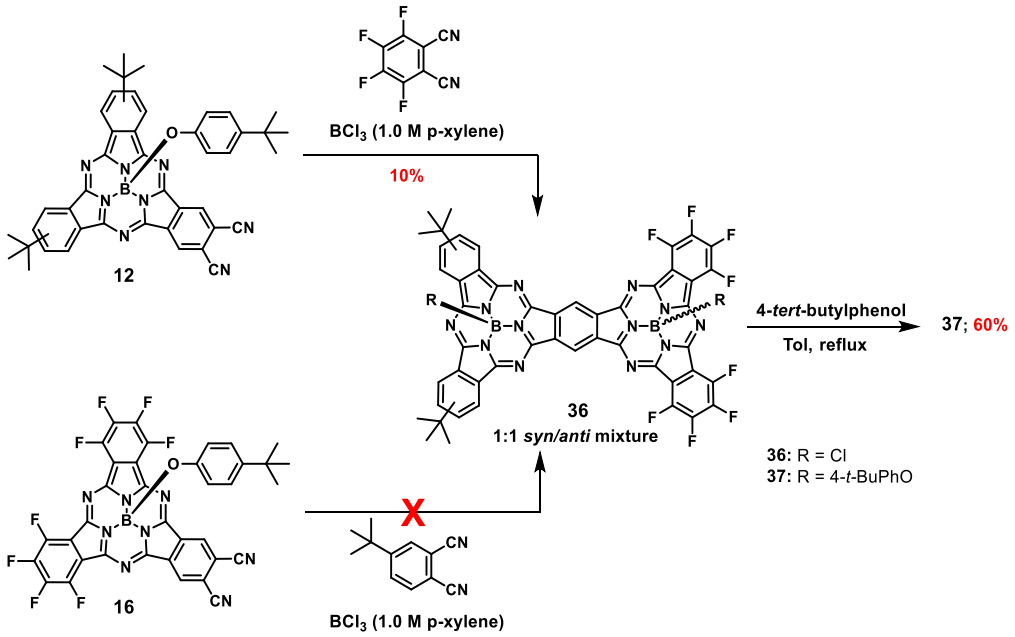

Scheme 18. Synthesis of dimers **36** and **37**.

Interestingly, ^{1}H-NMR and MS spectra revealed that the full substitution of the axial phenoxy ligand in the starting *ortho*-dicyano-SubPc **12** by a chlorine atom takes place during the reaction, rendering a dimer **36** with two chlorine atoms in axial positions. This axial substitution reaction of phenoxy ligands in the presence of BCl_3[189] and the related substitution by fluorine have already been described.[42b,64]

Replacement of the two chlorine atoms in **36** by 4-*tert*-butylphenol was carried out in order to increase the stability of the compound in silica gel and to ease the separation of *syn* and *anti* topoisomers. Dimer **37** was obtained in 60% yield from dimer **36**, but its topoisomers could not be isolated by column chromatography.

The results achieved in the synthesis of dimer **36** starting from dicyano-SubPc **12** prompted us to test the reaction of this SubPc with other phthalonitrile derivatives bearing electron-withdrawing groups, such as 4-iodo-, 4,5-diiodo- and 4,5-dichlorophthalonitrile. The reactions of **12** with 4-iodophthalonitrile or 4,5-diiodophthalonitrile in the same experimental conditions led mainly to decomposition products and symmetrical iodinated SubPcs. Only in the reaction of **12** with 4,5-diiodophthalonitrile, a tiny fraction of blue compound could be isolated by size exclusion chromatography where the peak corresponding to the corresponding unsymmetrical dimer **38** could be identified by MS.

On the other hand, condensation of SubPc **12** with previously activated 4,5-dichlorophthalonitrile in the presence of BCl_3 proceeded in better yields, rendering unsymmetrical dimer **39** in 16% yield with the optimized SubPc/phthalonitrile/BCl_3 ratio of 1:4:6. Dimer **39** was purified by column chromatography on silica gel, where the product was found to be stable, as a *syn*/*anti* 1:1 mixture. Separation of the two topoisomers of dimer **39** was not possible during the chromatographic purification step. However, substitution reaction of the two axial chlorine atoms by 4-*tert*-butylphenol allowed for the separation of both topoisomers ***anti*-40** and ***syn*-40** in 90% overall yield (Scheme 19). In this case, dimer **39** could also be obtained in the reaction of SubPc **15** with 4-*tert*-butyphthalonitrile with similar yields (Scheme 19).

In ^{1}H-NMR spectra, ***anti*-40** and ***syn*-40** exhibit several diagnostic singlets at high chemical shifts, around 10.33-10.27 ppm, corresponding to the highly deshielded protons of the central benzene ring (Figure 68). The appearance of more than one singlet for each topoisomer evidences that ***anti*-40** and ***syn*-40** are in fact a mixture of three different regioisomers depending on the position of *tert*-butyl groups in the electron-donating SubPc moiety. Besides, a comparative study of both spectra allows the assignment of *syn* and *anti* topologies by means of the shift of the proton signals of axial phenol groups.[107a,108a] Thus, ***anti*-40**, showing

chemical shifts of the aromatic phenolic protons around 5.3 ppm, very similar to those of the constituent SubPcs, Cl_6-SubPc-OPh^{t}Bu and ^{t}Bu$_3$-SubPc-OPh^{t}Bu, is identified as topoisomer *anti*, while in ***syn*-40**, these signals are significantly downfield shifted (*ca.* 0.15 ppm) due to the proximity of the axial groups and their resulting interaction (Figure 68).

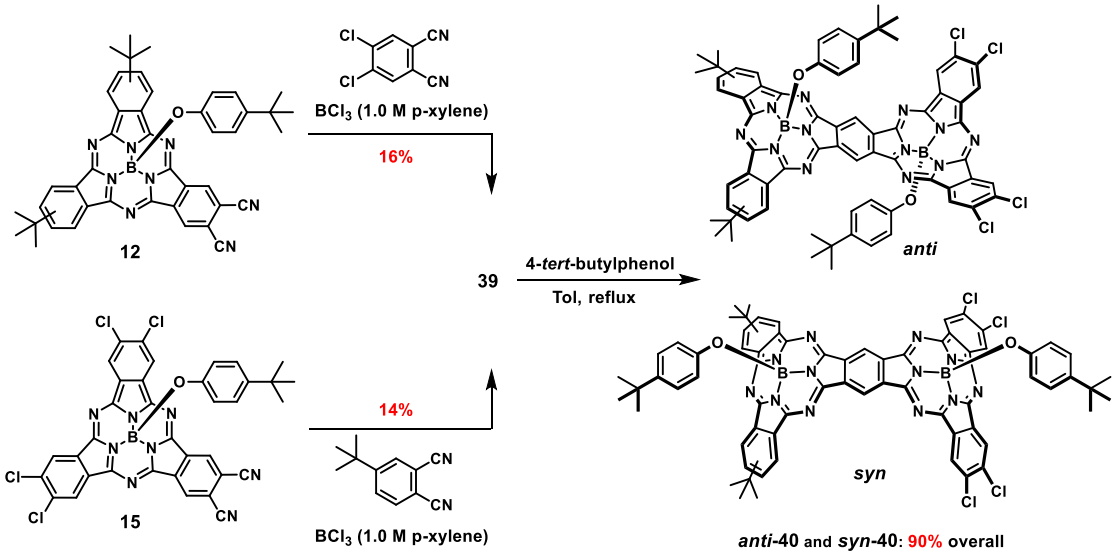

Scheme 19. Synthesis of dimers **39**, ***anti*-40** and ***syn*-40**.

With the aim of preparing regioisomerically and topoisomerically pure dimers, separation of the three regioisomers of diiodo-SubPc **4b** and dicyano-SubPc **12** was carried out by column chromatography on silica gel. The unequivocal assignment of the structure of each regioisomer was determined by NMR techniques, namely COSY, NOE and HMQC, and on the basis of the number of different signals of the α-protons adjacent to iodo/cyano substituents, as they face different or similar environments. Finally, the three regioisomers of dimer **39** were individually synthesized with similar yields (see *Experimental Section*). Unfortunately, small amounts of each dimer **39** regioisomer obtained in this process precluded the synthesis and separation of regioisomerically pure topoisomers ***anti*-40** and ***syn*-40**.

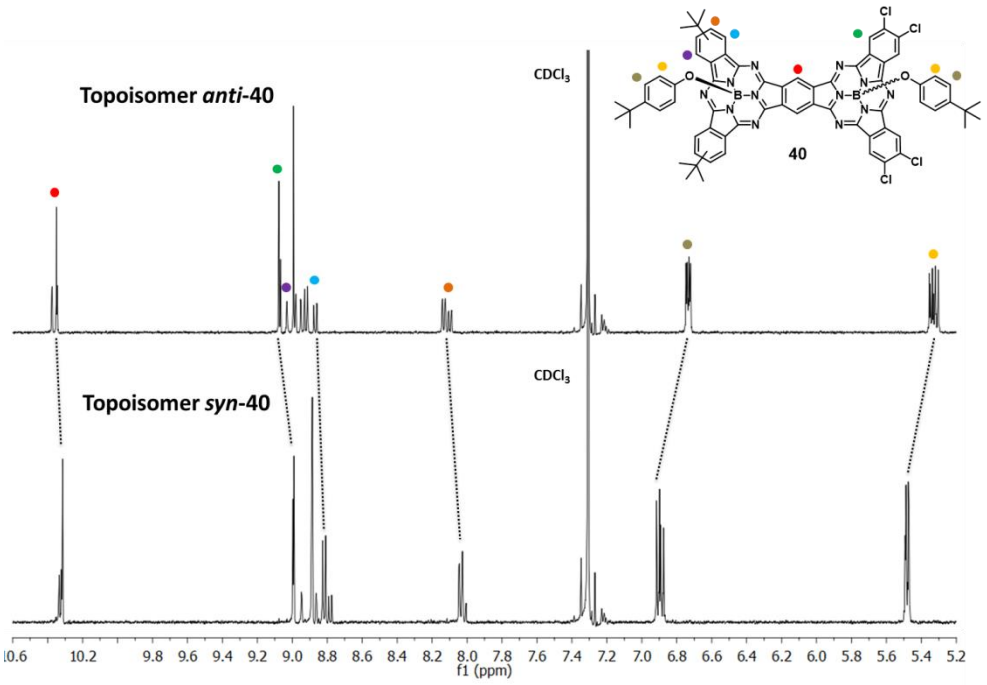

Figure 68. Partial ^{1}H-NMR (500 MHz) spectra in $CDCl_3$ of dimer ***anti*-40** (top) and topoisomer ***syn*-40** (down).

Next step was focused on the preparation of an unsymmetrical dimer that would not render a mixture of regioisomers to ease the isolation of the *syn* and *anti* topoisomers. The synthesis of a new unsymmetrical dimer **41** bearing no substituents in the first SubPc unit and chloro atoms in the second unit was devised. Reaction of either 1 equiv of SubPc **14** with 4 equiv of 4,5-dichlorophthalonitrile or 1 equiv of SubPc **15** with 4 equiv of phthalonitrile, in the presence of 6 equiv of BCl_3, led to the formation of dimer **41** as a *ca.* 4:1 mixture of *syn* and *anti* topoisomers in 14% yield (Scheme 20).

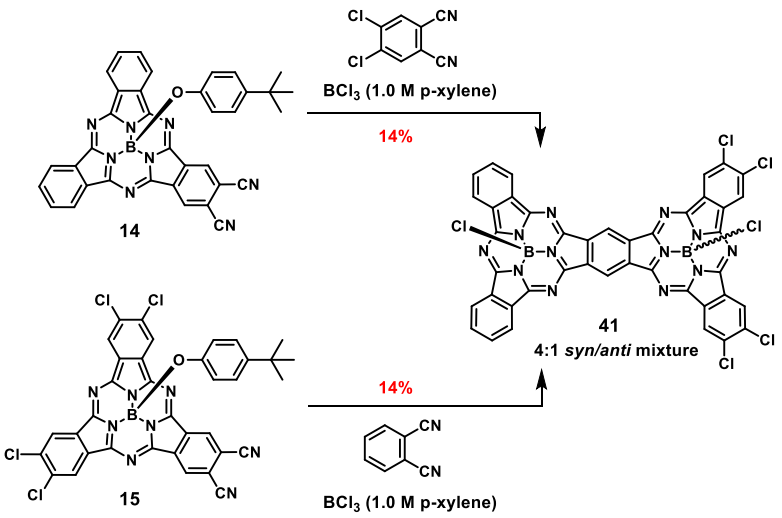

Scheme 20. Synthesis of dimer **41**.

The presence of two clearly discernible blue products spotted by TLC, identified as the *syn* and *anti* topoisomers of **41**, encouraged us to attempt the separation of both isomers without further substitution of the axial chlorine atoms. Unfortunately, both topoisomers could not be isolated either by column chromatography on silica gel or by size exclusion chromatography, mainly due to low stability of the compound in silica gel, evidenced by a remarkable mass loss during the work up. Only a small fraction of the topoisomer eluting last **41b** could be obtained in high purity, as it could be observed by ^{1}H-NMR (Figure 69). At this point, it must be noticed that, in an effort to provide more stability or a better resolution of the two topoisomers in chromatographic conditions, the exchange of the axial chlorine atoms in **41** by other substituents (namely fluorine atoms and phenol derivatives) has been tested, with unproductive results.

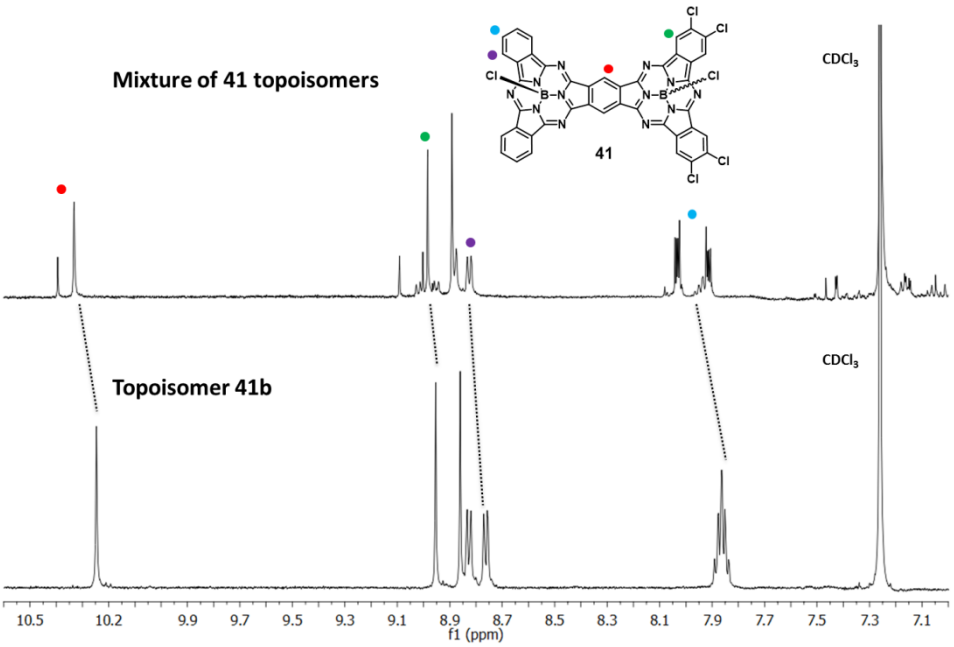

Figure 69. Partial ^{1}H-NMR (300 MHz) spectra in $CDCl_3$ of dimer **41** (mixture of topoisomers) (top) and topoisomer **41b** (down).

Finally, the syntheses of unsymmetrical SubPc fused dimers bearing thiooctyl substituents in the electron-donating SubPc moiety were addressed. First, cross condensation of SubPc **13** with 4,5-dichlorophthalonitrile or dicyanobenzene in BCl_3 was conducted in order to obtain dimer **42**. However, SubPc **13** exhibited lack of reactivity as phthalonitrile derivative and only exchange of the axial phenoxy group by a chlorine atom was observed by monitoring the reaction by TLC. Addition of a higher excess of BCl_3 led to total decomposition of **13**. We attributed this low reactivity to a decreased electrophilicity of the *ortho*-dicyano functionality owing to the presence of electron-donating thiooctyl groups in this SubPc derivative.

Therefore, preparation of unsymmetrical dimer **42** was tackled *via* reaction between SubPc **15** and 4,5-dioctylthiophthalonitrile (Scheme 21). The formation of a greenish compound showing hints of aggregation in TLC was promptly verified. Thus, *in situ* treatment of the reaction mixture with 4-*tert*-butylphenol was performed to decrease aggregation and increase stability. Interestingly, two well-defined green compounds with considerably distinct R_f values could be now spotted by TLC (Scheme 21).

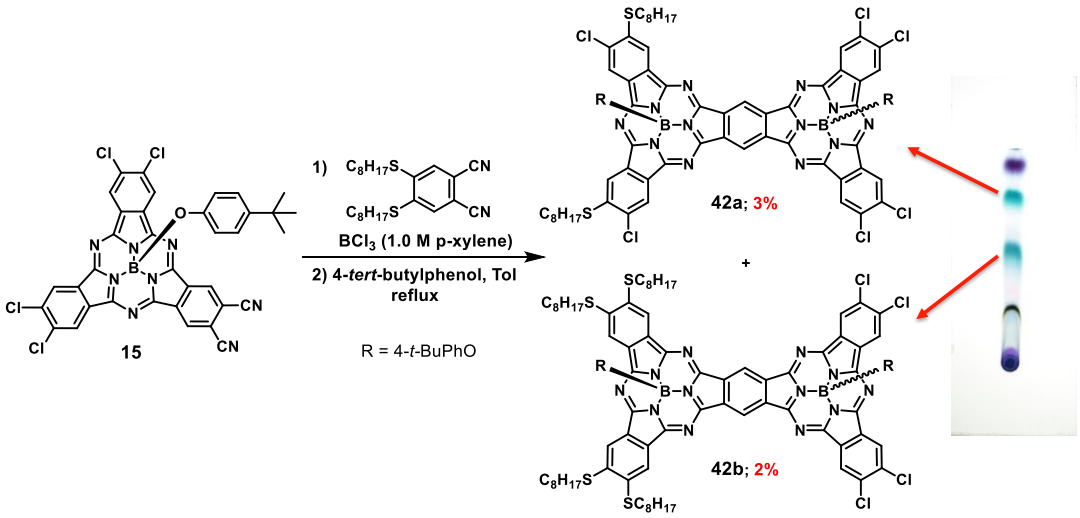

Scheme 21. Cross condensation reaction of SubPc **15** and 4,5-dioctylthiophthalonitrile. Two green compounds at Rf ~0.8 and 0.5 can be easily spotted by TLC, corresponding to **42a** and **42b** respectively.

In the belief that each spot corresponded to each **42** topoisomer, much effort was devoted to the separation of both products by tedious chromatographic work up, being able to isolate small fractions of each compound, obtaining **42a** and **42b** in 3% and 2% yield respectively. Surprisingly, ^{1}H-NMR and MS spectra revealed that an unexpected side reaction occurs: while compound **42b** matched in fact the sought unsymmetrical SubPc dimer bearing four thiooctyl substituents in one SubPc unit and four chloro atoms in the other unit, compound **42a** was identified as a highly unsymmetrical SubPc dimer where two thiooctyl substituents have been substituted by two chlorine atoms (Figure 70). Up to now, the displacement of thioalkyl peripheral substituents in the synthesis of SubPcs by chlorine atoms released by BCl_3 has never been reported. Although we do not have a clear explanation for this effect, it can only be hypothesized that a nucleophilic aromatic substitution by free chlorine atoms is favored by the presence of a second SubPc moiety bearing electron-withdrawing groups. Nevertheless, full displacement of thiooctyl groups was not observed upon treatment of **42a** with 100 equiv of BCl_3 at *p*-xylene reflux. Only axial substitution of phenoxy groups was observed. In this regard, it can be supposed that one substitution reaction takes place at each benzene ring of the first SubPc unit to render dimer **42a**, and that the presence of a second thioalkyl substituent in *ortho* position to reaction site is relevant for the substitution to happen.

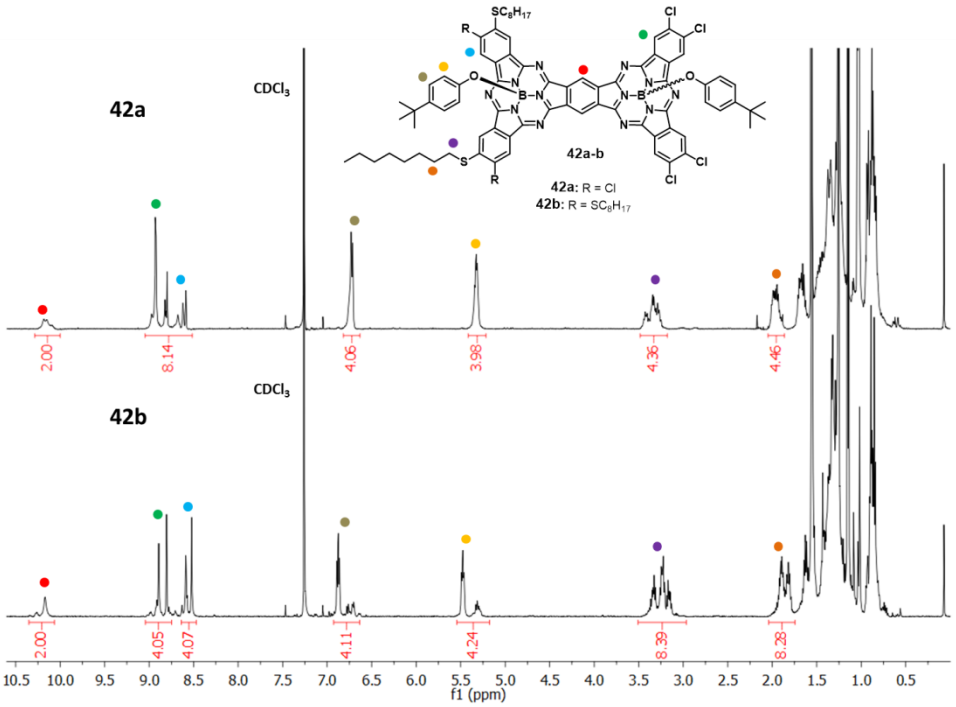

Figure 70. Partial ^{1}H-NMR (500 MHz) spectra in $CDCl_3$ of dimers **42a** (top) and **42b** (down). Splitting of some signals of aromatic protons and integration of the signals of aliphatic protons adjacent to sulfur atom enable structure elucidation of **42a**.

Reaction of SubPc **14** with 4,5-dioctylthiophthalonitrile proceeded in a similar manner, rendering a mixture of dimers in which one or two thiooctyl substituents have been displaced by chloro atoms.

2.3.1.2 Attempts on the synthesis of other symmetrical SubPc fused dimers

In order to assess the effectiveness of the novel stepwise synthesis of unsymmetrical SubPc fused dimers, a scope of the synthesis of symmetrical SubPc fused dimers through classical mixed condensation of a phthalonitrile derivative and tetracyanobenzene in the presence of BCl_3 was carried out. Reaction conditions previously optimized by Claessens *et al.*,[108a] namely 10:1 phthalonitrile/tetracyanobenzene ratio at *p*-xylene reflux temperature, were employed in the condensation reaction of tetracyanobenzene with a wide variety of phthalonitrile derivatives (Scheme 22).

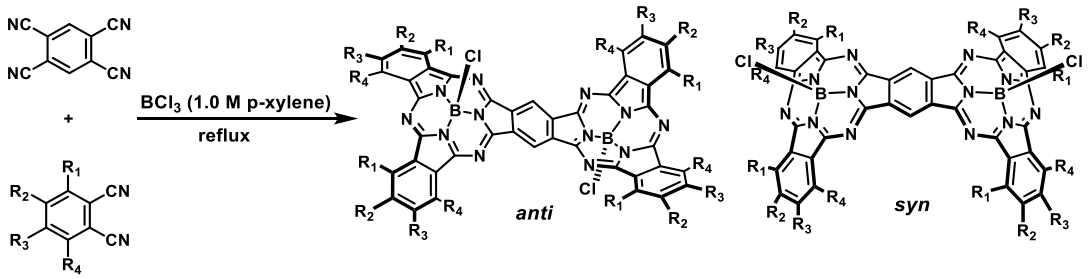

2: R_1-R_4 = F
43: R_1,R_4 = H, R_2,R_3 = F
44: R_1,R_4 = H, R_2,R_3 = Cl
45: R_1,R_4 = H, R_2,R_3 = I
46: R_2/R_3 = I, R_1,R_4,R_3/R_2 = H
47: R_1-R_4 = H
48: R_1,R_4 = H, R_2,R_3 = SC_8H_{17}
49: R_1,R_4 = H, R_2,R_3 = $C_4H_2Br_2$

Scheme 22. Synthesis of symmetrical SubPc dimers **2** and **43**-**49**.

As expected, dimers ***anti*-2** and ***syn*-2** could be obtained and individually isolated from the reaction between 3,4,5,6-tetrafluorophthalonitrile and tetracyanobenzene in 24% overall yield, comparable to previously reported ones.[108] From the condensation reaction of tetracyanobenzene with other electron deficient phthalonitriles such as 4,5-difluoro- and 4,5-dichlorophthalonitrile, dimers ***syn/anti*-43** and ***syn/anti*-44** were synthesized as a 1:1 mixture of *anti* and *syn* isomers in 4% and 5% yields, respectively. However, the low solubility that these dimers exhibited in most common solvents precluded the efficient separation of both topoisomers.

Dimers ***syn/anti*-45**, ***syn/anti*-46**, ***syn/anti*-47** and ***syn/anti*-49** could not be isolated from the condensation reaction of 4,5-diiodophthalonitrile, 4-iodophthalonitrile, dicyanobenzene or 2,3-dibromo-6,7-dicyanonaphthalene with tetracyanobenzene respectively, as a consequence of their poor solubility, though the formation of dimers could be confirmed by TLC in some cases. Finally, the synthesis of compounds ***syn/anti*-48** was carried out, but dimers formed in the reaction could not be isolated as a consequence of their quick decomposition on silica gel. In this case, axial substitution of dimers ***syn/anti*-48** with 4-*ter*t-butylphenol to increase their stability and reduce their tendency to form aggregates was not attempted.

From these results, it can be concluded that just a limited number of symmetrical SubPcs fused dimers can be synthesized and isolated, though in low yields. Dimers bearing electron-withdrawing groups in their periphery, such as ***syn/anti*-2**, ***syn/anti*-43** and ***syn/anti*-44** are the only derivatives that can be obtained and characterized. However, perfluorinated dimers ***syn/anti*-2** are produced in considerably larger yields than any other SubPc dimer, presumably due to their higher stability, both in solution and in the solid state, and their better solubility in common solvents allow for the separation of *syn* and *anti* topoisomers.[108a]

2.3.1.3 Attempts on the synthesis of larger SubPc fused oligomers

The stepwise synthesis of unsymmetrical SubPc fused trimers can be conceived through the cross condensation reaction between a phthalonitrile derivative and, in this case, a tetracyano-SubPc that presents two *ortho*-dicyano functionalities in its structure. Trimers obtained should be a mixture of three topoisomers, *syn,syn*, *syn,anti*, and *anti,anti*.

Our efforts were focused on the reaction of SubPc **17** with 4,5-dichlorophthalonitrile to yield SubPc trimer **50** (Scheme 23), inasmuch as the best results in the synthesis of unsymmetrical fused dimers were provided by the reaction between dicyano-SubPc **12** and the aforementioned phthalonitrile. It must be noted that the synthesis of trimer **50** requires the simultaneous cyclotrimerization of the two phthalonitrile-like units of SubPc **17** with two 4,5-dichlorophthalonitrile molecules each. Thus, this reaction can be seen as a challenging process where the sought-after compound is the product of two unsymmetrical SubPc syntheses occurring in the same system. Cross condensation reaction of 1 equiv of SubPc **17** and 6 equiv of 4,5-dichlorophthalonitrile in the presence of 8 equiv of BCl_3 rendered a complex reaction mixture, from which trimer **50** could be isolated in 4% yield. Surprisingly, a highly unsymmetrical SubPc dimer **51** corresponding to the cyclotrimerization of only one ortho-dicyano unit of **17** was also obtained. Unfortunately, poor reproducibility and scalability of this reaction did not allow the collection of appreciable amounts of **50**.

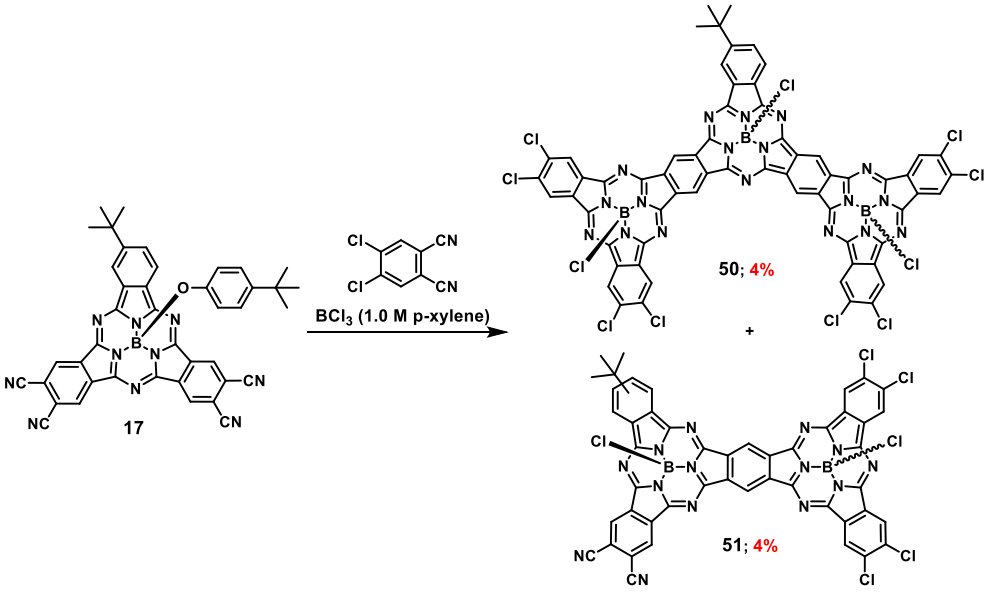

Scheme 23. Synthesis of trimer **50** and dimer **51**.

Structure of trimer **50** was confirmed on the basis of its spectroscopic features, namely ^{1}H-NMR and MS (Figure 71). Although no differentiation of the three possible topoisomers of **50** was spotted by TLC, the broad aromatic signals in ^{1}H-NMR spectrum suggests **50** is in fact a *syn,syn*, *syn,anti*, and *anti,anti* topoisomers mixture.

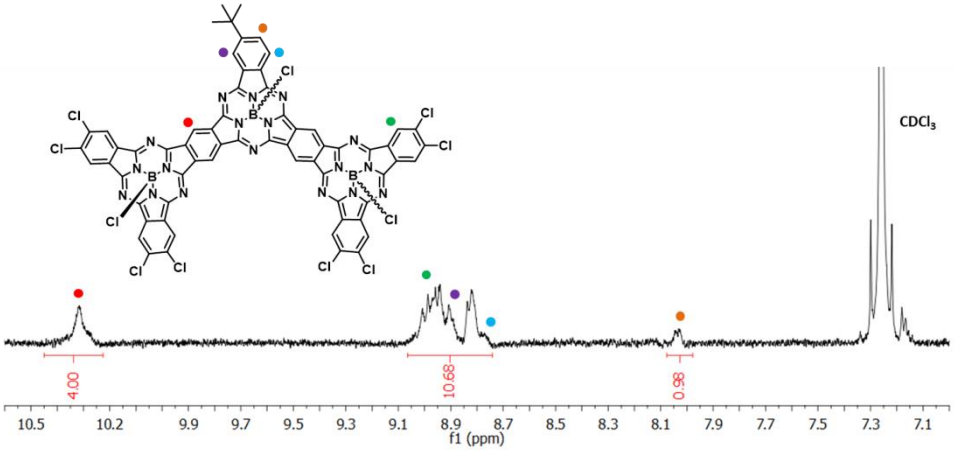

Figure 71. Partial ^{1}H-NMR (300 MHz) spectra in $CDCl_3$ of trimer **50**.

The syntheses of large multi-SubPc fused ensembles, namely a star-shaped SubPc fused tetramer, and a $(SubPc)_4ZnPc$ molecule consisting in a ZnPc core substituted with four SubPc macrocycles in the periphery, were attempted from dicyano-SubPc derivatives (Scheme 24). Self-condensation of SubPcs **12**, **15** or **16**, in standard cyclotrimerization conditions in the presence of stoichiometric amounts of a boron trihalide, either BCl_3 or BBr_3, only led to total and almost instantaneous decomposition of starting *ortho*-dicyano-SubPcs. On the other hand, heating SubPc **12** to reflux in a high boiling point solvent such as DMAE or DMF, in the presence of a zinc salt, namely $ZnCl_2$ or $Zn(OAc)_2$, only rendered green compounds that were identified as A_3B- and A_2B_2-type ZnPcs, products of the ring opening reaction of SubPc **12**.

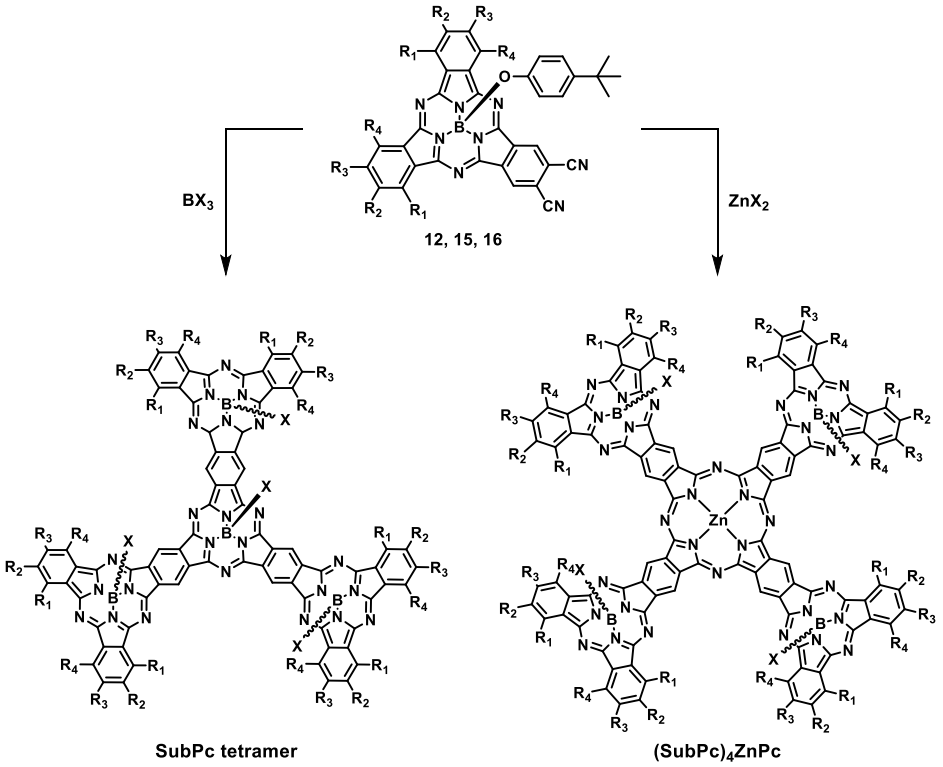

Scheme 24. Large SubPc fused ensembles that could be obtained from dicyano-SubPcs.

2.3.1.4 Optical properties of unsymmetrical SubPc fused oligomers

Unsymmetrical SubPc fused dimers **36-42** feature similar UV-vis absorption spectra in chloroform (Figures 72-73), all of them displaying a Soret band at *ca.* 320 nm and a *Q* band spanning from around 550 to 750 nm, with maxima at 700-720 nm. Compared to precursor dicyano-SubPcs, the *Q* band of dimers **36-42** presents a strong bathocromic shift of 100-130 nm that evidences the extended conjugation of the SubPc units within the dimer structure, and with higher ε values than SubPcs, in the order of 1.6-1.8 x 10^5 M^{-1} cm^{-1}, as a consequence of their larger molecular surface. Furthermore, the *Q* band exhibit a very characteristic shape, with three or four additional well-defined bands appearing in its blue region, due to the lower symmetry of these compounds.

The absorption spectra of unsymmetrical SubPc dimers are clearly influenced by both the electron-donating and the electron-withdrawing peripheral substituents of each SubPc moiety. In this regard, this effect is similar to the one observed when the peripheral substitution of

unsymmetrical dicyano-SubPcs is varied (Figure 72a). This way, comparison of absorption spectra of dimers **36** and **39**, bearing *tert*-butyl groups in one SubPc unit, shows a slight red shift in *Q* band maximum from 707 nm in dimer **36**, perfluorinated in the second SubPc unit, to 712 nm in dimer **39**, substituted with chlorine atoms, as was the case when going from dicyano-SubPc **16** (588 nm) to **15** (592 nm). Likewise, the modification of the substituents in the electron-donating SubPc moiety from dimer **39** to dimer **41** causes in this case a small hypsochromic shift from 712 to 707 nm, replicating the effect in the absorption features from SubPc **12** (598 nm) to SubPc **14** (593 nm). On the other hand, axial substitution of chlorine atoms in dimers **36** and **39** by phenoxy groups in dimers **37** and ***syn/anti*-40** respectively translates into a very small blue shift of only 2-3 nm (Figure 72b). Both topoisomers ***anti*-40** and ***syn*-40** exhibit the same absorption spectrum.

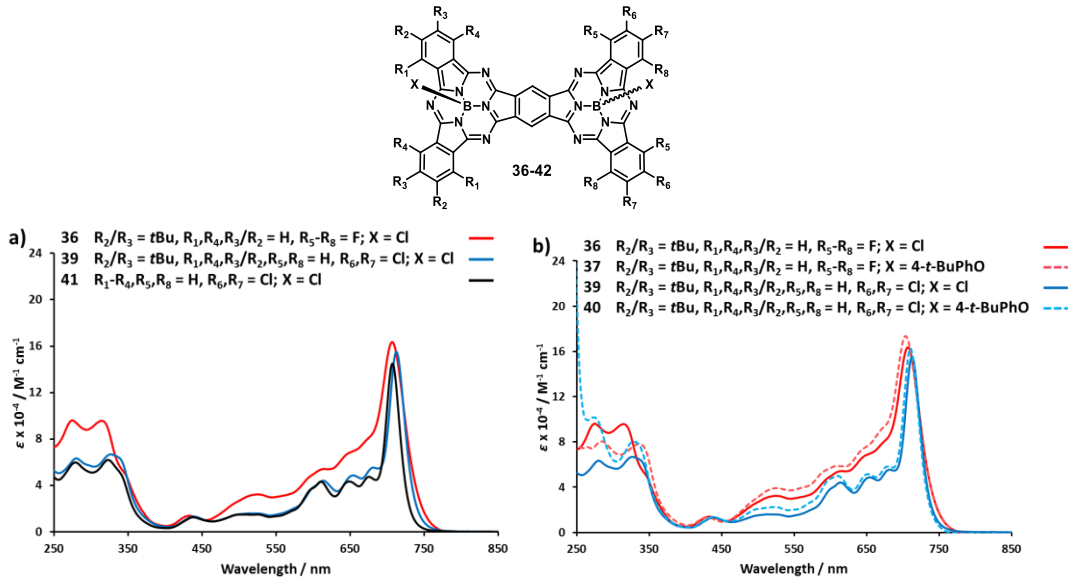

Figure 72. UV-vis absorption spectra in chloroform of: a) SubPc dimers **36**, **39**, and **41**, and b) SubPc dimers **36**, **37**, **39** and **40**.

Finally, trimer **50** features a Soret band at *ca.* 330 nm and a *Q* band that encompasses a broad area of the visible spectrum, from 550 to 800 nm, with a maximum at 783 nm, more than 70 nm bathochromically shifted with respect to dimer **39**, and six higher energy extra bands (Figure 73).

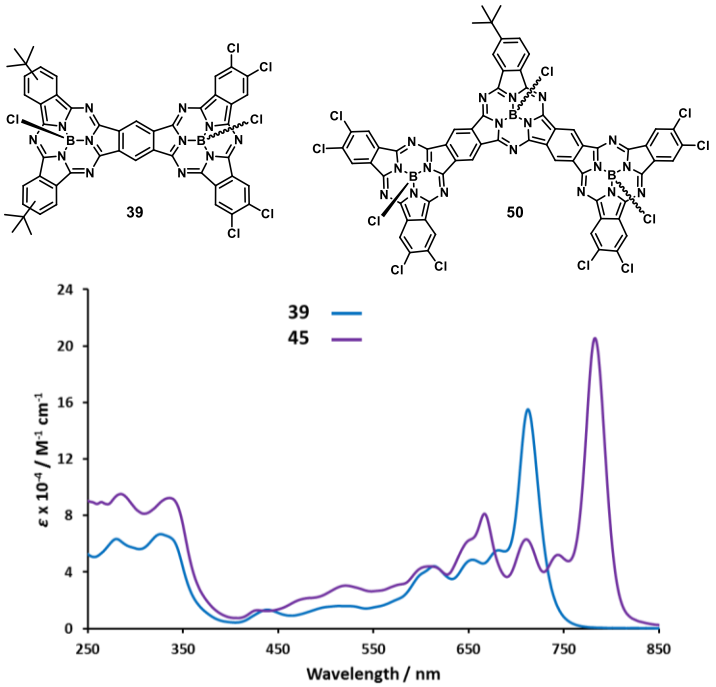

Figure 73. UV-vis absorption spectra in chloroform of: SubPc dimer **39** and SubPc trimer **50**.

2.3.1.5 Electrochemical studies and calculation of HOMO and LUMO levels of SubPc fused dimers 39-42

Electrochemical properties of unsymmetrical SubPc dimers **39**, ***syn/anti*-40**, **41** and **42b** were investigated by cyclic voltammetry, square-wave voltammetry and differential pulse voltammetry measurements in THF solution (0.1 M $TBAPF_6$). All potential values quoted throughout this section have been referred to the Fc/Fc^+ couple. Figure 74 shows the voltammograms of the compounds studied and the electrochemical data is summarized in Table 13.

All SubPc dimers present three or even four reversible reduction events and one irreversible oxidation process, as can be seen in Figure 74 SubPc dimer **39** displays reduction half-waves at -1088, -1392, and -1801 mV, and an oxidation event occurring at 640 mV. As it could be expected, axial substitution with donor 4-*tert*-butylphenoxy groups renders topoisomers ***anti*-40** and ***syn*-40** with slight differences in their reduction and oxidation processes compared to **39** and with exactly the same electrochemical behavior between them. Thus, first reduction

potential of ***syn/anti*-40** is cathodically shifted to -1215 mV and first oxidation peak appears at 50-70 mV lower potentials than **39**.

Modification of the peripheral substituents in the donor SubPc moiety does not seem to alter electrochemical properties of unsymmetrical SubPc dimers substantially. Dimer **41**, bearing no substituents in that SubPc unit instead of *tert*-butyl groups, exhibit a similar behavior to dimer **39**, with first reduction and oxidation potentials of -1060 and 645 mV respectively, barely shifted 28 and 5 mV with respect to dimer **39**. Furthermore, dimer **42b**, bearing thiooctyl substituents and axial 4-*tert*-butylphenoxy groups, presents easier reduction phenomena ($E^{1}_{1/2,red}$ = -1171 mV) and a similar oxidation event (E^{1}_{ox} = 577 mV) than topoisomers ***syn/anti*-40** (Table 13).

Interestingly, if we compare the electrochemical behavior of the unsymmetrical SubPc dimers with that of the dicyano-SubPc derivatives that resemble each of their SubPc units, these dimers have similar first reduction potentials than the dicyano-SubPcs related to the electron-donating SubPc unit. On the other hand, the extent of the conjugation in these larger fused systems renders easiest oxidation processes, inducing a rise in the HOMO energy and a reduction of the energy band gap to *ca.* 1.7 eV, in good agreement with the less energetic absorption of dimer compared to SubPcs and similar to the optical band gap estimated from the absorption-emission experiments.

Calculation of the energy level of LUMO and HOMO orbitals of dimers **39**, ***syn/anti*-40**, **41** and **42b** *vs.* vacuum were obtained from CV experiments and Equations 5 and 6 and are summarized in Table 13.

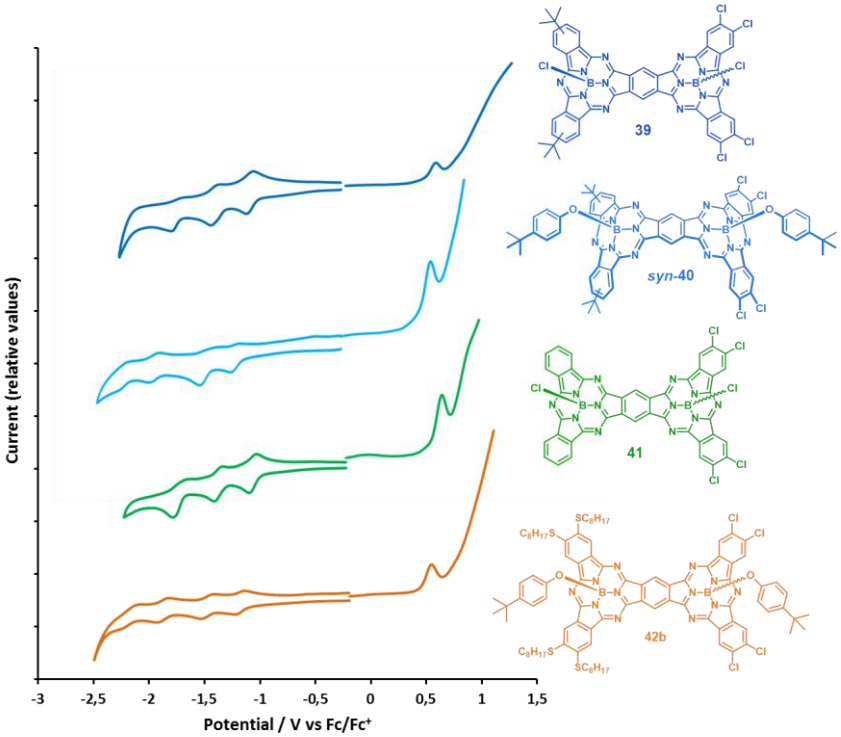

Figure 74. Cyclic voltammograms in the cathodic window and OSW voltammograms in the anodic window of SubPc dimers **39**, ***syn*-40**, **41** and **42b** in THF.

Table 13. Electrochemical data (in mV *vs.* Fc/Fc^{+}) in THF and experimental HOMO-LUMO energy levels data (in eV) of SubPc dimers **39**, ***syn/anti*-40**, **41** and **42b**.

SubPc	$E^{1}_{1/2,red}$ (mV)	$E^{2}_{1/2,red}$ (mV)	$E^{3}_{1/2,red}$ (mV)	E^{1}_{ox} [a] (mV)	E_{LUMO} (eV)	E_{HOMO} (eV)	$E_{g,opt}$ [b] (eV)
39	-1088	-1392	-1801	640[c]	-4.01	-5.74	1.73 (717)
***anti*-40**	-1215	-1487	-1953	589[c]	-4.04	-5.78	1.74 (714)
***syn*-40**	-1217	-1478	-1948	569[c]	-3.89	-5.61	1.73 (717)
41	-1060	-1369	-1739	645[c]	-3.88	-5.61	1.73 (717)
42	-1171	-1468	-1861	577[c]	-3.93	-5.63	1.71 (727)

[a] Since these oxidation processes are irreversible, only anodic peak potentials are reported. [b] Intersection wavelength in nm of the normalized absorption and emission spectra in brackets. [c] Peak oxidation potential by OSWV.

2.3.1.6 Assessment of the push-pull character of SubPc fused dimer 39

Among the distinct unsymmetrical SubPc fused dimers synthesized in this chapter, dimer **39**, bearing *tert*-butyl and chlorine substituents on each SubPc half, obtained in moderate yields as a 1:1 mixture of *syn* and *anti* topoisomers, which exhibit similar spectroscopic and electrochemical behavior, was chosen to study the potential push-pull character of these novel curved π-extended system by a series of physico-chemical studies. Two reference SubPc derivatives, namely hexachlorinated SubPc **29** and tri-*tert*-butyl SubPc **52** (Chart 8) were included in this study for comparison purposes.

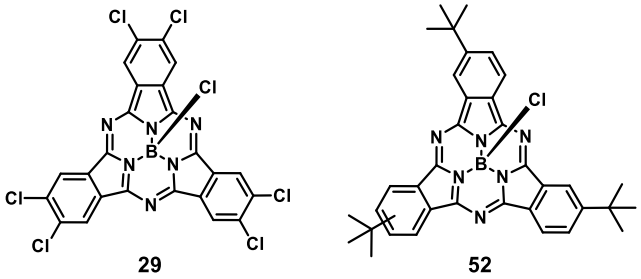

Chart 8. Structures of reference SubPcs **29** and **52** employed in this study.

First insights into potential push-pull interactions in the dimer **39** came from absorption and fluorescence measurements. In the two reference SubPcs, the long wavelength absorptions are seen at 574 for **29** and 569 nm for **52** in toluene (Figure 75). Importantly, changing the solvent polarity from toluene to benzonitrile exerts only a marginal impact on the vibrational progression of the absorption features. In direct contrast to the absorption, hexachlorinated SubPc **29** (2.15 eV) and tri-*tert*-butyl SubPc **52** (2.16 eV) exhibit fluorescence with distinct vibrational progression and with Stokes shifts of 211 and 229 cm^{-1}. Here, the fluorescence maxima, fluorescence quantum yields, and fluorescence lifetimes in toluene are 581 nm, 28.6 ± 2.5 %, and 3.65 ns, respectively, for the electron accepting chloro-substituted SubPc **29**, and 577 nm, 26.5 ± 2.5 %, and 3.29 ns for the electron donating *tert*-butyl-substituted SubPc **52**. It is notable that none of the fluorescence features change when the solvent polarity is varied systematically.

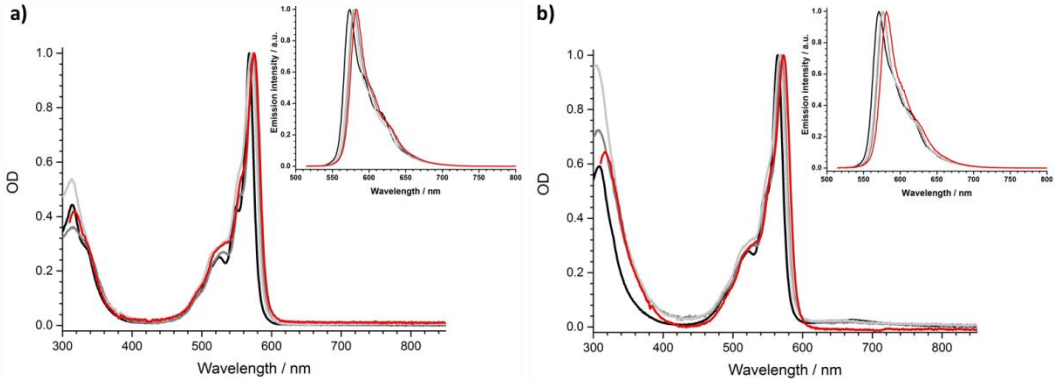

Figure 75. Absorption and fluorescence spectra (inset) upon 500 nm photoexcitation of a) SubPc **29** and b) SubPc **52**, in cyclohexane (black), toluene (dark grey), THF (light grey), and benzonitrile (red).

At first glance, the absorption and fluorescence of dimer **39** are similar to those seen for the references described above despite a substantial red shift (Figure 76). For example, in toluene the vibrationally fine structured absorption and fluorescence include a long wavelength maximum at 715 nm and a short wavelength maximum at 721 nm, respectively. In THF and benzonitrile, the corresponding features peak at 708/720 and at 716/727 nm, respectively. In contrast to the invariance of the maxima, the fluorescence quantum yields drop as the solvent polarity increases from cyclohexane (19.2%) and toluene (16.1%) to THF (8.3%) and benzonitrile (7.3%). A closer look reveals, however, that the fluorescence displays an additional, rather broad component, whose maximum is subject to some red shifts as the solvent polarity is increased, but determination of the exact location turned out to be difficult. We postulate that a delocalized singlet excited state (1.73 eV) is the origin of the former, while the latter is due to a polarized charge transfer state (< 1.7 eV).

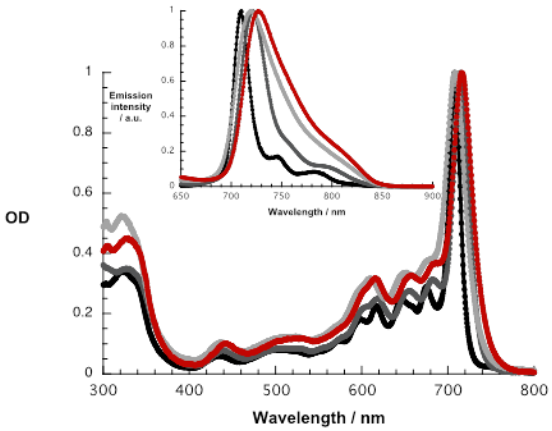

Figure 76. Absorption and fluorescence spectra (inset) upon 610 nm photoexcitation of **39** in cyclohexane (black), toluene (dark grey), THF (light grey), and benzonitrile (red).

This hypothesis was confirmed in pump probe experiments, in which chloro-substituted SubPc **29**, tert-butyl-substituted SubPc **52**, and SubPc dimer **39** were photoexcited at 530 and 656 nm. For **29** and **52**, differential absorption spectra can be found immediately upon photoexcitation (Figures 77 and 78). These include the features of the singlet excited states. For example, for **29** in toluene, transient bleaching from 510 to 608 nm with a minimum at 578 nm reflects the ground-state absorption. Maxima at 428 and 648 nm, a shoulder at 620 nm, and a broad NIR band complete the singlet excited state features of **29**. The differential absorption spectrum of **52** reveals a minimum at 574 and maxima at 446 and 620 nm, in addition to a shoulder at 645 nm. From multi-wavelength analyses, solvent-independent singlet excited state lifetimes of 2.9 ± 0.1 ns for **29** and 3.0 ± 0.15 ns for **52** were estimated. These decay lifetimes imply an efficient intersystem crossing to the corresponding triplet excited states. For the triplet excited state, the most prominent features in toluene are a 574 nm minimum with a 553 nm shoulder and 444, 617 and 672 nm maxima for chloro-substituted SubPc **29** and a 571 nm minimum with a shoulder at 550 nm and 458, 610 and 670 nm maxima for the *tert*-butyl-substituted SubPc **52**. They decay with lifetimes on the order of 7.7 ± 0.2 µs and 1.2 ± 0.1 µs and give place to the singlet ground state.

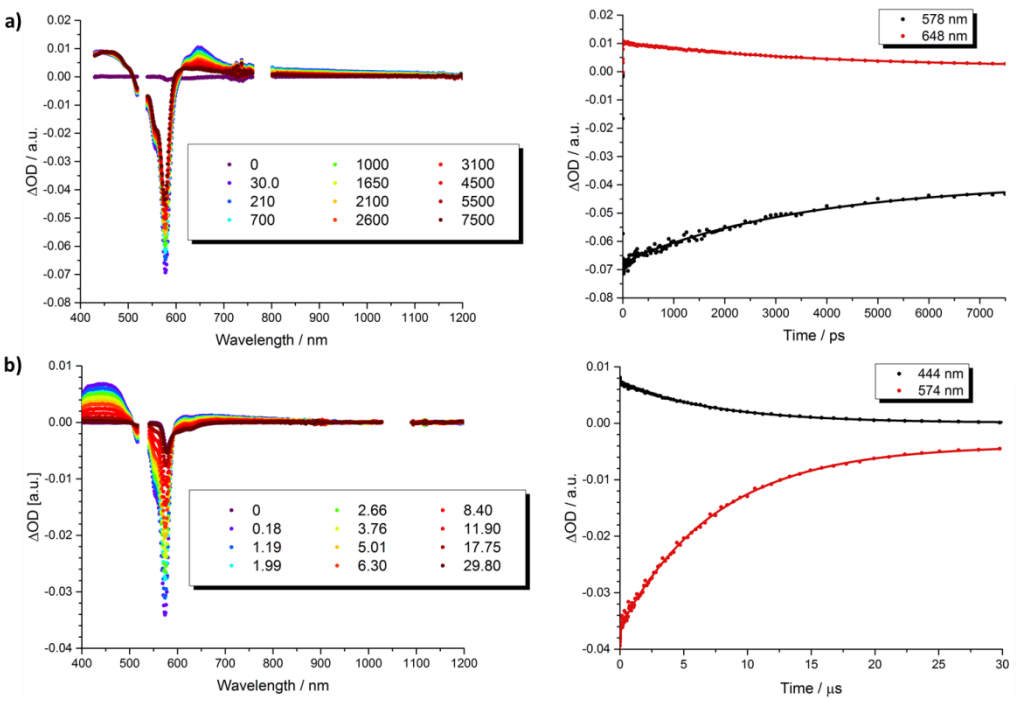

Figure 77. a) Differential absorption spectra (visible and near-infrared) obtained upon femtosecond pump probe experiments (530 nm) of SubPc **29** in toluene (left) with several time delays between 0 and 7500 ps at room temperature, and time absorption profiles of the spectra (right) at 578 (black spectrum) and 648 nm (red spectrum) monitoring the excited state dynamics. b) Differential absorption spectra (visible and near-infrared) obtained upon nanosecond pump probe experiments (530 nm) of SubPc **29** in toluene (left) with several time delays between 0 and 29.80 µs at room temperature, and time absorption profiles of the spectra (right) at 444 (black spectrum) and 574 nm (red spectrum) monitoring the excited state dynamics.

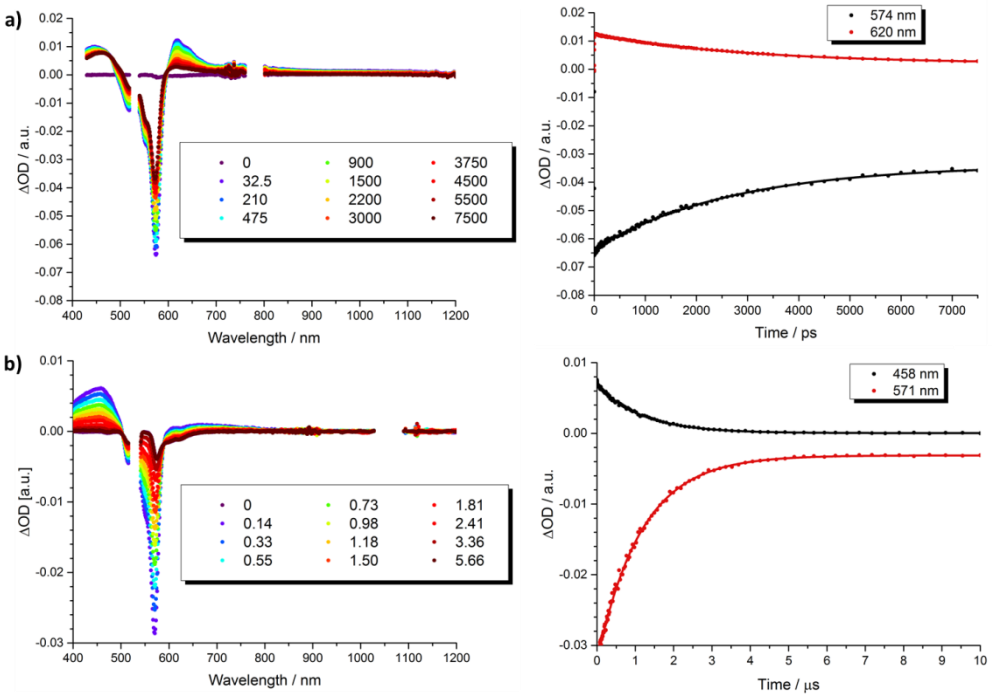

Figure 78. a) Differential absorption spectra (visible and near-infrared) obtained upon femtosecond pump probe experiments (530 nm) of SubPc **52** in toluene (left) with several time delays between 0 and 7500 ps at room temperature, and time absorption profiles of the spectra (right) at 574 (black spectrum) and 620 nm (red spectrum) monitoring the excited state dynamics. b) Differential absorption spectra (visible and near-infrared) obtained upon nanosecond pump probe experiments (530 nm) of SubPc **52** in toluene (left) with several time delays between 0 and 5.66 μs at room, and time absorption profiles of the spectra (right) at 458 (black spectrum) and 571 nm (red spectrum) monitoring the excited state dynamics.

The final set of experiments is concerned with the unsymmetrical SubPc dimer **39** in pump probe assays (Figure 79). In line with the absorption spectra, the ground-state bleaching in the singlet excited state (1.73 eV) is red shifted relative to those described above for chloro-substituted SubPc **29** (2.15 eV) and *tert*-butyl-substituted SubPc **52** (2.16 eV). In particular, minima develop immediately upon photoexcitation at 656 nm in toluene at 618, 684, and 716 nm, in THF at 611 and 710 nm, and in benzonitrile at 616 and 717 nm. Additionally, maxima are found at 468, 544, and 952 nm in toluene, 470, 541, and 948 nm in THF, and in benzonitrile at 470, 547, and 955 nm. The time evolution of these differential absorption spectra allowed to derive solvent-dependent intersystem crossing lifetimes for the delocalized singlet excited state with values that range from 2.28 ± 0.01 ns in cyclohexane to 1.69 ± 0.03 ns in

benzonitrile. These values are in close agreement with those determined in fluorescence lifetime measurements; 2.4 ns in cyclohexane and 1.7 ns in benzonitrile. Evidence for the shorter-lived polarized charge transfer state came in the form of ground-state bleaching at 710 nm and a 870 nm shoulder, but only in the polar solvents THF and benzonitrile. The lifetimes are 3.2 ± 0.3 ps in THF and 5.3 ± 0.5 ps in benzonitrile.

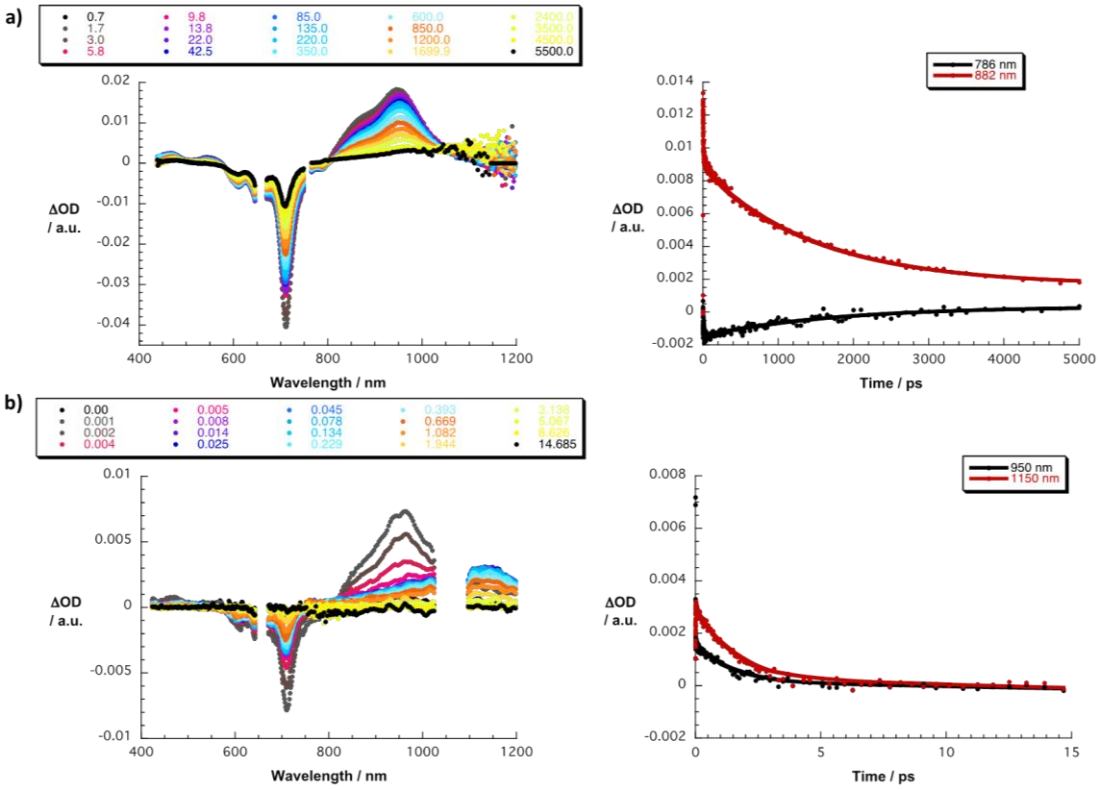

Figure 79. a) Differential absorption spectra (visible and near-infrared) obtained upon femtosecond pump probe experiments (656 nm) of SubPc dimer **39** in THF (left) with several time delays between 0.7 and 5500 ps at room temperature, and time absorption profiles of the spectra (right) at 786 (black spectrum) and 882 nm (red spectrum) monitoring the excited state dynamics. b) Differential absorption spectra (visible and near-infrared) obtained upon nanosecond pump probe experiments (656 nm) of SubPc dimer **39** in THF (left) with several time delays between 0 and 14.685 µs at room temperature, and time absorption profiles of the spectra (right) at 950 (black spectrum) and 1150 nm (red spectrum) monitoring the excited state dynamics.

In order to rationalize the experimental observations, computational modeling of the *syn* and *anti* topoisomers of dimer **39** and of a model unsymmetrical fused Pc dimer **39**, bearing *tert*-butyl and chlorine substituents on each Pc moiety, was carried out. A model unsymmetrical Pc dimer **53** was included in the study in order to quantify the effects of non-planarity on the SubPc dimers by comparison with a planar model compound. Optimized structures of these three compounds showed, as expected, strongly non-planar geometries for ***syn*-39** and ***anti*-39**, whereas **53** optimized to a planar structure. The calculated spectra of ***syn*-39** and ***anti*-39** turned out to be very similar, so that only that for the *anti* isomer will be discussed in the following. A simulation of the calculated UV-vis spectrum for ***anti*-39** displayed respectable agreement with the experiment, giving us confidence to reproduce the major features of the excited states of **39** and **53**.

A detailed analysis of the states involved in the excitations reveals that the S^1 to S^4 states have dipole moments that differ by less than 1.5 Debye from the ground state for both *syn* and *anti* topoisomers. A CT state is found in both isomers for S^5, which occurs close to 410 nm in both cases and gives an excited state with a dipole moment of 19.4 or 18.2 Debyes for *syn* and *anti*, respectively. The planar Pc dimer **53** shows similar behavior. S^1 to S^4 are π-π local excitations and S^5 (475 nm) is a CT state with a dipole moment of 36.5 Debyes. As the CT states are embedded energetically in a plethora of locally excited ones, strong solvent shifts of the CT state will not necessarily be evident in the experimental spectra. Figure 80 shows the calculated molecular electrostatic potentials on the 0.001 a.u. isodensity surface of the CT (S^5) states of ***anti*-39** and **53**. The color scale is the same in both cases, so that it is evident that CT is far more pronounced in the planar Pc dimer **53**. The oscillator strength calculated for the $S^0 \rightarrow S^5$ transition in **53** (0.27) is also slightly lower than those found for ***syn*-39** (0.31) and ***anti*-39** (0.36), which is consistent with lower charge-separation in the non-planar species **39**.

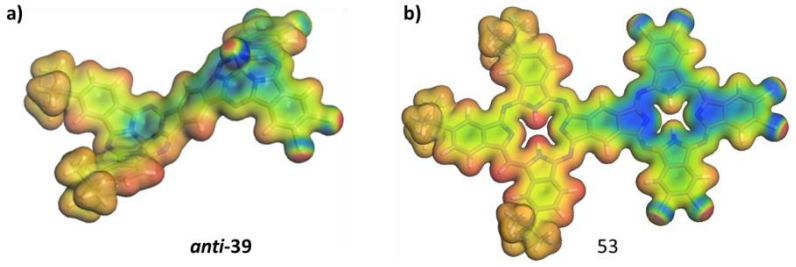

Figure 80. Molecular electrostatic potential calculated at the 0.001 a.u. isodensity surfaces of the S5 states of a) ***anti*-39** and b) **53**. The color scale ranges from -0.3 a.u. (blue) to 0.2 a.u (red).

The ground states of both isomers of **39** show a small amount of charge separation between the two unsymmetrical halves of the dimer. Figure 81 shows the calculated (DFT) HOMO and LUMO of ***anti*-39**. The slight polarization of the HOMO towards the donor monomer and of the LUMO towards the acceptor demonstrates nicely the effect of the donor and acceptor substituents. Self-consistent reaction field (SCRF) AM1-CIS calculations[271] in water suggest that the locally excite S^1 and a polar charge-shifted state close in energy are the first two excited states in solution.

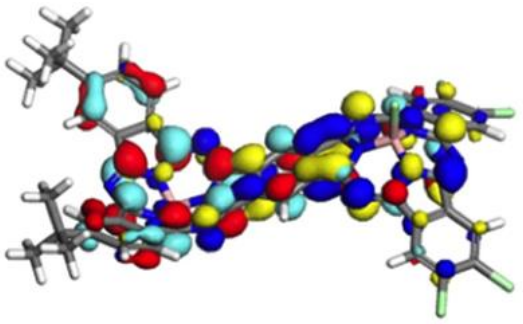

Figure 81. HOMO (red/cyan) and LUMO (blue/yellow) of ***anti*-39**.

[271] Rauhut, G.; Clark, T.; Steinke, T. *J. Am. Chem. Soc.* **1993**, *115*, 9174.

2.4 Subphthalocyanine based multicomponent systems for molecular recognition and artificial photosynthesis

2.4.1 Donor-acceptor systems for artificial photosynthesis

The direct light-to-electric energy conversion through solar cells as a possible solution to the increasing energy demand has been developed in the previous Chapter. On the other hand, the extraordinary performances observed in natural photosynthetic systems,[272] where luminous energy is efficiently transformed into chemical energy by cascades of energy and electron transfer occurring between well-arranged organic pigments, have boosted during the last several decades the construction of artificial photosynthetic systems that aim at mimicking the natural process for the conversion and storage of solar energy.[273]

In their most simple version, artificial photosystems are constituted by an electron donor unit (D) connected to an electron acceptor moiety (A) through a linker (L). This linker can connect both units either by covalent or supramolecular interactions. Photoexcitation of the donor or acceptor units can result in photoinduced electron or energy transfer. In the electron transfer process, upon photoexcitation, the electron travels from the donor to the acceptor, creating a charge separated pair involving a radical cation ($D^{\bullet+}$) and a radical anion ($A^{\bullet-}$). In the case of energy transfer, the energy of the excited state is transferred to the acceptor, leaving the donor molecule in the ground state and the acceptor molecule in the excited state. On the other hand, once a molecule is excited by the absorption of a photon, it can return to the ground state by many pathways, such as internal conversion, intersystem crossing, fluorescence, and phosphorescence. Therefore, the rates of the energy/electron transfer should be faster than those of the deactivation processes in order to achieve efficient energy or electron transfer.

In principle, for the construction of efficient artificial photoactive devices some major requirements should be met:

- High extinction coefficients in the visible range of the spectrum.

---

[272] a) Gingras, G. *The Photosynthetic Bacteria*; Clayton, R. K., Sistro, W. R., Eds.; Elsevier: Amsterdam, 1988. b) Pessarakli, M. *Handbook of Photosynthesis*, 2nd ed.; Taylor & Francis: Boca Raton, 2005. c) *Molecular Mechanisms of Photosynthesis*; Blankenship, R. E., Ed.; Blackwell Science: Malden, MA, 2002.

[273] a) *Photoinduced Electron Transfer*; Fox, M. A., Chanon, M., Eds.; Elsevier: Amsterdam, 1988. b) *Electron Transfer in Chemistry Vol. I-IV;* Balzani, V., Ed.; Wiley-VCH: Weinheim, 2001. c) Steiner, U. E. In *Photodynamic Therapy - From Theory to Application*; Abdel-Kader, M. H., Ed.; Springer-Verlag: Heidelberg, Germany, 2014.

- The charge separation processes quantum yield must be close to 1, so there are no losses of the excitation energy.
- The energetic level of the charge-separated state must be high and close to the energy level of the initial excited state, to minimize de energy loss.
- Recombination kinetics must be as slow as possible so the charge-separated state lifetime is as high as possible.

A basic description of the photoinduced charge transfer between donor and acceptor is shown in Figure 82.

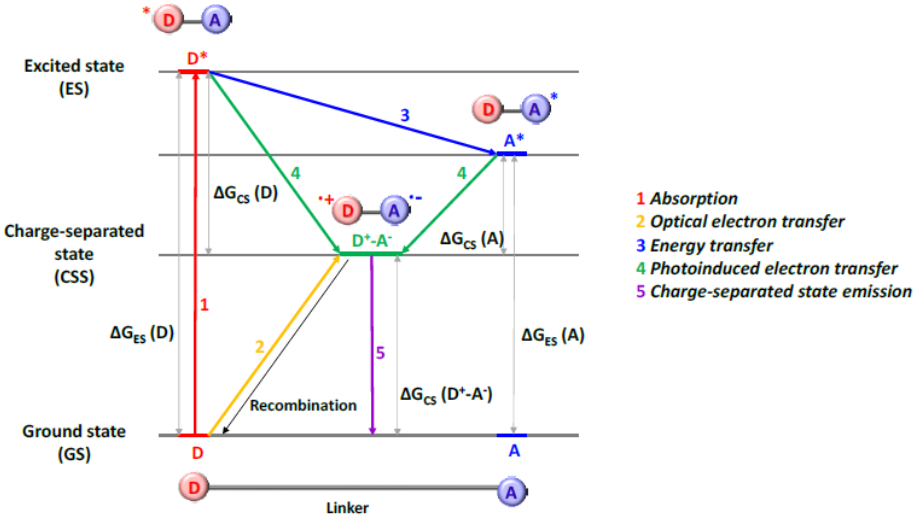

Figure 82. Representation of the photoinduced electron transfer between a donor and an acceptor connected through a linker.

Within this context, the appealing electrochemical and photophysical properties of SubPcs, together with their multiple options of functionalization at the peripheral or the axial positions, grant them ideal attributes for their integration as photoactive entities in D-A molecular models.

2.4.1.1 Subphthalocyanine-Fullerene ensembles as light harvesting systems

Among the myriad of electron accepting units employed in artificial photosystems, fullerenes and, to a lesser extent, carbon nanotubes, stand out, owing to their unique structural and redox features.

For this reason, assemblies of SubPcs, that can function as energy donors, energy acceptors, electron donors or electron acceptors in D-A systems,[35] covalently linked to C_{60} through SubPc axial or peripheral functionalization have been extensively explored, demonstrating that the SubPc-to-fullerene distance and the peripheral substitution of the SubPc units are the decisive factors that determine if either electron or energy transfer takes place.[72b,e,74,274,275]

However, natural photosynthetic reaction centers are based on highly organized supramolecular ensembles that allow obtaining long charge separation lifetimes. Thus, by making use of supramolecular interactions and molecular recognition, non-covalent D-A assemblies can be formed and studied for solar energy to electricity conversion applications.

In this regard, the aromatic concave faces of SubPcs form an excellent system for probing such interactions with complementary convex surfaces such as those of fullerenes. The utility of SubPcs as supramolecular fullerene receptors has been confirmed in the solid state. Kobayashi and co-workers have described the 2:1 complexes between fullerene and π-extended SubPc-based systems.[103b,105] The same co-crystallized structure in which the fullerene is embraced by two SubPcs has been more recently reported by Konarev *et al.*[276] with a dimeric SubPc and by Nemykin *et al.*[277] with a thiophenyl-substituted SubPc (Figure 83). Besides, several theoretical studies show a high degree of complementarity between SubPc and C_{60}.[278]

[274] KC, C. B.; Lim, G. N.; D'Souza, F. *Chem. Eur. J.* **2016**, *22*, 13301.
[275] Rudolf, M.; Trukhina, O.; Perles, J.; Feng, L.; Akasaka, T.; Torres, T.; Guldi, D. M. *Chem. Sci*. **2015**, *6*, 4141.
[276] Konarev, D. V.; Troyanov, S. I.; Lyubovskaya, R. N. *CrystEngComm* **2015**, *SubPc*, 3923.
[277] Rhoda, H. M.; Kayser, M. P.; Wang, Y.; Nazarenko, A. Y.; Belosludov, R. V.; Kiprof, P.; Blank, D. A.; Nemykin, V. N. *Inorg. Chem.* **2016**, *55*, 9549.
[278] a) Denis, P. A. *New J. Chem.* **2014**, *38*, 5608. b) Denis, P. A.; Yanney, M. *Chem. Phys. Lett.* **2015**, *640*, 140.

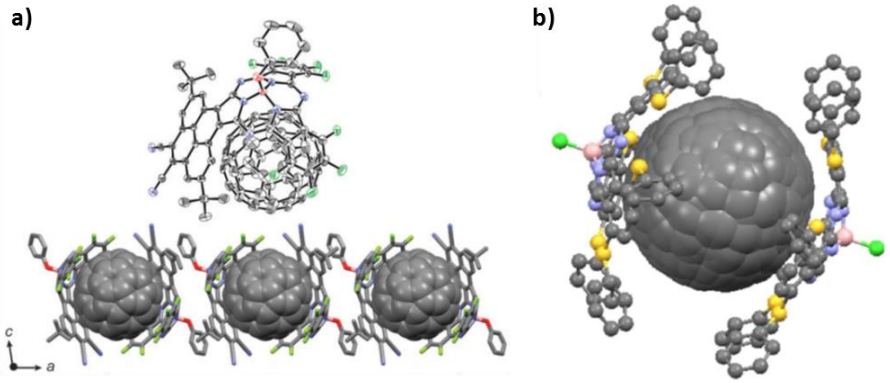

Figure 83. a) Crystal structure and packing diagram of a co-crystallate of a pyrene-fused SubPc with C_{60} as represented in ref. 103b. b) Crystal structure of the co-crystallate of a thiophenyl-substituted SubPc with C_{60} as represented in ref. 277.

In solution, first report of non-covalent interactions between fullerenes and SubPc systems came from the synthesis and study of SubPc homodimeric metallosupramolecular spherical cages capable to extract C_{60} into an acetone solution.[71b] A systematic study of the self-assembly, host-guest chemistry and photophysical properties of these systems with several fullerene derivatives revealed that SubPcs undergo a transduction of singlet excited-state energy to the fullerene inside the cavity upon photoexcitation.[88c] Formation of a 1:1 complex of an unsubstituted SubPc with C_{60} in solution has been also mentioned by Ziessel *et al*.[71c] even if no quantitative data were reported. In 2013, Torres and co-workers studied the 2:1 supramolecular complexes of hexaalkylthio-substituted SubPcs and C_{60} or C_{70} by UV-vis and fluorescence Job's plot and titration experiments, which yielded quantitative information on the stoichiometry, the strength and the kinetics of the assembly process in toluene solutions (Figure 84). Energy transfer, rather than electron transfer, was again assigned as the major deactivation pathway upon photoexcitation of the SubPc core.[279] Finally, very recently, non-covalent π–π interactions between different SubPc and SubNc derivatives with C_{60} and C_{70} fullerenes were studied by steady state and pump probe spectroscopy and DFT calculations, suggesting that only electron-rich SubPcs can facilitate an electron transfer to fullerenes and that van der Waals-type interaction energies tend to increase with an increase of the electron density at the SubPc core.[277]

[279] Sánchez-Molina, I.; Claessens, C. G.; Grimm, B.; Guldi, D. M.; Torres, T. *Chem. Sci.* **2013**, *4*, 1338.

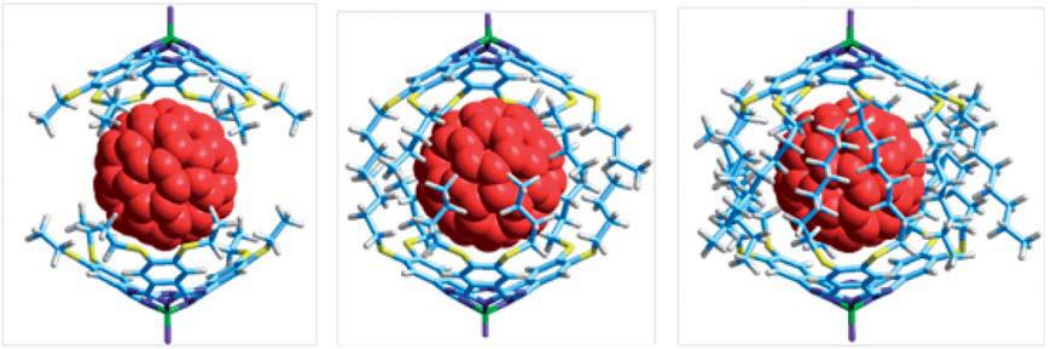

Figure 84. Molecular modelling of the 2:1 adducts of different hexaalkylthio-substituted SubPcs and C_{60} as represented in ref. 279.

2.4.2 Approach to the employment of SubPc fused dimer based systems as active units in molecular recognition and artificial photosynthetic systems

It has been then demonstrated that SubPcs, with their bowl-shaped structure, present not only the adequate shape complementarity to fullerenes, but also remarkable properties, such as intense absorption in the visible region, with high extinction coefficients, high electronic excitation energies, and intense fluorescence emissions with low reorganization energies, that turn them into compelling units for supramolecular photoactive systems.

On the other hand, the unique topologies of SubPc fused dimers, both *syn* and *anti* isomers, give rise to novel curved extended structures that might be also explored in molecular recognition to design D-A assemblies. Besides, the binuclear character of SubPc dimers provides them with two functionalizable axial positions. In this context, an example of perfluorinated SubPc *syn* dimer doubly connected through its axial positions to a fullerene molecule was described by Claessens *et al.*[267] This double connection through the convex face of the macrocycle forced the docking of the C_{60} unit in a relatively fixed position, suitable for through-space interaction between the donor SubPc dimer and the acceptor C_{60}.

Hence, attracted by the possibilities that these systems provide, our interest focused on the synthesis and study of SubPc fused dimers axially substituted with complexing molecular units specifically designed as photoactive supramolecular receptors for carbon nanostructures. Especially attractive for us was the idea of building rigid structures with three-dimensional conformations that would give rise to well-defined receptor sites for molecular recognition.

For this purpose, the introduction of alkynyl substituents directly linked to the boron atom of the SubPc first reported by Ziessel *et al.*[65] emerged as a useful synthetic tool. This linking

strategy, unlike the bent ether bond in the phenoxy SubPcs that reduces the symmetry and increases the flexibility of the molecular structure, would feature a linear carbon-carbon triple bond that would lead to more symmetrical and rigid receptor molecules. However, the attachment of an acetylide to the boron was performed *via* Grignard reactions, which preclude the use of base sensitive or electrophilic substrates.

Interestingly, very recently, a mild and versatile procedure described by Nielsen *et al.*[69b] for the functionalization of boron chloride SubPcs at the axial boron position with trimethylsilyl-protected alkyne nucleophiles appeared. This method allowed, inspired by previous works of Bender and Torres,[68,69a] the $AlCl_3$ assisted introduction of a large variety of R substituents on the alkyne units, including electron donating/withdrawing aryl groups, silyl-protected alkynyl groups, as well as ferrocenyl and azulenyl groups (Scheme 25).

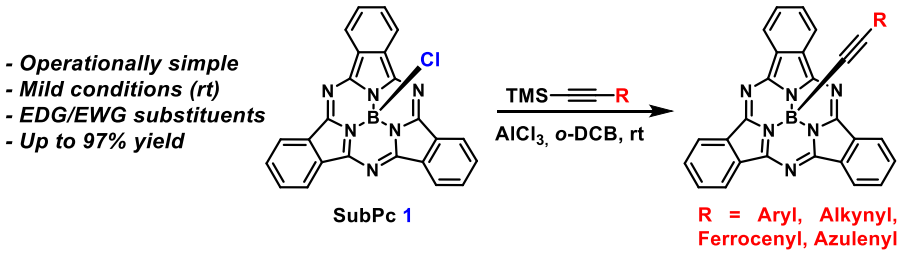

Scheme 25. Aluminum chloride mediated alkynylation of SubPcs using trimethylsilyl-capped acetylenes reported by Nielsen et al.[69b]

In the next section, several examples on the use of this novel synthetic strategy for the preparation of SubPc fused dimer based ensembles for the recognition of complementary carbon nanostructures and the creation of supramolecular D-A systems will be presented.

2.4.3 Functionalization of carbon nanotubes

Single wall carbon nanotubes (SWCNTs) are considered key materials in nanotechnology as a result of their nanometer-scale size and their extraordinary chemical, mechanical, thermal, and electronic properties.[280] However, their tendency to aggregate in bundles hinders their solubility in organic solvents and diminishes the special mechanical and electrical properties of the individual tubes.

With the aim of increasing their solubility and achieving stable dispersions, a number of covalent[281] and non-covalent[282] strategies have been developed in recent years for the functionalization of carbon nanotubes. While the covalent approach leads to more thermodynamically stable structures, the non-covalent functionalization presents the advantage that the electronic structure of the nanotube remains almost unaffected. Some functionalization possibilities for SWCNTs are shown in Figure 85: covalent functionalization by attaching functional groups to the nanotube ends or defect sites (A), covalent functionalization through sidewall functionalization (B), non-covalent functionalization with surfactants (C), non-covalent functionalization, for example, wrapping nanotubes by polymers (D), functionalization from inside (endohedral) by filling nanotubes with different nanoparticles (E).

[280] a) Reich, S.; Thomsen, C.; Maultzsch, J. *Carbon Nanotubes: Basic Concepts and Physical Properties*; Wiley-VCH: Weinheim, Germany, 2004. b) Fukuzumi, S.; Kojima, T. *J. Mater. Chem*. **2008**, *18*, 1427. c) *Carbon Nanotubes and Related Structures*; Guldi, D. M., Martin, N., Eds.; Wiley-VCH: Weinheim, Germany, 2010.
[281] Hirsch, A. *Angew. Chem. Int. Ed.* **2002**, *41*, 1853.
[282] a) Schuster, D. I.; Megiatto, J. D. *Nat. Chem.* **2009**, *1*, 182. b) Bottari, G.; Suanzes, J. A.; Trukhina, O.; Torres, T. *J. Phys. Chem. Lett.* **2011**, *2*, 905. c) Romero-Nieto, C.; Garcia, R.; Herranz, M. A.; Ehli, C.; Ruppert, M.; Hirsch, A.; Guldi, D. M.; Martin, N. *J. Am. Chem. Soc.* **2012**, *134*, 9183.

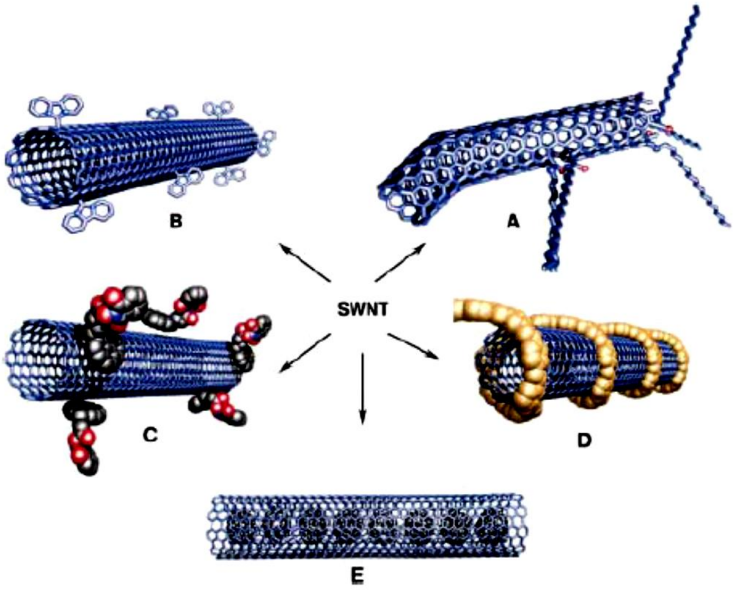

Figure 85. Schematic representation of the most common functionalization patterns of SWCNTs.

On the other hand, the combination of SWCNTs with electron donating[283] or electron accepting[284] photoactive units affords conjugates and/or hybrids that, upon photoexcitation, give rise to intramolecular energy and electron transfer events. Up to date, a variety of supramolecular assemblies based on Pcs or Ps and SWCNTs have been reported either by direct immobilization of the macrocycles cores onto the SWCNT sidewalls or by means of pyrene/SWCNT supramolecular interaction, taking advantage of the strong π-π interactions of pyrene to the SWCNT sidewalls.[285]

[283] a) D'Souza, F.; Ito, O. *Chem. Soc. Rev.* **2012**, *41*, 86. b) D'Souza, F.; Sandanayaka, A. S. D.; Ito, O. *J. Phys. Chem. Lett.* **2010**, *1*, 2586. c) Dirian, K.; Herranz, M. A.; Katsukins, G.; Malig, J.; Rodriguez-Perez, L.; Romero-Nieto, C.; Strauss, V.; Martin, N.; Guldi, D. M. *Chem. Sci.* **2013**, *4*, 4335. d) Bottari, G.; de la Torre, G.; Torres, T. *Acc. Chem. Res*. **2015**, *48*, 900.

[284] a) D'Souza, F.; Chitta, R.; Sandanayaka, A. S. D.; Subbaiyan, N. K.; D'Souza, L.; Araki, Y.; Ito, O. *J. Am. Chem. Soc.* **2007**, *129*, 15865. b) Hahn, U.; Engmann, S.; Oelsner, C.; Ehli, C.; Guldi, D. M.; Torres, T. *J. Am. Chem. Soc.* **2010**, *132*, 6392. c) Anaya-Plaza, E.; Oliva, M. M.; Kunzmann, A.; Romero-Nieto, C.; Costa, R. D.; de la Escosura, A.; Guldi, D. M.; Torres, T. *Adv. Funct. Mater.* **2015**, *25*, 7418.

[285] a) Chen, R. J.; Zhang, Y.; Wang, D.; Dai, H. *J. Am. Chem. Soc.* **2001**, *123*, 3838. b) Maligaspe, E.; Sandanayaka, A. S. D.; Hasobe, T.; Ito, O.; D'Souza, F. *J. Am. Chem. Soc.* **2010**, *132*, 8158. c) Bartelmess, J.; Ballesteros, B.; de la Torre, G.; Kiessling, D.; Campidelli, S.; Prato, M.; Torres, T.; Guldi, D. M. *J. Am. Chem. Soc.* **2010**, *132*, 16202. d) Ince, M.; Bartelmess, J.; Kiessling, D.; Dirian, K.; Martínez-Díaz, M. V.; Torres, T.; Guldi, D. M. *Chem. Sci.* **2012**, 3, 1472.

Taking the aforementioned into account, with the aim at increasing the solubility of SWCNTs *via* non-covalent pyrene-based interactions and combining them with a strong electron accepting photoactive system to obtain an electron donor SWCNT-based photosynthetic reaction center, the synthesis of *syn* and *anti* perfluorinated SubPc fused dimers **54** functionalized with pyrene units in its axial positions was envisioned (Scheme 26). Thus, the aluminum chloride mediated reaction of previously synthesized TMS-ethynylpyrene derivative **55** with a 1:1 *syn*/*anti* mixture of SubPc fused dimer **2** rendered dimers ***anti*-54** and ***syn*-54** separately in a 68% overall yield. Assignment of the *syn* and *anti* topoisomers of compound **54** could be confirmed by carrying out the same reaction from ***syn*-2** and ***anti*-2** individually.

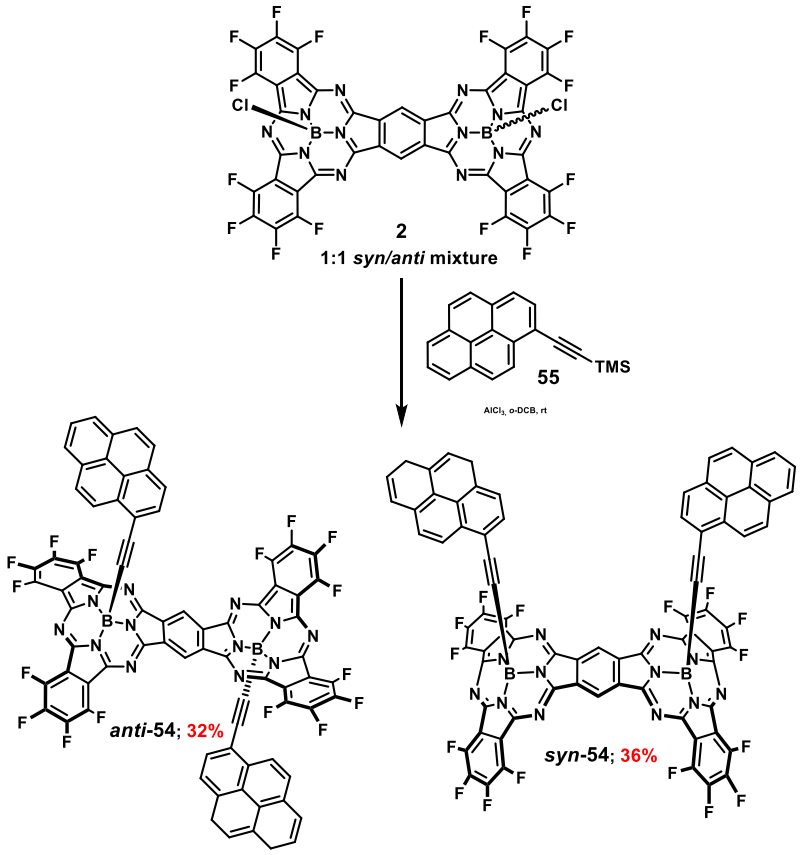

Scheme 26. Synthesis of dimers ***anti*-54** and ***syn*-54**.

Interestingly, the rigid and short alkynyl spacers endow dimer ***syn*-54** with an appealing restrained tweezer-like structure. Structural modeling and geometry optimization of this derivative at DFT level allowed us to estimate a distance between the two pyrene units of 1.68

nm when they are arranged facing one each other. This distance would presumably enable the accommodation of SWCNTs, with an average diameter of 0.7-1.4 nm, in the space defined by the pyrene units, ensuring a close supramolecular contact between SWCNT and perfluorinated SubPc fused dimer (Figure 86). On the other hand, the calculated distance between one boron atom and the center of the pyrene unit linked to the other boron atom in dimer ***anti*-54** was estimated as 1.40 nm.

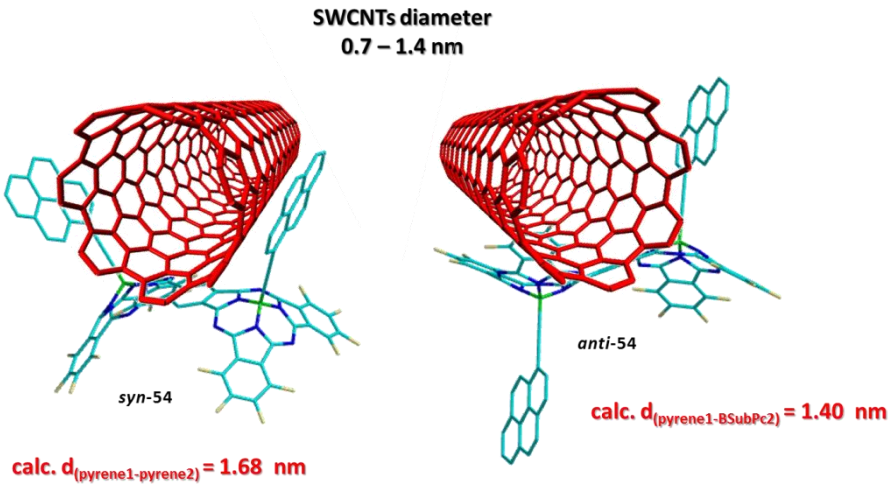

Figure 86. Models and calculated selected distances of dimer ***syn*-54** and ***anti*-54** for their non-covalent immobilization onto SWCNTs.

Immobilization assays onto SWCNTs and photophysical studies of dimers ***syn*-54** and ***anti*-54** will be carried out in the laboratory of Prof. Dirk Guldi at the Friederich-Alexander University in Erlangen, Germany, in the near future.

2.4.4 Approach to the synthesis of axially connected SubPc-SubPc fused dimer hybrids

Despite many examples of SubPc-containing dyads and triads can be found in the literature, the study of the interchromophoric interactions, both in the ground and excited state, of multi-SubPc systems is still limited to a couple of examples described by Shibata *et al.*[54g,h] of SubPc hetero-dimers and trimers axially connected via phenoxy linkers.

Thus, owing to the particular electronic properties of both SubPc and SubPc fused dimers, we considered to merge both units in ensembles suited for the study of intramolecular energy/electron transfer processes. Besides, since the absorption of each chromophore complements that of the other, a SubPc-SubPc dimer dyad would cover a very wide section of the UV-Vis spectrum. Finally, these multi-SubPc systems would present a variety of curved topologies in their structure useful for the recognition of complementary fullerene derivatives.

To this end, the synthesis of SubPc-SubPc fused dimer hybrids through an axial-axial substitution pattern (Figure 87) was first designed by consecutive aluminum chloride mediated reactions of a TMS-ethynyl derivative. Due to the aforementioned limitation in the number of symmetrical SubPcs fused dimers that can be synthesized in reasonable yields, perfluorinated SubPc dimer ***syn*-2** and ***anti*-2** was employed as platform in this study. For this reason, electronically complementary SubPc units, bearing no substituents or electron donating thioethers substituents, were chosen as axial substituents. Finally, different rigid spacers, namely a short ethynyl linker and two bis(ethynyl)-phenyl linkers, were tested.

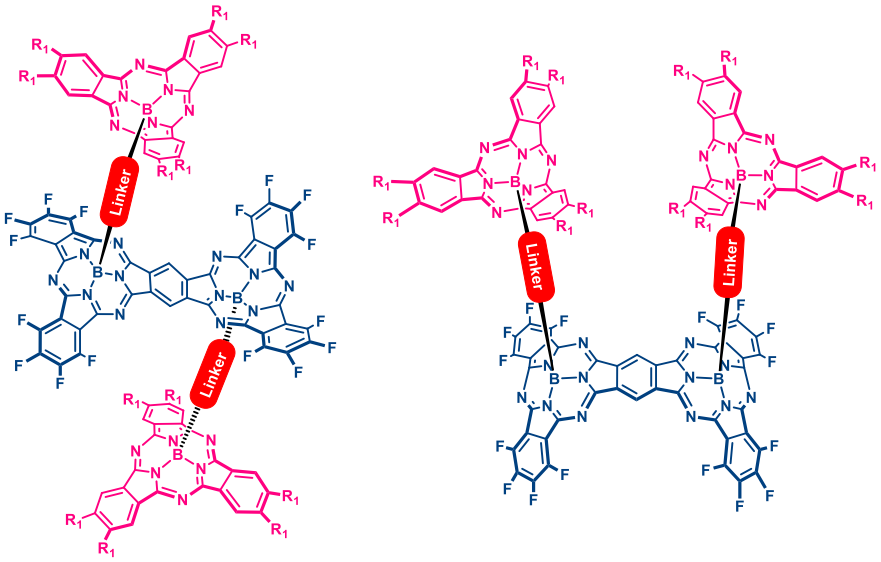

Figure 87. Proposed structure of the axial-to-axial SubPc-SubPc dimer hybrids obtained from both ***syn*-2** and ***anti*-2** dimer topoisomers.

The synthesis of ethynyl-boron functionalized dimers **56-58** was carried out by reacting a 1:1 *syn/anti* mixture of dimer **2** with of $AlCl_3$ and the corresponding previously synthesized TMS-protected alkynes **59-61** in o-dichlorobenzene at room temperature (Scheme 27). In all cases, topoisomers ***anti*-56-58** and ***syn*-56-58b** could be isolated and individually characterized. In a similar manner, axial alkynylation of SubPcs **1** and **62** with TMS-protected alkynes **59-61** led to the formation of SubPcs **63-68** in high yields (Scheme 28).

It must be noted that, in contrast to the observations of Nielsen *et al.*,[69b] that report the need for a large excess of the alkyne (8-10 equiv) and $AlCl_3$ (6 equiv) to lead reaction to completion in 2-18 h, dimers **56-58** and SubPcs **62-67** could be obtained in good yields after 30 min reaction time at 25 °C using a significantly lower excess of both reagents (2.5 equiv of alkyne and 1.5 equiv of $AlCl_3$ for SubPcs **62-67**; 5.0 equiv of alkyne and 2.5 equiv of $AlCl_3$ for the double substitution reaction of dimers **56-58**), probably due to the strict dry conditions employed during our syntheses.

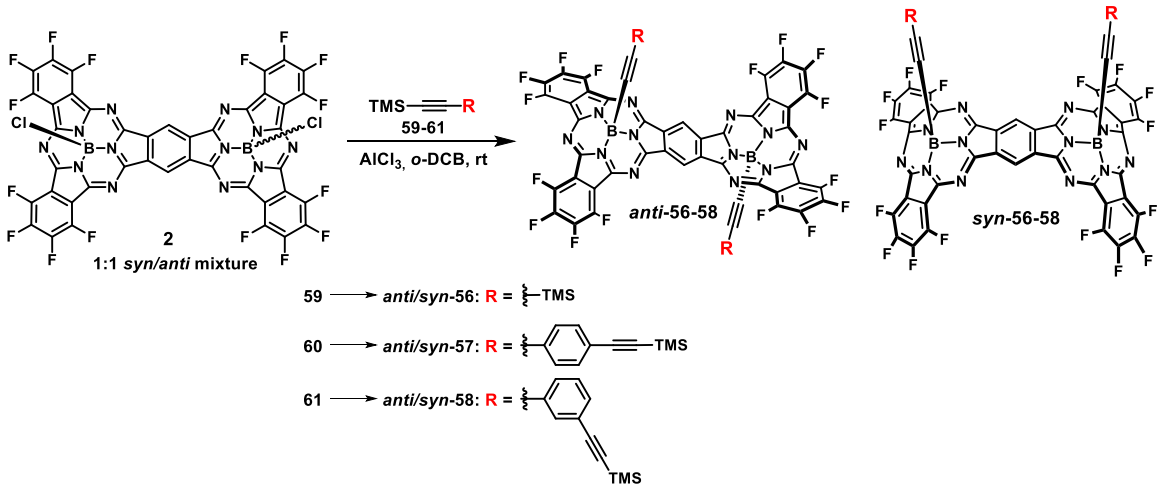

Scheme 27. Synthesis of SubPc dimers ***anti*-56-58** and ***syn*-56-58**.

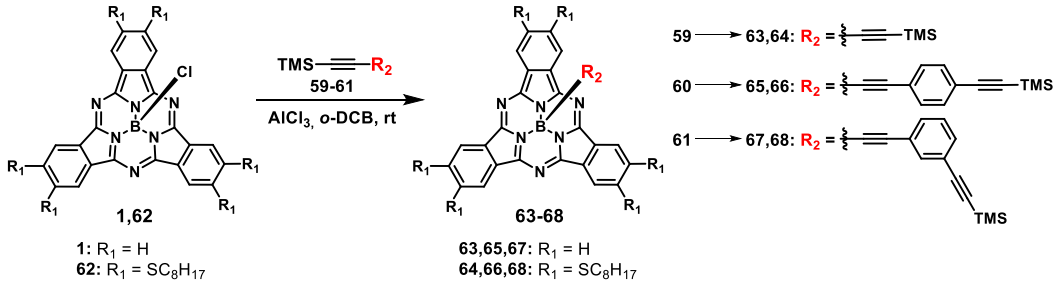

Scheme 28. Synthesis of SubPcs **63-68**.

Next step was the preparation of SubPc-SubPc fused dimer hybrids ***syn*-69-71** and ***anti*-69-71** starting either from dimers **56-58** or from SubPcs **63-68** (Scheme 29). These syntheses imply a new aluminum chloride mediated reaction of a TMS-ethynyl derivative with a chloro-boron SubPc derivative where, in this specific case, the TMS-protected alkyne nucleophiles are directly linked or indirectly linked through a π-conjugated spacer to the central boron atom of another SubPc derivative.

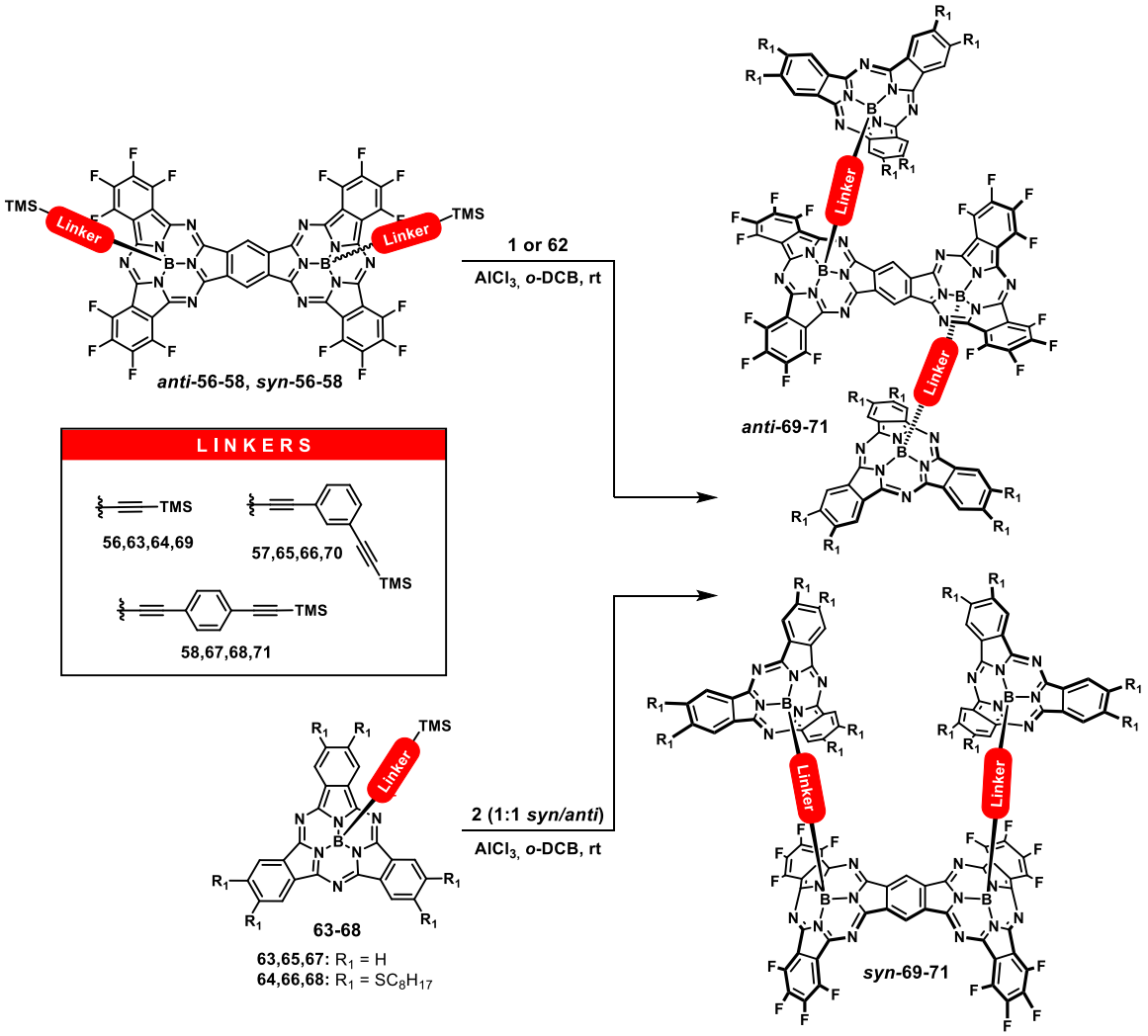

Scheme 29. Proposed synthetic routes for the preparation of SubPc-SubPc dimer hybrids ***anti*-69-71** and ***syn*-69-71**.

Initially, the synthesis of hybrids ***anti*-69** and ***syn*-69** was attempted either by reaction of dimer ***anti*-56** or ***syn*-56** with SubPcs **63-64** or by reaction of SubPcs **1** or **62** with a 1:1 *syn/anti* mixture of dimer **2**. However, and despite the good results obtained in the synthesis of the precursors, TMS-protected alkyne nucleophiles ***anti/syn*-56**, **63** and **64** displayed a total lack of reactivity. Forcing reaction conditions, like rising reaction temperature to 80 °C for 48 h, or using a large excess of reagents (up to 12 equiv of $AlCl_3$ and 20 equiv of TMS-ethynyl derivative), yielded starting materials unaltered. Even harsher conditions only led to gradual

decomposition of the starting SubPc derivatives. These results denote that these new SubPcs do not present the previously seen reactivity related with these TMS-alkyne nucleophiles, probably as a consequence of the electronic and/or steric effect exerted by the boron macrocycle.

Subsequently, aiming at reducing the steric hindrance of the SubPc core around the alkyne unit, reactions of *p*-(TMS-ethynyl)phenylethynyl-boron substituted SubPc dimers ***anti*-57** and ***syn*-57** with SubPcs **1** or **62** or SubPcs **65-66** with 1:1 *syn/anti* mixture of dimer **2** were tackled. Unfortunately, none of these reactions worked as desired, recovering starting materials after several hours or obtaining again decomposition products when modifying the reaction conditions. Nevertheless, we did observe that, upon employing an excess of $AlCl_3$ with respect to the corresponding TMS-ethynyl substituted SubPc derivatives, deprotection of the alkyne group took place to render the deprotected SubPc analogues. The formation of these products was undetected in the previous syntheses of hybrids ***anti/syn*-69**. In this case, the TMS-protected alkyne unit is located considerably far from the SubPc macrocycle to ascribe this lack of reactivity to steric effects only. Thus, it could only be conjectured that the unique nature of the highly electron deficient central boron atom of SubPc derivatives induce a critical decrease of the nucleophilic character of the TMS-ethynyl unit through the fully π-conjugated 1,4-diethynylphenyl linker.

For this reason, *m*-(TMS-ethynyl)phenylethynyl-boron substituted SubPcs **67-68** and SubPc dimers ***anti/syn*-58** were then tested as nucleophiles in the $AlCl_3$ mediated axial substitution of dimer **2** or SubPcs **1** and **62**, respectively. Unlike previous attempts, reaction of SubPc dimers ***anti*-58** or ***syn*-58** with 5 equiv of SubPc **1** in the presence of 8 equiv of $AlCl_3$ gave rise to a complex reaction mixture, mainly constituted by unreacted SubPc **1**, deprotected *m*-ethynylphenylethynyl-boron SubPc dimer and two new dark purple compounds. In both cases, either starting from the ***syn*-** or the ***anti*-58** topoisomer, these two derivatives could be isolated and identified as the product of the reaction of only one of the axial *m*-(TMS-ethynyl)phenylethynyl substituents of dimers ***anti/syn*-58** with one SubPc **1** unit and as the desired derivative ***anti/syn*-71**, consisting on *syn* or *anti* perfluorinated SubPc dimers **2** axially linked to two SubPc **1** units through 1,3-diethynylphenyl spacers. Nevertheless, compounds ***anti*-71** and ***syn*-71** could only be obtained in very low yields, namely 15% and 5% starting from 0.015 mmol of precursors ***anti/syn*-58** respectively, as the reaction could not be led to completion even with a large excess of SubPc **1**. On the other hand, the reaction of SubPc **67** with a 1:1 *syn/anti* dimer **2** rendered the same mono- and di-substituted products, but the isolation turned out to be more difficult due to the simultaneous presence of *syn* and *anti* derivatives in the reaction mixture.

Although the yields obtained for hybrids ***anti*-7 1** and ***syn*-7 1** were not very satisfactory, the observations made during the whole set of experiments suggest a dramatic influence of both the steric hindrance in the transition state and the aforementioned decrease of nucleophilicity of the TMS-alkynes linked to the SubPc boron atom in the lack of reactivity that TMS-protected alkyne groups at the axial position of SubPc derivatives display.

2.4.5 Design, synthesis and study of a SubPc-SubPc fused dimer hybrid for supramolecular complexation of fullerenes

Based on the use of the ethynyl linker as a rigid and short spacer for the synthesis of multi-SubPc systems, another SubPc-SubPc fused dimer hybrid that differs in the substitution pattern of the SubPc unit with respect to the ensembles of previous section was designed.

In this case, the SubPc periphery-to-SubPc dimer axial connection was chosen to originate conformationally fixed structures featuring well-defined cavities potentially useful for fullerenes complexation. Thus, in both *syn* and *anti* SubPc dimer topoisomers, the disposition that the two axial SubPc units would acquire in these assemblies, facing one each other in *syn* or facing each the concave side of the other SubPc dimer part in *anti*, would give rise to unique supramolecular recognition sites (Figure 88). Trying to enhance the complexation behavior of these molecules, the SubPc units employed were endowed with thiooctyl groups.[279]

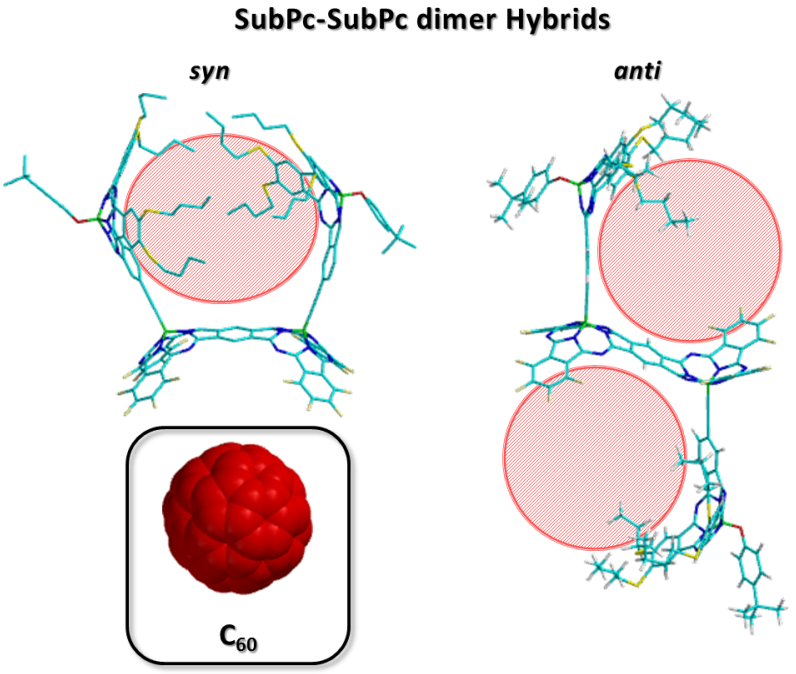

Figure 88. PM3 optimized structures of the proposed *syn* and *anti* SubPc-SubPc dimer hybrids, showing the three-dimensional cavities created by the substitution pattern. A model of C_{60} fullerene is also included for the sake of size comparison. In SubPc units, thiooctyl groups have been substituted by thiobutyl groups to speed up calculations.

2.4.5.1 Synthesis of SubPc-SubPc fused dimer hybrids *syn*-72 and *anti*-72

The synthesis of perfluorinated SubPc fused dimers ***anti/syn*-72** axially functionalized with octylthio-substituted SubPcs through the periphery was initially envisioned through the $AlCl_3$ mediated axial substitution of dimer **2** with unsymmetrical TMS-ethynyl-substituted SubPc derivative **73** (Scheme 30, Route A).

Precursor unsymmetrical monoiodo-SubPc **74** was obtained in 22% yield by statistical condensation of the 4,5-dioctylthiophthalonitrile and 4-iodophthalonitrile using BCl_3,[51g] followed by axial substitution by 4-*tert*-butylphenol. Palladium catalyzed crossed-coupling reaction of **74** with ethynyltrimethylsilane rendered SubPc **73** in 63%. Unfortunately, attempts to prepare compounds ***anti*-72** and ***syn*-72** by reaction of TMS-ethynyl-SubPc **73** with a 1:1 *syn/anti* mixture of dimer **2** in the presence of $AlCl_3$ were not successful, probably due to a lack of reactivity of SubPc **73**, observing only the formation of the corresponding TMS-deprotected derivative.

Thus, a second synthetic route (Scheme 30, Route B), consisting on the preparation of bis(ethynyl)boron-functionalized dimer **75** and subsequent double Sonogashira coupling reaction with unsymmetrical octylthio-substituted SubPc **74** was tackled. Axial substitution reaction of a 1:1 *syn/anti* mixture of dimer **2** with 5 equiv of ethynyltrimethylsilane and 4 equiv of $AlCl_3$ yielded dimer **75** as a 1:1 *syn/anti* mixture in 60% yield. This time, the small size of the ethynyl axial substituents precluded the separation of both topoisomers by chromatographic work up on silica gel. However, each topoisomer of compound **75** could be individually synthesized and characterized by starting from isomerically pure dimer **2**, ***syn*-75** and ***anti*-75** exhibiting identical ^{1}H-NMR and UV-vis features.

Finally, Pd-catalyzed crossed-coupling reaction of dimer **75** with SubPc **74** led to the formation of compounds ***syn*-72** and ***anti*-72**, as spotted by TLC. After tedious purification by column chromatography on silica gel and size exclusion chromatography, dark purple dimers ***syn*-72** and ***anti*-72** were obtained in 15% and 7% yields, respectively.

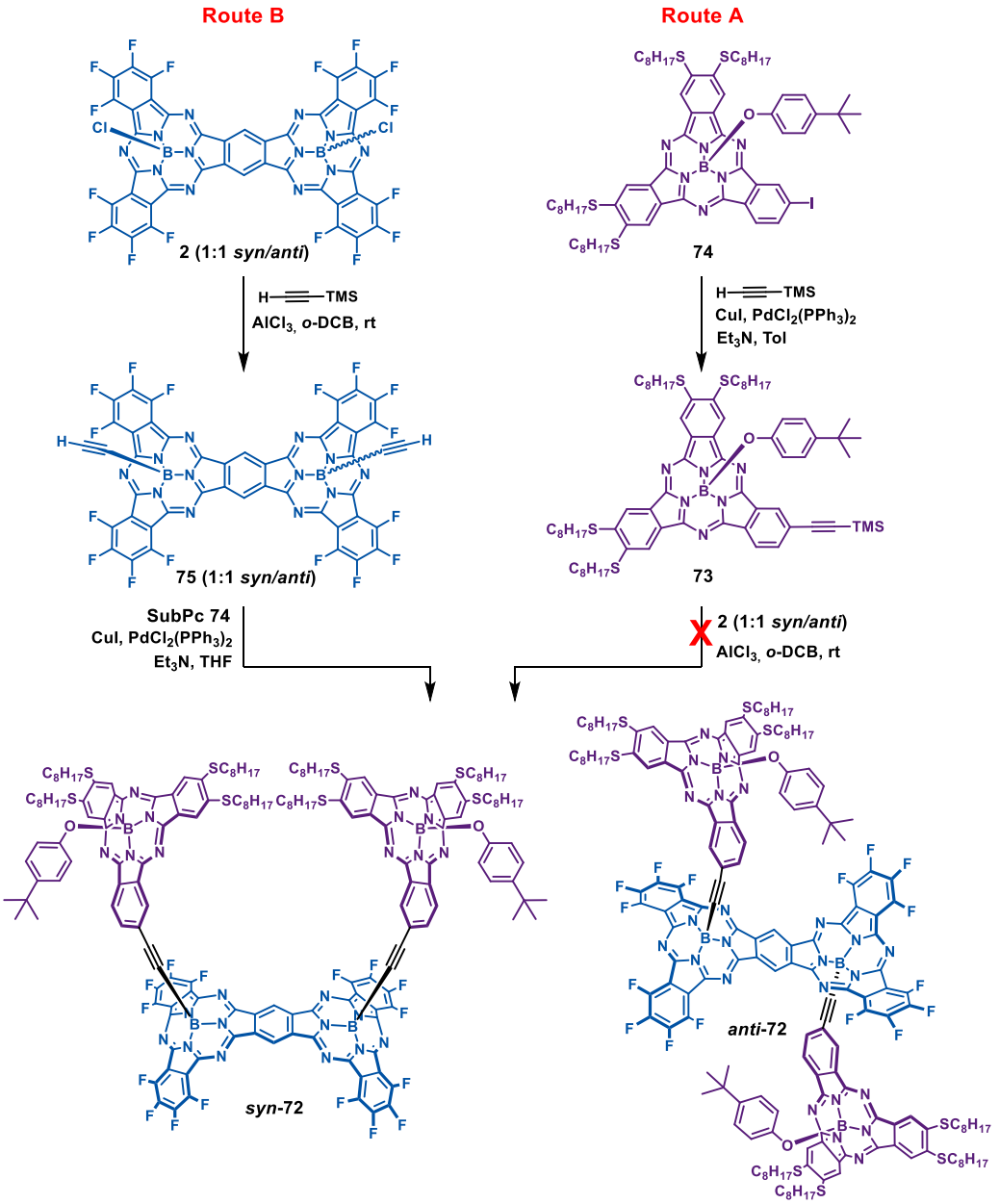

Scheme 30. Proposed synthetic routes for the preparation of SubPc-SubPc dimer hybrids ***anti*-72** and ***syn*-72**.

^{1}H-NMR spectra of both compounds in $CDCl_3$ agreed with the proposed structure of these compounds (Figure 89). Both spectra exhibit several diagnostic singlets at high chemical shifts, around 10.50-10.45 ppm in ***syn*-72** and 10.27-10.20 ppm in ***anti*-72**, corresponding to the protons of the central benzene ring of the dimer unit. The appearance of more than one singlet for each topoisomer might be a consequence of the presence of more than one regioisomer depending on the position through which each SubPc unit binds to each boron atom of the SubPc dimer fragment, relative to the other SubPc moiety. Besides, signals corresponding to the octylthio-substituted SubPc fragments are significantly upfield shifted in both ***syn*-72** and ***anti*-72** with respect to unsymmetrical SubPc **73**, due to the influence of the anisotropic ring current of the aromatic system of the SubPc dimer. In particular, protons in the ethynyl-substituted benzene ring of SubPcs appear notably shielded, from 8.94, 8.73 and 7.93 ppm in **73** to 8.22-8.16, 8.37-8.30 and 7.17-7.08 ppm in ***anti/syn*-72**.

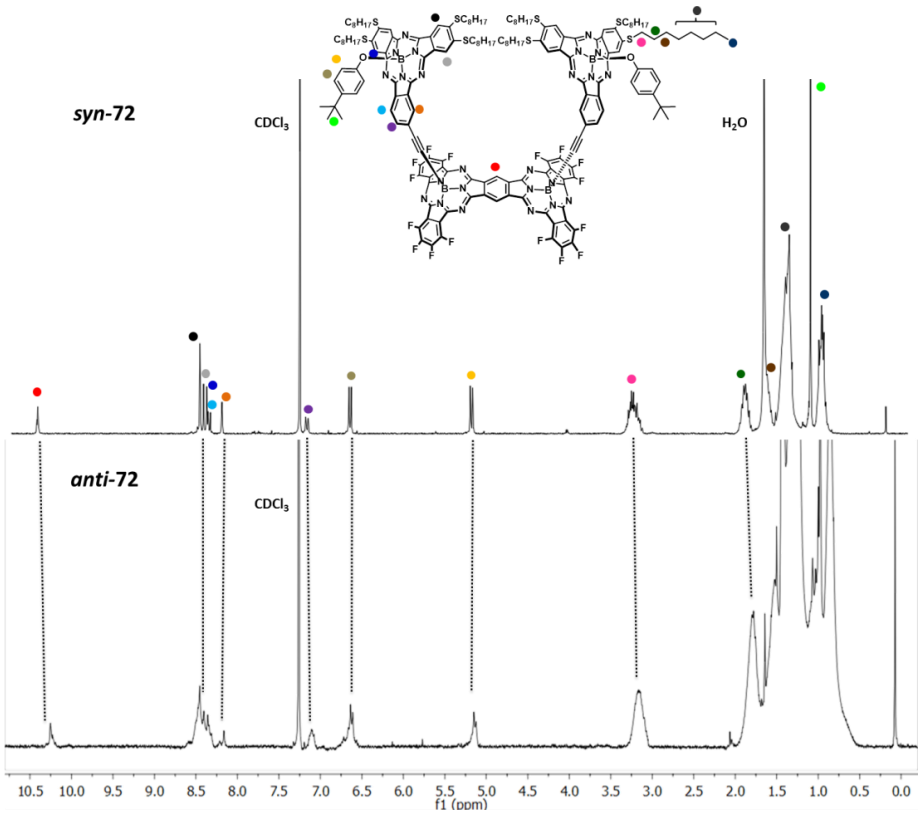

Figure 89. ^{1}H-NMR (300 MHz) spectra in $CDCl_3$ of compounds ***syn*-72** (top) and compounds ***anti*-72** (down).

UV-vis absorption spectra of SubPc-SubPc dimer hybrids ***syn*-72** and ***anti*-72** in chloroform are basically defined as the sum of the spectra of their macrocyclic components (Figure 90). Both compounds feature the characteristic *Q* band maximum of the perfluorinated SubPc dimer unit at 696 nm, with a number of less intense shoulders in its blue region, followed by *Q* band of octylthio-substituted SubPc units peaking at 596 nm. The high intensity of this band, approximately doubling that of SubPc **74**, supports the presence of two units of SubPc per unit of SubPc dimer **2** in the final structure of ***anti/syn*-72**.

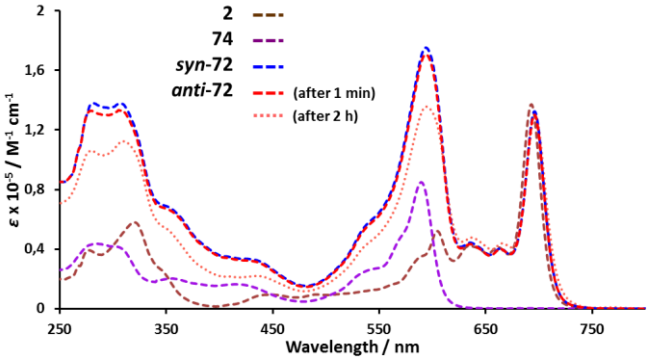

Figure 90. UV-vis absorption spectra in chloroform of: SubPc dimer **2**, SubPc **74**, compound ***syn*-72**, and compound ***anti*-72** after 1 minute and after 2 hours in solution.

It must be noted that, during the characterization of ***syn*-72** and ***anti*-72**, one of the topoisomers, namely ***anti*-72**, showed gradual decomposition in solution. Thus, it could be spotted by TLC that a pure fraction of ***anti*-72** gave rise to a number of new colored compounds after 2 hours in solution. After repurification of the main product of this mixture, UV-vis spectra of this fraction displayed a less intense SubPc units *Q* band, suggesting the presence of mono- and di-substituted SubPc dimers (Figure 90). This fact was supported by MS spectra, where mainly the presence of a monosubstituted dimer fragment and an unsymmetrical SubPc unit with an ethynyl peripheral substituent that must come from the cleavage of the C_{SubPc}-B_{Dimer} bond were spotted, even under soft ionization techniques. Topoisomer ***syn*-72** did not show these stability issues in solution.

Although ^{1}H-NMR, UV-vis and HR-MS spectra of compounds ***anti/syn*-72** unambiguously confirmed their characterization as *syn* and *anti* topoisomers of compound **72**, none of the spectroscopic features allowed for the assignment of each derivative to each of the two topoisomeric forms.

Therefore, with the aim at determining which topoisomer corresponds to each ***anti/syn*-72** hybrid, variable temperature ^{1}H-NMR experiments at low temperatures (298-188 K) of each fraction were performed. The reason to carry out these experiments came from the observation of the computationally optimized structures of both topoisomers. In the molecular model of topoisomer ***syn*-72**, free rotation around single B_{Dimer}-(C≡C) and (C≡C)-C_{SubPc} bonds implied going through a intermediate structural conformation where axial 4-*tert*-butylphenoxy groups of SubPc units are nearly in contact, impeding full rotation around those bonds. In topoisomer ***anti*-72**, however, the special orientation of both axial SubPc units to opposite sides of the SubPc dimer moiety would not affect the free rotation around the mentioned bonds (see Figure 88).

In ^{1}H-NMR spectra at room temperature, the rotational barrier around B_{Dimer}-(C≡C) and (C≡C)-C_{SubPc} was probably too small to observe any distinctive features between ***syn*-72** and ***anti*-72**. Nevertheless, by reducing the energy input to the system (*i.e.*, decreasing the temperature), we expected to see at some point a gradual shift of some of the protons of topoisomer ***syn*-72** that would not take place in ***anti*-72**. Variable temperature ^{1}H-NMR experiments in CD_2Cl_2 of compounds ***syn*-72** and ***anti*-72** are represented in Figure 91.

^{1}H-NMR spectra of ***syn*-72** clearly reflected appreciable changes in the chemical shifts of the protons of both the SubPc dimer and the SubPc unit during the experiment. Thus, SubPc dimer central benzene ring signals shifted towards upper fields, while aromatic protons of the SubPcs isoindole units were either upfield or downfield shifted during the experiment. On the other hand, despite ^{1}H-NMR spectra of ***anti*-72** displayed low resolution due to the aforementioned low stability of this compound in solution, it could be confirmed that none of the signals of either the SubPc dimer or the SubPc units shifted when decreasing temperature.

Hence, according to our reasoning, compound ***syn*-72** would correspond to *syn* topoisomer, and compound ***anti*-72** to *anti* topoisomer. Although, at this moment, we did not consider the conclusions drawn from variable temperature NMR experiments as absolutely certain, subsequent complexation studies of fullerene derivatives would confirm this assignment (*vide infra*).

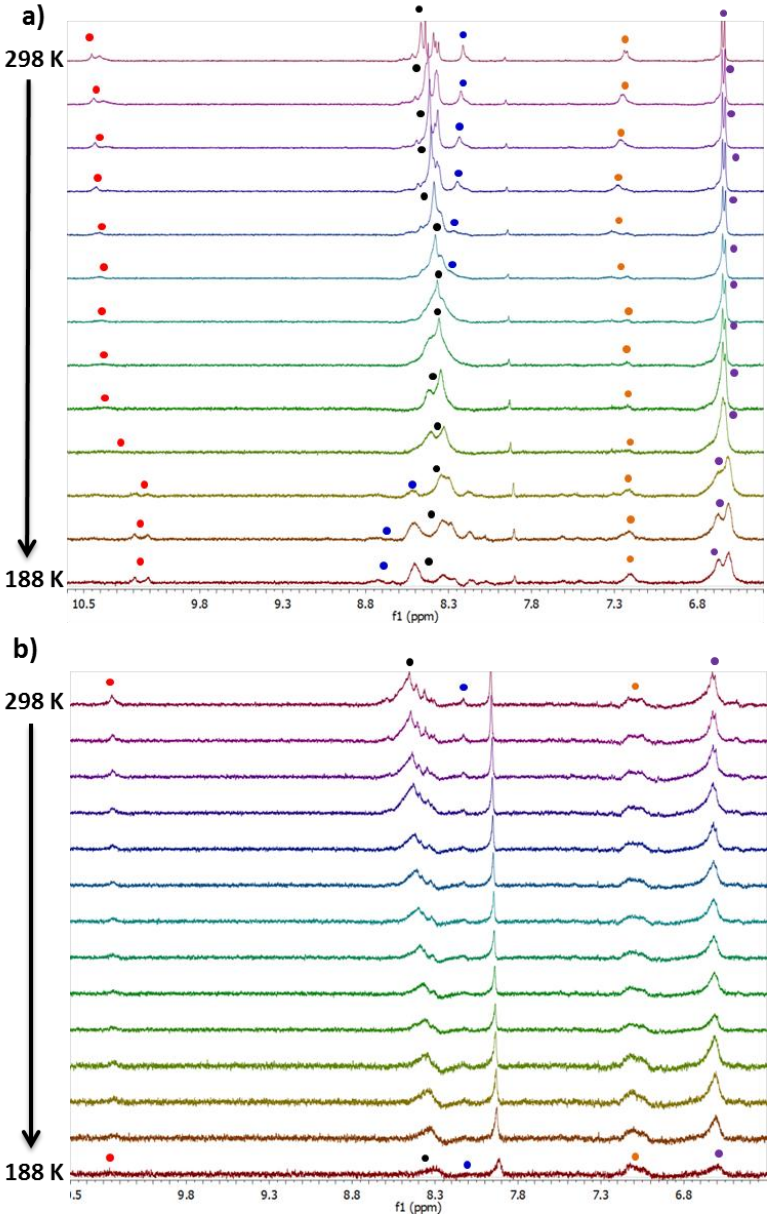

Figure 91. Partial ^{1}H-NMR (300 MHz) spectra at variable temperature in CD_2Cl_2 of compounds a) ***syn*-72** and b) ***anti*-72**.

From this point, the demonstrated lack of stability of derivative ***anti*-72** in solution prompted us to focus on the study of the properties and complexation ability of compound ***syn*-72**.

2.4.5.2 Electrochemical studies of compound *syn*-72

Electrochemical properties of compounds **74**, **75** and ***syn*-72** and fullerene derivatives **C_{60}/C_{70}** and **C_{60}-PCBM/C_{70}-PCBM** were investigated by cyclic voltammetry and square-wave voltammetry in *o*-dichlorobenzene solution (0.1 M $TBAPF_6$). All potential values quoted throughout this section have been referred to the Fc/Fc^+ couple. Figure 92 shows the OSW voltammograms of the compounds studied, as they display better resolved waves than the corresponding CV voltammograms, and the electrochemical data is summarized in Table 14.

Unsymmetrical SubPc **74** exhibits three reduction waves, with the first cathodic event at -1.53 V. Besides, a first anodic process appears at 0.54 V, due to the presence of thiooctyl groups in the SubPc periphery. On the other hand, perfluorinated SubPc dimer **75** (1:1 *syn/anti* mixture) display a rich electrochemistry, characterized by the presence of three reversible reduction waves at -1.01, -1.32 and -1.71 V and one irreversible oxidation peak at 0.75 V. It is interesting to note that dimer **75** shows both the first and the second reductions shifted toward more negative potentials with respect to SubPc **74**.

The voltammogram of SubPc-SubPc dimer hybrid ***syn*-72** shows the main features in common with their individual subunits. Although bonding of SubPc **74** to SubPc dimer **75** causes the electrochemical events of both subunits less resolvable, it is possible to assign each electrochemical process to one or other electroactive component. Thus, while first reduction wave in hybrid ***syn*-72**, peaking at -1.03 V, is centered on the SubPc dimer subunit, first cathodic event occurs at 0.55 V, corresponding to the oxidation of octylthio-substituted SubPc subunits. On sweeping to more negative or positive potentials, it can be observed that the redox behavior of each subunit alone remains almost unaltered in hybrid ***syn*-72**, indicating, together with steady-state absorption features, no appreciable electronic interactions between SubPc and SubPc dimer units in the ground state.

Finally, widely known electrochemical properties of fullerene derivatives **C_{60}/C_{70}** and **C_{60}-PCBM/C_{70}-PCBM** in *o*-DCB solution were investigated. As expected, PCBM derivatives present easier first oxidation and harder first reduction phenomena than the corresponding non-functionalized **C_{60}/C_{70}** fullerenes.

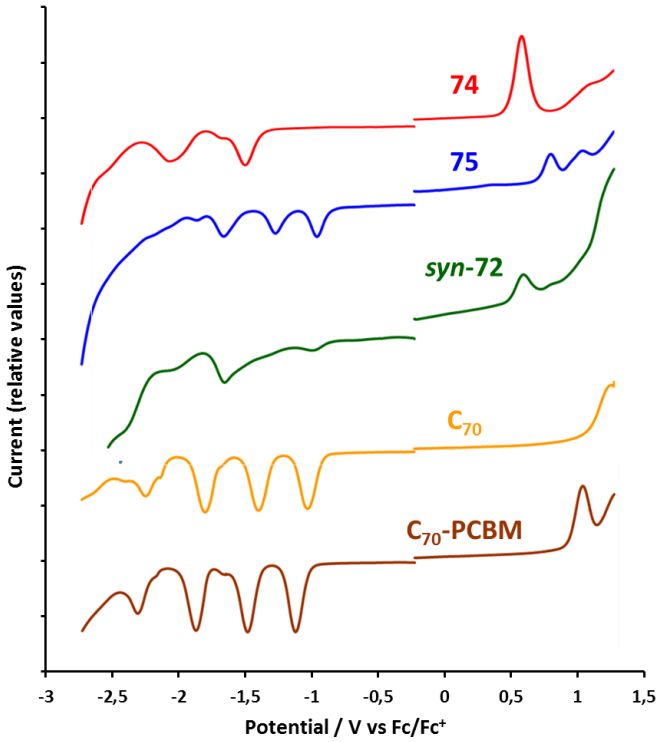

Figure 92. OSW voltammograms of compounds **74**, **75** and ***syn*-72** and fullerene derivatives **C_{70}** and **C_{70}-PCBM** in *o*-DCB.

Table 14. Electrochemical data (in V *vs.* Fc/Fc^+) in *o*-DCB of compounds **74**, **75**, ***syn*-72** and fullerene derivatives **C_{70}** and **C_{70}-PCBM** determined by CV and OSWV.

Compound	E^4_{red} (mV)	E^3_{red} (mV)	E^2_{red} (mV)	E^1_{red} (mV)	E^1_{ox} (mV)	E^2_{ox} (mV)
74		-2.09	-1.68	-1.53	0.54	
75		-1.71	-1.32	-1.01	0.75[b]	0.99[b]
***syn*-72**	-2.10[a]	-1.69[a]	-1.34[a]	-1.03[a]	0.55[b]	0.76[b]
C_{60}		-1.84	-1.46	-1.10	1.30	
C_{70}		-1.83	-1.43[c]	-1.06	1.24[b]	
C_{60}-PCBM		-1.95	-1.60[c]	-1.22	1.08[b]	
C_{70}-PCBM		-1.91	-1.52[c]	-1.16	1.00[b]	

[a] Peak reduction potential by OSWV. [b] Peak oxidation potential by OSWV.

2.4.5.3 Steady state photophysical studies of compound *syn*-72

Prior to the complexation studies of fullerene derivatives by compound ***syn*-72**, steady state absorption and emission spectra of the SubPc-SubPc dimer hybrid and its individual components, SubPc **74** and SubPc dimer ***syn*-2**, were compared.

As previously seen in chloroform solution, absorption spectra of ***syn*-72** in various solvents are best described as the superimposition of the absorption characteristics of the single components (Figure 93a), covering a huge range of the UV-vis spectra, since each individual chromophore fills regions of low absorption of the other. Thus, very small bathochromic shifts (1-3 nm) in *Q* bands of both SubPc **74** and SubPc dimer ***syn*-2** are observed when going to compound ***syn*-72**. Changing the solvent polarity barely affects both *Q* band absorption maxima of ***syn*-72**, peaking each at 592 and 700 nm in toluene, 594 and 696 nm in chloroform, 590 and 693 nm in THF, and 596 and 702 nm in benzonitrile, respectively (Figure 94a).

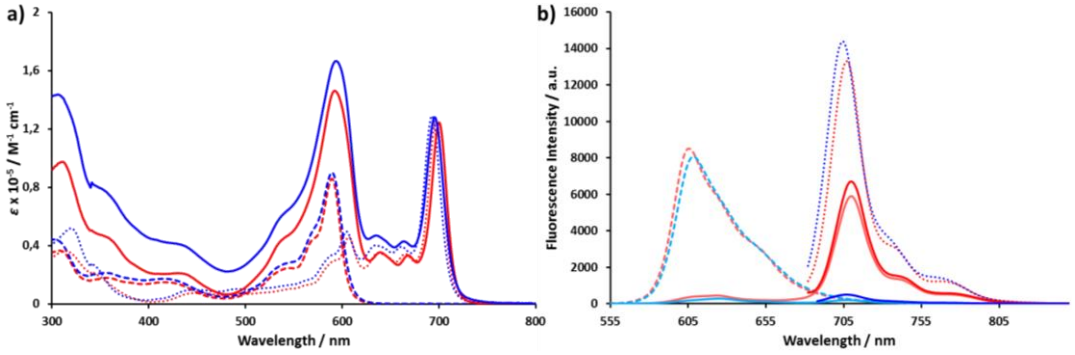

Figure 93. a) UV-vis absorption spectra of: SubPc **74** (dashed lines), SubPc dimer ***syn*-2** (dotted lines), and compound ***syn*-72** (solid lines) in chloroform (blue lines) and toluene (red lines). b) Emission spectra of: SubPc **74** (dashed lines), SubPc dimer ***syn*-2** (dotted lines), and compound ***syn*-72** (solid lines) in chloroform (λ_{exc} = 540 nm, light blue lines; λ_{exc} = 680 nm, dark blue lines) and toluene (λ_{exc} = 540 nm, light red lines; λ_{exc} = 680 nm, dark red lines).

In steady state fluorescence experiments, the absorption features of SubPc dimers, with several shoulders encompassing its *Q* band blue region, did not allow the selective excitation of the SubPc unit. Thus, each sample was irradiated at two different wavelengths: 540 nm, where a maximum part of the radiation is absorbed by the SubPc unit, and 680 nm, where only the SubPc dimer is able to absorb. Figure 93b displays the emission spectra of SubPc **74**, SubPc dimer ***syn*-2** and SubPc-SubPc dimer ensemble ***syn*-72** in toluene and chloroform solutions at both excitation wavelengths.

In toluene solution, excitation of either of the two subunits led to the detection of a major emission band peaking at 710 nm, consistent with the emission of the SubPc dimer component. An additional very weak band centered around 624 nm, corresponding to the SubPc fluorescence emission, can also be distinguished when exciting at 540 nm.

In chloroform solution, quenching of the SubPc fluorescence band was also observed. However, unlike in less polar toluene, emission spectra of the SubPc dimer component were almost totally quenched, either by exciting mainly the SubPc unit or selectively the SubPc dimer moiety (Figure 93b). The magnitude of this quenching was found to be dependent on solvent polarity, as it could be demonstrated by comparison with the emission spectra in more polar THF and benzonitrile (Figure 94b), where even less intense emission intensities for both the SubPc and the SubPc dimer components were detected.

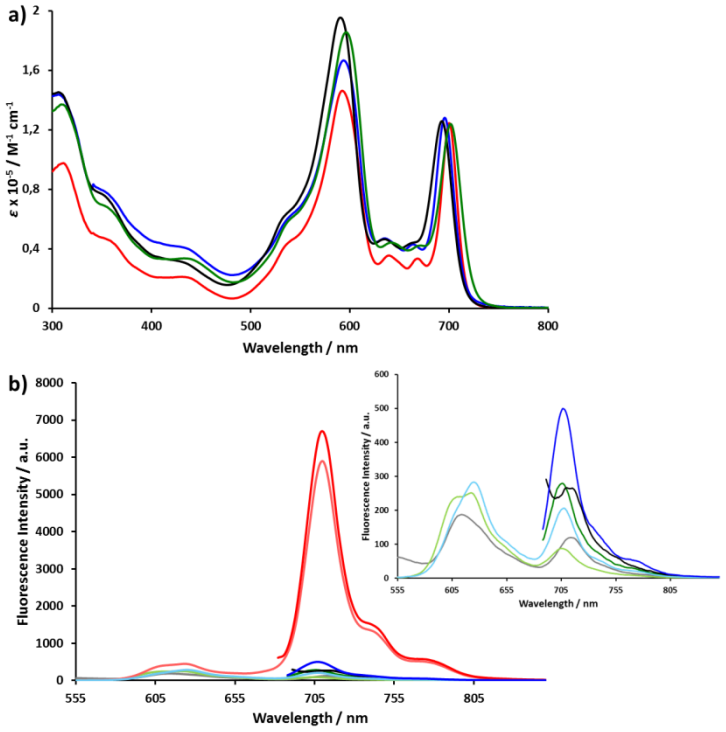

Figure 94. a) UV-vis absorption spectra of ***syn*-72** in toluene (red line), chloroform (blue line), THF (green line) and benzonitrile (black line). b) Emission spectra of compound ***syn*-72** in toluene (λ_{exc} = 540 nm, light red line; λ_{exc} = 680 nm, dark red line), chloroform (λ_{exc} = 540 nm, light blue line; λ_{exc} = 680 nm, dark blue line), THF (λ_{exc} = 540 nm, light green line; λ_{exc} = 680 nm, dark green line) and benzonitrile (λ_{exc} = 540 nm, grey line; λ_{exc} = 680 nm, black line) with matching absorption at the excitation wavelengths. Inset: detail of the low intensity area of the emission spectra.

Quantification of the singlet emission from both subunits in the ensemble ***syn*-72** in comparison to references SubPc **74** and SubPc dimer ***syn*-2** came from fluorescence quantum yield measurements in toluene and chloroform solutions. As reference compounds, zinc phthalocyanine ZnPc (ϕ_F = 0.30)[286] was employed for a λ_{exc} of 640 nm, subnaphthalocyanine SubNc (ϕ_F = 0.22)[287] for a λ_{exc} of 570 nm and SubPc **1** (ϕ_F = 0.71)[42b] for a λ_{exc} of 520 nm.

In reference experiments, a solvent independent fluorescence quantum yield of 0.11 was determined for unsymmetrical SubPc **74**, while ϕ_F values of 0.28 in toluene and 0.26 in chloroform were respectively measured for SubPc dimer ***syn*-2**. On the other hand, singlet emission from SubPc units in compound ***syn*-72** was estimated as 0.004 in toluene and 0.002 in chloroform. Finally, fluorescence quantum yields determined for SubPc dimer unit in compound ***syn*-72** were 0.09 for λ_{exc} = 570 nm and 0.10 for λ_{exc} = 640 nm, in toluene, and 0.003-0.004 for the two excitation wavelengths, in chloroform.

Based on these data, and given the energy values for the singlet excited state of both subunits (*ca.* 2.10 eV for SubPc **74** and 1.75 eV for SubPc dimer ***syn*-2**) and the energy level of the charge separation state (1.6 eV as determined from electrochemical measurements), a preliminary energy/electron transfer scenario for SubPc-SubPc dimer ensemble ***syn*-72** could be depicted. First, the fact that excitation at both 540 and 680 nm wavelengths results mainly in the population of the singlet SubPc dimer points to an efficient energy transfer process from the excited SubPc units to the SubPc dimer moiety. Second, the solvent dependent nonradiative deactivation of the singlet excited state of SubPc dimer unit suggest the existence of an electron transfer process from SubPc units to photoexcited SubPc dimer to generate a ($SubPc^{\bullet+}$-SubPc $Dimer^{\bullet-}$) radical pair.

However, it is obvious that the nature of the excited state interactions between the different subunits in ensemble ***syn*-72** should be probed by means of time-resolved transient absorption measurements to characterize and quantify the intramolecular processes that take place in the excited states. The transient state photophysical characterization of this system will be performed in due course.

[286] Murov, S. L.; Carmichael, I.; Hug, G. L. *Handbook of Photochemistry*; Marcel Dekker: New York, 1993; pp. 1-420.
[287] Nonell, S.; Rubio, N.; del Rey, B.; Torres, T. *J. Chem. Soc. Perkin Trans. 2* **2000**, 1091.

2.4.5.4 Complexation studies of fullerene derivatives with *syn*-72

The complexing ability of the SubPc-SubPc fused dimer ensemble ***syn*-72** towards different fullerene derivatives, namely **C_{60}**, **C_{70}**, **C_{60}-PCBM** and **C_{70}-PCBM**, was first analyzed employing UV-vis absorption and fluorescence spectrophotometry techniques. In this section, all the **C_{60}** and **C_{70}** fullerenes titration experiment were conducted in toluene and all the **C_{60}-PCBM** and **C_{70}-PCBM** titration experiment, in chloroform. No self-aggregation of any host compound in solution was observed by preliminary monitoring of their absorption at different concentrations.

Initially, host-guest behavior of the constituent subunits of ***syn*-72**, that is, perfluorinated SubPc dimer ***syn*-2** and unsymmetrical octylthio-substituted SubPc **74**, was studied. Topoisomer ***anti*-2** was also included in these experiments for the sake of comparison.

According to literature, significant supramolecular interactions of ***syn*-2** with fullerene derivatives in solution were not expected since, in theory, their electronic nature is not complementary. First, it was demonstrated that perfluorinated SubPc does not show any concave-convex interaction with **C_{60}** or **C_{70}** in toluene solution.[279] In addition, other perfluorinated expanded SubPc systems described by Kobayashi *et al.*[103b,105] capable of forming co-crystallates with **C_{60}** did not exhibit any evidence of fullerene complexation in solution either.

For this reason, it was our surprise to check the occurrence of measurable spectral changes in the UV-vis absorption and emission titrations of ***syn*-2** with **C_{60}**, **C_{70}**, **C_{60}-PCBM** and **C_{70}-PCBM** derivatives. Specifically, the addition of guest caused a bathochromic shift and decrease of intensity of ***syn*-2** *Q* band in the absorption spectra and a partial quenching of the emission band in fluorescence spectra. In all cases, Job's plot experiments confirmed the formation of 1:1 complexes with maxima at 0.5 mole fraction (except for **C_{60}**, where stoichiometry of the complex was not evident). Figure 95 displays the Job's plot experiment for the complexation of ***syn*-2** and **C_{70}-PCBM** in chloroform as a representative example.

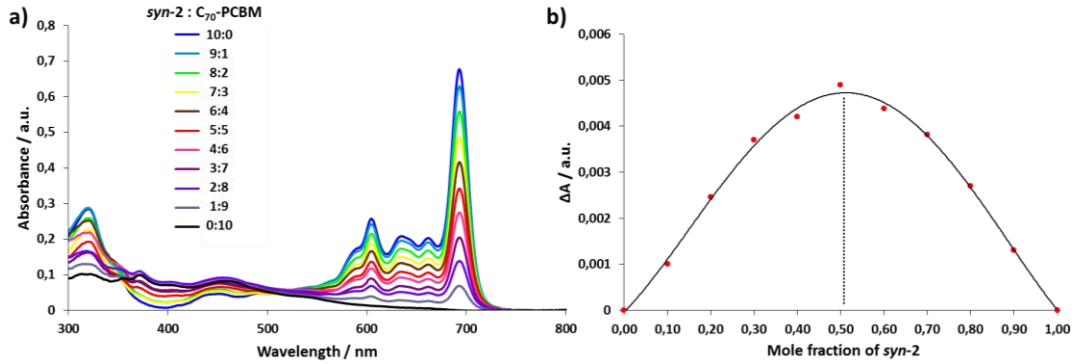

Figure 95. a) UV-vis titration spectral changes in various ratios of ***syn*-2** and **C_{70}-PCBM** in chloroform at 25 °C. The overall concentration stays constant during the experiments, at 5.0 x 10^{-6} M. b) Job's plot diagram of the complex ***syn*-2:C_{70}-PCBM** (monitored at 720 nm), centered at 0.5 (1:1 stoichiometry).

Titration experiments of ***syn*-2** with each fullerene derivative revealed a remarkably stronger host-guest interaction with **C_{70}-PCBM** than with the other derivatives (Figure 96). Thus, the appearance of a new absorption maximum corresponding to the complex formed and the almost complete quenching of the emission band of the host were especially noticeable in the former case.

Non-linear curve fitting of the spectroscopic changes in absorption and fluorescence titrations allowed determining the association constants value (K_{abs} and K_{em}, respectively) for each ***syn*-2**:fullerene complex, using two different softwares, namely ReactLab™ EQUILIBRIA software and the global fitting program created by Thordarson[288] for Matlab. Since values provided by both software properly matched, results from ReactLab™ EQUILIBRIA, obtained with lower uncertainties, are the ones presented here.

Furthermore, it must be taken into account that, in fluorescence experiments, quantitative analysis of solutions with optical density above 0.1 are subject to inner filter effects (IFEs).[289] To avoid this, all the fluorescence spectra were corrected according to Lakowicz equation:

$$F_{corr} = F_{obs} \times 10^{(Abs_{\lambda exc} + Abs_{\lambda emi})/2} \qquad \text{(Eqn. 16)}$$

[288] Thordarson, P. *Chem. Soc Rev.* **2011**, *40*, 1305.
[289] a) Miller, J. R.; Calcaterra, L. T.; Closs, G. L. *J. Am. Chem. Soc.* **1984**, *106*, 3047. b) Lakowicz, J. R. *Principles of Fluorescence Spectroscopy*, 3rd ed.; Springer-Verlag, 2006.

where F*corr* is the corrected fluorescence intensity, F_{obs} is the observed fluorescence intensity, $Abs_{\lambda exc}$ is the absorption at the excitation wavelength and $Abs_{\lambda emi}$ is the absorption at the emission wavelength.

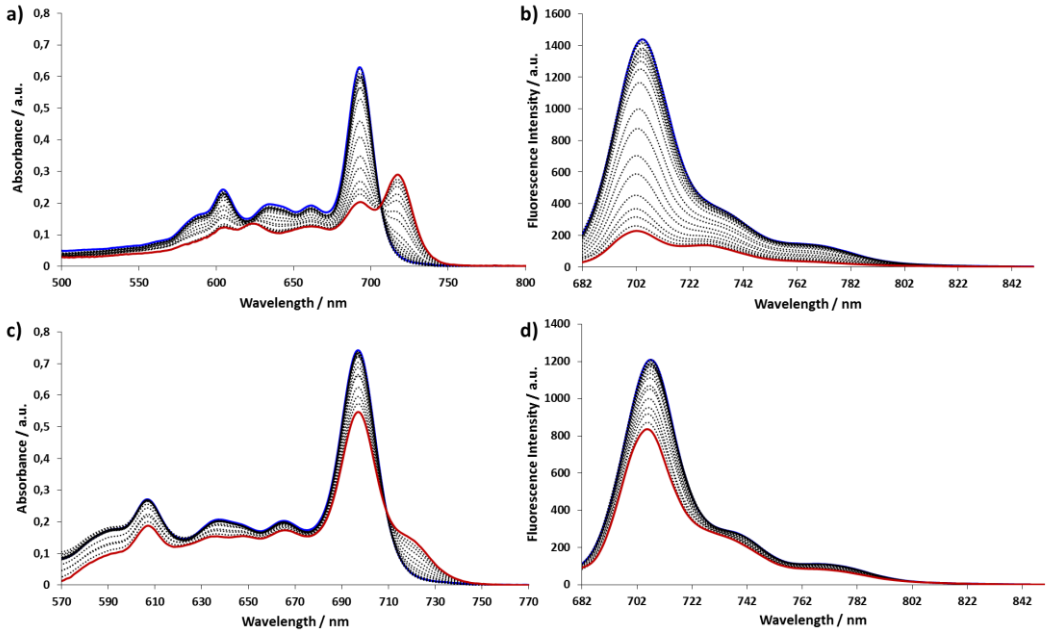

Figure 96. UV-vis titration a) absorption and b) emission spectra (λ_{exc} = 680 nm) of SubPc dimer ***syn*-2** (4.0×10^{-6} M) with **C_{70}-PCBM** from 0 (blue lines) to 3.7×10^{-4} M (90 equiv, red lines) in chloroform at 25 °C. UV-vis titration c) absorption and d) emission spectra (λ_{exc} = 680 nm) of SubPc dimer ***syn*-2** (4.0×10^{-6} M) with **C_{70}** from 0 (blue lines) to 4.0×10^{-4} M (100 equiv, red lines) in toluene at 25 °C.

Overall, association constants K_{abs} and K_{em} were respectively estimated as (1.26 ± 0.02) x 10^4 and (1.22 ± 0.02) x 10^4 M^{-1} for **C_{70}-PCBM**, (7.76 ± 0.03) x 10^2 and (1.31 ± 0.02) x 10^3 M^{-1} for **C_{60}-PCBM**, (1.11 ± 0.01) x 10^3 and (1.08 ± 0.02) x 10^3 M^{-1} for **C_{70}** and (9.61 ± 0.02) x 10^2 and (9.40 ± 0.02) x 10^2 M^{-1} for **C_{60}**. These values confirmed that **C_{70}-PCBM** forms more stable associates with ***syn*-2**, while the association constant governing the formation of 1:1 complexes with other fullerene derivatives are approximately one order of magnitude lower. These results suggest the binding affinity in this system is influenced not only by the size of the guest, **C_{70}** derivatives fitting better in the hemicircular cavity of ***syn*-2**, but also by solvent effects and/or host-guest electrostatic interactions.

Next, UV-vis absorption and emission titrations of topoisomer ***anti*-2** with **C_{60}-PCBM** and **C_{70}-PCBM** were carried out. First differences with respect to ***syn*-2** came from absorption spectra,

where no measurable changes in the absorption features of the host were observed after addition of 100 equiv of guests. On the other hand, a partial quenching of the emission of ***anti*-2** could be observed in fluorescence experiments with both PCBM derivatives during titrations (Figure 97).

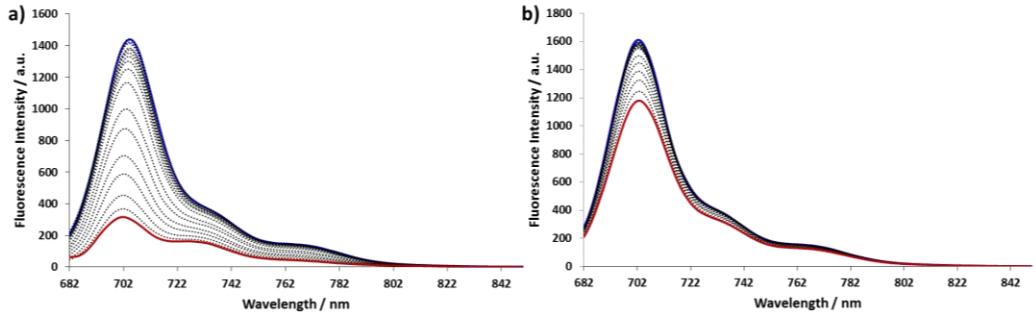

Figure 97. Fluorescence titration spectra (λ_{exc} = 680 nm) of SubPc dimer ***anti*-2** (4.0×10^{-6} M) with a) **C_{70}-PCBM** and b) **C_{60}-PCBM** from 0 (blue line) to 4×10^{-4} M (100 equiv, red line) in chloroform at 25 °C.

In this case, Job's plot fluorescence experiments did not render a clear stoichiometry of the complexes formed. However, fitting of the data obtained from titrations to different H:G binding models (namely 1:1, 2:1 and 1:2) did render useful information about the supramolecular interaction of ***anti*-2** with fullerenes. In particular, an association constant of K = (1.78 ± 0.08) x 10^3 M^{-1} was obtained for the formation of a 1:1 ***anti*-2**:**C_{70}-PCBM** complex. Interestingly, a change in stoichiometry to a 1:2 complex between ***anti*-2** and **C_{60}-PCBM** was inferred from the fitting of the emission experiments, obtaining binding constants of K_1 = (1.68 ± 0.03) x 10^3 M^{-1} and K_2 = (4.86 ± 0.06) x 10^2 M^{-1}. This finding is in good agreement with the host ***anti*-2** S-shaped geometry, which might be able to accommodate two **C_{60}-PCBM** molecules in each of its concave cavities. Although the 1:1 complex structure formed with **C_{70}-PCBM** is not clearly defined, it is rationale to think that the bigger size of this guest would prevent the formation of a similar 1:2 complex.

Last set of studies of the host-guest behavior of the subunits of ***syn*-72** came from UV-vis absorption and emission titrations of unsymmetrical octylthio-substituted SubPc **74** with **C_{70}** and **C_{70}-PCBM**. Previous complexation studies of **C_{60}** or **C_{70}** fullerenes in toluene solution with a number of symmetrical hexaalkylthio-substituted SubPcs resulted in the formation of 2:1 SubPc:fullerene complexes with binding constants K_1=K_2 ranging from 10^4 to 10^5 M^{-1}, displaying no significant differences between the guest employed.[279]

Although SubPc **74** presents an unsymmetrical structure with thioalkyl substituents in only two of the isoindole units, our results nicely agreed with the ones reported (Figure 98). Thus, a 2:1 stoichiometry was deducted for both SubPc complexes with $\mathbf{C_{70}}$ and $\mathbf{C_{70}}$**-PCBM**. Association constants obtained for both systems were also similar, with values of K_1 = (2.02 ± 0.03) x 10^4 M^{-1} and K_2 = (1.48 ± 0.02) x 10^4 M^{-1} for $\mathbf{C_{70}}$ and K_1 = (2.17 ± 0.02) x 10^4 M^{-1} and K_2 = (2.08 ± 0.03) x 10^4 M^{-1} for $\mathbf{C_{70}}$**-PCBM**. Similar values should be expected for smaller $\mathbf{C_{60}}$ derivatives, as extracted from literature. Thus, unlike dimer ***syn*-2**, supramolecular interactions between SubPc **74** and fullerenes do not seem to be dependent on the size of the guest or the solvent employed. Besides, comparing ***syn*-2** and **74** reveals higher affinities of all fullerene guests with the octylthio-substituted SubPc host than with the perfluorinated SubPc dimer except for $\mathbf{C_{70}}$**-PCBM**, where these values are almost equal.

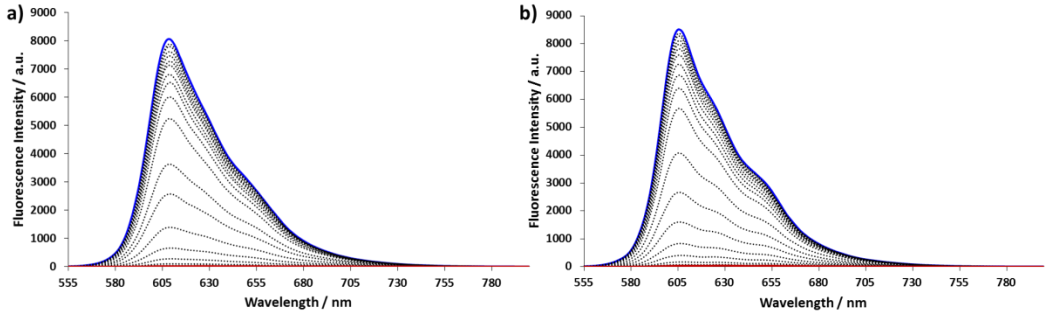

Figure 98. a) UV-vis titration emission spectra (λ_{exc} = 540 nm) of SubPc **74** (8.0×10^{-6} M) with $\mathbf{C_{70}}$**-PCBM** from 0 (blue line) to 4×10^{-4} M (50 equiv, red line) in chloroform at 25 °C. b) UV-vis titration emission spectra (λ_{exc} = 540 nm) of SubPc **74** (8.0×10^{-6} M) with $\mathbf{C_{70}}$ from 0 (blue line) to 4.0×10^{-4} M (50 equiv, red line) in toluene at 25 °C.

Finally, the complexing ability of the SubPc-SubPc dimer ensemble ***syn*-72** towards fullerenes was studied. From previous results, it could be expected the formation of a 1:2 complex where one of the fullerene units would be encapsulated by the two octylthio-substituted SubPc units and the second guest molecule would present concave-convex interactions with the perfluorinated SubPc dimer moiety. Particularly interesting from this study would be to observe the influence that the restricted spatial separation between the two SubPc units in ***syn*-72** would display in the formation of the supramolecular ensembles, compared with the previously performed complexation of fullerenes by "free" SubPc units.

Our hypothesis was confirmed by means of UV-vis absorption and emission titrations. Although Job's plot experiments did not show a clear stoichiometry for the complexes (here, it must be noted that Job's plot method is not considered fully reliable for 1:2 or 2:1 systems

where there is more than one complex present), monitoring of the titrations of ***syn*-72** with **C_{60}**, **C_{70}**, **C_{60}-PCBM** and **C_{70}-PCBM** revealed, in all cases, distinct changes in the spectroscopic features of the host that matched a two-step complex formation (Figures 99-100). Thus, the addition of guest first caused a bathocromic shift and decrease of intensity of *Q* bands of both SubPc and SubPc dimer units. These observations might imply that the first guest molecule is complexed by the two axial SubPc units of ***syn*-72**. This fact was supported by the changes produced at higher guest ratio, which resulted in an additional bathocromic shift of the *Q* band of the SubPc dimer, while the SubPcs *Q* band remained unaltered. This shift would then correspond to the less favored complexation of a second fullerene unit by the SubPc dimer.

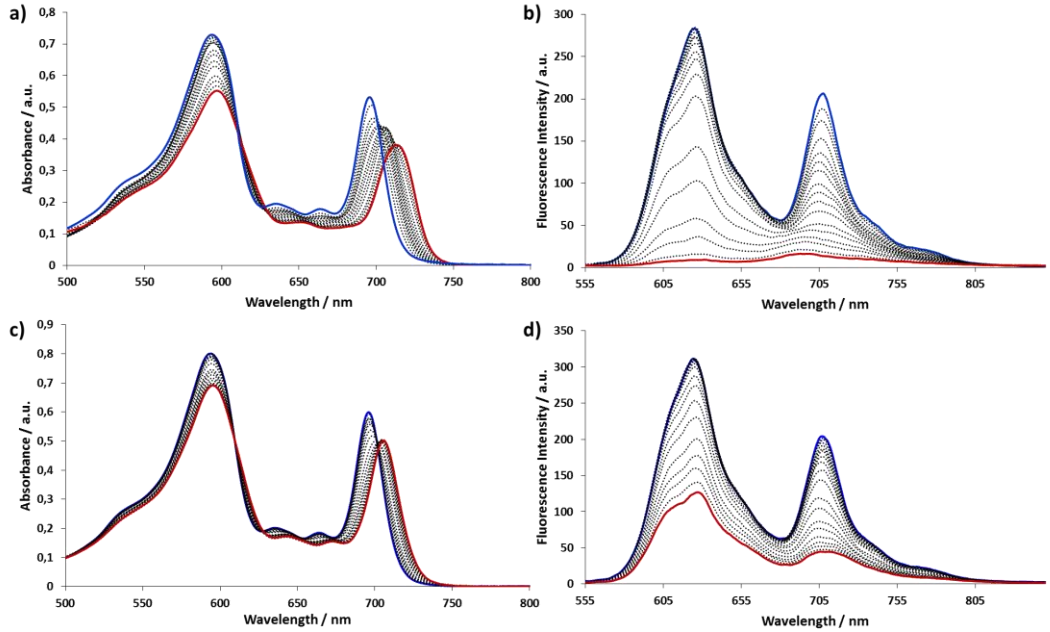

Figure 99. UV-vis titration a) absorption and b) emission spectra (λ_{exc} = 540 nm) of compound ***syn*-72** (4.0×10^{-6} M) with **C_{70}-PCBM** from 0 (blue lines) to 2.0×10^{-4} M (50 equiv, red lines) in chloroform at 25 °C. UV-vis titration c) absorption and d) emission spectra (λ_{exc} = 540 nm) of compound ***syn*-72** (4.0×10^{-6} M) with **C_{60}-PCBM** from 0 (blue lines) to 4.0×10^{-4} M (100 equiv, red lines) in chloroform at 25 °C.

In fluorescence titrations, a two-step process also takes place. In this case, only a decrease of intensity of the SubPc dimer unit emission was initially observed, but, again at higher guest ratio, the partial or almost total quenching of both SubPcs and SubPc dimer emissions followed. This fact is consistent with absorption experiments. If the first fullerene unit is accommodated in the cavity generated by the two octylthio-substituted SubPcs in the 1:1

complex, the energy transfer process from the excited SubPc units to the SubPc dimer moiety might be impeded by the presence of a new energy-accepting unit, justifying the initial quenching of the SubPc dimer emission band. When the second guest molecule is complexed by the perfluorinated SubPc dimer to form the 1:2 ensemble, a cascade of energy/electron transfer events involving all photoactive units in the system would explain the quenching in the emission of both SubPc and SubPc dimer entities.

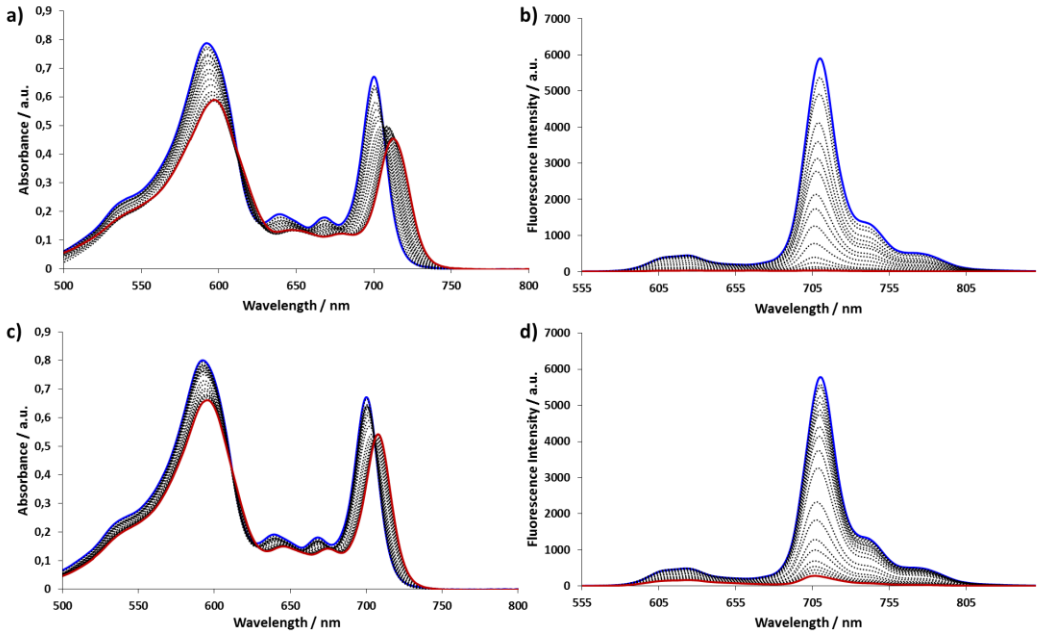

Figure 100. UV-vis titration a) absorption and b) emission spectra (λ_{exc} = 540 nm) of compound ***syn*-72** (4.0×10^{-6} M) with **C_{70}** from 0 (blue lines) to 2.0×10^{-4} M (50 equiv, red lines) in toluene at 25 °C. UV-vis titration c) absorption and d) emission spectra (λ_{exc} = 540 nm) of compound ***syn*-72** (4.0×10^{-6} M) with **C_{60}** from 0 (blue lines) to 4.0×10^{-4} M (100 equiv, red lines) in toluene at 25 °C.

Association constants of the 1:1 and 1:2 complexes of ***syn*-72** with each fullerene derivative were derived from both absorption and emission titrations. In fluorescence experiments, these values were estimated as $K_1 = (1.87 \pm 0.01) \times 10^6$ M^{-1} and $K_2 = (3.03 \pm 0.02) \times 10^4$ M^{-1} for **C_{70}-PCBM**, $K_1 = (5.64 \pm 0.03) \times 10^4$ M^{-1} and $K_2 = (3.78 \pm 0.03) \times 10^3$ M^{-1} for **C_{60}-PCBM**, $K_1 = (5.82 \pm 0.02) \times 10^5$ M^{-1} and $K_2 = (1.11 \pm 0.01) \times 10^4$ M^{-1} for **C_{70}** and $K_1 = (5.00 \pm 0.03) \times 10^4$ M^{-1} and $K_2 = (6.47 \pm 0.04) \times 10^3$ M^{-1} for **C_{60}**.

It is noteworthy to mention the difference in K_a values for the formation of the initial 1:1 complex depending on the fullerene guest employed. Thus, the spatially-defined cavity created by the two octylthio-substituted SubPcs embraces **C_{70}** and **C_{70}-PCBM** guests with remarkably high association constants of around 5 x 10^5 and 1 x 10^6 M^{-1}, respectively, that is, more than one order of magnitude higher values than the corresponding **C_{60}** and **C_{60}-PCBM** (*ca.* 5 x 10^4 M^{-1}). Besides, this cavity presents an enhanced binding ability of fullerenes with respect to the complexation by "free" SubPc **74** units, with slightly higher K_a values for **C_{60}** and **C_{60}-PCBM** and an increase of up to one order and two orders of magnitude for **C_{70}** and **C_{70}-PCBM**, respectively. This fact points out the positive effect that the particular disposition of the octylthio-substituted SubPcs in our system exerts in the fullerenes encapsulation. Finally, binding constants K_2 estimated for the formation of the 1:2 ensembles are very similar to the ones obtained for the ***syn*-2**:fullerene complexes, confirming that a secondary supramolecular interaction between the perfluorinated SubPc dimer unit and another fullerene molecule takes place in our system, with significant values that depend on the size and the host-guest electrostatic interactions.

In order to assess the quality of the data retrieved from UV-vis absorption and fluorescence measurements, the titration of reference compound ***syn*-2** and the SubPc-SubPc dimer ensemble ***syn*-72** with **C_{70}-PCBM** by ^{1}H-NMR and ^{19}F-NMR spectroscopy in CD_2Cl_2 were carried out at two orders of magnitude higher concentrations than spectrophotometry techniques.

Titrations of perfluorinated dimer ***syn*-2** with **C_{70}-PCBM** are represented in Figure 101. In this case, the saturation point appeared around 1.2 equiv of added guest. In ^{1}H-NMR, upon addition of fullerene, the central benzene ring protons of ***syn*-2** shifted towards upper fields, while in ^{19}F-NMR the signal corresponding to the fluor atoms in α position splitted and downfield shifted.

On the other hand, ^{1}H-NMR titration of ***syn*-72** with **C_{70}-PCBM** enabled to monitor the changes in the proton signals of both the SubPcs and the SubPc dimer units (Figure 102). Thus, it could be clearly observed that, while the protons of the SubPc dimer unit moved from 10.5 to 10.0 ppm during titration, reaching the saturation point at *ca.* 2.4 ppm, signals corresponding to the benzene ring of the SubPcs bearing the ethynyl linker shifted upon the addition of the first equivalent of guest and then stabilized. These results confirm the proposal of the initial formation of a 1:1 complex where the fullerene is in between the two SubPc units and a subsequent 1:2 system after complexation of a second guest molecule by the SubPc dimer.

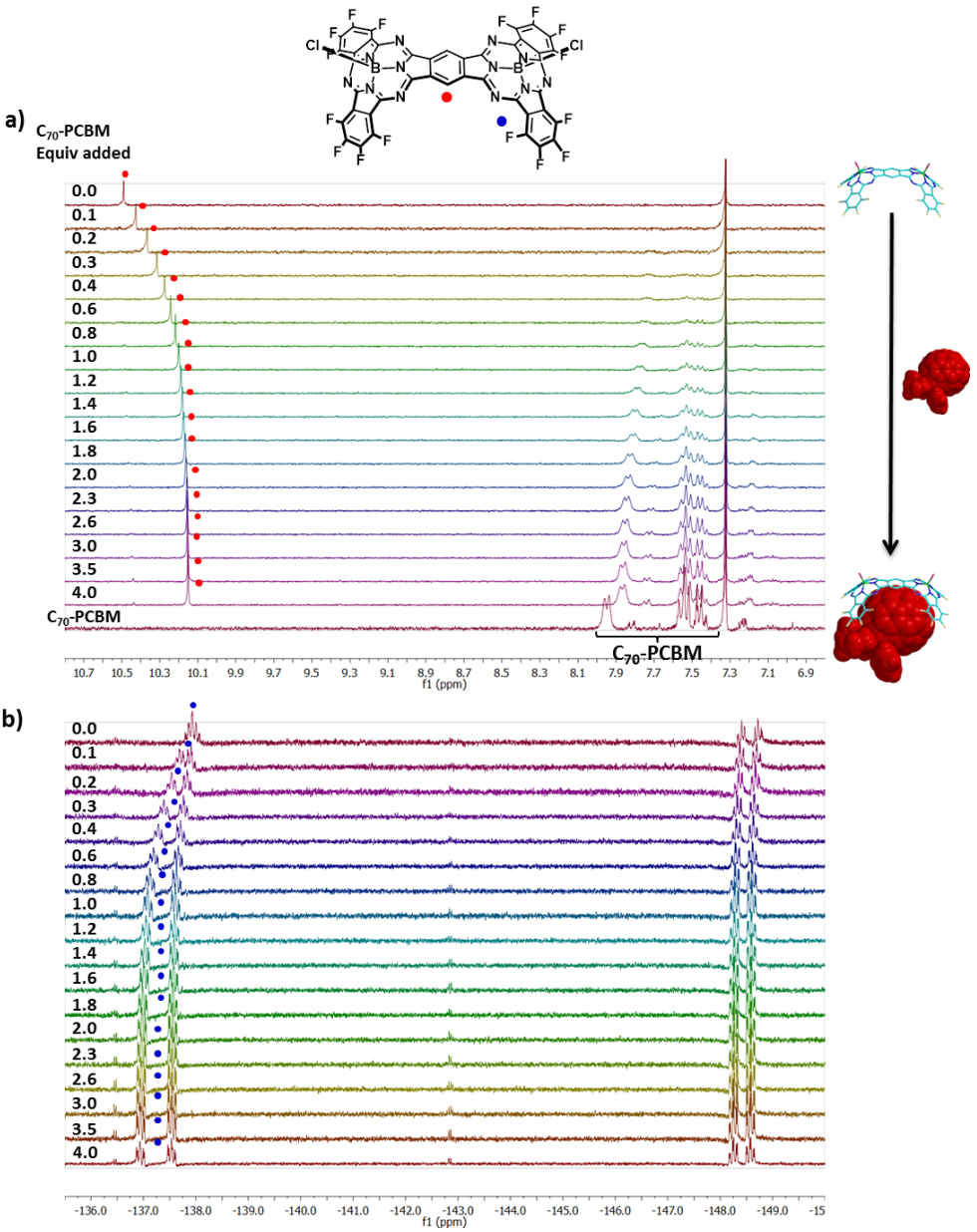

Figure 101. a) ^{1}H-NMR and b) ^{19}F-NMR titration of compound ***syn*-2** (8.0×10^{-4} M) with **C_{70}-PCBM** from 0 to 3.2×10^{-3} M (4 equiv) in CD_2Cl_2 at 25 °C.

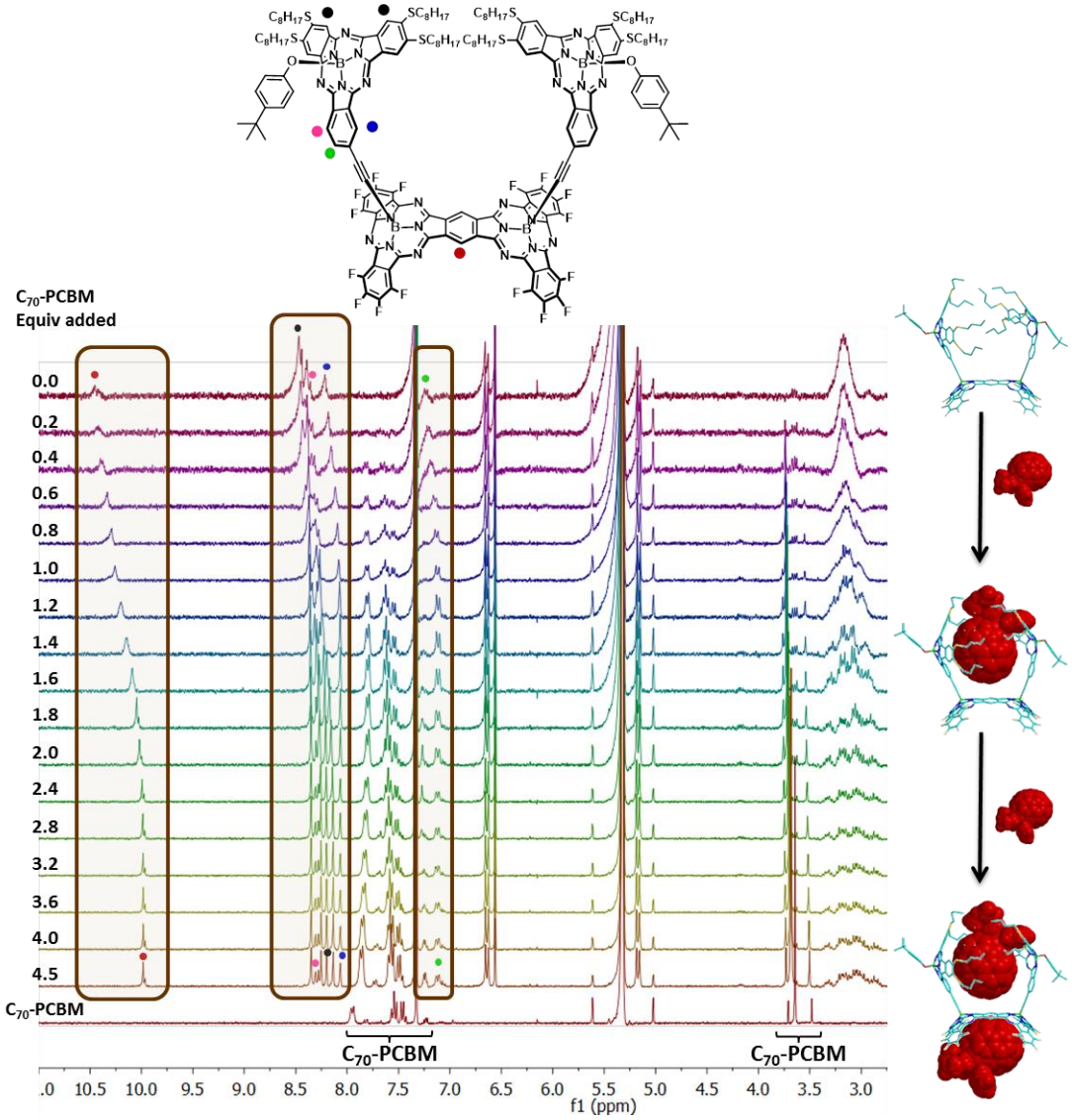

Figure 102. ^{1}H-NMR titration of compound ***syn*-72** (8.0×10^{-4} M) with **C_{70}-PCBM** from 0 to 3.6×10^{-3} M (4.5 equiv) in CD_2Cl_2 at 25 °C.

The high binding constants of the system allowed calculating the stoichiometry of the complexes using the mole ratio method.[290] This method uses a binding isotherm where the concentration of host is fixed and the concentration of guest is varied, representing the chemical shift of a proton versus the concentration of guest. The break point coming from the extrapolation of the apparently linear points at the beginning and the end of the curve corresponds to the guest:host stoichiometric ratio. By applying this method, the titrations with **C_{70}-PCBM** confirmed a 1:1 stoichiometry for ***syn*-2**, and a 2:1 stoichiometry for ***syn*-72** (Figure 103).

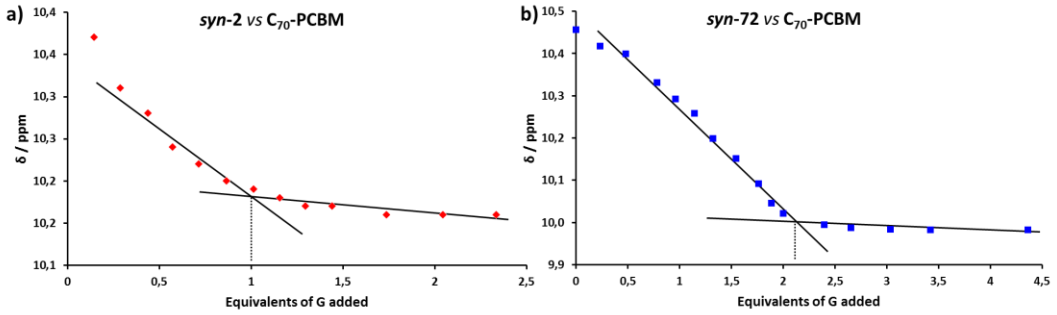

Figure 103. Plots of ^{1}H-NMR titrations of a) ***syn*-2** with **C_{70}-PCBM** and b) ***syn*-72** with **C_{70}-PCBM**, showing the changes in the chemical shifts of the SubPc dimer central benzene protons. The apparently linear portions at the beginning and the end of the curve are extrapolated to find a break point, corresponding to the **Host/C_{70}-PCBM** stoichiometric ratio.

The association constants for the formation of the complexes were determined by plotting the changes of the proton and fluor signals of ***syn*-2** and of three different protons and the fluor signals of ***syn*-72**, respectively, using HypNMR2008[291] and the global fitting program softwares. The calculated binding isotherms are in sound agreement with those determined in the experiments. Best quality values obtained by HypNMR2008 were estimated as 3.06×10^4 M^{-1} for ***syn*-2** and $K_1 = 1.95 \times 10^6$ M^{-1} and $K_2 = 3.98 \times 10^4$ M^{-1} for ***syn*-72,** with good standard deviation values ($\sigma = 0.08$). These results are very similar to the ones extracted from UV-vis measurements.

[290] Tsukube, H.; Furuta, H.; Odani, A.; Takeda, Y.; Kudo, Y.; Inoue, Y.; Liu, Y.; Sakamoto, H.; Kimura, K. In *Comprehensive Supramolecular Chemistry*; Atwood, J. L., Davies, J. E. D., MacNicol, D. D., Vögtle, F., Eds.; Pergamon: Oxford, 1996; Vol. 8, No. 10, pp 425−482.

[291] a) Frassineti, C.; Ghelli, S.; Gans, P.; Sabatini, A.; Moruzzi, M. S.; Vacca, A. *Anal. Biochem.* **1995**, *231*, 374. b) Frassineti, C.; Alderighi, L.; Gans, P.; Sabatini, A.; Vacca, A.; Ghelli, S. *Anal. Bioanal. Chem.* **2003**, *376*, 1041.

To sum up, all the binding constants of the diverse complexes calculated in this section by different spectroscopic techniques are summarized in Table 15.

Table 15. Calculated binding constants for the complexes formed by reference compounds, dimers ***syn*-2** and ***anti*-2**, SubPc **74**, and SubPc-SubPc dimer ensemble ***syn*-72**, with fullerene derivatives **C_{60}**, **C_{70}**, **C_{60}-PCBM** and **C_{70}-PCBM**, employing all the techniques discussed in the text.

Host	Guest	K_a / M^{-1}		
		UV-vis Absorption	**Fluorescence**	**NMR**
***syn*-2**	**C_{60}**	$(9.61 \pm 0.02) \times 10^2$	$(9.40 \pm 0.02) \times 10^2$	-
	C_{70}	$(1.11 \pm 0.01) \times 10^3$	$(1.08 \pm 0.02) \times 10^3$	-
	C_{60}-PCBM	$(7.76 \pm 0.03) \times 10^2$	$(1.31 \pm 0.02) \times 10^3$	-
	C_{70}-PCBM	$(1.26 \pm 0.02) \times 10^4$	$(1.22 \pm 0.02) \times 10^4$	3.06×10^4 ($\sigma = 0.08$)
***anti*-2**	**C_{60}-PCBM**		$K_1 = (1.68 \pm 0.03) \times 10^3$ $K_2 = (4.86 \pm 0.06) \times 10^2$	
	C_{70}-PCBM		$(1.78 \pm 0.08) \times 10^3$	
74	**C_{70}**		$K_1 = (2.02 \pm 0.03) \times 10^4$ $K_2 = (1.48 \pm 0.02) \times 10^4$	
	C_{70}-PCBM		$K_1 = (2.17 \pm 0.02) \times 10^4$ $K_2 = (2.08 \pm 0.03) \times 10^4$	
***syn*-72**	**C_{60}**	$K_1 = (4.01 \pm 0.02) \times 10^4$ $K_2 = (5.53 \pm 0.03) \times 10^3$	$K_1 = (5.00 \pm 0.03) \times 10^4$ $K_2 = (6.47 \pm 0.04) \times 10^3$	
	C_{70}	$K_1 = (3.16 \pm 0.02) \times 10^5$ $K_2 = (9.33 \pm 0.06) \times 10^3$	$K_1 = (5.82 \pm 0.02) \times 10^5$ $K_2 = (1.11 \pm 0.01) \times 10^4$	
	C_{60}-PCBM	$K_1 = (3.92 \pm 0.02) \times 10^4$ $K_2 = (4.32 \pm 0.03) \times 10^3$	$K_1 = (5.64 \pm 0.03) \times 10^4$ $K_2 = (3.78 \pm 0.03) \times 10^3$	
	C_{70}-PCBM	$K_1 = (1.13 \pm 0.01) \times 10^6$ $K_2 = (3.09 \pm 0.02) \times 10^4$	$K_1 = (1.87 \pm 0.01) \times 10^6$ $K_2 = (3.03 \pm 0.02) \times 10^4$	$K_1 = 1.95 \times 10^6$ $K_2 = 3.98 \times 10^4$ ($\sigma = 0.08$)

C_{60}/C_{70} UV-vis absorption and fluorescence titrations carried out in toluene solution at 25 °C, [H] = 4.0×10^{-6} M; **C_{60}-PCBM/C_{70}-PCBM** UV-vis absorption and fluorescence titrations carried out in chloroform solution at 25 °C, [H] = 4.0×10^{-6} M; NMR titrations carried out in CD_2Cl_2 at 25 °C, [H] = 8.0×10^{-4} M.

2.5 Summary and conclusions

In this chapter, the synthesis and characterization of novel π-extended systems based on SubPc fused oligomers peripherally and/or axially functionalized and the study of selected properties and potential applications have been expounded.

In the first part, unsymmetrical SubPc fused dimers have been synthesized by a stepwise methodology that makes use of the *ortho*-dicyano-SubPcs prepared in the first chapter of this *Thesis* as π-extended phthalonitrile derivatives. In particular, either electron-donating or electron-accepting substituents have been introduced on each SubPc constituent unit. However, several undesired processes, such as lack of reactivity, decomposition and/or polymerization of *o*-dicyano-SubPcs in the reaction conditions, have limited the number of unsymmetrical SubPc fused dimers achieved. In a specific case, separation of *syn* and *anti* isomers of a dimer bearing electron-donating *tert*-butyl and electron-withdrawing chloro groups in each SubPc moiety **39** has been achieved by further axial functionalization. On the other hand, an unsymmetrical SubPc fused trimer has been synthesized by condensation reaction of a tetracyano-SubPc with a phthalonitrile derivative, albeit in very low yields. Finally, other attempts on the synthesis of larger SubPc-based ensembles have failed.

The optical and electrochemical properties of the unsymmetrical SubPc fused dimers obtained have been studied, confirming that their electronic and redox features are modulated by their peripheral functionalization. In addition, physico-chemical studies of dimer **39** have allowed to probe the push-pull character of these unsymmetrical SubPc fused dimers and have provided evidence for a charge-polarized curved π-extended system. Thus, from steady state fluorescence and pump probe experiments, a dual nature of fluorescence, namely a delocalized singlet excited state (1.73 eV) and a polarized charge transfer state (<1.7 eV), has been concluded. The nature of the CT state has been visualized using the results of DFT calculations, showing a slight polarization of the HOMO towards the electron donor and of the LUMO towards the electron acceptor (Figure 104).

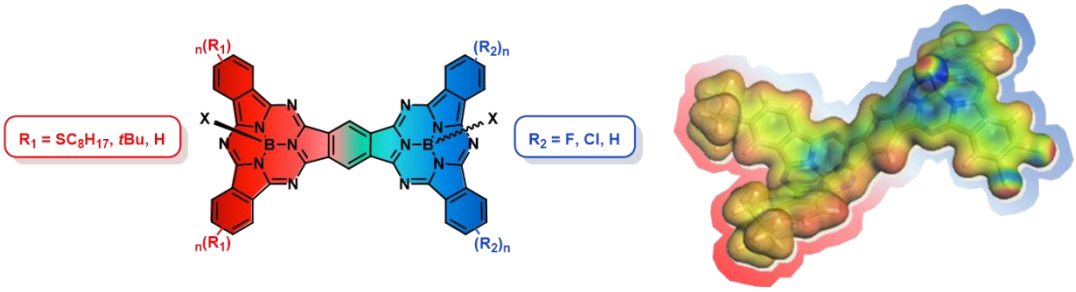

Figure 104. Graphical abstract of the results obtained in section 2.3.

In the second part of this chapter, an approach to the employment of SubPc fused dimer based systems as active units in molecular recognition and artificial photosynthetic systems has been presented.

A synthetic methodology based on the aluminum chloride mediated axial functionalization of SubPcs with TMS-alkynyl substituents has allowed for the preparation of a number of multichromophoric systems through the attachment of other photoactive units to the two axial positions of a perfluorinated SubPc fused dimer.

First, the synthesis of *syn* and *anti* SubPc dimers functionalized with axial ethynylpyrene units has been carried out. The rigid and short alkynyl spacers confer both topisomers appealing three-dimensional structures that can be exploited for the inmobilization of SWCNTs, potentially giving rise to electron donor SWCNT-based photosynthetic reaction center.

Second, the preparation of multi-SubPc systems constituted by SubPc and SubPc fused dimer units connected by their mutual axial positions has been explored. For this purpose, a series of SubPcs and SubPc dimers bearing different conjugated spacers linked by alkyne bonds to the SubPc or SubPc dimer boron atoms have been synthesized in good yields. Unfortunately, once attached to the SubPc axial position, TMS-alkynes display a remarkable lack of reactivity, ascribed to steric hindrance in the transition state and decrease of nucleophilicity, which precludes the obtainment of these ensembles.

Finally, a multi-SubPc hybrid **72** comprised of a perfluorinated SubPc fused dimer (*syn* or *anti* topoisomer) axially functionalized with unsymmetrical octylthio-substituted SubPcs linked through their periphery by ethynyl linkers to the boron atoms of the dimer has been prepared. Electrochemical and steady state photophysical studies of the ***syn*-72** hybrid suggest the existence of an electron transfer process from SubPc units to photoexcited SubPc dimer to generate a ($SubPc^{\bullet+}$-$SubPc\ Dimer^{\bullet-}$) radical pair.

Furthermore, the disposition that the two axial SubPc units acquire in this assembly gives rise to unique supramolecular recognition sites suitable for the complexation of shape and size complementary fullerenes. Thus, the binding ability of this hybrid towards different fullerene derivatives, namely **C_{60}**, **C_{70}**, **C_{60}-PCBM** and **C_{70}-PCBM**, has been analyzed through UV-vis absorption, fluorescence and NMR titrations. It has been demonstrated that compound ***syn*-72** displays a unique fullerene complexation mode. Initially, the formation of a 1:1 supramolecular complex involving the axial octylthio-substituted SubPcs embracing a guest molecule with remarkable association constants of around 10^6 - 10^5 M^{-1} is observed. This well-defined cavity generated by the SubPc dimer and the axial SubPcs shows higher affinity for the **C_{70}** fullerene derivatives. Then, a secondary supramolecular recognition event between the curved perfluorinated SubPc *syn* dimer unit and another fullerene molecule occurs, with significant binding constants of 10^4 - 10^3 M^{-1}, depending on the size and the host-guest electrostatic interactions, leading to the formation of the final 1:2 supramolecular ensemble.

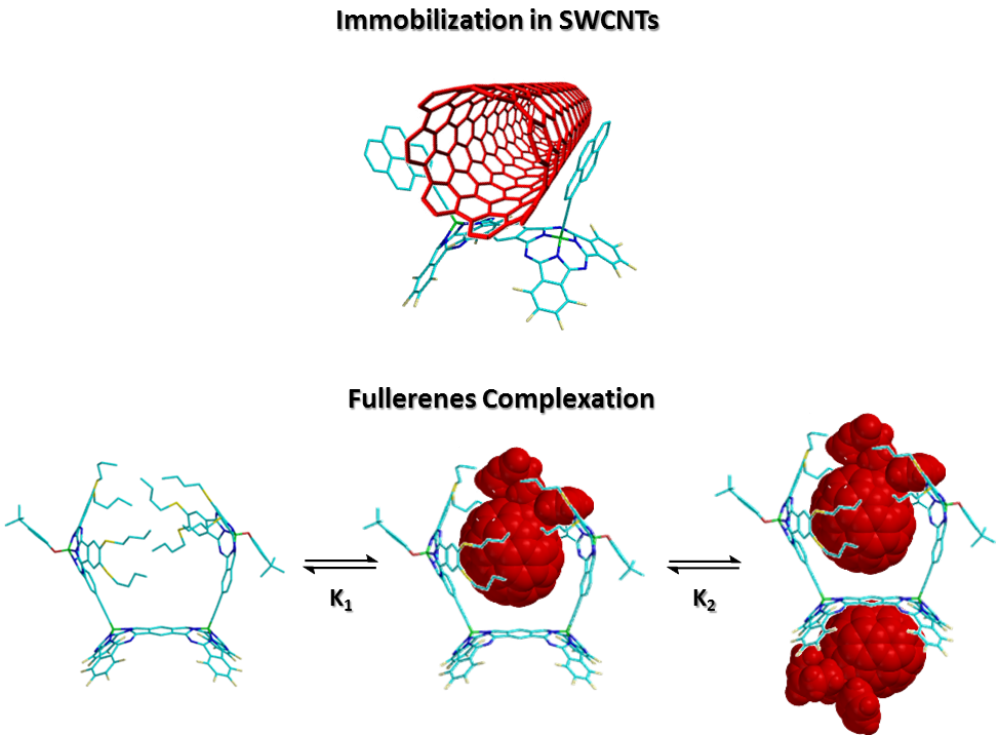

Figure 105. Graphical abstract of the results obtained in section 2.4.

2.6 Experimental section

2.6.1 Specific Methods in Chapter II

Femtosecond and nanosecond transient absorption spectroscopy: pump probe experiments were performed in Friederich-Alexander University in Erlangen, with an amplified Ti:Sapphire CPA-2110 fs laser system (Clark MXR: output 775 nm, 1 kHz, 150 fs pulse width) using transient absorption pump/probe detection systems (Helios and Eos, Ultrafast Systems). The 530 and 656 nm excitation wavelengths were generated with a noncolinear optical parametric amplifier (NOPA, Clark MXR). Fluorescence lifetimes were determined by the time correlated single photon counting technique using a FluoroLog3 emission spectrometer (Horiba JobinYvon) equipped with an R3809U-58 MCP (Hamamatsu) and a 405LH laser diode (Horiba JobinYvon) exciting at 403 nm (675 ps fwhm) as well as a 650L laser diode (Horiba JobinYvon) exciting at 647 nm (<200 ps fwhm).

Theoretical calculations: all theoretical calculations in *Section 2.3.1.5* were carried out in Friederich-Alexander University in Erlangen. Geometries were initially optimized using density-functional theory (DFT) with the B3LYP hybrid functional,[292] and the 6-31G(d) basis set.[293] All DFT calculations used the Gaussian09 program.[294] The optimized geometries were confirmed to be local minima by calculating their normal vibrations within the harmonic approximation. Electronic spectra were calculated for these geometries in the gas phase using the AM1 Hamiltonian[295] and a configuration-interaction with only single excitations (CIS). CIS

[292] a) Becke, A. D. *Phys. Rev. A: At., Mol., Opt. Phys.* **1988**, *38*, 3098. b) J. P. Perdew, Phys. Rev. B: Condens. Matter Mater. Phys. 1986, 33, 8822.

[293] a) Binkley, J. S.; Pople, J. A.; Hehre, W. J. *J. Am. Chem. Soc.* **1980**, *102*, 939. b) Gordon, M. S. *Chem. Phys. Lett.* **1980**, *76*, 163. c) Gordon, M. S.; Binkley, J. S.; Pople, J. A.; Pietro, W. J.; Hehre, W. J. *J. Am. Chem. Soc.* **1982**, *104*, 2797.

[294] Frisch, M. J.; Trucks, G. W.; Schlegel, H. B.; Scuseria, G. E.; Robb, M. A.; Cheeseman, J. R.; Scalmani, G.; Barone, V.; Mennucci, B.; Petersson, G. A.; Nakatsuji, H.; Caricato, M.; Li, X.; Hratchian, H. P.; Izmaylov, A. F.; Bloino, J.; Zheng, G.; Sonnenberg, J. L.; Hada, M.; Ehara, M.; Toyota, K.; Fukuda, R.; Hasegawa, J.; Ishida, M.; Nakajima, T.; Honda, Y.; Kitao, O.; Nakai, H.; Vreven, T.; Montgomery, J. J. A.; Peralta, J. E.; Ogliaro, F.; Bearpark, M.; Heyd, J. J.; Brothers, E.; Kudin, K. N.; Staroverov, V. N.; Kobayashi, R.; Normand, J.; Raghavachari, K.; Rendell, A.; Burant, J. C.; Iyengar, S. S.; Tomasi, J.; Cossi, M.; Rega, N.; Millam, J. M.; Klene, M.; Knox, J. E.; Cross, J. B.; Bakken, V.; Adamo, C.; Jaramillo, J.; Gomperts, R.; Stratmann, R. E.; Yazyev, O.; Austin, A. J.; Cammi, R.; Pomelli, C.; Ochterski, J. W.; Martin, R. L.; Morokuma, K.; Zakrzewski, V. G.; Voth, G. A.; Salvador, P.; Dannenberg, J. J.; Dapprich, S.; Daniels, A. D.; Farkas, O.; Foresman, J. B.; Ortiz, J. V.; Cioslowski, J.; Fox, D. J. Gaussian 09, Revision A.02, Gaussian, Inc. (Wallingford CT), 2009.

[295] a) Dewar, M. J. S.; Zoebisch, E. G.; Healy, E. F.; Stewart, J. J. P. *J. Am. Chem. Soc.* **1985**, *107*, 3902. b) Holder, A. J. AM1. In *Encyclopedia of Computational Chemistry*; Schleyer, P. v. R.; Allinger, N. L.; Clark, T.; Gasteiger, J.;

calculations used 100 occupied and 100 virtual orbitals in the active space. All semiempirical calculations were performed with a development version of VAMP.[296]

Kollman, P. A.; Schaefer, III, H. F.; Schreiner, P. R., Eds.; John Wiley & Sons Ltd.: Chichester, UK, 1998; Vol. 1, pp. 8-11.

[296] Clark, T.; Alex, A.; Beck, B.; Burkhardt, F.; Chandrasekhar, J.; Gedeck, P.; Horn, A. H. C.; Hutter, M.; Martin, B.; Rauhut, G.; Sauer, W.; Schindler, T.; Steinke, T. VAMP 11, Erlangen 2014.

2.6.2 Synthesis of subphthalocyanine fused oligomers

2.6.2.1 Synthesis of unsymmetrical subphthalocyanine fused dimers

*2.6.2.1.1 Dimers **36** and **37***

Dimer 36, mixture of *syn* and *anti* topoisomers

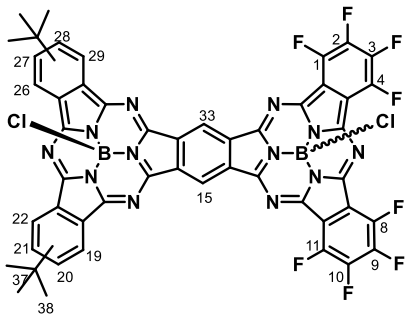

To a 10 mL round-bottom two-neck flask equipped with a reflux condenser and magnetic stirrer, a 1.0 M solution of BCl_3 in *p*-xylene (200 µL, 0.200 mmol) was added to 3,4,5,6-tetrafluorophthalonitrile (27 mg, 0.133 mmol), under argon atmosphere. The slurry was stirred at room temperature for 5 min. Then, a solution of SubPc **12** (23 mg, 0.033 mmol) in dry *p*-xylene (0.8 mL) was added and the mixture was heated to reflux (136-138 °C) for 1 h. The crude was cooled down to room temperature and flushed with argon, and solvent was removed by rotary evaporation. The resulting dark solid was first washed with abundant heptane, later dissolved in heptane/CH_2Cl_2 1:1 and passed through a short celite plug. The solvent was vacuum-evaporated and the resulting dark solid was subjected to size exclusion chromatography using $CHCl_3$ as eluent. By washing with hexane, 3.3 mg (0.0033 mmol) of compound **36** were obtained as a blue solid. Yield: 10% (*syn*/*anti* 1:1 mixture).

Mp > 250 °C.

^{1}H-NMR (300 MHz, $CDCl_3$): δ (ppm) = 10.47-10.41 (m, 2H; H-15, H-33), 9.08-8.77 (m, 4H; H-19, H-22, H-26, H-29), 8.18-8.02 (m, 2H; H-20/H-21, H-27/H-28), 1.63-1.60 (m, 18H; H-38).

MS (MALDI-TOF, DCTB): *m/z* = 1038.2 $[M]^+$.

UV-vis ($CHCl_3$): λ_{max} (nm) (log ε (dm^3 mol^{-1} cm^{-1})) = 707 (5.2), 679 (sh), 653 (sh), 615 (4.7), 600 (sh), 525 (4.5), 432 (4.1), 315 (5.0), 275 (5.0).

Dimer 37, mixture of *syn* and *anti* topoisomers

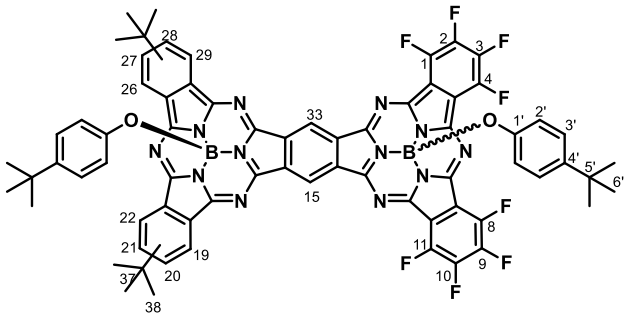

In a 10 mL round-bottom two-neck flask equipped with a reflux condenser and a magnetic stirrer, 4-*tert*-butylphenol (4 mg, 0.026 mmol) and dimer **36** (5 mg, 0.0047 mmol) were refluxed in toluene (0.5 mL) for 2 h. After cooling down to room temperature, the excess of phenol

was removed by washing the crude with a 5:1 MeOH/water solution. The resulting dark solid was purified by size exclusion chromatography using $CHCl_3$ as eluent. By washing with hexane and methanol, 3.6 mg (0.0028 mmol) of compound **37** were obtained as a blue solid. Yield: 60% (*syn*/*anti* 1:1 mixture).

Mp > 250 °C.

^{1}H-NMR (300 MHz, $CDCl_3$): δ (ppm) = 10.45-10.33 (m, 4H; H-15, H-33), 9.05-8.72 (m, 8H; H-19, H-22, H-26, H-29), 8.16-7.96 (m, 4H; H-20/H-21, H-27/H-28), 6.93-6.82 (d, J_o = 8.6 Hz, 2H; H-3' *syn*), 6.80-6.67 (d, J_o = 8.6 Hz, 2H; H-3' *anti*), 5.51-5.41 (d, J_o = 8.6 Hz, 2H; H-2' *syn*), 5.36-5.37 (d, J_o = 8.6 Hz, 2H; H-2' *anti*), 1.65-1.58 (m, 36H; H-38), 1.14 (s, 9H; H-6´ *syn*), 1.01 (s, 9H; H-6' *anti*).

MS (MALDI-TOF, DCTB): *m/z* = 1266.4 $[M]^+$.

UV-vis ($CHCl_3$): λ_{max} (nm) (log ε (dm^3 mol^{-1} cm^{-1})) = 704 (5.2), 677 (sh), 650 (sh), 611 (4.8), 600 (sh), 526 (4.6), 428 (4.1), 336 (4.9), 285 (4.9).

*2.6.2.1.2 Dimers **39**, **anti-40** and **syn-40***

Separation of the three regioisomers of SubPc 12

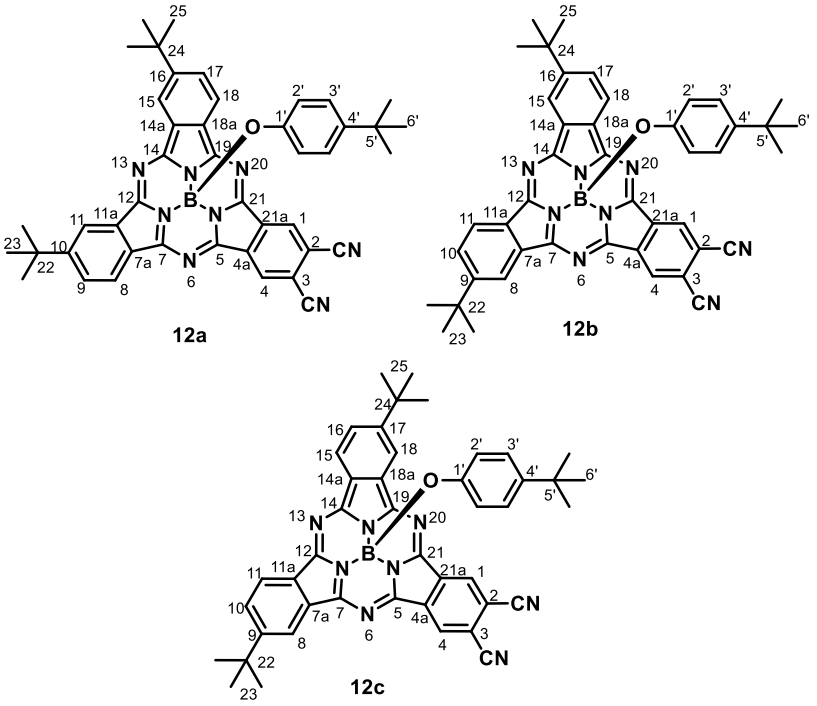

During the isolation and purification of diiodo-SubPc **4b** and dicyano-SubPc **12**, subsequent purification by column chromatography on silica gel using the eluents previously reported for the synthesis of each SubPc allows the separation of the three different regioisomers of compound **12** in similar yields.

Regioisomer 12a:

^{1}H-NMR (300 MHz, $CDCl_3$): δ (ppm) = 9.23 (s, 2H; H-1, H-4), 8.87 (d, J_m = 1.6 Hz, 2H; H-11, H-15), 8.72 (d, J_o = 8.3 Hz, 2H; H-8, H-18), 8.06 (dd, J_o = 8.3 Hz, J_m = 1.6 Hz, 2H; H-9, H-17), 6.77 (d, J_o = 8.8 Hz, 2H; H-3'), 5.33 (d, J_o = 8.8 Hz, 2H; H-2'), 1.56 (s, 18H; H-23, H-25), 1.09 (s, 9H; H-6´).

^{13}C-NMR (75.5 MHz, $CDCl_3$): δ (ppm) = 157.1 (C-12, C-14), 155.6 (C-7, C-19), 152.8 (C-5, C-21), 149.8 (C-1'), 145.9 (C-10, C-16), 144.3 (C-4'), 131.4 (C-7a, C-18a), 130.0 (C-11a, C-14a), 129.8 (C-9, C-17), 129.6 (C-4a, C-21a), 128.8 (C-1, C-4), 126.0 (C-3'), 122.4 (C-8, C-18), 119.7 (C-11, C-15), 117.9 (C-2'), 116.3 (C-2, C-3), 112.6 (C≡N), 36.1 (C-22, C-24), 34.0 (C-5'), 31.7 (C-23, C-25), 31.5 (C-6').

Regioisomer 12b:

^{1}H-NMR (300 MHz, $CDCl_3$): δ (ppm) = 9.22 (s, 1H; H-4), 9.20 (s, 1H; H-1), 8.86 (d, J_m = 1.6 Hz, 1H; H-15), 8.84 (d, J_m = 1.6 Hz, 1H; H-8), 8.77 (d, J_o = 8.3 Hz, 1H; H-11), 8.77 (d, J_o = 8.3 Hz, 1H; H-18), 8.07 (dd, J_o = 8.3 Hz, J_m = 1.6 Hz, 1H; H-17), 8.03 (dd, J_o = 8.3 Hz, J_m = 1.6 Hz, 1H; H-10), 6.80 (d, J_o = 8.7 Hz, 2H; H-3'), 5.37 (d, J_o = 8.7 Hz, 2H; H-2'), 1.56 (s, 9H; H-25), 1.55 (s, 9H; H-23), 1.10 (s, 9H; H-6´).

^{13}C-NMR (75.5 MHz, $CDCl_3$): δ (ppm) = 157.3 (C-14), 156.9 (C-12), 156.4 (C-16), 155.7 (C-9), 153.0, 152.9 (C-7, C-19), 149.8 (C-1'), 145.8, 145.7 (C-5, C-21), 144.3 (C-4'), 132.6 (C-11a), 131.4 (C-18a), 130.0 (C-7a, C-14a), 129.8 (C-17), 129.4 (C-4a, C-21a), 129.1 (C-10), 128.8 (C-4), 128.7 (C-1), 126.0 (C-3'), 122.9 (C-11), 122.4 (C-18), 119.7 (C-15), 119.3 (C-8), 117.9 (C-2'), 116.2 (C-2, C-3), 112.5 (C≡N), 36.2 (C-22), 36.1 (C-24), 34.0 (C-5'), 31.7 (C-23), 31.7 (C-25), 31.4 (C-6').

Regioisomer 12c:

^{1}H-NMR (300 MHz, $CDCl_3$): δ (ppm) = 9.25 (s, 2H; H-1, H-4), 8.83 (d, J_m = 1.7 Hz, 2H; H-8, H-18), 8.73 (d, J_o = 8.3 Hz, 2H; H-11, H-15), 8.03 (dd, J_o = 8.3 Hz, J_m = 1.7 Hz, 2H; H-10, H-16), 6.78 (d, J_o = 8.7 Hz, 2H; H-3'), 5.35 (d, J_o = 8.7 Hz, 2H; H-2'), 1.56 (s, 18H; H-23, H-25), 1.09 (s, 9H; H-6´).

^{13}C-NMR (75.5 MHz, $CDCl_3$): δ (ppm) = 157.1 (C-7, C-19), 156.4 (C-9, C-17), 153.2 (C-12, C-14), 149.8 (C-1'), 145.6 (C-5, C-21), 144.3 (C-4'), 132.7 (C-11a, C-14a), 129.4 (C-7a, C-18a), 129.1 (C-10, C-16), 128.8 (C-1, C-4), 128.4 (C-4a, C-21a), 126.0 (C-3'), 122.8 (C-11, C-15), 119.3 (C-8, C-18), 117.9 (C-2'), 116.3 (C-2, C-3), 112.5 (C≡N), 36.2 (C-22, C-24), 34.0 (C-5'), 31.7 (C-23, C-25), 31.5 (C-6').

Dimers 39, mixture of *syn* and *anti* topoisomers

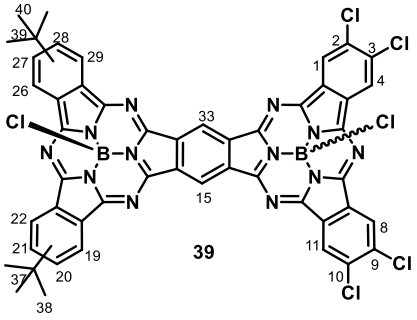

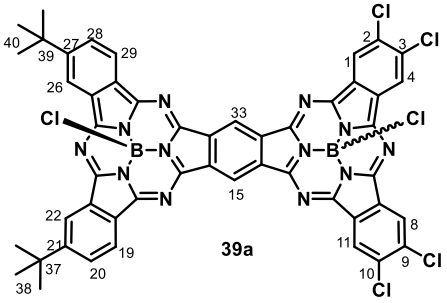

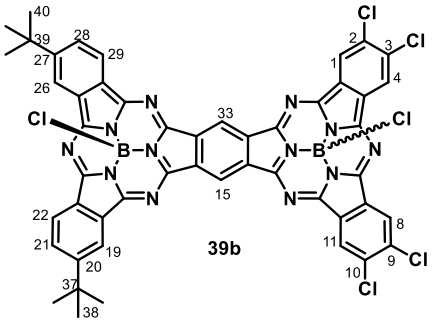

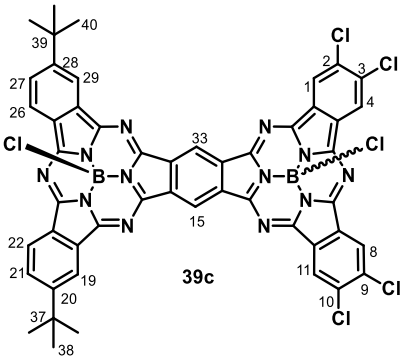

To a 10 ml round-bottom two-neck flask equipped with a reflux condenser and magnetic stirrer, a 1.0 M solution of BCl_3 in *p*-xylene (600 µL, 0.600 mmol) was added to 4,5-dichlorophthalonitrile (79 mg, 0.400 mmol), under argon atmosphere. The slurry was stirred at room temperature for 5 min. Then, a solution of SubPc **12a-c** (71 mg, 0.100 mmol) in dry *p*-xylene (1.4 mL) was added and the mixture was heated to reflux (136-138 °C) for 1 h. The crude was cooled down to room temperature and flushed with argon, and solvent was removed by rotary evaporation. The solid residue was purified by column chromatography on silica gel using toluene as eluent, yielding 17 mg (0.017 mmol) of product **39a-c** as a blue solid. Yield: 16% (*syn*/*anti* 1:1 mixture).

Mixture of regioisomers 39:

Mp > 250 °C.

^{1}H-NMR (500 MHz, $CDCl_3$): δ (ppm) = 10.40-10.35 (m, 2H; H-15, H-33), 9.09-8.74 (m, 8H; H-1, H-4, H-8, H-11, H-19, H-22, H-26, H-29), 8.16-8.01 (m, 2H; H-20/H-21, H-27/H-28), 1.64-1.53 (6s, 18H; H-38, H-40).

MS (MALDI-TOF, DCTB): *m/z* = 1032.1 $[M]^+$.

HRLSI-MS: m/z Calcd for $[C_{50}H_{30}B_2Cl_6N_{12}]$: 1032.1021; Found: 1032.1009.

UV-vis ($CHCl_3$): λ_{max} (nm) (log ε (dm^3 mol^{-1} cm^{-1})) = 712 (5.2), 682 (4.7), 654 (4.6), 614 (4.6), 515 (4.1), 439 (4.0), 326 (4.8), 280 (4.7).

FT-IR (KBr), ν (cm^{-1}): 2963, 2924, 2855, 1725, 1611, 1459, 1385, 1281, 1225, 1175, 1127, 1096, 1025, 975, 890, 793, 703.

Regioisomer 39a:

^{1}H-NMR (500 MHz, $CDCl_3$): δ (ppm) = 10.38 (s, 2H; H-15, H-33), 9.08, 9.00 (2s, 2H; H-22, H-26), 9.00, 8.93 (2s, 4H; H-1, H-4, H-8, H-11), 8.90, 8.82 (2d, J_o = 8.3 Hz, 2H; H-19, H-29), 8.14, 8.05 (2dd, J_o = 8.3 Hz, J_m = 1.7 Hz, 2H; H-20, H-28), 1.56-1.54 (m, 18H; H-38, H-40).

Regioisomer 39b:

^{1}H-NMR (500 MHz, $CDCl_3$): δ (ppm) = 10.39, 10.38, 10.37, 10.36 (4d, J_p = 0.8 Hz, 2H; H-15, H-33), 9.06, 8.99, 8.89 (3s, 4H; H-1, H-4, H-8, H-11), 9.02, 8.99, 8.97, 8.95 (4d, J_m = 1.7 Hz, 2H; H-19, H-26), 8.92, 8.88, 8.81, 8.79 (4d, J_o = 8.3 Hz, 2H; H-22, H-29), 8.14, 8.10, 8.04, 8.02 (4dd, J_o = 8.3 Hz, J_m = 1.7 Hz, 2H; H-21, H-28), 1.64, 1.61, 1.57, 1.53 (4s, 18H; H-38, H-40).

Regioisomer 39c:

^{1}H-NMR (500 MHz, $CDCl_3$): δ (ppm) = 10.40, 10.39 (2s, 2H; H-15, H-33), 9.06, 9.04 (2d, J_m = 1.7 Hz, 2H; H-19, H-29), 8.99, 8.95, 8.90 (3s, 4H; H-1, H-4, H-8, H-11), 8.86, 8.76 (2d, J_o = 8.3 Hz, 2H; H-22, H-26), 8.10, 8.02 (2dd, J_o = 8.3 Hz, J_m = 1.7 Hz, 2H; H-21, H-27), 1.58-1.54 (m, 18H; H-38, H-40).

Dimers *anti*-40 and *syn*-40, mixture of regioisomers

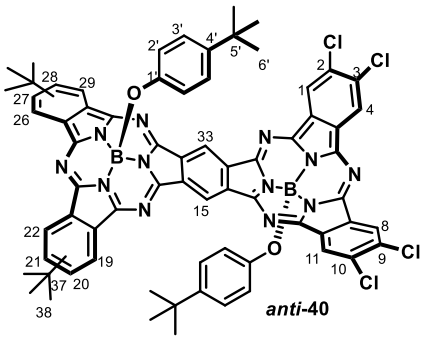

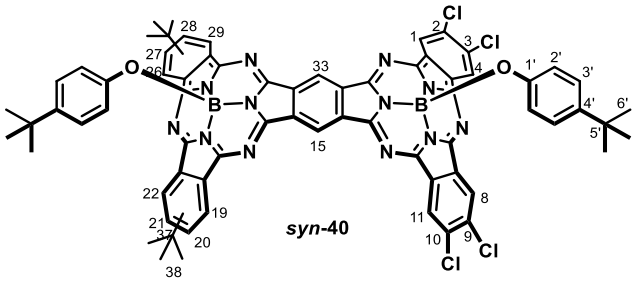

In a 25 ml round-bottom two-neck flask equipped with a reflux condenser and magnetic stirrer, dimer **39** (10 mg, 0.010 mmol) and 4-*tert*-butylphenol (15 mg, 0.100 mmol) were solved in dry toluene (1 mL). The mixture was refluxed for 2 hours. After cooling down to room temperature, the excess of phenol was removed by washing the crude with a 3:1 MeOH/water solution. The crude product was purified by column chromatography on silica gel using toluene as eluent. By washing with hexane, 5 mg (0.0039 mmol, 45%) of compound ***anti*-40** and 5 mg (0.0039, 45%) of compound ***syn*-40** were obtained as blue solids. Overall yield: 90%.

Topoisomer *anti*-40, mixture of regioisomers:

^{1}H-NMR (500 MHz, $CDCl_3$): δ (ppm) = 10.33-10.29 (m, 2H; H-15, H-33), 9.04-8.80 (m, 8H; H-1, H-4, H-8, H-11, H-19, H-22, H-26, H-29), 8.11-8.03 (m, 2H; H-20/H-21, H-27/H-28), 6.71-6.66 (2d, J_o = 8.7 Hz, J_o' = 8.7 Hz, 4H; H-3'), 5.32-5.24 (m, 4H; H-2'), 1.63-1.57 (3s, 18H; H-38), 1.02-0.99 (m, 18H; H-6´).

MS (MALDI-TOF, DCTB): *m/z* = 1260.3 $[M]^+$.

HRLSI-MS: m/z Calcd for $[C_{70}H_{56}B_2Cl_4N_{12}O_2]$: 1260.3584; Found: 1260.3588.

UV-vis ($CHCl_3$): λ_{max} (nm) (log ε (dm^3 mol^{-1} cm^{-1})) = 710 (5.2), 679 (4.7), 651 (4.6), 610 (4.6), 515 (4.1), 437 (4.0), 327 (4.8).

Topoisomer *syn*-40, mixture of regioisomers:

^{1}H-NMR (500 MHz, $CDCl_3$): δ (ppm) = 10.30-10.25 (m, 2H; H-15, H-33), 8.98-8.70 (m, 8H; H-1, H-4, H-8, H-11, H-19, H-22, H-26, H-29), 8.02-7.94 (m, 2H; H-20/H-21, H-27/H-28), 6.88-6.81 (2d, J_o = 8.7 Hz, J_o' = 8.7 Hz, 4H; H-3'), 5.46-5.41 (m, 4H; H-2'), 1.57-1.50 (3s, 18H; H-38), 1.15-1.13 (2s, 18H; H-6´).

MS (MALDI-TOF, DCTB): *m/z* = 1260.3 $[M]^+$.

HRLSI-MS: m/z Calcd for $[C_{70}H_{56}B_2Cl_4N_{12}O_2]$: 1260.3584; Found: 1260.3588.

UV-vis ($CHCl_3$): λ_{max} (nm) (log ε (dm^3 mol^{-1} cm^{-1})) = 710 (5.2), 679 (4.7), 651 (4.6), 610 (4.6), 515 (4.1), 437 (4.0), 327 (4.8).

*2.6.2.1.3 Dimer **41***

Dimer 41, 4:1 mixture of 41a and 41b topoisomers

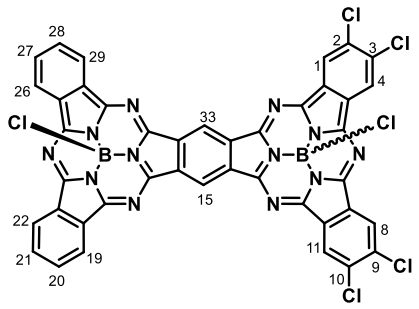

To a 10 ml round-bottom two-neck flask equipped with a reflux condenser and magnetic stirrer, a 1.0 M solution of BCl_3 in *p*-xylene (600 µL, 0.600 mmol) was added to the corresponding phthalonitrile (0.400 mmol of 4,5-dichlorophthalonitrile for SubPc **14**, 0.400 mmol of dicyanobenzene for SubPc **15**) under argon atmosphere. The slurry was stirred at room temperature for 5 min. Then, a solution of SubPc **14-15** (0.100 mmol) in dry *p*-xylene (1.4 mL) was added and the mixture was heated to reflux (136-138 °C) for 1 h. The crude was cooled down to room temperature and flushed with argon, and solvent was removed by rotary evaporation. The solid residue was purified by column chromatography on silica gel using toluene as eluent, yielding 13 mg (0.014 mmol) of product **41** as a blue solid. Yield: 14% (*syn*/*anti* 4:1 mixture).

Mp > 250 °C.

^{1}H-NMR (300 MHz, $CDCl_3$): δ (ppm) = 10.39 (s, 2H; H-15, H-33 **41a**), 10.33 (s, 2H; H-15, H-33 **41b**), 9.09 (s, 2H, H-1, H-11 **41a**), 9.03-8.94 (AA'BB' system, 4H; H-19, H-22, H-26, H-29 **41a**), 9.00 (s, 2H, H-4, H-8 **41a**), 8.98 (s, 2H, H-1, H-11 **41b**), 8.89 (s, 2H, H-4, H-8 **41b**), 8.90-8.81 (AA'BB' system, 4H; H-19, H-22, H-26, H-29 **41b**), 8.06-7.90 (AA'BB' system, 8H; H-20, H-21, H-27, H-28 **41a**/**41b**).

MS (MALDI-TOF, DCTB): *m/z* = 920.0 $[M]^+$.

HRLSI-MS: m/z Calcd for $[C_{42}H_{14}B_2Cl_6N_{12}]$: 919.9765; Found: 919.9747.

UV-vis ($CHCl_3$): λ_{max} (nm) (log ε (dm^3 mol^{-1} cm^{-1})) = 707 (5.2), 675 (4.7), 649 (4.6), 610 (4.6), 597 (sh), 500 (4.2), 438 (4.1), 323 (4.8), 279 (4.8).

*2.6.2.1.4 Dimers **42a** and **42b***

Dimers 42a and 42b, mixture of *syn* and *anti* topoisomers

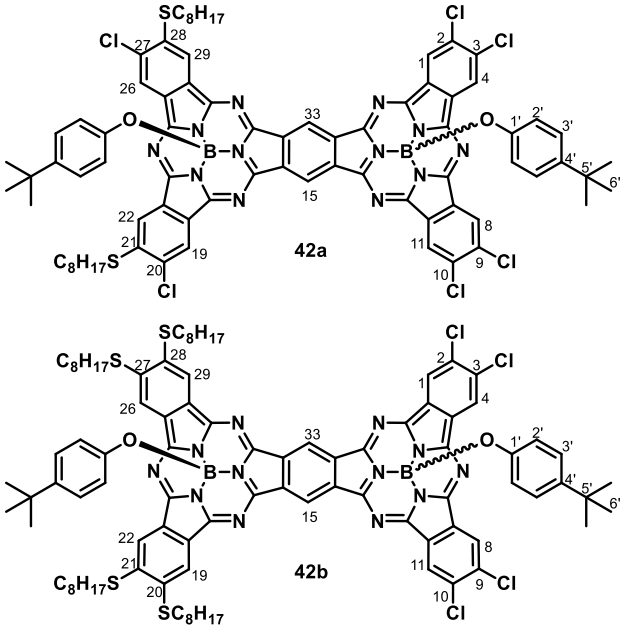

To a 10 ml round-bottom two-neck flask equipped with a reflux condenser and magnetic stirrer, a 1.0 M solution of BCl_3 in *p*-xylene (600 µL, 0.600 mmol) was added to 4,5-dioctylthiophthalonitrile (165 mg, 0.400 mmol), under argon atmosphere. The slurry was stirred at room temperature for 5 min. Then, a solution of SubPc **15** (73 mg, 0.100 mmol) in dry *p*-xylene (1.4 mL) was added and the mixture was heated to reflux (136-138 °C) for 2 h. The crude was cooled down to room temperature and flushed with argon. After evaporation of *p*-xylene, 4-*tert*-butylphenol (175 mg, 1.15 mmol) was added. The mixture was dissolved in *ca.* 1

mL of dry toluene and refluxed for 2 h. After cooling down to room temperature, the excess of phenol was removed by washing the crude with a 5:1 MeOH/water solution. Successive column chromatographies on silica gel using toluene/heptane 3:1 and $CHCl_3$/heptane 3:2 as eluents and purification by size exclusion chromatography using toluene as eluent rendered dimers **42a** (4.2 mg, 0.003 mmol, 3%) and **42b** (3.3 mg, 0.002 mmol, 2%) as *syn*/*anti* mixtures.

Dimer 42a, mixture of *syn* and *anti* topoisomers:

^{1}H-NMR (500 MHz, $CDCl_3$): δ (ppm) = 10.24-10.06 (m, 2H; H-15, H-33), 8.99-8.90 (m, 4H; H-1, H-4, H-8, H-11), 8.85-8.78 (m, 2H; H-19, H-26), 8.70-8.58 (m, 2H; H-22, H-29), 6.78-6.70 (m, 4H; H-3'), 5.37-5.29 (m, 4H; H-2'), 3.48-3.23 (m, 4H; $S\underline{CH_2}$), 2.02-1.86 (m, 4H; $SCH_2\underline{CH_2}$), 1.73-1.60 (m, 4H; $S(CH_2)_2\underline{CH_2}$), 1.49-1.16 (m, 16H; $S(CH_2)_3(\underline{CH_2})_4$), 1.04-1.02 (m, 18H; H-6'), 0.96-0.81 (m, 6H; $S(CH_2)_7\underline{CH_3}$).

MS (MALDI-TOF, DCTB): *m/z* = 1614.4 $[M - Cl + SC_8H_{17}]^+$, 1504.3 $[M]^+$.

HRLSI-MS: m/z Calcd for $[C_{78}H_{70}B_2Cl_6N_{12}O_2S_2]$: 1504.3501; Found: 1504.3517.

UV-vis ($CHCl_3$): λ_{max} (nm) (log ε (dm^3 mol^{-1} cm^{-1})) = 708 (5.2), 675 (4.8), 648 (4.8), 607 (4.9), 593 (5.0), 439 (4.4), 326 (5.1), 280 (5.3).

Dimer 42b, mixture of *syn* and *anti* topoisomers:

^{1}H-NMR (500 MHz, $CDCl_3$): δ (ppm) = 10.29-10.12 (m, 2H; H-15, H-33), 8.94-8.78 (m, 4H; H-1, H-4, H-8, H-11), 8.61-8.51 (m, 4H; H-19, H-22, H-26, H-29), 6.90-6.69 (m, 4H; H-3'), 5.51-5.27 (m, 4H; H-2'), 3.40-3.12 (m, 8H; $S\underline{CH_2}$), 2.00-1.74 (m, 8H; $SCH_2\underline{CH_2}$), 1.68-1.51 (m, 8H; $S(CH_2)_2\underline{CH_2}$), 1.46-1.21 (m, 32H; $S(CH_2)_3(\underline{CH_2})_4$), 1.16-1.14 (2s, 18H; H-6'), 0.95-0.82 (m, 12H; $S(CH_2)_7\underline{CH_3}$).

MS (MALDI-TOF, DCTB): *m/z* = 1724.6 $[M]^+$.

HRLSI-MS: m/z Calcd for $[C_{94}H_{104}B_2Cl_4N_{12}O_2S_4]$: 1724.6236; Found: 1724.6219.

UV-vis ($CHCl_3$): λ_{max} (nm) (log ε (dm^3 mol^{-1} cm^{-1})) = 720 (5.2), 696 (sh), 659 (4.8), 616 (4.9), 593 (4.9), 573 (sh), 524 (sh), 440 (4.5), 329 (sh), 281 (5.2).

2.6.2.2 Synthesis of symmetrical subphthalocyanine fused dimers

General procedure:

To a 25 ml round-bottom two-neck flask equipped with a reflux condenser and magnetic stirrer, a 1.0 M solution of BCl_3 in *p*-xylene (5.5 mL) was added to a mixture of 1,2,4,5-tetracyanobenzene (90 mg, 0.50 mmol) and of the corresponding dry phthalonitrile (5.00 mmol), under argon atmosphere. The mixture was stirred and heated to reflux (136-138 °C) for 2 hours. The crude was cooled down to room temperature and flushed with argon. The solvent was removed by rotary evaporation and the resulting dark solid was subjected to column chromatography on silica gel using a suitable eluent, as described in each case.

Dimers *anti*-2 and *syn*-2

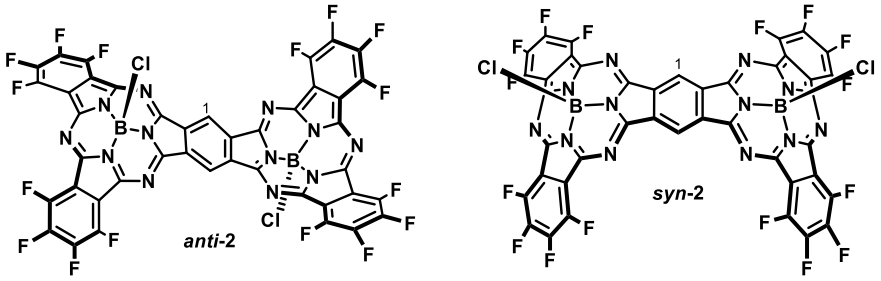

Dimers ***anti*-2** and ***syn*-2** were separated from perfluorinated SubPc **8c** by column chromatography on silica gel using CH_2Cl_2/heptane 3:2 as eluent. Mixture of *anti* and *syn* dimers was further subjected to column chromatography on silica gel using heptane/acetone 4:1 as eluent to afford 64 mg (0.060 mmol, 12%) of compound ***anti*-2** and 68 mg (0.062 mmol, 12%) of compound ***syn*-2** as blue solids. Overall yield: 24%.

Topoisomer *anti*-2:

^{1}H-NMR (300 MHz, $CDCl_3$): δ (ppm) = 10.48 (s, 2H; H-1).

^{19}F-NMR (470 MHz, $CDCl_3$): δ (ppm) = -137.7 (AA'BB' system, 6F), -146.0 (AA'BB' system, 6F).

MS (MALDI-TOF, DCTB): *m/z* = 1070.7 $[M]^+$.

HRLSI-MS: m/z Calcd for $[C_{42}H_2B_2Cl_2F_{16}N_{12}]$: 1069.9833; Found: 1069.9855.

UV-vis ($CHCl_3$): λ_{max} (nm) (log ε (dm^3 mol^{-1} cm^{-1})) = 692 (5.0), 662 (4.5), 636 (4.5), 605 (4.6), 592 (sh), 441 (4.0), 320 (4.6), 278 (4.5).

Topoisomer *syn*-2:

^{1}H-NMR (300 MHz, $CDCl_3$): δ (ppm) = 10.46 (m, 2H; H-1).

^{19}F-NMR (470 MHz, $CDCl_3$): δ (ppm) = -137.7 (AA'BB' system, 6F), -148.4 (AA'BB' system, 6F).

MS (MALDI-TOF, DCTB): *m/z* = 1070.7 $[M]^+$.

HRLSI-MS: m/z Calcd for $[C_{42}H_2B_2Cl_2F_{16}N_{12}]$: 1069.9833; Found: 1069.9825.

UV-vis ($CHCl_3$): λ_{max} (nm) (log ε (dm^3 mol^{-1} cm^{-1})) = 692 (5.0), 662 (4.5), 636 (4.5), 605 (4.6), 592 (sh), 441 (4.0), 320 (4.6), 278 (4.5).

Dimer 43, mixture of *syn* and *anti* topoisomers

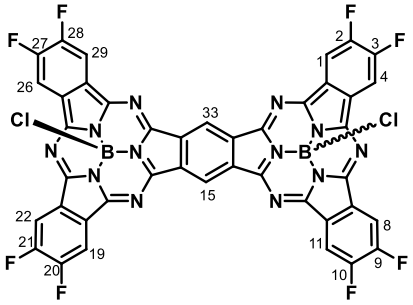

The solid residue was purified by column chromatography on silica gel using CH_2Cl_2/heptane from 1:1 to 3:1 as eluent, yielding 18 mg (0.020 mmol) of product **43** as a blue solid. Yield: 4% (*syn*/*anti* 1:1 mixture).

^{1}H-NMR (300 MHz, $CDCl_3$): δ (ppm) = 10.27 (s, 2H; H-15, H-33), 10.23 (s, 2H; H-15, H-33), 8.64-8.56 (m, 8H; H-4, H-8, H-22, H-26), 8.56-8.47 (m, 8H; H-1, H-11, H-19, H-29).

MS (MALDI-TOF, DCTB): *m/z* = 926.2 $[M]^+$.

HRLSI-MS: m/z Calcd for $[C_{42}H_{10}B_2Cl_2F_8N_{12}]$: 926.0596; Found: 926.0596.

UV-vis ($CHCl_3$): λ_{max} (nm) (log ε (dm^3 mol^{-1} cm^{-1})) = 693 (5.0), 662 (4.5), 639 (4.5), 603 (4.6), 590 (sh), 441 (4.0), 315 (4.6).

Dimer 44, mixture of *syn* and *anti* topoisomers

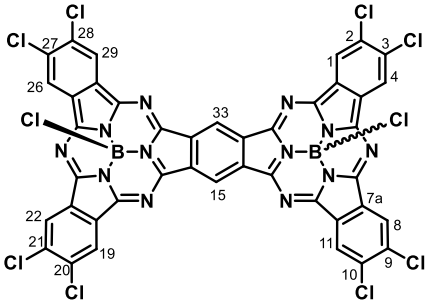

The solid residue was purified by column chromatography on silica gel using CH_2Cl_2/heptane from 1:1 to 2:1 as eluent, yielding 26 mg (0.025 mmol) of product **44** as a blue solid. Yield: 5% (*syn*/*anti* 1:1 mixture).

^{1}H-NMR (300 MHz, $CDCl_3$): δ (ppm) = 10.26 (2s, 2H; H-15, H-33), 8.92-8.84 (m, 8H; H-1, H-4, H-8, H-11, H-22, H-19, H-26, H-29).

MS (MALDI-TOF, DCTB): *m/z* = 1057.9 $[M]^+$.

HRLSI-MS: m/z Calcd for $[C_{42}H_{10}B_2Cl_{10}N_{12}]$: 1057.8178; Found: 1057.8207.

UV-vis ($CHCl_3$): λ_{max} (nm) (log ε (dm^3 mol^{-1} cm^{-1})) = 695 (5.0), 665 (4.4), 640 (4.4), 604 (4.5), 444 (4.0), 316 (4.7).

2.6.2.3 Synthesis of unsymmetrical subphthalocyanine fused trimer 50

Trimer 50 and dimer 51, mixture of topoisomers

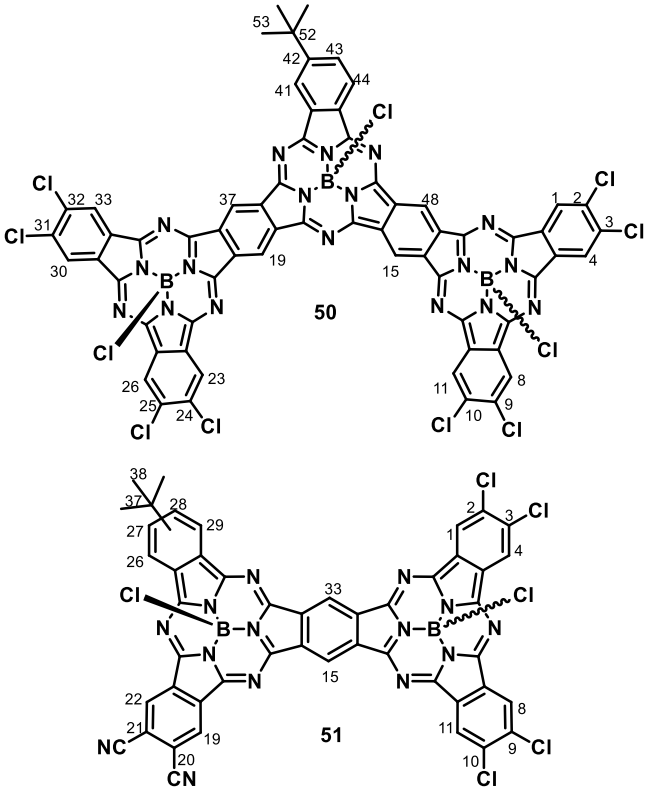

To a 10 ml round-bottom two-neck flask equipped with a reflux condenser and magnetic stirrer, a 1.0 M solution of BCl_3 in *p*-xylene (360 µL, 0.360 mmol) was added to 4,5-dichlorophthalonitrile (53 mg, 0.270 mmol), under argon atmosphere. The slurry was stirred at room temperature for 5 min. Then, a solution of SubPc **17** (32 mg, 0.045 mmol) in dry *p*-xylene (1.0 mL) was added and the mixture was heated to reflux (136-138 °C) for 1 h. The crude was cooled down to room temperature and flushed with argon, and solvent was removed by rotary evaporation. The solid residue was purified by column chromatography on silica gel using toluene as eluent, yielding trimer **50** (2.5 mg, 0.0018 mmol, 4%) and dimer **51** (1.9 mg, 0.0019 mmol, 4%) as blue solids.

Trimer 50, mixture of topoisomers:

^{1}H-NMR (500 MHz, $CDCl_3$): δ (ppm) = 10.39-10.26 (m, 4H; H-15, H-19, H-37, H-48), 9.07-8.75 (m, 10H; H-1, H-4, H-8, H-11, H-23, H-26, H-30, H-33, H-41, H-44), 8.03 (d, J_o = 8.3 Hz, 1H; H-43), 1.63-1.60 (m, 9H; H-53).

MS (MALDI-TOF, DCTB): *m/z* = 1467.9 $[M]^+$.

HRLSI-MS: m/z Calcd for $[C_{64}H_{24}B_3Cl_{11}N_{18}]$: 1467.9231; Found: 1467.9253.

UV-vis ($CHCl_3$): λ_{max} (nm) (log ε (dm^3 mol^{-1} cm^{-1})) = 783 (5.3), 744 (4.7), 711 (4.8), 667 (4.9), 651 (sh), 610 (4.6), 521 (4.5), 482 (sh), 428 (sh), 336 (5.0), 285 (4.0).

Dimer 51, mixture of topoisomers:

^{1}H-NMR (500 MHz, $CDCl_3$): δ (ppm) = 10.50-10.31 (m, 2H; H-15, H-33), 9.44-9.24 (m, 2H; H-19, H-22), 9.16-8.74 (m, 6H; H-1, H-4, H-8, H-11, H-26, H-29), 7.95 (m, 1H; H-27/H28), 1.63-1.60 (m, 9H; H-38).

MS (MALDI-TOF, DCTB): *m/z* = 1026.1 $[M]^+$.

HRLSI-MS: m/z Calcd for $[C_{48}H_{20}B_2Cl_6N_{14}]$: 1026.0299; Found: 1026.0320.

UV-vis ($CHCl_3$): λ_{max} (nm) (log ε (dm^3 mol^{-1} cm^{-1})) = 780 (4.4), 712 (5.2), 681 (4.8), 652 (4.8), 610 (4.8), 601 (4.8), 556 (sh), 482 (sh), 448 (4.3), 325 (5.0), 283 (5.0).

2.6.3 Synthesis of axially functionalized subphthalocyanine fused dimers

2.6.3.1 Synthesis of TMS-ethynyl functionalized axial substituents

*1-[(Trimethylsilyl)ethinyl)]pyrene (***55***)*[297]

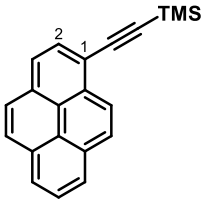

To a degassed solution of 1-bromopyrene (505 mg, 1.80 mmol) in dry Et_3N (60 mL), were successively added $Pd(PPh_3)_2Cl_2$ (126 mg, 0.180 mmol), CuI (126 mg, 0.180 mmol) and TMS-acetylene (1.26 mL, 8.98 mmol). The reaction mixture was stirred at 70 °C for 20 h. The solvent was evaporated under reduced pressure and the crude material was purified through silica gel column chromatography using heptane as eluent to give 526 mg (1.76 mmol) of **55** as a yellow oil. Yield: 98%.

^{1}H-NMR (300 MHz, $CDCl_3$): δ (ppm) = 8.57 (d, J_o = 9.1 Hz, 1H; H-2), 8.25-8.00 (m, 8H; Py-H), 0.40 (s, 9H; Si($\underline{CH_3}$)$_3$).

^{13}C-NMR (75.5 MHz, $CDCl_3$): δ (ppm) = 132.4, 131.5, 131.3, 131.2, 130.1, 128.5, 128.4, 127.4, 126.3, 125.8, 125.7, 125.7, 124.5, 124.4, 117.7, 104.2, 100.4, 0.3 (Si($\underline{CH_3}$)$_3$).

FT-IR (KBr), ν (cm^{-1}): 3041, 2957, 2898, 2149 (C≡C), 1738, 1600, 1582, 1487, 1407, 1365, 1248, 1184, 895, 836, 821, 756, 715, 633.

*1,4-Bis[(trimethylsilyl)ethynyl]benzene (***60***)*[298]

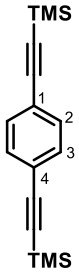

To a degassed solution of 1,4-dibromobenzene (2.0 g, 8.50 mmol) in dry Et_3N (25 mL), were successively added $Pd(PPh_3)_4$ (116 mg, 0.100 mmol), CuI (40 mg, 0.210 mmol) and TMS-acetylene (2.87 mL, 20.4 mmol). The reaction mixture was heated to reflux for 8 h. The solvent was evaporated under reduced pressure and the crude material was purified through silica gel column chromatography using heptane as eluent to give 2.07 g (7.65 mmol) of **60** as a white solid. Yield: 90%.

^{1}H-NMR (300 MHz, $CDCl_3$): δ (ppm) = 7.38 (s, 4H; H-2, H-3), 0.24 (s, 18H; Si($\underline{CH_3}$)$_3$).

^{13}C-NMR (75.5 MHz, $CDCl_3$): δ (ppm) = 131.7, 123.1, 96.3, 95.1, -0.1 (Si($\underline{CH_3}$)$_3$).

[297] Rocard, L.; Berezin, A.; de Leo, F.; Bonifazi, D. *Angew.Chem. Int.Ed.* **2015**, *54*,15739.
[298] Lim, S. H.; Cohen, S. M. *Inorg. Chem.* **2013**, *52*, 7862.

*1,3-Bis[(trimethylsilyl)ethynyl]benzene (***61***)*[299]

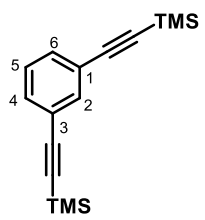

1,3-dibromobenzene (1 mL, 8.30 mmol), CuI (48 mg, 0.25 mmol) and $PdCl_2(PPh_3)2$ (155 mg, 0.22 mmol) were suspended in dry THF (30 mL). TMS-acetylene (3.60 mL, 25.50 mmol) and dry Et_3N (25 mL) were added and the resulting mixture was stirred at 50 °C in a pressure Schlenk tube under argon for 2 days. The crude product was filtered through celite. After removing the solvent, the solid obtained was purified through silica gel column chromatography using heptane as eluent to give 2.05 g (7.58 mmol) of **61** as a white solid. Yield: 89%.

^{1}H-NMR (300 MHz, $CDCl_3$): δ (ppm) = 7.59 (td, J_m = 1.7 Hz, J_p = 0.6 Hz, 1H; H-2), 7.39 (dd, J_o = 7.8 Hz, J_m = 1.7 Hz, 2H; H-4, H-6), 7.23 (td, J_o = 7.8 Hz, J_p = 0.6 Hz, 1H; H-5),0.24 (s, 18H; $Si(\underline{CH_3})_3$).

^{13}C-NMR (75.5 MHz, $CDCl_3$): δ (ppm) = 135.6, 131.9, 128.3, 123.5, 104.2, 95.0, 0.1 ($Si(\underline{CH_3})_3$).

2.6.3.2 Synthesis of bis-ethynylpyrene functionalized dimers

Dimers *anti*-54 and *syn*-54

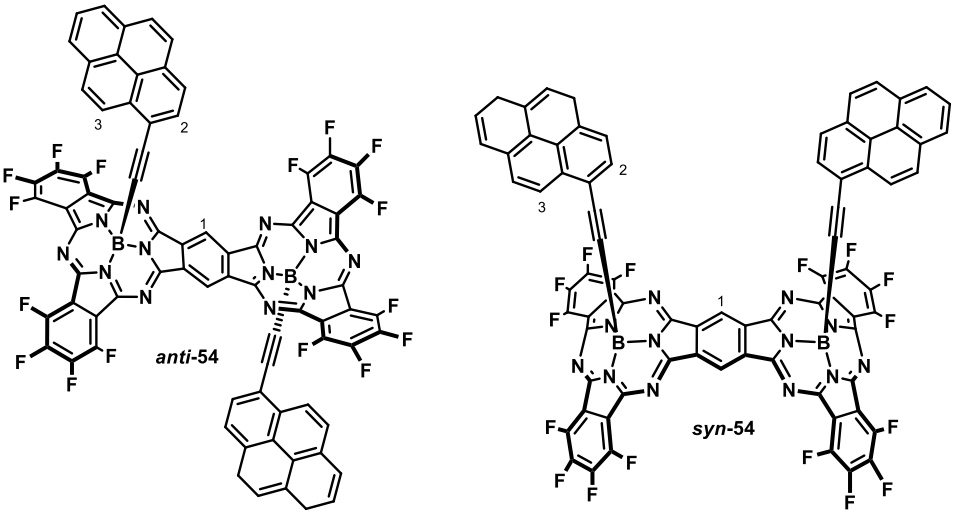

A 10 mL Schlenk flask was charged with dimer **2** (1:1 mixture of *syn* and *anti*, 160 mg, 0.150 mmol), 1-[(trimethylsilyl)ethinyl)]pyrene **55** (224 mg, 0.750 mmol) and *o*-dichlorobenzene (8 mL). The resulting solution was deoxygenated via three Freeze-Pump-Thaw cycles, $AlCl_3$ (80

[299] Asmus, S.; Beckendorf, S.; Zurro, M.; Mück-Lichtenfeld, C.; Fröhlich, R.; García-Mancheño, O. *Chem. Asian J.* **2014**, *9*, 2178.

mg, 0.600 mmol) was added and the suspension stirred at 25 °C for 30 min under argon atmosphere. Pyridine (0.1 mL) was added and solvent was removed by rotary evaporation. The dark blue reaction slurry was dissolved in CH_2Cl_2 and passed through a short silica plug. The solvent was removed by vacuum distillation and the resulting solid was subjected to column chromatography on silica gel using toluene/heptane 2:1 as an eluent to afford 69 mg (0.048 mmol, 32%) of compound ***anti*-54** and 78 mg (0.054 mmol, 36%) of compound ***syn*-54** as blue solids. Overall yield: 68%.

Topoisomer *anti*-54:

^{1}H-NMR (300 MHz, $CDCl_3$): δ (ppm) = 10.32 (s, 2H; H-1), 7.89-7.66 (m, 14H; Py-H), 7.52 (d, J_o = 9.1 Hz, 2H; H-3), 7.36 (d, J_o = 8.1 Hz, 2H; H-2).

MS (MALDI-TOF, DCTB): *m/z* = 1450.2 $[M]^+$.

HRLSI-MS: m/z Calcd for $[C_{78}H_{22}B_2F_{16}N_{12}]$: 1450.1881; Found: 1450.1887.

UV-vis ($CHCl_3$): λ_{max} (nm) (log ε (dm^3 mol^{-1} cm^{-1})) = 695 (5.1), 663 (4.6), 637 (4.6), 607 (4.7), 590 (sh), 451 (4.0), 366 (4.8), 348 (4.8), 322 (4.8), 285 (4.9), 276 (4.8).

Topoisomer *syn*-54:

^{1}H-NMR (300 MHz, $CDCl_3$): δ (ppm) = 10.18 (s, 2H; H-1), 8.17-8.06 (m, 4H; Py-H), 8.02-7.82 (m, 10H; Py-H), 7.73 (d, J_o = 9.1 Hz, 2H; H-3), 7.56 (d, J_o = 8.1 Hz, 2H; H-2).

MS (MALDI-TOF, DCTB): *m/z* = 1450.2 $[M]^+$.

HRLSI-MS: m/z Calcd for $[C_{78}H_{22}B_2F_{16}N_{12}]$: 1450.1881; Found: 1450.1889.

UV-vis ($CHCl_3$): λ_{max} (nm) (log ε (dm^3 mol^{-1} cm^{-1})) = 697 (5.1), 664 (4.6), 639 (4.6), 608 (4.7), 592 (sh), 454 (4.0), 366 (4.8), 348 (4.8), 323 (4.8), 285 (4.9), 276 (4.8).

2.6.3.3 Synthesis of ethynyl-boron subphthalocyanines and subphthalocyanine dimers

General procedure:

A 10 mL Schlenk flask was charged with SubPc **1** or **62** (0.100 mmol) or SubPc dimer **2** (1:1 mixture of *syn* and *anti*, 0.100 mmol), the corresponding bis(TMS-ethynyl) functionalized linker **59-61** (0.250 mmol for SubPcs **1,62**; 0.500 mmol for SubPc dimer **2**) and *o*-dichlorobenzene (5 mL). The resulting solution was deoxygenated via three Freeze-Pump-Thaw cycles, $AlCl_3$ (0.150 mmol for SubPcs **1,62**; 0.300 mmol for SubPc dimer **2**) was added and the suspension stirred at 25 °C for 30 min under argon atmosphere. Pyridine (0.1 mL) was added and solvent was removed by rotary evaporation. The reaction slurry was dissolved in CH_2Cl_2 and passed through a short silica plug. The solvent was removed by vacuum distillation and the resulting solid was subjected to column chromatography on silica gel using a suitable eluent, as described in each case.

*2.6.3.3.1 Subphthalocyanines **64-68***

Subphthalocyanine 64

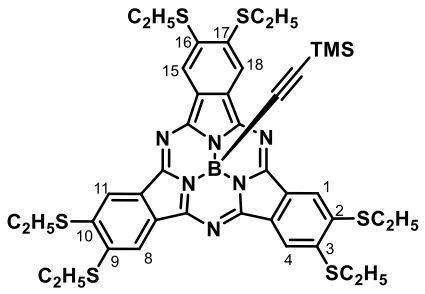

Eluent: heptane/EtOAc 7:1. Compound **64** was obtained as a greenish solid. Yield: 81%.

^{1}H-NMR (300 MHz, $CDCl_3$): δ (ppm) = 8.58 (s, 6H; H-1, H-4, H-8, H-11, H-15, H-18), 3.26 (t, J = 7.5 Hz, 12H; $S\underline{CH_2}$), 1.51 (t, J = 7.5 Hz, 18H; $SCH_2\underline{CH_3}$), -0.34 (s, 9H; $Si(\underline{CH_3})_3$).

MS (MALDI-TOF, DCTB): m/z = 852.2 $[M]^+$.

HRLSI-MS: m/z Calcd for $[C_{41}H_{45}BN_6S_6Si]$: 852.1894; Found: 852.1906.

UV-vis ($CHCl_3$): λ_{max} (nm) (log ε (dm^3 mol^{-1} cm^{-1})) = 599 (4.8), 575 (sh), 423 (4.4), 368 (4.5), 303 (4.8).

Subphthalocyanine 65

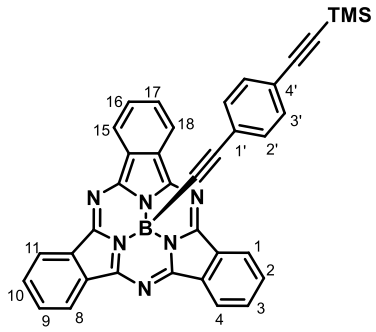

Eluent: heptane/EtOAc 4:1. Compound **65** was obtained as a pink solid. Yield: 90%.

^{1}H-NMR (300 MHz, $CDCl_3$): δ (ppm) = 8.90-8.83 (AA'BB' system, 6H; H-1, H-4, H-8, H-11, H-15, H-18), 7.93-7.86 (AA'BB' system, 6H; H-2, H-3, H-9, H-10, H-16, H-17), 7.03 (d, J_o = 8.6 Hz, 2H; H-3'), 6.66 (d, J_o = 8.6 Hz, 2H; H-2'), 0.14 (s, 9H; $Si(\underline{CH_3})_3$).

MS (MALDI-TOF, DCTB): m/z = 592.3 $[M]^+$.

HRLSI-MS: m/z Calcd for $[C_{37}H_{25}BN_6Si]$: 592.2004; Found: 592.1990.

UV-vis ($CHCl_3$): λ_{max} (nm) (log ε (dm^3 mol^{-1} cm^{-1})) = 566 (4.6), 529 (sh), 310 (4.4), 292 (4.6), 279 (4.6).

Subphthalocyanine 66

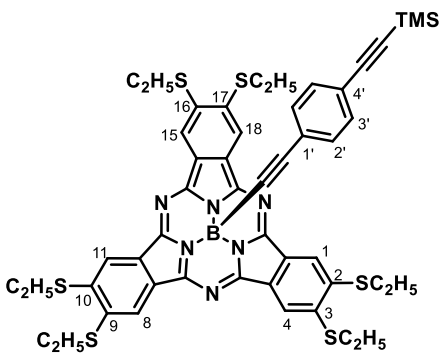

Eluent: heptane/EtOAc 5:1. Compound **66** was obtained as a greenish solid. Yield: 86%.

^{1}H-NMR (300 MHz, $CDCl_3$): δ (ppm) = 8.61 (s, 6H; H-1, H-4, H-8, H-11, H-15, H-18), 7.05 (d, J_o = 8.5 Hz, 2H; H-3'), 6.70 (d, J_o = 8.5 Hz, 2H; H-2'), 3.27 (t, J = 7.5 Hz, 12H; S$\underline{CH_2}$), 1.51 (t, J = 7.5 Hz, 18H; $SCH_2\underline{CH_3}$), 0.14 (s, 9H; Si($\underline{CH_3}$)$_3$).

MS (MALDI-TOF, DCTB): m/z = 952.3 $[M]^+$.

HRLSI-MS: m/z Calcd for $[C_{49}H_{49}BN_6S_6Si]$: 952.2208; Found: 952.2186.

UV-vis ($CHCl_3$): λ_{max} (nm) (log ε (dm^3 mol^{-1} cm^{-1})) = 598 (4.8), 572 (sh), 422 (4.4), 367 (4.5), 303 (4.8), 294 (4.7), 277 (4.6).

Subphthalocyanine 67

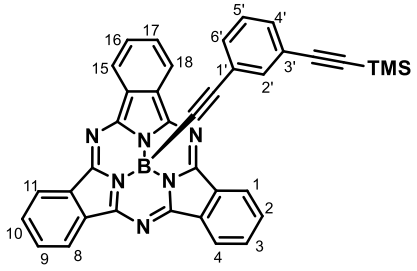

Eluent: heptane/EtOAc 3:1. Compound **67** was obtained as a pink solid. Yield: 82%.

^{1}H-NMR (300 MHz, $CDCl_3$): δ (ppm) = 8.84-8.78 (AA'BB' system, 6H; H-1, H-4, H-8, H-11, H-15, H-18), 7.85-7.76 (AA'BB' system, 6H; H-2, H-3, H-9, H-10, H-16, H-17), 7.09 (dd, J_o = 7.7 Hz, J_m = 1.5 Hz, 1H; H-4'), 6.90 (m, 1H; H-2'), 6.87 (t, J_o = 7.7 Hz, 1H; H-5'), 6.70 (dd, J_o = 7.7 Hz, J_m = 1.5 Hz, 1H; H-6'), 0.15 (s, 9H; Si($\underline{CH_3}$)$_3$).

MS (MALDI-TOF, DCTB): m/z = 592.3 $[M]^+$.

HRLSI-MS: m/z Calcd for $[C_{37}H_{25}BN_6Si]$: 592.2004; Found: 592.2011.

UV-vis ($CHCl_3$): λ_{max} (nm) (log ε (dm^3 mol^{-1} cm^{-1})) = 566 (4.6), 528 (sh), 308 (4.4), 273 (4.4).

Subphthalocyanine 68

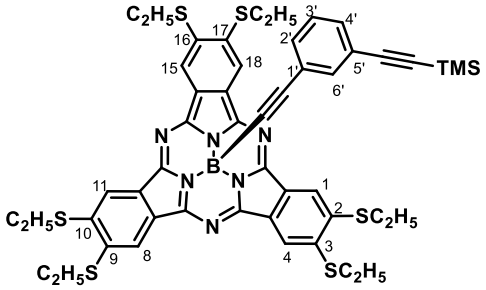

Eluent: heptane/EtOAc 7:1. Compound **68** was obtained as a greenish solid. Yield: 78%.

^{1}H-NMR (300 MHz, $CDCl_3$): δ (ppm) = 8.54 (s, 6H; H-1, H-4, H-8, H-11, H-15, H-18), 7.11 (dd, J_o = 7.7 Hz, J_m = 1.5 Hz, 1H; H-4'), 6.93 (m, 1H; H-2'), 6.90 (t, J_o = 7.7 Hz, 1H; H-5'), 6.78 (dd, J_o = 7.7 Hz, J_m = 1.5 Hz, 1H; H-6'), 3.26 (t, J = 7.5 Hz, 12H; S$\underline{CH_2}$),

1.51 (t, *J* = 7.5 Hz, 18H; $SCH_2\underline{CH_3}$), 0.13 (s, 9H; $Si(\underline{CH_3})_3$).

MS (MALDI-TOF, DCTB): *m/z* = 952.3 $[M]^+$.

HRLSI-MS: m/z Calcd for $[C_{49}H_{49}BN_6S_6Si]$: 952.2208; Found: 952.2208.

UV-vis ($CHCl_3$): λ_{max} (nm) (log ε (dm^3 mol^{-1} cm^{-1})) = 599 (4.8), 573 (sh), 422 (4.4), 362 (4.5), 304 (4.8).

*2.6.3.3.2 Dimers **56-58***

Dimers *anti*-56 and *syn*-56

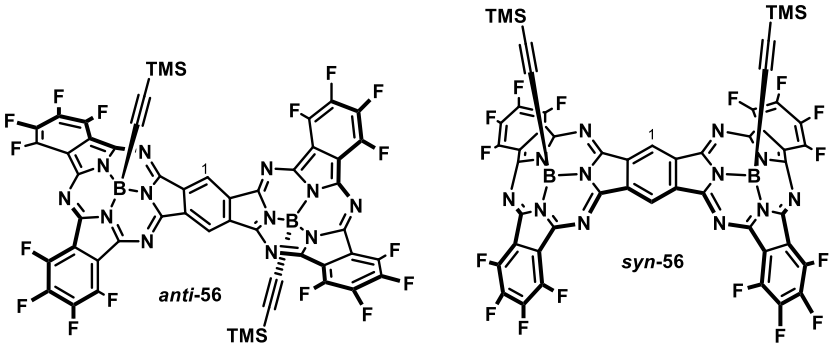

Eluent: $CHCl_3$/heptane 3:2. Compounds ***anti*-56** (0.045 mmol, 45%) and ***syn*-56** (0.045 mmol, 45%) were obtained as blue solids. Overall yield: 90%.

Topoisomer *anti*-56:

^{1}H-NMR (300 MHz, $CDCl_3$): δ (ppm) = 10.38 (s, 2H; H-1), -0.40 (s, 18H; $Si(\underline{CH_3})_3$).

MS (MALDI-TOF, DCTB): *m/z* = 1194.1 $[M]^+$.

HRLSI-MS: m/z Calcd for $[C_{52}H_{20}B_2F_{16}N_{12}Si_2]$: 1194.1415; Found: 1194.1423.

UV-vis ($CHCl_3$): λ_{max} (nm) (log ε (dm^3 mol^{-1} cm^{-1})) = 692 (5.1), 660 (4.7), 630 (4.6), 602 (4.7), 588 (sh), 448 (4.0), 318 (4.7), 259 (4.9).

Topoisomer *syn*-56:

^{1}H-NMR (300 MHz, $CDCl_3$): δ (ppm) = 10.34 (s, 2H; H-1), -0.27 (s, 18H; $Si(\underline{CH_3})_3$).

MS (MALDI-TOF, DCTB): *m/z* = 1194.1 $[M]^+$.

HRLSI-MS: m/z Calcd for $[C_{52}H_{20}B_2F_{16}N_{12}Si_2]$: 1194.1415; Found: 1194.1408.

UV-vis ($CHCl_3$): λ_{max} (nm) (log ε (dm^3 mol^{-1} cm^{-1})) = 692 (5.1), 661 (4.7), 633 (4.6), 605 (4.7), 591 (sh), 445 (4.0), 318 (4.7), 256 (4.9).

Dimers *anti*-57 and *syn*-57

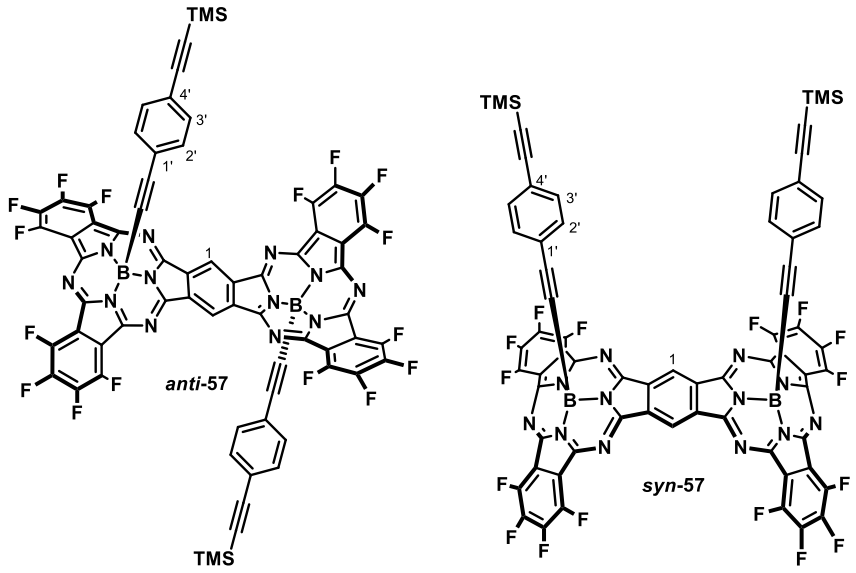

Eluent: $CHCl_3$/heptane 5:4. Compounds ***anti*-57** (0.040 mmol, 40%) and ***syn*-57** (0.035 mmol, 35%) were obtained as blue solids. Overall yield: 75%.

Topoisomer *anti*-57:

^{1}H-NMR (300 MHz, $CDCl_3$): δ (ppm) = 10.41 (s, 2H; H-1), 7.03 (d, J_o = 8.6 Hz, 4H; H-3'), 6.65 (d, J_o = 8.6 Hz, 4H; H-2'), 0.12 (s, 18H; Si($\underline{CH_3}$)$_3$).

MS (MALDI-TOF, DCTB): *m/z* = 1394.2 $[M]^+$.

HRLSI-MS: m/z Calcd for $[C_{68}H_{28}B_2F_{16}N_{12}Si_2]$: 1394.2044; Found: 1394.2041.

UV-vis ($CHCl_3$): λ_{max} (nm) (log ε (dm^3 mol^{-1} cm^{-1})) = 694 (5.1), 661 (4.8), 636 (4.8), 606 (4.8), 591 (sh), 444 (4.2), 320 (5.0), 291 (5.1), 278 (5.1).

Topoisomer *syn*-57:

^{1}H-NMR (300 MHz, $CDCl_3$): δ (ppm) = 10.25 (s, 2H; H-1), 7.13 (d, J_o = 8.5 Hz, 4H; H-3'), 6.82 (d, J_o = 8.5 Hz, 4H; H-2'), 0.18 (s, 18H; Si($\underline{CH_3}$)$_3$).

MS (MALDI-TOF, DCTB): *m/z* = 1394.2 $[M]^+$.

HRLSI-MS: m/z Calcd for $[C_{68}H_{28}B_2F_{16}N_{12}Si_2]$: 1394.2044; Found: 1394.2036.

UV-vis ($CHCl_3$): λ_{max} (nm) (log ε (dm^3 mol^{-1} cm^{-1})) = 696 (5.1), 663 (4.8), 638 (4.8), 607 (4.8), 590 (sh), 447 (4.2), 320 (5.0), 291 (5.1), 278 (5.1).

Dimers *anti*-58 and *syn*-58

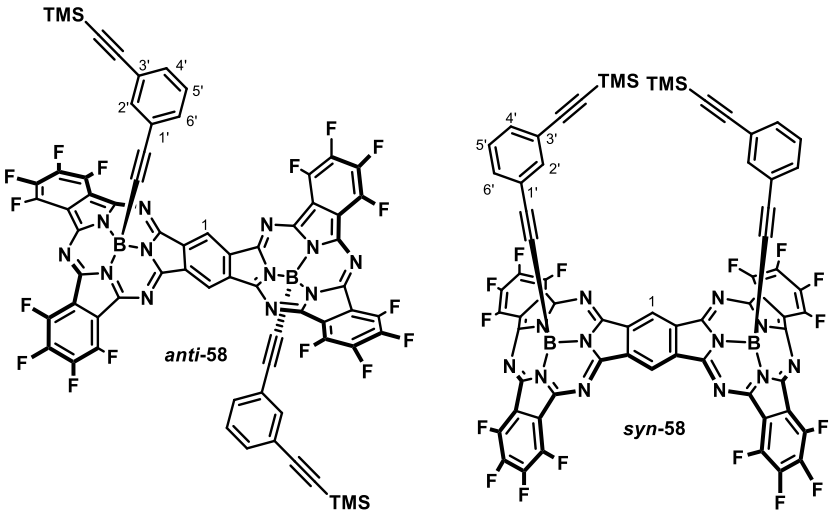

Eluent: $CHCl_3$/heptane 5:4. Compounds ***anti*-58** (0.043 mmol, 43%) and ***syn*-58** (0.033 mmol, 33%) were obtained as blue solids. Overall yield: 76%.

Topoisomer *anti*-58:

^{1}H-NMR (300 MHz, $CDCl_3$): δ (ppm) = 10.42 (s, 2H; H-1), 7.10 (dd, J_o = 7.8 Hz, J_m = 1.4 Hz, 2H; H-4'), 6.86 (t, J_o = 7.7 Hz, 2H; H-5'), 6.83 (s, 2H; H-2'), 6.64 (dd, J_o = 7.8 Hz, J_m = 1.4 Hz, 1H; H-6'), 0.09 (s, 18H; Si($\underline{CH_3}$)$_3$).

MS (MALDI-TOF, DCTB): *m/z* = 1394.2 $[M]^+$.

HRLSI-MS: m/z Calcd for $[C_{68}H_{28}B_2F_{16}N_{12}Si_2]$: 1394.2044; Found: 1394.2013.

UV-vis ($CHCl_3$): λ_{max} (nm) (log ε (dm^3 mol^{-1} cm^{-1})) = 693 (5.1), 662 (4.7), 636 (4.6), 606 (4.7), 591 (sh), 447 (4.0), 320 (4.7), 258 (4.9).

Topoisomer *syn*-58:

^{1}H-NMR (300 MHz, $CDCl_3$): δ (ppm) = 10.30 (s, 2H; H-1), 7.18 (dd, J_o = 7.7 Hz, J_m = 1.3 Hz, 2H; H-4'), 6.99 (s, 2H; H-2'), 6.97 (t, J_o = 7.7 Hz, 2H; H-5'), 6.80 (dd, J_o = 7.7 Hz, J_m = 1.3 Hz, 1H; H-6'), 0.17 (s, 18H; Si($\underline{CH_3}$)$_3$).

MS (MALDI-TOF, DCTB): *m/z* = 1394.2 $[M]^+$.

HRLSI-MS: m/z Calcd for $[C_{68}H_{28}B_2F_{16}N_{12}Si_2]$: 1394.2044; Found: 1394.2024.

UV-vis ($CHCl_3$): λ_{max} (nm) (log ε (dm^3 mol^{-1} cm^{-1})) = 695 (5.1), 663 (4.7), 637 (4.6), 607 (4.7), 591 (sh), 447 (4.0), 320 (4.7), 258 (4.9).

*2.6.3.3.3 Subphthalocyanine-Dimer Hybrids **71***

SubPc-Dimers *anti*-71

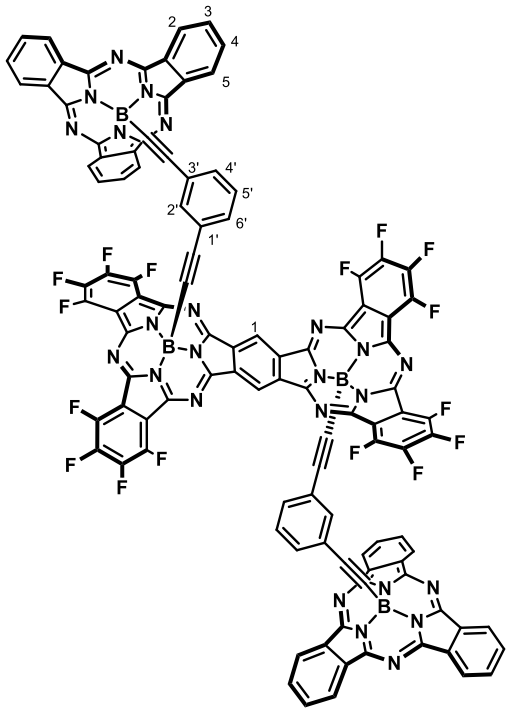

A 10 mL Schlenk flask was charged with dimer ***anti*-58** (20 mg, 0.015 mmol), SubPc **1** (15 mg, 0.036 mmol) and *o*-dichlorobenzene (2 mL). The resulting solution was deoxygenated via three Freeze-Pump-Thaw cycles, $AlCl_3$ (10 mg, 0.075 mmol) was added and the suspension stirred at 25 °C for 2 h under argon atmosphere. Pyridine (0.05 mL) was added and solvent was removed by rotary evaporation. The reaction slurry was dissolved in CH_2Cl_2 and passed through a short silica plug. The solvent was removed by vacuum distillation and the resulting solid was subjected to column chromatography on silica gel using toluene/THF 100:1 as an eluent to afford 3 mg (0.0015 mmol) of compound ***anti*-71** as a dark purple solid. Yield: 15%.

^{1}H-NMR (300 MHz, $CDCl_3$): δ (ppm) = 10.30 (s, 2H; H-1), 8.81-8.74 (AA'BB' system, 12H; H-2, H-5), 7.88-7.82 (AA'BB' system, 12H; H-3, H-4), 6.50-6.47 (m, 2H; H-5'), 6.38-6.30 (m, 4H; H-4', H-6'), 6.10 (m, 2H; H-2').

MS (MALDI-TOF, DCTB): *m/z* = 2038.3 $[M]^+$.

HRLSI-MS: m/z Calcd for $[C_{110}H_{34}B_4F_{16}N_{24}]$: 2038.3559; Found: 2038.3534.

UV-vis ($CHCl_3$): λ_{max} (nm) (log ε (dm^3 mol^{-1} cm^{-1})) = 694 (5.1), 662 (4.7), 636 (4.7), 606 (4.8), 568 (5.1), 524 (sh), 309 (5.1).

2.6.3.4 Synthesis of bis-ethynylSubPc functionalized dimers

Subphthalocyanine 74

To a 25 ml round-bottom two-neck flask equipped with a reflux condenser and magnetic stirrer, a 1.0 M solution of BCl_3 in *p*-xylene (3 mL) was added to a mixture of 4-iodophthalonitrile (255 mg, 1 mmol) and 4,5-dioctylthiophthalonitrile (833 mg, 2 mmol), under argon atmosphere. The mixture was stirred and heated to reflux for 45 min. The crude was cooled down to room temperature and flushed with argon. After evaporation of *p*-xylene, 4-

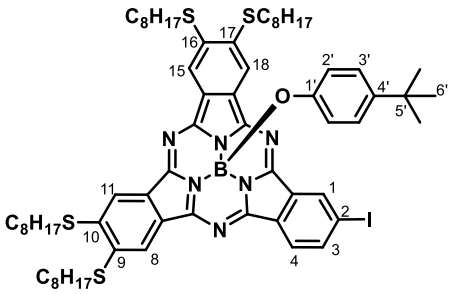

tert-butylphenol (750 mg, 5 mmol) was added. The mixture was dissolved in *ca.* 3 mL of dry toluene and refluxed for 4 hours. After cooling down to room temperature, the excess of phenol was removed by washing the crude with a 3:1 MeOH/water solution. The resulting dark solid was subjected to column chromatography on silica gel using heptane/EtOAc from 15:1 to 5:1 as an eluent to afford 271 mg (0.220 mmol) of compound **74** as a greenish oil. Yield: 22%.

^{1}H-NMR (300 MHz, $CDCl_3$): δ (ppm) = 9.19 (s, 1H; H-1), 8.59 (s, 4H; H-8, H-11, H-15, H-18), 8.54 (d, J_o = 8.8 Hz, 1H; H-4), 8.16 (d, J_o = 8.8 Hz, 1H; H-3), 6.75 (d, J_o = 8.7 Hz, 2H; H-3'), 5.30 (d, J_o = 8.7 Hz, 2H; H-2'), 3.33-3.15 (m, 8H; $S\underline{CH_2}$), 1.93-1.79 (m, 8H; $SCH_2\underline{CH_2}$), 1.67-1.51 (m, 8H; $S(CH_2)_2\underline{CH_2}$), 1.46-1.24 (m, 32H; $S(CH_2)_3(\underline{CH_2})_4$), 1.10 (s, 9H; H-6'), 0.93-0.85 (m, 12H; $\underline{CH_3}$).

MS (MALDI-TOF, DCTB): *m/z* = 1246.3 $[M]^+$, 1097.3 [M - axial group]$^+$.

UV-vis ($CHCl_3$): λ_{max} (nm) (log ε (dm^3 mol^{-1} cm^{-1})) = 589 (4.9), 544 (sh), 414 (4.5), 355 (4.6), 302 (4.8), 284 (4.8).

Subphthalocyanine 73

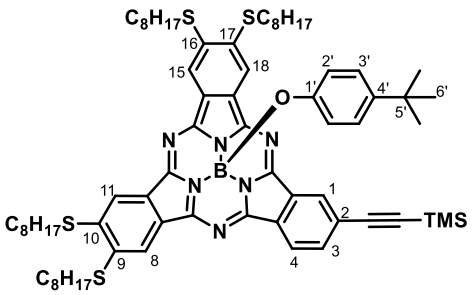

A 10 mL Schlenk flask was charged with SubPc **73** (150 mg, 0.120 mmol), CuI (2.3 mg, 0.012 mmol), $PdCl_2(PPh_3)_2$ (4.2 mg, 0.006 mmol), dry toluene (4 mL) and triethylamine (50 µL, 0.360 mmol) and the suspension was deoxygenated via three Freeze-Pump-Thaw cycles. Ethynyltrimethylsilane (83 µL, 0.600 mmol) was added and the suspension stirred at 25 °C for 1 h under argon atmosphere. Water was added and the product was extracted with CH_2Cl_2. The purple solution was then dried over Na_2SO_4. The solvent was removed by vacuum distillation and the resulting solid was subjected to column chromatography on silica gel using heptane/ EtOAc 8:1 as an eluent to afford 92 mg (0.076 mmol) of compound **73** as a dark purple solid. Yield: 63%.

^{1}H-NMR (300 MHz, $CDCl_3$): δ (ppm) = 8.94 (s, 1H; H-1), 8.73 (d, J_o = 8.2 Hz, 1H; H-4), 8.59-8.57 (2s, 4H; H-8, H-11, H-15, H-18), 7.93 (d, J_o = 8.2 Hz, 1H; H-3), 6.75 (d, J_o = 8.7 Hz, 2H; H-3'), 5.31 (d, J_o = 8.7 Hz, 2H; H-2'), 3.33-3.18 (m, 8H; $S\underline{CH_2}$), 1.92-1.79 (m, 8H; $SCH_2\underline{CH_2}$), 1.67-1.51 (m, 8H; $S(CH_2)_2\underline{CH_2}$), 1.46-1.23 (m, 32H; $S(CH_2)_3(\underline{CH_2})_4$), 1.08 (s, 9H; H-6'), 0.94-0.84 (m, 12H; $\underline{CH_3}$).

MS (MALDI-TOF, DCTB): *m/z* = 1216.6 $[M]^+$, 1067.6 [M - axial group]$^+$.

HRLSI-MS: m/z Calcd for $[C_{71}H_{97}BN_6OS_4Si]$: 1216.6475; Found: 1216.6440.

Dimer 75, mixture of *syn* and *anti* topoisomers

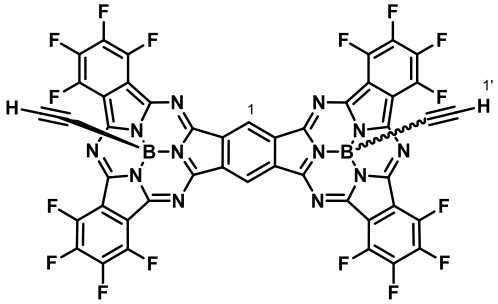

A 10 mL Schlenk flask was charged with dimer **75** (1:1 mixture of *syn* and *anti*, 160 mg, 0.150 mmol), ethynyltrimethylsilane (104 µL, 0.750 mmol) and *o*-dichlorobenzene (8 mL). The resulting solution was deoxygenated via three Freeze-Pump-Thaw cycles, $AlCl_3$ (80 mg, 0.600 mmol) was added and the suspension stirred at 25 °C for 30 min under argon atmosphere. Pyridine (0.1 mL) was added and solvent was removed by rotary evaporation. The dark blue reaction slurry was dissolved in CH_2Cl_2 and passed through a short silica plug. The solvent was removed by vacuum distillation and the resulting solid was subjected to column chromatography on silica gel using toluene/heptane 5:1 as an eluent to afford 94 mg (0.090 mmol) of compound **75** as a blue solid. Overall yield: 60% (*syn*/*anti* 1:1 mixture).

^{1}H-NMR (300 MHz, $CDCl_3$): δ (ppm) = 10.39 (s, 2H; H-1), 1.10 (s, 4H; H-1').

MS (MALDI-TOF, DCTB): *m/z* = 1050.1 $[M]^+$.

HRLSI-MS: m/z Calcd for $[C_{46}H_4B_2F_{16}N_{12}]$: 1050.0622; Found: 1050.0608.

UV-vis ($CHCl_3$): λ_{max} (nm) (log ε (dm^3 mol^{-1} cm^{-1})) = 692 (5.0), 662 (4.5), 636 (4.5), 605 (4.6), 592 (sh), 441 (4.0), 320 (4.6), 278 (4.5).

Dimer *syn*-72

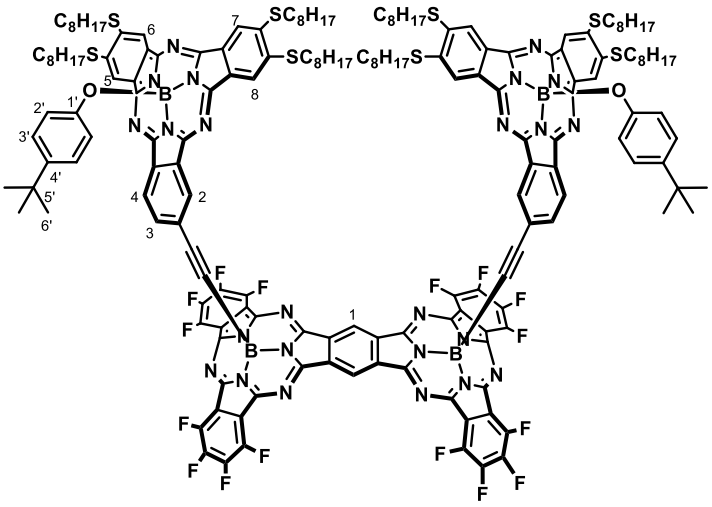

A 10 mL Schlenk flask was charged with SubPc dimer **75** (1:1 mixture of *syn* and *anti*, 50 mg, 0.048 mmol), CuI (1.9 mg, 0.010 mmol), $PdCl_2(PPh_3)_2$ (7.0 mg, 0.010 mmol), dry THF (4 mL) and triethylamine (1 mL) and the suspension was deoxygenated via three Freeze-Pump-Thaw cycles. SubPc **74** (125 mg, 0.100 mmol) was added and the suspension stirred at 25 °C for 1 h under argon atmosphere. The reaction slurry was dissolved in CH_2Cl_2 and passed through a short silica plug. The solvent was removed by vacuum distillation and the resulting solid was subjected to column chromatography on silica gel using $CHCl_3$/heptane 2:1 as an eluent and purification to obtain a pure fraction of dimer ***syn*-72** and a second fraction containing a mixture of dimers ***syn*-72**, ***anti*-72** and side products. By collecting the pure fractions of dimer ***syn*-72** obtained from several successive column chromatographies, a total amount of 24 mg (0.0073 mmol) of dimer ***syn*-72** was obtained as a dark purple solid. Yield: 15%.

^{1}H-NMR (300 MHz, $CDCl_3$): δ (ppm) = 10.50-10.45 (m, 2H; H-1), 8.49 (s, 4H; H-6, H-7), 8.44 (s, 2H; H-5), 8.40 (s, 2H; H-8), 8.37 (d, J_o = 8.8 Hz, 2H; H-4), 8.22 (d, J_m = 1.2 Hz, 2H; H-2), 7.17 (dd, J_o = 8.8 Hz, J_m = 1.2 Hz, 2H; H-3), 6.64 (d, J_o = 8.7 Hz, 4H; H-3'), 5.15 (d, J_o = 8.7 Hz, 4H; H-2'), 3.28-3.03 (m, 16H; $S\underline{CH_2}$), 1.89-1.72 (m, 16H; $SCH_2\underline{CH_2}$), 1.60-1.46 (m, 16H; $S(CH_2)_2\underline{CH_2}$), 1.40-1.20 (m, 64H; $S(CH_2)_3(\underline{CH_2})_4$), 0.99 (s, 18H; H-6'), 0.92-0.79 (m, 24H; $\underline{CH_3}$).

MS (MALDI-TOF, DCTB): *m/z* = 3288.3 $[M]^+$, 3139.3 [M - SubPc axial group]$^+$.

HRLSI-MS: m/z Calcd for $[C_{178}H_{178}B_4F_{16}N_{24}NaO_2S_8]$: 3311.2410; Found: 3311.2339.

UV-vis ($CHCl_3$): λ_{max} (nm) (log ε (dm^3 mol^{-1} cm^{-1})) = 696 (5.1), 664 (4.6), 635 (4.6), 594 (5.2), 543 (sh), 434 (4.5), 355 (sh), 308 (5.1), 281 (5.1).

Dimer *anti*-72

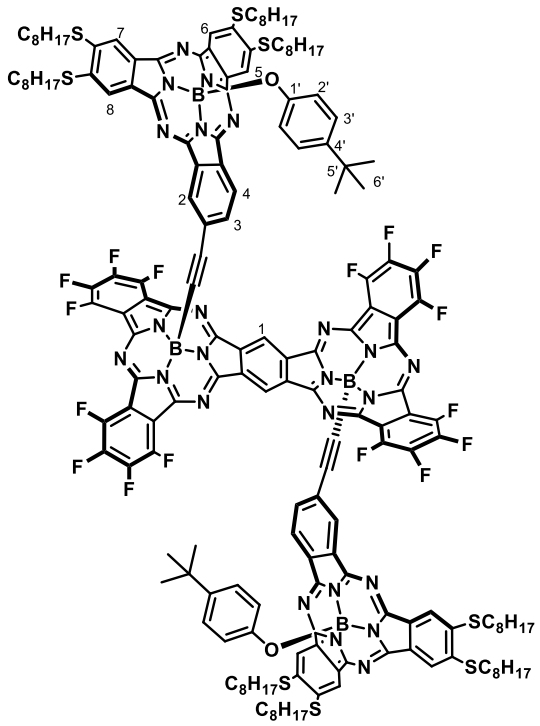

A mixture of dimers ***syn*-72**, ***anti*-72** and side products was subjected to size exclusion chromatography using THF as eluent to render 11 mg (0.0033 mmol) of dimer ***anti*-72** as a dark purple solid. Yield: 7%.

^{1}H-NMR (300 MHz, $CDCl_3$): δ (ppm) = 10.27-10.20 (m, 2H; H-1), 8.53-8.30 (m, 10H; H-4, H-5, H-6, H-7, H-8), 8.16 (s, 2H; H-2), 7.08 (d, J_o = 8.8 Hz, 2H; H-3), 6.62 (d, J_o = 8.5 Hz, 4H; H-3'), 5.14 (d, J_o = 8.5 Hz, 4H; H-2'), 3.29-3.05 (m, 16H; $S\underline{CH_2}$), 1.89-1.72 (m, 16H; $SCH_2\underline{CH_2}$), 1.60-1.45 (m, 16H; $S(CH_2)_2\underline{CH_2}$), 1.41-1.20 (m, 64H; $S(CH_2)_3(\underline{CH_2})_4$), 0.98 (s, 18H; H-6'), 0.92-0.79 (m, 24H; $\underline{CH_3}$).

MS (MALDI-TOF, DCTB): *m/z* = 3288.3 $[M]^+$, 3139.3 [M - SubPc axial group]$^+$, 2143.6 [M - SubPc unit]$^+$, 1144.6 [SubPc-ethynyl]$^+$, 1010.6 [SubPc-ethynyl- axial group + OH]$^+$.

HRLSI-MS: m/z Calcd for $[C_{178}H_{178}B_4F_{16}N_{24}NaO_2S_8]$: 3311.2410; Found: 3311.2296.

UV-vis ($CHCl_3$): λ_{max} (nm) (log ε (dm^3 mol^{-1} cm^{-1})) = 696 (5.1), 666 (4.6), 637 (4.6), 594 (5.2), 544 (sh), 434 (4.5), 353 (sh), 311 (5.1), 279 (5.1).

Resumen y Conclusiones

Las Subftalocianinas como Materiales Moleculares

Los Materiales Moleculares están constituidos por unidades moleculares de origen orgánico o metalorgánico que pueden ser sintetizadas individualmente y, en una segunda etapa, organizadas y/o polimerizadas en algún tipo de fase condensada (cristal líquido, película fina…). Estos materiales presentan propiedades eléctricas, ópticas y magnéticas no convencionales. La posibilidad de correlacionar las características estructurales de estos sistemas complejos con las propiedades observadas, así como la modificación de éstas por diseño molecular a través de síntesis orgánica convencional son, junto con la mayor facilidad de procesado, los puntos fuertes de este tipo de materiales. Los materiales moleculares y polímeros orgánicos han recibido una atención especial en los últimos años dirigida a sus aplicaciones tecnológicas.

Dentro de estos materiales, las ftalocianinas (Pcs) representan uno de los sistemas macrocíclicos más estudiados. Aunque su síntesis sigue siendo de gran interés científico, la preparación de nuevos análogos de tipo porfirinoide, tanto "expandidos" como "contraídos", resulta un amplio campo de estudio, aún en expansión, con un gran potencial.

Dentro de los análogos "contraídos", juegan un papel muy importante las subftalocianinas (SubPcs). Las SubPcs son macrociclos aromáticos que, a diferencia de las Pcs, presentan una estructura cóncava formada por tres unidades de diiminoisoindol.

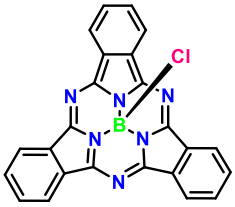

1

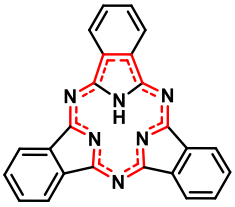

14 e⁻

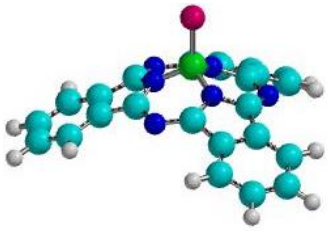

Las SubPcs poseen 28 electrones π que se extienden sobre 24 átomos de carbono y 6 átomos de nitrógeno. En su cavidad central, un átomo de boro se halla unido a tres átomos de nitrógeno de las unidades de isoindol y a un sustituyente que ocupa la posición axial de la molécula. La coordinación tetraédrica de este átomo central proporciona a las SubPcs su peculiar geometría. La deslocalización electrónica se produce preferentemente sobre los 14 electrones π del anillo interior, mientras que los anillos de benceno mantienen su estructura electrónica. Estas características convierten a las SubPcs en uno de los pocos ejemplos conocidos de compuestos aromáticos no planos compuestos por carbono y heteroátomos.

Las SubPcs se sintetizan generalmente mediante ciclotrimerización de un derivado de ftalonitrilo en presencia de un trihaluro de boro, BCl_3 o BBr_3, en cantidades estequiométricas, empleándose disolventes de alto punto de ebullición como *p*-xileno o clorobenceno. Debido a la limitación de grupos funcionales impuesta por el uso de reactivos de boro, el desarrollo de las modificaciones sintéticas de las SubPcs tanto en el ligando unido al átomo de boro como en los sustituyentes de las unidades aromáticas periféricas resulta de gran importancia. Estas variaciones estructurales permiten inducir cambios en sus propiedades físico-químicas, modificar su solubilidad, aumentar la extensión de su conjugación, incorporar estas unidades en sistemas electroactivos u organizarlas en ensamblajes supramoleculares.

Recientemente, se han desarrollado nuevas estrategias sintéticas que permiten una sustitución eficiente del átomo de halógeno axial original por diversos nucleófilos de naturaleza variada. Entre los numerosos sustituyentes axiales posibles, los derivados de fenol ofrecen, por motivos experimentales, numerosas ventajas: (i) están disponibles en grandes cantidades, (ii) aumentan la solubilidad del compuesto respecto a los derivados con un halógeno en posición axial y (iii) pueden resultar útiles para introducir nuevos grupos funcionales.

La reactividad periférica de las SubPcs engloba aquellas reacciones que provocan una modificación química en los sustituyentes de los anillos de isoindol. Dada la relativa inestabilidad química de estos macrociclos, los procedimientos sintéticos deben ser cuidadosamente seleccionados para mantener inalterada la estructura del anillo. Las reacciones de acoplamiento cruzado catalizadas por metales constituyen el método más empleado para funcionalizar las SubPcs en su periferia empleando SubPcs iodosustituidas como precursores.

Por otro lado, la condensación mixta de dos ftalonitrilos distintos en presencia de un haluro de boro conduce a la formación de derivados de SubPc con un patrón de sustitución diferente en cada una de las unidades de isoindol. Estas SubPcs asimétricamente sustituidas son compuestos de gran interés ya que pueden poseer no solo propiedades físicas intermedias entre las dos SubPcs simétricas correspondientes, sino también nuevas propiedades derivadas de la cooperación entre los distintos sustituyentes (por ejemplo, interacciones dador-aceptor).

El espectro de absorción característico de las SubPcs muestra una intensa banda en la región visible del espectro electromagnético, típicamente entre 550 y 600 nm, denominada banda *Q*, y una segunda banda de menor intensidad entre 260 y 370 nm, equivalente a la banda Soret de las Pcs. Los coeficientes de absorción ε, tanto de la banda Soret como de la banda *Q*, suelen oscilar entre 5-6 × 10^4 dm^3 mol^{-1} cm^{-1}.

Las SubPcs poseen excepcionales propiedades físico-químicas que las convierten en materiales de gran interés para su aplicación en multitud de dispositivos tecnológicos. Sus características electrónicas y fotofísicas permiten la generación de estados excitados de vida larga. Este hecho, junto con un creciente entendimiento de la morfología a escala nanométrica de los materiales moleculares basados en SubPcs, están permitiendo la aplicación de estos compuestos en campos como la óptica no lineal, la grabación óptica de información, la química supramolecular, la electrónica y la fotónica moleculares, la terapia fotodinámica y las células fotovoltaicas orgánicas (OPVs).

Materiales Orgánicos Activos en Fotovoltaica Molecular

El desarrollo y optimización de nuevas formas de energía se ha visto fuertemente impulsado en las últimas décadas, debido a una creciente preocupación sobre el impacto negativo en el medioambiente de los subproductos derivados de los combustibles fósiles. En este sentido, la conversión directa de energía solar en eléctrica a través de dispositivos fotovoltaicos ha sido extensamente estudiada. Complementariamente a las células inorgánicas, que se encuentran actualmente en uso comercial, se han desarrollado nuevas configuraciones basadas en materiales orgánicos o en la combinación de ambos, presentando varias ventajas como el hecho ser fáciles de preparar mediante técnicas de fabricación en disolución, lo que reduce su coste de producción, la ausencia de materiales activos tóxicos, y su flexibilidad y reducido peso, abriendo nuevas aplicaciones de las mismas.

Básicamente, las células solares orgánicas están constituidas por un material semiconductor orgánico dador y otro aceptor en contacto. En este sentido, la transformación de energía solar en energía eléctrica tiene lugar a través de una serie de procesos ópticos y electrónicos comunes a todo tipo de células solares orgánicas.

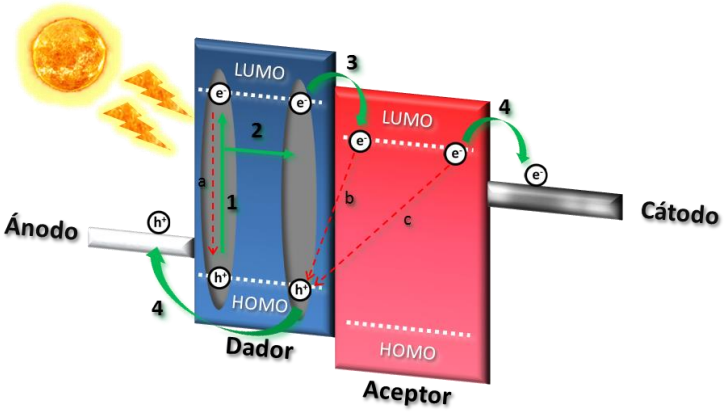

El funcionamiento de estas células es el siguiente: la luz incidente es inicialmente absorbida por el dador, lo que provoca el salto de un electrón del estado fundamental al excitado (paso 1), generándose un excitón. Este excitón difunde hacia la interfase dador/aceptor (paso 2), donde el electrón es transferido al estado excitado del aceptor, formándose un complejo de transferencia de carga. La disociación definitiva del excitón da lugar al estado de separación de carga (paso 3). Las cargas disociadas pueden entonces difundir a través del material dador y el aceptor hacia los electrodos, donde el ánodo recoge los huecos generados y el cátodo, los electrones (paso 4). Durante este proceso, también pueden ocurrir fenómenos no deseados que tienen lugar en la célula solar y que disminuyen su eficiencia, como son la recombinación del excitón o del par disociado en la interfase (procesos a y b), o la recombinación de la carga libre en su viaje al electrodo (proceso c).

En el desarrollo de nuevos compuestos orgánicos como materiales activos en células solares, contrasta el amplio número de materiales dadores investigados con la reducida variedad de materiales aceptores estudiados. En este sentido, los fullerenos y sus derivados dominan el panorama de materiales tipo n para células solares debido a que presentan una serie de propiedades muy convenientes para este fin, como su habilidad aceptora y transportadora de electrones, altos valores de movilidad electrónica, múltiples procesos de reducción reversibles, y capacidad para agregar en dominios adecuados para favorecer la separación de carga. Sin embargo, los aceptores fullerénicos poseen importantes limitaciones, como una débil absorción en el espectro visible, sus propiedades optoelectrónicas son difíciles de modular y su coste sintético es muy alto.

Por ello, en los últimos años, se está haciendo un gran esfuerzo en el desarrollo de nuevos tipos de materiales semiconductores orgánicos de tipo n para su empleo como materiales aceptores en células solares orgánicas. Estos compuestos, denominados aceptores no-fullerénicos, deben mantener las propiedades ventajosas de los fullerenos y, al mismo tiempo, permitir una variación más sencilla de sus propiedades a través de modificaciones sintéticas, presentar mejor solubilidad y procesabilidad en los disolventes adecuados y absorber energía solar intensamente en áreas amplias del espectro visible.

Entre los aceptores no-fullerénicos, las SubPcs poseen una serie de características optoelectrónicas que, junto con las múltiples opciones de funcionalización que presentan en sus posiciones periférica y axial, convierten estos compuestos en candidatos ideales para su estudio como materiales aceptores no-fullerénicos en células solares.

Capítulo 1: Derivados de SubPcs como Componentes Aceptores de Electrones en Células Solares Orgánicas

El **Capítulo 1** se centra en la síntesis, el estudio y la aplicación de diferentes derivados de SubPc como potenciales materiales aceptores de tipo no-fullerénico en células solares orgánicas.

En la primera sección se describe la síntesis de una nueva familia de SubPcs sustituidas en su periferia con grupos nitrilo. La introducción de estos sustituyentes π-conjugados aceptores de electrones en las unidades de isoindol se plantea como una estrategia interesante para modular las propiedades optoelectrónicas y el carácter semiconductor de tipo n de estos derivados.

La preparación de estos derivados de SubPc, que representa un reto sintético debido a la conocida inestabilidad de estos compuestos en presencia de bajas concentraciones de aniones cianuro en disolución, se ha conseguido por medio de una metodología sintética de dos pasos, consistente en la preparación de SubPcs iodosustituidas precursoras, seguida de una reacción de cianación catalizada por paladio. Se ha observado que el empleo de la técnica de microondas como fuente de calor en la etapa de cianación es esencial para el éxito de la reacción. La optimización de las condiciones de reacción de cada etapa de este procedimiento ha permitido la preparación con buenos rendimientos de una serie de derivados de SubPc asimétricos con uno o dos grupos *orto*-dinitrilo en sus bencenos periféricos, funcionalizados en las otras dos subunidades de isoindol con sustituyentes aceptores de electrones o dadores de electrones. Así mismo, se han sintetizado de la misma forma triciano-SubPcs con simetría C_3 y C_1 por separado.

Se han estudiado las características electrónicas y redox de estos nuevos derivados, así como la influencia de la introducción de los grupos nitrilo en sus propiedades. Se ha observado que la presencia de los sustituyentes nitrilo en la periferia de las SubPcs produce un notable desplazamiento batocrómico del máximo de absorción, unido a un incremento del coeficiente de extinción molar, y un aumento sustancial del carácter aceptor de la molécula. Todo ello confirma que la conjugación π está más extendida en estos derivados de SubPc que en sus análogos iodados, involucrando a los grupos *orto*-dinitrilo en la deslocalización electrónica. Además, cuanto mayor es el número de funcionalidades *orto*-dinitrilo que se introducen en la estructura, mayor es también el desplazamiento batocrómico que experimenta la banda *Q* y más fácilmente tienen lugar los fenómenos de reducción de la molécula.

Por otra parte, se han estimado los niveles de energía de los orbitales HOMO y LUMO de las ciano-SubPcs, tanto a partir de datos experimentales como por cálculos DFT. Los valores obtenidos demuestran que los derivados de SubPc sintetizados cubren un amplio rango de niveles energéticos de orbitales frontera, que varían gradualmente dependiendo del tipo de sustituyentes adicionales presentes en la periferia.

Finalmente, se ha medido la capacidad de conducción de portadores de carga de las nuevas SubPcs con grupos nitrilo y se ha comparado con la de otras SubPcs aceptoras ya conocidas, mediante técnicas novedosas sin contacto como la flash-photolysis time-resolved microwave conductivity (FP-TRMC), que permiten evaluar el movimiento de los portadores de carga sin el empleo de electrodos. Estas medidas se han llevado a cabo en el laboratorio del Prof. Shu Seki en la Universidad de Kyoto. Los valores de movilidad obtenidos para películas de ciano-SubPcs producidas por deposición de vapor se encuentran en el orden de 10^{-4} - 10^{-3} cm^2 V^{-1} s^{-1}, lo que supone una capacidad conductora similar o superior a la de las SubPcs empleadas como referencia.

Las destacables propiedades ópticas, la excelente capacidad aceptora de electrones y la habilidad conductora de carga de estos nuevos derivados de SubPc sustituidos con grupos nitrilo en la periferia constituyen una perspectiva prometedora para la aplicación de estos compuestos como semiconductores orgánicos de tipo n en la fabricación de dispositivos fotovoltaicos.

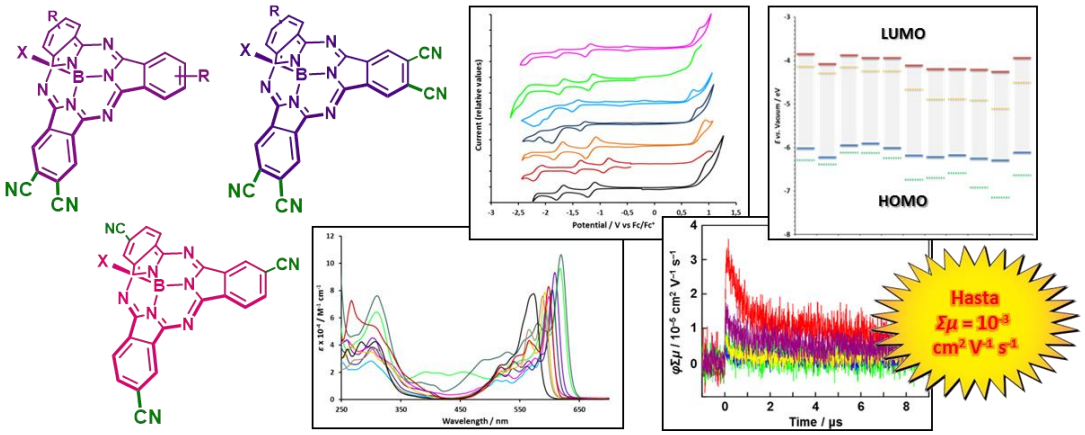

La segunda parte de este capítulo está dedicada al empleo de derivados de SubPc como aceptores no-fullerénicos en células solares de tipo heterounión plana.

Se espera que el uso de derivados de SubPc en estos dispositivos dé lugar a mayores eficiencias debido a un aumento del voltaje de circuito abierto V_{OC} y a una mejor absorción de la luz solar. Para este estudio, se han seleccionado cuatro SubPcs diferentemente funcionalizadas en su periferia basándose en sus propiedades optoelectrónicas. En concreto, se han escogido SubPcs evaporables que presentan sustituyentes aceptores de electrones de tipo halógeno (F, Cl) o grupos nitrilo, que permiten modular el nivel de energía de su orbital LUMO y su carácter semiconductor tipo n. Estos compuestos aceptores han sido combinados a su vez con cuatro materiales dadores con un "gap" energético y un nivel de energía HOMO adecuados y perfiles de absorción complementarios a los de los derivados de SubPc.

La fabricación de los dispositivos y las medidas pertinentes se han realizado en el laboratorio de Aernouts en el IMEC de Leuven. El estudio sistemático de la combinación de cada derivado de SubPc con cada material dador ha permitido crear una correlación entre el rendimiento del dispositivo fotovoltaico y los niveles energéticos de la interfase dador/aceptor. Las observaciones han confirmado que los valores de V_{OC} y de corriente fotoeléctrica muestran tendencias opuestas con respecto al valor de diferencia de energía en la interfase E_{DA}: mientras que la V_{OC} crece linealmente con la E_{DA}, la corriente fotoeléctrica decrece para mayores E_{DA}. Como resultado de esta compensación entre ambos factores, el aumento de la eficiencia de las células solares de heterounión plana reside en la optimización de los niveles energéticos de la interfase. La capacidad de modular de forma sencilla y predictiva el nivel LUMO de los derivados de SubPc aceptores constituye pues una gran ventaja para mejorar la eficiencia de estos dispositivos. Finalmente, se ha investigado la inserción de distintas capas adicionales, tanto para la extracción eficiente de carga en el cátodo como para el bloqueo de excitones en el ánodo, que permiten potenciar la generación de corriente fotoeléctrica del dispositivo. El ajuste y optimización de estas capas intermedias han dado lugar a un dispositivo fotovoltaico de heterounión plana con una eficiencia de 6.9% y una V_{OC} por encima de 1 V.

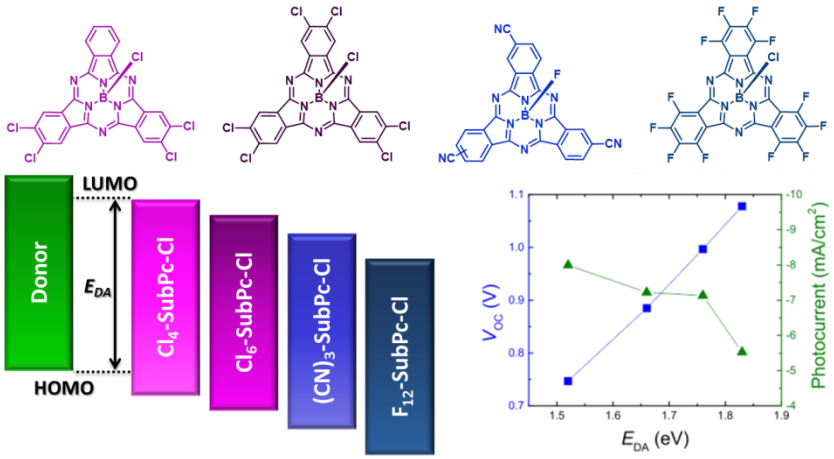

En la tercera sección, se presenta la fabricación de dispositivos fotovoltaicos de heterounión masiva procesados a partir de disoluciones de derivados de SubPc aceptores con materiales poliméricos dadores.

En concreto, se ha sintetizado para este propósito un conjunto de hexacloro-SubPcs funcionalizadas en posición axial con flúor, cloro y una serie de fenoles diferentemente sustituidos. El estudio de las propiedades optoelectrónicas de estos derivados evidencia que, mientras que la modificación del sustituyente axial de la SubPc apenas altera su espectro de absorción, el carácter aceptor de electrones del compuesto sí se ve ligeramente afectado por la naturaleza de dicho sustituyente.

La fabricación de los dispositivos y las medidas pertinentes se han realizado en el laboratorio del Prof. René Janssen en la Technische Universiteit de Eindhoven. De entre los diversos materiales dadores analizados, las mejores eficiencias se han obtenido con el polímero PTB7-Th. Además, se ha demostrado necesario el empleo de células solares de heterounión masiva con una arquitectura invertida para obtener mejores valores de eficiencia energética. Se ha registrado un rendimiento máximo del 4.0% para una combinación D/A con el derivado Cl_6-SubPc-Cl como material aceptor, lo que supone un récord de eficiencia para células solares basadas en SubPcs procesadas en disolución. Se ha verificado experimentalmente la contribución a la generación de corriente fotoeléctrica tanto por parte del polímero dador como de la SubPc aceptora. Además, se ha estudiado la influencia del sustituyente axial de la SubPc en su comportamiento de agregación y la relevancia que este hecho tiene en el resultado de eficiencia final del dispositivo. Las principal limitación que se ha encontrado en las células solares basadas en SubPcs aceptoras reside en el bajo valor del factor de forma *FF*

obtenido, como consecuencia de una reducida movilidad electrónica, una considerable recombinación bimolecular y una deficiente morfología de la heterounión masiva.

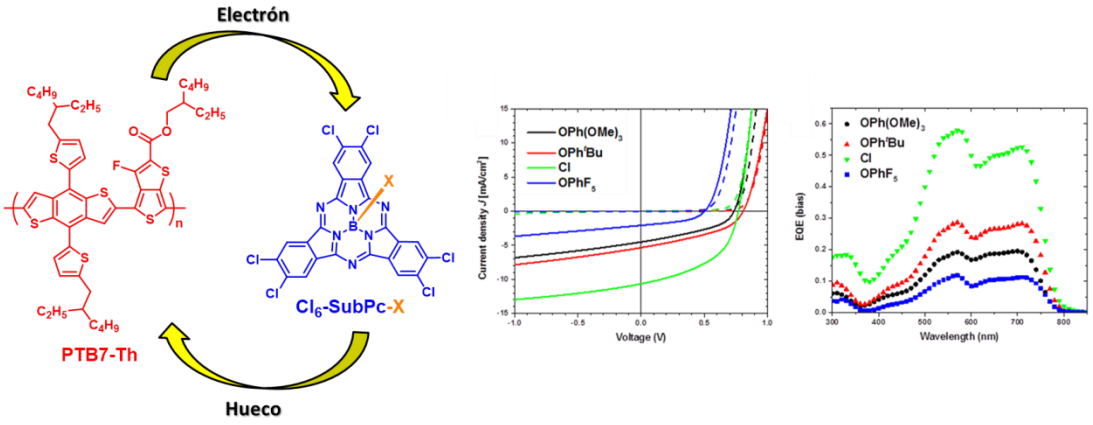

Capítulo 2: Funcionalización Axial y Periférica de Dímeros Fusionados de SubPc

El **Capítulo 2** se centra en la síntesis y caracterización de nuevos sistemas curvos π-extendidos basados en dímeros fusionados de SubPc y el estudio de sus propiedades y potenciales aplicaciones en el área de las tecnologías fotovoltaicas.

En la primera parte, se discute la preparación de una serie de oligómeros fusionados de SubPc con el objetivo de modular las propiedades optoelectrónicas de este tipo de materiales moleculares. Para ello, se ha diseñado una estrategia sintética basada en el empleo de los derivados de SubPc con funcionalidades *orto*-dinitrilo en la periferia descritos en el Capítulo 1 como ftalonitrilos extendidos. De esta forma, por condensación de derivados de diciano-SubPc o tetraciano-SubPc con otros ftalonitrilos, se podrían sintetizar respectivamente dímeros o trímeros fusionados de SubPc asimétricos. Además, la reacción de ciclotrimerización de una diciano-SubPc en condiciones de síntesis de SubPcs estándar daría lugar presuntamente a un tetrámero fusionado de SubPcs en forma de estrella. Este procedimiento ha permitido llevar a cabo la preparación de dímeros fusionados de SubPc asimétricos tanto con grupos dadores de electrones como aceptores de electrones en cada una de las unidades de SubPc constituyentes. Sin embargo, el número de dímeros que se ha podido sintetizar se ha visto limitado por diversos procesos indeseados, como la falta de reactividad, la descomposición y/o la polimerización de las *orto*-diciano-SubPcs en las condiciones de reacción. En el caso concreto del dímero asimétrico **39**, que presenta grupos *terc*-butilo dadores y sustituyentes cloro aceptores en cada unidad de SubPc, se ha conseguido la separación de los topoisómeros

sin y *anti* por medio de una reacción de funcionalización axial posterior. Por otra parte, se ha sintetizado un trímero de SubPc fusionado asimétrico por reacción de condensación mixta de un derivado de tetraciano-SubPc con otro ftalonitrilo, aunque en muy bajos rendimientos. Finalmente, los intentos por preparar oligómeros fusionados de SubPc de mayor tamaño han resultado infructuosos.

El estudio de las propiedades ópticas y electroquímicas de los dímeros fusionados de SubPc obtenidos confirma que las características electrónicas y redox de estos compuestos se pueden modular mediante su funcionalización periférica. Además, se han llevado a cabo estudios físico-químicos en el dímero **39** en el laboratorio del Prof. Dirk Guldi en la Universidad Friederich-Alexander de Erlangen para evaluar el carácter "push-pull" de los dímeros asimétricos. Estos experimentos han demostrado que la carga está polarizada en el sistema curvo π-extendido del dímero. Así, por medio de técnicas de fluorescencia de estado estacionario y espectroscopía de absorción transitoria, se ha establecido una naturaleza dual de su fluorescencia, caracterizada por un estado singlete excitado deslocalizado (1.73 eV) y un estado de transferencia de carga polarizado (<1.7 eV). La naturaleza de este estado de transferencia de carga se ha visualizado mediante cálculos DFT que muestran una ligera polarización del orbital HOMO hacia la unidad de SubPc con grupos dadores de electrones y del orbital LUMO hacia la unidad con grupos aceptores de electrones.

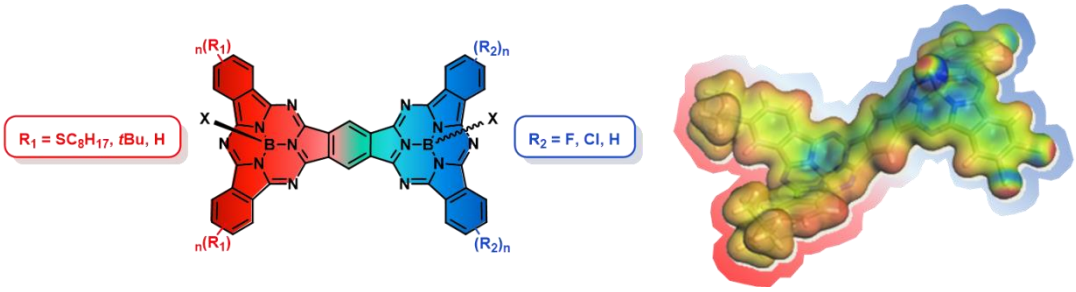

La segunda parte se centra en la preparación de sistemas multicomponente basados en dímeros fusionados de SubPc para su empleo en reconocimiento molecular y sistemas fotosintéticos artificiales supramoleculares. Para este fin, se ha explotado la funcionalización de las dos posiciones axiales disponibles que poseen estos compuestos para unir otras unidades fotoactivas a través de procedimientos sintéticos recientemente descritos en la química de las SubPcs. En concreto, la metodología basada en la funcionalización axial de SubPcs con sustituyentes TMS-alquinilo mediada por cloruro de aluminio ha permitido

preparar una serie de sistemas multicromofóricos basados en el uso de un dímero perfluorado de SubPc como plataforma.

En primer lugar, se han introducido dos unidades de etinilpireno en las posiciones axiales de los dímeros perfluorados de SubPc *sin* y *anti*. La rigidez y la corta longitud del espaciador alquinilo proporcionan a ambos topoisómeros una estructura tridimensional muy atractiva para la inmovilización de nanotubos de carbono, que daría lugar potencialmente a un centro de reacción fotosintético supramolecular basado en nanotubos de carbono como material dador.

Se han descrito los intentos para preparar sistemas constituidos por más de una unidad de derivado de SubPc o, como se han denominado en esta tesis, sistemas multi-SubPc. Se ha planteado la unión mutua de las posiciones axiales de derivados de SubPcs y un dímero fusionado de SubPc perfluorado. Para ello, se han sintetizado en buenos rendimientos una serie de SubPcs y dímeros de SubPc que presentan diferentes sustituyentes alquinilo conjugados unidos al átomo de boro. Desafortunadamente, una vez unidos a la posición axial de una SubPc, los sustituyentes TMS-alquino muestran una notable falta de reactividad, atribuida a un alto impedimento estérico en el estado de transición y a una disminución de su nucleofilia, lo que impide el ensamblado final de estos sistemas.

Por último, se han preparado híbridos multi-SubPc constituidos por un dímero fusionado de SubPc perfluorado (topoisómeros *sin* y *anti*) unido en sus posiciones axiales a la periferia de dos SubPcs asimétricas sustituidas con grupos tioéter a través de un enlace etinilo. Los estudios electroquímicos y fotofísicos de estado estacionario del híbrido ***syn*-72** sugieren la existencia de un proceso de transferencia electrónica desde las unidades de SubPc al dímero de SubPc excitado para general un par radical ($SubPc^{\bullet+}$-Dímero $SubPc^{\bullet-}$).

Además, la disposición que adquieren las dos unidades de SubPc en posición axial en este sistema da origen a sitios de reconocimiento molecular singulares en su estructura, que pueden ser empleados para la complejación de fullerenos. Por ello, se ha investigado la capacidad complejadora de los derivados de fullereno **C_{60}**, **C_{70}**, **C_{60}-PCBM** and **C_{70}-PCBM** por parte de este híbrido ***syn*-72** por medio de valoraciones utilizando las técnicas espectroscópicas de absorción, fluorescencia y RMN. Se ha demostrado que, inicialmente, ***syn*-72** forma un complejo supramolecular de estequiometría 1:1 con una unidad de fullereno en el que las SubPc sustituidas con grupos tioéter abrazan a la molécula huésped con constantes de asociación apreciables de entre 10^6 - 10^4 M^{-1}. En este proceso, la rigidez de los enlaces alquinilo provoca que esta cavidad, con un volumen bien definido, muestre una mayor afinidad por los derivados de fullereno de mayor tamaño. Posteriormente, se produce una

segunda interacción supramolecular entre la estructura cóncava del dímero de SubPc perfluorado *sin* y otra molécula de fullereno que depende tanto del tamaño como de las interacciones electrostáticas entre anfitrión y huésped. Se han calculado constantes de asociación entre 10^4 - 10^3 M^{-1} para este segundo proceso.

Inmovilización sobre SWCNTs

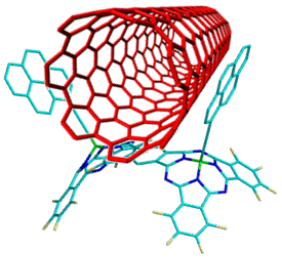

Complejación de Fullerenos